

UNIVERSITY OF TURIN

Department of Oncology

Phd School in life and Health Sciences

Molecular Medicine

XXIX Cycle

Academic Years: 2014-2017



TITLE

New pharmacological tools against doxorubicin-resistant osteosarcomas targeting mitochondria and endoplasmic reticulum of resistant cells

Tutor: Prof.ssa Chiara Riganti

Candidata: Dott.ssa Buondonno Ilaria

Coordinator: Prof. Francesco Novelli

Abstract

Osteosarcoma is the most frequent bone tumor. The presence of the drug efflux transporter P-glycoprotein (Pgp) is a negative prognostic factor in osteosarcoma patient because it impairs the efficacy of doxorubicin (Dox), the first-line treatment for this tumor.

In my PhD thesis I focused on two intracellular compartments – mitochondria and endoplasmic reticulum (ER) – that sporadic evidences from our reserach group and other groups have highlighted as key determinants in acquisition and maintenance of a chemoresistant phenotype due to Pgp expression. I validated the efficacy of synthetic multitarget Dox-derivatives, designed to be delivered in mitochondria and ER, respectively, and to impair the functions of these organelles, against Pgp-positive ostoesarcoma cells, refractory to parental Dox.

In the first part of this thesis I used a chemically modified Dox, called mtDox, characterized by a selective tropism for mitochondria. The novelty of the therapeutic strategy based on mtDox is related to two factors. First, we used a derivative of Dox, the efficacy of which is limited by the expression of Pgp and by the development of cardiotoxicity: mtDox did not induce toxicity in cardiomyocytes and was highly effective against Pgp-expressing osteosarcoma in vitro and in vivo, thus overcoming the main limitations encountered in patients treated with Dox-based regimens. Second, mtDox was particularly effective against Dox-resistant osteosarcomas because it exploited a metabolic signature typical of chemoresistant cells, i.e. the hyperactive oxidative mitochondrial metabolism. By impairing mitochondrial energy metabolism and redox balance, it altered an energy pathway that was crucial for drug resistant tumors, producing the mitochondria-triggered apoptosis of Pgp-expressing osteosarcoma cells.

In the second part of this PhD thesis I investigated the pharmacodynamic properties of the so-called Sdox, a H₂S-releasing Dox that was also less cardiotoxic beacuse of its ability to reduce the Dox-mediated oxidative stress in cardiomyocytes thanks to its H₂S-releasing moiety, but it retained its efficacy against Pgp-expressing osteosarcoma cells.

In osteosarcoma cells Sdox had a peculiar localization within ER: this finding may justify was Sdox was less available for Pgp efflux present on cell surface and was well retained within Pgp-expressing osteosarcoma cells. Moreover, the presence of Sdox, that can act either as pro- or anti-oxiadant agents within ER, the compartment where cellular proteins – including Pgp - are synthesized and folded, led us to investigate which effects were exerted by the drug on the physiological functions of ER.

Sdox induced a higher amount of sulfhydrated proteins in Dox-resistant cells than in sensitive cells. The sulfhydration was followed by protein ubiquitination. One of the protein sulfhydrated and ubiquitinated was Pgp, that was reduced in Sdox-treated cells. Sdox increased the expression of ER-associated degradation/ER quality control (ERAD/ERQC)-related genes in both sensitive and resistant cells, likely as a physiological consequence of the increased misfolded/unfolded proteins. Dox-resistant osteosarcoma cells had a defective ERAD/ERQC system compared to Dox-sensitive cells, and Sdox overflowed the buffering capacity of resistant cells inducing ER stress. As a consequence, Sdox triggered ER-dependent pro-apoptotic pathways. A preliminary in vivo experimental set validated the efficacy of Sdox in Dox-resistant osteosarcoma models as an effective tool able to reduce tumor growth, without inducing significant systemic toxicities.

My thesis demonstrated that alterations of physiological functions of mitochondria and ER are responsible for Dox-resistance mediated in osteosarcoma cells. Using mitochondria- and ER-targeting synthetic Dox, devoid of cardiotoxicity, reversed the resistance to Dox in Pgp-expressing osteosarcoma, in vitro and in vivo. These results may pave the way for the potential use of these synthetic Doxs in clinical settings, in particular for patients with Pgp-positive osteosarcomas or as a possible second-line treatment for relapsed patients.

1. Introduction.....	6
1.1 Osteosarcoma.....	6
1.1.1 Epidemiology.....	7
1.1.2 Treatment.....	8
1.1.3 Chemotherapy	9
1.1.4 Immunotherapy.....	10
1.2 Multidrug resistance.....	10
1.2.1 ATP binding cassette (ABC) transporters.....	12
1.2.2 P-glycoprotein.....	14
1.3 Approaches to overcome multidrug resistance.....	17
1.4 Doxorubicin.....	19
1.5 Mitochondria.....	21
1.6 Endoplasmic reticulum (ER).....	23
1.7 New synthetic doxorubicins targeting mitochondria and ER.....	26
2. Aims of the PhD thesis.....	29
3. Materials and Methods.....	30
3.1 Chemicals.....	30
3.2 Cells.....	30
3.3 ABCB1/Pgp and ABCC1/MRP1 expression.....	31
3.4 Doxorubicin accumulation.....	31
3.5 Cell viability and proliferation.....	31
3.6 Confocal microscope analysis.....	33
3.7 Immunogenic cell death assays.....	33
3.8 In vivo tumor growth, hematocemical parameters, and immunohistochemical analysis.....	33
3.9 Tumor cell phagocytosis.....	35
3.10 PCR arrays and qRT-PCR.....	35
3.11 Isolation of mitochondria, nuclei and microsomes	35
3.12 Mitochondrial DNA quantification	36
3.13 Mitochondria biogenesis.....	36
3.14 Tricarboxylic acid cycle.....	36
3.15 Fatty acids oxidation.....	37
3.16 Mitochondrial energy metabolism.....	37
3.17 Intramitochondrial reactive oxygen species levels	37
3.18 Mitochondrial electric potential ($\Delta\psi$) measurement.....	38
3.19 Immunoblotting.....	38
3.20 Kinetics of doxorubicin efflux.....	39
3.21 Quantification of sulphydrated microsomal proteins.....	40
3.22 Quantification of ubiquitinated microsomal proteins.....	40
3.23 Statistical analysis.....	41

4. Results	42
4.1 Expression of Pgp in doxorubicin-sensitive and doxorubicin-resistant osteosarcoma cells.....	42
4.2 Mitochondria targeting Dox.....	44
4.2.1 Mitochondria-targeting doxorubicin is effective against doxorubicin-resistant osteosarcoma in vitro	44
4.2.2 Mitochondria-targeting doxorubicin is effective against doxorubicin-resistant osteosarcoma in vivo.....	53
4.2.3 Mitochondria-targeting doxorubicin deeply alters the expression of mitochondria-related genes in doxorubicin-resistant osteosarcoma cells.....	58
4.2.4. Mitochondria-targeting doxorubicin reduces mitochondrial biogenesis, protein import and energy metabolism in doxorubicin-resistant osteosarcoma cells.....	86
4.2.5. Mitochondria-targeting doxorubicin triggers a mitochondria-dependent apoptosis in drug-resistant osteosarcoma cells	89
4.3 H ₂ S-releasing doxorubicin (Sdox).....	92
4.3.1 H ₂ S-releasing doxorubicin is not exert cytotoxicity on H9c2 cardiomyocytes.....	92
4.3.2 H ₂ S-releasing doxorubicin exerts cytotoxic effects against drug-resistant osteosarcoma cells.....	95
4.3.3 H ₂ S-releasing doxorubicin localizes within ER and up-regulates ERAD/ERQC-related genes.....	100
4.3.4 H ₂ S-releasing doxorubicin increases sulfhydrated proteins of ER and promotes their ubiquitination.....	114
4.3.5 H ₂ S-releasing doxorubicin decreases Pgp amount by promoting its sulfhydration and ubiquitination in resistant osteosarcoma cells.....	116
4.3.6 H ₂ S-releasing doxorubicin triggers ER-dependent apoptosis in drug-resistant osteosarcoma cells.....	119
4.3.7 H ₂ S-releasing doxorubicin is effective against doxorubicin-resistant osteosarcoma in vivo.....	124
5. Discussion	126
6. Future perspectives	134
7. References	136
8. Acknowledgments	145
9. Course and workshop	146
10. Oral and poster communication	147
11. Paper	148

1. Introduction

1.1 Osteosarcoma

Osteosarcoma (OS) is the most frequent bone tumor. Conventional OS (high-grade tumors, localized in the extremities in patients younger than 40 years without evidence of metastasis at diagnosis) are usually treated with pre- and post-operative chemotherapy, in association to the surgical removal of the tumor. Doxorubicin (Dox) is one of the leader drugs, together with cisplatin and methotrexate. Unfortunately, this multimodal treatment achieves control disease in no more than than 60% of OS patients. Despite alternative therapeutic strategies, the prognosis of OS has not significantly improved in the last decades (Hattinger CM, Expert Opin Emerg Drugs 2015; Hattinger CM, Future Oncol. 2017).

Symptoms of OS can vary depending on the size and location of tumour and include bone pain, particularly occurring at night, bone mass or swelling, restricted movement in a joint. Symptoms can be confused with more common problems such as a sports injury or growing pains in children and young people.

The diagnosis and grading of OS is usually performed by pathological analysis on bioptic samples and by imaging techniques. Identifying the stage and grade of OS is predictive of therapeutic response and outcome.

Grading:

Low-grade means that the cancer cells are slow-growing and look quite similar to normal cells. They are less aggressive and less likely to spread.

High-grade means the cancer cells are fast growing and look very anaplastic. They are more aggressive and more likely to spread.

Staging:

Stage 1 : The cancer is low-grade and has not grown outside the bone. Stage 1 is divided into:

- 1a The cancer is low-grade and is still completely within the bone it started in.
- 1b The cancer is low-grade and has grown through the bone wall.

Stage 2: The cancer is high-grade and has spread beyond the bone. Stage 2 is divided into:

- 2a The cancer is high-grade and is still completely in the bone it started in.
- 2b The cancer is high-grade and has grown outside the bone wall.

Stage 3: The cancer may be any grade and has metastasized to other tissues, such as the lungs.

(<https://sarcoma.org.uk/sarcoma-types/osteosarcoma>)

1.1.1 Epidemiology

The incidence rates (95% confidence intervals) of OS for all races and both sexes are 4.0 (3.5-4.6) for the range 0-14 years and 5.0 (4.6-5.6) for the range 0-19 years per year per million persons. OS accounts for 2.4% of all cancers in children and is the eighth cancer for incidence in childhood and young adolescent, after leukemias (30%), central nervous system cancers (22.3%), neuroblastoma (7.3%), Wilms tumor (5.6%), Non-Hodgkin lymphoma (4.5%), rhabdomyosarcoma (3.1%), retinoblastoma (2.8%). The incidence rates of childhood and adolescent OS has no geographical differences.

OS has a bimodal age distribution, having the first peak during adolescence and the second peak in older adulthood. The first peak is in the 10-14-year-old age group, coinciding with the pubertal growth spurt. This suggests a close relationship between the adolescent growth spurt and osteosarcoma. The second peak is in adults older than 65 years of age: it is likely a second malignancy, frequently related to Paget's disease.

OS commonly occurs in the long bones of the extremities near the metaphyseal growth plates. The most common sites are the femur (42%, with 75% of tumors in the distal femur), the tibia (19%, with 80% of tumors in the proximal tibia), and the humerus (10%, with 90% of tumors in the proximal humerus). Other locations are the skull or jaw (8%) and the pelvis (8%).

Cancer deaths due to bone and joint malignant neoplasms represent 8.9% of all childhood and adolescent cancer deaths. Death rates for OS have been declining by about 1.3% per

year. The overall 5-year survival rate for OS is 68%, without significant gender difference. The age of the patient is correlated with the survival, with the poorest survival among older patients. (Ottaviani G. *et Jaffe N* , Cancer Treat Res. 2009)

1.1.2 Treatment

Many clinical trials are focusing on treating OS using a variety of strategies.

Surgery: surgery, along with newer imaging tests that better define the extent of tumors, aims at removing cancer mass and sparing as much normal tissue as possible. For reconstruction, internal prostheses can now be expanded without the need for more surgery. This is especially important for children, who in the past often needed several operations to replace the prosthesis with a larger one as they grew.

Radiation therapy: OS cells are relatively radioresistant, so high doses are needed to obtain a therapeutic effect. This has limited the use of radiation, because high doses can often cause unacceptable side effects. Intensity-modulated radiation therapy (IMRT) is an example of an advanced form of radiotherapy. The intensity (strength) of the beams can also be adjusted to limit the dose reaching nearby normal tissues. A newer approach is to use radioactive particles instead of X-rays, such as protons beams. Unlike X-rays, which release energy both before and after they hit their target, protons cause little damage to tissues they pass through and then release their energy after traveling a certain distance. As with IMRT, proton beam therapy may be helpful for hard-to-treat tumors, such as those on the spine or pelvic bones.

Chemotherapy: Clinical trials are being done to determine the best combinations of chemotherapy drugs, as well as the best time to give them (see paragraph 1-1-3 for details on chemotherapy protocols).

Photodynamic therapy (PDT) is one of the most promising and minimally invasive treatments developed in the last years, for the treatment of superficial tumors. Three basic factors – choice of proper photosensitizer, choice of appropriate light source and ability to kill tumor cells by inducing oxidative stress - are responsible for tumor cell cytotoxicity. PDT in OS is still under evaluation (Wei Yu *et al.*, Oncotarget 2017)

1.1.3 Chemotherapy

Standard chemotherapy protocols for high-grade OS include doxorubicin, cisplatin, high-dose methotrexate and/or ifosfamide and/or etoposide. Clinical evidence collected in the past decades has allowed to understand that regimens based on the use of three drugs (doxorubicin, cisplatin, methotrexate) achieved significantly better results than two-drug treatments. The addition of a fourth drug - in most cases ifosfamide - has not significantly improved the clinical outcome, still leaving open the question whether this strategy should be considered for the first-line treatment of all OS patients or rather only for those patients who poorly respond to preoperative chemotherapy (Anninga JK *et al.*, Eur J Cancer 2011). The major clinical problem that chemotherapy encounters is the development of drug resistance (see paragraphs 1.2 for details). The second main problem is that chemotherapy often fails in preventing the development of metastasis, which usually occur within the first 24 - 36 months from diagnosis in high-grade OS. Later relapses in bone are also documented but they are less frequent (Anninga JK *et al.*, Eur J Cancer 2011 ; Ferrari S *et al.*, J Pediatr Hematol Oncol 2006).

The lungs are the most common site of OS metastasis: recently, inhaled forms of some chemo drugs (such as cisplatin) are being studied for patients with OS lung metastases.

(<https://www.cancer.org/cancer/osteosarcoma/about/new-research.html>)

Treatment of relapsed OS patients is based on different therapeutic approaches and second-line chemotherapy protocols, which, however, have not provided satisfactory results, being able to rescue no more than 20 - 25% of patients (Bacci G *et al.*, Acta Oncol 2006 ; Kempf-Bielack B *et al.*, J Clin Oncol 2005). It is therefore clear that new treatment approaches and drugs are needed to improve the results of the current chemotherapy protocols. Identification of new therapeutic markers and targeted drugs is even more important for relapsed OS patients, in order to improve the dismal results that are currently achievable with the available second-line treatment protocols (Hattinger CM *et al.*, Expert Opinion on Emerg Drugs 2015)

1.1.4 Immunotherapy

The key role played by the microenvironment in the disease increases the number of therapeutic targets (such as macrophages or osteoclasts), as well as the key proteins that control cell proliferation or cell death. (Heymann MF *et al.*, Expert Opin Invest Drugs 2016)

Recent evidence reveals that using dendritic cells (DC)-based immunotherapy may elicit cytotoxic T cell response in preclinical OS models (He YT *et al.*, Oncol Lett 2016). T cells play an essential role in mediating potent tumor-specific immune responses, and may provide a rational basis for tumor immunotherapies, such as adoptive cell transfer (ACT) (Yang JC *et al.*, Cancer Adv Immunol 2016)

Clinical investigations of immune checkpoint inhibitors have demonstrated activity in multiple types of neoplasms (Naidoo J *et al.*, Br J Cancer 2014). Checkpoint inhibitors are planned to be included in combination strategy for treatment of OS in the next future (Tsukahara T *et al.*, Expert Opin Biol Ther 2016).

Immunogenic cell death (ICD) is characterized by the early surface exposure of calreticulin (CRT). On the surface of apoptotic tumor cells CRT mediates the recognition and phagocytosis of tumor cells by antigen presenting cells. It has been demonstrated that capsaicin induces the translocation of CRT from intracellular compartments to the cell surface in human OS cells. CRT in turn promotes the DC-mediated phagocytosis of tumor cells, thereby mediating tumor cell ICD. (Tao Jin *et al.*, Exp Ther Med 2016)

Chemo-immunotherapy is a very promising approach in the treatment of the most aggressive cancers, refractory to the conventional anticancer drugs (Brady P *et al.*, J Immunother. 2009). Studies in this field are under development in particular for the treatment of metastatic or relapsed OS (Wan J *et al.*, Onco Lett, 2016)

1.2 Multidrug Resistance

About seven million people die of cancer and 12 million new cases arise every year (Garcia M *et al.*, Global cancer facts 2007). Over 90% of the deaths are caused by failure of chemotherapy, mostly due to multidrug resistance (MDR). MDR is a term describing the variety of the strategies that cancer cells use to avoid cytotoxic and immunogenic effects of anticancer drugs. Chemoresistance can be either acquired after exposure to chemotherapy

itself (induced or acquired MDR) or innate (constitutive MDR). A common feature is that tumor is cross-resistant to a wide range of structurally and functionally unrelated drugs (Longley DB *et al.*, J Pathol 2005). The resistance phenotype is heterogeneous and dynamic, involving a combination of independent molecular mechanisms that are functionally regulated during tumor progression and treatment (Szakács G *et al.*, Nat Rev Drug Discov 2006). Indeed, cancer cells escape chemotherapy by a number of different mechanisms that modulate genetic and epigenetic features of the tumor and its environment. These mechanisms include processes limiting anticancer drug concentrations (by decreased drug influx, increased drug efflux, vesicular sequestration and enhanced drug metabolism); change of ionic environment (by modification in pH and Ca²⁺ concentration); prevention of drug induced cell death (such as increased DNA repair mechanisms and decreased cell death apparatus); changes in the molecular targets (e.g. decreased topoisomerase II alpha activity for anthracyclines, mutated thymidylate synthase and/or folate reductase for anti-folate agents).

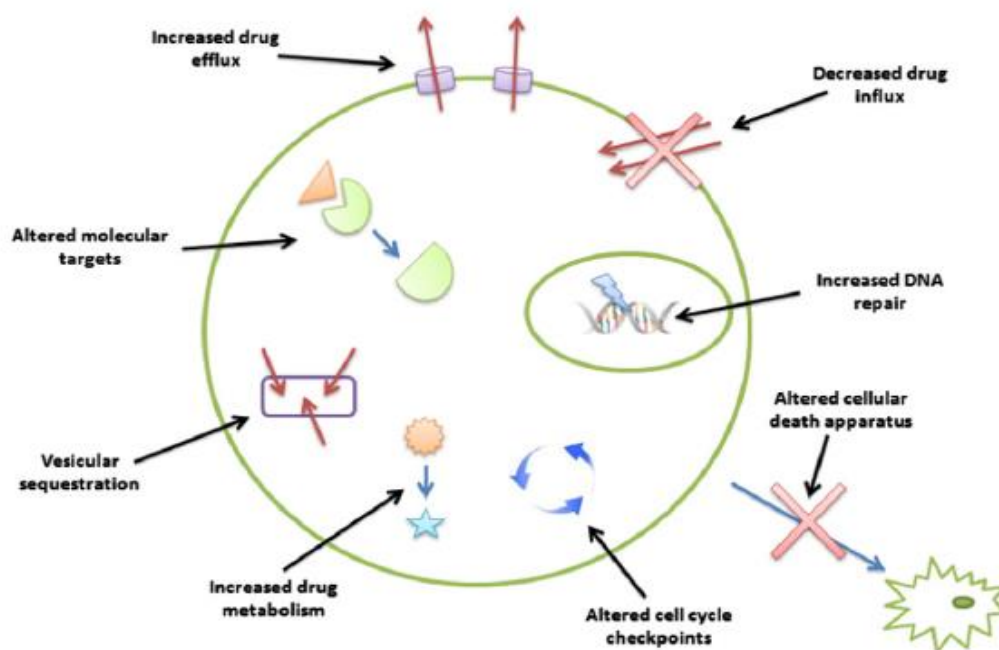


Figure 1. Mechanisms of drug resistance in cancer cells. Cancer cells can evade chemotherapeutic treatment by increasing active drug efflux, decreasing drug influx, increasing DNA repair mechanisms, altering apoptotic machinery and cell cycle checkpoints, enhancing drug metabolism, increasing vesicular sequestration or altering molecular drug targets (adapted from Gong J *et al.*, Cancer Treat Rev. 2012)

1.2.1 ATP binding cassette (ABC) transporters

One of the main mechanisms of MDR is the overexpression of transmembrane drug efflux transporters in resistant cancer cells: these efflux pumps reduce drug levels in the intracellular cancer cells, allowing cell survival. Most transporters involved in MDR utilize the energy of ATP hydrolysis to extrude drugs out of the cell against a concentration gradient and belong to the ATP Binding Cassette (ABC) superfamily, a conserved family of proteins, present in all living organisms from prokaryotes to mammals.

ABC transporters are integral membrane proteins, named after a conserved, specific domain of 200- to 250- aminoacids which can bind and hydrolyze ATP, known as nucleotide binding domain (NBD) (Ni Z *et* Mao Q, *Curr Pharm Biotechnol.* 2011 ; Zhou SF, *Xenobiotica*, 2008). ABC transporters contain transmembrane domains (TMD), composed in most cases of two modules of six membrane spanning helices forming a channel, whose opening and closing is regulated by the binding of ATP. Active ABC transporters contain a minimum of two NBDs and two TMDs. These four elements in many cases are present in one single polypeptide chain (Fig. 2; Hyde SC *et al.*, *Nature.* 1990). The mechanism of drug extrusion via ABC transporters is not completely understood. Structural, biochemical, genetic data suggest the “ATP-switch model” for substrate transport. Protein switch between two principal conformations of the NBD dimer: when ATP binds, it causes the rotation of NBD domains and formation of a closed dimer with two molecules of ATP attached. ATP hydrolysis allows protein to return to its open configuration (Szakács G *et al.*, *Nat Rev Drug Discov.* 2006).

In humans forty-eight ABC transporters have been identified, divided into seven groups (ABCA, ABCB, ABCC, ABCD, ABCE, ABCF, ABCG) (Ni Z *et* Mao Q, *Curr Pharm Biotechnol.* 2011). The three major types of MDR proteins include members of the ABCB (such as ABCB1/MDR1/Pgp, i.e. P-glycoprotein), the ABCC/Multidrug resistance Related Proteins (ABCC1/MRP1, ABCC2/MRP2, probably also ABCC3–6, and ABCC10–11) and the ABCG (ABCG2/BCRP, i.e. Breast Cancer Related Protein) subfamily (Szakács G *et al.*, *Nat Rev Drug Discov.* 2006; Damiani D *et al.*, *Br J Haematol.* 2002; Gilet JP *et al.*, *BBA-Rev. Cancer.* 2007).

MDR transporters have a large spectrum of substrate: typical drugs extruded include Vinca alkaloids (vinblastine and vincristine), anthracyclines (doxorubicin and daunorubicin), epipodophyllotoxines (etoposide, teniposide), antibiotics (actinomycin D) and taxanes (paclitaxel, docetaxel). Although structurally different, these compounds have similar

features. They are large hydrophobic/amphipathic molecules with molecular weight up to 800 Da, have a planar ring system and a positive charge at physiological pH (Lee CH *et al.*, *Curr Med Chem.* 2004).

MDR proteins are usually known as crucial actors in chemoresistance because they are overexpressed in tumors, but they are also present in normal tissue. Pgp, BCRP, MRPs in the placenta limit fetal exposure to toxins, drugs or xenobiotics, (Ni Z *et Mao Q*, *Curr Pharm Biotechnol.* 2011). In liver MDR transporters are involved in the regulation of bile formation and disposition for xenobiotics. In renal epithelial cells the transporters are responsible for the clearance of compounds from the cytoplasm of renal tubular cells to the urine (Ni Z *et Mao Q*, *Curr Pharm Biotechnol.* 2011). In brain blood–brain barrier they contribute to brain homeostasis by protecting the central nervous system parenchyma from potentially harmful endogenous and exogenous substances (Ni Z *et Mao Q*, *Curr Pharm Biotechnol.* 2011) (Fig 3.). Therein, finding pharmacological inhibitors that reduce Pgp activity only in tumors but not in healthy tissues has not been possible until now (Callaghan R *et al.*, *Drug Met Disp* 2014).

1.2.2 P-glycoprotein

P-glycoprotein is the most broadly studied protein involved in multidrug resistance. Pgp induces resistance to a wide spectrum of clinically and toxicologically relevant compounds, including anticancer drugs, human immunodeficiency virus-protease inhibitors, antiepileptics, antidepressants, analgesics and antibiotics (Luqmani YA *et al.*, *Med Princ Pract* 2005).

Pgp is glycosylated and has a molecular weight of 170-kDa, containing 1,280 amino acids. (Longley DB *et al.*, *J Pathol* 2005 ; Ni Z *et al.* Mao Q, *Curr Pharm Biotechnol.* 2011 ; Zhou SF, *Xenobiotica*, 2008). It is encoded by *MDR1* gene. Regulation of Pgp expression is highly complex: indeed, *MDR1* promoter has several overlapping binding sites for many different transcription factors. It has a “TATA-less” promoter, where the transcription complex is controlled by an initiator (Inr) element. The transcriptional factors interacting with the *MDR1* promoter include the inverted CCAAT-box (Y-box) binding proteins (NF-Y, YB-1, C/EBP β), the CAAT-box interacting proteins (c-fos, NF κ B), and the GC-box interacting proteins (Sp1–3, EGR1, WT1) (Ni Z *et al.* Mao Q, *Curr Pharm Biotechnol.* 2011 ; Zhou SF, *Xenobiotica*, 2008). The requirement of each transcriptional factor in the constitutive expression of Pgp has been demonstrated in several cell lines. Like most ‘TATAless’ genes, the *MDR1* promoter includes both an inverted CCAAT-box (Ni Z *et al.* Mao Q, *Curr Pharm Biotechnol.* 2011) that interacts with the trimeric transcription factor NF-Y (Ni Z *et al.* Mao Q, *Curr Pharm Biotechnol.* 2011) and a GC-rich element that interacts with members of the Sp-family of transcription factors, specifically Sp1 and Sp3 (Ni Z *et al.* Mao Q, *Curr Pharm Biotechnol.* 2011 ; Zhou SF, *Xenobiotica*, 2008). Pgp levels increase in response to stress signals, such as heat shock (Ni Z *et al.* Mao Q, *Curr Pharm Biotechnol.* 2011), hypoxia (Terasaki T *et al.*, *NeuroRx* 2005), inflammation (Zhou SF, *Xenobiotica*, 2008), exposure to xenobiotics, toxic metabolites, or UV irradiation (Szakács G *et al.*, *Nat Rev Drug Discov* 2006; Hu Z *et al.*, *J Biol Chem.* 2000). *MDR1* gene expression is also regulated at epigenetic levels, since it depends on DNA methylation, histone modification, chromosomal remodeling (Scotto KW *et al.*, *Oncogene* 2003). Moreover, Pgp activity can be modulated by post-translation events, such as phosphorylation and by the membrane microenvironment. The type of lipids, especially cholesterol in the plasma membrane in proximity of Pgp, is critical for the pump activity (Ni Z *et al.* Mao Q, *Curr Pharm Biotechnol.* 2011)

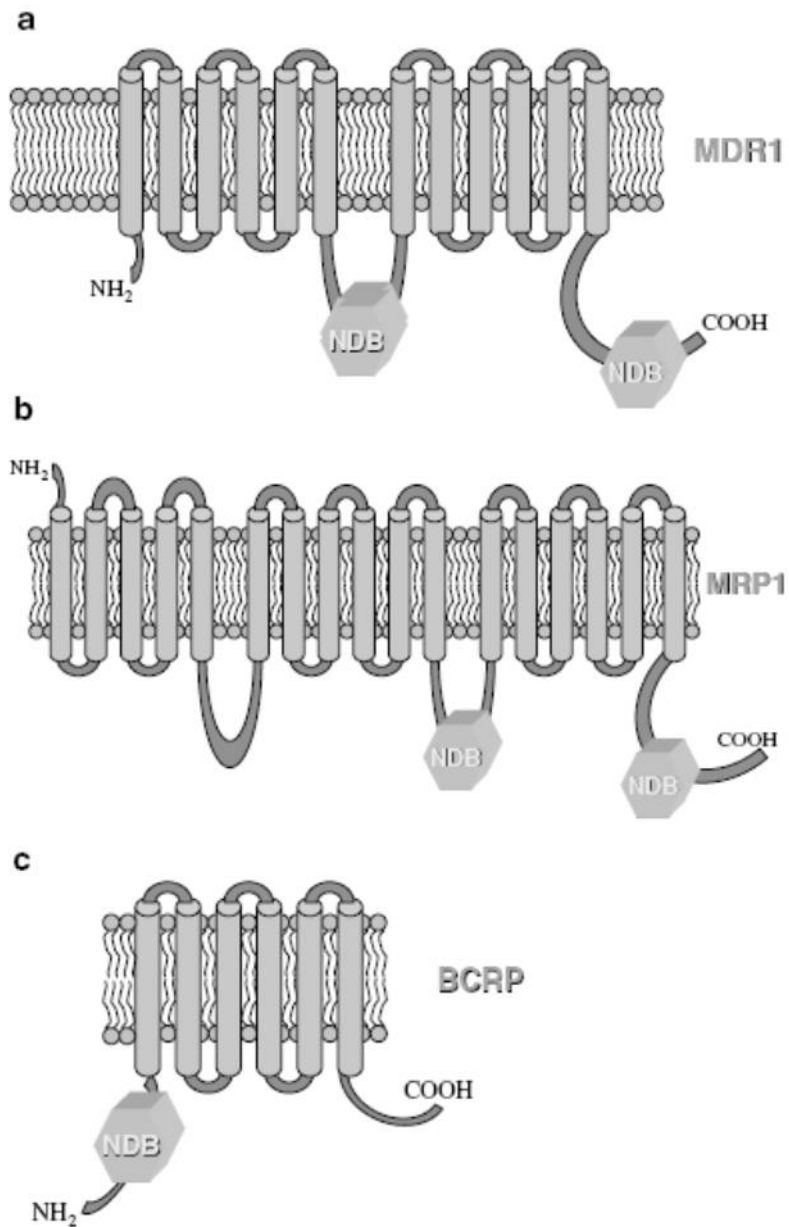


Figure 2. Predicted structure of representative drug transporters from each of the three classes: MDR1 contains 12 transmembrane domains and two nucleotide-binding domains (NBD). The amino-(NH₂) and carboxyl (COOH)-termina are designated. MRP1 is similar to MDR1, but includes an additional five transmembrane domains at the N-terminus. BCRP is a ‘half-transporter’ with one NBD located at the N-terminus (Scotto KW *et al.*, *Oncogene* 2003).

Common Name	Systematic name	Tissue	Non-chemotherapy substrates	Chemotherapy substrates (known and suspected)	Defects in human disease	References
PGP/MDR1	ABCB1	Intestine, liver, kidney, placenta, blood-brain barrier	Neutral and cationic organic compounds, many commonly used drugs	Doxorubicin, daunorubicin, vincristine, vinblastine, actinomycin-D, paclitaxel, docetaxel, etoposide, teniposide, bisantrene, homoharringtonine (STI-571)	None known; altered sensitivity to drugs	8
MDR2	ABCB4	Liver	Phosphatidylcholine, some hydrophobic drugs	Paclitaxel, vinblastine	Progressive familial intrahepatic cholestasis	31,33,66,67
MRP1	ABCC1	All tissues	Glutathione and other conjugates, organic anions, leukotriene C4	Doxorubicin, epirubicin, etoposide, vincristine, methotrexate	None known	20–24
MRP2, cMOAT	ABCC2	Liver, kidney, intestine	Similar to MRP1, non-bile salt organic anions	Methotrexate, etoposide, doxorubicin, cisplatin, vincristine, mitoxantrone	Dubin–Johnson syndrome	24,60–63
MRP3	ABCC3	Pancreas, kidney, intestine, liver, adrenal glands	Glucuronate and glutathione conjugates, bile acids	Etoposide, teniposide, methotrexate, cisplatin, vincristine, doxorubicin	None known	37,38
MRP4	ABCC4	Prostate, testis, ovary, intestine, pancreas, lung	Nucleotide analogues, organic anions	Methotrexate, thiopurines	None known	39,40
MRP5	ABCC5	Most tissues	Nucleotide analogues, cyclic nucleotides, organic anions	6-Mercaptopurine 6-Thioguanine	None known	41,42
MRP6	ABCC6	Liver, kidney	Anionic cyclic pentapeptide	Unknown	Pseudoxanthoma elasticum (substrate unknown)	43–46,58
MXR, BCRP, ABC-P	ABCG2	Placenta, intestine, breast, liver	Prazosin	Doxorubicin, daunorubicin, mitoxantrone, topotecan, SN-38	None known	25–29,54
BSEP, SPGP	ABCB11	Liver	Bile salts	Paclitaxel	Progressive familial intrahepatic cholestasis	30,47,48, 64,65
ABCA2	ABCA2	Brain, monocytes	Steroid derivatives, lipids	Estramustine	Intracellular steroid transport	7,34,35

Figure 3. ABC transporters involved in anti-cancer drug resistance (Ni Z *et* Mao Q, Curr Pharm Biotechnol. 2011)

Pgp has been found overexpressed in acute myeloid leukemia (65-80% of patient), chronic myeloid leukemia (14-26%), multiple myeloma (29-50%), ovarian cancer (15-47%), breast cancer (14-43%), renal cancer (75-80%), osteosarcoma and soft tissue sarcomas (23-50%), glioblastoma (18-57%). Bad prognosis is associated with high levels of Pgp in tumor cells (Ni Z *et* Mao Q, Curr Pharm Biotechnol. 2011)

1.3 Approaches to overcome multidrug resistance

Strategies to overcome MDR have been focused on increasing drug delivery, reducing ABC transporters transcription, and preventing drug efflux (Fig. 4).

For Pgp-overexpressing tumors, three main approaches have been experimented at least in pre-clinical models: new carriers of anticancer drugs, Pgp pharmacological inhibitors and Pgp down-regulation strategies.

Combining drugs or siRNA with nanocarriers such as nanoparticles, liposomes, micelles, dendrimers, magnetic nanoparticles, nanogolds, minicells and polymer-drug conjugates, provides an innovative and promising alternative to free chemotherapeutic drugs to overcome MDR (Gao Z *et al.*, *Journal of Controlled Release*. 2012). Liposomal drugs are particularly effective in chemoresistant cells, because they seem subjected to a reduced efflux through membrane transporters. Pegylated liposomal doxorubicin has been approved for the treatment of breast and ovary metastatic cancers resistant to conventional chemotherapy (Duggan ST *et Keating GM*, *Drugs*. 2011; Riganti C *et al.*, *Mol Pharm* 2011 ; Kopecka J *et al.*, *Nanomedicine*, 2014 ; Pedrini I *et al.*, *Mol Pharm*, 2014). The nanoparticle-mediated delivery of drugs is generally superior to free drug in inducing cell death in drug-resistant cells (Patil Y *et al.*, *J Control Release* 2009). The advantages of nanocarriers system include: enhanced particle penetration across physiological barriers, protection of labile drugs in systemic circulation, active tumor targeting, decreased drug clearance and regulated drug release.

Pharmacological inhibitors of Pgp can be categorized into three generations on a base of sequential refinements in the pharmacodynamic properties. First-generation Pgp inhibitors, such as cyclosporin A and verapamil, interact with substrate binding site of Pgp and are characterized by low specificity and high toxicity. Second-generation inhibitors, such as cinchonine and valspodar block ATPase activity of the transporters, but *in vivo* they cause many side effects because they affect cytochrome p450 3A4 activity. The third-generation of inhibitors (such as tariquidar and zosuquidar) were developed to elicit a high degree of specific Pgp inhibition with less toxicity. They are still in clinical development, but until now they did not shown any successful outcome (Takara K *et al.*, *Curr Pharm Des*. 2006 ; Ni Z *et Mao Q*, *Curr Pharm Biotechnol*. 2011; Zhou SF, *Xenobiotica*, 2008; Callaghan R *et al.*, *Drug Met Disp* 2014; Szakács G *et al.*, *Chem Reviews*, 2014).

Strategies focused on downregulation of *MDR1* gene expression using RNA interference (RNAi) technology (small interfering RNA (siRNA), short hairpin RNA (shRNA) (Ni Z *et Mao*

Q, *Curr Pharm Biotechnol.* 2011), knockdown or re-expression of specific microRNAs regulating Pgp expression by synthetic anti-sense oligonucleotides (Ni Z *et al.* *Curr Pharm Biotechnol.* 2011; Tsouris V. *et al.*, *Biotechnol* 2014) are currently under development in preclinical models, but the potential translation of these approaches into clinical practice is far.

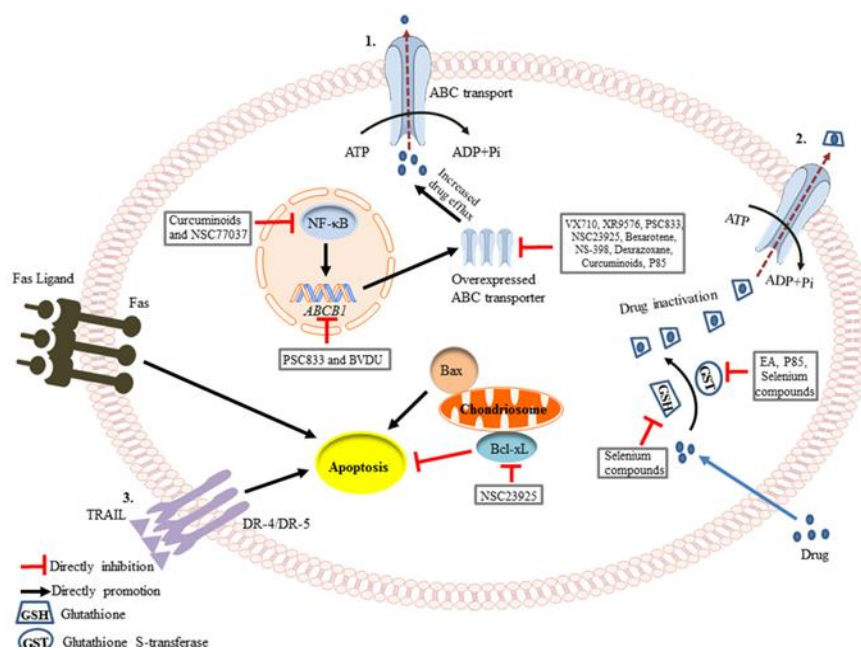


Figure 4. Mechanisms involved in the prevention or overcoming of drug resistance due to ABC transporters (Wang GY *et al.*, *Oncotarget* 2017)

1.4 Doxorubicin

Anthracyclines such as doxorubicin, daunorubicin, epirubicin, are among the most active and frequently used cytotoxic agents for treatment of solid tumors and hematological malignancies. All anthracyclines share a quinone-containing rigid planar aromatic ring structure bound by a glycosidic bond to an aminosugar, daunosamine (Fig. 5). Anthracyclines enter inside the cells via passive diffusion. Intracellular accumulation can result in concentrations that are 10–500 fold greater than extracellular drug levels (Minotti G *et al.*, *Pharm Rev* 2004). All anthracyclines are substrates of Pgp (Szakács G *et al.*, *Nat Rev Drug Discov.* 2006).

The main mechanisms of anthracycline-induced cell death is topoisomerase II inhibition that leads to DNA damage and induction of apoptosis, but also other mechanisms contribute to anthracyclines' cytotoxicity as: generation of free radicals (namely oxygen reactive species, ROS, and nitrogen reactive species, RNS), DNA binding, alkylation and cross-linking, alterations of calcium flux and mitochondria activity (Ni Z *et al.*, *Curr Pharm Biotechnol.* 2011; Zhou SF, *Xenobiotica*, 2008; Granados-Principal S *et al.*, *Food Chem. Toxicol.* 2010). Moreover, doxorubicin induces an immunogenic cell death (ICD), i.e. it induces the translocation of the endoplasmic-reticulum (ER)-associated protein calreticulin on plasmamembrane. Here calreticulin acts as an "eat-me" signals, making doxorubicin-treated cells easily phagocytized by dendritic cells. Following this process, dendritic cells activate autologous CD8⁺ T-lymphocytes endorsed with anti-tumor activity (Obeid M *et al.*, *Nat Med* 2007). Our group, however, has demonstrated that Pgp-expressing cells are refractory to doxorubicin-mediated ICD: on the one hand, Pgp effluxes doxorubicin, limiting the intracellular accumulation necessary to activate nitric oxide synthesis that mediates calreticulin translocation; on the other hand, Pgp is physically associated with calreticulin in ER and on plasmamembrane and impairs the calreticulin immunogenic functions (De Boo *et al.*, *Mol Cancer* 2009; Kopeckca J *et al.*, *J Cell Mol Med* 2011).

The main side-effects of doxorubicin is cardiotoxicity, either acute cardiotoxicity and chronic, dose-dependent cardiotoxicity (Ni Z *et al.*, *Curr Pharm Biotechnol.* 2011; Granados-Principal S *et al.*, *Food Chem. Toxicol.* 2010).

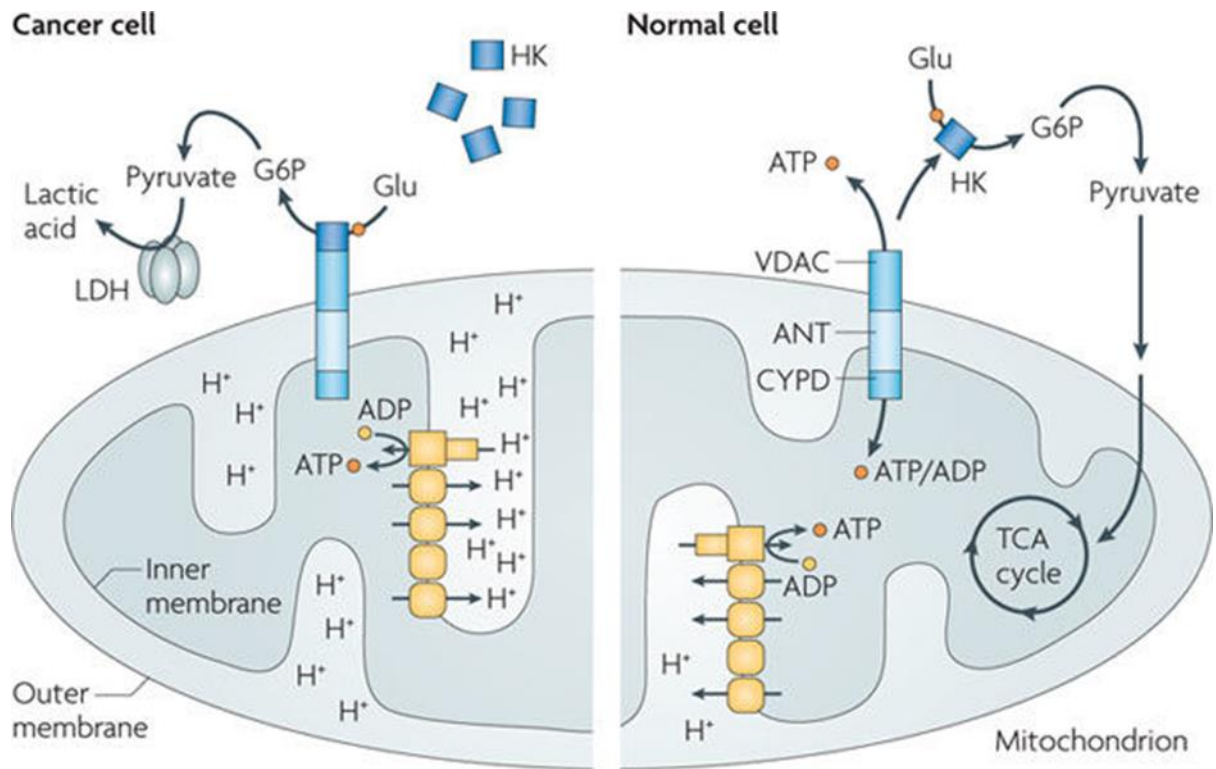
Basic molecular structure	Anthracycline	R1	R2	R3
	Daunorubicin	-H		-OCH3
	Doxorubicin	-OH		-OCH3
	Epirubicin	-OH		-OCH3
	Idarubicin	-H		-H

Figure 5. Molecular structures of different anthracyclines.

1.5. Mitochondria

Mitochondria plays a critical role in energy and redox balance, and represents key intracellular signaling hub of cancer progression, including metabolic reprogramming, acquisition of metastatic capability, and response to chemotherapeutic drugs (Trotta AP *et al.*, *Cell. Mol. Life Sci.* 2017 ; Caino MC *et al.*, *Proc. Natl. Acad. Sci. USA.* 2015 ; García-Ledo L *et al.*, *Front. Oncol.* 2017). Alteration in mitochondrial proteins and DNA, genomic DNA encoding for mitochondrial proteins, and mitochondrial dynamics are now considered critical events in cancer progression and aggressiveness (Guerra F *et al.*, *Biochim Biophys Acta.* 2017). Mitochondrial dynamics is characterized by fission and fusion, which allow cellular adaptation to specific metabolic states. Mitochondrial fission is helpful to segregate mitochondrial DNA and eliminate damaged/non-functioning mitochondria. Mitochondrial fusion with efficient ATP production and transport was more frequently observed in chemoresistant than chemosensitive gynecological cancer cells. Moreover, it is well known that during genomic DNA replication, mitochondria produce more ATP (Zheng HC, *Oncotarget* 2017).

Impairing mitochondria energetic metabolism and ATP synthesis, may reduce tumor cell proliferation and invasion, and trigger apoptosis (Trotta AP *et al.*, *Cell. Mol. Life Sci.* 2017). For this reason, targeting tumor cells mitochondria and impairing mitochondria energetic metabolism, became one of the promising strategy in the antitumor therapy (Wallace DC, *Nat. Rev. Cancer* 2012 ; Weinberg, SE et Chandel NS, *Nat. Chem. Biol.* 2015 ; Refaat A *et al.*, *Free Radic Res.* 2017). A typical feature of most solid tumors is that they have higher (i.e. more negative inside) mitochondrial transmembrane potential compared to their normal counterparts (Modica-Napolitano J *et al.*, *Adv. Drug. Deliv. Rev.* 2001). (Figure 6). We demonstrated that Pgp-expressing doxorubicin resistant cells has a constitutively more active mitochondrial metabolism but are also more susceptible to the damages produced by intramitochondrial ROS. The exposure to low and repeated doses to doxorubicin, a process that uncouples mitochondrial metabolism and increases intramitochondrial ROS, triggers a cytochrome c/caspase 9/caspase 3-dependent apoptosis of doxorubicin-resistant cells, notwithstanding the high levels of Pgp that remain unaffected (Riganti C *et al.*, *Cancer Lett.* 2015). The peculiar metabolism of mitochondria in drug-resistant cancer cell may be exploited to improved the response to antineoplastic drugs also in MDR tumors.



Nature Reviews | Drug Discovery

Figure 6. Mitochondrial membrane potential in cancer cells. Despite it has been generally accepted that most solid tumors obtain fuel from aerobic glycolysis (Warburg effects), the role of mitochondrial oxidative metabolism has been recently re-evaluated as a key contributor in tumor growth and progression. Active mitochondria of cancer cells have a higher mitochondrial transmembrane potential compared to normal cells (Gottesman MM *et al.*, Nat Reviews 2002)

1.6 Endoplasmic reticulum (ER)

Endoplasmic reticulum (ER) is the cellular site of protein synthesis, folding, modification, and trafficking of secretory and cell-surface proteins. ER is the major intracellular calcium storage compartment that maintains cellular calcium homeostasis. Several ER-specific molecular steps sense quantity and quality of synthesized proteins as well as proper folding into their native structures during the production of functionally effective proteins. An excessive accumulation of unfolded/misfolded proteins in the ER lumen results in ER stress, that activates an ER-specific adaptation program, (the unfolded protein response; UPR) to increase ER-associated degradation (ERAD) of structurally and/or functionally defective proteins, in the attempt to maintain ER protein homeostasis. If the attempt to adapt to ER stress fails, the UPR activates cell death programs that eliminate the damaged cells (Ohoka N et al., EMBO J. 2005 ; Hetz C, Nat Rev Mol Cell Biol. 2012). The detailed mechanisms of UPR response are depicted in Figure 7.

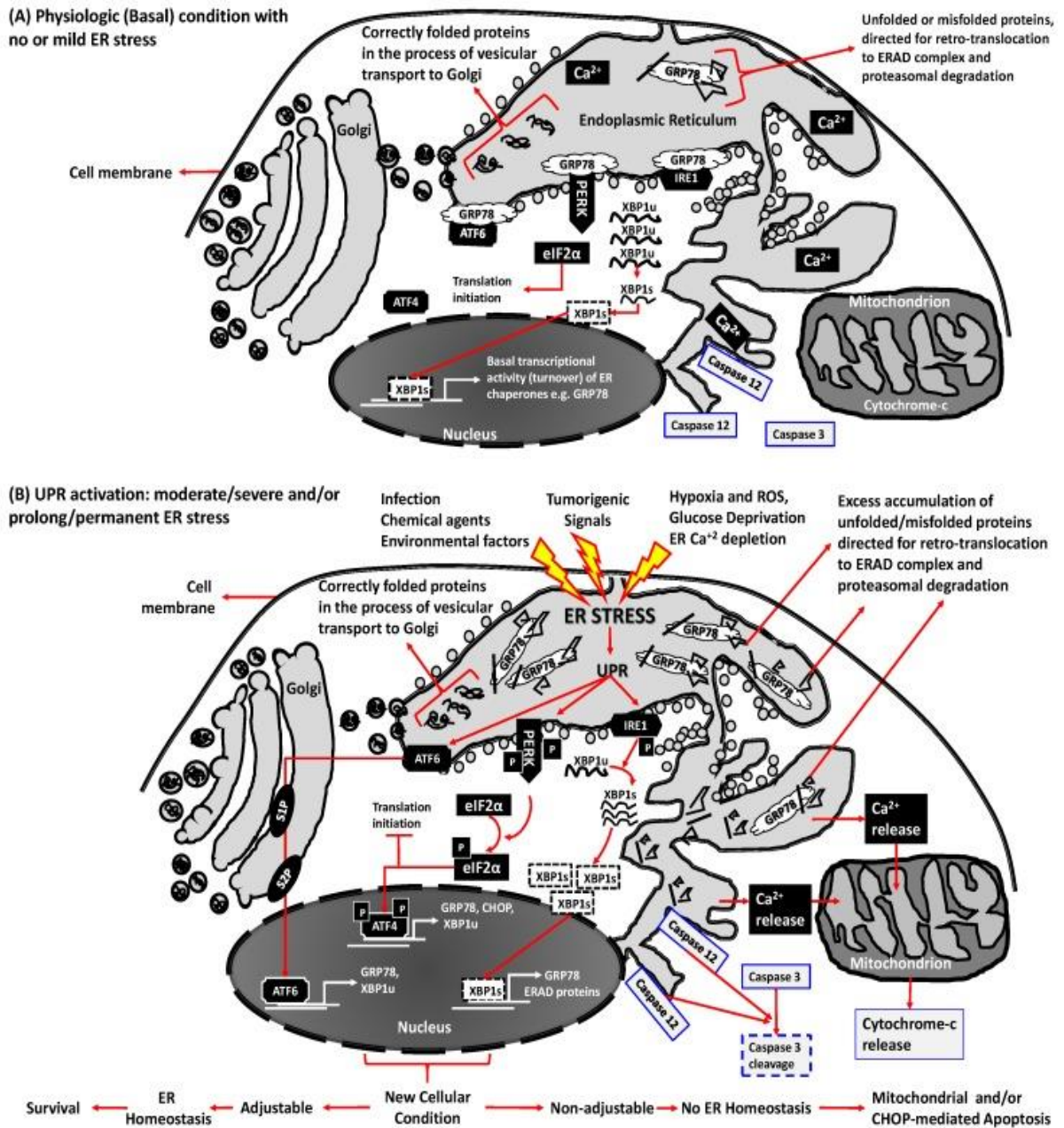


Figure 7 Endoplasmic Reticulum (ER) homeostasis/stress and the unfolded protein response (UPR) signaling in physiopathologic conditions. The UPR consists of three signaling pathways initiated by the detachment of ER stress sensors activating transcription factor 6 (ATF6), protein kinase R (PKR)-like endoplasmic reticulum kinase (PERK) and inositol-requiring enzyme 1 (IRE1) from glucose-regulated protein 78 (GRP78), a chaperone protein that monitors accumulation of unfolded and misfolded proteins inside the ER lumen. (A) In physiological (unstressed) states, these transducers bind to GRP78 and maintains ER protein homeostasis; (B) ER stress inducers accumulate unfolded/misfolded proteins in the ER lumen by impairing protein folding. Higher GRP78 affinity for unfolded/misfolded proteins

dissociates GRP78 from ATF6, PERK and IRE1, enabling cells to initiate three UPR signaling cascades that may results in cell adaptation and survival, or in cell apoptotic death (Guzel E *et al.*, Int J Mol Sci. 2017)

We recently demonstrated that cancer cells with constitutive or acquired resistance to chemotherapy are also resistant to ER stress-triggered cell death, owing to the reduced activation of C/EBP- β LIP/CHOP/Capsase 3 axis in resposne to ER stress inducers and chemotherapy and to the simultaneous up-regulation of Pgp (Riganti C *et al.*, J Natl Cancer Inst, 2015). On the other hand, canecr cell clones adapted to survive under mild and prolonged ER stressing conditions acuqire a MDR phenotype, beacuse of the up-regulation of PERK/Nrf2/MRP1 axis (Salaroglio IC *et al.*, Mol Canc 2017). These complimentary studies demosntrate that resistance to ER stress and to chemotherapy are strictly associated and suggest that altering ER protein homeostasis may influence the response to chemotherapy.

1.7 New synthetic doxorubicins targeting mitochondria and ER

As stated above, Dox is the most commonly chemotherapeutic drug used in OS, but many patients with high grade of OS are resistant because their high levels of Pgp. In my reserach I validated the efficacy of new synthetic Doxs targeting mitochondria and ER of Dox-resistant OS, in order to obtain effective tools against these resistant tumors.

The first synthetic Dox that I tested included a the Dox conjugated with a short peptide containing cationic and hydrophobic residues that deliver cargoes into mitochondria (Figure 8). This Dox, called mtDox, was a kind gift of Prof. Shana O. Kelley, Department of Pharmaceutical Sciences, Leslie Dan Faculty of Pharmacy, University of Toronto, Toronto, Ontario, Canada, and was synthesized as reported in (Chamberlain GR *et al.*, ACS Chem Biol. 2013). The selective delivery into the mitochondria, limited the availability of Dox for the Pgp on the plasma membrane in drug-resistant ovarian cancer cells, reducing the efflux of the drug from tumor cells (Chamberlain GR *et al.*, ACS Chem Biol. 2013).

Moreover, mtDox had no nuclear genotoxic effects in H9c2 rat cardiomyocytes: it induces a moderate mitochondrial damage in cardiomyocytes that was well compensated by increased mitochondrial biogenesis. Mice exposed to mtDox had no sign of cardiac toxicity. By contrast, MDR cells show a defective mitobiogenesis in response to mtDox and undergo to apoptosis (Jean SR *et al.*, ACS Chem Biol. 2015.)

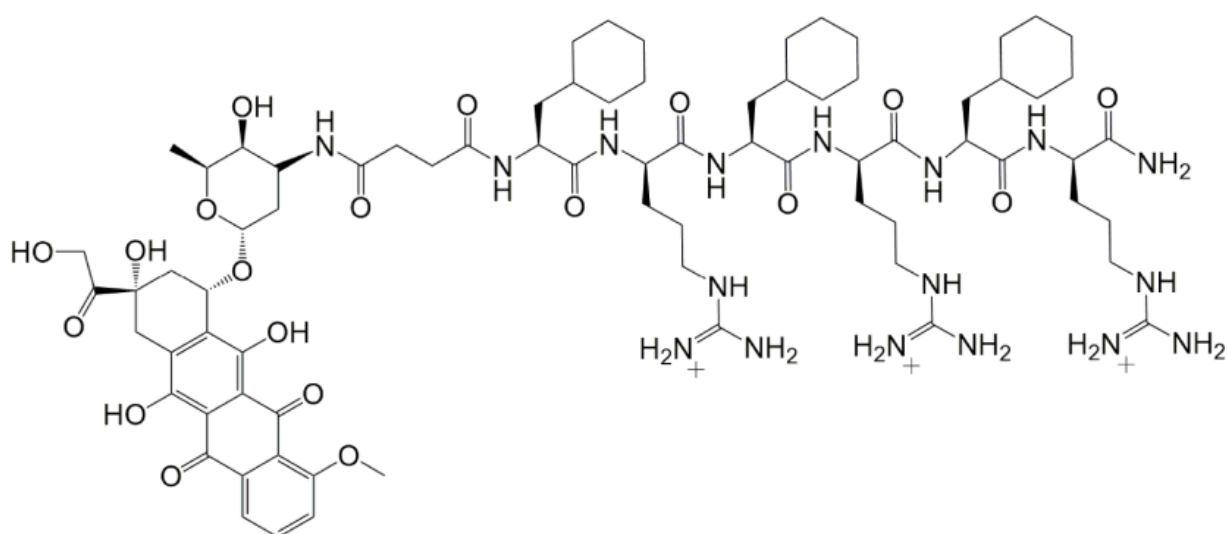


Figure 8 Chemical structure of mitochondria-targeted doxorubicin

The second type of synthetic Dox synthesized was a library of Doxs conjugated with H₂S-releasing groups (Fig 9). The library was produced in collaboration with the Department of Drug Science and Technology, University of Torino, Prof. Fruttero group. In a preliminary screening, most compounds resulted less cardiotoxic in rat H9c2 cells than Dox since the presence of H₂S prevented the increase of ROS (Chegaev K *et al.*, J Med Chem 2016 and Results section).

The role of H₂S in tumor biology is controversial, depending on the cancer cell line, the amount and the kinetics of H₂S release: some experimental evidences support a pro-tumor effect of H₂S, other works demonstrated the opposite (Szabo C et Hellmich MR, Cell Cycle 2013), fostering the synthesis of H₂S-releasing molecules with potential oncological applications (Ma K *et al.*, Plos One 2011; Kafshi K et Olson KR, Biochem. Pharmacol 2013; Li L *et al.*, Annu Rev Pharmacol Toxicol. 2011). H₂S-releasing Dox inhibited topoisomerase II and increased ROS levels less than Dox (Chegaev K *et al.*, J Med Chem 2016), suggesting that their higher cytotoxicity did not rely on these two classical effects exerted by anthracyclines (Granados-Principal S *et al.*, Food Chem. Toxicol. 2010).

Interestingly we observed that H₂S-releasing Doxs had a peculiar tropism for ER (see Results section). We hypothesize that by releasing H₂S and inducing protein sulfhydration, that may impair the correct protein folding, altering the ER protein homeostasis in MDR cells.

In my thesis I thus tested the *in vitro* and *in vivo* efficacy of mtDox and of the most effective H₂S-releasing Doxs (termed Sdox; compound **10** in Chegaev K *et al.*, J Med Chem 2016) in Pgp-overexpressing Dox-resistant OS cells.

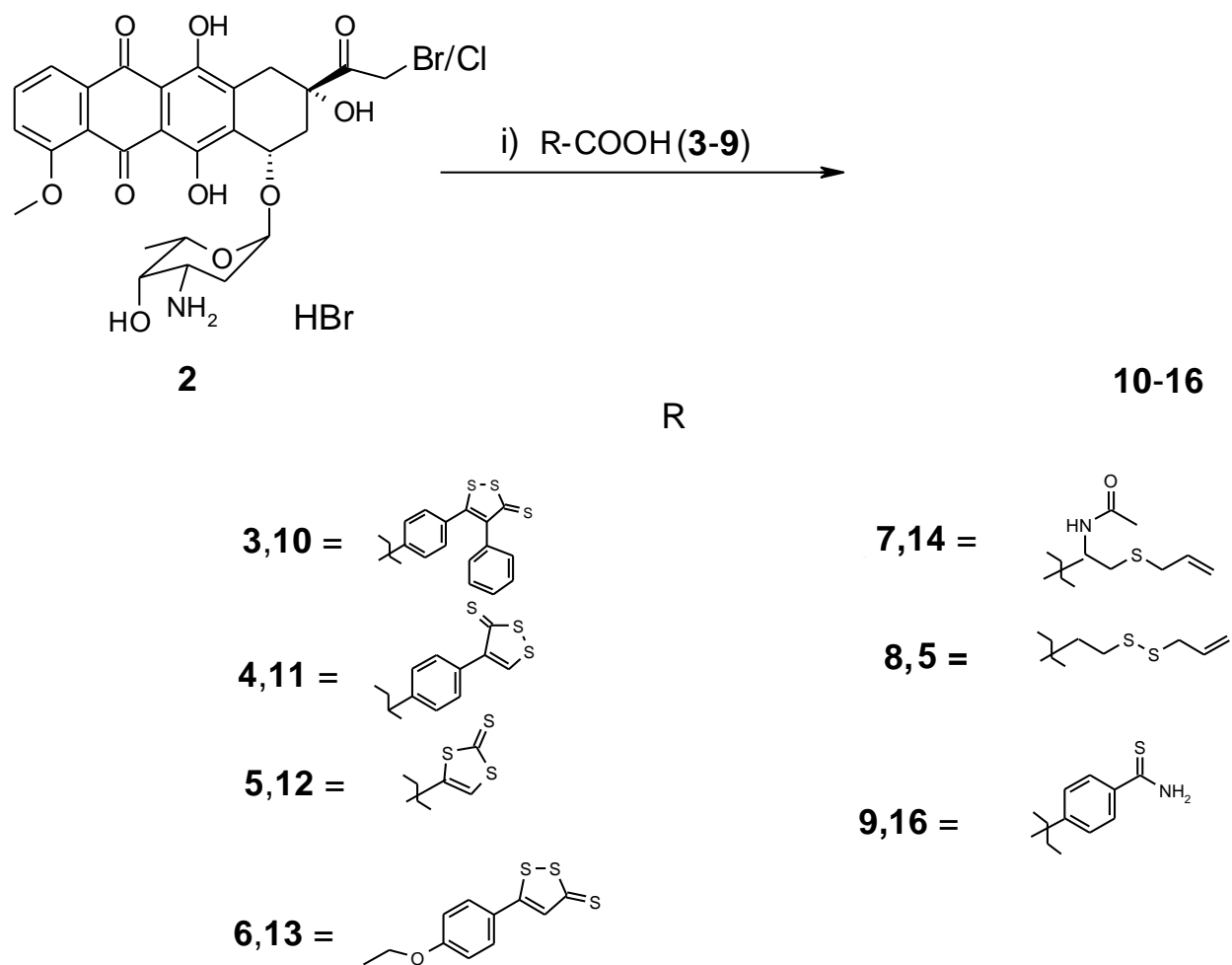


Figure 9 Chemical structure of H₂S-releasing doxorubicin (Chegaev K *et al.*, J Med Chem 2016)

2. Aims of the PhD thesis

The main aim of this work is to validate the efficacy of new synthetic Doxs against Pgp-positive human OS cells with progressively increased resistance to parental Dox.

Instead of using Pgp pharmacological inhibitors, I validated the efficacy of synthetic Doxs targeting intracellular compartments –namely mitochondria and ER – that –on the basis of preliminary works of our group – had different metabolic and functional features between chemosensitive and MDR cells (Riganti C *et al.*, *Cancer Lett* 2015 ; Kopecka J *et al.*, *Oncotarget* 2015 ; Riganti C *et al.*, *J Natl Cancer Inst* 2015 ; Salaroglio IC *et al.*, *Mol Cancer* 2017). Such features may be exploited to trigger cell death in MDR cells in a rather selective way, i.e. with the maximal efficacy against MDR cells and with few side-effects on not-transformed tissues.

In the first part of the thesis I analyzed the metabolic and functional differences in mitochondria between Dox-sensitive and Dox-resistant OS cells. I analyzed the genomic and biochemical effects produced by mtDox and its potential efficacy as a new cytotoxic drug against Dox-resistant OS cells.

In the second part of the thesis, I focused on the metabolic and functional differences in ER between Dox-sensitive and Dox-resistant OS cells. I next studied the molecular basis of the high efficacy of Sdox against OS cells refractory to parental Dox.

The final goal of my thesis was to perform the preclinical validation of new synthetic Dox as specific and effective tools against Pgp-expressing human OS, where the standard therapy with Dox fails.

3. Materials and Methods

3.1 Chemicals

Fetal bovine serum (FBS) and culture medium were from Invitrogen Life Technologies (Carlsbad, CA). Plasticware for cell cultures was from Falcon (Becton Dickinson, Franklin Lakes, NJ). The protein content in cell extracts in cell monolayers, mitochondrial, and nuclear extracts was assessed with the BCA kit from Sigma Chemical Co. (St. Louis, MO). Electrophoresis reagents were obtained from Bio-Rad Laboratories (Hercules, CA). Dox was purchased by Sigma Chemical Co. MtDox was synthesized as described in ref. (Chamberlain GR *et al.*, ACS Chem Biol 2013). Sdox was synthesized as described in (Chegaev K *et al.*, J Med Chem 2016): the Sdox used in the present thesis was namely compound **10** of (Chegaev K *et al.*, J Med Chem 2016). Unless otherwise specified, all the other reagents were purchased from Sigma Chemical Co.

3.2 Cells

Murine osteosarcoma K7M2 cells, human Dox-sensitive osteosarcoma U-2OS and Saos-2 cells, and rat neonatal H9c2 cardiomyocytes were purchased from the ATCC (Manassas, MA) in 2012. The corresponding variants with increasing resistance to Dox (U-2OS/ DX30, U-2OS/DX100, U-2OS/DX580, Saos-2/DX30, Saos-2/DX100 and Saos-2/DX580), selected by culturing parental cells in a medium with 30, 100, and 580 ng/mL Dox, were generated as reported in (Serra M *et al.*, Anticancer research 1993) and continuously cultured in presence of Dox. All cell lines were authenticated once a year by microsatellite analysis, using the PowerPlex Kit.

Primary non-transformed osteoblasts were obtained from mesenchymal stem cells of healthy subjects, grown in osteogenic conditions, as reported in (Gronthos S *et al.*, J Cell Sci 2003.). Fourteen days after culture, Bone Alkaline Phosphatase (BAP staining Kit; Sigma Chemicals Co.) was performed as authentication test for osteoblasts. Cells were maintained in IMDM medium (U-2OS and Saos-2 cells) or DMEM medium (K7M2 and H9c2 cells), supplemented with 10% v/v FBS, 1% v/v penicillin–streptomycin, and 1% v/v L-glutamine.

3.3 ABCB1/Pgp and ABCC1/MRP1 expression

For flow cytometry assays, cells were harvested, washed once in PBS, twice with 10 mM/L Hepes in Hank's balanced salt solution, and fixed with 4% paraformaldehyde in PBS for 5 minutes. After a wash in Hepes, cells were permeabilized in 0.1% w/v saponin and incubated with an anti-ABCB1/Pgp (clone MRK16; Kamiya) or anti-ABCC1/MRP1 (clone MRPm5; Abcam) antibodies. After washing with saponin, cells were incubated with a secondary anti-mouse FITC-conjugated antibody (Sigma Chemical Co.), washed twice with saponin and once with Hepes. In the negative control, primary antibody was replaced by 0.1% saponin. Samples were analyzed by flow cytometry (FACSCalibur; Becton Dickinson). For immunoblot analysis, 20 µg of proteins from cell lysates (see details in "Immunoblotting" paragraph) were probed with anti-Pgp (clone 17F9; BD Biosciences) antibody, using an anti-β-tubulin (Santa Cruz Biotechnology Inc.) antibody to check the equal control loading of proteins.

3.4 Doxorubicin accumulation

Cellular, nuclear, or mitochondrial extracts (see details below) were resuspended in 0.5 mL ethanol/0.3 N HCl. The amount of Dox, mtDox or Sdox was measured fluorimetrically after 6 h incubation with each drug (Riganti C *et al.*, Cancer Res 2005), using a Synergy HT Multi-Detection Microplate Reader (Bio-Tek). Excitation and emission wavelengths were 475 nm and 553 nm, respectively. A blank was prepared in the absence of cells in each set of experiments and its fluorescence was subtracted from that measured in each sample. Fluorescence was converted into nmol/mg cellular, nuclear, or mitochondrial proteins, using a previously set calibration curve with serial dilutions of the drug.

3.5 Cell viability and proliferation

The extracellular release of lactate dehydrogenase (LDH), considered an index of cell damage and necrosis, was measured in cells incubated for 24 h with Dox, mtDox or Sdox, as reported in (Riganti C *et al.*, Cancer Res 2005). 100 µl of supernatant from extracellular medium or 10 µl of cell lysate was incubated at 37 °C with 82.3 mM trietanolamine phosphate TRAP (pH 7.6) and 5mM NADH (final volume: 0.3 ml). The reaction was started by adding 20 mM pyruvic acid and was followed for 10 min, measuring absorbance at 340 nm with Synergy HT Multi-Detection Microplate Reader. The reaction kinetics was linear throughout the time of measurement. Both intracellular and extracellular enzyme activity

was expressed as mol NADH oxidized/min/dish, then extracellular LDH activity was calculated as percentage of the total LDH activity in the dish.

Cell viability was measured by the ATPlite Luminescence Assay System (PerkinElmer, Waltham, MA), as per manufacturer's instructions, using a Synergy HT Multi-Detection Microplate Reader to measure the relative luminescence units (RLU). The RLUs of untreated cells was considered as 100% viability; the results were expressed as a percentage of viable cells versus untreated cells. To determine the IC₅₀ of each drug, 1 x 10⁵ cells were incubated for 72 h with increasing concentrations of Dox, mtDox or Sdox (from 1 nM to 1 mM). IC₅₀ was considered the concentration of the drug that reduced cell viability to 50%.

In cell cycle analysis, cells were washed twice with PBS, incubated in 0.5 mL ice-cold ethanol 70 % v/v for 15 min, then centrifuged at 1200 x g for 5 min at 4°C and rinsed with 0.3 mL citrate buffer (50 mM Na₂HPO₄, 25 mM sodium citrate, and 0.01% Triton X-100) containing 10 mg/mL propidium iodide and 1 mg/mL RNase (from bovine pancreas). After a 15-min incubation in the dark, intracellular fluorescence was detected by a FACSCalibur flow cytometer. For each analysis, 10 000 events were collected and analyzed by Cell Quest software (Becton Dickinson).

Caspase 3 activity, as index of apoptosis, was measured by lysing 10⁵ cells in 0.5 mL of caspase lysis buffer (20 mM HEPES/KOH, 10 mM KCl, 1.5 mM MgCl₂, 1 mM EGTA, 1 mM EDTA, 1 mM DTT, 1 mM PMSF, 10 µg/mL leupeptin; pH 7.5). Then 20 µg cell lysates were incubated for 1 h at 37°C with 20 µM of the fluorogenic substrate of caspase 9, LEHD-7-amino-4-methylcumarine (LEHD-AMC), or of caspase 3, DEVD-7-amino-4-methylcumarine (DEVD-AMC), in 0.25 mL caspase assay buffer (25 mM HEPES, 0.1% w/v 3-[(3-cholamidopropyl) dimethylammonio] -1- propanesulfonate CHAPS, 10% w/v sucrose, 10 mM DTT, 0.01% w/v egg albumin; pH 7.5). The reaction was stopped by adding 0.75 mL ice-cold 0.1% w/v trichloroacetic acid and the fluorescence of the AMC fragment released by active caspase 9 or caspase-3 was read using a Synergy HT Multi-Detection Microplate Reader. Excitation and emission wavelengths were 380 nm and 460 nm respectively. Fluorescence was converted in pmol-mg⁻¹ cell protein using a calibration curve prepared previously with standard solutions of AMC.

3.6 Confocal microscope analysis.

5×10^5 cells were grown on sterile glass coverslips and transfected with the green fluorescence protein (GFP)-E1 α pyruvate dehydrogenase expression vector to label mitochondria or with GFP-KDEL fused-calreticulin expression vector to label ER (Cell Light BacMan 2.0, Invitrogen Life Technologies). After 24 h cells were incubated with 5 μ M Dox, mtDox (for mitochondria localization) or Sdox (for ER localization) for 6 h. Samples were rinsed with PBS, fixed with 4% w/v paraformaldehyde for 15 min, washed three times with PBS and once with water, mounted with 4 μ l of Gel Mount Aqueous Mounting. Slides were analysed using an Olympus FV300 laser scanning confocal microscope (Olympus Biosystems, Hamburg, Germany; ocular lens: 10X; objective: 60X). For each experimental condition, a minimum of 5 microscopic fields were examined.

3.7 Immunogenic cell death assays

To evaluate the ICD induced by Dox or mtDox the extracellular release of ATP was measured by a chemiluminescence-based assay using the ATP Bioluminescent Assay Kit (FL-AA; Sigma Chemical Co.), as per manufacturer's instruction. The extracellular release of high mobility group box 1 (HMGB1) protein was measured by immunoblotting on 25 μ L of cell culture medium. Following a procedure commonly used in the immunoblotting of extracellular proteins (Riganti C *et al.*, PLoS One 2013), we stained the blot with Red Ponceau and reported a band at the same level of the HMGB1 band, as the control of equal protein loading. Surface translocation of calreticulin, detected by flow cytometry, was measured as reported (Riganti C *et al.*, PLoS One 2013). The mean fluorescence intensity was calculated using Cell Quest software (Becton Dickinson).

3.8 In vivo tumor growth, hematochemical parameters, and immunohistochemical analysis

In a first experimental set, 1×10^6 K7M2 cells, stably transfected with the pGL4.51[luc2/CMV/Neo] Vector (Promega Corporation), mixed with 100 mL Matrigel, were injected s.c. in 6-week-old female BALB/c mice (weight: 20 g \pm 1.3; Charles River Laboratories Italia); 1×10^7 U-2OS cells, mixed with 100 mL Matrigel, were injected s.c. in 6-week-old female NOD SCID BALB/c mice (weight: 19.6 g \pm 1.6; Charles River Laboratories Italia). Animals were housed (5 per cage) under 12-hour light/dark cycles, with food and drinking provided ad libitum. Tumor growth was measured daily by caliper and calculated according to the equation $(L \times W^2)/2$, where L $\frac{1}{4}$ tumor length and W $\frac{1}{4}$ tumor width. When the tumor reached a volume of 50 mm³ (day 7 after injection), the mice were randomized

into 3 groups: (1) Control group, treated with 0.1 mL saline solution i.v. on days 7, 14, 21, and 28; (2) Dox group, treated with Dox i.v. on days 7, 14, 21, and 28; (3) mtDox group, treated with mitochondria-targeting Dox i.v. on days 7, 14, 21, and 28. This dosage of mtDox was chosen after a preliminary dose-dependence experiment using 0.5, 1, 2.5, 5 mg/Kg against K7M2 implanted tumors.

In vivo bioluminescence imaging was performed on days 7, 21, and 35 with a Xenogen IVIS Spectrum (PerkinElmer). Tumor volumes were monitored daily by caliper, and animals were euthanized by injecting lorazepam (0.2 mL/kg) and xylazine (16 mg/kg) i.m. at day 35. The inhibition rate was calculated as a percentage (i.e., the tumor weight of the control group minus that of the tumor weight of the test group) divided by the tumor weight of the control group.

In a second preliminary experimental set, 1×10^6 K7M2 cells, mixed with 100 mL Matrigel, were injected s.c. in 6-week-old female BALB/c mice (weight: $19.5 \text{ g} \pm 1.7$; Charles River Laboratories Italia). When the tumor reached a volume of 50 mm^3 , the mice were randomized into 3 groups: (1) Control group, treated with 0.1 mL saline solution i.v. on days 7, 14, 21, and 28; (2) Dox group, treated with Dox i.v. on days 7, 14, 21, and 28; (3) Sdox group, treated with Sdox i.v. on days 7, 14, 21, and 28. Tumor volumes were monitored daily by caliper, and animals were euthanized as reported above.

The hematochemical parameters LDH, aspartate aminotransferase (AST), alanine aminotransferase (ALT), alkaline phosphatase (AP), creatinine, creatine phosphokinase (CPK) were measured on 0.5 mL of blood collected immediately after mice sacrifice, using the respective kits from Beckman Coulter Inc. For immunohistochemical analysis, tumors were resected and fixed in 4% v/v paraformaldehyde. The paraffin sections were stained with hematoxylin/eosin or immunostained for Ki67 (Millipore), cleaved caspase 3-Asp175 (Cell Signaling Technology Inc.), calreticulin (Affinity Bioreagents), CD11c (BD Biosciences), followed by a peroxidase-conjugated secondary antibody (Dako). Nuclei were counterstained with hematoxylin. Sections were examined with a Leica DC100 microscope (Leica Microsystems GmbH; 10Xocular lens, 20X objective). All animal care and experimental procedures were approved by the Bio-Ethical Committee of the University of Torino, Italy.

3.9 Tumor cell phagocytosis.

Murine dendritic cells (DC) were obtained as reported by Obeid and colleagues (Obeid M *et al.*, Nat Med 2007). Tumor cell phagocytosis was performed by flow cytometry (Obeid M *et al.*, Nat Med 2007). In each set of experiments, a phagocytosis assay was performed by coincubating DCs and tumor cells at 4°C, instead of 37°C, and the percentage of phagocytized cells at 4°C was subtracted from values observed at 37°C. The phagocytosis rate was expressed as a phagocytic index, calculated as previously reported (Obeid M, *et al.*, Nat Med 2007).

3.10 PCR arrays and qRT-PCR

Total RNA was extracted and reverse-transcribed using the iScript[™] cDNA Synthesis Kit (Bio-Rad Laboratories). The PCR arrays were performed on 1 µg cDNA, using Mitochondria, Mitochondria Energy Metabolism Arrays and the Unfolded Protein Response Plus PCR Array (Bio-Rad Laboratories). The expression levels of specific genes, representative of the main biological categories screened by PCR arrays, were validated by qRT-PCR. Primer sequences were designed using qPrimerDepot software (<https://primerdepot.nci.nih.gov/>). *S14* was used as the housekeeping gene. Data analysis was performed with PrimePCR Analysis Software (Bio-Rad Laboratories).

3.11 Isolation of mitochondria, nuclei and microsomes

Mitochondrial fractions were isolated as reported in (Campia I *et al.*, J Pharmacol 2009), with minor modifications. Samples were lysed in 0.5 mL buffer A (50 mM Tris, 100 mM KCl, 5 mM MgCl₂, 1.8 mM ATP, 1 mM EDTA, pH 7.2), supplemented with protease inhibitor cocktail III (Calbiochem), 1 mM PMSF and 250 mM NaF. Samples were clarified by centrifuging at 650x *g* for 2 min at 4°C, and the supernatant was collected and centrifuged at 13 000 x *g* for 5 min at 4°C. This supernatant was discarded and the pellet containing mitochondria was washed in 0.5 mL buffer A and resuspended in 0.25 mL buffer B (250 mM sucrose, 15 mM K₂HPO₄, 2 mM MgCl₂, 0.5 mM EDTA, 5% w/v BSA). A 50 µL aliquot was sonicated and used for the measurement of protein content or Western blotting; the remaining part was stored at -80°C until the use. To confirm the presence of mitochondrial proteins in the extracts, 10 µg of each sonicated sample were subjected to SDS-PAGE and probed with an anti-porin antibody (Abcam; data not shown). To exclude any mitochondrial contamination in the cytosolic extracts, the absence of porin in the latter was analyzed by Western blotting (data not shown).

Nuclear proteins were extracted using the Nuclear Extract Kit (Active Motif), as per manufacturer's instructions. To exclude any cytosolic contamination in the nuclear extracts, the absence of actin (Sigma Chemical Co.) in the latter was analyzed by immunoblotting. Microsomal fractions were prepared using the Endoplasmic Reticulum Isolation Kit (Sigma Chemicals. Co), as per manufacturer's instructions. To exclude any cytosolic contamination, the absence of actin (Sigma Chemical Co.) in the latter was analyzed by immunoblotting.

3.12 Mitochondrial DNA quantification

Mitochondrial DNA was extracted, amplified, and quantified by PicoGreen (Invitrogen Life Technologies) staining as reported in (Jean SR *et al.*, ACS Chem Biol 2015.). The results are expressed as ng DNA/10⁵ cells.

3.13 Mitochondria biogenesis

The expression of peroxisome proliferator-activated receptor gamma coactivator-1a (PGC-1a), measured on 30 µg of nuclear proteins and considered an index of increased mitochondria biogenesis (LeBleu VS *et al.*, Nat Cell Biol 2014), was evaluated by Western blotting, using an anti-PGC-1a (#ab54481; Abcam) antibody. An anti-TATA-box binding protein (TBP; clone 58C9; Santa Cruz Biotechnology Inc.) was used to check equal protein loading. Mitochondria biogenesis was also evaluated by measuring the expressions of subunit I of complex IV (COX-I), which is encoded by mitochondrial DNA, and succinate dehydrogenase-A of complex II (SDHA), which is encoded by nuclear DNA, using the MitoBiogenesis In-Cell ELISA Kit (Abcam). The results are expressed as units (U) of each protein/mg mitochondrial proteins.

3.14 Tricarboxylic acid cycle

The glucose flux through tricarboxylic acid (TCA) cycle was measured by radiolabeling cells with 2 µCi/mL [6-¹⁴C]-glucose (55 mCi/mmol; PerkinElmer). Cell suspensions were incubated for 1 hour in a closed experimental system to trap the ¹⁴CO₂ developed from [¹⁴C]-glucose. The reaction was stopped by injecting 0.8 N HClO₄. The amount of glucose transformed into CO₂ through the TCA cycle was calculated as described by Riganti and colleagues (Riganti C *et al.*, J Biol Chem 2004). and expressed as pmol CO₂/h/mg cellular proteins.

3.15 Fatty acids β -oxidation

Long-chain fatty acids β -oxidation was measured as detailed earlier (Gaster M *et al.*, Diabetes 2004) with minor modifications. 100 μ l mitochondrial suspension were rinsed with in 100 μ l of 20 mM Hepes, containing 0.24 mM fatty acid-free BSA, 0.5 mM L-carnitine and 2 μ Ci [$1\text{-}^{14}\text{C}$]palmitic acid (3.3 mCi/mmol, PerkinElmer). Samples were incubated at 37°C for 1 h, then 100 μ l of 1:1 v/v solution phenylethylenamine 100 mM/methanol were added. After one hour at room temperature, the reaction was stopped by adding 100 μ L of 0.8 N HClO₄. Samples were centrifuged at 13,000 x g for 10 min. Both the precipitates containing ^{14}C -acid soluble metabolites (ASM) and the supernatants containing $^{14}\text{CO}_2$ -derived from oxidation (used as internal control and expected to be less than 10% of ASM) were counted by liquid scintillation. Results are expressed as nmol/min/mg cellular proteins. In each experimental set, cells were preincubated for 30 minutes with the carnitine palmitoyltransferase inhibitor etomoxir (1 mM) or with the AMPkinase activator 5-aminoimidazole-4-carboxamide ribonucleotide (AICAR; 1 mM), as negative and positive controls, respectively. In the presence of etomoxir, the rate of β -oxidation was less than 10% than in its absence; in the presence of AICAR, the rate of β -oxidation was increased 2-fold.

3.16 Mitochondrial energy metabolism

The oxygen consumption rate (OCR) was measured on 20,000 cells with the XFp Mito Stress Test Kit, using a Seahorse XFp Extracellular Flux Analyzer (Seahorse Bioscience, M&M Biotech). Carbonyl cyanide 4-(trifluoromethoxy) phenylhydrazone (FCCP) was used at a concentration of 0.3 mM/L to uncouple mitochondrial oxidative phosphorylation and induce maximal respiration. The data were analyzed using Wave Seahorse software.

The amount of ATP produced by oxidative phosphorylation was measured on 20 mg mitochondrial proteins with the ATP Bioluminescent Assay Kit (FL-AA; Sigma Chemical Co.). Data were converted into nmol/mg mitochondrial proteins, using a previously set calibration curve

3.17 Intramitochondrial reactive oxygen species levels

The amount of reactive oxygen species (ROS) in mitochondrial extracts was measured fluorimetrically incubating mitochondrial suspension at 37°C for 10 minutes with 10 μ M of 5-(and-6)-chloromethyl-2,7-dichlorodihydro-fluorescein diacetate-acetoxymethyl ester (DCFDA-AM), then washed, and resuspended in 0.5 mL of PBS. Results were expressed

as nmoles/mg mitochondrial proteins, using a calibration curve previously set with serial dilution of H₂O₂.

3.18 Mitochondrial electric potential ($\Delta\psi$) measurement

1 × 10⁶ cells, re-suspended in 0.5 mL PBS, were incubated for 30 min at 37 °C with 2 μmol/L of the fluorescent probe JC-1 (Biotium Inc., Hayward, CA), then centrifuged at 13,000 × g for 5 min and re-suspended in 0.5 mL PBS. The fluorescence of each sample was read using a Synergy HT Multi-Mode Microplate Reader: the red fluorescence, index of polarized mitochondria, was detected at 550 nm (λ excitation) and 600 nm (λ emission); the green fluorescence, index of depolarized and damaged mitochondria, was detected at 485 nm (λ excitation) and 535 nm (λ emission). The fluorescence units were used to calculate the percentage of green-fluorescent versus red-fluorescent mitochondria.

3.19 Immunoblotting

For whole cell lysates, cells were rinsed with ice-cold lysis buffer (50 mM Tris, 10 mM EDTA, 1% v/v Triton-X100; pH 7.5), supplemented with the protease inhibitor cocktail set III (80 μM aprotinin, 5 mM bestatin, 1.5 mM leupeptin, 1 mM pepstatin; Calbiochem, San Diego, CA), 2 mM phenylmethylsulfonyl fluoride, 1 mM Na₃VO₄. Cells were then sonicated (10 bursts of 10 sec, 4°C, 100 W, using a Labsonic sonicator, Hielscher, Teltow, Germany) and centrifuged at 13,000 × g for 10 min at 4°C. 20 μg of protein extracts were subjected to 4-20% gradient SDS-PAGE and probed with the following antibodies: anti-ABCB1/Pgp (1:500, Calbiochem); anti-BAD (Cell Signaling Technology, Danvers, MA); anti-BAK (Cell Signaling Technology); anti-BAX (Cell Signaling Technology); anti-BID (Cell Signaling Technology); anti-BIM (Cell Signaling Technology); anti-p53 up-regulated modulator of apoptosis (PUMA; Cell Signaling Technology); anti-BCL-2 (Cell Signaling Technology); anti-BCL-xL; anti-ER degradation enhancing α-mannosidase like protein 1 (EDEM1; Abcam); anti-UDP-glucose glycoprotein glucosyltransferase 1 (UGGT1; Abcam); anti-SEC62 homolog/preprotein translocation factor (SEC62; Abcam); anti-valosin containing protein (VCP; Abcam); anti-glucose-regulated protein 78/binding immunoglobulin protein (GRP78/BiP; Abcam), anti-inositol requiring kinase-1α (IRE1α; Thermo Scientific Inc., Rockford, IL), anti-X-box binding protein 1 (XBP1; Abcam), anti-protein kinase-like endoplasmic reticulum kinase (PERK; Santa Cruz Biotechnology Inc.), anti-phospho(Ser51)eukariotic initiation factor-2α (peIF2α; Abcam), anti-eIF2α (Abcam), anti-activating transcription factor (ATF4; Abcam), anti-activating transcription factor 6 (ATF6; Abcam), anti-CCAAT-enhancer-binding protein-β

(C/EBP- β , recognizing either LAP or LIP isoform; Santa Cruz Biotechnology Inc.), anti-C/EBP homologous protein/growth arrest and DNA damage 153 (CHOP/GADD153; Santa Cruz Biotechnology Inc.), anti-Tribbles homolog 3 (TRB3; Proteintech, Chicago, IL), anti-caspase 12 (Abcam), anti-caspase 7 (Abcam), anti-caspase 3 (GeneTex, Hsinhu City, Taiwan), The membranes were then incubated with peroxidase-conjugated secondary antibody (1:3,000, Bio-Rad Laboratories) and washed with Tris-buffered saline-Tween 0.1% v/v solutions. Protein bands were detected by enhanced chemiluminescence (Bio-Rad Laboratories).

After mitochondrial-cytosol separation, 10 μ g mitochondrial or cytosolic extracts were probed with anti-cytochrome c (BD Bioscience). 10 μ g mitochondrial extracts were probed with the antibodies for BAD, BAX, BAK, PUMA indicated above.

After nuclear separation, 10 μ g nuclear proteins were probed with anti-CHOP antibody.

After microsomal extraction, 100 μ g of microsomal proteins were probed with an anti-mono/poly-ubiquitin antibody (Axxora, Lausanne, Switzerland). To measure ubiquitinated Pgp, 100 μ g of microsomal proteins were immunoprecipitated with the anti-Pgp antibody, using 25 μ l of PureProteome Magnetic Beads (Millipore, Bedford, MA), then probed with the anti-mono/poly-ubiquitin antibody.

The control of equal protein loading was performed by using an anti- β -tubulin antibody (Santa Cruz Biotechnology Inc.) for whole cell lysates and cytosolic extracts, an anti-TATA box binding protein antibodies (TBP; Santa Cruz Biotechnology Inc.) for nuclear extracts, an anti-calreticulin antibody (Affinity Bioreagents, Rockford, IL) for microsomal extracts. Membranes were then washed with TBS-Tween 0.1%, incubated with the secondary horseradish-peroxidase conjugated antibody, washed and developed by enhanced chemiluminescence (Bio-Rad Laboratories). Images were acquired by Image Lab software (Bio-Rad Laboratories).

3.20 Kinetics of doxorubicin efflux

Dox efflux kinetics was measured as described elsewhere (Riganti C *et al.*, Cancer Res. 2005). Cells were incubated for 20 min with increasing (0–50 μ M) concentrations of parent or synthetic Doxs, then washed and analyzed for intracellular Dox concentration. A second series of dishes, incubated in the same experimental conditions, were left for a further 10 min at 37 $^{\circ}$ C, then washed and tested for intracellular drug content. The difference of Dox concentration between the two series, expressed as nmol Dox extruded/min/mg cell proteins, was plotted versus initial drug concentration. Values were fitted to the

Michaelis–Menten equation to calculate V_{max} and K_m , using the Enzfitter software (Biosoft Corporation, Cambridge, UK).

3.21 Quantification of sulfhydrated microsomal proteins.

The sulfhydration of 100 μg of microsomal proteins or 50 μg of immunopurified Pgp was measured according to (Sen N *et al.*, Mol Cell 2012), with minor modifications. Samples were re-suspended in 600 μl solubilization buffer (150 mM NaCl, 0.5% v/v Tween 20, 50 mM Tris 7.5, 1 mM EDTA) and incubated for 2 h at 4°C with 2 μM Alexa Fluor 680 conjugated C2 maleimide (Thermo Fisher Scientific, Waltham, MA), to label either sulfhydrated and unsulfhydrated cysteines. Samples were vortexed every 20 minutes. 300 μl were transferred in a new series of tubes and incubated for an additional 1 h at 4°C with 1 mM {DTT}, that removes maleimide adducts from sulfhydrated cysteines only, increasing labelling specificity. Fluorescence of samples (λ excitation=684 nm; λ emission=714 nm) was read with a Synergy HT Multi-Detection Microplate Reader. The fluorescence of samples treated with maleimide and DTT treated samples was divided per the fluorescence of the same sample without DTT (Sen N *et al.*, Mol Cell 2012). Results were expressed as relative fluorescence units (RFU)/mg of microsomal proteins or Pgp protein.

3.22 Quantification of ubiquitinated microsomal proteins.

The ubiquitination of 100 μg of microsomal proteins or 50 μg of immunopurified Pgp was measured with the E3Lite Customizable Ubiquitin Ligase kit (Life-Sensors Inc., Malvern, PA). Samples were diluted in 100 μl of ubiquitination assay buffer (1 M Tris/HCl, 500 mM MgCl_2 , 10 mM DTT; pH 8), and incubated for 30 min at 37°C, in the presence of 5 nM E1 activating enzyme provided by the kit, 100 nM E2 conjugating enzyme Ube2g2 (LifeSensors Inc.), 200 μM ATP, 6 mM human recombinant ubiquitin. Samples were washed twice with PBS-Tween 0.1% v/v containing 5% w/v BSA and incubated with the biotinylated anti-ubiquitin antibody of the kit, followed by streptavidin/horseradish peroxidase-conjugated polymer and enhanced chemiluminescence detection reagent. The chemiluminescent signal was read using a Synergy HT Multi-Detection Microplate Reader. The results were expressed as RLU/mg of microsomal proteins or Pgp protein.

3.23 Statistical analysis

All data in the text and figures are provided as means \pm SD. The results were analyzed by a one-way analysis of variance (ANOVA) and Tukey's test. $p < 0.05$ was considered significant.

4. Results

4.1 Expression of Pgp in doxorubicin-sensitive and doxorubicin-resistant osteosarcoma cells

The expression of Pgp/ABCB1 and MRP1/ABCC1, the main transporters involved in Dox efflux, was measured in parental U-2OS and Saos-2 cells, and in their resistant clones DX30, DX100 and DX580 by flow cytometry. As shown in Figure 10, ABCB1/Pgp progressively increased with the progressive increase in Dox-resistance, while ABCC1/MRP1 had a less clear trend. The progressive increase in Pgp in resistant clones was confirmed by immunoblot (Figure 11).

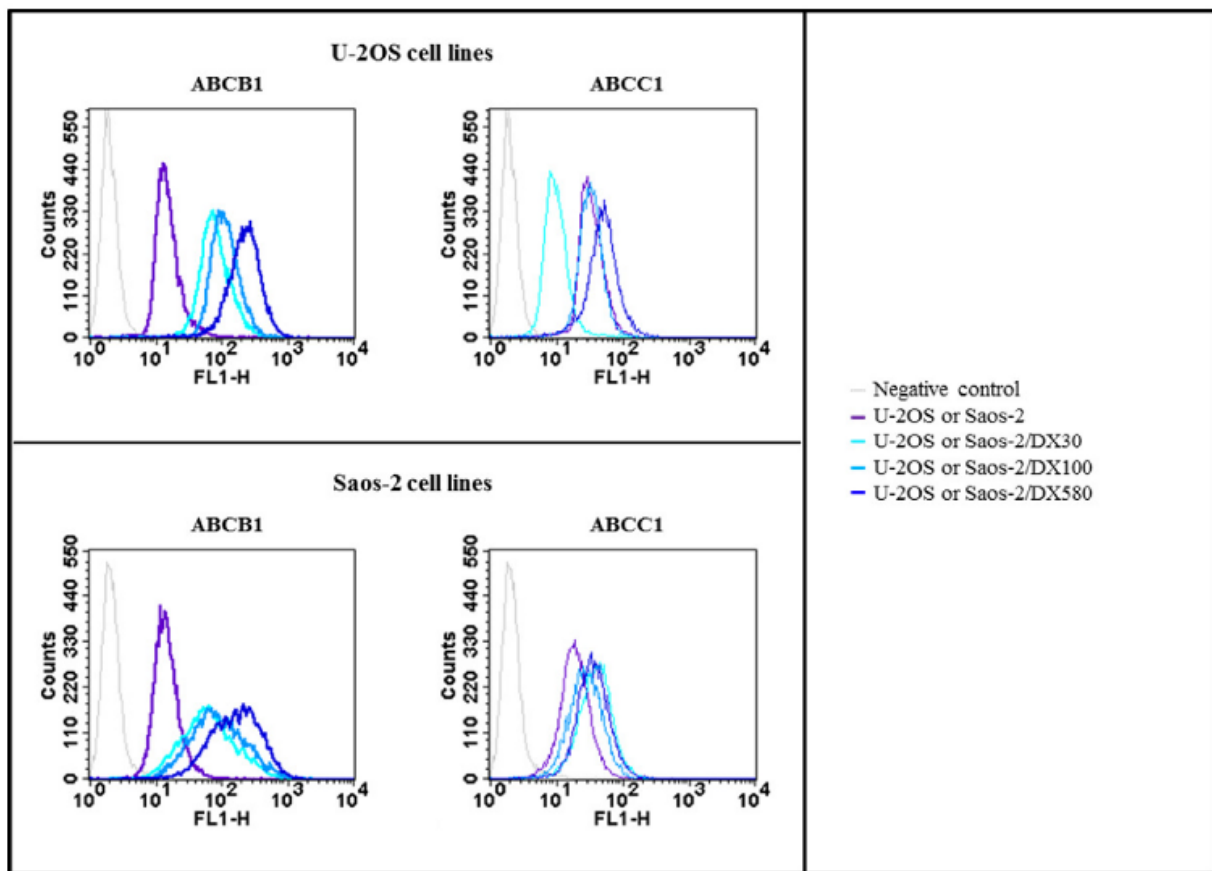


Figure 10 Human Dox-sensitive U-2OS cells and Dox-resistant variants (U-2OS/DX30, U-2OS/DX100, U-2OS/DX580), human Dox-sensitive Saos-2 cells and Dox-resistant variants (Saos-2/DX30, Saos-2/DX100, Saos-2/DX580) were analyzed for the surface expression of ABCB1/Pgp by flow cytometry in duplicate. The figure is representative of 1 out of 3 experiments.

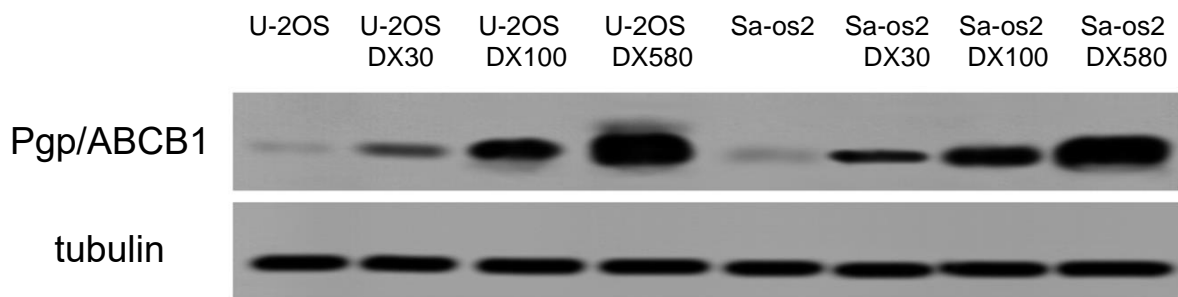


Figure 11 Expression Pgp/ABCB1 in Dox-sensitive U-2OS cells and Dox-resistant variants (U-2OS/DX30, U-2OS/DX100, U-2OS/DX580), human Dox-sensitive Saos-2 cells and Dox-resistant variants (Saos-2/DX30, Saos-2/DX100, Saos-2/DX580) by immunoblotting. β -tubulin was used as control of equal protein loading. The figure is representative of 1 out of 3 experiments.

Part one

4.2 Mitochondria targeting Dox

4.2.1 Mitochondria-targeting doxorubicin is effective against doxorubicin-resistant osteosarcoma in vitro

We compared the anti-tumor efficacy of Dox and mtDox in the Dox-sensitive cells and in their resistant variants. Dox had a typical nuclear localization in U-2OS cell line (Figure 12A) and a progressively lower intramitochondrial accumulation in the resistant variants (Figure 12B). By contrast, mtDox had a peculiar mitochondrial localization in U-2OS cells (Figure 12A): intramitochondrial mtDox accumulation was significantly higher than Dox and was progressively increased in the resistant cells (Figure 12B). Dox retention in the whole cell was progressively lower (Figure 12C) and the inhibition of cell survival was lost (Figure 12D) in the resistant variants. Although mtDox was slightly less accumulated within whole cell in the most resistant variants (Figure 12C), it was still able to reduce cell survival (Figure 12D).

Dox is one of the few chemotherapeutic drugs able to induce direct cytotoxicity on tumor cell, indicated by the extracellular release of LDH (Riganti C *et al.*, J Biol Chem 2004), and to elicit tumor immunogenic cell death, indicated by the extracellular release of ATP and HMGB1, and by the exposure on cell surface of the immune-activating protein calreticulin/CRT (Keep O *et al.*, Oncoimmunology 2014). In U-2OS cells Dox increased the extracellular release of LDH (Figure 12E), ATP (Figure 12F) and HMGB1 (Figure 12G), and the exposure of CRT (Figure 12H), but it progressively lost these properties in the resistant variants. By contrast, mtDox increased all these parameters in sensitive and resistant cells (Figure 12E-H). The effects of mtDox were not cell line- or species-specific: indeed, mtDox was more accumulated and more cytotoxic than doxorubicin in human sensitive Saos-2 cells and in the corresponding resistant variants Saos-2/DX30, Saos-2/DX100, Saos-2/DX580 cells as well as in murine Pgp-expressing K7M2 cells (Figure 13 A-E). In K7M2 cells, mtDox – but not Dox – increased the percentage of apoptotic sub-G₀ cells and decreased the percentage of cells in S-phase (Figure 13F), increased the activation of caspase 3 (Figure 13G), the exposure of CRT (Figure 13H) and the rate of cell phagocytosis (Figure 13I), recapitulating the main cell death mechanisms induced by Dox, i.e. necrosis, reduced proliferation, apoptosis and ICD.

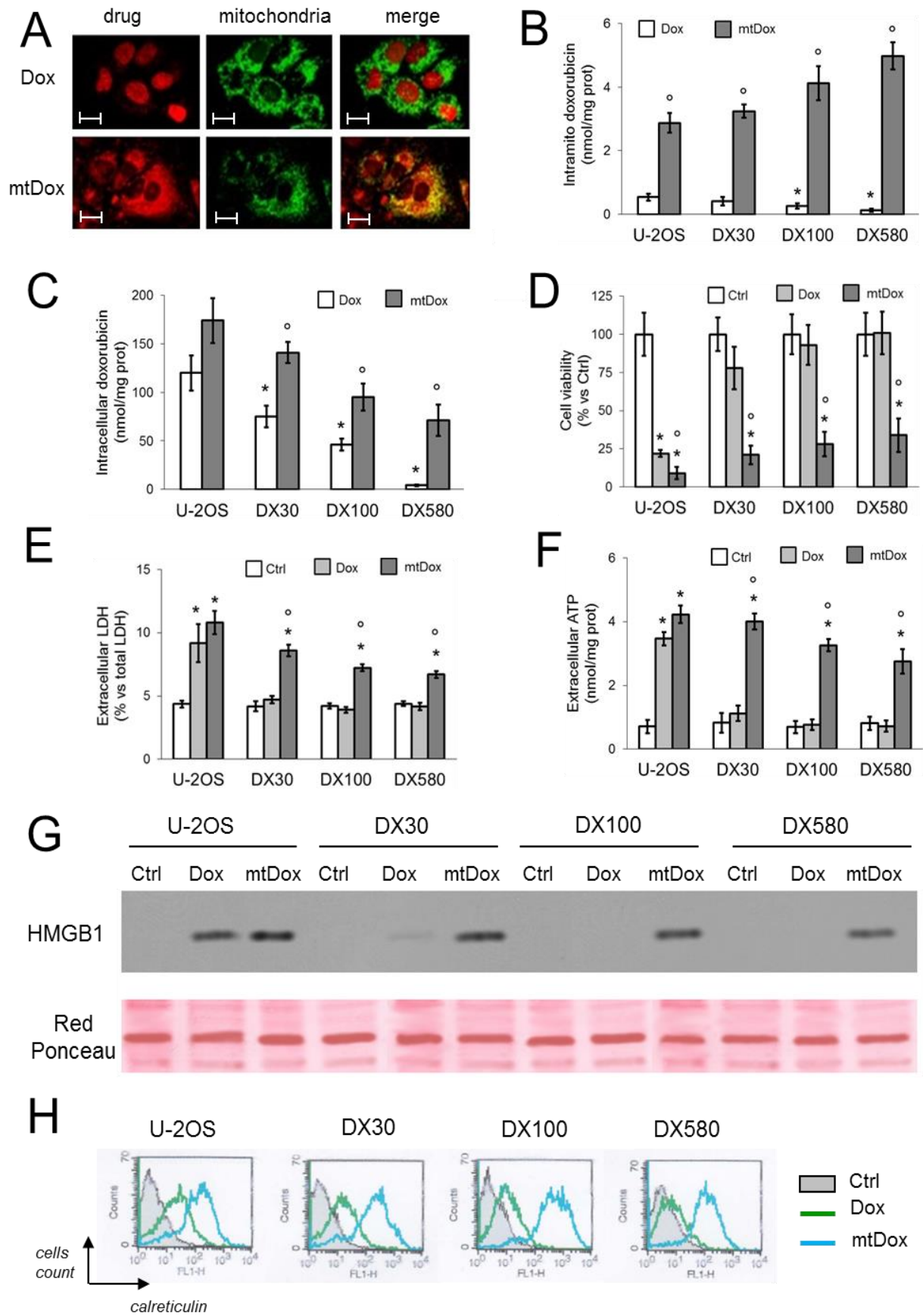


Figure 12. Dox-sensitive U-2OS cells and Dox-resistant variants (U-2OS/DX30, U-2OS/DX100, U-2OS/DX580) were incubated in the absence (Ctrl) or in the presence of 5 $\mu\text{mol/L}$ Dox or mtDox for 6 h (panels A, B), 24 h (panels C, E, F, G) or 72 h (panel D). **A.** Dox-sensitive U-2OS cells were incubated for 24 h with the GFP-E1 α pyruvate dehydrogenase expression vector to label mitochondria, then treated with Dox or mtDox. The intracellular localization of the drugs was analyzed by confocal microscopy. Bar: 10 μm . The micrographs are representative of 3 experiments with similar results. **B.** The amount of Dox was measured spectrofluorimetrically in isolated mitochondria in duplicate. Data are presented as means \pm SD (n= 3). Versus U-2OS cells: * p < 0.02; mtDox versus Dox: ° p < 0.001. **C.** The content of doxorubicin in whole cell lysates was measured spectrofluorimetrically in duplicate. Data are presented as means \pm SD (n= 4). Versus U-2OS cells: * p < 0.05; mtDox versus Dox: ° p < 0.002. **D.** Cell viability was measured in quadruplicate. The results were expressed as percentage of viable cells versus untreated cells. Data are presented as means \pm SD (n= 3). Versus respective Ctrl cells: * p < 0.001; mtDox versus Dox: ° p < 0.01. **E.** The release of LDH in the extracellular medium was measured spectrophotometrically in duplicate. Data are presented as means \pm SD (n= 4). Versus respective Ctrl cells: * p < 0.005; mtDox versus Dox: ° p < 0.001. **F.** The extracellular release of ATP was measured in duplicate by a chemiluminescence-based assay. Data are presented as means \pm SD (n = 3). Versus respective Ctrl cells: * p < 0.001; mtDox versus Dox: ° p < 0.001. **G.** The release of HMGB1 in the cell supernatants was analyzed by Western blotting. Red Ponceau staining was used to check the equal loading of proteins. The figure is representative of 3 experiments with similar results. **H.** The amount of surface calreticulin was measured by flow cytometry in duplicate. The figure is representative of 3 experiments with similar results.

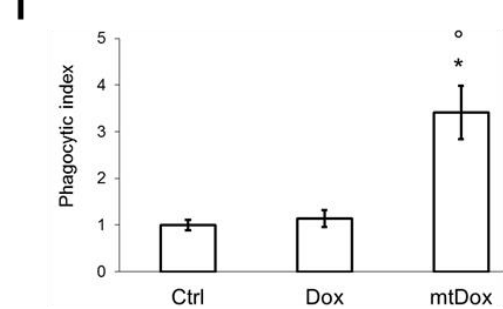
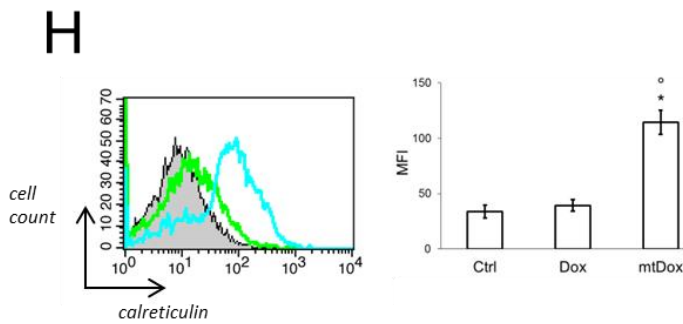
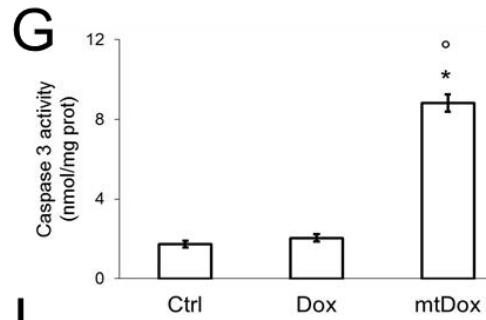
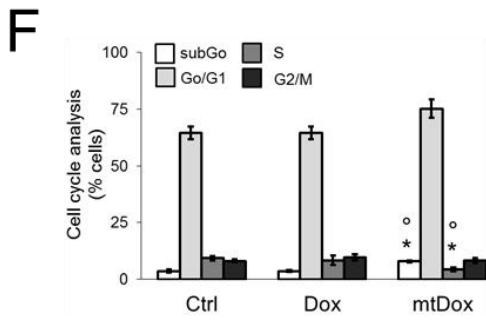
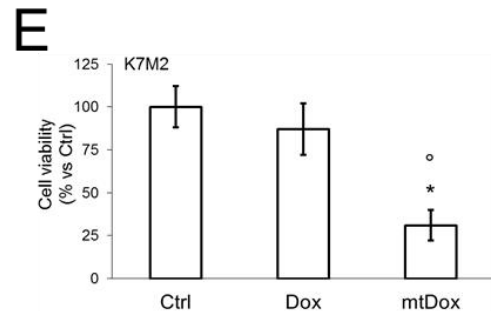
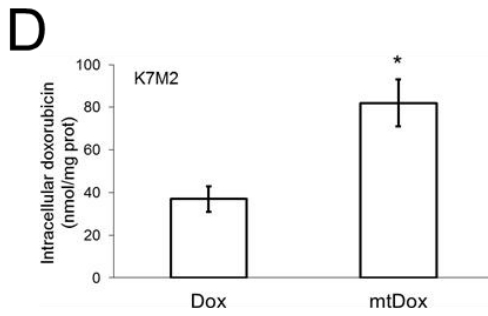
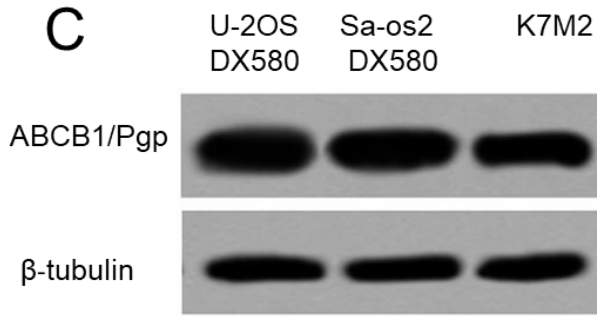
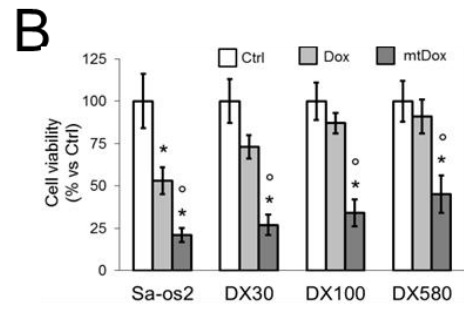
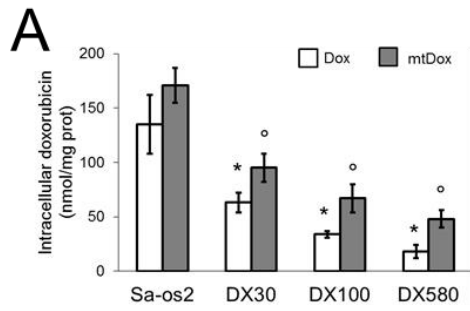


Figure 13. Intracellular accumulation and cytotoxicity of mitochondria-targeted doxorubicin in drug-sensitive Saos-2 cells and in their resistant variants, and in K7M2 cells

A. Dox-sensitive Saos-2 cells and Dox-resistant variants (Saos-2/DX30, Saos-2/DX100, Saos-2/DX580) were incubated with 5 μ M/L Dox or mtDox for 24 h. The amount of Dox in whole cell lysates was measured spectrofluorimetrically in duplicate. Data are presented as means \pm SD (n= 3). Versus Saos-2 cells: * p < 0.01; mtDox versus Dox: \circ p < 0.05. **B.** Cells were grown for 72 h in fresh medium (Ctrl), in medium containing 5 μ M/L Dox or mtDox, then ATPLite kit was used to measure viability in quadruplicate. The results were expressed as a percentage of viable cells versus untreated cells. Data are presented as means \pm SD (n= 3). Versus respective Ctrl: * p < 0.005; mtDox versus Dox: \circ p < 0.005. **C.** Murine osteosarcoma K7M2 cells were lysed and subjected to the Western blot analysis of ABCB1/Pgp. The resistant U-2OS/DX580 and Saos-2/DX580 variants were included as control of Pgp-overexpressing cells. The β -tubulin expression was used as a control of equal protein loading. The figure is representative of 1 out of 2 experiments. **D.** K7M2 cells were incubated for 24 h with 5 μ M/L Dox or mtDox. The amount of Dox was measured spectrofluorimetrically in duplicate. Data are presented as means \pm SD (n= 3). mtDox versus Dox: * p < 0.01. **E.** Cells were grown for 72 h in fresh medium (Ctrl), in medium containing 5 μ M/L Dox or mtDox, then their viability was measured in quadruplicate. The results were expressed as a percentage of viable cells versus untreated cells. Data are presented as means \pm SD (n= 3). Versus Ctrl: * p < 0.002; mtDox versus Dox: \circ p < 0.002. **F.** Cell cycle analysis was measured by flow cytometry. Data are presented as means \pm SD (n = 3). Versus Ctrl: * p < 0.01; mtDox versus Dox: \circ p < 0.001. **G.** The activity of caspase 3 was measured fluorimetrically in duplicate in the cytosolic extracts. Data are presented as means \pm SD (n = 4). Versus Ctrl: * p < 0.001; mtDox versus Dox: \circ p < 0.001. **H.** The amount of surface calreticulin was measured by flow cytometry in duplicate. Left panel: histograms representative of 1 out of 3 experiments; right panel: mean fluorescence intensity (MFI) of calreticulin-positive cells. Data are presented as means \pm SD (n = 3). Versus Ctrl: * p < 0.001; mtDox versus Dox: \circ p < 0.001. **I.** DC-mediated phagocytosis of K7M2 cells was measured by flow cytometry. Data are presented as means \pm SD (n = 4). The phagocytic index of untreated cells was considered as 1. Versus Ctrl: * p < 0.002; mtDox versus Dox: \circ p < 0.005.

In not-transformed osteoblast, mtDox was less accumulated (Figure 14A) and less cytotoxic than Dox, in terms of release of LDH (Figure 14B), and cell viability reduction (Figure 14C). Similarly, mtDox significantly less accumulated in rat H9c2 cardiomyocytes (Figure Suppl. 14D) and less cytotoxic at short (Figure 14E) and long term (Figure 14F).

This scenario grants a good therapeutic windows for mtDox that showed a preferential cytotoxic effect against osteosarcoma cells rather than against not-transformed bone cells or cardiomyocytes.

In line with these results, IC₅₀ of Dox increased in the resistant variants of U2-OS and SaoS-2 cells and in K7M2, wherease the IC₅₀ of mtDox was significantly lower. By contrast, mtDox had higher IC₅₀ than Dox in not-transformed osteoblasts and cardiomyocytes (Table 1).

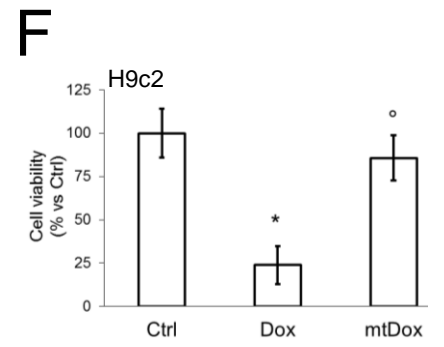
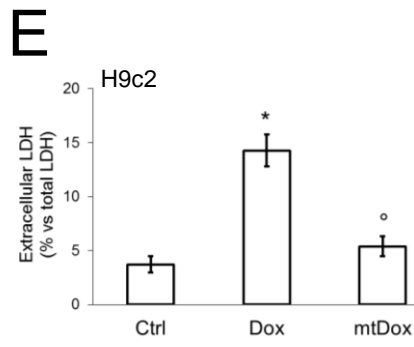
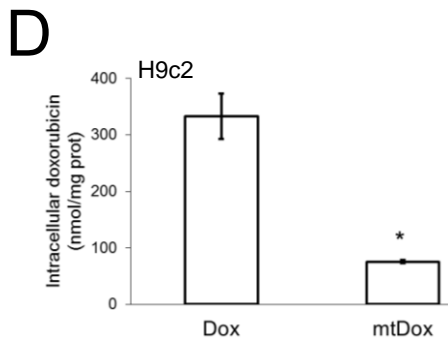
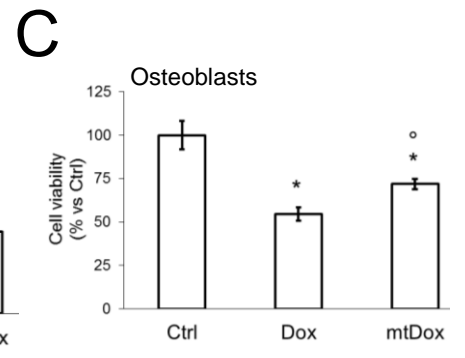
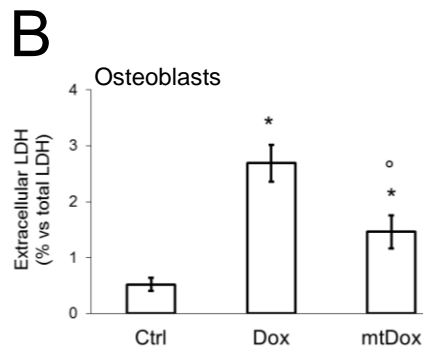
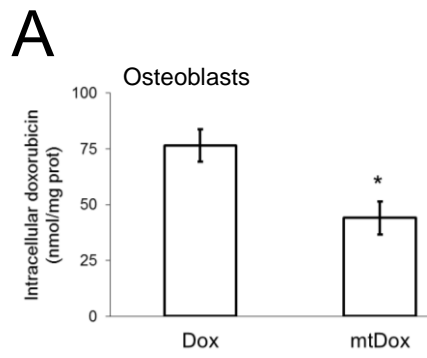


Figure 14 Intracellular accumulation and cytotoxicity of mitochondria targeted doxorubicin in non-transformed osteoblasts and cardiomyocytes

Human non-transformed osteoblasts and rat neonatal H9c2 cardiomyocytes were cultured for 24 h (panels **A, B, D, E**) or 72 h (panels **C, F**) in fresh medium (Ctrl), in medium containing 5 $\mu\text{mol/L}$ Dox or mtDox. **A** and **D**. The amount of Dox in whole cell lysates was measured spectrofluorimetrically in duplicate. Data are presented as means \pm SD (n= 3). mtDox versus Dox: * p < 0.02. **B** and **E**. The release of LDH in the extracellular medium was measured spectrophotometrically in duplicate. Data are presented as means \pm SD (n= 3). Versus respective Ctrl: * p < 0.005; mtDox versus Dox: ° p < 0.01. **C** and **F**. Cells were stained with neutral red solution in quadruplicate. The results were expressed as a percentage of viable cells versus untreated cells. Data are presented as means \pm SD (n= 4). Versus respective Ctrl: * p < 0.01; mtDox versus Dox: ° p < 0.02.

Table 1. IC50 ($\mu\text{M/L}$) of doxorubicin and mitochondria-targeted doxorubicin

Cell line	Dox	mtDox
U-2OS	3.91 ± 0.43	$1.09 \pm 0.12^\circ$
U-2OS/DX30	$25.62 \pm 1.16^*$	$2.35 \pm 0.28^\circ$
U-2OS/DX100	$79.67 \pm 6.17^*$	$4.68 \pm 0.99^\circ$
U-2OS/DX580	$124.18 \pm 11.07^*$	$10.71 \pm 0.87^\circ$
Saos-2	4.55 ± 0.71	$2.31 \pm 0.23^\circ$
Saos-2/DX30	$18.78 \pm 2.37^*$	$3.81 \pm 0.42^\circ$
Saos-2/DX100	$53.29 \pm 8.93^*$	$6.17 \pm 0.52^\circ$
Saos-2/DX580	$109.82 \pm 21.09^*$	$9.71 \pm 0.87^\circ$
K7M2	75.71 ± 4.77	$8.54 \pm 0.41^\circ$
Primary osteoblasts	4.93 ± 0.29	$27.52 \pm 4.11^\circ$
H9c2	0.72 ± 0.08	$12.39 \pm 5.27^\circ$

Cells were incubated for 72 h with increasing concentrations (1 nM/L-1 mM/L) of Dox or mtDox, then viability was measured in quadruplicate. Data are presented as means \pm SD (n = 3). Dox-resistant variants versus their parental cells: * p < 0.001; mtDox versus Dox: $^\circ$ p < 0.001

4.2.2 Mitochondria-targeting doxorubicin is effective against doxorubicin-resistant osteosarcoma *in vivo*

mtDox dose-dependently decreased tumor growth of Dox-resistant K7M2 cells implanted in syngeneic mice (Figure 15): the maximal efficacy was reached using 5mg/kg, once a week for 3 consecutive weeks

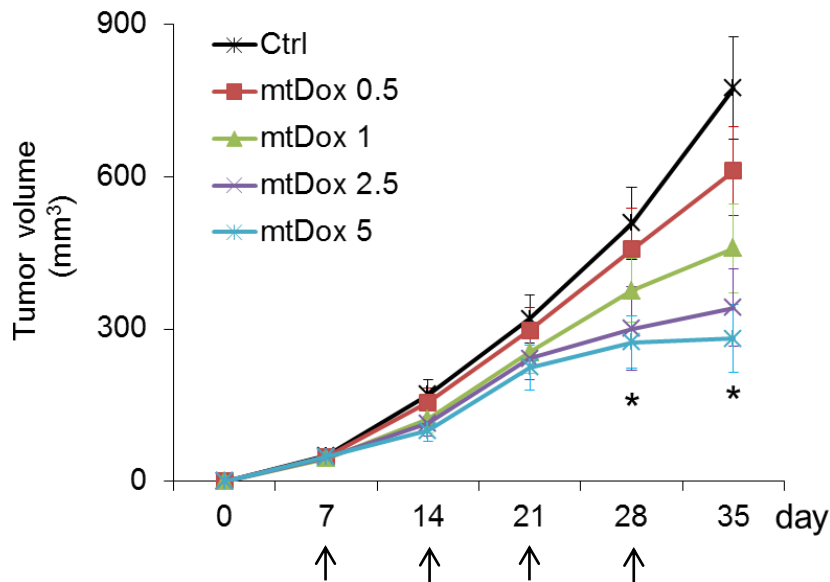


Figure 15 Dose-response effects of mitochondria-targeted doxorubicin on drug-resistant osteosarcoma *in vivo*

Six week-old female BALB/c mice were inoculated s.c. with 1×10^6 K7M2 cells. When the tumor reached the volume of 50 mm³ (day 7), the animals (10 mice/group) were randomized and treated on days 7, 14, 21, 28 with 0.1 mL saline solution i.v. (Ctrl group) or with 0.5, 1, 2.5, 5 mg/kg mtDox. Tumor growth monitored by caliper measurements. Arrows represent saline or mtDox injections. Data are presented as means \pm SD. 1, 2.5, 5 mg/kg mtDox group versus Ctrl group: * $p < 0.01$

At this dosage, mtDox was as effective as Dox in sensitive U2-OS cells implanted in NOD SCID BALB/c mice (Figure 16).

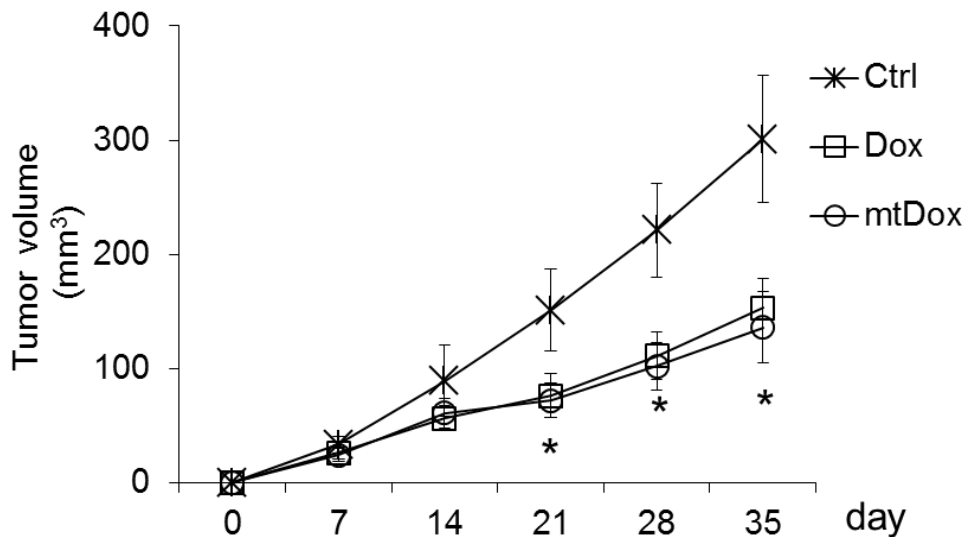


Figure 16 Effects of mitochondria-targeted doxorubicin on drug-sensitive osteosarcoma *in vivo*

Six week-old female NOD SCID BALB/c mice were inoculated s.c. with 1×10^7 U-2OS cells. When the tumor reached the volume of 50 mm³ (day 7), the animals were randomized and treated on days 7, 14, 21, 28 as it follows: 1) Ctrl group, treated with 0.1 mL saline solution i.v.; 2) Dox group, treated with 5 mg/kg Dox i.v.; 3) mtDox group, treated with 5 mg/kg mitochondria-targeted Dox i.v. Arrows represent saline or drug injections. Data are presented as means \pm SD. Dox/mtDox group versus Ctrl group: * $p < 0.001$.

As expected, resistant K7M2 tumors implanted in immunocompetent BALB/c mice did not respond to doxorubicin (Figure 17A-C), which did not reduce tumor cell proliferation nor increased the activation of caspase 3, the amount of CRT on tumor cells, the intratumor infiltration of DC (Figure 17D). On the contrary, mtDox significantly decreased tumor growth and cell proliferation, increased the percentage of apoptotic and calreticulin-positive tumor cells, and the number of DC within the tumor bulk (Figure 17 C). According to the hematochemical parameters of the animals at the time of sacrifice, mtDox was significantly less cardiotoxic than doxorubicin and did not elicit liver or kidney toxicity (Table 2).

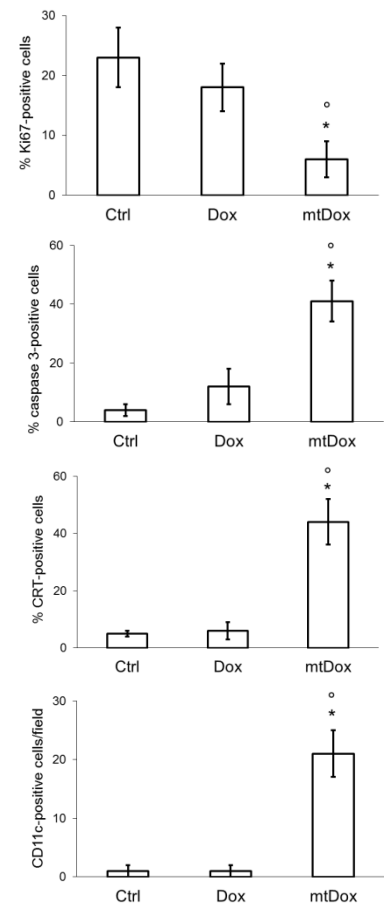
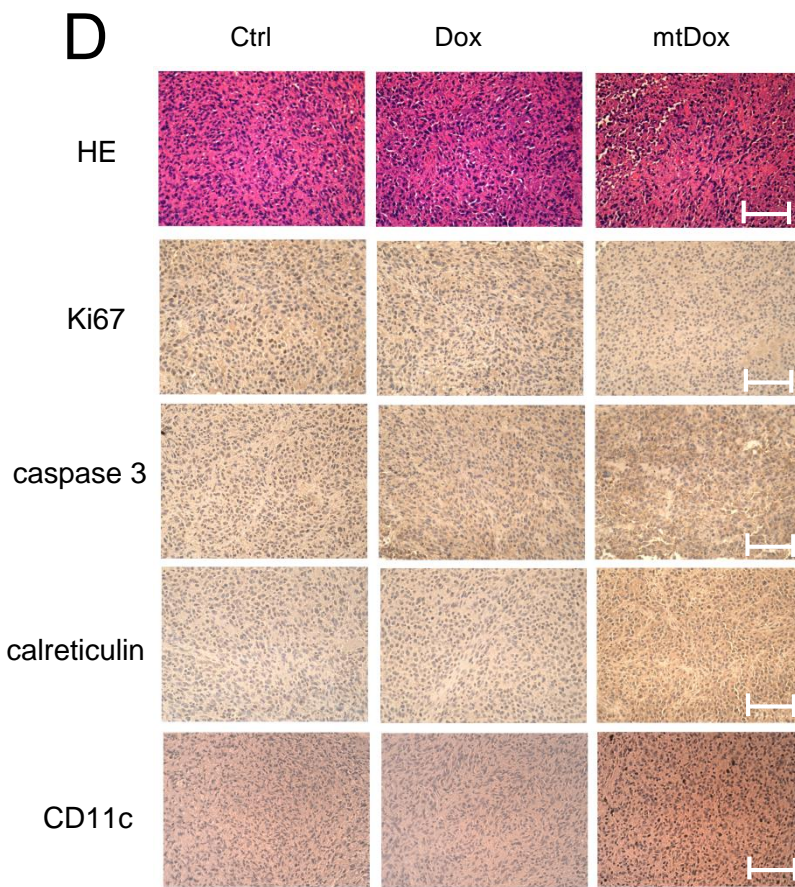
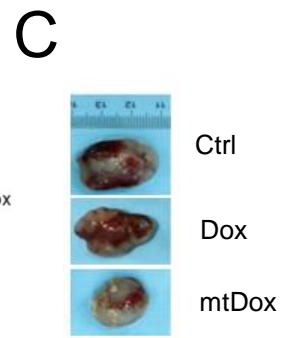
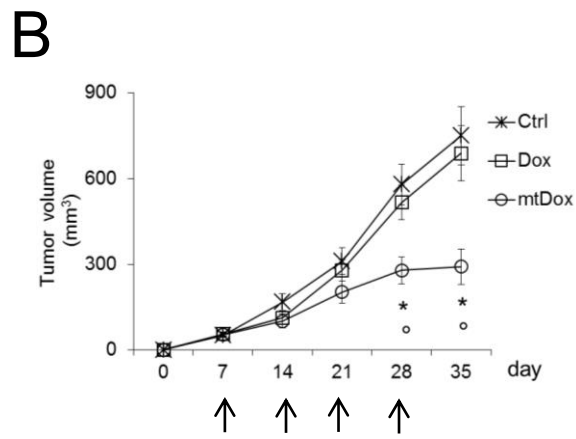
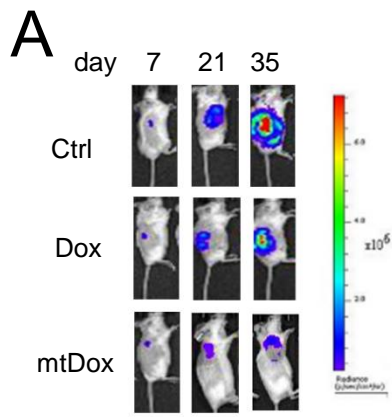


Figure 17 Mitochondria-targeting doxorubicin is effective against drug-resistant osteosarcoma *in vivo*

Six weeks-old female BALB/c mice were inoculated s.c. with 1×10^6 K7M2 cells. When the tumor reached the volume of 50 mm³ (day 7), the animals were randomized and treated as detailed under Materials and methods (10 mice/group). **A.** Representative *in vivo* bioluminescence imaging, performed on days 7, 21, 35 after implant. **B.** Tumor growth monitored by caliper measure. Arrows represent saline, doxorubicin or mitochondria-targeting doxorubicin injections. Data are presented as means \pm SD. Versus Ctrl group: * $p < 0.001$; mtDox group versus Dox group: ° $p < 0.001$. The inhibition rate in Dox-treated animals was 16.86%, in mtDox-treated animals was 45.49%. **C.** Photograph of representative tumors from each treatment group after mice sacrifice. **D. Left panels:** sections of tumors from each group of animals were stained with hematoxylin and eosin (HE) or immunostained for the proliferation marker Ki67, the activated cleaved caspase 3, the immunogenic death marker CRT, the DC marker CD11c. Nuclei were counterstained with hematoxylin. Bar = 10 μ m. The photographs are representative of sections from 5 tumors/group. **Right panels:** quantification of immunohistochemistry images, performed on sections from 5 animals of each group (106-71 nuclei/field). The percentage of proliferating cells was determined by the ratio of Ki67-positive nuclei and the total number of nuclei (hematoxylin-positive nuclei) using ImageJ software (<http://imagej.nih.gov/ij/>). Ctrl group percentage was considered 100%. The percentage of caspase 3-positive and calreticulin-positive cells was determined by Photoshop program. The number of CD11c-positive cells/field was calculated by ImageJ software. Data are presented as means + SD. Versus Ctrl group: * $p < 0.01$; mtDox group versus Dox group: ° $p < 0.02$.

Table 2. Hematochemical parameters of animals

	Ctrl	Dox	mtDox
LDH (U/L)	6231 ± 1098	6234 ± 724	6198 ± 821
AST (U/L)	187 ± 52	234 ± 27	212 ± 82
ALT (U/L)	38 ± 9	41 ± 5	43 ± 10
AP (U/L)	87 ± 13	94 ± 15	91 ± 13
Creatinine (mg/L)	0.041 ± 0.006	0.039 ± 0.008	0.037 ± 0.009
CPK (U/L)	321 ± 93	850 ± 150 *	453 ± 83 °

Animals (n = 10/group) were treated as reported under Materials and methods. Blood was collected immediately after mice euthanasia and analyzed for lactate dehydrogenase (LDH), aspartate aminotransferase (AST), alanine aminotransferase (ALT), alkaline phosphatase (AP), creatinine, creatine phosphokinase (CPK). Ctrl: mice treated with saline solution; Dox: mice treated with doxorubicin; mtDox: mice treated with mitochondria-targeting doxorubicin. Versus Ctrl group: *p < 0.005; mtDox group versus Dox group: ° p < 0.01.

4.2.3 Mitochondria-targeting doxorubicin deeply alters the expression of mitochondria-related genes in doxorubicin-resistant osteosarcoma cells

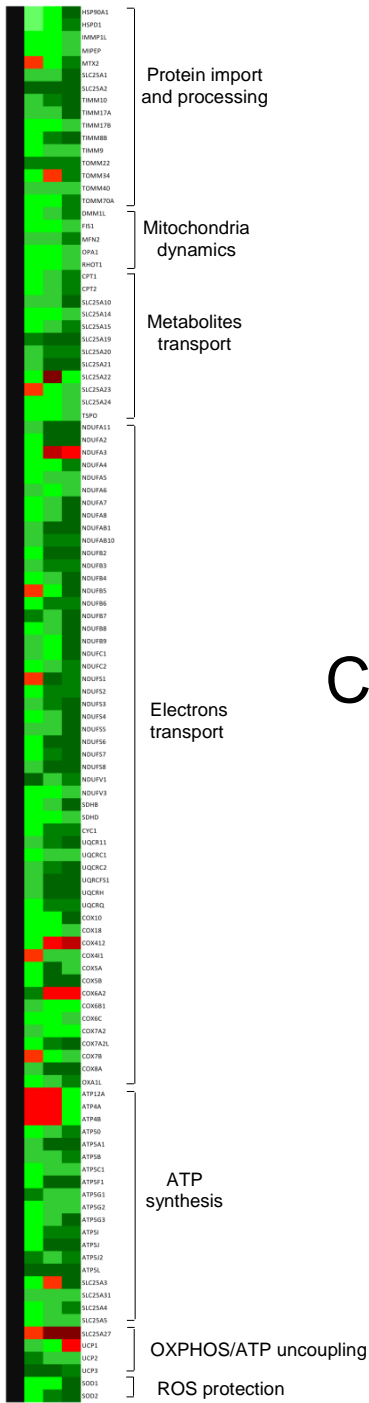
We next analyzed the expression of genes involved in mitochondria functions and mitochondria-dependent apoptosis. As shown in Figure 18 and in Table 3, the progressive increase in Dox resistance was paralleled by the up-regulation of genes controlling processing, import and folding of mitochondrial proteins; mitochondrial fusion, fission and trafficking; transport of metabolites and co-factors across the mitochondrial membranes; mitochondrial metabolic pathways, such as TCA cycle, fatty acids β -oxidation, electron transport; ATP synthesis; ROS protection, such as superoxide dismutase (*SOD*) 1 and 2. *SLC25A27* and *UCP1*, which encode for proteins uncoupling oxidative phosphorylation and ATP synthesis, were instead progressively down-regulated.

In drug-sensitive U-2OS cells, either Dox or mtDox down-regulated at least two-fold 25 genes encoding for metabolite transporters, subunits of respiratory chain complexes and ATP synthase, *SOD1*, *SOD2*, anti-apoptotic genes such as *BCL2* and *BCL2L1* (also known as *Bcl-xL*). They both up-regulated genes encoding for the uncoupling proteins *SLC25A27*, *UCP1*, *UCP2*, *UCP3* and the pro-apoptotic genes *BAK1*, *BBC3* (also known as *Puma*), *BNIP3* (Figure 18B; Table 4). In U-2OS/DX580 cells, Dox up- or down-regulated less than one-fold most of these genes, consistently with the low drug accumulation and efficacy. By contrast, mtDox down-regulated at least two-fold the vast majority of genes involved in proteins import and processing, mitochondria fusion and fission, metabolites transport, electron transport, ATP synthesis, ROS protection, apoptosis inhibition. In parallel, it up-regulated genes encoding for uncoupling proteins (e.g. *SLC25A27*, *UCP1* and *UCP3*) and pro-apoptotic factors (e.g. *BAK1*, *BBC3*, *BID*, *BNIP3*; Figure 18C; Table 5).

A

```

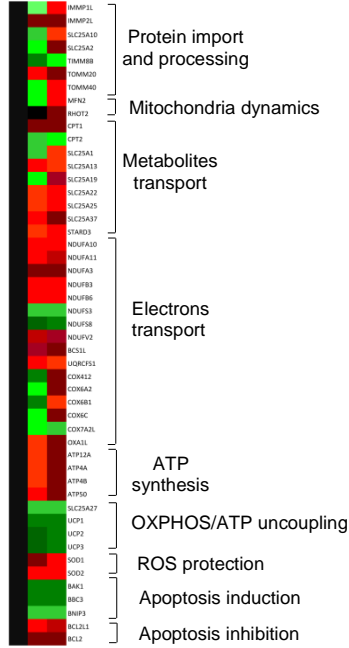
U D D D
- X X X
  2 3 1 5
O O O 8
S   0 0
  
```



B

```

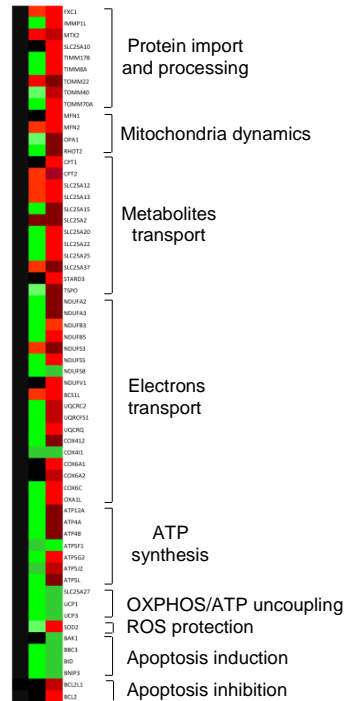
U-2OS
C m
t D D
r o o
l x x
  
```



C

```

DX580
C m
t D D
r o o
l x x
  
```



Fold change <math><-4</math> -4 -3 -2 -1 0 1 2 3 4 >4

Figure 18 Modulation of mitochondria-related genes by doxorubicin and mitochondria-targeting doxorubicin in drug-sensitive and drug-resistant osteosarcoma cells **A**. The cDNA from doxorubicin-sensitive U-2OS cells and doxorubicin-resistant variants (U-2OS/DX30, U-2OS/DX100, U-2OS/DX580) was analyzed by PCR arrays specific for mitochondria-related genes, as reported under Materials and methods. The figure reports the genes up- or down-regulated two-fold or more in at least one cell line, in a colorimetric scale, and is the mean of 4 experiments. **B-C**. U-2OS cells (panel **B**) or U-2OS/DX580 cells (panel **C**) were grown for 24 h in fresh medium (Ctrl), in medium containing 5 $\mu\text{mol/L}$ doxorubicin (Dox) or mitochondria-targeting doxorubicin (mtDox). The cDNA was analyzed by the same PCR arrays of panel **A**. The figures report the genes up- or down-regulated two-fold or more in at least one experimental condition, in a colorimetric scale, and are the means of 4 experiments. OXPHOS: oxidative phosphorylation.

Table 3. Expression of mitochondrial-related genes in U-2OS cells and resistant variants

Gene	Fold change DX30 versus U-2OS	p value	Fold change DX100 versus U-2OS	p value	Fold change DX580 versus U-2OS	p value	Biological function
<i>AIFM2</i>	1.66	0.02	1.42	0.005	1.04	Ns	Apoptosis induction
<i>ATP12A</i>	0.34	0.005	0.45	0.02	1.70	Ns	H ⁺ /ATP exchange
<i>ATP4A</i>	0.33	0.005	0.45	0.02	1.70	Ns	H ⁺ /ATP exchange
<i>ATP4B</i>	0.34	0.005	0.45	0.02	1.67	Ns	H ⁺ /ATP exchange
<i>ATP50</i>	1.29	Ns	2.40	0.001	3.71	0.001	ATP synthase subunit
<i>ATP5A1</i>	2.24	0.002	5.82	0.001	6.38	0.001	ATP synthase subunit
<i>ATP5B</i>	2.09	0.005	2.96	0.001	3.93	0.001	ATP synthase subunit
<i>ATP5C1</i>	1.38	0.05	2.91	0.001	2.26	0.001	ATP synthase subunit
<i>ATP5F1</i>	1.70	0.01	4.62	0.001	4.91	0.001	ATP synthase subunit
<i>ATP5G1</i>	3.40	0.001	2.53	0.001	2.42	0.001	ATP synthase subunit
<i>ATP5G2</i>	1.72	0.01	2.24	0.001	2.42	0.001	ATP synthase subunit
<i>ATP5G3</i>	1.80	0.01	2.29	0.001	5.41	0.001	ATP synthase subunit
<i>ATP5I</i>	1.82	0.005	3.4	0.001	3.93	0.001	ATP synthase subunit
<i>ATP5J</i>	1.59	0.001	5.92	0.001	6.38	0.001	ATP synthase subunit
<i>ATP5J2</i>	3.17	0.001	2.06	0.001	3.93	0.001	ATP synthase subunit
<i>ATP5L</i>	4.41	0.001	4.49	0.001	10.38	0.001	ATP synthase subunit

<i>BAK1</i>	1.55	0.02	1.10	Ns	1.42	Ns	Apoptosis induction
<i>BBC3</i>	1.44	Ns	1.52	Ns	0.88	Ns	Apoptosis induction
<i>BCL2</i>	1.35	0.05	0.88	Ns	1.13	Ns	Apoptosis inhibition
<i>BCL2L1</i>	1.78	0.001	0.73	Ns	1.17	Ns	Apoptosis induction
<i>BCS1L</i>	1.82	0.005	1.82	0.001	1.39	0.01	Ubiquinol-cytochrome c reductase assembly
<i>BID</i>	1.55	0.02	1.19	Ns	1.59	Ns	Apoptosis induction
<i>BNIP3</i>	1.18	Ns	1.99	Ns	1.90	Ns	Apoptosis induction
<i>COX10</i>	1.66	0.01	1.41	Ns	4.02	0.05	Cytochrome c oxidase assembly
<i>COX18</i>	1.78	0.02	1.40	Ns	2.05	0.02	Cytochrome c oxidase assembly
<i>COX412</i>	1.70	Ns	0.45	0.02	0.34	0.01	Cytochrome c oxidase subunit
<i>COX411</i>	0.79	Ns	2.40	0.001	2.39	0.01	Cytochrome c oxidase assembly
<i>COX5A</i>	1.95	0.005	4.16	0.001	2.59	0.001	Cytochrome c oxidase subunit
<i>COX5B</i>	1.95	0.005	4.16	0.001	5.81	0.001	Cytochrome c oxidase subunit
<i>COX6A1</i>	1.70	0.01	0.81	0.001	0.71	0.02	Cytochrome c oxidase subunit
<i>COX6A2</i>	3.32	0.01	0.41	0.001	0.34	0.001	Cytochrome c oxidase subunit
<i>COX6B1</i>	2.41	0.005	1.16	0.001	1.71	0.001	Cytochrome c oxidase assembly/regulation
<i>COX6C</i>	1.38	0.05	1.49	0.05	2.26	0.001	Cytochrome c oxidase assembly/regulation
<i>COX7A2</i>	2.24	0.005	1.86	0.001	1.71	0.001	Cytochrome c oxidase assembly/regulation
<i>COX7A2 L</i>	1.29	Ns	3.81	0.001	4.21	0.001	Cytochrome c oxidase assembly/regulation
<i>COX7B</i>	0.85	0.002	1.96	0.001	2.11	0.001	Cytochrome c oxidase subunit
<i>COX8A</i>	2.09	0.001	4.53	0.001	4.51	0.001	Cytochrome c oxidase regulation
<i>CPT1</i>	1.66	0.01	2.05	0.05	3.30	0.05	Long chain fatty acylCoA import/ β -oxidation
<i>CPT2</i>	1.55	0.02	2.04	0.05	3.42	0.01	Long chain fatty acylCoA import/ β -oxidation
<i>CYC1</i>	1.95	0.005	3.24	0.001	3.98	0.001	Electron transport
<i>DMM1L</i>	1.91	0.01	2.16	0.02	3.18	0.05	Control of mitochondria morphology
<i>FIS1</i>	1.35	0.05	1.52	Ns	2.71	0.05	Control of mitochondria fission

<i>FXC1</i>	1.45	0.05	0.78	Ns	1.05	Ns	Mitochondrial proteins import
<i>HSP90A</i> 1	1.26	Ns	2.26	0.05	4.40	0.05	Proteins chaperon
<i>HSPD1</i>	1.26	Ns	2.16	0.05	3.33	0.05	Mitochondrial proteins chaperon
<i>IMMP1L</i>	1.45	0.05	1.24	0.05	2.01	0.05	Mitochondrial proteins processing/import
<i>IMMP2L</i>	0.59	0.001	0.80	Ns	1.56	Ns	Mitochondrial proteins processing/import
<i>LRPPRC</i>	1.10	Ns	1.42	Ns	1.59	Ns	Mitochondrial transcription factor
<i>MFN1</i>	0.63	0.02	0.86	Ns	1.15	Ns	Control of mitochondria fusion
<i>MFN2</i>	2.19	0.002	2.43	0.05	3.49	0.05	Control of mitochondria fusion
<i>MIPEP</i>	1.78	0.01	1.39	Ns	2.47	0.05	Mitochondrial proteins processing
<i>MPV17</i>	1.66	0.01	1.18	Ns	1.45	0.005	Metabolism of mitochondrial ROS
<i>MTX2</i>	0.72	0.05	1.18	Ns	3.11	0.001	Mitochondrial proteins import
<i>NDUFA1</i>	1.82	0.005	1.40	0.001	1.71	0.001	NADH:ubiquinone oxidoreductase subunit
<i>NDUFA1</i> 0	1.70	0.01	1.38	0.001	1.70	0.002	NADH:ubiquinone oxidoreductase subunit
<i>NDUFA1</i> 1	2.58	0.001	5.29	0.001	6.84	0.001	NADH:ubiquinone oxidoreductase subunit
<i>NDUFA2</i>	1.70	0.01	5.16	0.001	6.41	0.001	NADH:ubiquinone oxidoreductase assembly
<i>NDUFA3</i>	1.95	0.005	0.29	0.001	0.40	0.05	NADH:ubiquinone oxidoreductase subunit
<i>NDUFA4</i>	1.82	0.005	1.91	0.001	3.96	0.001	NADH:ubiquinone oxidoreductase subunit
<i>NDUFA5</i>	1.70	0.01	2.19	0.001	2.26	0.001	NADH:ubiquinone oxidoreductase subunit
<i>NDUFA6</i>	2.09	0.005	1.91	0.001	2.11	0.001	NADH:ubiquinone oxidoreductase subunit
<i>NDUFA7</i>	1.48	0.02	2.24	0.001	4.21	0.001	NADH:ubiquinone oxidoreductase subunit

<i>NDUFA8</i>	1.70	0.01	2.78	0.001	8.38	0.001	NADH:ubiquinone subunit	oxidoreductase
<i>NDUFAB1</i>	2.76	0.001	4.12	0.001	6.35	0.001	NADH:ubiquinone subunit	oxidoreductase
<i>NDUFAB10</i>	2.76	0.001	3.91	0.001	3.93	0.001	NADH:ubiquinone subunit	oxidoreductase
<i>NDUFB2</i>	1.95	0.005	5.92	0.001	6.38	0.001	NADH:ubiquinone subunit	oxidoreductase
<i>NDUFB3</i>	2.09	0.005	3.81	0.001	3.97	0.001	NADH:ubiquinone subunit	oxidoreductase
<i>NDUFB4</i>	1.82	0.005	2.59	0.001	5.16	0.001	NADH:ubiquinone subunit	oxidoreductase
<i>NDUFB5</i>	0.79	Ns	1.71	0.001	4.19	0.001	NADH:ubiquinone subunit	oxidoreductase
<i>NDUFB6</i>	1.59	0.01	3.67	0.001	3.91	0.001	NADH:ubiquinone subunit	oxidoreductase
<i>NDUFB7</i>	3.65	0.005	2.24	0.001	7.86	0.001	NADH:ubiquinone subunit	oxidoreductase
<i>NDUFB8</i>	1.82	0.005	2.42	0.001	8.38	0.001	NADH:ubiquinone subunit	oxidoreductase
<i>NDUFB9</i>	2.96	0.001	1.83	0.001	6.35	0.001	NADH:ubiquinone subunit	oxidoreductase
<i>NDUFC1</i>	2.24	0.002	1.26	0.001	4.19	0.001	NADH:ubiquinone subunit	oxidoreductase
<i>NDUFC2</i>	1.38	0.05	2.26	0.001	3.40	0.001	NADH:ubiquinone subunit	oxidoreductase
<i>NDUFS1</i>	0.85	Ns	4.81	0.001	3.67	0.001	NADH:ubiquinone subunit	oxidoreductase
<i>NDUFS2</i>	1.29	Ns	3.65	0.001	3.19	0.001	NADH:ubiquinone subunit	oxidoreductase
<i>NDUFS3</i>	2.41	0.002	3.19	0.001	5.53	0.001	NADH:ubiquinone subunit	oxidoreductase

<i>NDUFS4</i>	1.59	0.01	2.59	0.001	4.49	0.001	NADH:ubiquinone oxidoreductase subunit
<i>NDUFS5</i>	2.24	0.002	2.78	0.001	5.16	0.001	NADH:ubiquinone oxidoreductase subunit
<i>NDUFS6</i>	2.24	0.005	4.81	0.001	4.84	0.001	NADH:ubiquinone oxidoreductase subunit
<i>NDUFS7</i>	1.82	0.001	3.93	0.001	4.49	0.001	NADH:ubiquinone oxidoreductase subunit
<i>NDUFS8</i>	2.76	0.001	14.49	0.001	16.76	0.001	NADH:ubiquinone oxidoreductase subunit
<i>NDUFV1</i>	4.19	0.001	2.98	0.001	3.65	0.001	NADH:ubiquinone oxidoreductase subunit
<i>NDUFV2</i>	1.59	0.01	1.29	0.001	1.05	Ns	NADH:ubiquinone oxidoreductase subunit
<i>NDUFV3</i>	1.20	Ns	1.49	0.002	2.24	0.001	NADH:ubiquinone oxidoreductase subunit
<i>OPA1</i>	1.45	0.05	1.79	0.05	2.01	0.05	Control of mitochondria network
<i>OXA1L</i>	1.59	0.005	2.11	0.001	3.65	0.001	Cytochrome c oxidase assembly
<i>RHOT1</i>	1.55	0.02	1.39	Ns	2.71	0.05	Control of mitochondria fission and fusion
<i>RHOT2</i>	1.91	0.005	0.62	Ns	1.15	Ns	Control of mitochondria fission and fusion
<i>SDHA</i>	1.17	Ns	1.48	0.005	1.83	0.001	Succinate dehydrogenase subunit
<i>SDHB</i>	1.59	0.01	2.29	0.001	4.21	0.001	Succinate dehydrogenase subunit
<i>SDHC</i>	1.38	0.05	1.58	0.001	1.83	0.001	Succinate dehydrogenase subunit
<i>SDHD</i>	1.29	Ns	1.35	0.001	2.98	0.001	Succinate dehydrogenase subunit
<i>SH3SGL</i> <i>B1</i>	1.45	0.05	1.84	Ns	1.53	Ns	Apoptosis induction
<i>SLC25A</i> <i>1</i>	2.52	0.002	2.74	0.02	5.29	0.05	Tricarboxylic acids import
<i>SLC25A</i> <i>10</i>	2.35	0.005	2.66	0.02	6.22	0.05	Dicarboxylic acids import

SLC25A 12	1.78	0.01	1.39	0.02	1.96	0.02	Aspartatic acid/glutamic acid carrier 1
SLC25A 13	1.02	Ns	1.50	Ns	1.87	Ns	Aspartic acid/glutamic acid exchange
SLC25A 14	1.91	0.01	1.42	Ns	2.30	0.02	Aspartic acid/glutamic acid exchange
SLC25A 15	1.55	0.02	2.01	0.05	3.57	0.05	Ornithine import
SLC25A 19	3.10	0.002	4.01	0.05	6.93	0.05	Thiamine pyrophosphate import
SLC25A 2	4.09	0.001	4.53	0.05	4.70	0.05	Mitochondrial proteins import
SLC25A 20	2.46	0.002	3.10	0.05	3.74	0.001	Carnitine/acylcarnitine translocation
SLC25A 21	2.76	0.01	5.07	0.05	5.77	0.05	Oxodicarboxylic acids import
SLC25A 22	1.35	0.05	0.14	0.05	1.29	0.05	Glutamate import
SLC25A 23	0.72	0.05	1.39	Ns	2.01	0.05	Phosphate import
SLC25A 24	1.66	0.01	1.71	0.01	2.77	0.05	Phosphate import
SLC25A 25	1.35	0.05	0.96	0.01	1.07	Ns	Phosphate import
SLC25A 27	0.59	0.01	0.16	0.01	0.13	0.001	OXPPOS/ATP synthesis uncoupling
SLC25A 3	1.78	0.01	0.82	Ns	4.30	0.05	Phosphate/hydroxyl ions exchange
SLC25A 31	2.44	0.01	2.52	0.05	2.41	0.005	Adenine nucleotide translocation
SLC25A 37	1.55	0.02	0.92	Ns	0.74	Ns	Iron import

<i>SLC25A</i> 4	1.10	Ns	2.98	0.05	3.18	0.05	Adenine nucleotide translocation
<i>SLC25A</i> 5	1.26	Ns	2.72	0.05	2.65	0.05	Adenine nucleotide translocation
<i>SOD1</i>	1.26	Ns	1.09	Ns	4.01	0.05	ROS protection (cytosol)
<i>SOD2</i>	1.48	0.005	3.39	0.001	4.30	0.001	ROS protection (mitochondria)
<i>STARD3</i>	1.02	Ns	0.94	Ns	1.07	Ns	Cholesterol import
<i>TIMM10</i>	2.05	0.005	3.34	0.05	4.30	0.05	Protein insertion in the inner membrane
<i>TIMM17</i> A	2.35	0.005	2.78	0.02	4.72	0.05	Protein insertion in the inner membrane
<i>TIMM17</i> B	1.10	Ns	1.45	Ns	2.01	0.05	Protein insertion in the inner membrane
<i>TIMM8A</i>	1.91	0.01	1.88	Ns	3.66	0.05	Protein insertion in the inner membrane
<i>TIMM8B</i>	1.66	0.01	3.58	0.02	5.54	0.05	Protein insertion in the inner membrane
<i>TIMM9</i>	1.26	Ns	2.84	0.05	2.30	0.05	Protein insertion in the inner membrane
<i>TOMM2</i> 0	1.35	0.05	1.46	Ns	1.35	0.05	Mitochondrial proteins import
<i>TOMM2</i> 2	3.35	0.01	3.13	0.05	3.01	0.05	Mitochondrial proteins import
<i>TOMM3</i> 4	1.45	0.05	0.90	Ns	3.66	0.05	Mitochondrial proteins import
<i>TOMM4</i> 0	2.19	0.005	2.48	0.02	2.65	0.01	Mitochondrial proteins import
<i>TOMM7</i> 0A	1.78	0.01	1.75	0.01	3.74	0.002	Mitochondrial proteins import
<i>TSPO</i>	1.18	Ns	1.42	Ns	2.25	0.05	Cholesterol import
<i>UCP1</i>	2.44	0.05	1.34	Ns	0.42	0.05	OXPHOS/ATP synthesis uncoupling
<i>UCP2</i>	3.34	0.005	2.12	0.05	2.10	0.05	OXPHOS/ATP synthesis uncoupling
<i>UCP3</i>	9.19	0.001	9.01	0.05	3.12	0.05	OXPHOS/ATP synthesis uncoupling

<i>UQCR11</i>	2.58	0.001	3.42	0.001	4.81	0.001	Ubiquinol-cytochrome c reductase subunit
<i>UQCRC1</i>	1.29	Ns	2.22	0.001	2.96	0.001	Ubiquinol-cytochrome c reductase subunit
<i>UQCRC2</i>	2.41	0.002	3.67	0.001	5.53	0.001	Ubiquinol-cytochrome c reductase subunit
<i>UQCRFS1</i>	2.09	0.002	8.42	0.001	15.63	0.001	Ubiquinol-cytochrome c reductase subunit
<i>UQCRH</i>	2.41	0.002	5.56	0.001	10.31	0.001	Ubiquinol-cytochrome c reductase subunit
<i>UQCRQ</i>	1.95	0.005	1.71	0.001	3.40	0.001	Ubiquinol-cytochrome c reductase subunit

OXPHOS: oxidative phosphorylation.

Fold-Change ($2^{(-\Delta\Delta Ct)}$) is the normalized gene expression ($2^{(-\Delta Ct)}$) in U-2OS/DX30, U-2OS/DX100 or U-2OS/DX580 cells, divided the normalized gene expression ($2^{(-\Delta Ct)}$) in U-2OS cells (n= 4), where Ct is the threshold cycle in qRT-PCR; when fold-change is less than 1, the value is the negative inverse of the fold-change. Ns: not significant. Bold characters: up- or down-regulation more than two-fold.

Table 4. Expression of mitochondrial-related genes in U-2OS cells untreated and treated with doxorubicin or mitochondria-targeting doxorubicin

Gene	Fold change Dox versus Ctrl	p value	Fold change mtDox versus Ctrl	p value	Biological function
<i>AIFM2</i>	1.83	0.05	0.71	0.02	Apoptosis induction
<i>ATP12A</i>	0.80	0.001	0.21	0.001	H ⁺ /ATP exchange
<i>ATP4A</i>	0.71	0.001	0.22	0.001	H ⁺ /ATP exchange
<i>ATP4B</i>	0.80	0.001	0.21	0.001	H ⁺ /ATP exchange
<i>ATP50</i>	0.35	0.001	0.06	0.001	ATP synthase subunit
<i>ATP5A1</i>	1.29	0.005	1.99	0.005	ATP synthase subunit
<i>ATP5B</i>	1.21	0.02	1.39	0.002	ATP synthase subunit
<i>ATP5C1</i>	0.86	0.05	1.13	Ns	ATP synthase subunit
<i>ATP5F1</i>	1.39	0.005	1.26	0.01	ATP synthase subunit
<i>ATP5G1</i>	1.30	0.01	1.06	Ns	ATP synthase subunit
<i>ATP5G2</i>	0.65	0.001	1.39	0.02	ATP synthase subunit
<i>ATP5G3</i>	0.99	0.05	1.21	0.05	ATP synthase subunit
<i>ATP5I</i>	0.70	0.002	0.68	0.01	ATP synthase subunit
<i>ATP5J</i>	1.49	0.002	1.11	0.01	ATP synthase subunit
<i>ATP5J2</i>	1.06	Ns	1.97	0.001	ATP synthase subunit
<i>ATP5L</i>	1.84	0.001	1.21	0.02	ATP synthase subunit
<i>BAK1</i>	3.42	0.05	3.72	0.001	Apoptosis induction
<i>BBC3</i>	3.46	0.05	3.17	0.001	Apoptosis induction
<i>BCL2</i>	0.20	0.05	0.10	0.001	Apoptosis inhibition
<i>BCL2L1</i>	0.48	0.05	0.31	0.005	Apoptosis inhibition
<i>BCS1L</i>	0.28	0.001	0.21	0.001	Ubiquinol-cytochrome c reductase assembly
<i>BID</i>	1.65	0.05	2.76	0.05	Apoptosis induction
<i>BNIP3</i>	2.48	0.05	2.06	0.05	Apoptosis induction
<i>COX10</i>	1.01	Ns	1	Ns	Cytochrome c oxidase assembly
<i>COX18</i>	0.54	0.05	0.66	0.005	Cytochrome c oxidase assembly
<i>COX412</i>	3.20	0.001	0.21	0.001	Cytochrome c oxidase subunit
<i>COX411</i>	0.92	Ns	1.97	0.001	Cytochrome c oxidase assembly

<i>COX5A</i>	1.30	0.01	0.99	0.005	Cytochrome c oxidase subunit
<i>COX5B</i>	1.06	Ns	1.60	0.001	Cytochrome c oxidase subunit
<i>COX6A1</i>	0.70	0.002	0.57	0.001	Cytochrome c oxidase subunit
<i>COX6A2</i>	1.13	0.005	0.10	0.001	Cytochrome c oxidase subunit
<i>COX6B1</i>	3.20	0.001	0.92	Ns	Cytochrome c oxidase assembly/regulation
<i>COX6C</i>	1.21	0.02	0.21	0.001	Cytochrome c oxidase assembly/regulation
<i>COX7A2</i>	0.75	0.005	1.21	0.02	Cytochrome c oxidase assembly/regulation
<i>COX7A2</i> <i>L</i>	1.81	0.001	2.26	0.002	Cytochrome c oxidase assembly/regulation
<i>COX7B</i>	0.80	0.01	1.30	0.01	Cytochrome c oxidase subunit
<i>COX8A</i>	1.71	0.001	1.30	0.01	Cytochrome c oxidase regulation
<i>CPT1</i>	0.18	0.001	0.18	0.001	Long chain fatty acylCoA import/ β -oxidation
<i>CPT2</i>	2.06	0.05	0.54	0.005	Long chain fatty acylCoA import/ β -oxidation
<i>CYC1</i>	0.98	Ns	1.06	Ns	Electron transport
<i>DMM1L</i>	0.96	Ns	1.06	Ns	Control of mitochondria morphology
<i>FIS1</i>	1.42	0.05	1.24	Ns	Control of mitochondria fission
<i>FXC1</i>	0.56	0.05	0.60	0.05	Mitochondrial proteins import
<i>HSP90A</i> <i>1</i>	0.92	Ns	1.20	Ns	Proteins chaperon
<i>HSPD1</i>	0.58	Ns	1.09	Ns	Mitochondrial proteins chaperon
<i>IMMP1L</i>	0.66	0.05	0.41	0.001	Mitochondrial proteins processing/import
<i>IMMP2L</i>	0.16	0.001	0.24	0.001	Mitochondrial proteins processing/import
<i>LRPPRC</i>	0.58	Ns	0.95	Ns	Mitochondrial transcription factor
<i>MFN1</i>	0.55	0.05	1.09	Ns	Control of mitochondria fusion
<i>MFN2</i>	1.39	0.05	0.36	0.001	Control of mitochondria fusion
<i>MIPEP</i>	1.13	Ns	0.79	0.01	Mitochondrial proteins processing

<i>MPV17</i>	1.33	Ns	0.83	0.05	Metabolism of mitochondrial ROS
<i>MTX2</i>	1.63	0.005	1.15	Ns	Mitochondrial proteins import
<i>NDUFA1</i>	0.75	0.005	1.30	0.01	NADH:ubiquinone oxidoreductase subunit
<i>NDUFA10</i>	0.46	0.001	0.35	0.005	NADH:ubiquinone oxidoreductase subunit
<i>NDUFA11</i>	0.43	0.001	0.27	0.001	NADH:ubiquinone oxidoreductase subunit
<i>NDUFA2</i>	1.71	0.001	1.91	0.005	NADH:ubiquinone oxidoreductase assembly
<i>NDUFA3</i>	0.24	0.001	0.10	0.001	NADH:ubiquinone oxidoreductase subunit
<i>NDUFA4</i>	0.70	0.002	1.13	Ns	NADH:ubiquinone oxidoreductase subunit
<i>NDUFA5</i>	0.75	0.005	1.06	Ns	NADH:ubiquinone oxidoreductase subunit
<i>NDUFA6</i>	1.06	Ns	1.30	0.01	NADH:ubiquinone oxidoreductase subunit
<i>NDUFA7</i>	0.86	0.05	1.30	0.01	NADH:ubiquinone oxidoreductase subunit
<i>NDUFA8</i>	1.26	0.002	1.42	0.001	NADH:ubiquinone oxidoreductase subunit
<i>NDUFAB1</i>	1.39	0.005	1.71	0.001	NADH:ubiquinone oxidoreductase subunit
<i>NDUFAB10</i>	0.86	0.05	1.13	Ns	NADH:ubiquinone oxidoreductase subunit
<i>NDUFB2</i>	0.79	0.001	1.46	0.005	NADH:ubiquinone oxidoreductase subunit
<i>NDUFB3</i>	0.42	0.001	0.36	0.001	NADH:ubiquinone oxidoreductase subunit
<i>NDUFB4</i>	0.98	Ns	1.84	0.005	NADH:ubiquinone oxidoreductase subunit

<i>NDUFB5</i>	1.06	Ns	1.26	0.01	NADH:ubiquinone subunit	oxidoreductase
<i>NDUFB6</i>	0.36	Ns	0.37	0.001	NADH:ubiquinone subunit	oxidoreductase
<i>NDUFB7</i>	3.20	0.001	1.97	0.001	NADH:ubiquinone subunit	oxidoreductase
<i>NDUFB8</i>	1.13	Ns	1.30	0.005	NADH:ubiquinone subunit	oxidoreductase
<i>NDUFB9</i>	1.20	0.05	0.75	0.005	NADH:ubiquinone subunit	oxidoreductase
<i>NDUFC1</i>	1.06	Ns	1.49	0.002	NADH:ubiquinone subunit	oxidoreductase
<i>NDUFC2</i>	1.30	0.01	1.60	0.001	NADH:ubiquinone subunit	oxidoreductase
<i>NDUFS1</i>	0.86	0.05	1.11	Ns	NADH:ubiquinone subunit	oxidoreductase
<i>NDUFS2</i>	0.92	Ns	1.60	0.001	NADH:ubiquinone subunit	oxidoreductase
<i>NDUFS3</i>	2.11	0.001	2.11	0.001	NADH:ubiquinone subunit	oxidoreductase
<i>NDUFS4</i>	0.70	0.002	0.97	0.001	NADH:ubiquinone subunit	oxidoreductase
<i>NDUFS5</i>	1.30	0.01	1.39	0.02	NADH:ubiquinone subunit	oxidoreductase
<i>NDUFS6</i>	1.84	0.005	1.84	0.001	NADH:ubiquinone subunit	oxidoreductase
<i>NDUFS7</i>	1.60	0.001	1.84	0.001	NADH:ubiquinone subunit	oxidoreductase
<i>NDUFS8</i>	4.22	0.001	3.43	0.001	NADH:ubiquinone subunit	oxidoreductase
<i>NDUFV1</i>	0.98	Ns	0.70	0.02	NADH:ubiquinone subunit	oxidoreductase

<i>NDUFV2</i>	0.30	0.001	0.25	0.001	NADH:ubiquinone oxidoreductase subunit
<i>NDUFV3</i>	0.92	Ns	1.49	0.002	NADH:ubiquinone oxidoreductase subunit
<i>OPA1</i>	0.84	Ns	0.60	0.005	Control of mitochondria network
<i>OXA1L</i>	0.80	0.001	0.21	0.001	Cytochrome c oxidase assembly
<i>RHOT1</i>	0.56	0.05	1	Ns	Control of mitochondria fission and fusion
<i>RHOT2</i>	1.03	Ns	0.22	0.02	Control of mitochondria fission and fusion
<i>SDHA</i>	0.65	0.001	0.94	Ns	Succinate dehydrogenase subunit
<i>SDHB</i>	1.49	0.002	1.65	0.01	Succinate dehydrogenase subunit
<i>SDHC</i>	0.91	Ns	1.71	0.02	Succinate dehydrogenase subunit
<i>SDHD</i>	1.71	0.001	1.42	0.01	Succinate dehydrogenase subunit
<i>SH3SGL</i> <i>B1</i>	1.27	0.005	1.51	Ns	Apoptosis induction
<i>SLC25A</i> <i>1</i>	2.42	0.001	0.76	0.005	Tricarboxylic acids import
<i>SLC25A</i> <i>10</i>	2.98	0.001	0.69	0.005	Dicarboxylic acids import
<i>SLC25A</i> <i>12</i>	0.59	0.05	0.62	0.005	Aspartic acid/glutamic acid carrier 1
<i>SLC25A</i> <i>13</i>	0.41	0.01	0.52	0.02	Aspartic acid/glutamic acid exchange
<i>SLC25A</i> <i>14</i>	1.15	Ns	0.66	0.05	Aspartic acid/glutamic acid exchange
<i>SLC25A</i> <i>15</i>	1.48	0.05	1.06	Ns	Ornithine import
<i>SLC25A</i> <i>19</i>	1.88	0.05	0.29	0.01	Thiamine pyrophosphate import
<i>SLC25A</i> <i>2</i>	1.88	0.02	0.19	0.001	Mitochondrial proteins import

<i>SLC25A</i> 20	0.98	Ns	0.55	0.01	Carnitine/acylcarnitine translocation
<i>SLC25A</i> 21	0.91	Ns	0.76	0.005	Oxodicarboxylic acids import
<i>SLC25A</i> 22	0.82	Ns	0.40	0.001	Glutamate import
<i>SLC25A</i> 23	0.96	Ns	1.26	Ns	Phosphate import
<i>SLC25A</i> 24	1.10	Ns	0.91	Ns	Phosphate import
<i>SLC25A</i> 25	0.56	0.05	0.41	0.02	Phosphate import
<i>SLC25A</i> 27	2.10	0.001	2.55	0.05	OXPPOS/ATP synthesis uncoupling
<i>SLC25A</i> 3	1.49	0.05	1.51	Ns	Phosphate/hydroxyl ions exchange
<i>SLC25A</i> 31	1.01	Ns	1.09	Ns	Adenine nucleotide translocation
<i>SLC25A</i> 37	0.41	0.01	0.19	0.001	Iron import
<i>SLC25A</i> 4	1.60	0.05	1.58	Ns	Adenine nucleotide translocation
<i>SLC25A</i> 5	1.05	Ns	1.34	Ns	Adenine nucleotide translocation
<i>SOD1</i>	0.20	0.001	0.38	0.02	ROS protection (cytosol)
<i>SOD2</i>	0.42	0.001	0.40	0.05	ROS protection (mitochondria)
<i>STARD3</i>	0.86	0.02	0.45	0.02	Cholesterol import
<i>TIMM10</i>	1.56	0.01	1.20	Ns	Protein insertion in the inner membrane
<i>TIMM17</i> A	1.71	0.001	0.95	Ns	Protein insertion in the inner membrane
<i>TIMM17</i> B	1.63	0.02	0.79	0.01	Protein insertion in the inner membrane

<i>TIMM8A</i>	1.67	0.02	1.00	Ns	Protein insertion in the inner membrane
<i>TIMM8B</i>	3.63	0.001	1.74	0.05	Protein insertion in the inner membrane
<i>TIMM9</i>	0.60	Ns	1.20	Ns	Protein insertion in the inner membrane
<i>TOMM20</i>	0.41	0.01	0.20	0.001	Mitochondrial proteins import
<i>TOMM22</i>	1.67	0.01	1.20	Ns	Mitochondrial proteins import
<i>TOMM34</i>	1.21	Ns	1.51	Ns	Mitochondrial proteins import
<i>TOMM40</i>	1.67	0.02	0.40	0.02	Mitochondrial proteins import
<i>TOMM70A</i>	1.21	Ns	1.09	Ns	Mitochondrial proteins import
<i>TSPO</i>	1.13	Ns	1.15	Ns	Cholesterol import
<i>UCP1</i>	3.46	0.001	3.17	0.002	OXPPOS/ATP synthesis uncoupling
<i>UCP2</i>	4.12	0.001	3.44	0.001	OXPPOS/ATP synthesis uncoupling
<i>UCP3</i>	4.12	0.001	3.18	0.005	OXPPOS/ATP synthesis uncoupling
<i>UQCRC1</i>	1.39	0.005	1.60	0.001	Ubiquinol-cytochrome c reductase subunit
<i>UQCRC1</i>	1.49	0.002	1.30	0.01	Ubiquinol-cytochrome c reductase subunit
<i>UQCRC2</i>	1.06	Ns	1.60	0.001	Ubiquinol-cytochrome c reductase subunit
<i>UQCRFS1</i>	0.42	0.001	0.68	0.001	Ubiquinol-cytochrome c reductase subunit
<i>UQCRC</i>	1.60	0.001	1.11	0.05	Ubiquinol-cytochrome c reductase subunit
<i>UQCRC</i>	1.13	Ns	0.92	Ns	Ubiquinol-cytochrome c reductase subunit

Ctrl: untreated cells; Dox: cells treated with 5 μ M/L doxorubicin for 24 h; mtDox: cells treated with 5 μ M/L mitochondria-targeting doxorubicin for 24 h; OXPHOS: oxidative phosphorylation.

Fold-Change ($2^{(-\Delta\Delta Ct)}$) is the normalized gene expression ($2^{(-\Delta Ct)}$) in Dox- or mtDox-treated U-2OS cells, divided the normalized gene expression ($2^{(-\Delta Ct)}$) in untreated cells (n= 4), where Ct is the threshold cycle in qRT-PCR; when fold-change is less than 1, the value was the negative inverse of the fold-change. Ns: not significant. Bold characters: up- or down-regulation more than two-fold.

Table 5. Expression of mitochondrial-related genes in U-2OS/DX580 cells untreated and treated with doxorubicin or mitochondria-targeting doxorubicin

Gene	Fold change Dox versus Ctrl	p value	Fold change mtDox versus Ctrl	p value	Biological function
<i>AIFM2</i>	1.58	Ns	0.71	0.002	Apoptosis induction
<i>ATP12A</i>	1.22	Ns	0.23	0.001	H ⁺ /ATP exchange
<i>ATP4A</i>	1.26	Ns	0.21	0.001	H ⁺ /ATP exchange
<i>ATP4B</i>	1.28	Ns	0.21	0.001	H ⁺ /ATP exchange
<i>ATP50</i>	1.66	0.05	1.62	0.001	ATP synthase subunit
<i>ATP5A1</i>	1.67	0.01	1.46	0.001	ATP synthase subunit
<i>ATP5B</i>	1.34	0.02	1.31	0.01	ATP synthase subunit
<i>ATP5C1</i>	1.22	Ns	1.44	0.001	ATP synthase subunit
<i>ATP5F1</i>	2.01	0.02	1.76	0.002	ATP synthase subunit
<i>ATP5G1</i>	1.26	Ns	0.76	0.005	ATP synthase subunit
<i>ATP5G2</i>	1.37	Ns	0.41	0.001	ATP synthase subunit
<i>ATP5G3</i>	0.89	Ns	0.51	0.001	ATP synthase subunit
<i>ATP5I</i>	1.11	Ns	1.23	Ns	ATP synthase subunit
<i>ATP5J</i>	1.26	0.05	1.62	0.005	ATP synthase subunit
<i>ATP5J2</i>	2.07	0.01	0.22	0.001	ATP synthase subunit
<i>ATP5L</i>	1.21	0.02	0.33	0.001	ATP synthase subunit
<i>BAK1</i>	1.00	Ns	2.72	0.001	Apoptosis induction
<i>BBC3</i>	1.23	Ns	2.19	0.001	Apoptosis induction
<i>BCL2</i>	1.03	0.05	0.43	0.001	Apoptosis inhibition
<i>BCL2L1</i>	0.93	Ns	0.29	0.005	Apoptosis inhibition

<i>BCS1L</i>	0.66	0.05	0.41	0.001	Ubiquinol-cytochrome c reductase assembly
<i>BID</i>	1.89	0.05	2.76	0.01	Apoptosis induction
<i>BNIP3</i>	1.26	Ns	2.09	0.05	Apoptosis induction
<i>COX10</i>	1.44	Ns	1	Ns	Cytochrome c oxidase assembly
<i>COX18</i>	0.72	0.02	0.66	0.05	Cytochrome c oxidase assembly
<i>COX412</i>	1.21	Ns	0.20	0.001	Cytochrome c oxidase subunit
<i>COX411</i>	2.11	0.01	2.14	0.001	Cytochrome c oxidase assembly
<i>COX5A</i>	1.78	0.005	1.86	0.001	Cytochrome c oxidase subunit
<i>COX5B</i>	1.09	Ns	1.11	Ns	Cytochrome c oxidase subunit
<i>COX6A1</i>	0.98	Ns	0.41	0.001	Cytochrome c oxidase subunit
<i>COX6A2</i>	1.00	Ns	0.29	0.001	Cytochrome c oxidase subunit
<i>COX6B1</i>	0.92	Ns	1.20	0.05	Cytochrome c oxidase assembly/regulation
<i>COX6C</i>	1.21	Ns	0.43	0.001	Cytochrome c oxidase assembly/regulation
<i>COX7A2</i>	1.23	Ns	1.23	Ns	Cytochrome c oxidase assembly/regulation
<i>COX7A2 L</i>	1.26	Ns	1.28	0.02	Cytochrome c oxidase assembly/regulation
<i>COX7B</i>	1.39	Ns	1.41	0.02	Cytochrome c oxidase subunit
<i>COX8A</i>	1.30	Ns	1.51	0.02	Cytochrome c oxidase regulation
<i>CPT1</i>	1.04	0.05	0.24	0.05	Long chain fatty acylCoA import/ β -oxidation
<i>CPT2</i>	0.81	Ns	0.37	0.02	Long chain fatty acylCoA import/ β -oxidation
<i>CYC1</i>	1.51	0.002	1.23	Ns	Electron transport
<i>DMM1L</i>	1.04	Ns	1.24	Ns	Control of mitochondria morphology
<i>FIS1</i>	1.44	Ns	1.06	Ns	Control of mitochondria fission
<i>FXC1</i>	1.55	0.02	0.40	0.05	Mitochondrial proteins import
<i>HSP90A 1</i>	1.44	Ns	1.20	Ns	Proteins chaperon
<i>HSPD1</i>	1.15	Ns	1.09	Ns	Mitochondrial proteins chaperon

<i>IMMP1L</i>	1.79	0.01	0.41	0.005	Mitochondrial proteins processing/import
<i>IMMP2L</i>	1.81	Ns	1.82	Ns	Mitochondrial proteins processing/import
<i>LRPPRC</i>	0.91	Ns	0.95	Ns	Mitochondrial transcription factor
<i>MFN1</i>	0.95	Ns	0.36	0.05	Control of mitochondria fusion
<i>MFN2</i>	0.83	0.05	0.39	0.02	Control of mitochondria fusion
<i>MIPEP</i>	1.05	Ns	0.79	Ns	Mitochondrial proteins processing
<i>MPV17</i>	0.79	0.01	1.15	Ns	Metabolism of mitochondrial ROS
<i>MTX2</i>	0.45	0.02	0.31	0.02	Mitochondrial proteins import
<i>NDUFA1</i>	0.77	0.01	1.23	0.005	NADH:ubiquinone oxidoreductase subunit
<i>NDUFA10</i>	0.97	Ns	0.76	0.005	NADH:ubiquinone oxidoreductase subunit
<i>NDUFA11</i>	1.56	0.005	1.62	0.001	NADH:ubiquinone oxidoreductase subunit
<i>NDUFA2</i>	1.34	0.01	0.29	0.001	NADH:ubiquinone oxidoreductase assembly
<i>NDUFA3</i>	1.51	0.01	0.08	0.001	NADH:ubiquinone oxidoreductase subunit
<i>NDUFA4</i>	1.13	Ns	1.29	Ns	NADH:ubiquinone oxidoreductase subunit
<i>NDUFA5</i>	1.78	0.02	1.63	0.001	NADH:ubiquinone oxidoreductase subunit
<i>NDUFA6</i>	1.30	0.05	1.51	0.001	NADH:ubiquinone oxidoreductase subunit
<i>NDUFA7</i>	1.24	Ns	1.17	0.05	NADH:ubiquinone oxidoreductase subunit
<i>NDUFA8</i>	1.61	0.001	1.02	Ns	NADH:ubiquinone oxidoreductase subunit
<i>NDUFAB1</i>	1.23	Ns	1.41	0.001	NADH:ubiquinone oxidoreductase subunit

<i>NDUFAB10</i>	1.45	0.05	1.15	Ns	NADH:ubiquinone subunit	oxidoreductase
<i>NDUFB2</i>	1.42	0.05	1.71	0.05	NADH:ubiquinone subunit	oxidoreductase
<i>NDUFB3</i>	1.26	0.05	0.50	0.02	NADH:ubiquinone subunit	oxidoreductase
<i>NDUFB4</i>	1.84	0.02	0.63	0.05	NADH:ubiquinone subunit	oxidoreductase
<i>NDUFB5</i>	1.23	Ns	0.40	0.01	NADH:ubiquinone subunit	oxidoreductase
<i>NDUFB6</i>	1.56	Ns	1.14	Ns	NADH:ubiquinone subunit	oxidoreductase
<i>NDUFB7</i>	1.56	0.05	1.41	0.01	NADH:ubiquinone subunit	oxidoreductase
<i>NDUFB8</i>	1.29	0.05	1.99	0.005	NADH:ubiquinone subunit	oxidoreductase
<i>NDUFB9</i>	0.78	0.05	0.81	0.02	NADH:ubiquinone subunit	oxidoreductase
<i>NDUFC1</i>	1.42	0.01	1.41	0.001	NADH:ubiquinone subunit	oxidoreductase
<i>NDUFC2</i>	1.60	0.01	1.23	0.005	NADH:ubiquinone subunit	oxidoreductase
<i>NDUFS1</i>	1.72	0.002	1.46	0.001	NADH:ubiquinone subunit	oxidoreductase
<i>NDUFS2</i>	1.11	Ns	1.74	0.001	NADH:ubiquinone subunit	oxidoreductase
<i>NDUFS3</i>	0.78	Ns	0.24	0.001	NADH:ubiquinone subunit	oxidoreductase
<i>NDUFS4</i>	1.62	0.001	1.13	Ns	NADH:ubiquinone subunit	oxidoreductase
<i>NDUFS5</i>	1.28	0.05	0.38	0.005	NADH:ubiquinone subunit	oxidoreductase

<i>NDUFS6</i>	1.36	Ns	1.46	0.001	NADH:ubiquinone oxidoreductase subunit
<i>NDUFS7</i>	1.17	Ns	1.51	0.002	NADH:ubiquinone oxidoreductase subunit
<i>NDUFS8</i>	2.11	0.05	3.46	0.001	NADH:ubiquinone oxidoreductase subunit
<i>NDUFV1</i>	1.01	Ns	0.37	0.001	NADH:ubiquinone oxidoreductase subunit
<i>NDUFV2</i>	1.32	Ns	1.12	Ns	NADH:ubiquinone oxidoreductase subunit
<i>NDUFV3</i>	0.71	Ns	0.81	Ns	NADH:ubiquinone oxidoreductase subunit
<i>OPA1</i>	1.02	0.002	0.16	0.001	Control of mitochondria network
<i>OXA1L</i>	1.56	0.02	0.46	0.005	Cytochrome c oxidase assembly
<i>RHOT1</i>	0.63	0.01	0.52	0.05	Control of mitochondria fission and fusion
<i>RHOT2</i>	1.16	0.001	0.22	0.05	Control of mitochondria fission and fusion
<i>SDHA</i>	1.32	Ns	0.61	0.001	Succinate dehydrogenase subunit
<i>SDHB</i>	1.89	0.001	1.34	0.001	Succinate dehydrogenase subunit
<i>SDHC</i>	1.42	0.002	0.87	0.05	Succinate dehydrogenase subunit
<i>SDHD</i>	1.70	0.002	1.99	0.001	Succinate dehydrogenase subunit
<i>SH3SGL</i> <i>B1</i>	1.32	Ns	1.51	0.05	Apoptosis induction
<i>SLC25A</i> <i>1</i>	0.79	0.005	0.56	0.01	Tricarboxylic acids import
<i>SLC25A</i> <i>10</i>	1	Ns	0.46	0.005	Dicarboxylic acids import
<i>SLC25A</i> <i>12</i>	0.83	0.05	0.49	0.005	Aspartic acid/glutamic acid carrier 1
<i>SLC25A</i> <i>13</i>	0.76	0.01	0.42	0.01	Aspartic acid/glutamic acid exchange

SLC25A 14	1.91	0.005	0.56	0.005	Aspartic acid/glutamic acid exchange
SLC25A 15	1.71	Ns	0.29	0.001	Ornithine import
SLC25A 19	1.32	Ns	1.09	Ns	Thiamine pyrophosphate import
SLC25A 2	0.10	0.05	0.19	0.05	Mitochondrial proteins import
SLC25A 20	1.07	Ns	0.45	0.05	Carnitine/acylcarnitine translocation
SLC25A 21	0.72	0.01	0.76	0.05	Oxodicarboxylic acids import
SLC25A 22	1.69	0.01	0.40	0.05	Glutamate import
SLC25A 23	1.32	Ns	1.26	Ns	Phosphate import
SLC25A 24	1.15	Ns	0.70	Ns	Phosphate import
SLC25A 25	1.45	0.002	0.41	0.05	Phosphate import
SLC25A 27	1.18	Ns	2.45	0.02	OXPPOS/ATP synthesis uncoupling
SLC25A 3	1.38	Ns	1.51	Ns	Phosphate/hydroxyl ions exchange
SLC25A 31	0.72	0.005	1.09	Ns	Adenine nucleotide translocation
SLC25A 37	0.81	0.05	0.21	0.002	Iron import
SLC25A 4	1.74	0.05	1.32	Ns	Adenine nucleotide translocation
SLC25A 5	1.26	Ns	1.58	Ns	Adenine nucleotide translocation
SOD1	1.38	Ns	0.38	Ns	ROS protection (cytosol)

<i>SOD2</i>	1.09	Ns	0.40	0.05	ROS protection (mitochondria)
<i>STARD3</i>	1.00	0.02	0.45	0.02	Cholesterol import
<i>TIMM10</i>	1.26	Ns	1.20	Ns	Protein insertion in the inner membrane
<i>TIMM17A</i>	1.04	Ns	0.75	Ns	Protein insertion in the inner membrane
<i>TIMM17B</i>	1.26	Ns	0.49	0.01	Protein insertion in the inner membrane
<i>TIMM8A</i>	1.15	Ns	0.41	0.005	Protein insertion in the inner membrane
<i>TIMM8B</i>	1.58	Ns	1.74	0.05	Protein insertion in the inner membrane
<i>TIMM9</i>	1.32	Ns	1.20	Ns	Protein insertion in the inner membrane
<i>TOMM20</i>	0.87	Ns	1.20	Ns	Mitochondrial proteins import
<i>TOMM22</i>	0.40	0.02	0.21	0.001	Mitochondrial proteins import
<i>TOMM34</i>	1.51	Ns	1.51	Ns	Mitochondrial proteins import
<i>TOMM40</i>	1.06	0.005	0.33	0.05	Mitochondrial proteins import
<i>TOMM70A</i>	1.20	Ns	0.47	0.02	Mitochondrial proteins import
<i>TSPO</i>	1.09	Ns	0.17	0.005	Cholesterol import
<i>UCP1</i>	1.21	Ns	2.19	0.05	OXPPOS/ATP synthesis uncoupling
<i>UCP2</i>	1.66	0.05	1.44	Ns	OXPPOS/ATP synthesis uncoupling
<i>UCP3</i>	1.21	Ns	2.18	0.05	OXPPOS/ATP synthesis uncoupling
<i>UQCRC1</i>	1.34	Ns	0.93	Ns	Ubiquinol-cytochrome c reductase subunit
<i>UQCRC1</i>	1.65	0.005	1.62	0.001	Ubiquinol-cytochrome c reductase subunit

<i>UQCRC2</i>	1.32	0.05	0.32	0.001	Ubiquinol-cytochrome c reductase subunit
<i>UQCRF1S1</i>	1.72	0.05	0.30	0.001	Ubiquinol-cytochrome c reductase subunit
<i>UQCRH</i>	1.19	Ns	1.15	Ns	Ubiquinol-cytochrome c reductase subunit
<i>UQCRQ</i>	0.89	Ns	0.46	0.01	Ubiquinol-cytochrome c reductase subunit

Ctrl: untreated cells; Dox: cells treated with 5 μ M/L doxorubicin for 24 h; mtDox: cells treated with 5 μ M/L mitochondria-targeting doxorubicin for 24 h; OXPHOS: oxidative phosphorylation.

Fold-Change ($2^{(-\Delta\Delta Ct)}$) is the normalized gene expression ($2^{(-\Delta Ct)}$) in Dox- or mtDox-treated U-2OS/DX580 cells, divided the normalized gene expression ($2^{(-\Delta Ct)}$) in untreated cells (n= 4), where Ct is the threshold cycle in qRT-PCR; when fold-change is less than 1, the value is the negative inverse of the fold-change. Ns: not significant. Bold characters: up- or down-regulation more than two-fold.

The expression levels of specific genes, representative of the main biological categories screened by PCR arrays, were validated by qRT-PCR (Tables 6-7-8)

Table 6. qRT-PCR validation of PCR-arrays results in U-2OS, U-2OS/DX30, U-2OS/DX100, U-2OS/DX580 cells

Gene name	Relative expression U-2OS/DX30 vs U-2OS	Relative expression U-2OS/DX30 vs U-2OS	Relative expression U-2OS/DX30 vs U-2OS	Biological function
<i>TIMM8B</i>	1.92 \pm 0.32 *	2.89 \pm 0.34 *	5.01 \pm 0.47 *	Protein insertion in the inner membrane
<i>TOMM70A</i>	1.72 \pm 0.21 *	1.81 \pm 0.29 *	3.34 \pm 0.27 *	Mitochondrial proteins import
<i>MFN2</i>	2.92 \pm 0.37 *	2.82 \pm 0.71 *	3.72 \pm 0.52 *	Control of mitochondria fusion
<i>OPA1</i>	1.26 \pm 0.12	1.54 \pm 0.12 *	2.91 \pm 0.43 *	Control of mitochondria network

<i>SLC25A10</i>	2.12 ± 0.61 *	2.73 ± 0.37 *	5.88 ± 0.34 *	Dicarboxylic acids import
<i>CPT1</i>	1.52 ± 0.26	2.44 ± 0.23 *	3.17 ± 0.28 *	Long chain fatty acylcoA import/ β -oxidation
<i>NDUFA2</i>	1.43 ± 0.21	5.03 ± 0.47 *	5.99 ± 0.71 *	NADH:ubiquinone oxidoreductase assembly
<i>NDUFS5</i>	2.35 ± 0.36 *	2.67 ± 0.11 *	5.56 ± 0.43 *	NADH:ubiquinone oxidoreductase subunit
<i>UQRQC</i>	1.76 ± 0.33 *	1.82 ± 0.32 *	2.47 ± 0.55 *	Ubiquinol-cytochrome c reductase subunit
<i>UQRFCFS1</i>	2.21 ± 0.65 *	7.13 ± 1.29 *	13.09 ± 2.24 *	Ubiquinol-cytochrome c reductase subunit
<i>OXA1L</i>	1.26 ± 0.21	2.53 ± 0.12 *	4.82 ± 0.33 *	Cytochrome c oxidase assembly
<i>ATP5L</i>	3.67 ± 0.56 *	4.45 ± 0.87 *	8.33 ± 1.21 *	ATP synthase subunit
<i>UCP1</i>	2.02 ± 0.35 *	1.18 ± 0.21	0.19 ± 0.05 *	OXPHOS/ATP synthesis uncoupling
<i>SLC25A27</i>	0.62 ± 0.12 *	0.26 ± 0.11 *	0.13 ± 0.06 *	OXPHOS/ATP synthesis uncoupling
<i>SOD2</i>	1.54 ± 0.31	2.28 ± 0.54 *	3.66 ± 0.29 *	ROS protection (mitochondria)
<i>BAK1</i>	1.23 ± 0.22	1.09 ± 0.03	0.98 ± 0.15	Apoptosis induction
<i>BCL2</i>	0.93 ± 0.21	1.22 ± 0.11	1.32 ± 0.09	Apoptosis inhibition

The expression level of specific mitochondria-related genes, representative of the main biological categories screened by PCR arrays, was validated by qRT-PCR (n = 3). The expression level of each gene in U-2OS cells was considered as 1. The relative expression of the other genes was calculated with the PrimePCR™ Analysis Software. S14 gene was used as housekeeping gene. Versus U-2OS cells: * p < 0.05.

Table 7. qRT-PCR validation of PCR-arrays results in U-2OS cells treated with doxorubicin or mitochondria-targeting doxorubicin

Gene name	Relative expression Dox vs Ctrl	Relative expression mtDox vs Ctrl	Biological function
<i>TIMM8B</i>	3.56 ± 0.34 *	1.65 ± 0.41	Protein insertion in the inner membrane
<i>TOMM70A</i>	1.12 ± 0.11	1.34 ± 0.26	Mitochondrial proteins import
<i>MFN2</i>	1.11 ± 0.19	0.27 ± 0.11 *	Control of mitochondria fusion
<i>OPA1</i>	0.79 ± 0.27	0.51 ± 0.09 *	Control of mitochondria network
<i>SLC25A10</i>	3.09 ± 0.45 *	0.62 ± 0.20 *	Dicarboxylic acids import
<i>CPT1</i>	0.32 ± 0.11 *	0.19 ± 0.08 *	Long chain fatty acylCoA import/ β -oxidation
<i>NDUFA2</i>	1.83 ± 0.14 *	1.89 ± 0.25 *	NADH:ubiquinone oxidoreductase assembly
<i>NDUFS5</i>	1.27 ± 0.06	1.35 ± 0.09	NADH:ubiquinone oxidoreductase subunit
<i>UQCRCQ</i>	1.01 ± 0.28	1.14 ± 0.28	Ubiquinol-cytochrome c reductase subunit
<i>UQCRCF1</i>	0.59 ± 0.18 *	0.63 ± 0.12 *	Ubiquinol-cytochrome c reductase subunit
<i>OXA1L</i>	0.92 ± 0.31	0.42 ± 0.11 *	Cytochrome c oxidase assembly
<i>ATP5L</i>	1.57 ± 0.33	1.26 ± 0.05	ATP synthase subunit
<i>UCP1</i>	3.01 ± 0.72 *	3.35 ± 0.61 *	OXPPOS/ATP synthesis uncoupling
<i>SLC25A27</i>	2.13 ± 0.27 *	2.61 ± 0.64 *	OXPPOS/ATP synthesis uncoupling
<i>SOD2</i>	0.61 ± 0.18 *	0.42 ± 0.19 *	ROS protection (mitochondria)
<i>BAK1</i>	2.93 ± 0.34 *	3.37 ± 0.71 *	Apoptosis induction
<i>BCL2</i>	0.39 ± 0.12 *	0.18 ± 0.08 *	Apoptosis inhibition

The expression level of specific mitochondria-related genes, representative of the main biological categories screened by PCR arrays, was validated by qRT-PCR (n = 3). The expression level of each gene in untreated U-2OS cells was considered as 1. The relative expression of the other genes was calculated with the PrimePCR™ Analysis Software. S14 gene was used as housekeeping gene. Versus untreated U-2OS cells: * p < 0.05.

Table 8. Supplementary Tables S7. qRT-PCR validation of PCR-arrays results in U-2OS/DX580 cells treated with doxorubicin or mitochondria-targeting doxorubicin

Gene name	Relative expression Dox vs Ctrl	Relative expression mtDox vs Ctrl	Biological function
<i>TIMM8B</i>	1.28 ± 0.21	1.54 ± 0.33	Protein insertion in the inner membrane
<i>TOMM70A</i>	1.07 ± 0.21	0.52 ± 0.13 *	Mitochondrial proteins import
<i>MFN2</i>	0.95 ± 0.13	0.43 ± 0.18 *	Control of mitochondria fusion
<i>OPA1</i>	0.91 ± 0.08	0.21 ± 0.10 *	Control of mitochondria network
<i>SLC25A10</i>	1.14 ± 0.21	0.33 ± 0.06 *	Dicarboxylic acids import
<i>CPT1</i>	0.95 ± 0.18	0.26 ± 0.05 *	Long chain fatty acylcoA import/ β -oxidation
<i>NDUFA2</i>	1.04 ± 0.12	0.21 ± 0.03 *	NADH:ubiquinone oxidoreductase assembly
<i>NDUFS5</i>	1.04 ± 0.19	0.41 ± 0.23 *	NADH:ubiquinone oxidoreductase subunit
<i>UQRCQ</i>	1.08 ± 0.11	0.61 ± 0.15 *	Ubiquinol-cytochrome c reductase subunit
<i>UQRCFS1</i>	1.52 ± 0.13	0.33 ± 0.07 *	Ubiquinol-cytochrome c reductase subunit
<i>OXA1L</i>	1.24 ± 0.11	0.61 ± 0.17 *	Cytochrome c oxidase assembly
<i>ATP5L</i>	1.06 ± 0.14	0.41 ± 0.19 *	ATP synthase subunit
<i>UCP1</i>	1.17 ± 0.25	2.49 ± 0.36 *	OXPPOS/ATP synthesis uncoupling
<i>SLC25A27</i>	0.97 ± 0.21	2.27 ± 0.31 *	OXPPOS/ATP synthesis uncoupling
<i>SOD2</i>	0.87 ± 0.11	0.36 ± 0.14 *	ROS protection (mitochondria)
<i>BAK1</i>	1.32 ± 0.22	3.11 ± 0.39 *	Apoptosis induction
<i>BCL2</i>	1.059 ± 0.19	0.37 ± 0.13 *	Apoptosis inhibition

The expression level of specific mitochondria-related genes, representative of the main biological categories screened by PCR arrays, was validated in qRT-PCR (n = 3). The expression level of each gene in untreated U-2OS/DX580 cells was considered as 1. The relative expression of the other genes was calculated with the PrimePCR™ Analysis

Software. S14 gene was used as housekeeping gene. Versus untreated U-2OS/DX580 cells: * $p < 0.05$.

4.2.4 Mitochondria-targeting doxorubicin reduces mitochondrial biogenesis, protein import and energy metabolism in doxorubicin-resistant osteosarcoma cells

Given the peculiar signature of drug-sensitive versus drug-resistant variants and the different effects of Dox versus mtDox in resistant cells, we then investigated the impact of mtDox on mitochondria biogenesis and energy metabolism in our osteosarcoma models. For sake of simplicity, I only show the results obtained in U-2OS and U-2OS/DX580 cells. The effects of Dox and mtDox on gene expression and mitochondrial functions of U-2OS/DX30 and U-2OS/DX100 variants were intermediate between the effects produced in U-2OS and U-2OS/DX580 cells (data not shown).

Compared with U-2OS cells, U-2OS/DX580 cells had a higher content of mitochondrial DNA (Figure 19A) and proteins (Figure 19), a higher nuclear translocation of PGC-1 α (Figure 19C) and a higher expression of COX-I (Figure 19D), which is encoded by mitochondrial DNA. This scenario is suggestive of increased mitochondria biogenesis in the resistant variant. Also SDH-A, which is encoded by nuclear DNA, was increased (Figure 19E), likely in consequence of the higher expression of mitochondrial protein importers in U-2OS/DX580 cells. In keeping with the gene expression profiling signature, U-2OS/DX580 cells had higher metabolic flux through the TCA cycle (Figure 19F), higher rate of fatty acids β -oxidation (Figure 19G), ATP-linked OCR (Figure 19H, 19I), maximal respiration capacity (Figure 19H, 19J), ATP synthesis by oxidative phosphorylation (Figure 19K) Dox and mtDox decreased all these parameters in drug-sensitive cells; only mtDox decreased them in drug-resistant cells (Figure 19). The experiment on Saos-2 cells and in the corresponding resistant variants Saos-2/DX30, Saos-2/DX100, Saos-2/DX580 cells confirm that not only the U-2OS cell line have that behavior (not shown).

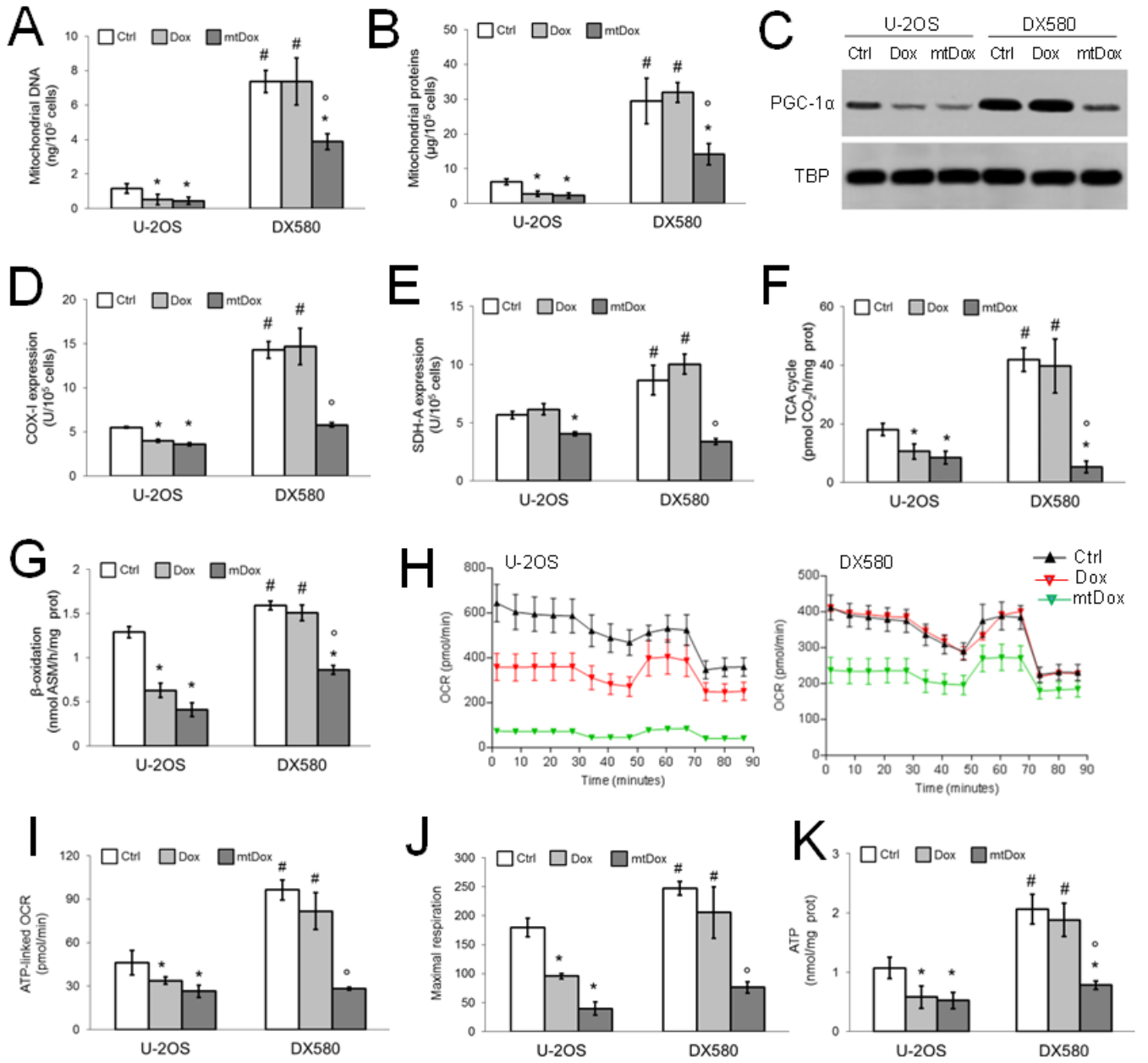


Figure 19 Mitochondria biogenesis and energy metabolism in cells treated with doxorubicin or mitochondria-targeting doxorubicin

Dox-sensitive U-2OS cells and Dox-resistant U-2OS/DX580 cells were incubated in the absence (Ctrl) or in the presence of 5 mM/L Dox or mtDox for 24 hours. Data are presented as mean \pm SD (n $\frac{1}{4}$ 4). **A** and **B**, the amount of mitochondrial DNA (A) and proteins (B) was measured in duplicate after mitochondria isolation, as described under Materials and Methods. For both panels, versus U-2OS Ctrl cells: *, P < 0.05; versus U-2OS/DX580 Ctrl cells: *, P < 0.02; U-2OS/DX580 versus U-2OS cells: #, P < 0.001. **C**, nuclear extracts were analyzed for the levels of PGC-1a by Western blotting. The TBP expression was used as the control of equal protein loading. The figure is representative of 1 of 3 experiments. **D** and **E**, the expression of subunit I of complex IV (COX-I, D) and succinic acid dehydrogenase-A of complex II (SDH-A, E) was measured by quantitative immunocytochemistry in duplicate. For both panels, versus U-2OS Ctrl cells: *, P < 0.05; versus U-2OS/DX580 Ctrl cells: °, P < 0.001; U-2OS/DX580 versus U-2OS cells: #, P < 0.05. **F**, the glucose flux through the TCA cycle was measured in duplicate in cells radiolabeled with [6-¹⁴C]-glucose. Versus U-2OS Ctrl cells: *, P < 0.05; versus U-2OS/DX580 Ctrl cells: °, P < 0.001; U-2OS/DX580 versus U-2OS cells: #, P < 0.002. **G**, the amount of ¹⁴C-ASM derived from fatty acids β -oxidation was measured in duplicate in cells labeled with [1-¹⁴C]-palmitoyl coenzyme A. Versus U-2OS Ctrl cells: *, P < 0.001; versus U-2OS/DX580 Ctrl cells: °, P < 0.001; U-2OS/DX580 versus U-2OS cells: #, P < 0.05. **H**, mitochondrial bioenergetic profiles generated using the Seahorse XFp Analyzer, in U-2OS cells (left) and U-2OS/DX580 cells (right). The figures are representative of 1 of 4 experiments, each performed in triplicate. **I** and **J**, ATP-linked OCR rates (I) and maximal respiration (J) were determined from the bioenergetic profiles in H. ATP-linked OCR represents the difference between basal and oligomycin-treated OCR, whereas maximal respiration represents the difference between FCCP- and rotenone/antimycin-treated OCR. Versus U-2OS Ctrl cells: *, P < 0.05; versus U-2OS/DX580 Ctrl cells: °, P < 0.001; U-2OS/DX580 versus U-2OS cells: #, P < 0.05. **K**, ATP levels in isolated mitochondria were measured in duplicate by a chemiluminescence-based assay. Versus U-2OS Ctrl cells: *, P < 0.05; versus U-2OS/DX580 Ctrl cells: °, P < 0.005; U-2OS/DX580 versus U-2OS cells #P < 0.01.

4.2.5 Mitochondria-targeting doxorubicin triggers a mitochondria-dependent apoptosis in drug-resistant osteosarcoma cells

We did not detect any significant difference in intramitochondrial ROS levels between U-2OS and U-2OS/DX580 cells (Figure 20A). Again, Dox increased ROS in drug-sensitive cells but not in drug-resistant ones; mtDox significantly increased intramitochondrial ROS in both cell populations (Figure 20A). The higher level of ROS was paralleled by mitochondrial depolarization (Figure 20B). Dox increased pro-apoptotic proteins such as Bak, active Bid (tBid) and Puma, and decreased anti-apoptotic proteins such as Bcl-2 and Bcl-xL in U-2OS cells only. mtDox elicited these effects in both variants (Figure 20C), in line with the gene expression profile. Consistently with the change in mitochondria polarization, Dox increased the mitochondria-associated Bad, Bak, Bax, tBid, BimL and Puma, the release of cytochrome c into the cytosol (Figure 20D), the activity of caspase 9 (Figure 20E) and caspase 3 (Figure 20F) only in drug-sensitive cells, whereas mtDox was effective in both U-2OS and U-2OS/DX580 cells (Figure 20D-F).

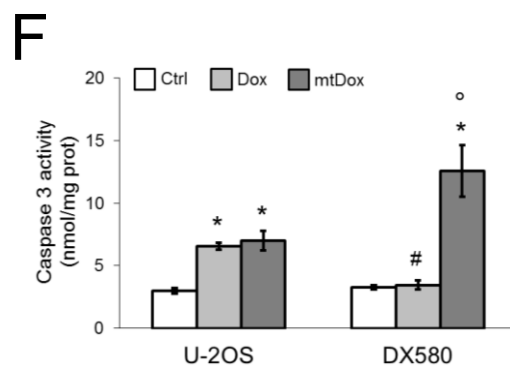
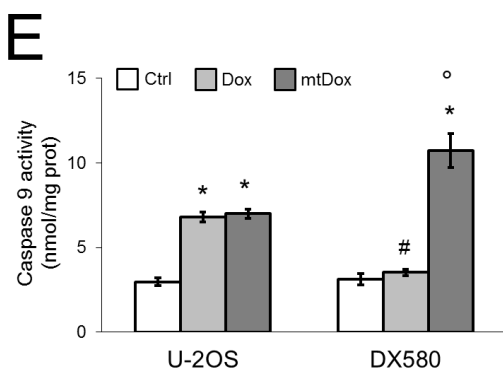
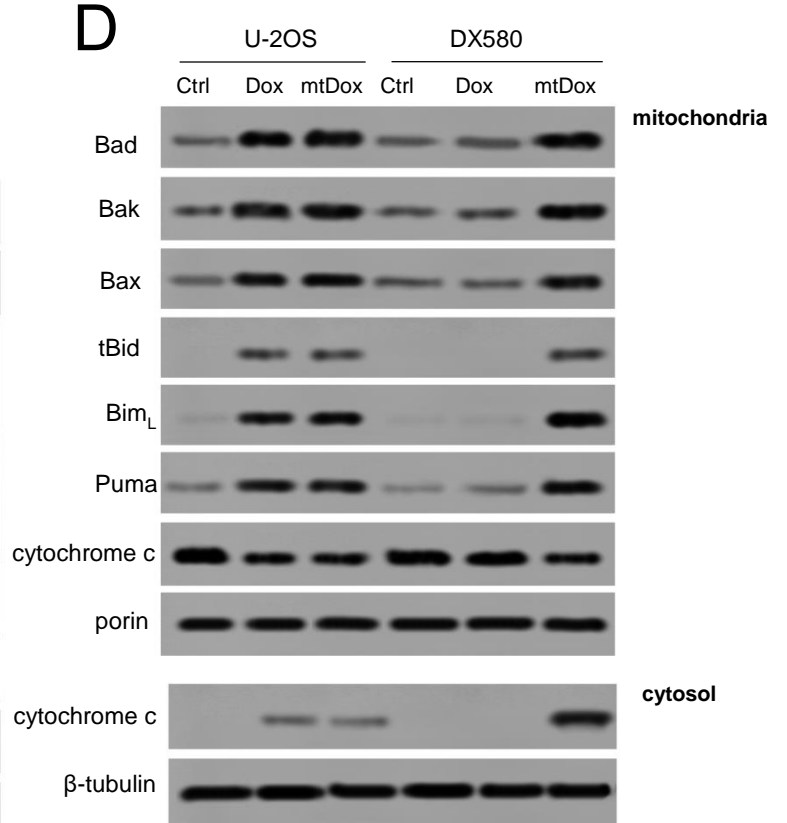
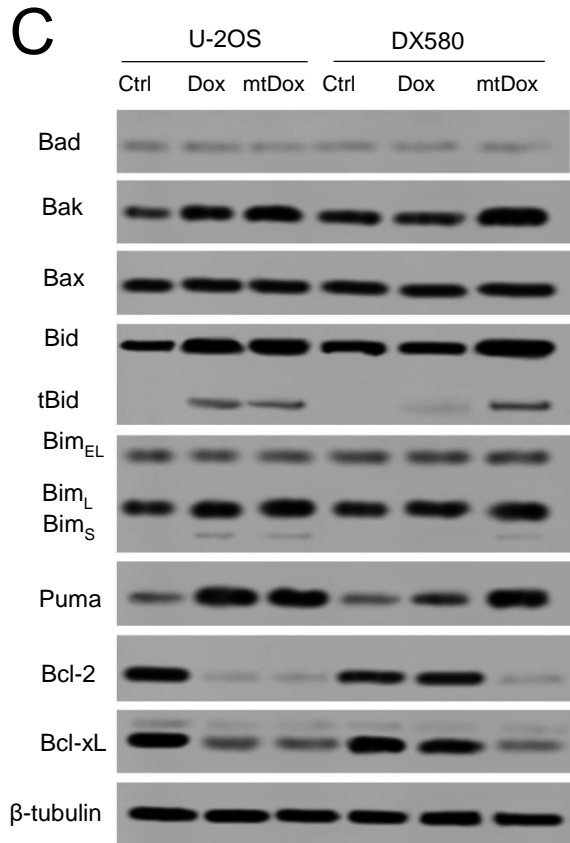
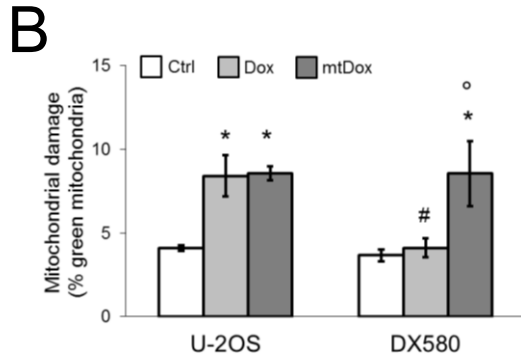
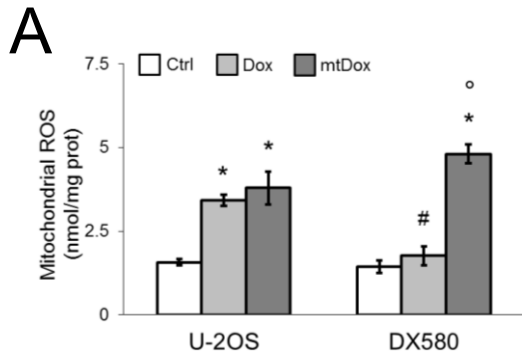


Figure 20 Effects of doxorubicin and mitochondria-targeting doxorubicin on mitochondria integrity and mitochondria-dependent apoptosis. Dox-sensitive U-2OS cells and Dox-resistant U-2OS/DX580 cells were incubated in the absence (Ctrl) or in the presence of 5 $\mu\text{mol/L}$ Dox or mitochondria-targeting doxorubicin (mtDox) for 24 h. **A.** Intramitochondrial ROS levels were measured fluorimetrically in triplicate using the DCFDA-AM probe. Data are presented as means \pm SD ($n = 4$). Versus U-2OS Ctrl cells: * $p < 0.001$; versus U-2OS/DX580 Ctrl cells: $^{\circ} p < 0.001$; U-2OS/DX580 versus U-2OS cells: # $p < 0.001$. **B.** The mitochondrial membrane potential was assessed in duplicate by the JC-1 staining method. The percentage of green versus red mitochondria was considered an index of mitochondrial depolarization and permeability transition. Data are presented as means + SD ($n = 4$). Versus U-2OS Ctrl cells: * $p < 0.005$; versus U-2OS/DX580 Ctrl cells: $^{\circ} p < 0.005$; U-2OS/DX580 versus U-2OS cells: # $p < 0.002$. **C.** Whole cell lysates were probed with the indicated antibodies. BID full-length and truncated (tBID) protein and BIM isoforms BIMEL, BIML, BIMS are shown. The β -tubulin expression was used as control of equal protein loading. The figure is representative of 3 experiments with similar results. **D.** Mitochondrial and cytosolic extracts were subjected to Western blotting and probed with the indicated antibodies. tBID and BIML isoforms are shown. Porin and β -tubulin expression were used as control of equal protein loading in the respective extracts. The figure is representative of 3 experiments with similar results. **E-F.** The activity of caspase 9 (panel **E**) and caspase 3 (panel **F**) was measured fluorimetrically in duplicate in the cytosolic extracts. Data are presented as means \pm SD ($n = 4$). For both panels, versus U-2OS Ctrl cells: * $p < 0.001$; versus U-2OS/DX580 Ctrl cells: $^{\circ} p < 0.001$; U-2OS/DX580 versus U-2OS cells: # $p < 0.001$.

Part two

4.3 H₂S-releasing doxorubicin (Sdox)

4.3.1 H₂S-releasing doxorubicin is not exert cytotoxicity on H9c2 cardiomyocytes

In a preliminary screening of different H₂S-releasing Doxs (Chegaev K *et al.*, J Med Chem 2016), we identified compound **10** (termed Sdox in the following paragraph) as the compound with the lowest cytotoxicity in H9c2 cardiomyocytes, notwithstanding the same intracellular accumulation (Figure 21 A-B).

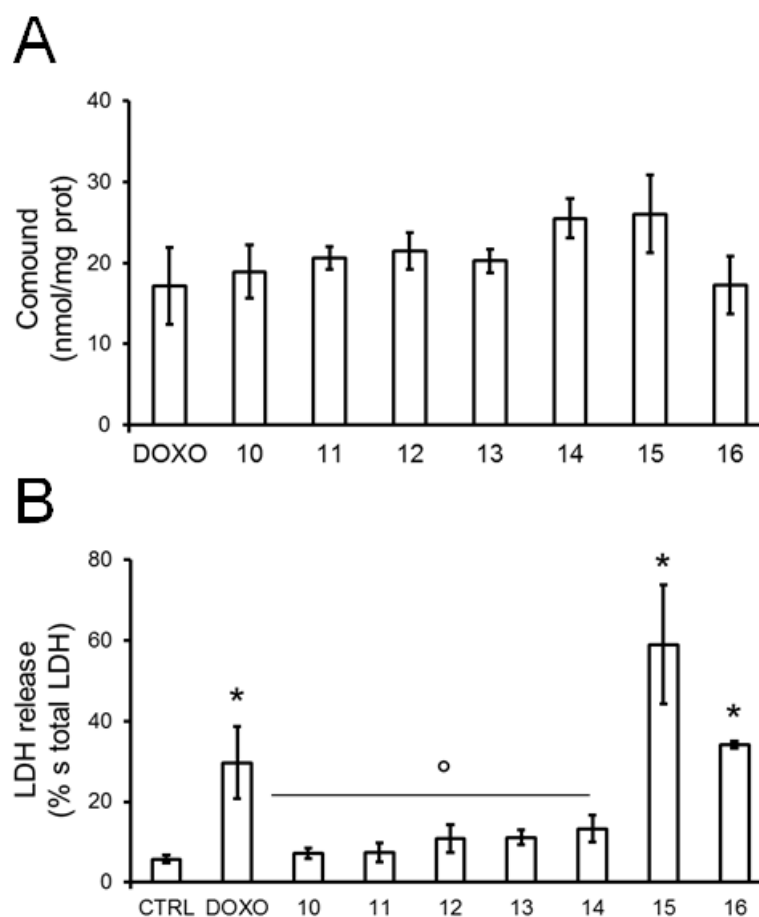


Figure 21 Intracellular accumulation and cytotoxicity of H₂S-releasing Doxorubicins in cardiomyocytes. H9c2 cardiomyocytes were incubated for 24 h in fresh medium (CTRL) or in medium containing 5 μ M Dox (DOXO) or different H₂S-releasing doxorubicins (compound 10–16). (A) The amount of intracellular Dox was measured fluorimetrically in cell lysates in duplicate (n = 3). Data are presented as means \pm SD. (B) The release of extracellular LDH in the culture medium was measured spectrophotometrically in duplicate (n = 3). Vs CTRL: * p < 0.001; vs DOXO: ° p < 0.05.

The lack of cytotoxicity was due to the low levels of ROS in cells exposed to H₂S-releasing doxorubicins (Figure 22A). Low ROS levels were likely due to the presence of H₂S that may buffer the ROS increase elicited by Dox. Indeed, in cells treated with H₂S-scavenger hydroxycobalamin intracellular ROS and cytotoxicity induced by H₂S-releasing doxorubicins were increased (Figure 22 A-B).

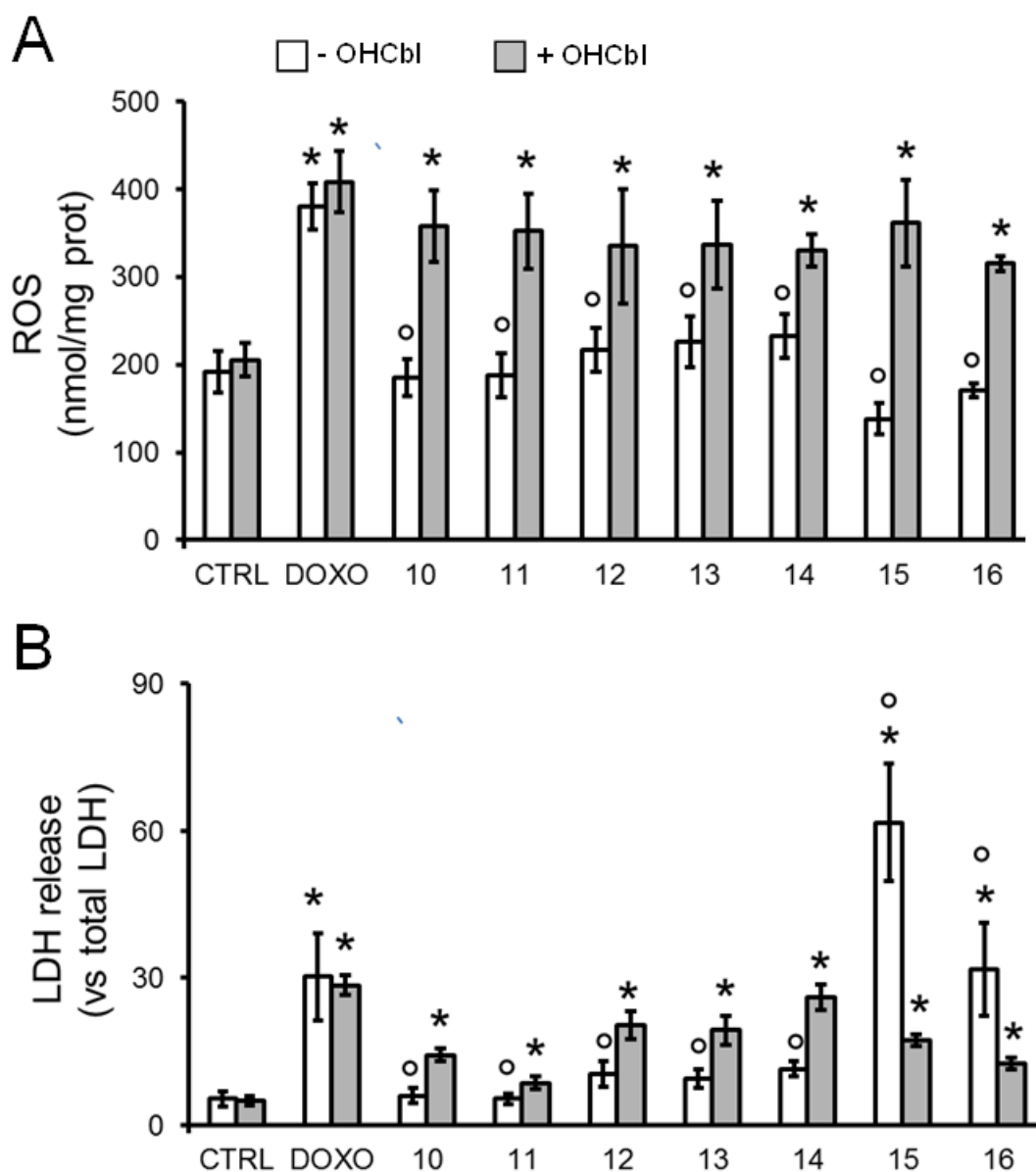


Figure 22 Intracellular ROS and cytotoxicity of H₂S-releasing doxorubicins in cardiomyocytes treated with the H₂S scavenger hydroxocobalamin (OHCbl). H9c2 cardiomyocytes were incubated for 24 h in fresh medium (CTRL) or in medium containing 5 μ M Dox (DOXO) or H₂S-releasing doxorubicins (compounds 10-16), in the absence (-) or in the presence (+) of 100 μ M OHCbl, chosen as H₂S scavenger. (A) The amount of intracellular ROS was measured fluorimetrically in cell lysates in duplicate (n = 3). Data are presented as means \pm SD. Vs respective CTRL: * p < 0.01; vs DOXO: ° p < 0.002; - OHCbl vs + OHCbl: p < 0.01 for all compounds (not shown). (B) The release of extracellular LDH in the culture medium was measured spectrophotometrically in duplicate (n = 3). Vs respective CTRL: * p < 0.05; vs DOXO: ° p < 0.05; - OHCbl vs + OHCbl: p < 0.05 for all compounds (not shown).

4.3.2 H₂S-releasing doxorubicin exerts cytotoxic effects against drug-resistant osteosarcoma cells

We next analyzed if the poorly cardiotoxic compound **10**/Sdox still exerted cytotoxic and anti-proliferative effects against U-2OS and Saos-2 cells, and in the respective resistant variants. As expected, Dox was well retained in U-2OS and Saos-2 cells (Figure 23A-B), where it induced cell damage (Figure 23C-D) and reduced cell viability (Figure 23E-F), but it was progressively less accumulated and less toxic in resistant cells (Figure 23A-F). Although the accumulation and the release of LDH were also progressively decreased in resistant cells treated with Sdox, such decrease was less pronounced: overall, Sdox was significantly more accumulated and cytotoxic than Dox in all cell populations. Notably, Sdox reduced cell viability to the same extent in sensitive and resistant cells (Figure 23A-F). In keeping with these data, the IC₅₀ to dox was at least 15-fold higher in DX580 sublines than in parental U-2OS or Saos-2 cells, while the IC₅₀ to Sdox increased less than 4-fold (Table 9). The IC₅₀ to Sdox was higher in not-transformed osteoblasts than in osteosarcoma cells (Table 9), suggesting again the existence of a good therapeutic window to target tumor cells, with limited toxicity on healthy osteoblasts.

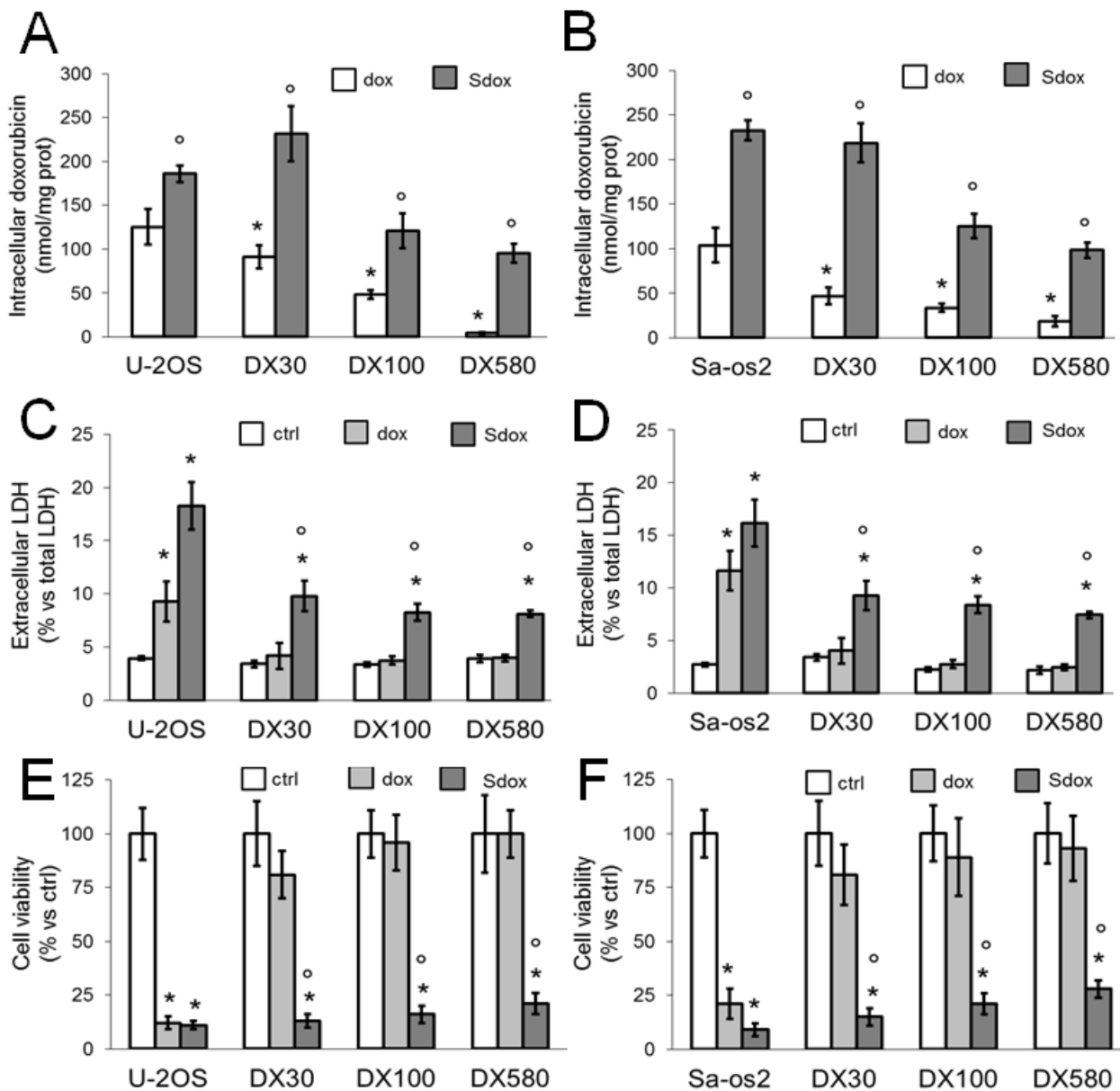


Figure 23 H₂S-releasing doxorubicin is effective against resistant osteosarcoma cells

Human dox-sensitive U-2OS cells and Saos-2 cells, and dox-resistant variants (DX30, DX100, DX580) were grown in fresh medium (ctrl) or in medium containing 5 μ M doxorubicin (dox) or H₂S-releasing doxorubicin (Sdox) for 6 h (panels **A-B**), 24 h (panels **C-D**) or 72 h (panels **E-F**). **A-B**. Intracellular doxorubicin accumulation, measured in duplicates by a fluorimetric assay. Data are means \pm SD (n=6). *p<0.05 for DX-cells vs. parental U-2OS or Saos-2 cells; $^{\circ}$ p<0.001 for Sdox vs. dox. **C-D**. Extracellular release of LDH measured spectrophotometrically in triplicates. Data are means \pm SD (n=6). *p<0.001 for treated vs.

untreated cells; °p<0.001 for Sdox vs. dox. **E-F.** Cell viability measured by a chemiluminescence-based assay in quadruplicates. Data are means±SD (n=6). *p<0.001 for treated vs. untreated cells; °p<0.001 for Sdox vs. dox.

Table 9. IC50 to doxorubicin and H₂S-releasing doxorubicin

Cell line	dox	Sdox
U-2OS	4.15 ± 0.37	3.09 ± 0.19
U-2OS/DX30	19.21 ± 2.02 *	4.35 ± 0.82 °
U-2OS/DX100	50.39 ± 8.33 *	9.34 ± 1.21 °
U-2OS/DX580	102.34 ± 22.09 *	11.88 ± 2.33 °
Saos-2	6.21 ± 1.09	4.88 ± 0.79
Saos-2/DX30	16.21 ± 1.97 *	7.45 ± 0.81 °
Saos-2/DX100	44.37 ± 8.01 *	10.22 ± 1.98 °
Saos-2/DX580	98.52 ± 15.01 *	15.23 ± 2.19 °
Primary osteoblasts	6.09 ± 0.77	28.98 ± 2.11 °

Cells were incubated for 72 h with increasing concentrations (1 nM-1 mM) of doxorubicin (dox) or H₂S-releasing doxorubicin (Sdox). Cell viability was measured in quadruplicates by a chemiluminescence-base assay (ATPlite kit). Data are means±SD (n=6). * p < 0.001 for dox-resistant variants vs.their parental cells; °p < 0.001 for Sdox versus dox.

Interestingly, whereas Dox accumulation was significantly increased in resistant cells treated with the Pgp inhibitor verapamil (Figure 24A), Sdox accumulation was not affected (Figure 24B), suggesting that the drug competed was not effluxed or less effluxed by Pgp.

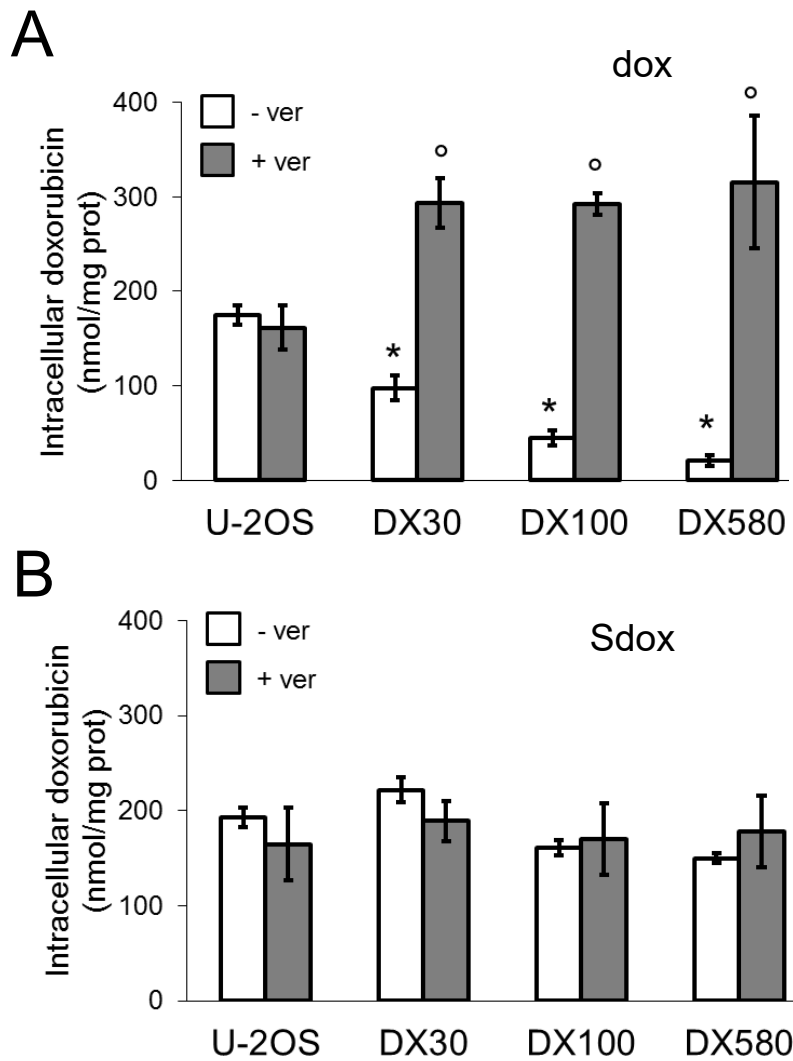


Figure 24 Effects of verapamil on H₂S-releasing doxorubicin accumulation

Human doxorubicin-sensitive U-2OS cells and doxorubicin-resistant variants (DX30, DX100, DX580) were cultured for 6 h with 5 μ M doxorubicin (dox; panel **A**) or H₂S-releasing doxorubicin (Sdox; panel **B**), in the absence (-) or presence (+) of 50 mM verapamil (ver). The intracellular drug accumulation was measured by a fluorimetric assay in duplicates. Data are means \pm SD (n=6). *p<0.001 for DX-cells vs. parental U-2OS cells; °p<0.001 for verapamil-treated vs. untreated cells.

Kinetic efflux of doxorubicin and S-dox/compound **10** from U-2OS/DX580 cells showed that S-dox had a higher K_m for Pgp, suggestive of poor affinity for the transporter (Figure 25). This issue is in line with the lack of effect of verapamil on S-dox retention. Moreover, S-dox had a significantly lower V_{max} of efflux from U-2OS/DX580 cells, suggesting that these cells may have a lower amount of Pgp on cell surface. The co-incubation of parental dox with the only H₂S-releasing moiety (compound **3**) contained in S-dox/compound **10** did not affect K_m , but reduced V_{max} of drug efflux (Figure 25). This experimental set suggests that part of the increased toxicity of S-dox may be due to the reduced efflux through Pgp, as a consequence of lower affinity of the drug and lower amount of the transporter on cell surface. This may result in increased intracellular retention of S-dox that induces increased cytotoxicity than dox.

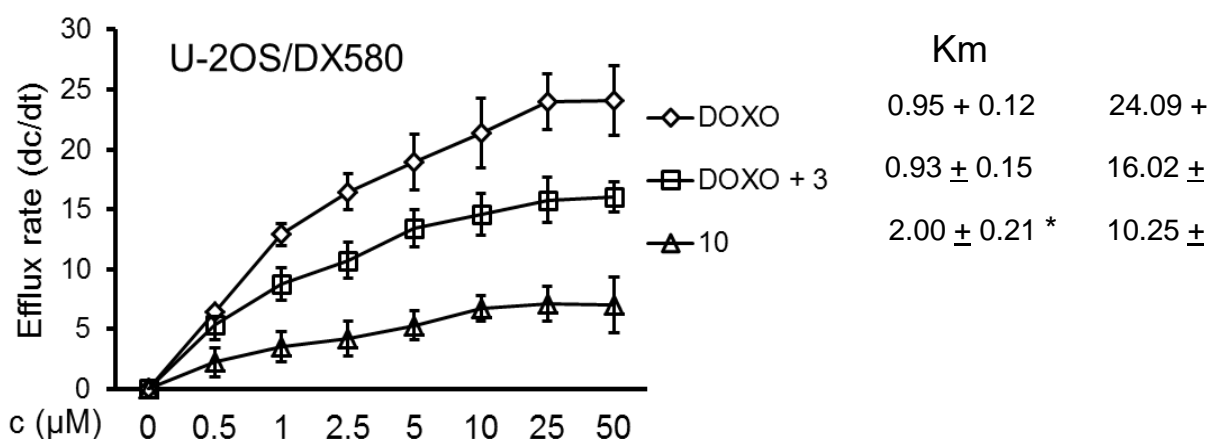


Figure 25 Efflux kinetics of doxorubicin from drug-resistant osteosarcoma cells. Dox-resistant U-2OS/DX580 cells were incubated for 20 min with increasing concentrations (0–50 μ M) of DOXO, DOXO with the H₂S-releasing moiety (compound **3**), or S-dox/compound **10**. Cells were washed and tested fluorimetrically for their intracellular drug content. The procedure was repeated on a second series of dishes, incubated under the same experimental conditions and analyzed after 10 min. Data are presented as means \pm SD ($n = 3$). The rate of DOXOs efflux (dc/dt) was plotted versus the initial concentration of the drug. V_{max} (nmol/min/mg proteins), and K_m (nmol/mg proteins) values were calculated with the Enzfitter software. DOXO + 3 vs DOXO: $p \leq 0.001$, for concentrations 1–50 μ M; 10 vs DOXO: $p \leq 0.001$, for concentrations 0.5–50 μ M; 10 vs DOXO + 3: $p \leq 0.01$, for concentrations 0.5–50 μ M (not shown). For K_m , vs DOXO: * $p < 0.01$; for V_{max} , vs DOXO: * $p < 0.001$; vs DOXO + 3: ° $p < 0.05$.

4.3.3 H₂S-releasing doxorubicin localizes within ER and up-regulates ERAD/ERQC-related genes

We next investigated possible mechanisms of Sdox cytotoxicity in resistant osteosarcoma cells.

As already observed in cardiomyocytes, also in osteosarcoma Sdox/compound 10 did not increase ROS production: the lower levels of ROS were due to the presence of H₂S-releasing moiety, since ROS were increased by the H₂S-scavenger hydroxycobalamin (Figure 26).

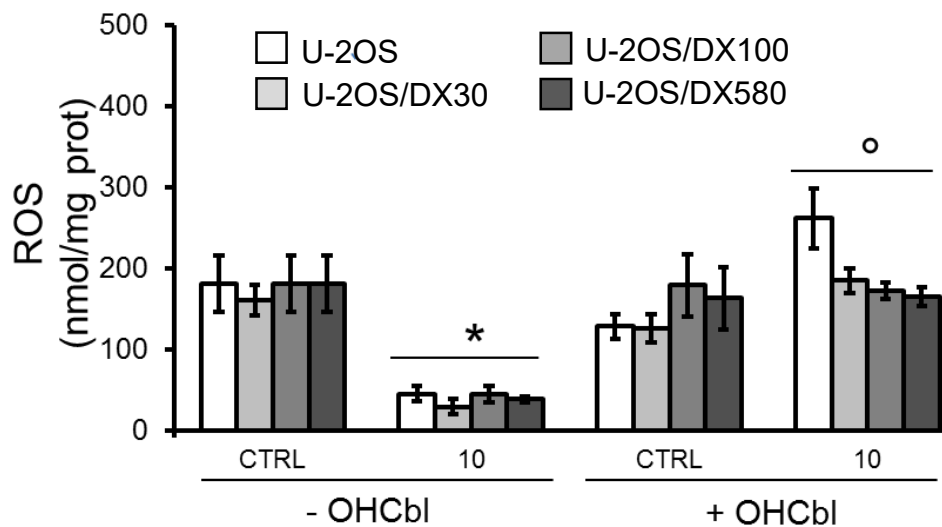


Figure 26 Intracellular ROS in cells treated with of H₂S-releasing doxorubicin and hydroxycobalamin. Dox-sensitive U-2OS cells and the Dox-resistant variants (U-2OS/DX30, U-2OS/DX100, U-2OS/DX580) were incubated for 24 h in fresh medium (CTRL) or in medium containing 5 μ M dox (DOXO) or Sdox (compound 10), in the absence (-) or in the presence (+) of 100 μ M OHCbl. The amount of intracellular ROS was measured fluorimetrically in cell lysates in duplicate (n = 3). Data are presented as means \pm SD. Vs respective CTRL: * p < 0.001; - OHCbl vs + OHCbl: p < 0.001

Differently from dox that had a nuclear accumulation, Sdox was mainly localized within ER (Figure 26).

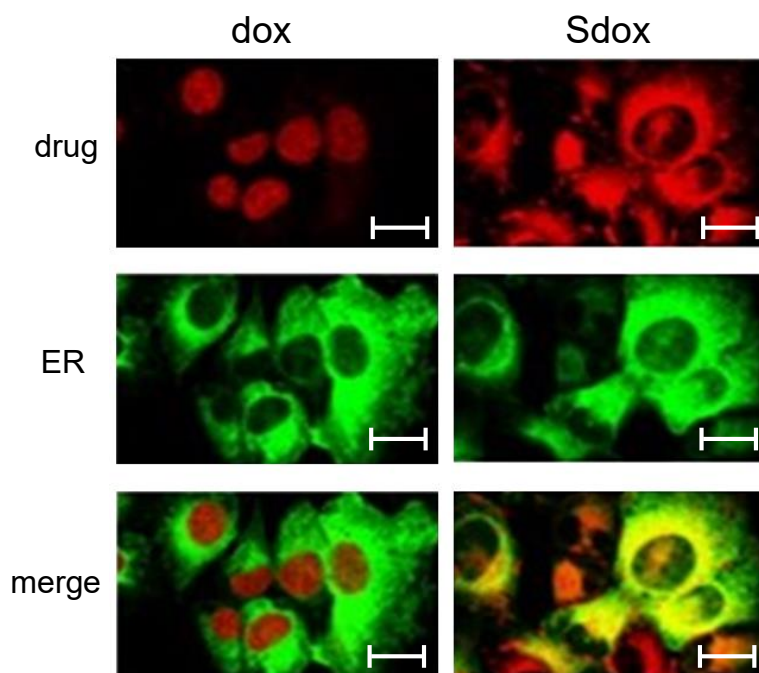


Figure 27 H₂S-releasing doxorubicin localizes within endoplasmic reticulum. U-2OS cells were incubated for 24 h with the GFP-KDEL-calreticulin expression vector to label endoplasmic reticulum (ER), then treated with 5 μ M doxorubicin (dox) or H₂S-releasing doxorubicin (Sdox) for the last 6 h. The intracellular localization of the drugs was analyzed by confocal microscopy. Bar: 10 μ m. The micrographs are representative of 4 experiments with similar results.

We thus investigated whether the cytotoxic effects of Sdox were mediated by alterations of ER functions.

A baseline gene profiling of U2-OS and resistant clones revealed a remarkable number of genes related to ER-associated protein degradation (ERAD) and ER-quality control (ERQC), two processes that check protein folding and remove irreversibly damaged proteins (Kim I *et al.*, *Nat Rev Drug Discov* 2008 ; Chevet E *et al.*, *Cancer Discov* 2015), down-regulated with the increase of dox-resistance (Table 10, Figure 28A). We detecte either up- or down-regulation of genes controlling the unfolded protein response (UPR; Table 10, Figure 28B), a series of events triggered by misfolded/unfolded proteins accumulated within ER lumen, leading to protein degradation and cell survival, or ER stress and cell death (Kim I *et al.*, *Nat Rev Drug Discov* 2008 ; Chevet E *et al.*, *Cancer Discov* 2015). Consistently, genes

mediating cell death or survival consequent to UPR were either up- or down-regulated in untreated sensitive and resistant cells (Table 10, Figure 28C).

Table 10. Unfolded protein response (UPR)-related genes in doxorubicin-sensitive and doxorubicin-resistant osteosarcoma cells

Ref Seq	Gene name	Biological function	Fold change (U-2OS/DX30 vs U-2OS)	p value	Fold change (U2OS/DX10 vs U-2OS)	p value	Fold change (U2OS/DX10 vs U-2OS)	p value
NM_001144	ADM2	Protein synthesis	1.13	ns	1.14	0.001	0.62	0.02
NM_024866	AMFR	ERAD; cholesterol homeostasis	1.27	0.01	1.33	0.002	1.51	0.001
NM_183356	ASNS	Protein synthesis	0.78	0.01	0.76	0.005	0.18	0.001
NM_001675	ATF4	UPR	1.46	0.002	1.16	0.02	0.93	ns
NM_007348	ATF6	UPR	0.63	0.001	0.62	0.001	0.75	0.05
NM_004381	ATF6B	UPR	0.42	0.001	0.46	0.005	0.53	0.001
NM_004993	ATXN3	ERQC/ERAD	1.03	ns	0.58	0.001	0.06	0.001
NM_004324	BAX	Cell death	0.85	ns	1.13	ns	1.11	ns
NM_032621	BEX2	Cell death	0.96	ns	0.94	ns	0.93	ns
NM_004343	CALR	ERQC	0.84	ns	0.94	ns	1.01	ns
NM_001746	CANX	ERQC	0.96	ns	1.01	ns	1.11	ns
NM_006430	CCT4	ERQC	0.74	0.01	0.39	0.001	0.12	0.01
NM_005194	CEBPB	UPR	0.84	0.05	0.76	0.005	0.65	0.001
NM_006368	CREB3	Cell death	1.59	0.001	1.65	0.001	1.06	ns
NM_032607	CREB3L3	UPR	1.17	ns	2.27	0.001	2.87	0.001
NM_004083	DDIT3	UPR; cell death	0.17	0.001	0.62	0.001	0.40	0.001
NM_024295	DERL1	ERAD	0.61	0.005	0.42	0.001	0.22	0.01
NM_012328	DNAJB9	Cell survival	0.78	0.01	0.76	0.005	0.65	0.001
NM_018981	DNAJC10	ERAD	0.68	0.002	0.41	0.001	0.07	0.001
NM_006260	DNAJC3	ERQC; UPR	0.73	0.005	0.48	0.001	0.14	0.001
NM_014674	EDEM1	ERAD	0.63	0.001	0.46	0.001	0.16	0.001
NM_032025	EIF2A	UPR	1.11	ns	0.50	0.001	0.53	0.001
NM_004836	EIF2AK3	UPR	0.78	0.01	0.31	0.001	0.21	0.001
NM_001433	ERN1	UPR	0.26	0.001	0.66	0.001	0.99	ns
NM_033266	ERN2	UPR; Cell death	0.36	0.001	0.38	0.002	1.62	0.02
NM_014584	ERO1L	ERQC; cell death	1.27	ns	0.84	0.05	0.57	0.001

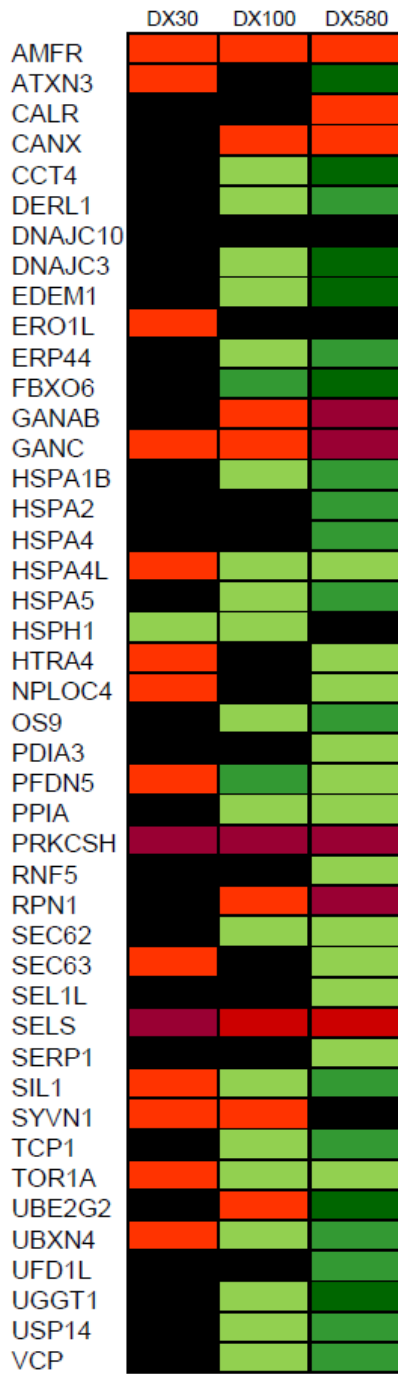
NM_019891	ERO1LB	Cell death	0.88	ns	0.73	0.01	0.53	0.001
NM_015051	ERP44	ERQC	0.73	0.05	0.50	0.001	0.33	0.001
NM_018438	FBXO6	ERAD	0.75	0.01	0.33	0.001	0.05	0.005
NM_198334	GANAB	ERQC	0.68	0.02	1.16	0.02	3.24	0.001
NM_198141	GANC	ERQC	1.36	ns	1.24	ns	3.72	0.001
NM_016095	GINS2	Cell survival	0.40	0.001	0.72	0.01	0.49	0.001
NM_014685	HERPUD1	UPR	2.13	0.005	3.65	0.001	5.26	0.001
NM_005346	HSPA1B	ERQC	0.80	0.05	0.46	0.001	0.15	0.001
NM_021979	HSPA2	ERQC	0.83	ns	0.67	0.01	0.22	0.001
NM_002154	HSPA4	ERQC	0.84	ns	0.62	0.001	0.22	0.001
NM_014278	HSPA4L	ERQC	1.10	ns	0.46	0.001	0.41	0.001
NM_005347	HSPA5	ERQC; UPR	0.83	ns	0.47	0.001	0.18	0.001
NM_006644	HSPH1	ERQC; UPR	0.36	0.001	0.38	0.002	0.62	0.02
NM_013247	HTRA2	Cell death	0.96	ns	0.92	ns	1.29	ns
NM_153692	HTRA4	ERQC	1.56	0.01	0.56	0.001	0.47	0.001
NM_031479	INHBE	Cell death	1.80	0.001	2.17	0.001	1.22	0.001
NM_016133	INSIG2	Cholesterol homeostasis	1.76	0.01	2.38	0.002	3.82	0.001
NM_014407	KCNMB3	Calcium flux	0.11	0.001	0.54	0.001	0.32	0.001
NM_006010	MANF	Cell death	1.27	0.01	0.88	0.05	0.81	0.01
NM_002750	MAPK8	Cell survival	0.52	0.001	1.76	0.001	3.24	0.001
NM_002752	MAPK9	Cell survival	2.06	0.001	1.64	0.001	2.13	0.001
NM_003791	MBTPS1	Cholesterol homeostasis	1.27	0.01	1.33	0.002	1.99	0.001
NM_015884	MBTPS2	Cholesterol homeostasis	6.70	0.001	5.34	0.001	4.58	0.001
NM_005914	MCM4	Cell survival	2.21	0.001	1.33	0.002	0.49	0.001
NM_017921	NPLOC4	ERAD	1.46	0.002	0.88	0.05	0.26	0.001
NM_006184	NUCB1	UPR	8.25	0.001	7.05	0.001	6.48	0.001
NM_006812	OS9	ERAD	0.84	ns	0.47	0.01	0.16	0.001
NM_182649	PCNA	Cell survival	0.34	0.001	0.50	0.001	0.14	0.001s
NM_005313	PDIA3	ERQC	0.86	ns	0.88	ns	0.36	0.001
NM_002624	PFDN5	ERQC	1.11	ns	0.29	0.001	0.45	0.001
NM_021130	PPIA	ERQC	0.72	0.01	0.42	0.001	0.29	0.001
NM_014330	PPP1R15A	Cell death	1.03	ns	0.94	ns	2.63	0.001
NM_002743	PRKCSH	ERQC	6.25	0.001	6.58	0.001	7.44	0.001
NM_006913	RNF5	ERAD	0.99	ns	0.76	0.01	0.44	0.001
NM_002950	RPN1	ERQC	0.73	0.005	1.16	ns	3.24	0.001
NM_001034	RRM2	Cell survival	0.36	0.001	0.38	0.002	0.62	0.02
NM_012235	SCAP	Cholesterol homeostasis	0.63	0.001	0.82	0.01	0.86	ns

NM_003262	SEC62	ERQC	0.70	0.01	0.45	0.001	0.27	0.001
NM_007214	SEC63	ERQC	1.03	ns	0.91	ns	0.31	0.001
NM_005065	SEL1L	ERQC	0.96	ns	0.94	ns	0.40	0.001
NM_203472	SELS	ERAD	3.13	0.001	2.49	0.001	2.63	0.001
NM_014445	SERP1	ERQC	0.70	0.002	0.62	0.001	0.45	0.002
NM_022464	SIL1	ERQC	1.18	ns	0.32	0.001	0.13	0.001
NM_005835	SLC17A2	Phosphate transport	0.55	0.001	0.50	0.001	2.45	0.001
NM_004176	SREBF1	Cholesterol homeostasis	0.36	0.001	0.38	0.002	1.62	0.02
NM_172230	SYVN1	ERQC; cell survival	1.15	ns	1.25	ns	0.86	0.05
NM_030752	TCP1	ERQC	0.66	0.001	0.46	0.001	0.14	0.001
NM_000113	TOR1A	ERQC	1.35	ns	0.49	0.001	0.45	0.001
NM_021158	TRIB3	UPR; cell death	0.70	0.01	1.29	ns	1.13	ns
NM_001071	TYMS	Cell survival	1.72	0.001	1.67	0.001	1.06	ns
NM_182688	UBE2G2	ERAD	0.96	ns	1.24	0.005	0.09	0.001
NM_014607	UBXN4	ERAD	1.25	ns	0.45	0.001	0.13	0.001
NM_005659	UFD1L	ERAD	0.63	0.001	0.66	0.001	0.23	0.001
NM_020120	UGGT1	ERQC	0.96	ns	0.46	0.002	0.12	0.01
NM_013282	UHRF1	Cell death	1.40	0.01	0.75	0.05	0.98	ns
NM_005151	USP14	ERAD	0.98	ns	0.49	0.001	0.17	0.001
NM_007126	VCP	ERAD	0.93	ns	0.42	0.001	0.19	0.001
NM_005080	XBP1	UPR	5.44	0.001	5.34	0.001	2.13	0.001

Baseline gene expression in U-2OS cells and in their resistant variants U-2OS/DX30, U-2OS/DX100 and U-2OS/DX580 cells. Fold-Change ($2^{(-\Delta\Delta Ct)}$) is the normalized gene expression ($2^{(-\Delta Ct)}$) in U-2OS/DX30, U-2OS/DX100 or U-2OS/DX580 cells, divided the normalized gene expression ($2^{(-\Delta Ct)}$) in U-2OS cells, where Ct is the threshold cycle in qRT-PCR (n=6). Fold-change values greater than 1 indicate up-regulation, fold-change values less than 1 indicate down-regulation. The p values are calculated based on a Student's t-test of the replicate $2^{(-\Delta Ct)}$ values for each gene. p<0.05 was considered significant. ERAD: ER-associated degradation; UPR: unfolded protein response; ERQC: ER-quality control.

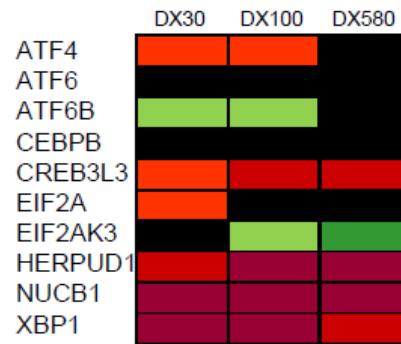
A

ERAD/ERQC



B

UPR



C

Cell death/survival

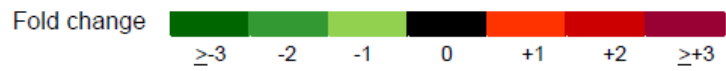
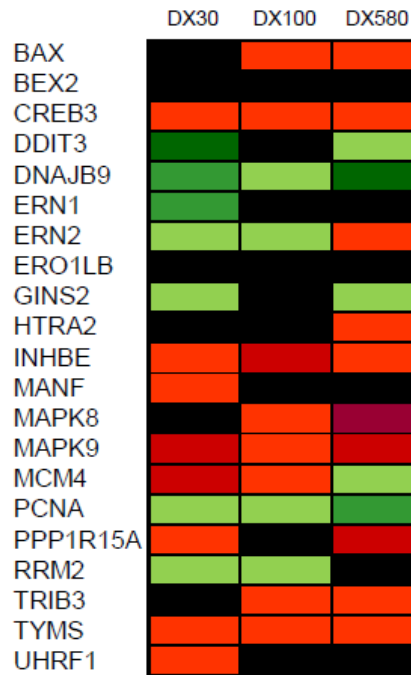


Figure 28 Expression of ERAD/ERQC and UPR-related genes in doxorubicin-sensitive and doxorubicin-resistant osteosarcoma cells

A-C. Hitmap of unfolded protein response (UPR)-related genes, cell death/survival related genes, ER-associated degradation/endoplasmic reticulum quality control (ERAD/ERQC)-related genes in U-2OS/DX30, U-2OS/DX100 and U-2OS/DX580 cells. The figure reports genes up-or down-regulated at least two-fold, in at least one cell line, compared to untreated U-2OS cells (n=6). The expression of each gene in U-2OS cells was considered 1 (not shown). The whole list of genes analyzed is reported in Table 10.

Both dox and Sdox up-regulated most of ERAD/ERQC-related genes in U-2OS cells (Table 11, Figure 29A). As expected in consequence of the low intracellular accumulation, dox produced minor changes in the expression of this gene set in U-2OS/DX580 cells. By contrast, Sdox still up-regulated most ERAD/ERQC-related genes in drug-resistant cells (Table 12, Figure 29A). The key proteins of ERAD pathway EDEM1, UGGT1, SEC62 and VCP were lower in U-2OS/DX580 cells compared to U-2OS cells (Figure 29B). In keeping with gene profiling results, dox increased these proteins in drug-sensitive but not in drug-resistant cells, Sdox increased them in both cell populations (Figure 29B).

These data suggests that Sdox forces resistant cells to up-regulate the ERAD/ERQC apparatus, likely as a consequence of an increased burden of unfolded/misfolded proteins in ER.

Table 11. Unfolded protein response (UPR)-related genes in doxorubicin-sensitive osteosarcoma cells treated with doxorubicin or H₂S-releasing doxorubicin

Ref Seq	Gene name	Biological function	Fold change (dox-treated cells vs untreated cells)	p value	Fold change (Sdox- treated cells vs untreated cells)	p value
NM_001144	ADM2	Protein synthesis	2.75	0.001	0.73	0.02
NM_024866	AMFR	ERAD; cholesterol homeostasis	1.44	0.001	0.62	0.001
NM_183356	ASNS	Protein synthesis	0.02	0.001	0.43	0.001
NM_001675	ATF4	UPR	2.17	0.001	3.53	0.001
NM_007348	ATF6	UPR	2.15	0.001	4.33	0.001
NM_004381	ATF6B	UPR	1.56	0.002	2.17	0.001
NM_004993	ATXN3	ERQC/ERAD	1.42	0.001	2.16	0.01
NM_004324	BAX	Cell death	1.82	0.001	2.66	0.001
NM_032621	BEX2	Cell death	1.12	ns	4.33	0.001
NM_004343	CALR	ERQC	0.74	0.05	1.22	ns
NM_001746	CANX	ERQC	1.28	ns	1.27	ns
NM_006430	CCT4	ERQC	1.12	ns	2.86	0.001
NM_005194	CEBPB	UPR	1.30	0.05	1.56	0.02
NM_006368	CREB3	Cell death	1.58	0.001	2.01	0.001
NM_032607	CREB3L3	UPR	1.17	ns	2.16	0.001
NM_004083	DDIT3	UPR; cell death	2.16	0.001	2.16	0.002
NM_024295	DERL1	ERAD	1.40	0.02	2.44	0.001
NM_012328	DNAJB9	Cell survival	0.34	0.001	0.64	0.001
NM_018981	DNAJC10	ERAD	2.26	0.001	2.66	0.001
NM_006260	DNAJC3	ERQC; UPR	1.52	0.001	2.88	0.001
NM_014674	EDEM1	ERAD	1.49	0.002	3.47	0.001
NM_032025	EIF2A	UPR	1.12	ns	1.35	ns
NM_004836	EIF2AK3	UPR	2.32	0.001	2.54	0.001
NM_001433	ERN1	UPR	0.40	0.001	0.44	0.001
NM_033266	ERN2	UPR; Cell death	2.75	0.001	2.41	0.002
NM_014584	ERO1L	ERQC; cell death	1.30	0.05	1.13	ns
NM_019891	ERO1LB	Cell death	2.09	0.002	0.94	ns
NM_015051	ERP44	ERQC	1.21	ns	1.38	ns

NM_018438	FBXO6	ERAD	2.11	0.001	2.10	0.001
NM_198334	GANAB	ERQC	1.37	ns	1.31	0.001
NM_198141	GANC	ERQC	1.85	0.02	2.62	0.001
NM_016095	GINS2	Cell survival	1.20	ns	1.02	ns
NM_014685	HERPUD1	UPR	2.26	0.001	2.15	0.001
NM_005346	HSPA1B	ERQC	1.32	ns	1.43	0.05
NM_021979	HSPA2	ERQC	1.64	0.005	4.64	0.001
NM_002154	HSPA4	ERQC	1.91	0.001	4.64	0.001
NM_014278	HSPA4L	ERQC	1.98	0.001	3.06	0.001
NM_005347	HSPA5	ERQC; UPR	1.38	0.02	3.06	0.001
NM_006644	HSPH1	ERQC; UPR	2.75	0.001	2.41	0.001
NM_013247	HTRA2	Cell death	1.37	ns	1.54	0.02
NM_153692	HTRA4	ERQC	1.82	0.001	5.33	0.001
NM_031479	INHBE	Cell death	0.91	ns	0.94	ns
NM_016133	INSIG2	Cholesterol homeostasis	2.75	0.001	0.48	0.002
NM_014407	KCNMB3	Calcium flux	1.11	ns	1.24	ns
NM_006010	MANF	Cell death	0.28	0.001	0.24	0.001
NM_002750	MAPK8	Cell survival	0.32	0.001	0.31	0.001
NM_002752	MAPK9	Cell survival	1.20	ns	0.76	0.005
NM_003791	MBTPS1	Cholesterol homeostasis	0.34	0.001	0.82	ns
NM_015884	MBTPS2	Cholesterol homeostasis	0.95	ns	1.53	ns
NM_005914	MCM4	Cell survival	0.56	0.001	0.33	0.001
NM_017921	NPLOC4	ERAD	1.42	0.005	1.58	0.002
NM_006184	NUCB1	UPR	1.20	ns	1.53	0.005
NM_006812	OS9	ERAD	0.91	ns	0.82	ns
NM_182649	PCNA	Cell survival	0.25	0.001	0.08	0.001
NM_005313	PDIA3	ERQC	1.52	0.001	2.22	0.001
NM_002624	PFDN5	ERQC	3.16	0.001	4.04	0.001
NM_021130	PPIA	ERQC	1.12	ns	1.76	0.001
NM_014330	PPP1R15A	Cell death	0.59	0.0001	0.33	0.001
NM_002743	PRKCSH	ERQC	1.20	ns	2.02	0.001
NM_006913	RNF5	ERAD	1.21	ns	2.02	0.001
NM_002950	RPN1	ERQC	0.37	0.001	0.10	0.001
NM_001034	RRM2	Cell survival	0.75	0.05	0.41	0.001
NM_012235	SCAP	Cholesterol homeostasis	0.24	0.001	0.17	0.001
NM_003262	SEC62	ERQC	1.34	0.05	2.76	0.001
NM_007214	SEC63	ERQC	0.79	ns	2.41	0.001

NM_005065	SEL1L	ERQC	1.34	ns	1.82	0.01
NM_203472	SELS	ERAD	1.42	0.005	1.43	0.005
NM_014445	SERP1	ERQC	1.23	ns	1.41	0.05
NM_022464	SIL1	ERQC	1.38	0.05	3.52	0.001
NM_005835	SLC17A2	Phosphate transport	0.30	0.001	0.58	0.001
NM_004176	SREBF1	Cholesterol homeostasis	2.75	0.001	0.41	0.002
NM_172230	SYVN1	ERQC; cell survival	0.07	0.001	0.06	0.001
NM_030752	TCP1	ERQC	1.40	0.005	1.17	ns
NM_000113	TOR1A	ERQC	1.56	0.002	2.08	0.001
NM_021158	TRIB3	UPR; cell death	1.97	0.001	2.49	0.001
NM_001071	TYMS	Cell survival	1.04	ns	0.94	ns
NM_182688	UBE2G2	ERAD	1.08	ns	1.64	0.001
NM_014607	UBXN4	ERAD	1.47	0.001	2.49	0.001
NM_005659	UFD1L	ERAD	1.11	ns	1.38	0.05
NM_020120	UGGT1	ERQC	1.42	0.01	3.08	0.001
NM_013282	UHRF1	Cell death	3.16	0.0018	4.04	0.001
NM_005151	USP14	ERAD	0.40	0.001	0.35	0.001
NM_007126	VCP	ERAD	1.49	0.001	2.44	0.001
NM_005080	XBP1	UPR	1.85	0.002	3.66	0.001

U-2OS cells were grown in fresh medium (ctrl) or in the presence of 5 μ M doxorubicin (dox) or H₂S-releasing doxorubicin (Sdox) for 24 h. Fold-Change ($2^{(-\Delta\Delta Ct)}$) is the normalized gene expression ($2^{(-\Delta Ct)}$) in dox- or Sdox-treated cells, divided the normalized gene expression ($2^{(-\Delta Ct)}$) in untreated U-2OS cells, where Ct is the threshold cycle in qRT-PCR (n=6). Fold-change values greater than 1 indicate up-regulation, fold-change values less than 1 indicate down-regulation. The p values are calculated based on a Student's t-test of the replicate $2^{(-\Delta Ct)}$ values for each gene. p<0.05 was considered significant. ERAD: ER-associated degradation; UPR: unfolded protein response; ERQC: ER-quality control.

Table 12. Unfolded protein response (UPR)-related genes in doxorubicin-resistant osteosarcoma cells treated with doxorubicin or H₂S-releasing doxorubicin

Ref Seq	Gene name	Biological function	Fold change (dox-treated cells vs untreated cells)	p value	Fold change (Sdox- treated cells vs untreated cells)	p value
NM_001144	ADM2	Protein synthesis	1.45	ns	0.52	0.002
NM_024866	AMFR	ERAD; cholesterol homeostasis	1.41	0.05	0.47	0.001
NM_183356	ASNS	Protein synthesis	1.33	ns	0.55	0.001
NM_001675	ATF4	UPR	0.91	ns	2.54	0.001
NM_007348	ATF6	UPR	0.92	ns	1.67	0.001
NM_004381	ATF6B	UPR	0.82	ns	1.88	0.005
NM_004993	ATXN3	ERQC/ERAD	0.97	ns	2.09	0.001
NM_004324	BAX	Cell death	1.16	ns	1.54	0.02
NM_032621	BEX2	Cell death	1.66	0.01	3.31	0.001
NM_004343	CALR	ERQC	0.87	ns	1.22	0.001
NM_001746	CANX	ERQC	1.31	ns	1.29	0.001
NM_006430	CCT4	ERQC	0.82	ns	2.34	0.001
NM_005194	CEBPB	UPR	1.01	ns	1.18	ns
NM_006368	CREB3	Cell death	1.01	ns	1.02	ns
NM_032607	CREB3L3	UPR	0.78	ns	1.09	ns
NM_004083	DDIT3	UPR; cell death	0.88	ns	2.51	0.001
NM_024295	DERL1	ERAD	1.58	0.02	2.33	0.001
NM_012328	DNAJB9	Cell survival	1.53	0.05	0.24	0.001
NM_018981	DNAJC10	ERAD	0.88	ns	1.72	0.001
NM_006260	DNAJC3	ERQC; UPR	1.19	ns	2.36	0.001
NM_014674	EDEM1	ERAD	0.94	ns	1.82	0.005
NM_032025	EIF2A	UPR	1.24	ns	1.09	ns
NM_004836	EIF2AK3	UPR	1.20	ns	1.41	0.05
NM_001433	ERN1	UPR	0.41	0.001	0.62	0.001
NM_033266	ERN2	UPR; Cell death	1.17	ns	2.22	0.001
NM_014584	ERO1L	ERQC; cell death	1.64	0.05	2.69	0.001
NM_019891	ERO1LB	Cell death	1.20	ns	1.72	0.001
NM_015051	ERP44	ERQC	1.14	ns	1.14	ns

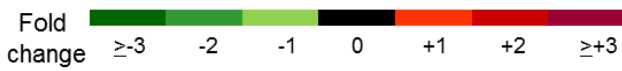
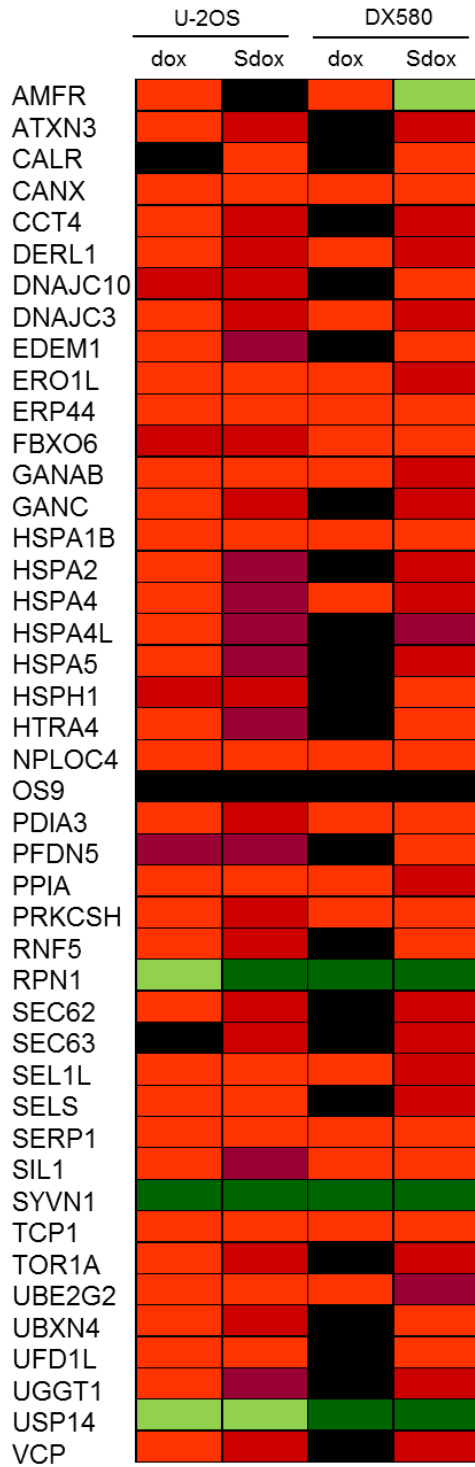
NM_018438	FBXO6	ERAD	1.17	ns	1.16	ns
NM_198334	GANAB	ERQC	1.11	ns	2.16	0.001
NM_198141	GANC	ERQC	0.92	ns	2.29	0.001
NM_016095	GIN52	Cell survival	1.01	ns	0.77	0.05
NM_014685	HERPUD1	UPR	0.86	ns	2.31	0.001
NM_005346	HSPA1B	ERQC	1.76	0.002	1.54	0.005
NM_021979	HSPA2	ERQC	0.88	ns	2.34	0.001
NM_002154	HSPA4	ERQC	1.16	ns	2.27	0.001
NM_014278	HSPA4L	ERQC	0.91	ns	3.31	0.001
NM_005347	HSPA5	ERQC; UPR	0.53	0.05	2.34	0.001
NM_006644	HSPH1	ERQC; UPR	0.87	ns	1.22	ns
NM_013247	HTRA2	Cell death	1.16	ns	1.14	ns
NM_153692	HTRA4	ERQC	0.76	ns	1.77	0.001
NM_031479	INHBE	Cell death	1.33	ns	0.95	ns
NM_016133	INSIG2	Cholesterol homeostasis	1.17	ns	0.39	0.002
NM_014407	KCNMB3	Calcium flux	0.88	ns	0.95	ns
NM_006010	MANF	Cell death	0.71	0.05	0.42	0.001
NM_002750	MAPK8	Cell survival	0.19	0.001	0.16	0.001
NM_002752	MAPK9	Cell survival	0.79	ns	1.47	0.02
NM_003791	MBTPS1	Cholesterol homeostasis	1.20	ns	1.58	0.005
NM_015884	MBTPS2	Cholesterol homeostasis	1.04	ns	1.54	0.002
NM_005914	MCM4	Cell survival	0.88	ns	0.72	0.02
NM_017921	NPLOC4	ERAD	1.38	0.01	1.41	0.01
NM_006184	NUCB1	UPR	0.87	ns	1.33	ns
NM_006812	OS9	ERAD	0.95	ns	0.81	ns
NM_182649	PCNA	Cell survival	1.16	ns	0.27	0.001
NM_005313	PDIA3	ERQC	1.19	ns	1.18	ns
NM_002624	PFDN5	ERQC	0.88	ns	1.72	0.005
NM_021130	PPIA	ERQC	1.08	ns	2.19	0.001
NM_014330	PPP1R15A	Cell death	1.16	ns	0.44	0.001
NM_002743	PRKCSH	ERQC	1.11	ns	1.88	0.001
NM_006913	RNF5	ERAD	0.96	ns	1.38	ns
NM_002950	RPN1	ERQC	0.12	0.001	0.14	0.001
NM_001034	RRM2	Cell survival	1.17	ns	0.22	0.001
NM_012235	SCAP	Cholesterol homeostasis	0.47	0.001	0.38	0.001
NM_003262	SEC62	ERQC	0.95	ns	2.34	0.001
NM_007214	SEC63	ERQC	0.91	ns	2.44	0.001

NM_005065	SEL1L	ERQC	1.08	ns	2.25	0.001
NM_203472	SELS	ERAD	0.92	ns	1.72	0.002
NM_014445	SERP1	ERQC	1.27	ns	1.41	0.05
NM_022464	SIL1	ERQC	1.13	ns	1.65	0.005
NM_005835	SLC17A2	Phosphate transport	0.14	0.001	0.20	0.001
NM_004176	SREBF1	Cholesterol homeostasis	1.17	ns	0.22	0.001
NM_172230	SYVN1	ERQC; cell survival	0.08	0.001	0.14	0.001
NM_030752	TCP1	ERQC	1.44	0.05	1.18	ns
NM_000113	TOR1A	ERQC	0.95	ns	2.41	0.001
NM_021158	TRIB3	UPR; cell death	0.93	ns	2.02	0.001
NM_001071	TYMS	Cell survival	1.33	ns	1.34	ns
NM_182688	UBE2G2	ERAD	1.04	ns	9.38	0.001
NM_014607	UBXN4	ERAD	0.93	ns	1.44	0.01
NM_005659	UFD1L	ERAD	0.97	ns	1.13	ns
NM_020120	UGGT1	ERQC	0.87	ns	2.25	0.001
NM_013282	UHRF1	Cell death	1.43	0.05	2.09	0.001
NM_005151	USP14	ERAD	0.11	0.001	0.16	0.001
NM_007126	VCP	ERAD	0.91	ns	2.12	0.001
NM_005080	XBP1	UPR	0.82	ns	1.92	0.001

U-2OS/DX580 cells were grown in fresh medium (ctrl) or in the presence of 5 μ M doxorubicin (dox) or H₂S-releasing doxorubicin (Sdox) for 24 h. Fold-Change ($2^{(-\Delta\Delta Ct)}$) is the normalized gene expression ($2^{(-\Delta Ct)}$) in dox- or Sdox-treated cells, divided the normalized gene expression ($2^{(-\Delta Ct)}$) in untreated U-2OS/DX580 cells, where Ct is the threshold cycle in qRT-PCR (n=6). Fold-change values greater than 1 indicate up-regulation, fold-change values less than 1 indicate down-regulation. The p values are calculated based on a Student's t-test of the replicate $2^{(-\Delta Ct)}$ values for each gene. $p < 0.05$ was considered significant. ERAD: ER-associated degradation; UPR: unfolded protein response; ERQC: ER-quality control.

A

ERAD/ERQC



B

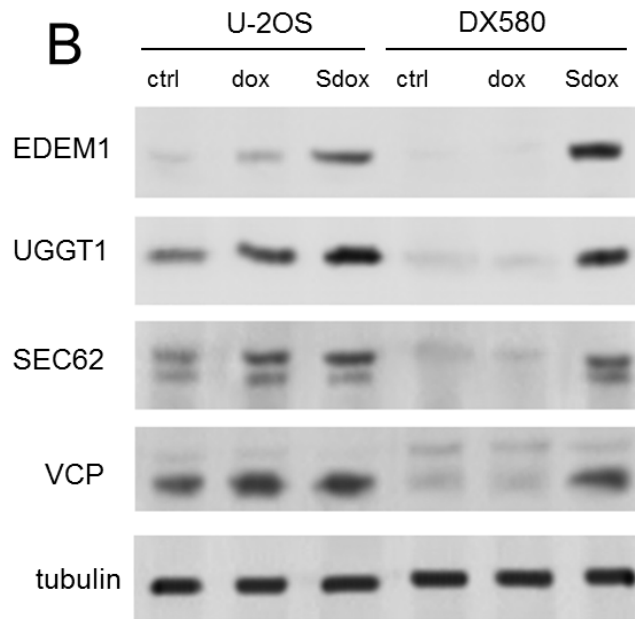


Figure 29 A. Hitmap of ER-associated degradation/endoplasmic reticulum quality control (ERAD/ERQC)-related genes in U-2OS and U-2OS/DX580 cells, after 24 h treatment with fresh medium, 5 μ M dox or Sdox. The figure reports genes up-or down-regulated at least two-fold, in at least one cell line, compared to untreated U-2OS cells (n=6). The expression of each gene in U-2OS cells was considered 1 (not shown in the figure). The whole list of genes analyzed is reported in Tables 11-12. **B.** Expression of the indicated ERAD/ERQC-related proteins measured by immunoblotting in U-2OS and U-2OS/DX580 cells, treated as in **A**. The β -tubulin expression was used as control of equal protein loading. The figure is representative of 1 out of 4 experiments. Ctrl: fresh medium.

3.3.4 H₂S-releasing doxorubicin increases sulfhydrated proteins of ER and promotes their ubiquitination

Since Sdox releases H₂S (Chegaev K *et al.*, J Med Chem 2016) that sulfhydrates cysteines and impairs the formation of disulfide bonds (Li L *et al.*, Annu Rev Toxicol 2011), we hypothesized that this property induces a significant misfolding of proteins synthesized within ER. We did not detect any appreciable difference of protein sulfhydration between U-2OS and U2-OS/DX580 cells, either under baseline conditions or after dox treatment (Figure 30A). By contrast, Sdox significantly increased the amount of sulfhydrated proteins in both sensitive and resistant cells: this effect was due to the release of H₂S, since it was abrogated by the co-incubation with the H₂S-scavenger hydroxy-cobalamin (Figure 30A).

U2-OS cells had low basal ubiquitination of ER-associated proteins; this ubiquitination rate was not affected by dox (Figure 30B-C). By contrast, the microsomal ubiquitinated proteins of U2-OS/DX580 cells were significantly higher, either in untreated or in dox-treated cells (Figure 30B-C), likely as a consequence of the basally low activity of ERAD/ERQC apparatus in the resistant population. Sdox increased ubiquitination of ER-associated proteins and this effect was abolished by H₂S-scavenging (Figure 30B-C), suggesting that sulfhydration was necessary to promote protein ubiquitination. The extent of ubiquitination exerted by Sdox was greater in U2-OS/DX580 cells than in U-2OS cells (Figure 30B-C), as a further confirmation of the lower efficiency of ERAD/ERQC system in U2-OS/DX580 cells.

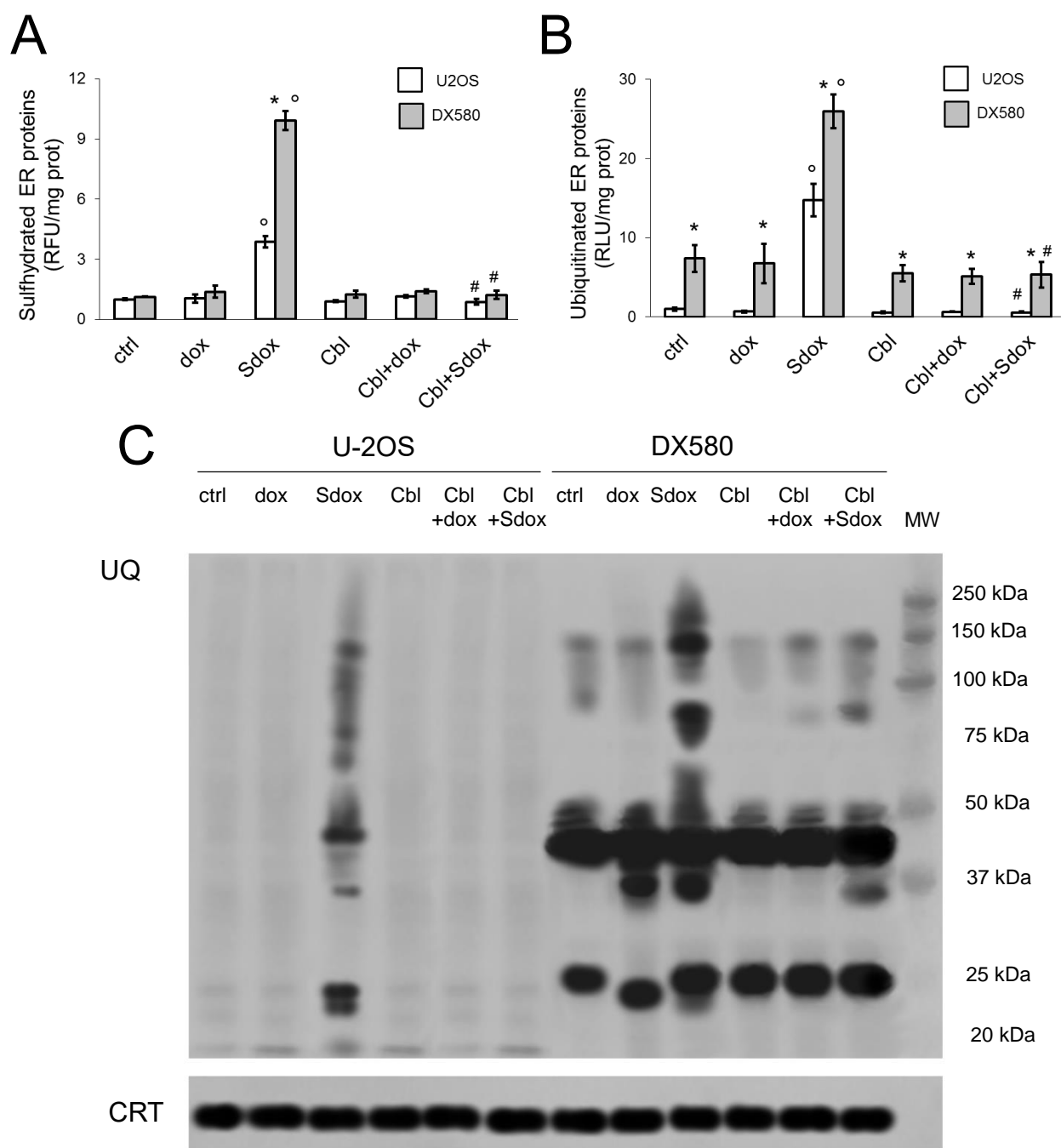


Figure 30 H₂S-releasing doxorubicin increases sulfhydrylation and ubiquitination of ER-associated proteins

U-2OS and U-2OS/DX580 cells were grown in fresh medium (ctrl) or in the presence of 5 μ M doxorubicin (dox) or H₂S-releasing doxorubicin (Sdox) for 24 h. When indicated, the H₂S-scavenger hydroxy-cobalamin (100 μ M, Cbl) was co-incubated. Cells were lysed and microsomal fractions were isolated. **A**. Fluorimetric analysis of sulfhydrated microsomal proteins, performed in triplicates. Data are means \pm SD (n=5). *p<0.001 for U-2OS/DX580

cells vs. U-2OS cells; °p<0.001 for Sdox-treated cells vs untreated (ctrl) or dox-treated cells; #p<0.001 for Cbl-treated cells vs. corresponding cells without Cbl. **B.** Ubiquitination of microsomal proteins, measured in triplicates by a chemiluminescence-based assay. Data are means±SD (n=5). *p<0.001 for U-2OS/DX580 cells vs. U-2OS cells; °p<0.001 for Sdox-treated cells vs untreated (ctrl) or dox-treated cells; #p<0.001 for Cbl-treated cells vs. corresponding cells without Cbl. **C.** Microsomal proteins were resolved by SDS-PAGE and probed with an anti-mono/poly-ubiquitin antibody. The calreticulin expression was used as control of equal protein loading. MW: molecular weight. The figure is representative of 1 out of 4 experiments.

4.3.5 H₂S-releasing doxorubicin decreases Pgp amount by promoting its sulfhydration and ubiquitination in resistant osteosarcoma cells

Pgp is synthesized in ER where it undergoes to folding and formation of disulfide bonds. This process is relevant for Pgp functions, since several cysteine residues are critical to preserve structure and catalytic activity of the protein (Pan L et Aller SG, Sci Rep. 2015 2015). Sdox strongly increased the sulfhydration of Pgp extracted from ER of U-2OS/DX580 cells (Figure 31A). This process was followed by Pgp ubiquitination (Figure 31B-C) and resulted in a decrease of Pgp amount in whole cell lysates (Figure 31D). The abrogation of all these effects by hydroxy-cobalamin indicated that H₂S is responsible for the sulfhydration and subsequent ubiquitination of Pgp. As a result, the amount of Pgp on cell surface, that was higher in U-2OS/DX580 cells compared to U-2OS cells, returned to the same levels of sensitive cells in resistant cells treated with Sdox (Figure 31E). The lower amount of Pgp on cell surface may explain the lower V_{max} of dox-efflux observed in U-2OS/DX580 cells treated with Sdox.

Figure 31 H₂S-releasing doxorubicin decreases Pgp by inducing its sulfhydration and ubiquitination

U-2OS/DX580 cells were grown in fresh medium (ctrl) or in the presence of 5 μ M doxorubicin (dox) or H₂S-releasing doxorubicin (Sdox) for 24 h. When indicated, the H₂S-scavenger hydroxy-cobalamin (100 μ M, Cbl) was co-incubated. **A.** Pgp was isolated by immunoprecipitation; the amount of sulfhydrated Pgp was measured fluorimetrically in triplicates. Data are means \pm SD (n=5). *p<0.001 for Sdox-treated cells vs untreated (ctrl) or dox-treated cells; °p<0.001 for Cbl-treated cells vs. corresponding cells without Cbl. **B.** Ubiquitinated Pgp, measured in triplicates by a chemiluminescence-based assay. Data are means \pm SD (n=5). *p<0.001 for Sdox-treated cells vs untreated (ctrl) or dox-treated cells; °p<0.001 for Cbl-treated cells vs. corresponding cells without Cbl. **C.** Microsomal proteins were immunoprecipitated (IP) with an anti-Pgp antibody, then immunoblotted (IB) with an anti-mono/poly-ubiquitin antibody. The caltreticulin expression was used as control of equal protein loading. The figure is representative of 1 out of 4 experiments. no Ab: untreated U-2OS/DX580 cell lysate immunoprecipitated in the absence of antibody, to check the specificity of the procedure. MW: molecular weight. The figure is representative of 1 out of 4 experiments. **D.** Expression of Pgp in whole lysate derived from cells treated as reported in **A.** U-2OS cells were used as control of lowly-expressing Pgp. **E.** Surface Pgp in U-2OS and U-2OS/DX580 cells, treated as reported in **A.**, measured in duplicates as per flow cytometry. Blank: cells incubated with not-immune isotypic antibody. Histograms are representative of 1 out of 5 experiments.

4.3.6 H₂S-releasing doxorubicin triggers ER-dependent apoptosis in drug-resistant osteosarcoma cells

Since UPR may trigger either cell death or cell survival (Kim, 2008; Chevet, 2015), we finally investigated which type of response was induced by Sdox.

As shown in Tables 11-12 and Figure 32A, Sdox up-regulated the expression of UPR sensors (e.g. *HSPA5/GRP78*, *EIF2AK3/PERK*, *ERN1/IRE1 α* , *ATF6*) and effectors (e.g. *ATF4*, *XBP1*, *CEBPB*, *DDIT3/CHOP*, *TRIB3*, *HERPUD1*) in both U-2OS and U2-OS/DX580 cells. A similar trend was elicited by dox in sensitive cells, not in resistant ones (Tables 11-12; Figure 32A). Sdox-treated cells increased the expression of the GRP78/Bip, an upstream sensor of UPR (Chevet E *et al.*, *Cancer Discov* 2015) (Figure 32B), suggesting that cells exposed to the drug underwent to ER stressing conditions. GRP78/Bip increase was paralleled by the increase of the main ER stress effectors, as demonstrated by the activation of IRE1 α /XBP-1 axis, PERK/phosphor(Ser51)eiF2 α /ATF4 axis and ATF6 (Figure 32B). ATF6 was clearly cleaved (Figure 32B), a step that up-regulates several ERAD-related and UPR-related genes (Kim I *et al.*, *Nat Rev Drug Discov* 2008).

It is known that a huge ER stress due to oxidative protein damages elicits ICD (Galluzzi L *et al.*, *Nat Rev Immunol.* 2017): contrarily to what observed with mtDox, cells treated with Sdox did not show significant increase of CRT translocation nor were more phagocytized than untreated cells (data not shown). Although we did not investigate this issue, we cannot exclude that the “reductive stress” induced by Sdox within ER lumen alter CRT folding and proper translocation on cell surface. Since Sdox did not mediate cytotoxicity through ICD, we focused on possible pro-apoptotic pathways activated in response to ER stress that may be induced by Sdox.

Prolonged activation of UPR effectors increases the expression of the pro-apoptotic isoform of C/EBP- β (i.e. C/EBP- β LIP) and of its downstream effector CHOP (Chiribau C *et al.*, *Mol Cell Biol* 2010; Riganti C *et al.*, *J Natl Cancer Inst* 2015). CHOP is known to activate TRB3 (Li T *et al.*, *Autophagy* 2013) and PUMA (Cazanave SC *et al.*, *Am J Physiol Gastrointest Liver Physiol.* 2010) that trigger caspase-mediated apoptosis (Li J *et al.*, *JBC* 2006; Cazanave SC *et al.*, *J Lipid Res* 2011). In U-2OS/DX580 cells Sdox increased the amount of C/EBP- β LIP and CHOP levels (Figure 32B), the nuclear translocation of CHOP (Figure 32C), the expression of TRB3 and PUMA, and the cleavage of caspase 12, 7 and 3 (Figure 32D). Interestingly, all Sdox effects were exerted with the same extent in dox-sensitive and dox-resistant cells. By contrast, dox activated these pathways only in sensitive population (Figure 32B-D).

The ER stress-triggered apoptosis induced by S-dox was confirmed by the up-regulation of several cell death-inducing genes (e.g. *BAX*, *BEX2*, *CREB3*, *ERN2*, *HTRA2*, *UHRF1*) coupled with the concomitant down-regulation of pro-survival genes (e.g. *DNAJB9*, *MAPK8*, *PCNA*, *PPP1R15A*, *RRM2*) (Tables 11-12; Figure 33) in both sensitive and resistant osteosarcoma cells. Once again, dox induced a gene signature similar to Sdox in sensitive cells, while its effects in resistant cells were not univocal, since it increased either cell death-related or cell survival-related genes (Tables 11-12; Figure 33).

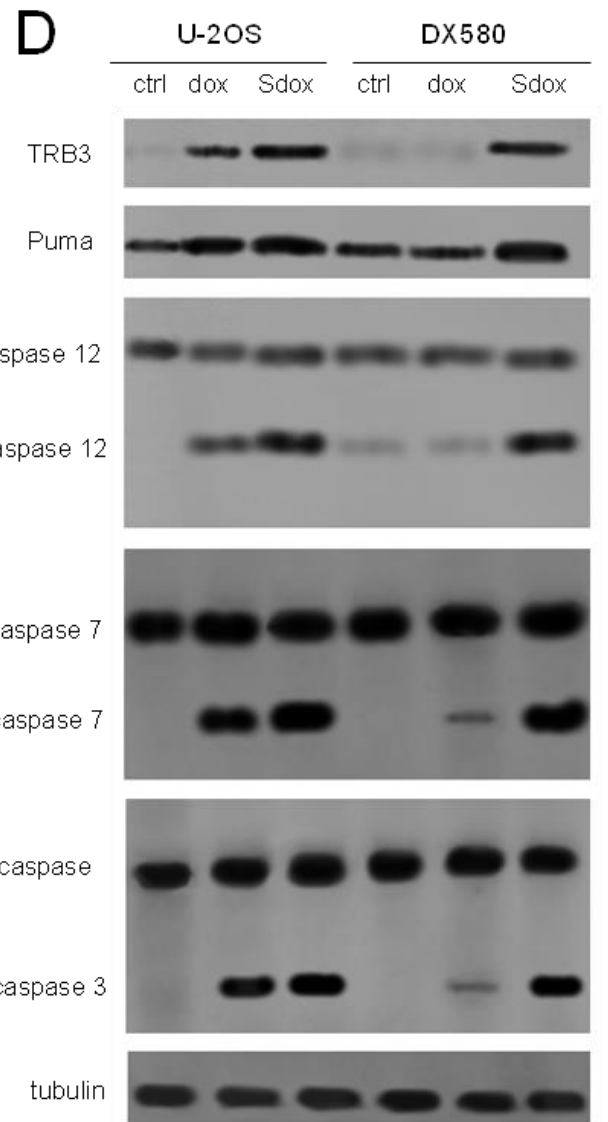
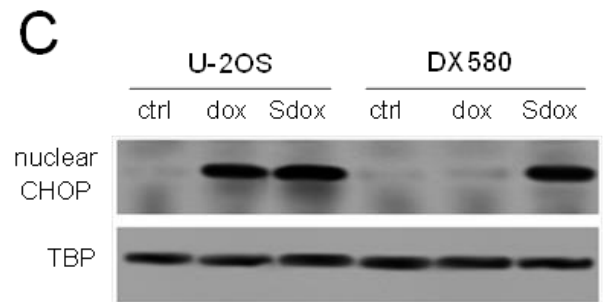
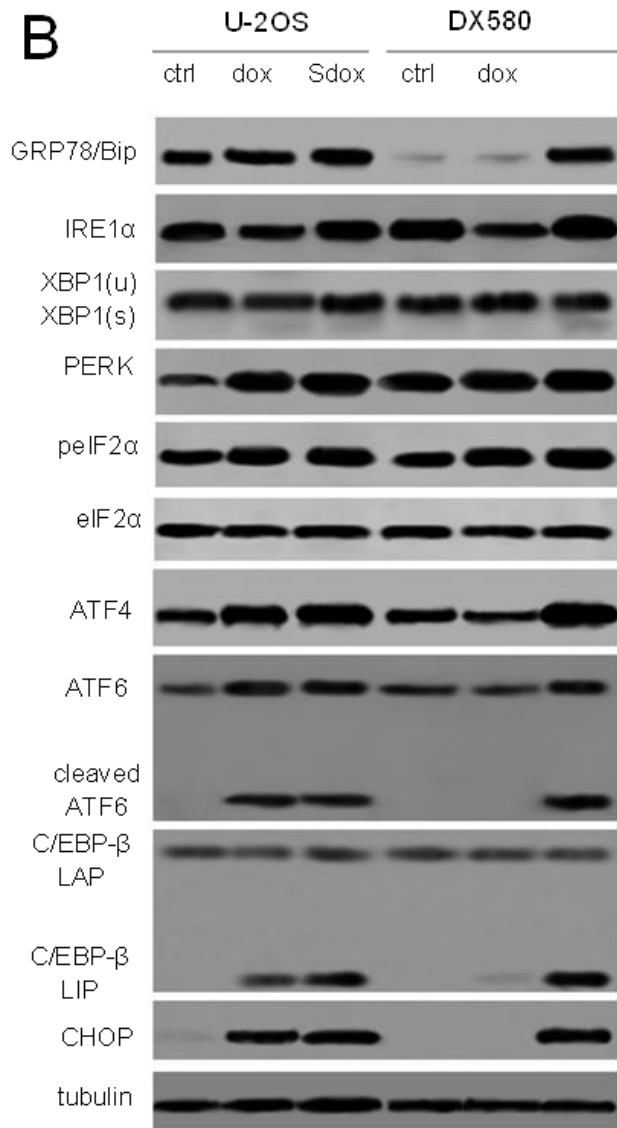
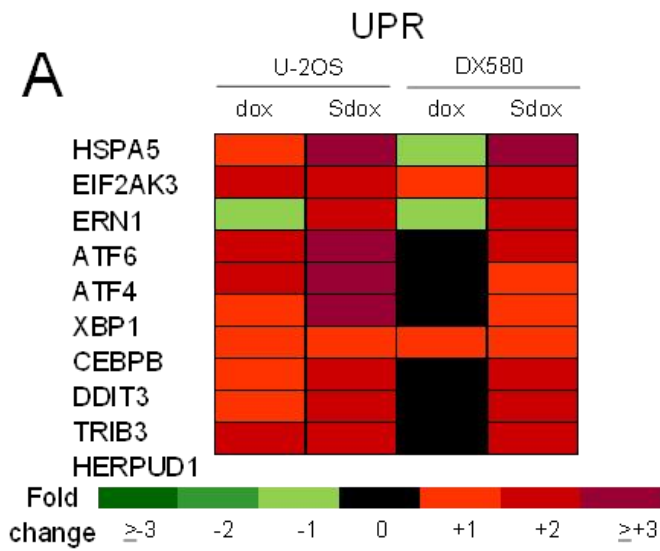


Figure 32 H₂S-releasing doxorubicin triggers ER-dependent pro-apoptotic pathways in resistant osteosarcoma cells

A. Hitmap of unfolded protein response (UPR)-related genes in U-2OS and U-2OS/DX580 cells, after 24 h treatment with fresh medium, 5 μ M doxorubicin (dox) or H₂S-releasing doxorubicin (Sdox). The figure reports genes up-or down-regulated at least two-fold, in at least one cell line, compared to untreated U-2OS cells (n=6). The expression of each gene in U-2OS cells was considered 1 (not shown). The whole list of genes analyzed is reported in Supplementary Tables 11-12. **B.** Cells treated as in **A** were lysed and probed with the indicated antibodies. The β -tubulin expression was used as control of equal protein loading. The figure is representative of 1 out of 4 experiments. XBP1(u): unspliced; XBP1(s): spliced. **C.** CHOP amount measured in nuclear extracts of cells treated as reported in **A**. The TBP expression was used as control of equal protein loading. The figure is representative of 1 out of 4 experiments **D.** Whole cell lysates from cells treated as indicated in **A** were probed with the indicated antibodies. The β -tubulin expression was used as control of equal protein loading. The figure is representative of 1 out of 4 experiments. Ctrl: fresh medium.

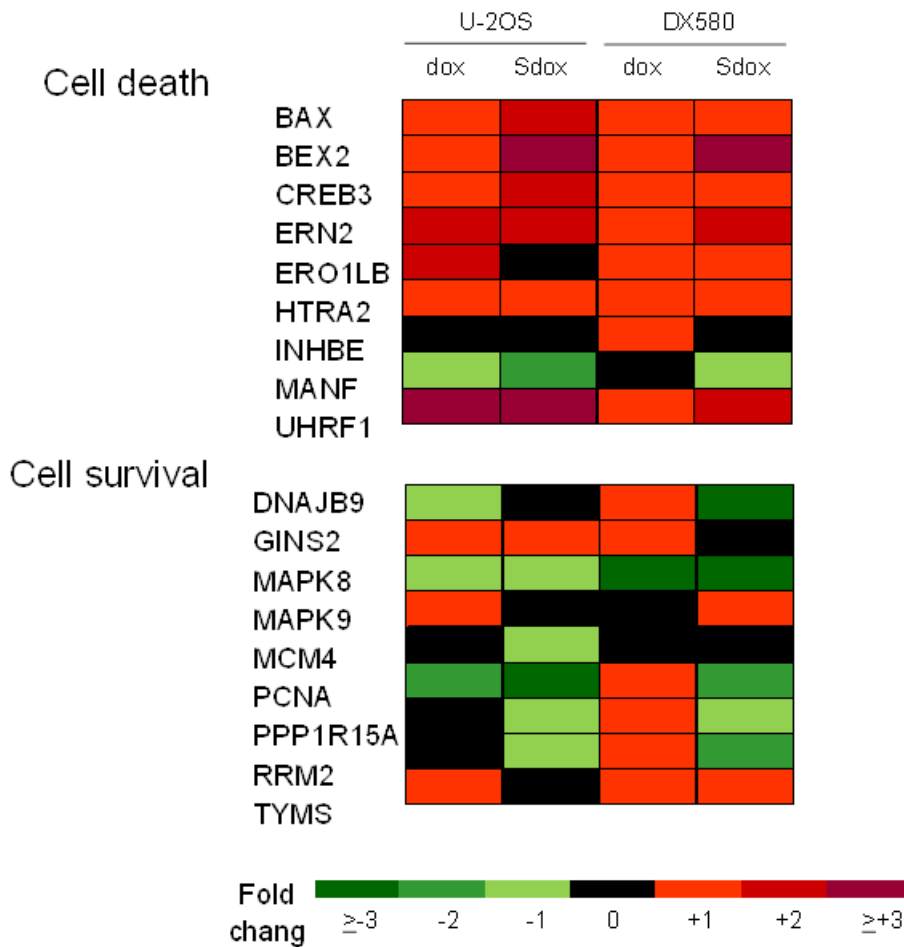


Figure 33 Expression of genes related to cell death and survival in doxorubicin-sensitive and doxorubicin-resistant osteosarcoma cells

Hitmap of genes related to cell death/survival in U-2OS and U-2OS/DX580 cells, after 24 h treatment with fresh medium, 5 μ M doxorubicin (dox) or H₂S-releasing doxorubicin (Sdox). The figure reports genes up-or down-regulated at least two-fold, in at least one cell line, compared to untreated U-2OS cells (n=6). The expression of each gene in U-2OS cells was considered 1 (not shown). The whole list of genes analyzed is reported in Tables 11-12.

4.3.7 H₂S-releasing doxorubicin is effective against doxorubicin-resistant osteosarcoma *in vivo*

We finally validated the efficacy of Sdox *in vivo*, using the model of dox-resistant K7M2 subcutaneously implanted in BALB/c mice. In this model, 5 mg/kg, one a week for 3 consecutive weeks, a dosage that was near the maximum tolerated dose for animals, did not reduce tumor growth (Figure 34A-B). By contrast, Sdox at the same dosage drastically reduced tumor development (Figure 34A-B). Moreover, while Dox induced cardiotoxicity as indicated by the increase in CPK, a sensitive index of cardiac damage, Sdox did not display any sign of cardiac or systemic toxicity, according to the hematochemical parameters measured at the end of treatment (Table 13).

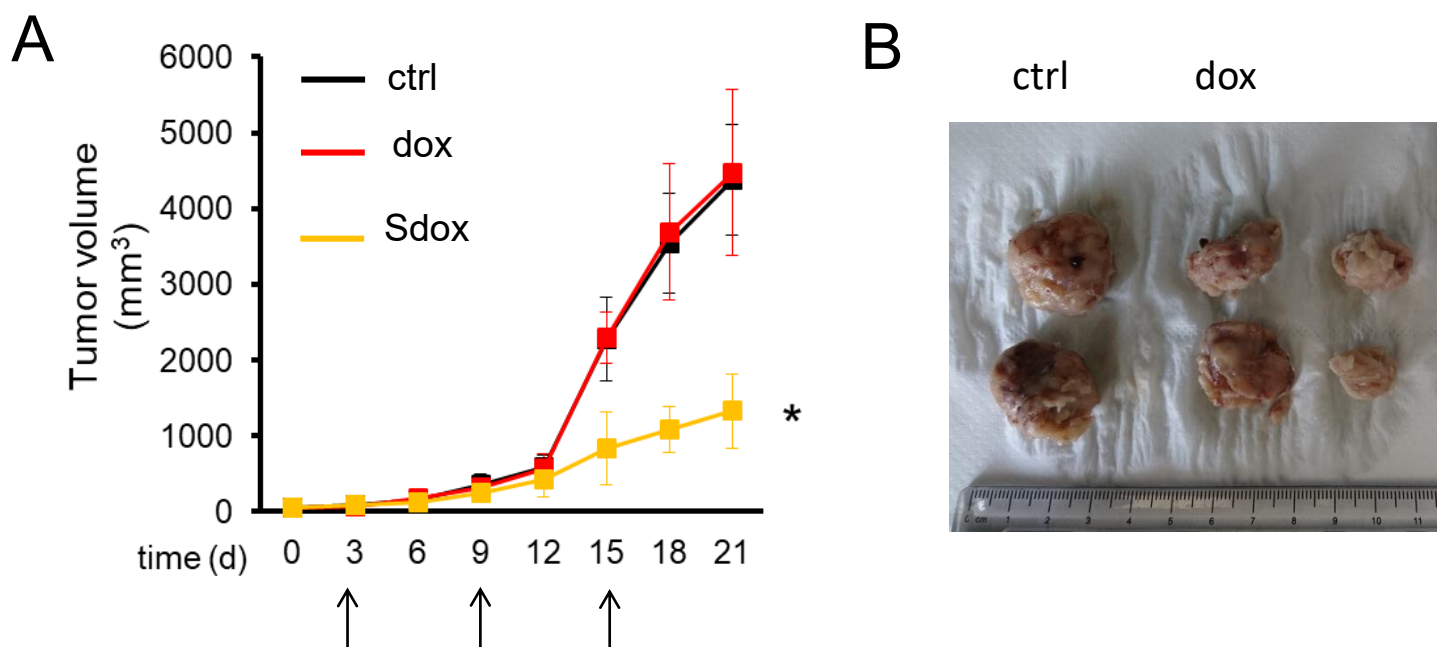


Figure 34 H₂S-releasing doxorubicin is effective against drug-resistant osteosarcoma *in vivo*. Six weeks-old female BALB/c mice were inoculated s.c. with 1×10^6 K7M2 cells. When the tumor reached the volume of 50 mm³ (day 7), the animals were randomized and treated as detailed under Materials and methods (10 mice/group). A. Tumor growth monitored by caliper measure. Arrows represent saline, doxorubicin (dox) or H₂S-releasing doxorubicin injections (Sdox). Data are presented as means \pm SD. Versus Ctrl group: * $p < 0.001$; Sdox group versus Dox group: ° $p < 0.001$. B. Photograph of representative tumors from each treatment group after mice sacrifice.

Table 13. Hematochemical parameters of animals

	Ctrl	dox	Sdox
LDH (U/L)	6211 ± 678	6273± 1082	5872 ± 428
AST (U/L)	109 ± 37	128 ± 43	134 ± 56
ALT (U/L)	45 ± 10	37 ± 11	41 ± 8
AP (U/L)	97 ± 14	89 ± 6	88 ± 12
Creatinine (mg/L)	0.037 ± 0.009	0.041 ± 0.010	0.034 ± 0.006
CPK (U/L)	289 ± 109	768 ± 132 *	311 ± 48 °

Animals (n = 10/group) were treated as reported under Materials and methods. Blood was collected immediately after mice euthanasia and analyzed for lactate dehydrogenase (LDH), aspartate aminotransferase (AST), alanine aminotransferase (ALT), alkaline phosphatase (AP), creatinine, creatine phosphokinase (CPK). Ctrl: mice treated with saline solution; dox: mice treated with doxorubicin; Sdox: mice treated with H₂S-releasing doxorubicin. Versus Ctrl group: *p < 0.005; Sdox group versus Dox group: ° p < 0.005.

5. Discussion

Osteosarcoma is the most frequent bone tumor and is usually treated with multiagent pre- and post-operative chemotherapy, in which Dox is one of the leader drugs, together with cisplatin and methotrexate, in association to the surgical removal of the tumor. Unfortunately, this multimodal treatment achieves control disease in no more than 60% of conventional osteosarcoma patients. The presence of Pgp is a negative prognostic factor in osteosarcoma patient because it impairs the efficacy of Dox. Despite alternative therapeutic strategies, the prognosis of osteosarcoma has not significantly improved in the last decades (Hattinger CM *et al.*, Expert Opin Emerg Drugs 2015; Hattinger CM *et al.*, Future Oncol. 2017).

In my PhD thesis I focused on two intracellular compartments – mitochondria and ER – that sporadic evidences from our research group and other groups has highlighted as key determinants in acquisition and maintenance of a chemoresistant phenotype. Instead of using a conventional approach – i.e. the use of pharmacological inhibitors of Pgp that have repeatedly failed in improving chemotherapy outcome – I validated the efficacy of synthetic multitarget Dox-derivatives, designed to be delivered in mitochondria and ER, respectively, and to impair the functions of these organelles. The goal of this thesis was the in vitro and preclinical validation of these synthetic chemotherapeutic drugs as agents that:

- bypass the resistance mediated by Pgp without direct targeting the transporters, but exploiting the peculiar biochemical and functional processes related to mitochondria and ER of chemoresistant cells that sustain Pgp activity, thus obtaining the reduction of Pgp activity/expression in osteosarcoma cells expressing this transporter;
- are particularly effective against Pgp-expressing/Dox-resistant osteosarcoma cells;
- have reduced cytotoxicity against not-transformed tissues and less side-effects than Dox.

Targeting mitochondria of osteosarcoma cells has been proposed as an effective therapeutic strategy (Armstrong J *et al.*, Curr Drug Targets 2015).

We used chemically modified Dox with a mitochondrial tropism against Dox-sensitive and Dox-resistant osteosarcoma cells. This modified mtDox was effective against osteosarcoma cells overexpressing Pgp and showing resistance to Dox.

The selective delivery into the mitochondria, due to the conjugation of the anthracycline moiety with a peptide containing cationic and hydrophobic residues that deliver cargoes into mitochondria, may limit the availability of Dox for the Pgp on the plasma membrane, reducing the efflux of the drug from tumor cells (Chamberlain GR *et al.*, ACS Chem Biol 2013). Our work supports this hypothesis. Unlike Dox, mtDox was well retained within

mitochondria in both drug-sensitive and drug-resistant/Pgp-overexpressing osteosarcoma cells. Although Dox accumulation and cytotoxic efficacy dramatically decreased in the Pgp-overexpressing variants, mtDox accumulation within resistant cells was only slightly lower, and its cytotoxicity remained high in Pgp-overexpressing cells. Although these data might suggest that Pgp effluxes both mtDox and Dox, the preferential intramitochondrial delivery of the former preserves its high intracellular retention.

The higher the intracellular accumulation of Dox, the higher the ability of the drug to kill cancer cells due to the induction of necro-apoptotic death and activation of the host immune system against the tumor, via the release of ATP and HMGB1, and the exposure on the plasma membrane of calreticulin/CRT, which activates the local DCs to phagocytize tumor cells (De Boo S *et al.*, Mol Cancer 2009). Mitochondrial depolarization, changes in calcium homeostasis, and increased ROS levels have also been correlated with CRT upregulation and translocation from (ER) to the plasma membrane (Biswas G *et al.*, Gene 2005 ; Zhang Y *et al.*, J Invest Dermatol 2014). Indeed, changes in intramitochondrial calcium and ROS are "sensed" by the ER membrane-associated to mitochondria (MAM) compartment, which is rich in CRT and controls the protein trafficking to the plasma membrane (Poston CN *et al.*, J Proteomics 2013). Because mtDox depolarized mitochondria and increased ROS in both drug-sensitive and drug-resistant osteosarcoma cells, these events likely trigger the upregulation of CRT and/or its translocation from ER/MAM to the plasma membrane.

The efficacy of mtDox was validated in a preclinical model of Dox-resistant osteosarcoma implanted in immunocompetent animals, i.e., the Pgp-expressing K7M2 cells that are syngeneic with BALB/c mice. In both in vitro and in vivo assays, mtDox exerted direct cytotoxicity on tumor cells (as indicated by the reduced tumor growth and cell proliferation, and by the increased apoptosis) and primed tumor cells for the recognition by the host immune system (as suggested by the increased percentage of CRT-positive tumor cells, tumor cell phagocytosis, and intratumor DC infiltration). Moreover, mtDox retained antitumor efficacy at 1/2 to 1/5 of the Dox maximum tolerated dose (5 mg/kg, once/week, for 3 consecutive weeks) that was ineffective in vivo against Dox-resistant osteosarcomas. Importantly, unlike the mice treated with Dox, those treated with mtDox did not show any increase in CPK. These results are in accordance with previous observations, showing that mtDox did not exert systemic and cardio-specific toxicity in vivo (Jean SR *et al.*, ACS Chem Biol 2015), and with the reduced toxicity observed by us in cultured cardiomyocytes. In preclinical models, mtDox was more advantageous than Dox in drug-resistant tumors, not in drug-sensitive ones, leading to hypothesize that the greater efficacy of mtDox was due to

the targeting of pathways which are crucial for the survival of drug-resistant cells. The increase of Dox resistance was associated with the upregulation of genes controlling mitochondrial biogenesis, the import of proteins, metabolites and cofactors, and energy metabolism, and with the downregulation of genes encoding for uncoupling proteins. This signature made the mitochondrial metabolism of Dox-resistant osteosarcoma cells more efficient, as confirmed by the higher content of mitochondrial DNA and proteins, and by the higher metabolic flux through the main energy pathways in U-2OS/DX580 cells. It is noteworthy that genes encoded by both nuclear and mitochondrial DNA were upregulated in drug-resistant cells. These results suggest that the higher mitochondrial metabolism of drug-resistant cells was supported partly by the increased mitochondria biogenesis and partly by the increased import of cytosolic proteins and metabolites within mitochondria. This process may favor a more efficient assembly of mitochondrial complexes involved in the TCA cycle, fatty acids β -oxidation, electron transport, and ATP synthesis, and may supply all these pathways with anaplerotic metabolites and essential cofactors. Contrarily to most tumor cells, which obtain energy from anaerobic glycolysis, chemoresistant cells often simultaneously activate glycolysis and oxidative phosphorylation to meet their energy requirements (Martinez-Outschoorn UE *et al.*, Cell Cycle 2011). The higher ATP level produced by mitochondrial oxidative phosphorylation may support the ATP-dependent efflux activity of ABC transporters, contributing to the chemoresistant phenotype.

On the other hand, a high proton motive force induces a high production of ROS from mitochondria (Mailloux RJ et Harper ME, Trends Endocrinol Metab 2012). We did not detect any differences in intramitochondrial ROS between U-2OS and U-2OS/DX580 cells, which was most likely due to the upregulation of mitochondrial SOD2 in the latter: this feature may also contribute to chemoresistance.

Dox acts through pleiotropic mechanisms on tumor cells, including mitochondrial-dependent mechanisms. For example, it reduces the activity of complexes I, II, and III (Marcillat O *et al.*, Biochem J 1989) and the synthesis of ATP (Strigun A *et al.*, Toxicol Sci 2012), and increases intramitochondrial ROS through iron-catalyzed redox cycles within complex I (Simunek T *et al.*, Pharmacol Rep 2009). In sensitive osteosarcoma cells, Dox downregulated specific metabolite transporters, subunits of mitochondrial respiratory complexes and ATP synthase, cytosolic and mitochondrial isoforms of SOD, and upregulated uncoupling proteins and proapoptotic factors. The consequent reduction of mitochondria biogenesis and ATP synthesis, coupled with the increase in intramitochondrial ROS, triggered a mitotoxicity-dependent apoptosis. None of these events occurred in the

drug-resistant U-2OS/DX580 variant, where Dox did not reach an intracellular concentration sufficient to elicit effects at genomic and metabolic levels.

By contrast, mtDox produced genomic and metabolic signatures that were similar in drug-sensitive and drug-resistant osteosarcoma cells. By downregulating genes involved in mitochondria biogenesis and mitochondrial protein import, it significantly reduced mitochondrial DNA and protein contents. Previously, it was reported that in cardiomyocytes, mtDox decreased mitochondrial DNA after 6 hours and increased it after 24 hours: this trend suggests a recovery from the initial damage due to mitochondrial biogenesis. On the contrary, in ovarian cancer cells, mitochondrial DNA levels remained significantly lower after 24 hours of treatment with mtDox, indicating that tumor cells are not able to increase mitochondria biogenesis in response to mtDox (Jean SR *et al.*, ACS Chem Biol 2015). These findings are in line with the results obtained in osteosarcoma cells. The different response of cardiomyocytes and tumor cells to the mitochondrial damage elicited by mtDox may explain the key properties of mtDox, i.e., its antitumor efficacy and its cardiac safety.

By decreasing the expression of several transporters and subunits of oxidative phosphorylation complexes, mtDox strongly reduced the mitochondrial energy metabolism. It is noteworthy that it upregulated the expression of uncoupling proteins and proapoptotic factors, and markedly decreased the expression of mitochondrial SOD2. These events uncoupled oxidative phosphorylation from ATP synthesis and increased the intramitochondrial levels of ROS, which were not buffered by SOD2. This metabolic dysfunction causes the opening of the mitochondrial permeability transition pore and triggers a mitochondria-dependent apoptosis. The simultaneous downregulation of antiapoptotic genes further supported the apoptotic process. The events described above were more pronounced in Dox-resistant cells than in Dox-sensitive ones, in accordance with the higher mitochondrial metabolic activity of the former. Of note, mtDox was relatively nontoxic in nontransformed osteoblasts.

On the one hand, the lower uptake of mtDox by nontransformed cells may explain the reduced toxicity; on the other hand, osteoblasts are more dependent on anaerobic glycolysis than on mitochondrial metabolism for their growth and differentiation (Esen E *et al.*, Cell Metab 2013 ; Regan JN *et al.*, Proc Natl Acad Sci U S A 2014). These factors may explain the relatively selective cytotoxicity of mtDox for tumor cells over nontransformed cells. Despite their resistance to chemotherapy, drug-resistant tumors are more susceptible than drug-sensitive ones to the depletion of ATP and to the increase of ROS, an event known as "collateral sensitivity" (Pluchino KM *et al.*, Drug Resist Updat 2012). Agents that lower

intracellular ATP and/or increase ROS levels are effective against chemoresistant cells in vitro. Unfortunately, the intrinsic toxicity of these agents limits their use in vivo (Callaghan R *et al.*, Drug Metab Dispos 2014). However, thanks to its ability to lower the levels of ATP produced by oxidative phosphorylation and increase ROS levels within drug-resistant cells, mtDox is an excellent inducer of CS. Unlike the other compounds exerting CS, it did not produce appreciable toxicity for the liver, kidneys, or heart in our preclinical model of resistant osteosarcoma, thus appearing suitable for being used in vivo.

The novelty of the therapeutic strategy based on mtDox relates to two factors. First, we used a derivative of the first-line drug Dox, the efficacy of which is limited by the expression of Pgp in osteosarcoma cells and by the development of cardiotoxicity: by chemically modifying Dox to achieve its selective delivery into mitochondria, we overcame a key limitation frequently encountered in patients treated with Dox-based regimens. Second, mtDox exploited a metabolic signature typical of chemoresistant cells—i.e., the hyperactive mitochondrial metabolism—and hit energy pathways that are crucial for drug resistant tumors. This drug conjugate produced promising results that may be applied to the treatment of Pgp-expressing osteosarcomas. These results may pave the way for the potential use of mtDox in clinical settings, in particular for patients with Pgp-positive osteosarcomas or as a possible second-line treatment for relapsed patients

In the second part of this PhD thesis we investigated the pharmacodynamic properties of Sdox, a H₂S-releasing dox that was less cardiotoxic thanks to its ability to reduce the Dox-mediated increase in intracellular ROS via the H₂S-releasing moiety, but it retained its efficacy against Pgp-expressing osteosarcoma cells.

Sdox intracellular retention was only slightly decreased notwithstanding the increase of Pgp in resistant sublines, where Dox accumulation was dramatically reduced. The results with the Pgp-inhibitor verapamil – that increased the intracellular accumulation of Dox but not of Sdox – suggested that Sdox is not likely effluxed by Pgp and may explain why the retention of Sdox was minimally affected by the presence of Pgp. This hypothesis is supported by the experimental findings of kinetics efflux: Sdox had a significantly higher K_m for Pgp compared to dox, suggesting that it is a poorer substrate than Dox for Pgp. Interestingly, the V_{max} of Sdox efflux, that reflects the amount of active Pgp, was also lower for Sdox, suggesting that the drug may also affect the levels of Pgp present on cell surface. Being less effluxed than Dox, the intracellular concentration of Sdox likely was above the „threshold” concentration

to induce toxicity, as demonstrated by the fact that Sdox induced cell damage and reduced cell viability in all the resistant populations.

It has been reported that H₂S may induce chemoresistance, by reducing the oxidative damages induced by many chemotherapeutic drugs (Sen, FRBM2015). In contrast with these observations, we found that Sdox was cytotoxic notwithstanding the reduction of intracellular ROS and that the drug's cytotoxicity was reduced by H₂S scavenging. Differently from most works using H₂S donors, we used a hybrid compound containing a H₂S-releasing group linked with Dox, which can trigger redox cycles and increase the synthesis of reactive nitrogen species like nitric oxide (Simunek T *et al.*, Pharmacol Rep 2009) Under these conditions, H₂S shifts from an anti-oxidant to a pro-oxidant molecule, promotes the synthesis of radical species and induces cell damage (Bruce King S *et al.*, Free Radic Biol Med 2013). In line with our data, H₂S-releasing valproic acid exerted cytotoxic effects in lung cancer cells, by impairing the mitochondrial redox balance (Tesei A *et al.*, 2012).

Altering the homeostasis of intracellular compartments of drug-resistant cells is an effective strategy to overcome resistance, as demonstrated in the first part of my thesis.

Sdox had a peculiar localization within ER: this finding may justify why Sdox was less available for Pgp efflux and thus still retained within Pgp-expressing cells. Moreover, the presence of Sdox, that can act either as pro- or anti-oxidant agents within ER, the compartment where cellular proteins are synthesized and folded, led us to investigate which effects were exerted by the drug on ER functions.

We first analyzed potential differences in ER functions between sensitive and resistant osteosarcoma cells. As demonstrated by our research group, multiple linkages exist between ER functions and chemoresistance. On the one hand, cells with constitutive or acquired chemoresistance due to Pgp expression are refractory to ER stress-triggered cell death, because they fail to activate ER-dependent apoptotic pathways (Riganti C *et al.*, J Natl Cancer Inst 2015). On the other hand, cancer cells adapted to survive under chronic ER stressing conditions acquire a chemoresistant phenotype (Salaroglio IC *et al.*, Mol Cancer 2017). Cells able to survive under stressing conditions moderately activate the ERQC program and/or promote ERAD pathways to remove misfolded proteins. If these integrated programs fail, ER stress induces apoptotic pathways such as the C/EBP- β /CHOP/TRB3/caspase 3 axis (Meir O *et al.*, Plos One 2011; Hetz C *et al.*, Nat Rev Mol Cell B 2012; Riganti C *et al.*, J Natl Cancer Inst 2015).

We found that the progressive increase of Dox-resistance in osteosarcoma cells was associated with the progressive down-regulation of ERAD/ERQC-related genes. This signature is similar to that found in Dox-resistant colon and lung cancer cells (Riganti C *et al.*, J Natl Cancer Inst 2015), suggesting that different tumor types resistant to Dox share defects in the mechanisms controlling protein folding and/or degradation of misfolded proteins. We hypothesized that these defects make resistant cells more susceptible to the apoptosis triggered by elevated unfolded proteins within ER, as it occurs in VCP-defective cells upon stress induction (Bastola P *et al.*, Mol Oncol 2016).

Dox is known to induce ER stress (Panaretakis T *et al.*, Embo J. 2009), but this response is limited to sensitive cells (Riganti C *et al.*, J Natl Cancer Inst 2015). In U-2OS cells, indeed, Dox up-regulated ERAD/ERQC system genes and proteins, suggesting that it likely damaged ER proteins that must be extracted from ER and degraded. Such compensatory response, however, was not sufficient to protect sensitive cells, that – upon Dox treatment – activated ER-dependent pro-apoptotic pathways. Differently from Dox, Sdox produced ER-dependent apoptosis in both sensitive and resistant cells. Multiple reasons may explain Sdox efficacy in both cell populations.

First, the predominant accumulation within ER increased the amount of H₂S and Dox sequestered within this compartment. Although U-2OS/DX580 cells retained less intracellular Sdox than U-2OS cells, we may suppose that the amount of Sdox retained within ER was still sufficient to elicit cytotoxic effects in resistant cells.

Second, Sdox induces a huge sulfhydrylation of ER-associated proteins. By changing the pattern of disulfide bonds and the consequent tertiary structures of proteins, sulfhydrylation can either activate or inhibit the target proteins (Li L *et al.*, Annu Rev Toxicol, 2011; Sen N *et al.*, Mol Cell 2012). In our model, sulfhydrylation is paralleled by increased ubiquitination of ER-associated proteins, suggesting that Sdox increased misfolded/unfolded proteins that are primed for the degradation.

Pgp has several cysteines whose mutations can alter catalytic function, ATP binding and protein stability (Pan L *et al.*, Sci Rep 2011; Swartz DJ *et al.*, Biosci Rep 2014). Sdox induced sulfhydrylation and ubiquitination of Pgp; these events were paralleled by reduced Pgp amount that was comparable to the amount found in U-2OS cells. This is an additional mechanism explaining why Sdox was well accumulated in Pgp-expressing U-2OS/DX580 and Sa-os2/DX580 cells. The result also explains the lower V_{max} of Sdox compared to Dox, indicative of a reduced amount of Pgp from U-2OS/DX580 cell surface.

Interestingly, Sdox induced a higher amount of sulfhydrated and ubiquitinated proteins in resistant cells than in sensitive cells. In the case of Pgp, this difference can be justified by the higher amount of the protein in U-2OS/DX580 cells. In the case of other proteins, the defective ERAD/ERQC pathways of Dox-resistant cells may explain the different phenotype, representing an Achille's heel of resistant osteosarcoma cells. As Dox did in sensitive cells, Sdox increased the expression of ERAD/ERQC-related genes in both sensitive and resistant cells, likely as a physiological consequence of the increased misfolded/unfolded proteins. Since resistant cells have a defective ERQC/ERAD system, the attempt to compensate the misfolding produced by Sdox was much more difficult than in sensitive cells. Therein, although Sdox was less accumulated in resistant cells, it was sufficient to trigger ER-dependent apoptosis.

ER stress is usually associated to conditions promoting oxidative stress, such as radiotherapy, chemotherapy, ionizing radiations, viral infections (Galluzzi L *et al.*, *Nat Rev Immunol* 2017). Our work suggests that also a strongly reductive environment within ER lumen – e.g. produced by H₂S – induces ER stress. Such ER stress was not sufficient to trigger CRT translocation from ER to cell surface followed by ICD, but was still sufficient to induce cell death.

It has been reported that H₂S activates the UPR sensor PERK by sulfhydrating the PERK activator protein tyrosine phosphatase 1B (Krishnan N *et al.*, *Sci Signal.* 2011) and modulates the expression of genes involved in UPR, metabolism, cell death and survival, by activating ATF4-dependent pathways (Gao XH *et al.*, *Elife* 2015). Consistently, Sdox up-regulated UPR-related genes and increased the ratio cell death-related genes/cell survival-related genes. The ER-dependent pro-apoptotic pathways induced by Sdox in sensitive and resistant cells were the same pathways induced by Dox in sensitive cells, suggesting that both drugs activated the same ER stress-dependent cell death effectors, although they have different upstream mechanisms (Panaretakis T *et al.*, *Embo J.* 2009 ; Riganti C *et al.*, *J Natl Cancer Inst* 2015).

A preliminary *in vivo* experimental set validated the efficacy of Sdox in Dox-resistant osteosarcoma models as an effective tool able to reduce tumor growth, without inducing significant systemic toxicities. These data open the way to further investigations to assess whether also *in vivo* the higher efficacy of Sdox was due to the same ER stress-dependent mechanisms observed *in vitro*.

Conclusions and future perspectives

Overall, the novelty of using mtDox and Sdox as therapeutic strategies for osteosarcoma relies on this point: by chemically modifying the first-line option Doxorubicin to achieve its selective delivery into mitochondria or ER, we limited the drug efflux via Pgp and triggered a mitochondria- or ER-dependent cell death, exploiting specific metabolic features of Dox-resistant cells (such as the increased mitochondrial metabolism that was coupled with increased susceptibility to mitochondrial-ROS damages; the defective ERAD/ERQC system that make resistant cells less susceptible to be damaged by increased unfolded/misfolded proteins within ER lumen). Targeting these peculiar features of Dox-resistant osteosarcoma allowed to spare not-transformed bone or other organs, such as heart, from the undesired side-effects exerted by Dox. Thus, our strategies overcame the two limitations most frequently encountered in patients treated with Dox-based regimens, i.e. cardiotoxicity and drug resistance. These results may pave the way to the potential use of mtDox and Sdox in clinical settings, in particular for patients with Pgp-positive osteosarcomas or as a possible second-line treatment for relapsed patients.

Our results will be developed into three further directions.

First, in preclinical models of resistant osteosarcoma we will investigate the efficacy of mtDox and Sdox in combination with cisplatin and methotrexate (the other two first-line treatments for osteosarcoma) or cyclophosphamide (used as second-line treatment in unresponsive patients), to exclude the presence of undesired and unfavourable drug-drug interactions and validate our approach as more effective than the standard therapeutic regimens.

Second, since – at least in the case of mtDox – part of the efficacy relies on the induction of ICD, we will investigate the effects of the drug on the tumor immune-environment, by:

1) using ex vivo cocultures of human osteosarcoma cells and peripheral blood mononuclear cells (PBMC) and performing functional assays of adaptive immunity (DC maturation, expansion and activation of CD8⁺ T-lymphocytes endowed with anti-tumor activity), multiplex PCR arrays of immune-activating vs. Immune-suppressive cytokines, immunophenotyping analysis (e.g. qualitative and quantitative analysis of CD4⁺ and CD8⁺ T-lymphocytes, T-regulatory cells, Natural Killer cells, granulocytic- and monocytic-myeloid derived suppressor cells, M1- versus M2-polarized macrophages, analysis of immune-suppressive immunecheckpoints);

2) using immunocompetent mice bearing Dox-resistant osteosarcoma (i.e. K7M2 model implanted in BALB/c mice) and analyzing the intratumor immune-infiltrate and the signs of anti-tumor immune response (e.g. expansion of CD8⁺ CD107a⁺ T-lymphocytes in tumor microenvironment and IFN- γ production from draining lymph nodes).

Until now, immunotherapy or immune-adjuvant agents had obtained low success against chemoresistance osteosarcoma (Hattinger C *et al.*, Future Oncology, 2017). This study may open the field to new combination therapy based on mtDox plus immunotherapeutic agents (e.g. immunecheckpoint inhibitors that are under evaluation in Phase I trials for osteosarcoma patients), effective against the osteosarcoma refractory to conventional chemotherapy.

Third, in order to maximize the delivery of mtDox and Sdox to tumor and increase their systemic stability, we are producing liposomal formulations of these drugs, in collaboration with the Department of Drug Science and Technology, University of Torino, Prof. Silvia Arpicco. Liposomal encapsulation of a drug allows an increased passive delivery to tumor thanks to the disrupted tumor vasculature that promotes a "sink" effect toward tumor tissues, the so-called "enhanced permeability retention" (EPR) effects. An active targeting of liposomes, i.e. the conjugation of liposomes with ligands binding receptors or transporters specifically overexpressed on osteosarcoma cells will further maximize the delivery of the liposome into tumor. We are currently exploring the proteome surfaceome of human primary Dox-resistant osteosarcoma by cell-surface-capture/mass spectrometry technology, in order to pick-up suitable targets to produce conjugated-liposomes. We will then validate in vivo the efficacy of our formulations, with the goal to further reduce the minimally efficacy dose of synthetic-Doxs effective against osteosarcoma. This is particularly important, since the liposomal formulation of Dox currently used in clinical practice (Caelyx) did not show any superior benefit compared to free Dox against Pgp-expressing osteosarcoma, apart from a reduced cardiotoxicity (Hattinger C *et al.*, Future Oncology, 2017). Our formulations, that contain synthetic Doxs specifically effective against Pgp-expressing osteosarcoma cells may represent a step forward over Caelyx in the treatment of these refractory tumors.

These three future research lines will allow to better characterize the proposed synthetic Doxs, in the perspective of translating them from preclinical studies to clinical applications.

7. References

- Anninga JK, Gelderblom H, Fiocco M, Kroep JR, Taminiau AH, Hogendoorn PC, Egeler RM. Chemotherapeutic adjuvant treatment for osteosarcoma: where do we stand? *Eur J Cancer*. 2011
- Armstrong J, Dass CR. Doxorubicin action on mitochondria: relevance to osteosarcoma therapy? *Curr Drug Targets* 2015
- Bacci G, Longhi A, Ferrari S, Mercuri M, Versari M, Bertoni F. Prognostic factors in non-metastatic Ewing's sarcoma tumor of bone: an analysis of 579 patients treated at a single institution with adjuvant or neoadjuvant chemotherapy between 1972 and 1998 *Acta Oncol*. 2006
- Bastola P, Neums L, Schoenen FJ, Chien J. VCP inhibitors induce endoplasmic reticulum stress, cause cell cycle arrest, trigger caspase-mediated cell death and synergistically kill ovarian cancer cells in combination with Salubrinal. *Mol Oncol*. 2016
- Biswas G, Guha M, Avadhani NG. Mitochondria-to-nucleus stress signaling in mammalian cells: Nature of nuclear gene targets, transcription regulation, and induced resistance to apoptosis. *Gene* 2005
- Braly P, Nicodemus CF, Chu C, Collins Y, Edwards R, Gordon A, McGuire W, Schoonmaker C, Whiteside T, Smith LM, Method M. The Immune adjuvant properties of front-line carboplatin-paclitaxel: a randomized phase 2 study of alternative schedules of intravenous oregovomab chemoimmunotherapy in advanced ovarian cancer. *J Immunother*. 2009
- Bruce King S. Potential biological chemistry of hydrogen sulfide (H₂S) with the nitrogen oxides. *Free Radic Biol Med*. 2013
- Caino MC, Ghosh, JC, Chae YC, Vaira V, Rivadeneira DB, Favarsani A, Rampini P, Kossenkov AV, Aird KM, Zhang R, Webster MR, Weeraratna AT, Bosari S, Languino LR, Altieri DC. PI3K therapy reprograms mitochondrial trafficking to fuel tumor cell invasion. *Proc. Natl. Acad. Sci. USA*. 2015
- Callaghan R, Luk F, Bebawy M. Inhibition of the multidrug resistance P-glycoprotein: time for a change of strategy? *Drug Metab Dispos* 2014
- Campia I, Lussiana C, Pescarmona G, Ghigo D, Bosia A, Riganti C. Geranylgeraniol prevents the cytotoxic effects of mevastatin in THP-1 cells, without decreasing the beneficial effects on cholesterol synthesis. *Br J Pharmacol*. 2009.

- *Cazanave SC, Elmi NA, Akazawa Y, Bronk SF, Mott JL, Gores GJ. CHOP and AP-1 cooperatively mediate PUMA expression during lipoapoptosis. Am J Physiol Gastrointest Liver Physiol. 2010*
- *Cazanave SC, Mott JL, Elmi NA, Bronk SF, Masuoka HC, Charlton MR, Gores GJ. A role for miR-296 in the regulation of lipoapoptosis by targeting PUMA. J Lipid Res. 2011*
- *Chamberlain GR, Tulumello DV, Kelley SO. Targeted delivery of doxorubicin to mitochondria. ACS Chem Biol. 2013*
- *Chegaev K, Rolando B, Cortese D, Gazzano E, Buondonno I, Lazzarato L, Fanelli M, Hattinger CM, Serra M, Riganti C, Fruttero R, Ghigo D, Gasco A. H2S-Donating Doxorubicins May Overcome Cardiotoxicity and Multidrug Resistance. J Med Chem. 2016*
- *Chevet E, Hetz C, Samali A. Endoplasmic reticulum stress-activated cell reprogramming in oncogenesis. Cancer Discov 2015*
- *Chiribau C, Gaccioli F, Huang C, Yuan C, Hatzoglou M. Molecular symbiosis of chop and c/ebp beta isoform lip contributes to endoplasmic reticulum stress-induced apoptosis. Mol Cell Biol 2010*
- *Damiani D, Michelutti A, Michieli M, et al. P-glycoprotein, lung resistance related protein and multidrug resistance-associated protein in de novo adult acute lymphoblastic leukaemia. Br J Haematol. 2002*
- *De Boo S, Kopecka J, Brusa D, Gazzano E, Matera L, Ghigo D, Bosia A, Riganti C. iNOS activity is necessary for the cytotoxic and immunogenic effects of doxorubicin in human colon cancer cells. Mol Cancer. 2009.*
- *Duggan ST, Keating GM. Pegylated liposomal doxorubicin: a review of its use in metastatic breast cancer, ovarian cancer, multiple myeloma and AIDS-related Kaposi's sarcoma Drugs. 2011*
- *Esen E, Chen J, Karner CM, Okunade AL, Patterson BW, Long F. WNT-LRP5 signaling induces Warburg effect through mTORC2 activation during osteoblast differentiation. Cell Metab 2013*
- *Ferrari S, Briccoli A, Mercuri M, Bertoni F, Cesari M, Longhi A, Bacci G. Late relapse in osteosarcoma. J Pediatr Hematol Oncol. 2006*

- Galluzzi L, Buqué A, Kepp O, Zitvogel L, Kroemer G. Immunogenic cell death in cancer and infectious disease. *Nat Rev Immunol.* 2017
- Gao XH, Krokowski D, Guan BJ, Bederman I, Majumder M, Parisien M, Diatchenko L, Kabil O, Willard B, Banerjee R, Wang B, Bebek G, Evans CR, Fox PL, Gerson SL, Hoppel CL, Liu M, Arvan P, Hatzoglou M. Quantitative H₂S-mediated protein sulfhydrylation reveals metabolic reprogramming during the integrated stress response. *Elife.* 2015
- Gao Z, Zhang L, Sun Y. Nanotechnology applied to overcome tumor drug resistance. *J Control Release.* 2012
- García-Ledo L, Nuevo-Tapióles C, Cuevas-Martín C, Martínez-Reyes I, Soldevilla B, González-Llorente L, Cuezva J.M. Overexpression of the ATPase Inhibitory Factor 1 Favors a Non-metastatic Phenotype in Breast Cancer. *Front. Oncol.* 2017
- Garcia M, Jemal A, Ward EM, Center MM, Hao Y, Siegel RL, Thun MJ. Global cancer facts and figures. Atlanta, GA: *American Cancer Society*; 2007.
- Gaster M, Rustan AC, Aas V, Beck-Nielsen H. Reduced lipid oxidation in skeletal muscle from type 2 diabetic subjects may be of genetic origin evidence from cultured myotubes. *Diabetes* 2004
- Gillet JP, Efferth T, Remacle J. Chemotherapy-induced resistance by ATPbinding cassette transporter genes. *BBA-Rev. Cancer.* 2007.
- Gong J, Jaiswal R, Mathys JM, Combes V, Grau GER, Bebawy M. Microparticles and their emerging role in cancer multidrug resistance. *Cancer Treatment Reviews.* 2012
- Gottesman MM, Fojo T, Bates SE. Multidrug resistance in cancer: role of ATP-dependent transporters. *Nat Reviews* 2002
- Granados-Principal S, Quiles JL, Ramirez-Tortosa CL, Sanchez-Rovira P, Ramirez-Tortosa MC. New advances in molecular mechanisms and the prevention of adriamycin toxicity by antioxidant nutrients. *FoodChemToxicol.* 2010
- Gronthos S, Zannettino AC, Hay SJ, Shi S, Graves SE, Kortessidis A, et al. Molecular and cellular characterisation of highly purified stromal stem cells derived from human bone marrow. *J Cell Sci* 2003
- Guerra F, Arbini AA, Moro L. Mitochondria and cancer chemoresistance. *Biochim Biophys Acta.* 2017
- Guzel E, Arlier S, Guzeloglu-Kayisli O, Tabak MS, Ekiz T, Semerci N, Larsen K, Schatz F, Lockwood CJ, Kayisli UA. Endoplasmic Reticulum Stress and Homeostasis in Reproductive Physiology and Pathology. *Int J Mol Sci.* 2017

- *Hattinger CM, Fanelli M, Tavanti E, Vella S, Ferrari S, Picci P, et al. Advances in emerging drugs for osteosarcoma. Expert Opin Emerg Drugs 2015*
- *Hattinger CM, Fanelli M, Tavanti E, Vella S, Riganti C, Picci P, Serra M. Doxorubicin-resistant osteosarcoma: novel therapeutic approaches in sight? Future Oncol. 2017*
- *He YT, Zhang QM, Kou QC, Tang B In vitro generation of cytotoxic T lymphocyte response using dendritic cell immunotherapy in osteosarcoma. Oncol Lett. 2016*
- *Hetz C The unfolded protein response: controlling cell fate decisions under ER stress and beyond. Nat Rev Mol Cell Biol. 2012 .*
- *Heymann MF, Brown HK, Heymann D Drugs in early clinical development for the treatment of osteosarcoma Expert Opin Investig Drugs. 2016*
- *Hu Z, Jin S, Scotto KW. Transcriptional activation of the MDR1 gene by UV irradiation. Role of NF-Y and Sp1. J Biol Chem. 2000*
- *Hyde SC, Emsley P, Hartshorn MJ, Mimmack MM, Gileadi U, Pearce SR, Gallagher MP, Gill DR, Hubbard RE, Higgins CF. Structural model of ATP-binding proteins associated with cystic fibrosis, multidrug resistance and bacterial transport. Nature. 1990*
- *Jean SR, Tulumello DV, Riganti C, Liyanage SU, Schimmer AD, Kelley SO. Mitochondrial Targeting of Doxorubicin Eliminates Nuclear Effects Associated with Cardiotoxicity. ACS Chem Biol. 2015*
- *Kashfi K, Olson KR. Biology and therapeutic potential of hydrogen sulphide and hydrogen sulphide-releasing chimeras. Biochem. Pharmacol. 2013*
- *Kepp O, Senovilla L, Vitale I, Vacchelli E, Adjemian S, Agostinis P, Apetoh L, Aranda F, Barnaba V, Bloy N, Bracci L, Breckpot K, Brough D, Buqué A, Castro MG, Cirone M, Colombo MI, Cremer I, Demaria S, Dini L, Eliopoulos AG, Faggioni A, Formenti SC, Fučíková J, Gabriele L, Gaipf US, Galon J, Garg A, Ghiringhelli F, Giese NA, Guo ZS, Hemminki A, Herrmann M, Hodge JW, Holdenrieder S, Honeychurch J, Hu HM, Huang X, Illidge TM, Kono K, Korbelik M, Krysko DV, Loi S, Lowenstein PR, Lugli E, Ma Y, Madeo F, Manfredi AA, Martins I, Mavilio D, Menger L, Merendino N, Michaud M, Mignot G, Mossman KL, Multhoff G, Oehler R, Palombo F, Panaretakis T, Pol J, Proietti E, Ricci JE, Riganti C, Rovere-Querini P, Rubartelli A, Sistigu A, Smyth MJ, Sonnemann J, Spisek R, Stagg J, Sukkurwala AQ, Tartour E, Thorburn A, Thorne SH, Vandenabeele P, Velotti F, Workenhe ST, Yang H, Zong WX, Zitvogel L, Kroemer G, Galluzzi L. Consensus guidelines for the detection of immunogenic cell death. Oncoimmunology. 2014*

- *Kempf-Bielack B, Bielack SS, Jürgens H, Branscheid D, Berdel WE, Exner GU, Göbel U, Helmke K, Jundt G, Kabisch H, Kevric M, Klingebiel T, Kotz R, Maas R, Schwarz R, Semik M, Treuner J, Zoubek A, Winkler K. Osteosarcoma relapse after combined modality therapy: an analysis of unselected patients in the Cooperative Osteosarcoma Study Group (COSS). J Clin Oncol. 2005*
- *Kim I, Xu W, Reed J. Cell death and endoplasmic reticulum stress: Disease relevance and therapeutic opportunities. Nat Rev Drug Discov 2008*
- *Kopecka J, Campia I, Brusa D, Doublie S, Matera L, Ghigo D, Bosia A, Riganti C. Nitric oxide and P-glycoprotein modulate the phagocytosis of colon cancer cells J Cell Mol Med. 2011*
- *Kopecka J, Salzano G, Campia I, Lusa S, Ghigo D, De Rosa G, Riganti C. Insights in the chemical components of liposomes responsible for P-glycoprotein inhibition Nanomedicine. 2014*
- *Kopecka J, Porto S, Lusa S, Gazzano E, Salzano G, Giordano A, Desiderio V, Ghigo D, Caraglia M, De Rosa G, Riganti C. Self-assembling nanoparticles encapsulating zoledronic acid revert multidrug resistance in cancer cells. Oncotarget. 2015*
- *Krishnan N, Fu C, Pappin DJ, Tonks NK. H₂S-Induced sulfhydration of the phosphatase PTP1B and its role in the endoplasmic reticulum stress response. Sci Signal. 2011*
- *LeBleu VS, O'Connell JT, Gonzalez Herrera KN, Wikman H, Pantel K, Haigis MC, de Carvalho FM, Damascena A, Domingos Chinen LT, Rocha RM, Asara JM, Kalluri RPGC-1 α mediates mitochondrial biogenesis and oxidative phosphorylation in cancer cells to promote metastasis. Nat Cell Biol. 2014*
- *Lee CH. Reversing agents for ATP-binding cassette (ABC) transporters: application in modulating multidrug resistance (MDR). Curr Med Chem. 2004*
- *Li J, Lee B, Lee AS. Endoplasmic reticulum stress-induced apoptosis: multiple pathways and activation of p53-up-regulated modulator of apoptosis (PUMA) and NOXA by p53. J Biol Chem. 2006*
- *Li L, Rose P, Moore PK. Hydrogen sulfide and cell signaling. Annu Rev Pharmacol Toxicol. 2011*
- *Li T, Su L, Zhong N, Hao X, Zhong D, Singhal S, Liu X. Salinomycin induces cell death with autophagy through activation of endoplasmic reticulum stress in human cancer cells. Autophagy. 2013*
- *Longley DB, Johnston PG. Molecular mechanisms of drug resistance J Pathol. 2005*

- *Luqmani YA. Mechanisms of Drug Resistance in Cancer Chemotherapy. Med Princ Pract. 2005*
- *Ma K, Liu Y, Zhu Q, Liu CH, Duan JL, Tan BK, et al. H2S donor, S-propargylcysteine, increases CSE in SGC-7901 and cancer-induced mice: evidence for a novel anti-cancer effect of endogenous H2S? PLoS One 2011*
- *Mailloux RJ, Harper ME. Mitochondrial proticity and ROS signaling: Lessons from the uncoupling proteins. Trends Endocrinol Metab 2012*
- *Marcillat O, Zhang Y, Davies KJ. Oxidative and non-oxidative mechanisms in the inactivation of cardiac mitochondrial electron transport chain components by doxorubicin. Biochem J 1989*
- *Martinez-Outschoorn UE, Pestell RG, Howell A, Tykocinski ML, Nagajyothi F, Machado FS, et al. Energy transfer in "parasitic" cancer metabolism: mitochondria are the powerhouse and Achilles' heel of tumor cells. Cell Cycle 2011*
- *Meir O, Dvash E, Werman A, Rubinstein M. C/ebp-beta regulates endoplasmic reticulum stress-triggered cell death in mouse and human models. Plos One. 2010*
- *Minotti G, Menna P, Salvatorelli E, Cairo G, Gianni L. Anthracyclines: Molecular Advances and Pharmacologic Developments in Antitumor Activity and Cardiotoxicity. Pharmacological reviews. 2004*
- *Modica-Napolitano J, Aprille J. Delocalized lipophilic cations selectively target the mitochondria of carcinoma cells. Adv. Drug. Deliv. Rev. 2001*
- *Naidoo J, Page DB, Wolchok JD Immune modulation for cancer therapy Br J Cancer. 2014*
- *Ni Z and Mao Q ATP-Binding Cassette Efflux Transporters in Human Placenta. Curr Pharm Biotechnol. 2011*
- *Obeid M, Tesniere A, Ghiringhelli F, Fimia GM, Apetoh L, Perfettini JL, Castedo M, Mignot G, Panaretakis T, Casares N, Métivier D, Larochette N, van Endert P, Ciccocanti F, Piacentini M, Zitvogel L, Kroemer G: Calreticulin exposure dictates the immunogenicity of cancer cell death. Nature Medicine 2007*
- *Ohoka N, Yoshii S, Hattori T, Onozaki K, Hayashi H. TRB3, a novel ER stress-inducible gene, is induced via ATF4-CHOP pathway and is involved in cell death. EMBO J. 2005*
- *Ottaviani G, Jaffe N. The etiology of osteosarcoma. Cancer Treat Res. 2009*
- *Pan L, Aller SG. Equilibrated atomic models of outward-facing P-glycoprotein and effect of ATP binding on structural dynamics. Sci Rep. 2015*

- *Panaretakis T, Kepp O, Brockmeier U, et al. Mechanisms of pre-apoptotic calreticulin exposure in immunogenic cell death. *Embo J.* 2009*
- *Patil Y, Sadhukha T, Ma L, Panyam J. Nanoparticle-mediated simultaneous and targeted delivery of paclitaxel and tariquidar overcomes tumor drug resistance. *J Control Release.* 2009*
- *Pedrini I, Gazzano E, Chegaev K, Rolando B, Marengo A, Kopecka J, Fruttero R, Ghigo D, Arpicco S, Riganti C. Liposomal nitrooxy-doxorubicin: one step over caelyx in drug-resistant human cancer cells. *Mol Pharm.* 2014*
- *Pluchino KM, Hall MD, Goldsborough AS, Callaghan R, Gottesman MM. Collateral sensitivity as a strategy against cancer multidrug resistance. *Drug Resist Updat* 2012*
- *Poston CN, Krishnan SC, Bazemore-Walker CR. In-depth proteomic analysis of mammalian mitochondria-associated membranes (MAM). *J Proteomics* 2013.*
- *Refaat A, Pararasa C, Arif M, Brown JE, Carmichael A, Ali SS, Sakurai H, Griffiths H.R. Bardoxolone-methyl inhibits migration and metabolism in MCF7 cells. *Free Radic Res.* 2017*
- *Regan JN, Lim J, Shi Y, Joeng KS, Arbeit JM, Shohet RV, et al. Upregulation of glycolytic metabolism is required for HIF1a-driven bone formation. *Proc Natl Acad Sci U S A* 2014*
- *Riganti C, Gazzano E, Polimeni M, Costamagna C, Bosia A, Ghigo D. Diphenyleneiodonium inhibits the cell redox metabolism and induces oxidative stress. *J Biol Chem* 2004.*
- *Riganti C, Miraglia E, Viarisio D, Costamagna C, Pescarmona G, Ghigo D, et al. Nitric oxide reverts the resistance to doxorubicin in human colon cancer cells by inhibiting the drug efflux. *Cancer Res* 2005*
- *Riganti C, Voena C, Kopecka J, Corsetto PA, Montorfano G, Enrico E, Costamagna C, Rizzo AM, Ghigo D, Bosia A. Liposome-encapsulated doxorubicin reverses drug resistance by inhibiting P-glycoprotein in human cancer cells. *Mol Pharm.* 2011*
- *Riganti C, Castella B, Kopecka J, Campia I, Coscia M, Pescarmona G, et al. Zoledronic acid restores doxorubicin chemosensitivity and immunogenic cell death in multidrug-resistant human cancer cells. *PLoS One* 2013*
- *Riganti C, Gazzano E, Gulino GR, Volante M, Ghigo D, Kopecka J. Two repeated low doses of doxorubicin are more effective than a single high dose against tumors overexpressing P-glycoprotein. *Cancer Lett.* 2015*

- *Riganti C, Kopecka J, Panada E, Barak S, Rubinstein M. The role of C/EBP- β LIP in multidrug resistance. J Natl Cancer Inst. 2015*
- *Salaroglio IC, Panada E, Moiso E, Buondonno I, Provero P, Rubinstein M, Kopecka J, Riganti C. PERK induces resistance to cell death elicited by endoplasmic reticulum stress and chemotherapy. Mol Cancer. 2017*
- *Scotto KW. Transcriptional regulation of ABC drug transporters. Oncogene 2003*
- *Sen N, Paul BD, Gadalla MM, Mustafa AK, Sen T, Xu R, Kim S, Snyder SH. Hydrogen sulfide-linked sulfhydration of NF- κ B mediates its antiapoptotic actions. Mol Cell. 2012*
- *Serra M, Scotlandi K, Manara MC, Maurici D, Lollini PL, De Giovanni C, et al. Establishment and characterization of multidrug-resistant human osteosarcoma cell lines. Anticancer Res 1993*
- *Simunek T, Sterba M, Popelova O, Adamcova M, Hrdina R, Gersl V. Anthracycline-induced cardiotoxicity: overview of studies examining the roles of oxidative stress and free cellular iron. Pharmacol Rep 2009*
- *Strigun A, Wahrheit J, Niklas J, Heinzle E, Noor F. Doxorubicin increases oxidative metabolism in HL-1 cardiomyocytes as shown by ¹³C metabolic flux analysis. Toxicol Sci 2012*
- *Swartz DJ, Mok L, Botta SK, Singh A, Altenberg GA, Urbatsch IL. Directed evolution of P-glycoprotein cysteines reveals site-specific, non-conservative substitutions that preserve multidrug resistance. Biosci Rep. 2014*
- *Szabo C, Hellmich MR. Endogenously produced hydrogen sulfide supports tumor cell growth and proliferation Cell Cycle. 2013*
- *Szakács G, Paterson JK, Ludwig JA, Booth-Genthe C, Gottesman MM. Targeting multidrug resistance in cancer. Nat Rev Drug Discov. 2006*
- *Szakács G, Hall MD, Gottesman MM, Boumendjel A, Kachadourian R, Day BJ, Baubichon-Cortay H, Di Pietro A. Targeting the Achilles heel of multidrug-resistant cancer by exploiting the fitness cost of resistance. Chem Rev. 2014*
- *Takara K, Sakaeda T, Okumura K. An update on overcoming MDR1-mediated multidrug resistance in cancer chemotherapy. Curr Pharm Des. 2006.*
- *Tao J, Shen X, Ai Y, Han X. Tea polyphenols protect against ischemia/reperfusion-induced liver injury in mice through anti-oxidative and anti-apoptotic properties. Exp Ther Med. 2016*

- Terasaki T, Ohtsuki S. Brain-to-blood transporters for endogenous substrates and xenobiotics at the blood–brain barrier: An overview of biology and methodology. *NeuroRx*. 2005
- Tesei A, Briigliadori G, Carloni S, Fabbri F, Ulivi P, Arienti C, Sparatore A, Del Soldato P, Pasini A, Amadori D, Silvestrini R, Zoli W. Organosulfur derivatives of the HDAC inhibitor *J Cell Physiol* 2012
- Tsouris V, Joo MK, Kim SH, Kwon IC, WonYY. Nano carriers that enable co-delivery of chemotherapy and RNAi agents for treatment of drug-resistant cancers, *Biotechnol. Adv.* 2014
- Tsukahara T, Emori M, Murata K, Mizushima E, Shibayama Y, Kubo T, Kanaseki T, Hirohashi Y, Yamashita T, Sato N, Torigoe T. The future of immunotherapy for sarcoma *Expert Opin Biol Ther.* 2016
- Trotta AP, Chipuk JE. Mitochondrial dynamics as regulators of cancer biology. *Cell Mol. Life Sci.* 2017
- Wallace DC Mitochondria and cancer. *Nat Rev Cancer.* 2012
- Wan J, Zhang X, Liu T, Zhang X Strategies and developments of immunotherapies in osteosarcoma *Oncol Lett.* 2016
- Wang GY, Wood CN, Dolorito JA, Libove E, Epstein EH. Differing tumor-suppressor functions of arf and p53 in murine basal cell carcinoma initiation and progression. *Oncogene.* 2017
- Wei Yu, Jian Zhu, Yitian Wang, Junjie Wang, Weijing Fang, Kaishun Xia, Jianlin Shao, Minzu Wu, Bing Liu, Chengzhen Liang, Chengyi Ye, and Huimin Tao A review and outlook in the treatment of osteosarcoma and other deep tumors with photodynamic therapy: from basic to deep *Oncotarget.* 2017
- Weinberg SE, Chandel NS. Targeting mitochondria metabolism for cancer therapy *Nat Chem Biol.* 2015
- Yang JC, Rosenberg SA. Adoptive T-Cell Therapy for Cancer. *Adv Immunol.* 2016
- Zhang Y, Liu L, Jin L, Yi X, Dang E, Yang Y, et al. Oxidative stress-induced calreticulin expression and translocation: New insights into the destruction of melanocytes. *J Invest Dermatol* 2014
- Zheng HC The molecular mechanisms of chemoresistance in cancers. *Oncotarget.* 2017
- Zhou SF. Structure, function and regulation of P-glycoprotein and its clinical relevance in drug disposition *Xenobiotica* 2008

8. Acknowledgments

I am recipients of PhD scholarships from the Italian Institute for Social Security (INPS)

I am grateful to Professor Chiara Riganti, Department of Oncology, University of Torino, for the fruitful discussion, for the support and for the patience.

I am also grateful, regretfully expire, to Professor Dario Ghigo, Department of Oncology, University of Torino, for the support.

I would like to thank Professor Patrizia D'Amelio, Department of Medical Sciences, University of Torino, for the support all these years.

I would like to thank my mentor, now a dear friend, Dr. Francesca Sassi, Department of Medical Sciences, University of Torino, for all.

I would like to thank Dr. Joanna Kopecka, Department of Oncology, University of Torino for the assistant in all stages of my work for this thesis.

A special thanks to my parents that always supported me.

Special thanks to my dear boyfriend and future husband Marco for the support, for the patience and strength.

Thanks to my dear friends Massimiliano, Stefania, Francesca, Viola, Simona for support and distractions in these years.

I dedicate this thesis to my darling grandfather and my sweet great-aunt that are always in my heart

9. Course and workshop

- “Targeted Therapy of Cancer: where we are heading” Workshop SIC, Turin ,27 June 2014
- "Introduzione alla ricerca bibliografica" Turin, 16/23 September 2014
- Multiplexing Elispot Workshop. Verona, 24-25 September 2014
- “Il trasferimento di conoscenze in Ateneo: dalla ricerca alla valorizzazione dell’innovazione” 3 february 2015 Turin
- Corso di Biostatistica. Turin , June 2015
- Immuno-Oncology Workshop. Paris, 9 September 2015, France
- Fellow-Day-SIOMMMS. Bologna, 11 November 2015
- Workshop “Polysaccharides in drug delivery” Turin, 27 october 2015
- “Optimization of oncology therapy novel drugs affecting multidrug resistance” Siena, 3-4 november 2016

10. Oral and poster communications

ORAL COMMUNICATIONS

- XVII National Congress SIOMMMS- Bologna 19-21 October 2017, Italy
- FORUM IN BONE AND MINERAL RESEARCH, 24-25 March 2017, Roma, Italy
- Pharmacology 2016 British Pharmacological Society's flagship annual meeting , 14-17 December 2016, London, United Kingdom (*Travel Grant*)
- FORUM BONE AND MINERAL RESEARCH- Torino, 15-16 giugno 2016 Italy
- Annual Conference of Italian Association of Cell Cultures, 16-18 November 2015, Napoli, Italy
- XV National Congress SIOMMMS, 12-14 November 2015, Bologna, Italy (*Best Oral Communication*)
- FORUM IN BONE AND MINERAL RESEARCH, 6-7 March 2015, Turin, Italy
- FORUM IN BONE AND MINERAL RESEARCH, Siena 23-24 May 2014, Italy

POSTER COMMUNICATIONS

- 3rd International Symposium of the Cancer Research Center of Lyon, 25-27 September 2017 Lyon, France
- 8th EORTC-NCI-AACR Symposium on Molecular Targets and Cancer Therapeutics 29 November 2 December 2016, Munich, Germany
- 4th World Congress on Controversies, Debates & Consensus in Bone, Muscle & Joint Diseases (BMJD), 20-22 October 2016 Barcellona, Spain
- Pharmacology 2015 British Pharmacological Society's flagship annual meeting, 15-17 December 2015, London, United Kingdom
- 2nd International Symposium of the Cancer Research Center of Lyon, 21-23 Settembre 2015 Lyon, France
- 9th International Conference of Anticancer Research, 6-10 Ottobre 2014, Sithonia, Greece

11. Papers

-D'Amelio P, Sassi F, **Buondonno I**, Spertino E, Tamone C, Piano S, Zugna D, Richiardi L, Isaia GC. *Effect of intermittent PTH treatment on plasma glucose in osteoporosis: A randomized trial*. Bone. 2015

-Campia I, **Buondonno I**, Castella B, Kopecka J, Gazzano E, Ghigo D, Riganti C. *An autocrine cytokine/JAK/STAT-signaling induces kynurenine synthesis in multidrug resistant human cancer cells*. Plos One 2015

-D'Amelio P, Sassi F, **Buondonno I**, Fornelli G, Spertino E, D'Amico L, Marchetti M, Lucchiarri M, Roato I, Isaia GC. *Treatment with intermittent PTH increases Wnt10b production by T cells in osteoporotic patients*. Osteoporos Int. 2015

-Rigoni M, Riganti C, Vitale C, Griggio V, Campia I, Robino M, Foglietta M, Castella B, Sciancalepore P, **Buondonno I**, Drandi D, Ladetto M, Boccadoro M, Massaia M, Coscia M. *Simvastatin and downstream inhibitors circumvent constitutive and stromal cell-induced resistance to doxorubicin in ighv unmutated cll cells*. Oncotarget. 2015

-Li J.Y, D'Amelio P., Robinson J. , Walker L.D. , Vaccaro C. , Luo T. , Tyagi A.M. , Yu M. , Reott M. , Sassi F. , **Buondonno I** , Adams J. , Weitzmann M.N., Isaia G.C. , Pacifici *IL- 17 a is increased in humans with primary hyperparathyroidism and mediates PTH induced bone loss in mice*. Cell Metab. 2015

-Chegaev K, Rolando B, Cortese D, Gazzano E, **Buondonno I**, Lazzarato L, Fanelli M, Hattinger CM, Serra M, Riganti C, Fruttero R, Ghigo D, Gasco A *H2S-Donating Doxorubicins May Overcome Cardiotoxicity and Multidrug Resistance*. J Med Chem. 2016

- **Buondonno I**, Gazzano E, Jean SR, Audrito V, Kopecka J, Fanelli M, Salaroglio IC, Costamagna C, Roato I, Mungo E, Hattinger CM, Deaglio S, Kelley SO, Serra M, Riganti C *Mitochondria-targeted doxorubicin: a new therapeutic strategy against doxorubicin-resistant osteosarcoma*. Mol Cancer Ther. 2016

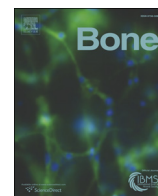
-Maffini E, Giaccone L, Festuccia M, Brunello L, **Buondonno I**, Ferrero D, Boccadoro M, Dellacasa C, Busca A, Novero D, Bruno B *Ruxolitinib in steroid refractory graft-vs.-host disease: a case report*. J Hematol Oncol. 2016

-Salaroglio IC, Panada E, Moiso E, **Buondonno I**, Provero P, Rubinstein M, Kopecka J, Riganti C. *PERK induces resistance to cell death elicited by endoplasmic reticulum stress and chemotherapy* Mol Cancer. 2017

-**Buondonno I**, Rovera G, Sassi F, Rigoni MM, Lomater C, Parisi S, Pellerito R, Isaia GC, D'Amelio P. *Vitamin D and immunomodulation in early rheumatoid arthritis: A randomized double-blind placebo-controlled study*. PLoS One. 2017

-Yu M, D'Amelio P, Tyagi A, Vaccaro C, Li J, Hsu E, **Buondonno I**, Sassi F, Adams J, Weitzmann MN, DiPaolo R, Pacifici R. *Regulatory T cells are expanded by Teriparatide treatment in humans and mediate intermittent PTH induced bone anabolism in mice* EMBO Reports 2017 DOI 10.15252/embr.201744421

-Gazzano E, Rolando B, Chegaev K, Salaroglio IC, Kopecka J, Pedrini I, Saponara S, Sorge M, **Buondonno I**, Stella B, Marengo A, Valoti M, Brancaccio M, Fruttero R, Gasco A, Arpicco S, Riganti C. Folate-targeted liposomal nitrooxy-doxorubicin: an effective tool against P-glycoprotein-positive and folate receptor-positive tumors. *J Control Release*, 2017 *in press*



Original Full Length Article

Effect of intermittent PTH treatment on plasma glucose in osteoporosis: A randomized trial [☆]



Patrizia D'Amelio ^{a,*}, Francesca Sassi ^a, Ilaria Buondonno ^a, Elena Spertino ^a, Cristina Tamone ^a, Simonetta Piano ^a, Daniela Zugna ^b, Lorenzo Richiardi ^b, Giovanni Carlo Isaia ^a

^a Gerontology Section, Department of Medical Science, University of Torino, Italy

^b Unit of Cancer Epidemiology, Department of Medical Science, University of Torino, Italy

ARTICLE INFO

Article history:

Received 7 November 2014

Revised 4 March 2015

Accepted 20 March 2015

Available online 27 March 2015

Edited by: Mark Cooper

Keywords:

PTH

Osteoporosis

Osteocalcin

Glucose

Adipokines

ABSTRACT

We investigated the effect of bone turnover on glucose homeostasis, fat distribution and adipokine production during anabolic treatment with PTH.

This is a parallel, randomized controlled, open label, trial. The randomization was done by computer generated tables to allocate treatments. Forty-six postmenopausal osteoporotic non-diabetic women were assigned to treatment with calcium and colecalciferol with (24) or without (22) PTH 1–84. Patients were recalled after 3, 6, 12 and 18 months of treatment and markers of bone turnover, glucose metabolism, adipokine secretion and fat distribution were analyzed. Markers of bone turnover and adipokines were measured by ELISA. Glucose metabolism was evaluated by an oral glucose load test and insulin resistance and secretion were calculated. Fat and lean mass were evaluated by anthropometric measures. The effect of treatment on measured variables was analyzed by repeated measure test, and its effect on glucose was also evaluated by mediation analysis after correction for possible confounders. Twenty patients in the calcium and vitamin D groups and 19 in the group treated with PTH 1–84 completed the study. There were no significance adverse events.

Treatment with PTH increases osteocalcin, both total (OC) and undercarboxylated (uOC), and decreases blood glucose, without influence on insulin secretion, resistance and pancreatic β cell function. Treatment with PTH does not influence fat distribution and adipokine production. The results of the mediation analyses suggest a total effect of PTH on blood glucose, moderately mediated by OC and to a less extent by uOC.

Here we suggest that treatment with PTH influences glucose metabolism partially through its effect on bone turnover, without influence on insulin secretion, resistance, pancreatic β cell function and fat mass.

© 2015 Elsevier Inc. All rights reserved.

Introduction

Glucose metabolism depends on a complex signal network that involves pancreatic islet cells, liver, fat, muscle, kidney and brain. In recent years the role of the skeleton in glucose and energy homeostasis has been studied. In particular the osteoblast-specific protein osteocalcin (OC), in its undercarboxylated form (uOC) appears to influence fat and glucose homeostasis in animal models. Mice knockout of both OC alleles had slightly increased fat mass and appear mildly hyperglycemic

because of decreased β -cell proliferation, insulin secretion, and insulin resistance [1]. Conversely, the opposite phenotype null for the *Esp* gene, which encodes a tyrosine phosphatase that hampers glucose metabolism by inhibiting OC functions, had small fat pads, increased β -cell proliferation, enhanced insulin sensitivity, improved glucose tolerance and increased expression and serum levels of adiponectin. The mice with high levels of uOC did not become obese or glucose intolerant under conditions that would usually induce these metabolic abnormalities.

In vitro experiments showed that uOC induced adiponectin expression in cultured adipocytes; adiponectin acts like an insulin sensitizing adipokine. Administration of recombinant uOC to wild-type mice decreased fat mass, increased adiponectin expression, improved glucose handling, and attenuated weight gain and glucose intolerance in the setting of a high-fat diet [2].

An even more intimate relationship between skeleton and energy metabolism was demonstrated by recent genetic experiments that found that leptin, an adipocyte derived hormone, inhibits insulin secretion by decreasing the production of uOC and is also involved in osteoblast differentiation [3].

Abbreviations: OC, osteocalcin; uOC, undercarboxylated osteocalcin; iPTH, intermittent PTH; BAP, bone alkaline phosphatase; TRAP5b, Serum Tartrate Resistant Acid Phosphatase 5b; BMD, bone mineral density; OGTT, oral glucose tolerance test; IS_{OGTT} , insulin sensitivity index; HOMA-IR, homeostasis model assessment of insulin resistance; FPG, fasting plasma glucose; FPI, fasting plasma insulin; IGI, insulinogenic index.

[☆] Trial registration EudraCT 2009-012397-12.

* Corresponding author at: Department of Medical Science, Corso Bramante 88/90, 10126 Torino, Italy. Fax: +39 116636033.

E-mail address: patrizia.damelio@unito.it (P. D'Amelio).

In human subjects, cross-sectional studies suggested an association between OC, glucose metabolism, and fat mass [4–10]. Total serum OC was inversely associated with body fat, fasting glucose, and fasting insulin in older adults [5] and in obese children [11]. In patients affected by type 2 diabetes mellitus, uOC was inversely correlated with abdominal fat and with hemoglobin A1c [10].

The administration of intermittent subcutaneous PTH is approved for osteoporosis treatment and increases bone formation in humans [12,13]; it has been shown that treatment with PTH 1–34 in diabetic rats increased the serum OC levels and decreased the serum glucose levels without changing insulin levels [14]. In humans an interventional study suggested that early increase in uOC induced by treatment with PTH 1–84 is associated with reduction in body fat and glucose level after 12 months [15].

The aims of this study were to investigate the effect of treatment with PTH 1–84 on bone turnover, glucose homeostasis, fat distribution and adipokine production in non-diabetic osteoporotic patients.

Materials and methods

The study was approved by the Ethical Committee of our Hospital (“Comitato Etico Interaziendale A.O.U. Città della Salute e della Scienza di Torino - A.O. Ordine Mauriziano - A.S.L. TO1”). Each patient signed an informed consent prior to the recruitment.

Trial design

This is a parallel, randomized controlled, open label, trial (registered as PTH 1–84 EudraCT 2009-012397-12). The randomization was done by computer generated tables to allocate treatments.

Randomization was done by the principal investigator, patients were enrolled by participants in the study, and lab measurement and statistical analyses were done by those blind to treatment.

Participants

Forty-six women affected by postmenopausal osteoporosis followed at our hospital were enrolled in the study between January 2010 and March 2012. Patients affected by secondary osteoporosis, by diabetes or taking drugs active on bone, glucose or fat metabolism were not considered eligible for the study.

Patients were randomly assigned to treatment with calcium 1200 mg/day and colecalciferol 800 UI/day with (24 patients, iPTH) or without (22 patients, controls) PTH 1–84 100 µg/day s.c. (Preotact®, kindly provided by Nycomed). This sample size provided an 80% power, assuming a two-sided significance level of 0.05, to detect differences in uOC greater than 1.71 (T-test on log-scale), considering previously reported median and interquartile ranges for uOC after iPTH treatment [15]. This effect is smaller than the one found in the randomized trial by Schafer et al. [15], in order to have enough power to focus also on the effect of uOC and OC on glucose metabolism. In the calcium and colecalciferol treatment group 2 patients dropped out for adverse gastrointestinal events after the first 3 months of treatment, whereas in the PTH 1–84 there were 3 dropouts after the first month for low compliance to sub-cutaneous injection and 2 patients did not come back at 18 months visit for personal problems. Data from patients who dropped out within the first 3 months were not considered in the statistics, whereas data from patients who completed 12 months were included (Fig. 1).

The main outcome measures were markers of bone turnover, glucose metabolism, adipokine secretion and fat distribution. The measurements were done at baseline and after 3, 6, 12 and 18 months of treatment.

Secondary outcome measure was evaluation of bone mineral density (BMD).

At baseline 25-OH vitamin D levels were measured by ELISA technique (DLD, Hamburg, Germany). Patients treated with iPTH get their injection at least 24 h before the blood exams in order to avoid the possible acute effect of PTH administration.

Bone turnover and bone density

As markers of bone formation we measured by ELISA technique: total OC (eBioscience, San Diego, CA), uOC (Takara, Shiga, JAP) and bone alkaline phosphatase (BAP, measured by QUIDEL kit, San Diego, CA).

Serum Tartrate Resistant Acid Phosphatase 5b (TRAP5b) was measured as marker of bone resorption by ELISA technique (QUIDEL, San Diego, CA). Markers of bone turnover were measured at enrollment and after 3, 6, 12 and 18 months of treatment, after overnight fasting.

The effect of treatment on BMD was assessed by bone densitometry on spine and femur performed at enrollment and after 18 months of treatment by Hologic QDR 4500 X-Ray densitometer.

Glucose metabolism

An oral glucose tolerance test (OGTT) with 75 g of glucose and blood sampling for glucose and insulin at 0 min, 30 min, 60 min, 90 min, and 120 min has been conducted at enrollment and after at 6, 12 and 18 months of therapy.

Insulin resistance was measured by Matsuda's insulin sensitivity index (IS_{OGTT}) [16] and the homeostasis model assessment of insulin resistance (HOMA-IR) [17]. IS_{OGTT} was calculated as $10,000 / \sqrt{(FPG * FPI) * (G * I)}$, where FPG represents the fasting plasma glucose, FPI the fasting plasma insulin, G the mean plasma glucose during the OGTT and I the mean plasma insulin during the OGTT [16] HOMA-IR was calculated as $FPG * FPI / 22.5$ [17].

Insulinogenic index (IGI) was calculated as $[(30 \text{ min FPI} - FPI) / (30 \text{ min G} - FPG)]$ divided by the HOMA-IR (IGI/IR) [18].

Adipokine and fat distribution

In order to evaluate the possible effect of iPTH treatment on adipokine production we measured serum leptin and adiponectin by ELISA technique (R&D Duoset, Minneapolis, MN) at enrollment and after 3, 6, 12 and 18 months of treatment, after overnight fasting.

Body fat was assessed by plicometry (Mahr GMBH Esslingen) at each visit, and the Pollock, Schmidt and Jackson's formula on three sites (triceps, subscapular and abdomen) was applied to calculate fat percentage [19]. Fat distribution was also measured by the waist/hip ratio. Muscle mass was measured by brachial and calf circumferences.

In order to exclude the possible biases due to variation in caloric intake, dietetic intake was investigated through personal interview and caloric and nutrient intakes were calculated using the PROGE software (Progeo S.r.l. Italy) at each visit.

The study flow chart is shown in Fig. 1.

Statistical analyses

The effect of treatment on markers of bone turnover, glucose metabolism parameters and adipokines was analyzed by repeated measure ANOVA. In order to evaluate the relationship between OC, uOC and FPG a linear regression model adjusted for treatment was carried out.

A mediation analysis was performed to evaluate if the effect of treatment on glucose level was mediated by OC level. Specifically we estimated separately:

- i) the direct (unmediated) and indirect (mediated) effects of treatment on the glucose level at 6 months mediated by OC at 3 months
- ii) the direct and indirect effects of treatment on the glucose level at 12 months mediated by OC at 6 months.

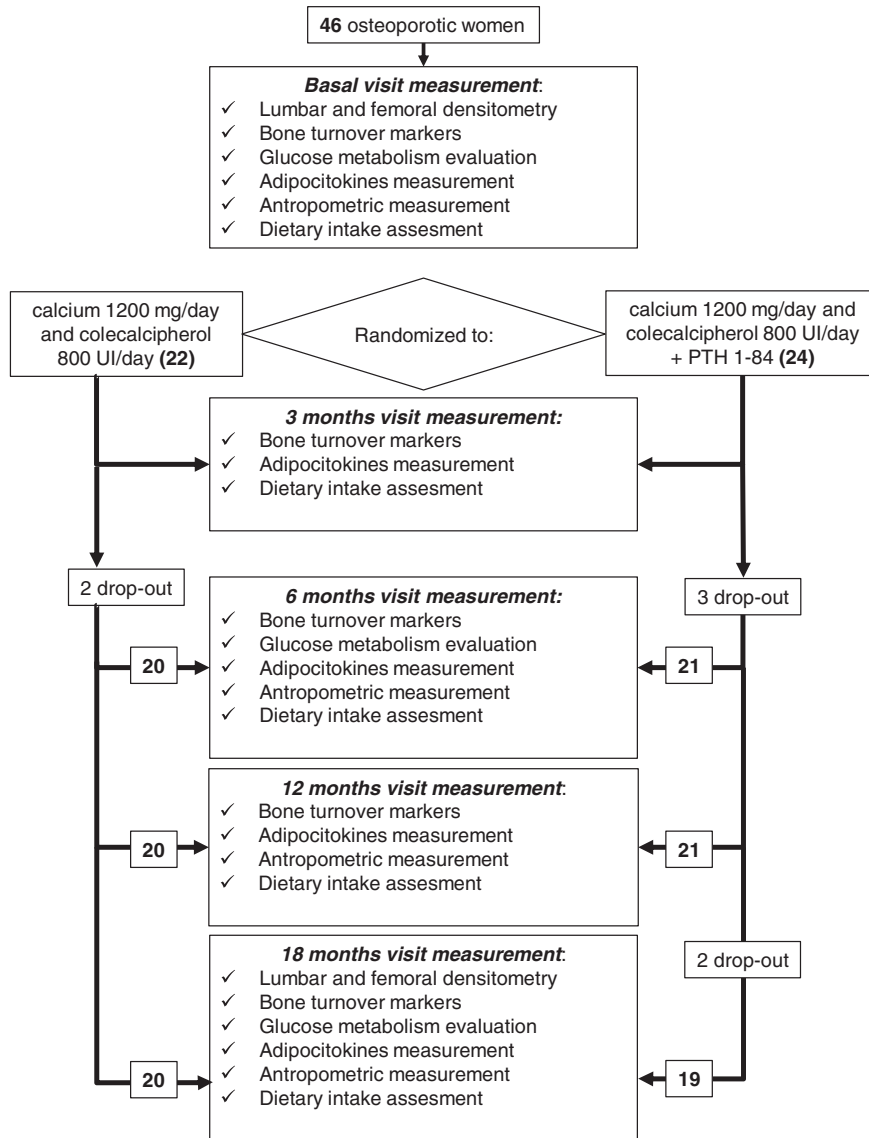


Fig. 1. The diagram shows the study design and the number of patients at each visit in bold. The tests performed at each visit are specified.

In order to obtain these estimates, two linear regression models on logarithmic scale were fitted, the first for glucose level dependent on treatment, OC level and their interaction and the second for OC level dependent on treatment; hence direct and indirect effects were estimated from the regression parameters in both models, provided certain identifiability assumptions and models are correctly specified [20]. A similar analysis was conducted by considering the association between glucose levels and uOC. The use of more sophisticated method to analyze repeated measures was not used because of low number of subjects included in this analysis.

The repeated measurements ANOVA testing the effect of treatment as well as the mediation analysis were adjusted for biomarkers that were unbalanced between the two treatment groups at baseline (uOC and TRAP5b). Statistical analysis was performed using statistical software STATA 11.1.

Results

There were no significant differences between the two treatment groups for the analyzed baseline variables with the exception of uOC and TRAP5b, that were higher in PTH treated patients (Table 1).

As expected the administration of iPTH increased markers of bone turnover, OC, BAP, TRAP5b (Figs. 2A–B–C) and uOC (Fig. 2D), whereas the treatment with calcium and vitamin D did not.

In secondary analyses, we found that iPTH increases lumbar BMD ($0.710 \pm 0.101 \text{ g/cm}^2$ at baseline vs $0.784 \pm 0.110 \text{ g/cm}^2$ after 18 months $p < 0.001$), and total femur BMD ($0.556 \pm 0.089 \text{ g/cm}^2$ at baseline vs $0.677 \pm 0.075 \text{ g/cm}^2$ after 18 months, $p = 0.001$), whereas there was weaker evidence on an effect of iPTH on femoral neck BMD ($0.556 \pm 0.084 \text{ g/cm}^2$ at baseline vs $0.576 \pm 0.098 \text{ g/cm}^2$ after 18 months, $p \text{ value} = 0.071$). Calcium and vitamin D treatment did not increase BMD in any of the analyzed sites.

Effect of iPTH on glucose level and mediation by OC and uOC

In patients treated with iPTH there was a decrease in FPG, the decrease was significant after 6 months of treatment and last for all the period analyzed, in patients treated with calcium and vitamin D alone there was no decrease in FPG (Fig. 3A). Treatment with iPTH seems not to influence the other parameters of glucose metabolism analyzed, we found no variation in insulin secretion and resistance as measured by OGTT derived parameters (Figs. 3B, C, D).

Table 1
Baseline characteristics of the study participants. Mean and standard deviations are shown for Gaussian variables, for non-Gaussian ones median and 25–75 centiles are shown in parentheses. p values were calculated by one way ANOVA.

	All	Calcium and vitamin plus iPTH	Calcium and vitamin D	p
Age (years)	62 ± 6	62 ± 6	61 ± 6	0.757
Post-menopausal period (years)	14 ± 8	13 ± 5	14 ± 9	0.431
BMI (kg/m ²)	22.7 ± 1.9	22.2 ± 6.1	23.2 ± 1.6	0.073
Body fat percentage	33.9 ± 5.1	33.4 ± 5.9	34.4 ± 4.3	0.558
Caloric intake (kcal/day)	1624 ± 407	1606 ± 398	1642 ± 425	0.784
Femoral neck BMD	0.574 ± 0.09	0.555 ± 0.08	0.590 ± 0.09	0.434
Total femur BMD	0.701 ± 0.08	0.714 ± 0.07	0.686 ± 0.09	0.494
Lumbar BMD	0.726 ± 0.093	0.701 ± 0.10	0.748 ± 0.08	0.136
25-OH vitamin D (ng/mL)	40.5 ± 14.9	41.6 ± 13.8	39.4 ± 16.2	0.646
BAP (UI/L)	59.5 ± 14.1	59.8 ± 13.3	59.3 ± 15.1	0.911
TRAP5b (UI/L)	3.3 ± 1	3.6 ± 1	2.9 ± 0.9	0.025
OC (ng/mL)	4.1 (2.8–6.1)	4 (3.4–6.9)	4.1 (2.1–5.9)	0.536
uOC (ng/mL)	4.29 ± 2.1	5 ± 2.2	3.6 ± 1.8	0.036
FPG (mg/dL)	81.4 ± 8.8	81.4 ± 7.4	81.5 ± 10.1	0.972
FPI (mUI/L)	3.2 ± 2.3	3.1 ± 2.0	3.3 ± 2.7	0.863
HOMA-IR	10.6 ± 9.6	10.4 ± 8.5	10.9 ± 10.8	0.866
IS _{OGTT}	1.0 ± 0.003	1.01 ± 0.004	1.01 ± 0.004	0.866
IGI	0.59 ± 0.5	0.58 ± 0.5	0.61 ± 0.5	0.718
IGI/IR	0.12 ± 0.04	0.11 ± 0.04	0.12 ± 0.05	0.535
Adiponectin (ng/mL)	4.4 ± 0.4	4.5 ± 0.3	4.4 ± 0.4	0.488
Leptin (ng/mL)	3 ± 0.5	3 ± 0.4	3 ± 0.5	0.819

Out of the 41 subjects, 3 patients had no data on OC and uOC at 3 and 12 months, whereas 4 patients (3 + 1) had no data on OC and uOC at 6 months. Hence linear regression models and mediation analyses were performed on patients having complete data on OC and uOC.

The linear regression analysis suggested that fasting plasma glucose is associated with OC (Table 2) and uOC mainly because of the treatment;

only the association between uOC and FPG measured at 12 months was not influenced by treatment with iPTH (Table 2).

The mediation analysis suggested that the effect of iPTH on FPG at 6 months was moderately mediated by its effect on OC (45% of total effect), but not on uOC at 3 months (15% of total effect) (Table 3). However the effect of iPTH on FPG at 12 months was more markedly

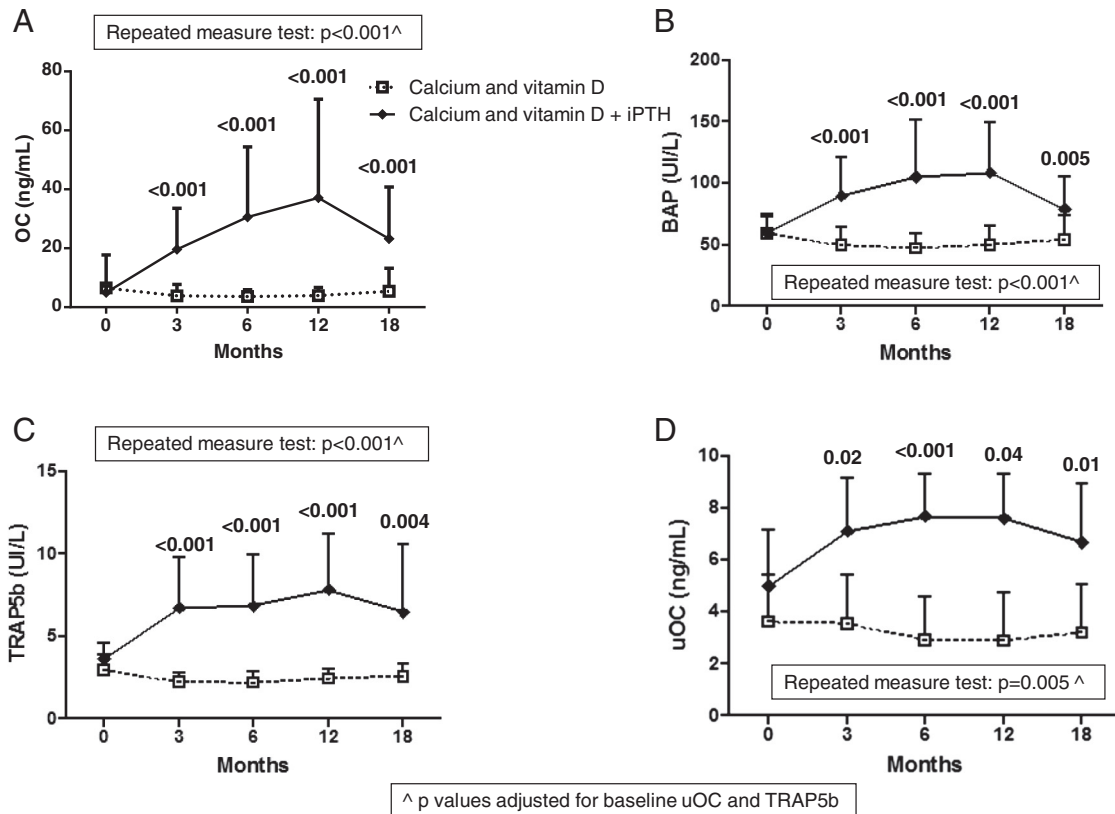


Fig. 2. The graphs show the effect of treatment with iPTH with respect to calcium and vitamin D alone on markers of bone turnover: OC panel A, BAP panel B, TRAP5b panel C and uOC panel D. Mean and SD are shown, significant p values calculated by paired T test vs baseline and repeated measure test after adjustment for basal values of uOC and TRAP5b (in box) is shown.

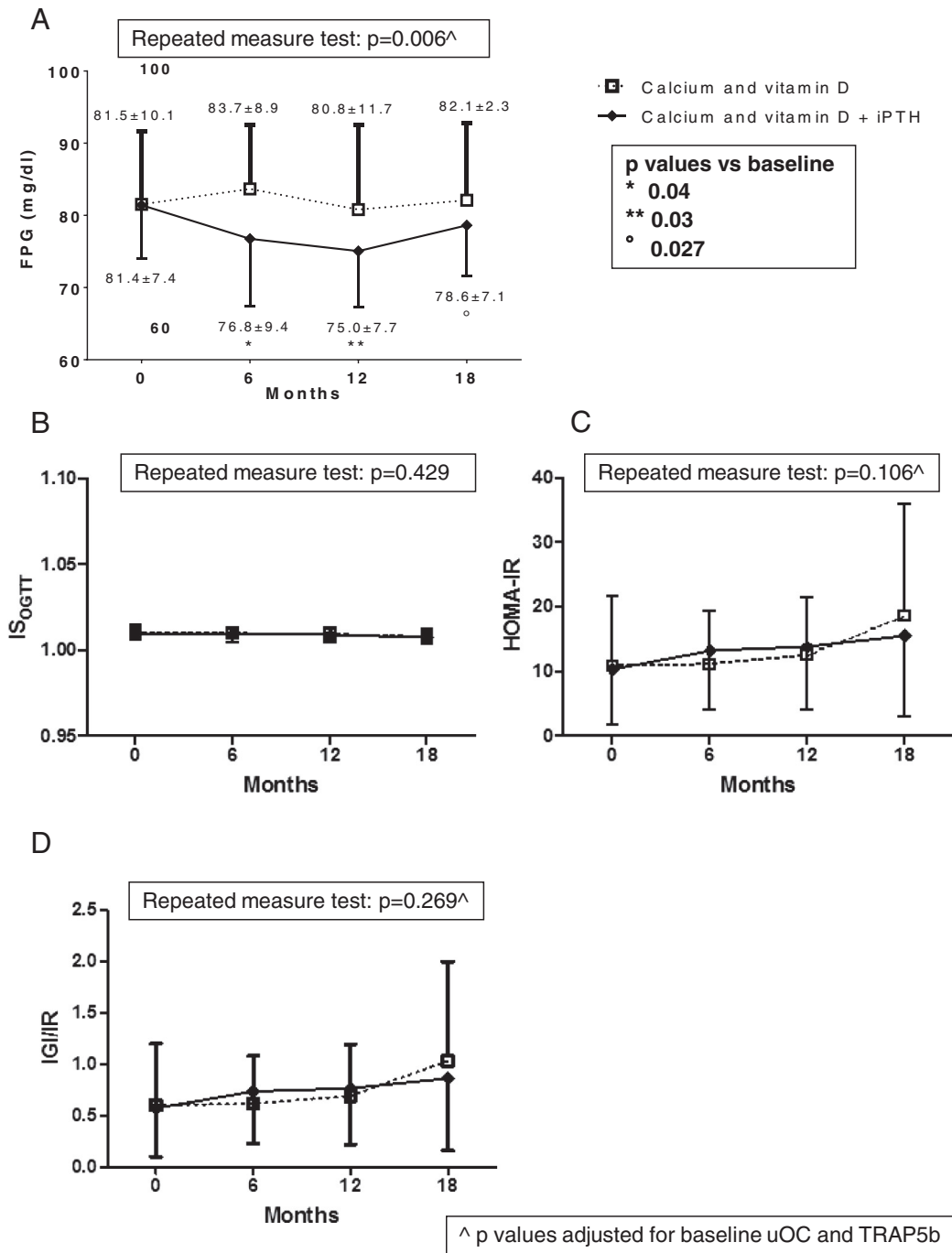


Fig. 3. The graphs show the effect of treatment with iPTH with respect to calcium and vitamin D alone on glucose metabolism parameters: fasting plasma glucose (FPG, panel A), insulin resistance (ISOGTT, panel B and HOMA-IR, panel C) and pancreatic β cell function (IGI/IR, panel D). Mean and SD are shown, significant p values calculated by paired T test vs baseline and repeated measure test after adjustment for basal values of uOC and TRAP5b (in box) is shown.

mediated by its effect on OC (62% of total effect) and uOC at 6 months (48% of total effect) (Table 3). Overall there was evidence of a total effect of iPTH on FPG, partially mediated by OC and to a less extent by uOC. If the interaction between treatment and OC/uOC levels was not taken into account, direct effects were emphasized compared to indirect effects.

Effect of iPTH on body fat

Treatment with calcium and vitamin D with or without iPTH had no effect on total fat ($p = 0.528$), on waist/hip ratio ($p = 0.300$) and on muscle mass (arm, $p = 0.302$, calf, $p = 0.480$).

The fat mass did not correlate with bone turnover markers nor with uOC, whereas it correlates with leptin ($r = 0.67, p < 0.001$). The amount of leptin and adiponectin measured in the serum was not modified by treatment with calcium and vitamin D with or without iPTH (data not shown). Patients' dietary intake evaluated as total caloric intake and as macronutrients intake per kg of body weight was not influenced by treatment (data not shown).

Discussion

In recent years animal studies suggested that uOC influences glucose metabolism through multiple pathways: it increases insulin secretion

Table 2

Linear regression models between fasting plasma glucose (FPG), OC and uOC measured after 3, 6 and 12 months of treatment. The table shows the regression coefficient, the 95% confidence interval (CI) and the p-values (p) in the crude and the adjusted analyses for treatment.

Regression coefficients for FPG ^a level vs OC ^a level				
	Crude analysis		Adjusted ^b analysis	
	Coefficient	95% CI (p-Value)	Coefficient	95% CI (p-Value)
FPG at 6 months				
OC at 3 months	−0.034	−0.067, −0.001 (p = 0.04)	0.009	−0.041, 0.058 (p = 0.73)
OC at 6 months	−0.036	−0.066, −0.005 (p = 0.02)	−0.011	−0.060, 0.039 (p = 0.67)
FPG at 12 months				
OC at 3 months	−0.021	−0.056, 0.015 (p = 0.24)	−0.008	−0.054, 0.039 (p = 0.74)
OC at 6 months	−0.027	−0.060, 0.005 (p = 0.10)	−0.004	−0.057, 0.050 (p = 0.89)
OC at 12 months	−0.026	−0.055, 0.003 (p = 0.08)	−0.007	−0.054, 0.041 (p = 0.77)
Regression coefficients for FPG level vs uOC ^a level				
	Crude analysis		Adjusted ^b analysis	
	Coefficient	95% CI (p-Value)	Coefficient	95% CI (p-Value)
FPG at 6 months				
uOC at 3 months	−0.048	−0.114, 0.018 (p = 0.15)	0.004	−0.075, 0.084 (p = 0.91)
uOC at 6 months	−0.052	−0.109, 0.004 (p = 0.07)	0.009	−0.077, 0.096 (p = 0.83)
FPG at 12 months				
uOC at 3 months	−0.065	−0.129, −0.001 (p = 0.05)	−0.040	−0.122, 0.042 (p = 0.33)
uOC at 6 months	−0.041	−0.101, 0.019 (p = 0.18)	0.012	−0.082, 0.106 (p = 0.80)
uOC at 12 months	−0.080	−0.129, −0.031 (p = 0.002)	−0.087	−0.160, −0.013 (p = 0.02)

Bold text indicates P significant values.

^a Regression models are performed on logarithmic transformation of FPG, OC and uOC.

^b Adjusted for treatment.

[21,22], both directly and indirectly by increasing the gut secretion of glucagon-like peptide-1 [23]; moreover uOC promotes β -cell proliferation [2] and increases insulin sensitivity in peripheral tissues [1].

Table 3

Mediation analysis model for OC and uOC measured at 3 and 6 months vs fasting plasma glucose (FPG) measured at 6 and 12 months adjusted for basal level of uOC and TRAP5b.

	Direct and indirect effects of treatment on glucose level at 6 months mediated by OC at 3 months (n = 38)		Direct and indirect effects of treatment on Glucose level at 6 months mediated by uOC at 3 months (n = 38)	
	Estimate	95% confidence interval	Estimate	95% confidence interval
Natural direct effect	−0.056	−0.196, 0.083	−0.087	−0.216, 0.041
Natural indirect effect	−0.046	−0.164, 0.072	−0.015	−0.119, 0.089
Total effect	−0.102	−0.178, −0.026	−0.102	−0.178, −0.026
<i>Adjusted for Trap and uOC at baseline</i>				
Natural direct effect	−0.066	−0.199, 0.067	−0.109	−0.226, 0.07
Natural indirect effect	−0.019	−0.126, 0.087	0.026	−0.058, 0.109
Total effect	−0.085	−0.169, −0.001	−0.084	−0.167, −0.001
	Direct and indirect effects of treatment on glucose level at 12 months mediated by OC at 6 months (n = 37)		Direct and indirect effects of treatment on glucose level at 12 months mediated by uOC at 6 months (n = 37)	
	Estimate	95% confidence interval	Estimate	95% confidence interval
Natural direct effect	−0.032	−0.187, 0.124	0.039	−0.188, 0.268
Natural indirect effect	−0.052	−0.187, 0.082	−0.124	−0.340, 0.093
Total effect	−0.084	−0.167, −0.001	−0.084	−0.169, 0.001
<i>Adjusted for Trap and uOC at baseline</i>				
Natural direct effect	−0.033	−0.186, 0.121	0.013	−0.201, 0.228
Natural indirect effect	−0.050	−0.178, 0.078	−0.085	−0.271, 0.102
Total effect	−0.082	−0.174, 0.009	−0.071	−0.162, 0.019

However, human studies found conflicting results: in some works uOC has been found to be related with fasting plasma glucose levels and to influence insulin sensitivity [24–26], whereas other researchers found no association [27–29]. The stronger association between insulin resistance and uOC in humans has been found in obese and/or diabetic patients [24–26], whereas in lean subjects this relation is less evident [27]. The suppression of bone turnover with antiresorptive drugs in humans does not influence glucose metabolism [28,29], whereas the role of bone turnover in the control of glucose metabolism has been demonstrated in mice [30].

Here we studied if anabolic treatment with iPTH could influence glucose metabolism, fat amount and distribution and the production of adipocytokines by increasing bone turnover.

As expected iPTH significantly increases bone turnover along the 18-months of treatment, whereas calcium and vitamin D do not. Treatment with iPTH is effective in increasing the undercarboxylated fraction of OC as also shown by Schafer et al. [15]; the increase in uOC is evident after 3 months of treatment and last for all the treatment period. As demonstrated in animal studies OC and uOC affect glucose metabolism, hence a treatment able to influence these parameters may affect glucose homeostasis. Our results show that fasting plasma glucose is decreased in patients treated with iPTH, but not in patients treated with calcium and vitamin D alone. A previous study by Anastasilakis et al. [31] showed an adverse effect of treatment with teriparatide on glucose metabolism. In particular these authors showed an increased glucose and insulin level immediately after the injection of teriparatide and 6 months after treatment. To explain the differences between our result and this study, it is important to consider that Anastasilakis et al. evaluated the effect of the 1–34 fragment of PTH and not of the entire molecule as we did, the two molecules may have a different effect on glucose metabolism. Furthermore Anastasilakis et al. included in their study patients affected by diabetes or by impaired glucose tolerance, whereas we enrolled only non-diabetic patients. In another study from the same group the administration of teriparatide in non-diabetic patients did not affect glucose metabolism, whereas chronic hypersecretion in primary hyperparathyroidism increases insulin secretion after glucose oral load [32].

Schafer et al. [15] showed that the increase in uOC after 3 months of iPTH treatment correlates with the changes in body mass and adipokines after at 12 months, whereas Anastasilakis et al. [31] demonstrated a different effect of acute teriparatide administration with respect to chronic administration. Our study suggests that the increase in OC and uOC after 3 and 6 months of iPTH partially influences glucose measured at

12 months, this delayed effect is in line with the findings by Schafer et al. [15]. This observation allows us to hypothesize a metabolic control exerted on a long period more than an acute effect of iPTH, partially mediated by its effect on OC and uOC.

Literature data on the effect of uOC on insulin secretion are quite controversial, some animal and human studies show that uOC influences glucose levels without affecting insulin secretion and sensitivity [14,15], whereas others suggested an inverse relationship between uOC and insulin resistance [11,33–36]. Some studies show that uOC influences β cell proliferation and activity [2,21,22], whereas others do not [37].

A recent paper suggests that OC may be associated specifically with skeletal muscle insulin action, more than on its hepatic metabolism [38]; furthermore a study on patients affected by type 1 diabetes demonstrated that OC level is inversely correlated with glycemic control and BMI independently from residual pancreatic function [39]. The abovementioned studies could explain our data on the effect of iPTH on glucose metabolism partially mediated by osteocalcin, and to a less extent by uOC without influence on insulin secretion. This result is in contrast with animal data [1,2], whereas it confirms a human study by Díaz-López et al. [25]. In animal models uOC has a deeper effect on glucose metabolism with respect to OC [1,2], whereas in humans OC, but not uOC, was inversely associated with insulin resistance and with FPG [25].

In this study the higher effect of OC on glucose level could be due to the higher increase of this molecule following iPTH and to the low cohort size. The reduction in fasting glucose in our patients has no direct clinical effect, but this observation may be useful to confirm the role of the skeleton on glucose metabolism in humans.

The human studies on the effect of uOC on insulin resistance have been obtained mainly in diabetic subjects, it is well known that diabetes influences bone metabolism per se [40] and thus can alter the relationship between bone turnover and glucose metabolism; we enrolled in the study only lean women (mean BMI 23) without diabetes in order to exclude the influences of fat and high glucose levels on bone turnover and density.

In this study the mediation analysis suggests that iPTH has a direct effect on FPG beyond its effect on bone turnover, previous studies allow to hypothesize a direct effect of PTH on glucose metabolism as it has been suggested that continuous increase in PTH levels could impair glucose tolerance through: (i) increased intracellular free Ca concentration, which decreases insulin sensitivity by decreasing insulin-dependent glucose transport [38,41], (ii) decreased plasma phosphate levels which decrease insulin sensitivity, as insulin-dependent glucose uptake is closely related to phosphate uptake [42], and (iii) downregulation of glucose uptake following insulin stimulus [43]. All the abovementioned data suggested that continuous PTH secretion influences glucose metabolism by reducing insulin secretion whereas there are no previous experimental data on the effect of iPTH on glucose metabolism per se, without the mediation of bone anabolic effect.

Here we show no effect of iPTH on body fat amount and distribution, this result disagrees with the previous human study of Schafer et al. [15] that shows a decrease in body weight and fat mass after iPTH treatment; on the other hand a recent animal study by Hamann et al. [37] shows no effect of iPTH on rat body weight. Differently from Schafer et al. [15] we included in the study leaner patients (mean BMI was 22.7 in our study vs 25.3) this may influence the possible effect of iPTH on body weight, through its possible different effects on uOC. In fact a recent human study shows that the levels of uOC are influenced by weight, being lower in overweight and obese women [44]. Differently from Schafer et al. [15] we control the data on fat mass and distribution by an accurate dietary intake interview, this excludes any change in dietary habits during treatment.

We do not find any effect of iPTH on fat production of leptin and adiponectin whereas Schafer and colleagues [15] show a decrease in adiponectin after treatment with iPTH; this discrepancy could be explained by the lack of effect of iPTH on body weight and fat mass in

our study. We also find no correlation between marker of bone turnover, fat amount and adipokines; previous literature found conflicting results on this point: some studies suggested an inverse relationship [1,6,10], whereas others did not find any correlation [40]. The direct correlation between leptin and fat mass in our study confirms the measure reliability.

The main limits of our study are the low sample size and the lack of more direct measure of insulin resistance as, for example, the glucose clamp technique. Moreover we do not include in the study a placebo controlled group, anyway it is unlikely that this methodological limitation can influence our results as in other human studies no placebo group has been included [15,31,32]. The higher level of TRAP5b and uOC detected at basal level in the group treated with iPTH is presumably due to chance and to the small sample size, anyway this datum does not influence our results as shown by statistical analyses.

Conclusion

In conclusion here we show that iPTH decreases fasting glucose without affecting insulin resistance and secretion and has no effect on fat mass and distribution and on adipokine production. We also suggest that the iPTH effect on glucose metabolism is partially mediated through its effect on OC production.

Disclosure statement

The authors have nothing to disclose.

Funding

Unconditioned grant from Nycomed SpA.

Acknowledgments

This work was supported by an unconditioned grant from Nycomed SpA (ISAG02AP13) which also provided the PTH 1–84 and calcium and vitamin D supplements.

Appendix A. Supplementary data

Supplementary data to this article can be found online at <http://dx.doi.org/10.1016/j.bone.2015.03.018>.

References

- [1] Lee NK, Sowa H, Hinoi E, Ferron M, Ahn JD, Confavreux C, et al. Endocrine regulation of energy metabolism by the skeleton. *Cell* 2007;130:456–69.
- [2] Ferron M, Hinoi E, Karsenty G, Ducy P. Osteocalcin differentially regulates beta cell and adipocyte gene expression and affects the development of metabolic diseases in wild-type mice. *Proc Natl Acad Sci U S A* 2008;105:5266–70. <http://dx.doi.org/10.1073/pnas.0711119105>.
- [3] D'Amelio P, Panico A, Spertino E, Isaia GC. Energy metabolism and the skeleton: reciprocal interplay. *World J Orthop* 2012;3:190–8. <http://dx.doi.org/10.5312/wjov.v3.i11.190>.
- [4] Kanazawa I, Yamaguchi T, Yamamoto M, Yamauchi M, Kurioka S, Yano S, et al. Serum osteocalcin level is associated with glucose metabolism and atherosclerosis parameters in type 2 diabetes mellitus. *J Clin Endocrinol Metab* 2009;94:45–9. <http://dx.doi.org/10.1210/jc.2008-1455>.
- [5] Pittas AG, Harris SS, Eliades M, Stark P, Dawson-Hughes B. Association between serum osteocalcin and markers of metabolic phenotype. *J Clin Endocrinol Metab* 2009;94:827–32. <http://dx.doi.org/10.1210/jc.2008-1422>.
- [6] Kindblom JM, Ohlsson C, Ljunggren O, Karlsson MK, Tivesten A, Smith U, et al. Plasma osteocalcin is inversely related to fat mass and plasma glucose in elderly Swedish men. *J Bone Miner Res* 2009;24:785–91. <http://dx.doi.org/10.1359/jbmr.081234>.
- [7] Yeap BB, Chubb SA, Flicker L, McCaul KA, Ebeling PR, Beilby JP, et al. Reduced serum total osteocalcin is associated with metabolic syndrome in older men via waist circumference, hyperglycemia, and triglyceride levels. *Eur J Endocrinol* 2010;163:265–72. <http://dx.doi.org/10.1530/EJE-09-0585>.
- [8] Zhou M, Ma X, Li H, Pan X, Tang J, Gao Y, et al. Serum osteocalcin concentrations in relation to glucose and lipid metabolism in Chinese individuals. *Eur J Endocrinol* 2009;161:723–72. <http://dx.doi.org/10.1530/EJE-09-0585>.
- [9] Im JA, Yu BP, Jeon JY, Kim SH. Relationship between osteocalcin and glucose metabolism in postmenopausal women. *Clin Chim Acta* 2008;396:66–9. <http://dx.doi.org/10.1016/j.cca.2008.07.001>.

- [10] Kanazawa I, Yamaguchi T, Yamauchi M, Yamamoto M, Kurioka S, Yaho S, et al. Serum undercarboxylated osteocalcin was inversely associated with plasma glucose level and fat mass in type 2 diabetes mellitus. *Osteoporos Int* 2011;22:187–94. <http://dx.doi.org/10.1007/s00198-010-1184-7>.
- [11] Garanty-Bogacka B, Syrenicz M, Rać M, Krupa B, Czaja-Bulsa G, Walczak M, et al. Association between serum osteocalcin, adiposity and metabolic risk in obese children and adolescents. *J Invest Med* 2014;62:33–6. <http://dx.doi.org/10.231/JIM.0000000000000015>.
- [12] Neer RM, Arnaud CD, Zanchetta JR, Prince R, Gaich GA, Reginster JY, et al. Effect of parathyroid hormone (1–34) on fractures and bone mineral density in postmenopausal women with osteoporosis. *N Engl J Med* 2001;344:1434–41.
- [13] Greenspan SL, Bone HG, Ettinger MP, Hanley DA, Lindsay R, Zanchetta JR, et al. Effect of recombinant human parathyroid hormone (1–84) on vertebral fracture and bone mineral density in postmenopausal women with osteoporosis: a randomized trial. *Ann Intern Med* 2007;146:326–39.
- [14] Kimura S, Sasase T, Ohta T, Sato E, Matsushita M. Parathyroid hormone (1–34) improves bone mineral density and glucose metabolism in spontaneously diabetic Torii–Leprfa rats. *J Vet Med Sci* 2012;74:103–5.
- [15] Schafer AL, Sellmeyer DE, Schwartz AV, Rosen CJ, Vittinghoff E, Palermo L, et al. Change in undercarboxylated osteocalcin is associated with changes in body weight, fat mass, and adiponectin: parathyroid hormone (1–84) or alendronate therapy in postmenopausal women with osteoporosis (the PaTH study). *J Clin Endocrinol Metab* 2011;96:E1982–9. <http://dx.doi.org/10.1210/jc.2011-0587>.
- [16] Matsuda M, DeFronzo RA. Insulin sensitivity indices obtained from oral glucose tolerance testing: comparison with the euglycemic insulin clamp. *Diabetes Care* 1999;22:1462–70.
- [17] Matthews DR, Hosker JP, Rudenski AS, Naylor BA, Treacher DF, Turner RC. Homeostasis model assessment: insulin resistance and beta-cell function from fasting plasma glucose and insulin concentration in man. *Diabetologia* 1985;28:412–9.
- [18] Wareham NJ, Phillips DI, Byrne CD, Hales CN. The 30 minute insulin incremental response in an oral glucose tolerance test as a measure of insulin secretion. *Diabet Med* 1995;12:931.
- [19] Jackson AS, Pollock ML, Ward A. Generalized equations for predicting body density of women. *Med Sci Sports Exerc* 1980;12:175–81.
- [20] VanderWeele T, Vansteelandt S. Conceptual issues concerning mediation, interventions and composition. *Stat Interface* 2009;2:457–68.
- [21] Hinoi E, Gao N, Jung DY, Yadav V, Yoshizawa T, Myers Jr MG, et al. The sympathetic tone mediates leptin's inhibition of insulin secretion by modulating osteocalcin bioactivity. *J Cell Biol* 2008;183:1235–42. <http://dx.doi.org/10.1083/jcb.200809113>.
- [22] Pi M, Wu Y, Quarles LD. GPRC6A mediates responses to osteocalcin in beta-cells in vitro and pancreas in vivo. *J Bone Miner Res* 2011;26:1680–3. <http://dx.doi.org/10.1002/jbmr.390>.
- [23] Mizokami A, Yasutake Y, Gao J, Matsuda M, Takahashi I, Takeuchi H, et al. Osteocalcin induces release of glucagon-like peptide-1 and thereby stimulates insulin secretion in mice. *PLoS One* 2013;8:e57375. <http://dx.doi.org/10.1371/journal.pone.0057375>.
- [24] Buday B, Pach FP, Literati-Nagy B, Vítai M, Vecsei Z, Koranyi L. Serum osteocalcin is associated with improved metabolic state via adiponectin in females versus testosterone in males. Gender specific nature of the bone–energy homeostasis axis. *Bone* 2013;57:98–104. <http://dx.doi.org/10.1016/j.bone.2013.07.018>.
- [25] Díaz-López A, Bulló M, Juanola-Falgarona M, Martínez-González MA, Estruch R, Covas MI, et al. Reduced serum concentrations of carboxylated and undercarboxylated osteocalcin are associated with risk of developing type 2 diabetes mellitus in a high cardiovascular risk population: a nested case–control study. *J Clin Endocrinol Metab* 2013;98:4524–31. <http://dx.doi.org/10.1210/jc.2013-2472>.
- [26] Sarkar PD, Choudhury AB. Relationships between serum osteocalcin levels versus blood glucose, insulin resistance and markers of systemic inflammation in central Indian type 2 diabetic patients. *Eur Rev Med Pharmacol Sci* 2013;17:1631–5.
- [27] Mori K, Emoto M, Motoyama K, Lee E, Yamada S, Morioka T, et al. Undercarboxylated osteocalcin does not correlate with insulin resistance as assessed by euglycemic hyperinsulinemic clamp technique in patients with type 2 diabetes mellitus. *Diabetol Metab Syndr* 2012;4:53. <http://dx.doi.org/10.1186/1758-5996-4-53>.
- [28] Hong SH, Koo JW, Hwang JK, Hwang YC, Jeong IK, Ahn KJ, et al. Changes in serum osteocalcin are not associated with changes in glucose or insulin for osteoporotic patients treated with bisphosphonate. *J Bone Metab* 2013;20:37–41. <http://dx.doi.org/10.11005/jbm.2013.20.137>.
- [29] Schwartz AV, Schafer AL, Grey A, Vittinghoff E, Palermo L, Lui LY, et al. Effects of antiresorptive therapies on glucose metabolism: results from the FIT, HORIZON-PFT, and FREEDOM trials. *J Bone Miner Res* 2013;28:1348–54. <http://dx.doi.org/10.1002/jbmr.1865>.
- [30] Lacombe J, Karsenty G, Ferron M. In vivo analysis of the contribution of bone resorption to the control of glucose metabolism in mice. *Mol Metab* 2013;2:498–504. <http://dx.doi.org/10.1016/j.molmet.2013.08.004> [eCollection 2013].
- [31] Anastasilakis A, Goulis DG, Koukoulis G, Kita M, Slavakis A, Avramidis A. Acute and chronic effect of teriparatide on glucose metabolism in women with established osteoporosis. *Exp Clin Endocrinol Diabetes* 2007;115:108–11.
- [32] Anastasilakis AD, Efsthadiadou Z, Plevraki E, Koukoulis GN, Slavakis A, Kita M, et al. Effect of exogenous intermittent recombinant human PTH 1–34 administration and chronic endogenous parathyroid hormone excess on glucose homeostasis and insulin sensitivity. *Horm Metab Res* 2008;40:702–7. <http://dx.doi.org/10.1055/s-2008-1078729>.
- [33] Choudhury AB, Sarkar PD, Sakalley DK, Petkar SB. Role of adiponectin in mediating the association of osteocalcin with insulin resistance and type 2 diabetes: a cross sectional study in pre- and post-menopausal women. *Arch Physiol Biochem* 2014;120:73–9. <http://dx.doi.org/10.3109/13813455.2013.877488>.
- [34] Villafán-Bernal JR, Llamas-Covarrubias MA, Muñoz-Valle JF, Rivera-León EA, González-Hita ME, Bastidas-Ramírez BE, et al. A cut-point value of undercarboxylated to carboxylated index is associated with glycemic status markers in type 2 diabetes. *J Invest Med* 2014;62:33–6. <http://dx.doi.org/10.231/JIM.0000000000000015>.
- [35] Kim S, Lee JY, Im JA, Kim DW, Lee HS, Kim SH, et al. Association between serum osteocalcin and insulin resistance in postmenopausal, but not premenopausal, women in Korea. *Menopause* 2013;20:1061–6. <http://dx.doi.org/10.1097/GME.0b013e31828838e8>.
- [36] Lucey AJ, Paschos GK, Thorsdottir I, Martínéz JA, Cashman KD, Kiely M. Young overweight and obese women with lower circulating osteocalcin concentrations exhibit higher insulin resistance and concentrations of C-reactive protein. *Nutr Res* 2013;33:67–75. <http://dx.doi.org/10.1016/j.nutres.2012.11.011>.
- [37] Hamann C, Picke AK, Campbell GM, Balyura M, Rauner M, Bernhardt R, et al. Effects of parathyroid hormone on bone mass, bone strength, and bone regeneration in male rats with type 2 diabetes mellitus. *Endocrinology* 2014;155:1197–206. <http://dx.doi.org/10.1210/en.2013-1960>.
- [38] Gower BA, Pollock NK, Casazza K, Clemens TL, Goree LL, Granger WM. Associations of total and undercarboxylated osteocalcin with peripheral and hepatic insulin sensitivity and β -cell function in overweight adults. *J Clin Endocrinol Metab* 2013;98:E1173–80. <http://dx.doi.org/10.1210/jc.2013-1203>.
- [39] Maddaloni E, D'Onofrio L, Lauria A, Maurizi AR, Strollo R, Palermo A, et al. Osteocalcin levels are inversely associated with HbA1c and BMI in adult subjects with long-standing type 1 diabetes. *J Endocrinol Invest* 2014;37:661–6. <http://dx.doi.org/10.1007/s40618-014-0092-7>.
- [40] Hamann C, Kirschner S, Günther KP, Hofbauer LC. Bone, sweet bone—osteoporotic fractures in diabetes mellitus. *Nat Rev Endocrinol* 2012;8:297–305. <http://dx.doi.org/10.1038/nrendo.2011.233>.
- [41] Rountree AM, Neal AS, Lisowski M, Rizzo N, Radtke J, White S, et al. Control of insulin secretion by cytochrome c and calcium signaling in islets with impaired metabolism. *J Biol Chem* 2014;2014 [in press].
- [42] Haap M, Heller E, Thamer C, Tschritter O, Stefan N, Fritsche A. Association of serum phosphate levels with glucose tolerance, insulin sensitivity and insulin secretion in non-diabetic subjects. *Eur J Clin Nutr* 2006;60:734–9.
- [43] Chang EI, Donkin SS, Teegarden D. Parathyroid hormone suppresses insulin signaling in adipocytes. *Mol Cell Endocrinol* 2009;307:77–82. <http://dx.doi.org/10.1016/j.mce.2009.03.024>.
- [44] Pepene CE. Serum under-carboxylated osteocalcin levels in women with polycystic ovary syndrome: weight-dependent relationships with endocrine and metabolic traits. *J Ovarian Res* 2013. <http://dx.doi.org/10.1186/1757-2215-6-4>.



Published in final edited form as:

Cell Metab. 2015 November 3; 22(5): 799–810. doi:10.1016/j.cmet.2015.09.012.

IL-17A IS INCREASED IN HUMANS WITH PRIMARY HYPERPARATHYROIDISM AND MEDIATES PTH-INDUCED BONE LOSS IN MICE

Jau-Yi Li^{1,*}, Patrizia D'Amelio^{2,*}, Jerid Robinson¹, Lindsey D. Walker¹, Chiara Vaccaro¹, Tao Luo¹, Abdul Malik Tyagi¹, Mingcan Yu¹, Michael Reott¹, Francesca Sassi², Ilaria Buondonno², Jonathan Adams¹, M. Neale Weitzmann^{1,3}, Giovanni Carlo Isaia², and Roberto Pacifici^{1,4}

¹Division of Endocrinology, Metabolism and Lipids, Department of Medicine, Emory University, Atlanta, GA

²Gerontology Section, Department of Medical Sciences, University of Torino, Corso Bramante 88/90, 10126 Torino, Italy

³Atlanta Department of Veterans Affairs Medical Center, Decatur, GA 30033

⁴Immunology and Molecular Pathogenesis Program, Emory University, Atlanta, GA

SUMMARY

Primary hyperparathyroidism (PHPT) is a common cause of bone loss that is modeled by continuous PTH (cPTH) infusion. Here we show that the inflammatory cytokine IL-17A is upregulated by PHPT in humans and cPTH in mice. In humans IL-17A is normalized by parathyroidectomy. In mice treatment with anti-IL-17A antibody and silencing of IL-17A receptor IL-17RA prevent cPTH induced osteocytic and osteoblastic RANKL production and bone loss. Mechanistically, cPTH stimulates conventional T cell production of TNF α (TNF), which increases the differentiation of IL-17A producing Th17 cells via TNF receptor 1 (TNFR1) signaling in CD4⁺ cells. Moreover, cPTH enhances the sensitivity of naïve CD4⁺ cells to TNF via G α S/ cAMP/Ca⁺⁺ signaling. Accordingly, conditional deletion of G α S in CD4⁺ cells and treatment with the calcium channel blocker diltiazem prevents Th17 cell expansion and blocks cPTH induced bone loss. Neutralization of IL-17A and calcium channel blockers may thus represent novel therapeutic strategies for hyperparathyroidism.

Address correspondence to: Roberto Pacifici, M.D., Division of Endocrinology, Metabolism and Lipids, Emory University School of Medicine, 101 Woodruff Circle, Room 1309, Atlanta, GA 30322, Telephone: 404-712-8420, Fax: 404-727-1300, roberto.pacifici@emory.edu.

*These authors have contributed equally

Publisher's Disclaimer: This is a PDF file of an unedited manuscript that has been accepted for publication. As a service to our customers we are providing this early version of the manuscript. The manuscript will undergo copyediting, typesetting, and review of the resulting proof before it is published in its final citable form. Please note that during the production process errors may be discovered which could affect the content, and all legal disclaimers that apply to the journal pertain.

AUTHOR CONTRIBUTIONS: PDA, FS, IB and GCI designed the human studies, performed the human research, and analyzed the human data. RP, JYL and MNW designed the animal study/protocols. JYL, JR, LDW, CV, TL, AMT, MY, MR, and JA performed the animal research and analyzed the data. RP wrote the manuscript and was the principle investigator.

DISCLOSURES

The authors state that they have no conflicts of interest.

Keywords

PTH; Hyperparathyroidism; T cells; Th17 cells; IL-17; IL-17R; IL-17 antibody; bone

INTRODUCTION

Parathyroid hormone (PTH) is a major regulator of calcium metabolism and bone homeostasis. PHPT, a condition characterized by chronic overproduction of PTH, is a common cause of osteoporosis (Parisien et al., 2001; Potts, 1998; Silverberg et al., 1989) that is modeled in animals by continuous PTH (cPTH) infusion. Both PHPT and cPTH treatment stimulate bone resorption and, to a lesser extent, bone formation (Qin et al., 2004) causing cortical bone loss and often trabecular bone loss (Iida-Klein et al., 2005; Potts, 1998).

The effects of cPTH on bone result from its binding to the PTH/PTH-related protein (PTHrP) receptor (PPR or PTHR1), which is expressed on bone marrow (BM) stromal cells, osteoblasts and osteocytes (Calvi et al., 2001; Saini et al., 2013), but also T cells (Terauchi et al., 2009) and macrophages (Cho et al., 2014). Early consensus held that the catabolic effect of cPTH is mediated by altered production of RANKL and OPG by stromal cells and osteoblasts (Ma et al., 2001). Osteocytes have now emerged as essential targets of PTH, as osteocyte-produced RANKL is pivotal for cPTH induced bone loss (Ben-awadh et al., 2014; Saini et al., 2013; Xiong et al., 2014). cPTH fails to induce bone loss in T cell null mice and mice with conditional deletion of PPR in T cells (Gao et al., 2008; Tawfeek et al., 2010), thus revealing that T cells contribute to the mechanism of action of PTH in bone. PPR activation in T cells stimulates TNF production by BM conventional CD4⁺ and CD8⁺ cells (Tawfeek et al., 2010) and cPTH fails to induce bone loss in mice specifically lacking TNF production by T cells (Tawfeek et al., 2010). TNF upregulates CD40 expression in SCs, allowing T cell expressed CD40L to regulate the responsiveness of SCs to cPTH (Gao et al., 2008). However, TNF is likely to contribute to the bone catabolic activity of cPTH via additional effects. Moreover, the mechanisms by which cPTH regulates T cell function, the specific population of T cells that mediate the activity of cPTH, and the role of T cells in the activity of PTH in humans remain to be determined.

Th17 cells are an osteoclastogenic population of CD4⁺ cells (Miossec et al., 2009; Sato et al., 2006) defined by the capacity to produce IL-17A and other minor members of the IL-17 family of cytokines (Basu et al., 2013). Th17 cells reside in the BM (Kappel et al., 2009) and play a pathogenic role in inflammatory conditions such as psoriasis, rheumatoid arthritis, multiple sclerosis and Crohn's disease (Martinez et al., 2008; Miossec et al., 2009). Moreover, Th17 cells contribute to the bone wasting caused by estrogen deficiency in mice (DeSelm et al., 2012; Tyagi et al., 2012) and humans (Molnar et al., 2014; Zhang et al., 2014). Th17 cells potently induce osteoclastogenesis by secreting IL-17A, RANKL, TNF, IL-1 and IL-6, along with low levels of IFN γ (Jovanovic et al., 1998; Komatsu and Takayanagi, 2012; Waisman, 2011). IL-17A stimulates the release of RANKL by all osteoblastic cells including osteocytes (Komatsu and Takayanagi, 2012; Kotake et al., 1999;

Sato et al., 2006) and potentiates the osteoclastogenic activity of RANKL by upregulating RANK (Adamopoulos et al., 2010).

cPTH stimulates bone and immune cells to release growth factors and cytokines. Among them are TGF β , IL-6, and TNF (Koh et al., 2011; Lowik et al., 1989; Tawfeek et al., 2010), factors that direct the differentiation of naïve CD4⁺ cells into Th17 cells (Basu et al., 2013; Bettelli et al., 2006; Nakae et al., 2007; Sugita et al., 2012). Therefore, it is plausible that cPTH may induce Th17 cell differentiation in the BM, and that IL-17A produced by BM Th17 cells may act as an upstream cytokine that plays a pivotal role in the bone loss induced by cPTH and PHPT.

This study was designed to determine the effects of PHPT and cPTH on the production of IL-17A in humans and mice and to investigate the contribution of IL-17A to the bone loss induced by cPTH in mice. We report that PHPT increases peripheral blood cell expression of IL-17A mRNA, which is normalized by parathyroidectomy. We also show that in mice, cPTH promotes Th17 cell differentiation via TNFR1 signaling in T cells. In addition, cPTH enhances the sensitivity of naïve CD4⁺ cells to TNF via the G α S/cAMP/Ca⁺⁺ signaling pathway. Attesting to relevance of IL-17A and PTH signaling in T cells, silencing of IL-17RA or G α S and treatment with neutralizing anti IL-17A antibody or the calcium channel blocker diltiazem prevent cPTH induced bone loss.

RESULTS AND DISCUSSION

Increased production of IL-17A in humans affected by PHPT

To investigate the effects of PHPT on the production of cytokines, unfractionated peripheral blood nucleated cells were obtained from 57 healthy controls and 20 subjects affected by PHPT of similar gender, age and years since menopause. The demographic characteristics of the study population and the serum levels of calcium, phosphorous, PTH and 25-hydroxy Vitamin D are shown in table 1. In PHPT patient's blood samples were obtained before surgery and 1 month after successful resolution of PHPT by parathyroidectomy. Overproduction of IL-17A has been documented in inflammatory conditions associated with local and systemic bone loss such as psoriasis, rheumatoid arthritis and Crohn's disease (Martinez et al., 2008; Miossec et al., 2009) but the effects of PHPT on IL-17A are unknown. Analysis by real time RT-PCR revealed that the mRNA levels of IL-17A in unfractionated peripheral blood nucleated cells were ~ 3 fold higher in PHPT patients than in healthy controls (fig.1a). Moreover, surgical restoration of normal parathyroid function was associated with the normalization of IL-17A levels, as demonstrated by the finding at 1 month after parathyroidectomy of similar IL-17A mRNA levels in healthy subjects and former PHPT patients. Furthermore, the mRNA levels of the IL-17-inducing transcription factor RORC were ~ 3 fold higher in PHPT patients before surgery than in healthy controls (fig.1b) and parathyroidectomy was followed by a decrease in RORC mRNA levels. As a result, levels of RORC mRNA in healthy controls and PHPT patients after surgery were not significantly different. Whether PHPT increases levels of IL-17A protein in the peripheral circulation and in the BM remains to be determined.

In the entire study population PTH levels were directly correlated with mRNA levels of IL-17A ($r=0.38$, $p<0.005$) and RORC ($r=0.27$, $p<0.05$). Moreover, disease status (healthy or PHPT) and age were independent predictors of IL-17A and RORC mRNA levels, whereas gender was not (tables S1,S2). These differences in IL-17A and RORC levels between healthy controls and PHPT patients remained significant even after adjustment for age and gender by a multiple regression model.

These findings suggest that increased IL-17A gene expression in PHPT patients is due to increased levels of circulating PTH. However, we cannot exclude the possibility that IL-17A might be regulated by factors modified by PTH, such as serum levels of calcium, phosphate and calcitriol. A previous cross-sectional study in patients on dialysis with hyperparathyroidism secondary to end-stage renal disease revealed a direct correlation between phosphate levels and frequency of peripheral blood Th17 cells (Lang et al., 2014). By contrast, in our study IL-17A levels were increased in PHPT patients who have decreased phosphate levels. Moreover, we found no correlation between IL-17A and RORC expression and serum phosphate levels.

PHPT was also associated with increased mRNA levels of TNF and IL-23, which were normalized by parathyroidectomy. By contrast all groups had similar mRNA levels of IFN γ and IL-4 suggesting that PHPT does not expand Th1 cells, Th2 cells (fig. S1).

Treatment with cPTH expands Th17 cells and IL-17A production in the mouse

To investigate the effect of PTH in mice, human PTH 1–34 was continuously infused at the rate of 80 $\mu\text{g}/\text{kg}/\text{day}$ for 2 weeks, a treatment modality referred to hereafter as cPTH. Analysis by flow cytometry of unfractionated peripheral blood nucleated cells harvested at sacrifice revealed that cPTH increased the relative and absolute frequency of peripheral blood Th17+ cells (fig.2a–c). Moreover, cPTH increased IL-17A mRNA levels in purified peripheral blood CD4+ cells (fig. 2d) and unfractionated peripheral blood nucleated cells, but not in CD4+ cell-depleted peripheral blood nucleated cells (fig.2e), indicating that CD4+ cells represent the major source of IL-17 mRNA in peripheral blood cells.

Mirroring its activity in peripheral blood, cPTH increased by ~2 fold the relative and absolute frequency of Th17 cells in the BM (fig.2f,g), by ~5 fold the levels of IL-17A mRNA in purified BM CD4+ cells (fig. 2h), and by 2 fold the levels of IL-17A protein in the culture media of BM CD4+ cells (fig.2i). Moreover, cPTH increased the expression of the Th17-inducing transcription factors ROR α and ROR γT in BM CD4+ T cells (fig.2j). cPTH treatment was also associated with a ~2 fold increase in the relative and absolute frequency of splenic Th17 cells (fig.2k,l) and a ~4 fold increase in the levels of IL-17A mRNA in purified splenic CD4+ cells (fig. 2m). By contrast, cPTH did not increase the relative and absolute frequency of IFN γ +CD4+ cells, IL-4+CD4+ cells, and FoxP3+CD4+ cells in the peripheral blood, BM and spleen (fig. S2), indicating that cPTH does not expand murine Th1 cells, Th2 cells and regulatory T cells.

Although IL-17A is mostly produced by Th17 cells, $\gamma\delta$ T cells, innate lymphoid cells, NK cells, NKT cells, neutrophils and eosinophils also produce IL-17 (Korn et al., 2009; Lockhart et al., 2006; Sutton et al., 2009). Our data do not support a role for $\gamma\delta$ T cell

produced IL-17A in the bone catabolic activity of cPTH because TCR β ^{-/-} mice, a strain lacking $\alpha\beta$ but not $\gamma\delta$ T cells are completely protected against cPTH induced bone loss (Gao et al., 2008).

Neutralization of IL-17A or silencing of IL-17RA block cPTH induced bone loss

To investigate whether IL-17A contributes to the bone catabolic activity of cPTH, WT mice were treated with vehicle or cPTH and either a neutralizing antibody directed against murine IL-17A (IL-17A Ab) or isotype matched irrelevant Ab (Irr. Ab), at the dose of 2.5 mg/kg, twice per week for 2 weeks. To assess the differential effects of cPTH on cortical and trabecular bone, micro-computed tomography (μ CT) was utilized to analyze femurs harvested at sacrifice. cPTH induced significant loss of cortical thickness (Ct.Th) and volume (Ct.Vo) and trabecular bone volume (BV/TV) in mice treated with Irr. Ab, but not in those treated with IL-17A Ab (fig.3a). Analysis of indices of trabecular structure revealed that cPTH had opposite effects in trabecular number (Tb.N) in mice treated with Irr. Ab and those treated with IL-17A Ab. A similar trend was observed for trabecular space (Tb.Sp). By contrast, cPTH induced decreased trabecular thickness (Tb.Th) in all mice (fig. S3a–c).

Analysis of femoral cancellous bone by histomorphometry revealed that neutralization of IL-17A blunts the bone catabolic activity of cPTH by decreasing bone resorption. In fact, cPTH treatment increased two indices of bone resorption, the number of OCs per bone surface (N.Oc/BS) and the percentage of surfaces covered by OCs (Oc.S/BS), in mice treated with Irr. Ab but not in those treated with IL-17Ab (fig.3b). Analysis of dynamic indices of bone formation revealed that cPTH increased mineral apposition rate (MAR) and bone formation rate (BFR) in mice treated with Irr. Ab and in those treated with IL-17A Ab (fig.3c). Two static indices of bone formation, the number of OBs per bone surface (N.Ob/BS) and the percentage of surfaces covered by OBs (Ob.S/BS) increased significantly in response to treatment with cPTH in both mice treated with Irr. Ab and those treated with IL-17A Ab (fig.3c). These indices were unexpectedly higher in the vehicle/IL-17A Ab group as compared to the vehicle/Irr. Ab group. Confirmation that neutralization of IL-17A blunts the bone catabolic activity of cPTH by decreasing bone resorption was provided by measurements of serum levels of C-terminal telopeptide of collagen (CTX), a marker of bone resorption, and total procollagen type 1 N-terminal propeptide (P1NP), a marker of bone formation. These assays revealed that treatment with IL-17A Ab significantly blunted the increase in serum CTX levels induced by cPTH, while it did not diminish the cPTH induced increase in P1NP levels (fig.3d).

The blockade of bone resorption induced by IL-17 Ab was of greater magnitude when estimated by serum levels of CTX than when measured by bone histomorphometry. The likely explanation for this phenomenon is that CTX levels reflect both cortical and trabecular bone resorption while histomorphometric indices were calculated only in the trabecular compartment. This is relevant because cortical bone accounts for most of the total bone mass and cPTH affects primarily the cortical compartment of the skeleton.

In summary, the data demonstrate neutralization of IL-17A blunts the capacity of cPTH to stimulate bone resorption without affecting bone formation. These changes in bone turnover

prevented bone loss but did not cause a significant increase in bone volume presumably because of the short duration of the IL-17Ab treatment.

Osteocytes and the pool of RANKL produced by osteocytes are crucial for the activity of cPTH. In fact, not only does silencing of PPR expression in osteocytes blunts the bone catabolic activity of cPTH (Saini et al., 2013), but increased production of RANKL by osteocytes is now known to play a pivotal role in cPTH induced bone loss (Ben-awadh et al., 2014; Saini et al., 2013; Xiong et al., 2014). Reports from our laboratory have led to the hypothesis that T cells are also an important target of PTH (Pacifci, 2013), primarily because silencing of PPR in T cells protects against cPTH induced bone loss (Tawfeek et al., 2010). The fact that silencing of PPR signaling in T cells and osteocytes induces similar bone sparing effects is in keeping with a “serial circuit” regulatory model, where signals from one population affect the response to cPTH of the other. Since T cells and osteocytes have limited physical contacts, the cross talk between these populations is likely mediated by a soluble factor. IL-17A is a likely candidate because it is a potent inducer of RANKL in organ cultures containing osteoblasts and osteocytes (Nakashima et al., 2000). In support of this hypothesis we found IL-17A Ab to completely block the increase in osteocytic RANKL mRNA levels induced by cPTH (fig.3e). Further attesting to causal role of IL-17A, we found that treatment with IL-17A Ab completely blocked the capacity of cPTH treatment to increase the expression of RANKL, TNF, IL-1 β and IL-6 mRNAs in purified osteoblasts and the increase in the expression of TNF mRNA in purified BM T cells (fig. S4a). These data indicate that IL-17A may mediate the bone catabolic activity of cPTH by upregulating the production of RANKL by osteocytes and osteoblasts.

IL-17A binds to the heterodimeric receptor IL-17RA/IL-17RC known as IL-17RA (Iwakura et al., 2011; Zepp et al., 2011). IL-17A signaling is silenced in IL-17RA $^{-/-}$ mice (Ye et al., 2001). We made use of IL-17RA $^{-/-}$ mice to further investigate whether IL-17A contributes to the bone catabolic activity of cPTH. 16 week-old IL-17RA $^{-/-}$ mice and WT littermates were treated with vehicle or cPTH for 2 weeks. In vitro μ CT analysis of femurs harvested at sacrifice revealed that cPTH induced significant losses of Ct.Th, Ct.Vo and BV/TV in WT mice but not in IL-17RA $^{-/-}$ mice (fig.3f). For reasons that remain undetermined, Ct.Th was lower in vehicle treated IL-17RA $^{-/-}$ mice as compared to vehicle treated WT mice. Parameters of trabecular structure (Tb.N, Tb.Th, and Tb.Sp) were altered by cPTH in WT but not in IL-17RA $^{-/-}$ mice (fig. S3d-f).

Serum CTX levels were increased by cPTH in WT but not in IL-17RA $^{-/-}$ mice (fig.3g). By contrast serum P1NP levels were increased by cPTH in WT and IL-17RA $^{-/-}$ mice (fig.3g). Osteocytic RANKL mRNA levels were increased by cPTH in WT but not in IL-17RA $^{-/-}$ mice (fig.3h). Finally, cPTH treatment increased the osteoblastic expression of RANKL, TNF, IL-1 β and IL-6 mRNAs and the T cell expression of TNF mRNA in WT but not IL-17RA $^{-/-}$ mice (fig. S4b). These findings demonstrate that silencing of IL-17RA prevents the loss of cortical and trabecular bone, and the increase in bone resorption and the osteoblastic/osteocytic RANKL production induced by cPTH. Importantly, the data confirm that IL-17A acts as an upstream cytokine that drives bone loss by increasing the sensitivity of osteoblasts and osteocytes to cPTH, thus enabling these lineages to release RANKL when stimulated by cPTH. Parallel deletions of PPR in T cells, osteocytes and osteoblasts as well

as conditional deletion of IL-17RA in osteocytes and osteoblasts will be necessary to conclusively confirm this hypothesis.

cPTH increases the differentiation of Th17 cells via TNF and GαS signaling

IL-6 and TGFβ initiate Th17 differentiation (Basu et al., 2013; Martinez et al., 2008) while TNF, IL-1, and IL-23 amplify it (Veldhoen et al., 2006). The relevance of TNF for Th17 cell expansion has emerged by investigations on the effects of TNF blockers, which have demonstrated that TNF contributes to the expansion of Th17 cells in inflammatory conditions in humans and rodents (Nakae et al., 2007; Sugita et al., 2012). Accumulation of cAMP in CD4+ cells and the resulting Ca²⁺ influx further promote Th17 cell differentiation and activity (Li et al., 2012). Treatment with cPTH induces the production of IL-6 and TGFβ by bone and immune cells (Koh et al., 2011; Lowik et al., 1989) and the release of TNF by BM CD4+ and CD8+ cells (Tawfeek et al., 2010). PTH binding to PPR activates the G protein-coupled receptor subunit GαS, leading to the generation of cAMP (Datta and Abou-Samra, 2009). Therefore, several mechanisms could account for the capacity of cPTH to expand Th17 cells.

We utilized BM cells, which are essential for the regulation of bone homeostasis, and cells from the spleen, an organ not known to regulate bone remodeling to determine the mechanism by which cPTH expands Th17 cells. BrdU incorporation studies revealed that cPTH did not increase the proliferation of Th17 cells in the BM and the spleen (fig. S5a,b). IL-17A-eGFP mice were utilized to investigate the differentiation of naïve CD4+ cells into Th17 cells. IL-17A-eGFP reporter mice possess an IRES-eGFP sequence after the stop codon of the IL17A gene so that eGFP expression is limited to IL-17A expressing cells, allowing Th17 cells to be detected by measuring eGFP by flow cytometry. Splenic naïve CD4+ cells (CD4⁺CD44^{lo}CD62L^{hi}eGFP-cells) were FACS sorted from IL-17A-eGFP mice and transferred into congenic T cell deficient TCRβ^{-/-} mice. Recipient mice were treated with vehicle or cPTH for 2 weeks starting 2 weeks after the T cell transfer, and newly produced Th17 cells (CD4⁺eGFP⁺ cells) counted. Since TCRβ^{-/-} mice were reconstituted with eGFP- cells, the number of eGFP⁺ cells in host mice at sacrifice provides a direct quantification of the differentiation of naïve CD4+ cells into Th17 cells. cPTH treated mice had a higher number eGFP⁺ cells than controls in the BM and the spleen (fig. S5c,d) demonstrating that cPTH increases Th17 cell differentiation in the BM and the spleen.

TNF expands Th17 cells and mediates the catabolic activity of cPTH (Chen et al., 2011; Nakae et al., 2007; Sugita et al., 2012). Therefore, we investigated the overall contribution of TNF and the specific role of T cell produced TNF in the expansion of Th17 cells induced by cPTH. WT and TNF^{-/-} mice were treated with cPTH for 2 weeks and the relative frequency of BM Th17 cells determined. cPTH increased the frequency of Th17 cells in the spleen and the BM in WT mice, but not in TNF^{-/-} mice (fig.4a,b). Analysis of purified BM CD4+ cells revealed that cPTH increased IL-17A mRNA levels (fig.4c) and the expression of RORα and RORγt (fig. 4d,e) in BM CD4+ cells from WT but not in those from TNF^{-/-} mice. Thus, cPTH induces Th17 cells via TNF. Next, splenic T cells from WT and TNF^{-/-} mice were transferred into TCRβ^{-/-} mice. Recipient mice were treated with vehicle or cPTH for 2 weeks starting 2 weeks after the T cell transfer. cPTH increased the number of Th17

cells (fig.4f), IL-17A mRNA levels in CD4⁺ cells (fig.4g) and the expression of ROR α and ROR γ t in CD4⁺ cells (fig.4h,i) in the BM of host mice with WT T cells but not in those with TNF^{-/-} T cells. These findings demonstrate that the production of TNF by T cells is required for cPTH to expand Th17 cells.

To determine whether TNF directly targets Th17 precursors, splenic CD4⁺ cells from TNFR1^{-/-} and TNFR2^{-/-} mice were transferred into TCR β ^{-/-} mice. Host mice were treated with vehicle or cPTH for 2 weeks starting 2 weeks after the T cell transfer. cPTH expanded BM Th17 cells in mice with TNFR2^{-/-} T cells but not in those with TNFR1^{-/-} T cells (fig. 4f). Moreover, cPTH increased IL-17A mRNA levels in BM CD4⁺ cells (fig.4g) and the BM CD4⁺ cell expression of ROR α and ROR γ t (fig.4h,i) in mice with TNFR2^{-/-} T cells but not in those with TNFR1^{-/-} T cells. These findings demonstrate that cPTH expands the pool of BM Th17 cells through direct TNFR1 signaling in T cells.

In addition to TNF, several cytokines are known to promote Th17 cell expansion. Among them are the T cell produced factor IL-21 and the macrophage/dendritic cell produced cytokine IL-23. We found that cPTH treatment increased the mRNA levels of IL-21, and IL-23R in BM and spleen CD4⁺ cells from WT but not TNF^{-/-} mice (fig. S6a,b). Moreover, cPTH increased the mRNA levels of IL-23 in BM CD11c⁺ cells from WT but not TNF^{-/-} mice (fig. S6c). These findings suggest that IL-21 and IL-23 may contribute to expansion of Th17 cells induced by cPTH. However, cPTH upregulates these factors via TNF.

In summary, our human and murine data indicate that TNF acts directly by upregulating the Th17 inducing factors IL-21 and IL-23. However, our findings do not exclude the possibility that PTH mediated stimulation of IL-6 and TGF β production may contribute to the expansion of Th17 cells induced by cPTH.

Conditional deletion of the G protein-coupled receptor subunit G α S in T cells impairs the generation of Th17 cells (Li et al., 2012). Since PTH binding to PPR activates G α S (Datta and Abou-Samra, 2009), cPTH could further upregulate Th17 differentiation by activating G α S in naïve CD4⁺ T cells. To investigate the role of G α S we generated G α S^{CD4,8} mice by crossing C57BL6 G α S fl/fl mice with C57BL6 CD4-Cre mice, as previously described (Li et al., 2012). The targeted genetic deletion of G α S with CD4-Cre occurs at the CD4⁺CD8⁺ double positive stage of T cell development (Li et al., 2012). Consequently, both CD4⁺ and CD8⁺ T cells from G α S^{CD4,8} mice lack G α S expression. G α S^{CD4,8}, G α S fl/fl, and WT mice have similar numbers of CD4⁺ and CD8⁺ cells, and similar percentages of effector, memory, and naïve CD4⁺ and CD8⁺ cells (Li et al., 2012).

One mechanism by which activation of G α S in CD4⁺ cells could promote Th17 cell differentiation is increased sensitivity to TNF. To investigate this hypothesis, naïve splenic CD4⁺ cells from vehicle and cPTH treated WT, G α S fl/fl and G α S^{CD4,8} mice were cultured *in vitro* in anti-CD3 Ab and anti-CD28 coated wells for 3 days in the presence of TNF at 10–50 ng/ml to induce the conversion of CD4⁺ cells into Th17 cells. Cultures of CD4⁺ cells from cPTH treated WT and G α S fl/fl mice yielded a higher number of Th17 cells as compared to those from vehicle treated mice (fig.5a). By contrast cultures of CD4⁺

cells from vehicle and cPTH treated $G\alpha S^{CD4,8}$ mice yielded similar numbers of Th17 cells, demonstrating that cPTH increases the sensitivity of nascent Th17 cells to TNF via $G\alpha S$ signaling in CD4+ cells. Mechanistic studies revealed that treatment with cPTH for 2 weeks increased the mRNA levels of TNFR1 and the TNFR1 activated signaling molecule TRAF2 (Qin et al., 2012) in BM CD4+ cells from WT and $G\alpha S$ fl/fl mice but not in those from $G\alpha S^{CD4,8}$ mice (fig.5b,c) indicating that activation of $G\alpha S$ signaling by cPTH increases the sensitivity of nascent Th17 cells to TNF by upregulating TNFR1 expression and TNFR1 signaling.

Treatment of $G\alpha S^{CD4,8}$ and $G\alpha S$ fl/fl control mice with cPTH for 2 weeks increased the frequency of BM Th17 cells (fig.5d), and induced significant losses of Ct.Th, Ct.Vo, and BV/TV (fig.5e–g), and Tb.Th (fig. S7a) in $G\alpha S$ fl/fl mice but not $G\alpha S^{CD4,8}$ mice. Unexpectedly, cPTH did not affect Tb.Sp and Tb.N in all mice (fig. S7b,c). cPTH also increased serum CTX levels in $G\alpha S$ fl/fl but not $G\alpha S^{CD4,8}$ mice (fig. 5h). Serum P1NP and osteocalcin (OCN) levels were increased by cPTH in $G\alpha S$ fl/fl and $G\alpha S^{CD4,8}$ mice (fig. 5i,j). These findings demonstrate that silencing of $G\alpha S$ in T cells prevents the expansion of Th17 cells, the loss of cortical and trabecular bone, and the increase in bone resorption induced by cPTH.

Signaling events downstream of $G\alpha S$ include cAMP generation (Li et al., 2012) and activation of L-type calcium channels (Hell, 2010). The latter contributes to Th17 cell differentiation (Oh-hora, 2009). Accordingly, *in vitro* treatment with the L-type calcium channel blocker diltiazem blunts the differentiation of CD4+ cells into Th17 cells (Li et al., 2012). We fed mice with or without diltiazem in their drinking water (Mieth et al., 2013; Semsarian et al., 2002) and infused them with vehicle or cPTH. Diltiazem blocked the increase in the number of BM Th17 cells (fig.6a), the BM mRNA levels of IL-17A (fig.6b), and the BM CD4+ cell expression of ROR α and ROR γ t (fig.6c,d) induced by cPTH. Moreover, diltiazem completely blocked the decrease in Ct.Vo, Ct.Th and BV/TV induced by cPTH (fig.6e–g) and altered the response to cPTH of parameters of trabecular structure (fig.6h–j). Diltiazem blocked the increase in serum CTX levels but not the increase in serum P1NP induced by cPTH (fig.6k,l). These data demonstrate that diltiazem prevents the loss of cortical and trabecular bone induced by cPTH by blunting bone resorption. The finding that *in vivo* treatment with diltiazem blocks Th17 cell expansion and prevents cPTH induced bone loss may suggest a potential therapeutic role for L-type calcium channel blockers in the treatment of hyperparathyroidism, even though the available data do not exclude the possibility of additional effects of diltiazem on immune cells that may contribute to its bone sparing activity.

A striking and unexpected finding of this investigation is that neutralization of IL-17A and deletion of IL-17RA block the capacity of cPTH to increase the production of RANKL by osteocytes and osteoblasts. These findings and the published literature suggest that T cells, osteoblasts and osteocytes are all required for the high levels of PTH characteristic of PHPT to induce bone loss. By contrast, osteocytes, but not T cells and IL-17A, are required for physiologic levels of endogenous PTH to regulate bone remodeling. In fact, mice lacking PPR signaling in osteocytes have high baseline bone volume (Saini et al., 2013), while

IL-17RA null mice and those lacking PPR signaling in T cells (Bedi et al., 2012; Tawfeek et al., 2010) have a normal bone volume.

Direct clinical applications of the current study arise because L-type calcium channel blocker are available, while anti-human IL-17A Abs and IL-17 receptor Abs are under investigation as therapeutic agents in psoriasis and spondyloarthritis (Leonardi et al., 2012; Martin et al., 2013; Mease et al., 2014; Yeremenko et al., 2014). Therefore our findings demonstrate a novel role for IL-17A in the mechanism of action of cPTH and provide a proof of principle for the use of L-type calcium channel blocker and IL-17A Ab in the treatment of primary hyperparathyroidism.

EXPERIMENTAL PROCEDURES

Human Study population

All human studies were approved by the Ethical Committee of the A.O.U. Città della Salute e della Scienza - A.O. Ordine Mauriziano - A.S.L. TO1, Turin Italy and informed consent was obtained from all participants. The study population was recruited from the patients of A.O.U. Città della Salute e della Scienza, Turin Italy and healthy volunteers. The study population included 20 patients (16 women and 4 men) affected by primary hyperparathyroidism (PHPT) and 57 healthy subjects (25 males and 32 females) comparable for age and years since menopause. The demographic characteristics of the study population are shown in table 1. The diagnosis of PHPT was established based on the finding of elevated circulating levels of calcium and PTH in at least 2 instances and the presence of normal renal function. PHPT patients were subjected to parathyroidectomy and restoration of normal parathyroid function was demonstrated by the finding of normal serum PTH levels 1 month after surgery. Inclusion and exclusion criteria are provided in supplemental experimental procedures.

Measurements of IL-17A, TNF α , IL-23, IL-4, IFN γ and RORC mRNAs in human samples

Red cells were lysed in all peripheral blood samples and total nucleated cells collected and dissolved in TRIzol reagent (Ambion, Huntingdon, UK) and frozen at -80°C until RNA extraction. RNA was isolated using chloroform extraction, and subsequent isopropanol precipitation according to the manufacturer's protocol. 1 μg of RNA was reverse transcribed to cDNA using a High Capacity cDNA Reverse Transcription Kit (Applied-Biosystems). Real time RT-PCR was performed with IQ SYBR Green Supermix (BIORAD). Relative IL-17A, RORC, IFN γ , IL-4, IL-23, and TNF α gene expression was determined using the $2^{-\text{CT}}$ method with normalization to β -Actin. The primers used are listed as supplemental information.

Animals

All the animal procedures were approved by the Institutional Animal Care and Use Committee of Emory University. Female C57BL6 WT, TNF $^{-/-}$, TNFR1 $^{-/-}$, TNFR2 $^{-/-}$, TCR $\beta^{-/-}$ and IL17A-GFP knock-in (IL17a^{tm1Bcgen/J}) mice were purchased from Jackson Laboratories (Bar Harbor, ME). C57BL6 IL-17RA $^{-/-}$ were provided by Amgen, Inc. C57BL6 G α S fl/fl mice were provided by Dr. Lee Weinstein (NIH). C57BL/6 CD4-Cre

mice were purchased from Taconic. GαS^{CD4,8} mice were generated by crossing C57BL6 GαS fl/fl mice with C57BL6 CD4-Cre mice. All mice were maintained under specific pathogen free conditions and fed sterilized food and autoclaved water ad libitum.

In vivo cPTH treatment

80 µg/kg/day of hPTH1–34 (Bachem California Inc., Torrance, CA) or vehicle were infused for 2 weeks in 16 weeks old female mice by implanting ALZET osmotic pump model-1002 (DURECT corporation Cupertino, CA) with a delivery rate of 0.24 ml/hr, as previously described (Gao et al., 2008; Tawfeek et al., 2010).

IL-17A Ab treatment

16 week-old WT mice were infused with vehicle or PTH for 2 weeks. These mice were also injected with mouse IL-17A neutralizing antibody (IL-17A Ab) (R&D Systems, MAB421) or isotype matched irrelevant Ab (Irr.Ig) at 2.5 mg/kg, twice per week.

Diltiazem treatment

16 week-old WT mice were infused with vehicle or PTH for 2 weeks. These mice received regular water or 100mg/kg body weight/day Diltiazem (Enzo life Science, Inc. Farmingdale, NY) with the drinking water.

T cell transfers

Splenic naïve CD4⁺ cells (CD4⁺CD44^{lo}CD62L^{hi}) from IL-17A–eGFP– mice were FACS sorted. WT, TNF^{–/–}, TNFR1^{–/–} and TNFR2^{–/–} spleen T cells were purified by negative immunoselection using MACS Pan T cell isolation kit (Miltenyi Biotech, Auburn, CA). These cells were injected (5×10^6 cells per mouse) IV into TCRβ^{–/–} recipient mice 2 weeks before treatment. Successful T cell engraftment was confirmed by flow cytometry of the spleens of the recipient mice harvested at sacrifice.

BrdU incorporation

Mice were injected IP with 1 mg of BrdU solution 48 hours before sacrifice. The detection of BrdU incorporation for proliferating cells was performed by using BrdU Flow Kit (BD Biosciences, San Diego, CA) and analyzed by FACS. The percentage of IL-17A⁺ BrdU⁺ cells was quantified by gating IL-17A⁺ CD4⁺ T cells in CD3⁺ cells.

In vivo and in vitro Th17 cell differentiation and IL-17A ELISA

Sorted splenic naïve (CD62L^{hi}CD44^{low}) CD4⁺ T cells from IL17A–GFP knock-in mice (IL17a^{tm1Bcgen/J} mice) were injected IV into 14 weeks old TCRβ^{–/–} mice (2×10^6 per mouse). Host mice were treated with vehicle or cPTH for 2 weeks starting 2 weeks after the adoptive transfer of T cells. Mice were then sacrificed and spleen and BM cells were harvested and incubated with phorbol 12-myristate 13-acetate (50ng/ml, Sigma) and ionomycin (1µg/ml, Sigma) in the presence of GolgiStop (1 µg/ml, Biolegend) for 4 hours. The cells were further stained with surface marker and analyzed for GFP expression. For *in vitro* studies, naïve CD4⁺ T cells from mice treated with vehicle or cPTH for 2 weeks were activated with plate bound anti-CD3 (2µg/ml) and anti-CD28 (2µg/ml) in the presence of

TNF (10–50 ng/ml) for 3 days. Cells were then harvested for FACS analysis of CD4+IL-17A+ cells.

IL-17A ELISA

CD4⁺ T cells were purified using CD4-specific MACS Microbeads (Miltenyi Biotec) following the manufacturer's instructions. Cells were cultured for 48 hours with 1 µg/ml anti-CD28 (Biolegend, San Diego, CA) on anti-CD3-coated plates. Supernatants were collected and assayed for IL-17 by ELISA kit (R&D Systems, Minneapolis, MN) according to the manufacturer's directions.

µCT measurements

µCT scanning and analysis was performed as reported previously (Tawfeek et al., 2010; Terauchi et al., 2009) using a Scanco µCT-40 scanner. Additional information as supplemental information.

Quantitative bone histomorphometry

The measurements, terminology and units used for histomorphometric analysis, were those recommended by the Nomenclature Committee of the American Society of Bone and Mineral Research (Dempster et al., 2013). Non-consecutive longitudinal sections of the femur were prepared and analyzed as described previously (Robinson et al., 2015). Additional information is provided as supplemental information.

Osteoblast and dendritic cell purification

BM cells were collected at sacrifice and OBs were purified as previously described (Bedi et al., 2012; Gao et al., 2008). Additional information is provided as supplemental information.

RNA isolation from enriched osteocytes

The distal end of a tibia was cut off and BM cells were removed by centrifuging at 12000 rpm for 2 minutes. The surfaces of the bone shafts were scraped to remove the periosteum and the bone was cut into a few small pieces. Bone pieces were then digested with 1 ml of Hank's solution containing 0.1 % bovine serum albumin, 1 mM CaCl₂, and 1 mg/ml of collagenase (type I:II, ratio 1:3) in a 12-well-plate. A total of 6 digestions for 15 minutes were performed at 37°C on a rocking platform at 90 oscillations per minute to remove the cells on the bone surface. After the final digestion, bone pieces were washed with PBS and frozen in liquid nitrogen. For RNA isolation, bone pieces were transferred into a tube of 1 mL TRIzol reagent with 5 stainless steel beads and the sample was spun in a refrigerated bullet blender centrifuge at 12000 rpm for 10 minutes. The supernatant was transferred into a new tube, and RNA extracted.

Markers of bone turnover

Serum CTX, PINP and Osteocalcin were measured by rodent specific ELISA assays (Immunodiagnostic Systems, Scottsdale, AZ).

Flow cytometry and cell sorting

For surface staining, cells were stained with anti-mouse CD3, CD4, CD62L, and CD44 antibodies (Biolegend, San Diego, CA). For intracellular staining, cells were incubated with phorbol 12-myristate 13-acetate (50ng/ml, Sigma) and ionomycin (1µg/ml, Sigma) in the presence of GolgiStop (1 µg/ml, Biolegend) at 37°C for 4 hours. Cells were then stained with anti-mouse CD3 and CD4 antibodies followed by intracellular staining with anti-mouse IL-17A, IFN γ , IL-4 and Foxp3 antibodies (Biolegend). Cells were then subjected to FACS analysis on an LSRII (BD Biosciences, Franklin Lakes, NJ) and analyzed using FlowJo software (TreeStar).

Real-time RT-PCR and murine primers

The expression levels of murine IL-17A, I ROR α , ROR γ t, IL-21, IL-23, IL-23R, TNFR1, TRAF2, IL-1 β , IL-6, RANKL and TNF α mRNAs levels were quantified by real-time RT-PCR. Murine RNAs levels were measured in BM and spleen CD4+ cells, as well as unfractionated nucleated peripheral blood cells. All the primers used were designed by Primer Express Express® Software v2.0 (PE Biosystems). Changes in relative gene expression between vehicle and cPTH groups were calculated using the 2^{-CT} method with normalization to 18S rRNA. The primers used are provided in supplemental experimental procedures.

Statistical Analysis

Human cytokines and RORC mRNA levels and serum Ca, PTH, and 25OH Vitamin D levels were analyzed by Mann Whitney (healthy controls vs. PHPT before surgery and healthy controls vs. PHPT after surgery) and Wilcoxon matched pairs signed rank tests (PHPT vs. PHPT after surgery), as the data were not normally distributed according to the Shapiro-Wilk normality test. Serum levels of phosphorous and the demographic data were analyzed by one-way ANOVA, as these data were normally distributed. To evaluate the effects of age and gender on IL-17A and RORC levels, multivariate general linear regression models (GLMs) on logarithmic scale were fitted for age, gender and IL-17A or RORC mRNA levels at baseline and their interactions. The relationship between serum PTH levels and IL-17A and RORC mRNA levels were further analyzed by nonparametric Spearman correlations.

Murine data were normally distributed according to the Shapiro-Wilk normality test and analyzed by unpaired t-tests or two-way analysis-of-variance as appropriate. Additional information is provided as supplemental information.

Supplementary Material

Refer to Web version on PubMed Central for supplementary material.

ACKNOWLEDGEMENTS

We are grateful to Prof. L. Richiardi (University of Turin, Italy) for his assistance with the statistical analysis of the human data, Dr. Weinstein (NIH) for providing the Gas fl/fl mice and to Amgen, Inc for providing the IL-17RA $^{-/-}$ mice. This study was supported by grants from the National Institutes of Health (AR54625, DK007298 and RR028009). JYL was supported by a grant from the National Institutes of Health (AR061453). MNW was

supported in part, by a grant from the Biomedical Laboratory Research & Development Service of the VA Office of Research and Development (5101BX000105) and by NIH grants R01AR059364 and R01AG040013.

Nonstandard abbreviations used

BM	Bone marrow
cPTH	Continuous PTH
OBs	Osteoblasts
OCYs	Osteocytes
PTH	Parathyroid hormone
PHPT	Primary Hyperparathyroidism
PPR	PTH/PTHrP receptor
SCs	Stromal Cells
TNF	Tumor necrosis factor α

REFERENCES

- Adamopoulos IE, Chao CC, Geissler R, Laface D, Blumenschein W, Iwakura Y, McClanahan T, Bowman EP. Interleukin-17A upregulates receptor activator of NF-kappaB on osteoclast precursors. *Arthritis Res Ther.* 2010; 12:R29. [PubMed: 20167120]
- Basu R, Hatton RD, Weaver CT. The Th17 family: flexibility follows function. *Immunol Rev.* 2013; 252:89–103. [PubMed: 23405897]
- Bedi B, Li JY, Tawfeek H, Baek KH, Adams J, Vangara SS, Chang MK, Kneissel M, Weitzmann MN, Pacifici R. Silencing of parathyroid hormone (PTH) receptor 1 in T cells blunts the bone anabolic activity of PTH. *Proc Natl Acad Sci U S A.* 2012; 109:E725–E733. [PubMed: 22393015]
- Ben-awadh AN, Delgado-Calle J, Tu X, Kuhlenschmidt K, Allen MR, Plotkin LI, Bellido T. Parathyroid hormone receptor signaling induces bone resorption in the adult skeleton by directly regulating the RANKL gene in osteocytes. *Endocrinology.* 2014; 155:2797–2809. [PubMed: 24877630]
- Betelli E, Carrier Y, Gao W, Korn T, Strom TB, Oukka M, Weiner HL, Kuchroo VK. Reciprocal developmental pathways for the generation of pathogenic effector TH17 and regulatory T cells. *Nature.* 2006; 441:235–238. [PubMed: 16648838]
- Calvi LM, Sims NA, Hunzelman JL, Knight MC, Giovannetti A, Saxton JM, Kronenberg HM, Baron R, Schipani E. Activated parathyroid hormone/parathyroid hormone-related protein receptor in osteoblastic cells differentially affects cortical and trabecular bone. *J Clin Invest.* 2001; 107:277–286. [PubMed: 11160151]
- Chen DY, Chen YM, Chen HH, Hsieh CW, Lin CC, Lan JL. Increasing levels of circulating Th17 cells and interleukin-17 in rheumatoid arthritis patients with an inadequate response to anti-TNF- α therapy. *Arthritis Res Ther.* 2011; 13:R126. [PubMed: 21801431]
- Cho SW, Soki FN, Koh AJ, Eber MR, Entezami P, Park SI, van Rooijen N, McCauley LK. Osteal macrophages support physiologic skeletal remodeling and anabolic actions of parathyroid hormone in bone. *Proc Natl Acad Sci U S A.* 2014
- Datta NS, Abou-Samra AB. PTH and PTHrP signaling in osteoblasts. *Cell Signal.* 2009; 21:1245–1254. [PubMed: 19249350]
- Dempster DW, Compston JE, Drezner MK, Glorieux FH, Kanis JA, Malluche H, Meunier PJ, Ott SM, Recker RR, Parfitt AM. Standardized nomenclature, symbols, and units for bone histomorphometry: a 2012 update of the report of the ASBMR Histomorphometry Nomenclature Committee. *J Bone Miner Res.* 2013; 28:2–17. [PubMed: 23197339]

- DeSelm CJ, Takahata Y, Warren J, Chappel JC, Khan T, Li X, Liu C, Choi Y, Kim YF, Zou W, et al. IL-17 mediates estrogen-deficient osteoporosis in an Act1-dependent manner. *Journal of cellular biochemistry*. 2012; 113:2895–2902. [PubMed: 22511335]
- Gao Y, Wu X, Terauchi M, Li JY, Grassi F, Galley S, Yang X, Weitzmann MN, Pacifici R. T cells potentiate PTH-induced cortical bone loss through CD40L signaling. *Cell metabolism*. 2008; 8:132–145. [PubMed: 18680714]
- Hell JW. Beta-adrenergic regulation of the L-type Ca²⁺ channel Ca(V)_{1.2} by PKA rekindles excitement. *Science signaling*. 2010; 3:pe33. [PubMed: 20876870]
- Iida-Klein A, Lu SS, Kapadia R, Burkhart M, Moreno A, Dempster DW, Lindsay R. Short-term continuous infusion of human parathyroid hormone 1–34 fragment is catabolic with decreased trabecular connectivity density accompanied by hypercalcemia in C57BL/J6 mice. *J Endocrinol*. 2005; 186:549–557. [PubMed: 16135674]
- Iwakura Y, Ishigame H, Saijo S, Nakae S. Functional specialization of interleukin-17 family members. *Immunity*. 2011; 34:149–162. [PubMed: 21349428]
- Jovanovic DV, Di Battista JA, Martel-Pelletier J, Jolicoeur FC, He Y, Zhang M, Mineau F, Pelletier JP. IL-17 stimulates the production and expression of proinflammatory cytokines, IL-beta and TNF-alpha, by human macrophages. *J Immunol*. 1998; 160:3513–3521. [PubMed: 9531313]
- Kappel LW, Goldberg GL, King CG, Suh DY, Smith OM, Ligh C, Holland AM, Grubin J, Mark NM, Liu C, et al. IL-17 contributes to CD4-mediated graft-versus-host disease. *Blood*. 2009; 113:945–952. [PubMed: 18931341]
- Koh AJ, Novince CM, Li X, Wang T, Taichman RS, McCauley LK. An irradiation-altered bone marrow microenvironment impacts anabolic actions of PTH. *Endocrinology*. 2011; 152:4525–4536. [PubMed: 22045660]
- Komatsu N, Takayanagi H. Autoimmune arthritis: the interface between the immune system and joints. *Advances in immunology*. 2012; 115:45–71. [PubMed: 22608255]
- Korn T, Bettelli E, Oukka M, Kuchroo VK. IL-17 and Th17 Cells. *Annual review of immunology*. 2009; 27:485–517.
- Kotake S, Udagawa N, Takahashi N, Matsuzaki K, Itoh K, Ishiyama S, Saito S, Inoue K, Kamatani N, Gillespie MT, et al. IL-17 in synovial fluids from patients with rheumatoid arthritis is a potent stimulator of osteoclastogenesis. *J Clin Invest*. 1999; 103:1345–1352. [PubMed: 10225978]
- Lang CL, Wang MH, Hung KY, Hsu SH, Chiang CK, Lu KC. Correlation of interleukin-17-producing effector memory T cells and CD4⁺CD25⁺Foxp3 regulatory T cells with the phosphate levels in chronic hemodialysis patients. *TheScientificWorldJournal*. 2014; 2014:593170.
- Leonardi C, Matheson R, Zachariae C, Cameron G, Li L, Edson-Heredia E, Braun D, Banerjee S. Anti-interleukin-17 monoclonal antibody ixekizumab in chronic plaque psoriasis. *N Engl J Med*. 2012; 366:1190–1199. [PubMed: 22455413]
- Li X, Murray F, Koide N, Goldstone J, Dann SM, Chen J, Bertin S, Fu G, Weinstein LS, Chen M, et al. Divergent requirement for Galphas and cAMP in the differentiation and inflammatory profile of distinct mouse Th subsets. *J Clin Invest*. 2012; 122:963–973. [PubMed: 22326954]
- Lockhart E, Green AM, Flynn JL. IL-17 production is dominated by gammadelta T cells rather than CD4 T cells during Mycobacterium tuberculosis infection. *J Immunol*. 2006; 177:4662–4669. [PubMed: 16982905]
- Lowik CWGM, van der Pluijm G, Bloys H, Hoekman K, Bijvoet OL, Aarden LA, Papapoulos SE. Parathyroid hormone (PTH) and PTH-like protein (PLP) stimulate IL-6 production by osteogenic cells: a possible role of interleukin-6 in osteoclastogenesis. *Biochem.Biophys.Res.Commun*. 1989; 162:1546–1552. [PubMed: 2548501]
- Ma YL, Cain RL, Halladay DL, Yang X, Zeng Q, Miles RR, Chandrasekhar S, Martin TJ, Onyia JE. Catabolic effects of continuous human PTH (1–38) in vivo is associated with sustained stimulation of RANKL and inhibition of osteoprotegerin and gene-associated bone formation. *Endocrinology*. 2001; 142:4047–4054. [PubMed: 11517184]
- Martin DA, Churchill M, Flores-Suarez L, Cardiel MH, Wallace D, Martin R, Phillips K, Kaine JL, Dong H, Salinger D, et al. A phase Ib multiple ascending dose study evaluating safety, pharmacokinetics, and early clinical response of brodalumab, a human anti-IL-17R antibody, in

- methotrexate-resistant rheumatoid arthritis. *Arthritis Res Ther.* 2013; 15:R164. [PubMed: 24286136]
- Martinez GJ, Nurieva RI, Yang XO, Dong C. Regulation and function of proinflammatory TH17 cells. *Ann N Y Acad Sci.* 2008; 1143:188–211. [PubMed: 19076351]
- Mease PJ, Genovese MC, Greenwald MW, Ritchlin CT, Beaulieu AD, Deodhar A, Newmark R, Feng J, Erondy N, Nirula A. Brodalumab, an anti-IL17RA monoclonal antibody, in psoriatic arthritis. *N Engl J Med.* 2014; 370:2295–2306. [PubMed: 24918373]
- Mieth A, Revermann M, Babelova A, Weigert A, Schermuly RT, Brandes RP. L-type calcium channel inhibitor diltiazem prevents aneurysm formation by blood pressure-independent anti-inflammatory effects. *Hypertension.* 2013; 62:1098–1104. [PubMed: 24082061]
- Miossec P, Korn T, Kuchroo VK. Interleukin-17 and type 17 helper T cells. *N Engl J Med.* 2009; 361:888–898. [PubMed: 19710487]
- Molnar I, Bohaty I, Somogyine-Vari E. IL-17A-mediated sRANK ligand elevation involved in postmenopausal osteoporosis. *Osteoporos Int.* 2014; 25:783–786. [PubMed: 24337660]
- Nakae S, Suto H, Berry GJ, Galli SJ. Mast cell-derived TNF can promote Th17 cell-dependent neutrophil recruitment in ovalbumin-challenged OTII mice. *Blood.* 2007; 109:3640–3648. [PubMed: 17197430]
- Nakashima T, Kobayashi Y, Yamasaki S, Kawakami A, Eguchi K, Sasaki H, Sakai H. Protein expression and functional difference of membrane-bound and soluble receptor activator of NF- κ B ligand: modulation of the expression by osteotropic factors and cytokines. *Biochem Biophys Res Commun.* 2000; 275:768–775. [PubMed: 10973797]
- Oh-hora M. Calcium signaling in the development and function of T-lineage cells. *Immunol Rev.* 2009; 231:210–224. [PubMed: 19754899]
- Pacifici R. Role of T cells in the modulation of PTH action: physiological and clinical significance. *Endocrine.* 2013; 44:576–582. [PubMed: 23729167]
- Parisien, M.; Dempster, DW.; Shane, E.; Bilezikian, JP. The parathyroids. Basic and clinical concepts. San Diego: Academic Press; 2001. Histomorphometric analysis of bone in primary hyperparathyroidism; p. 423-436.
- Potts, J. Primary hyperparathyroidism. In: Avioli, LV.; Krane, S., editors. *Metabolic Bone Diseases.* San Diego: Academic Press; 1998. p. 411-442.
- Qin J, Shang L, Ping AS, Li J, Li XJ, Yu H, Magdalou J, Chen LB, Wang H. TNF/TNFR signal transduction pathway-mediated anti-apoptosis and anti-inflammatory effects of sodium ferulate on IL-1 β -induced rat osteoarthritis chondrocytes in vitro. *Arthritis Res Ther.* 2012; 14:R242. [PubMed: 23134577]
- Qin L, Raggatt LJ, Partridge NC. Parathyroid hormone: a double-edged sword for bone metabolism. *Trends Endocrinol Metab.* 2004; 15:60–65. [PubMed: 15036251]
- Robinson JW, Li JY, Walker LD, Tyagi AM, Reott MA, Yu M, Adams J, Weitzmann MN, Pacifici R. T cell-expressed CD40L potentiates the bone anabolic activity of intermittent PTH treatment. *J Bone Miner Res.* 2015; 30:695–705. [PubMed: 25359628]
- Saini V, Marengi DA, Barry KJ, Fulzele KS, Heiden E, Liu X, Dedic C, Maeda A, Lotinun S, Baron R, et al. Parathyroid hormone (PTH)/PTH-related peptide type 1 receptor (PPR) signaling in osteocytes regulates anabolic and catabolic skeletal responses to PTH. *The Journal of biological chemistry.* 2013; 288:20122–20134. [PubMed: 23729679]
- Sato K, Suematsu A, Okamoto K, Yamaguchi A, Morishita Y, Kadono Y, Tanaka S, Kodama T, Akira S, Iwakura Y, et al. Th17 functions as an osteoclastogenic helper T cell subset that links T cell activation and bone destruction. *J Exp Med.* 2006; 203:2673–2682. [PubMed: 17088434]
- Semsarian C, Ahmad I, Giewat M, Georgakopoulos D, Schmitt JP, McConnell BK, Reiken S, Mende U, Marks AR, Kass DA, et al. The L-type calcium channel inhibitor diltiazem prevents cardiomyopathy in a mouse model. *J Clin Invest.* 2002; 109:1013–1020. [PubMed: 11956238]
- Silverberg SJ, Shane E, de la Cruz L, Dempster DW, Feldman F, Seldin D, Jacobs TP, Siris ES, Cafferty M, Parisien MV, et al. Skeletal disease in primary hyperparathyroidism. *J Bone Miner Res.* 1989; 4:283–291. [PubMed: 2763869]

- Sugita S, Kawazoe Y, Imai A, Yamada Y, Horie S, Mochizuki M. Inhibition of Th17 differentiation by anti-TNF-alpha therapy in uveitis patients with Behcet's disease. *Arthritis Res Ther.* 2012; 14:R99. [PubMed: 22546542]
- Sutton CE, Lalor SJ, Sweeney CM, Brereton CF, Lavelle EC, Mills KH. Interleukin-1 and IL-23 induce innate IL-17 production from gammadelta T cells, amplifying Th17 responses and autoimmunity. *Immunity.* 2009; 31:331–341. [PubMed: 19682929]
- Tawfeek H, Bedi B, Li JY, Adams J, Kobayashi T, Weitzmann MN, Kronenberg HM, Pacifici R. Disruption of PTH Receptor 1 in T Cells Protects against PTH-Induced Bone Loss. *PLoS ONE.* 2010; 5:e12290. [PubMed: 20808842]
- Terauchi M, Li JY, Bedi B, Baek KH, Tawfeek H, Galley S, Gilbert L, Nanes MS, Zayzafoon M, Guldberg R, et al. T lymphocytes amplify the anabolic activity of parathyroid hormone through Wnt10b signaling. *Cell metabolism.* 2009; 10:229–240. [PubMed: 19723499]
- Tyagi AM, Srivastava K, Mansoori MN, Trivedi R, Chattopadhyay N, Singh D. Estrogen deficiency induces the differentiation of IL-17 secreting Th17 cells: a new candidate in the pathogenesis of osteoporosis. *PLoS ONE.* 2012; 7:e44552. [PubMed: 22970248]
- Veldhoen M, Hocking RJ, Atkins CJ, Locksley RM, Stockinger B. TGFbeta in the context of an inflammatory cytokine milieu supports de novo differentiation of IL-17-producing T cells. *Immunity.* 2006; 24:179–189. [PubMed: 16473830]
- Waisman A. T helper cell populations: as flexible as the skin? *European journal of immunology.* 2011; 41:2539–2543. [PubMed: 21952814]
- Xiong J, Piemontese M, Thostenson JD, Weinstein RS, Manolagas SC, O'Brien CA. Osteocyte-derived RANKL is a critical mediator of the increased bone resorption caused by dietary calcium deficiency. *Bone.* 2014; 66C:146–154. [PubMed: 24933342]
- Ye P, Rodriguez FH, Kanaly S, Stocking KL, Schurr J, Schwarzenberger P, Oliver P, Huang W, Zhang P, Zhang J, et al. Requirement of interleukin 17 receptor signaling for lung CXC chemokine and granulocyte colony-stimulating factor expression, neutrophil recruitment, and host defense. *J Exp Med.* 2001; 194:519–527. [PubMed: 11514607]
- Yeremenko N, Paramarta JE, Baeten D. The interleukin-23/interleukin-17 immune axis as a promising new target in the treatment of spondyloarthritis. *Current opinion in rheumatology.* 2014; 26:361–370. [PubMed: 24827753]
- Zepp J, Wu L, Li X. IL-17 receptor signaling and T helper 17-mediated autoimmune demyelinating disease. *Trends in immunology.* 2011; 32:232–239. [PubMed: 21493143]
- Zhang J, Fu Q, Ren Z, Wang Y, Wang C, Shen T, Wang G, Wu L. Changes of serum cytokines-related Th1/Th2/Th17 concentration in patients with postmenopausal osteoporosis. *Gynecological endocrinology : the official journal of the International Society of Gynecological Endocrinology.* 2014:1–8. [PubMed: 25211539]

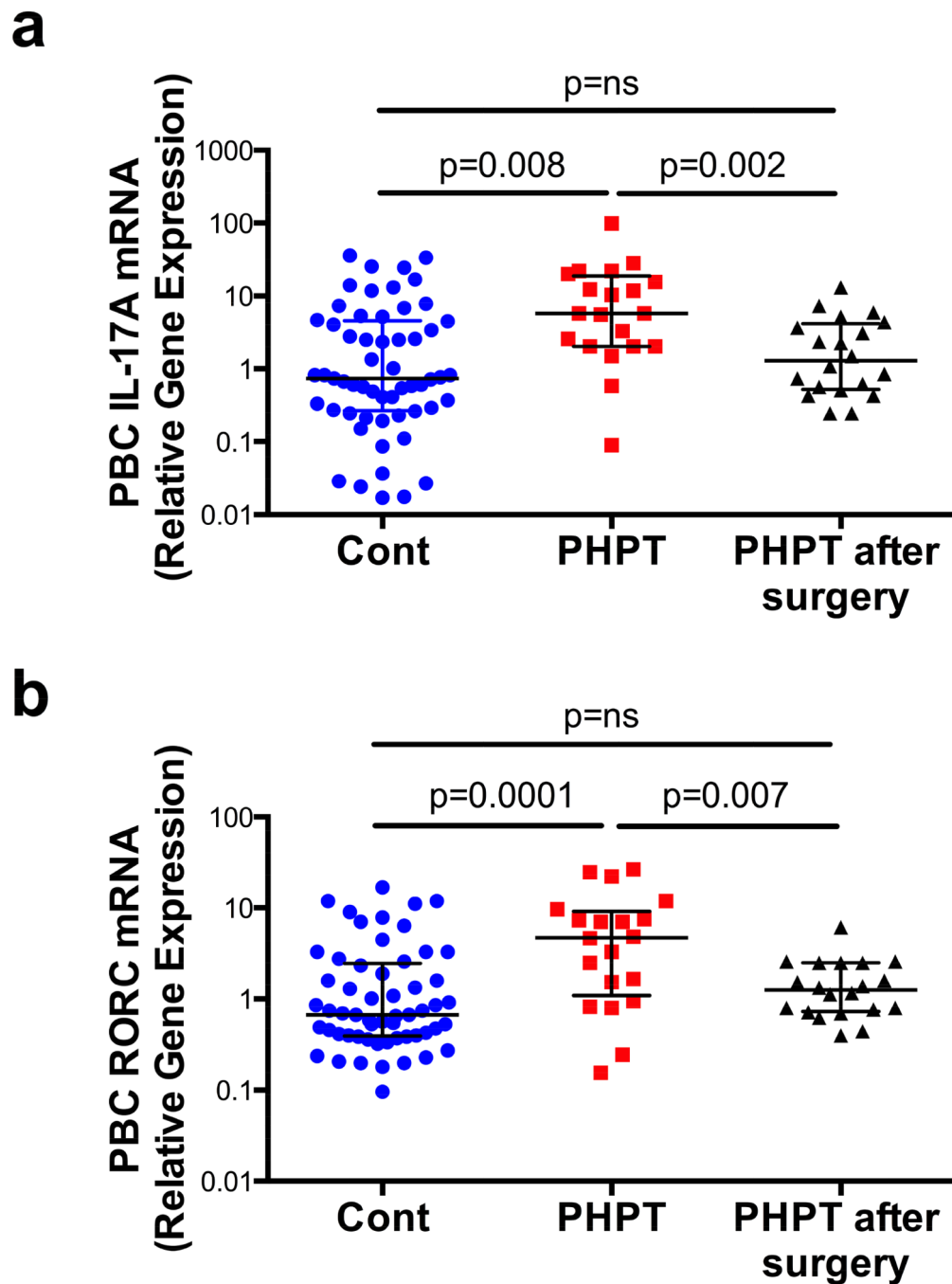


Figure 1. Primary hyperparathyroidism increases IL-17A and RORC mRNA levels in humans
 Levels (Median \pm interquartile range) of IL-17A and RORC mRNAs in healthy controls ($n = 57$) and subjects with PHPT before ($n = 20$) and after parathyroidectomy ($n = 20$). Data were analyzed by Mann Whitney (healthy controls vs. PHPT before surgery and healthy controls vs. PHPT after surgery) and Wilcoxon matched pairs signed rank tests (PHPT vs. PHPT after surgery) as the data were not normally distributed according to the Shapiro-Wilk normality test.

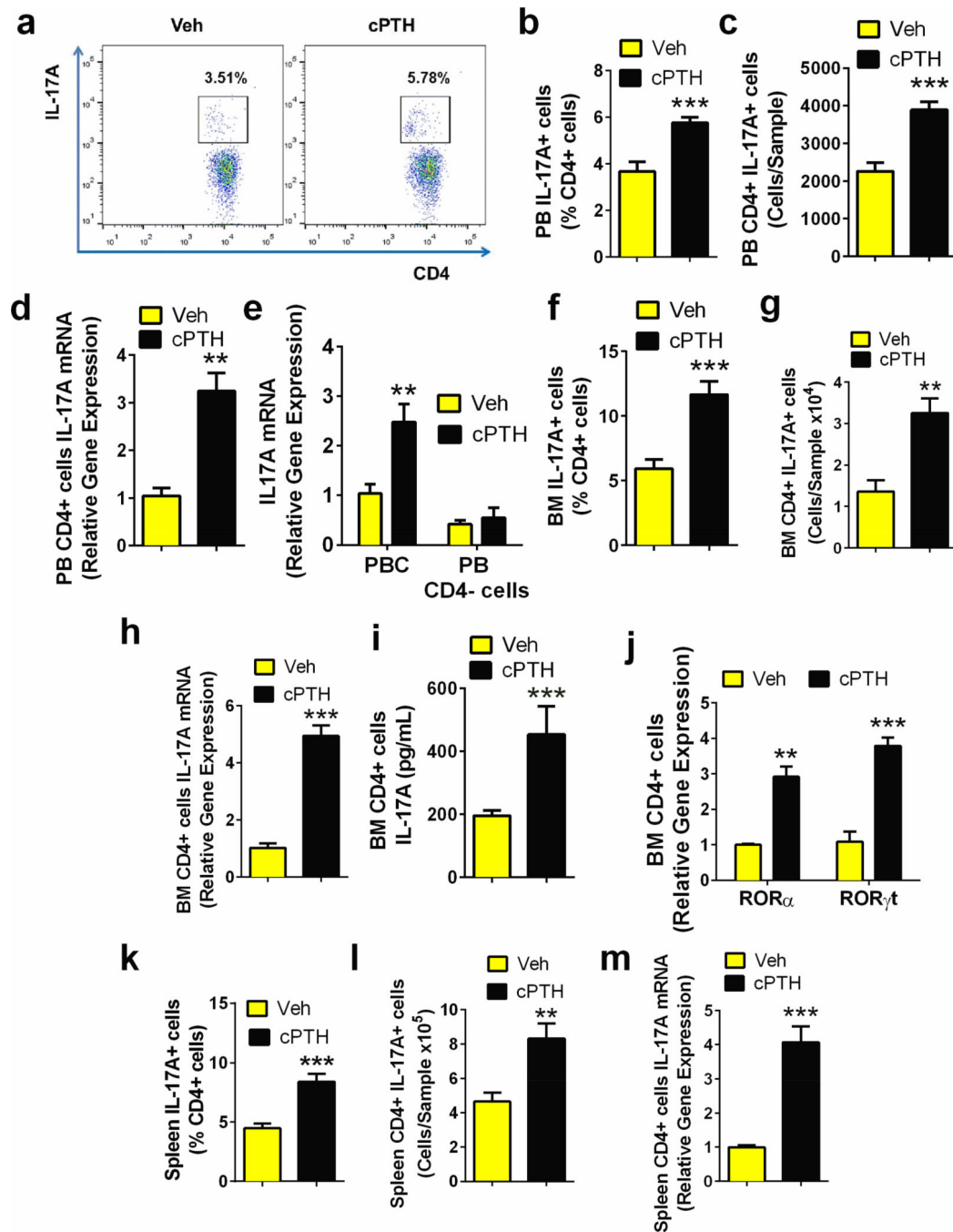


Figure 2. cPTH treatment expands Th17 cells and increases L-17A production

a-c. Frequency of IL-17A producing Th17 cells in unfractionated peripheral blood (PB) cells (PBC). Panel a shows representative flow cytometric dot plots from 1 mouse per group. Panel b shows the relative frequency of CD4+IL-17A+ PBC. Data are expressed as % of CD4+ cells. Panel c shows the absolute number of CD4+IL-17A+ PBCs per sample. **d.** IL-17A mRNA levels in PB CD4+ cells. **e.** IL-17A mRNA levels in unfractionated PBC and CD4+ cell-depleted PBC. **f.** Relative frequency of Th17 cells in the BM. **g.** Absolute number of BM Th17 cells per sample. **h.** IL-17A mRNA levels in BM CD4+ cells. **i.** IL-17A protein

levels in BM CD4⁺ cells. **j.** mRNA levels of the Th17 cells-inducing transcription factors ROR α and ROR γ t in BM CD4⁺ cells. **k.** Relative frequency of Th17 cells in the spleen. **l.** Absolute number of Th17 cells in the spleen **m.** IL-17A mRNA levels in spleen CD4⁺ cells. Data in panels b-m are shown as mean \pm SEM. n = 8 mice per group in all panels. All data passed the Shapiro-Wilk normality test and were analyzed by unpaired t-tests **= $p < 0.01$ and ***= $p < 0.001$ compared to the corresponding vehicle group.

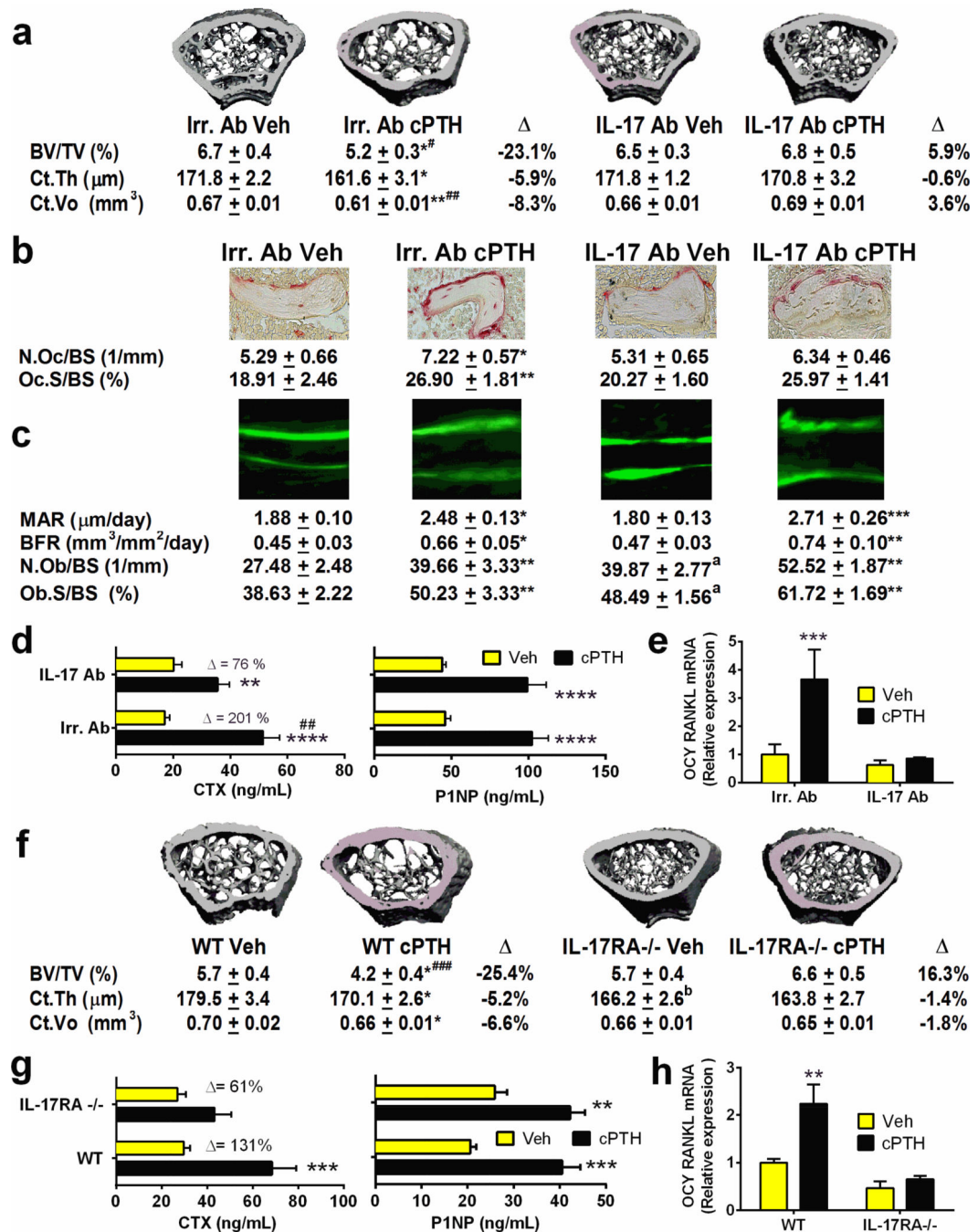


Figure 3. Silencing of IL-17A or IL-17A signaling prevents the bone catabolic effect of cPTH
 Effects (mean ± SEM) of cPTH on bone volume, structure and turnover in mice treated with IL-17A Ab or lacking IL-17A. **a.** In vitro measurements of cortical and trabecular bone indices of volume and structure by μ CT scanning in WT mice treated with vehicle or cPTH and Irrelevant Ab (Irr. Ab) or anti IL-17A Ab. n = 12 mice per group. Representative 3-dimensional μ CT reconstructions of the femurs are shown above the data. **b.** Histomorphometric indices of bone resorption (obtained in the first 10 of the 12 mice per group enrolled in the study). The images show TRAP stained sections of the distal femur

used to compute the number of OCs per mm bone surface (N.Oc/BS) and the percentage of bone surface covered by OCs (Oc.S/BS), which are indices of bone resorption. Original magnification $\times 40$. **c.** Dynamic indices of bone formation. The images show calcein double-fluorescence labeling used to compute mineral apposition rate (MAR) and bone formation rate (BFR), which are indices of bone formation. Original magnification $\times 20$. The number of OBs per mm bone surface (N.Ob/BS) and the percentage of bone surface covered by OBs (Ob.S/BS), which are static indices of formation, were measured on trichrome-stained sections. **d.** Serum levels of CTX and P1NP. $n = 12$ mice per group. **e.** mRNA levels of RANKL in purified osteocytes (OCYs). $n = 5$ mice per group. **f.** μ CT measurements of cortical and trabecular bone volume and structure in samples from WT and IL-17RA $^{-/-}$ mice. $n = 14$ mice per group. The images are 3-dimensional reconstructions of the femurs. **g.** Serum levels of CTX and P1NP. $n = 14$ mice per group. **h.** mRNA levels of RANKL in purified OCYs from WT and IL-17RA $^{-/-}$ mice. $n = 5$ mice per group. All data passed the Shapiro-Wilk normality test and were analyzed by 2-Way ANOVA. * = $p < 0.05$, ** = $p < 0.01$ and *** = $p < 0.001$ compared to the corresponding vehicle treated group. # = $p < 0.05$, and ## = $p < 0.01$ compared to IL-17 Ab cPTH. ### = $p < 0.001$ compared to IL-17RA $^{-/-}$ cPTH. a = $p < 0.05$ compared to Irr. Ab Veh. b = $p < 0.05$ compared to WT Veh.

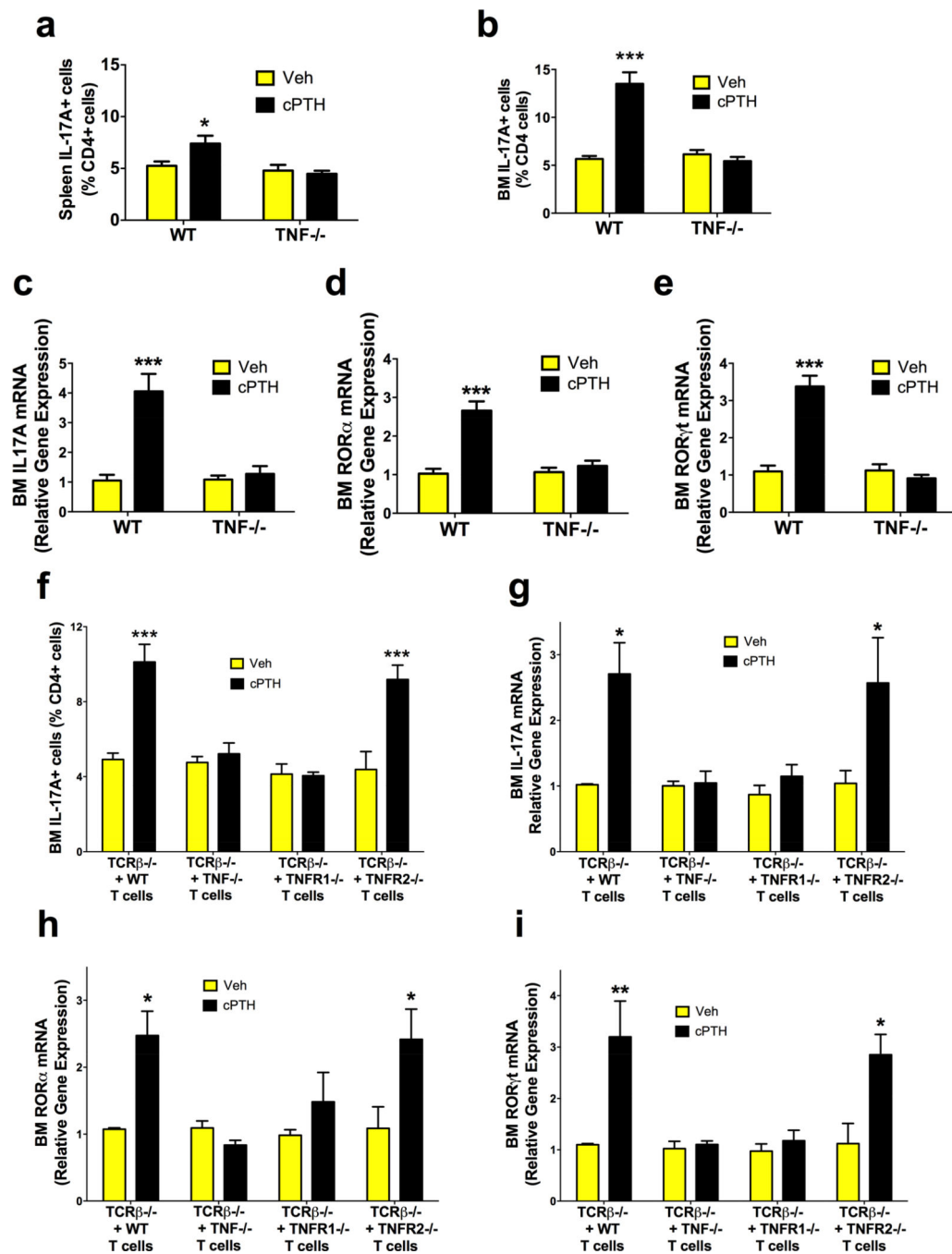


Figure 4. cPTH expands Th17 cells through TNF and TNFR1 signaling

a-b. Relative frequency of Th17 cells in the spleen and BM of WT and TNF^{-/-} mice. **c.** IL-17A mRNA levels in BM CD4⁺ cells of WT and TNF^{-/-} mice. **d,e.** ROR α and ROR γ t mRNA levels in BM CD4⁺ cells of WT and TNF^{-/-} mice. **f.** Relative frequency of Th17 cells in the BM of TCR β ^{-/-} mice previously subjected to adoptive transfer of WT T cells, TNF^{-/-} T cells, TNFR1^{-/-} T cells, or TNFR2^{-/-} T cells. **g.** IL-17A mRNA levels in BM CD4⁺ cells of TCR β ^{-/-} mice previously subjected to adoptive transfer of WT T cells, TNF^{-/-} T cells, TNFR1^{-/-} T cells, or TNFR2^{-/-} T cells. **h,i.** Levels of ROR α and ROR γ t

mRNA in BM CD4⁺ cells of TCR β ^{-/-} mice previously subjected to adoptive transfer of WT T cells, TNF^{-/-} T cells, TNFR1^{-/-} T cells, or TNFR2^{-/-} T cells. Data are expressed as the mean \pm SEM. n = 8 mice per group. All data passed the Shapiro-Wilk normality test and were analyzed by 2-Way ANOVA. *= $p < 0.05$, **= $p < 0.01$ and ***= $p < 0.001$ compared to the corresponding vehicle group.

Author Manuscript

Author Manuscript

Author Manuscript

Author Manuscript

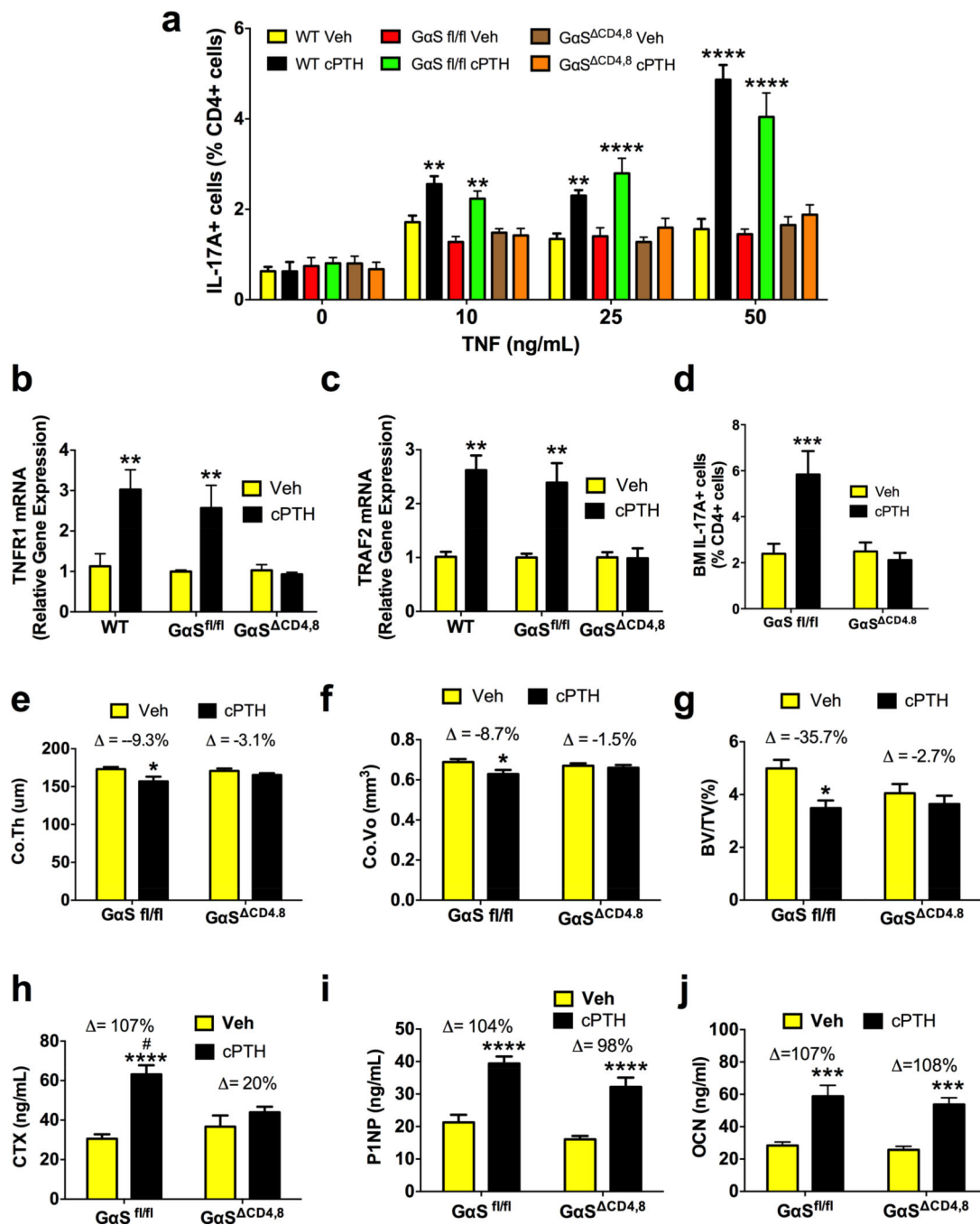


Figure 5. cPTH expands Th17 cells, causes bone loss and stimulates bone resorption through activation of G α S in naïve CD4+ cells

a. cPTH increases the sensitivity to TNF of naïve CD4+ cells from WT and G α S fl/fl mice but not of those from G α S ^{ΔCD4,8} mice. Naïve CD4+ cells were sorted from vehicle and cPTH treated mice and cultured with TNF (10–50 ng/ml) to induce their differentiation into Th17 cells. **b.** TNFR1 mRNA levels in BM CD4+ cells. **c.** TRAF2 mRNA levels in BM CD4+ cells **d.** Frequency of BM Th17 cells. **e-g.** mCT indices of bone volume and structure. **h-j.** Serum levels of CTX, P1NP and osteocalcin (OCN). Data are shown as mean \pm SEM. n

= 5 mice per group for panels b-c. n = 16 G α S fl/fl mice per group and 21 G α S^{CD4,8} mice per group for panels d-j. All data passed the Shapiro-Wilk normality test and were analyzed by 2-Way ANOVA. * = p < 0.05, ** = p < 0.01, *** = p < 0.001 and **** = p < 0.0001 compared to the corresponding vehicle group. # = p < 0.05 compared to the G α S^{CD4,8} cPTH group.

Author Manuscript

Author Manuscript

Author Manuscript

Author Manuscript

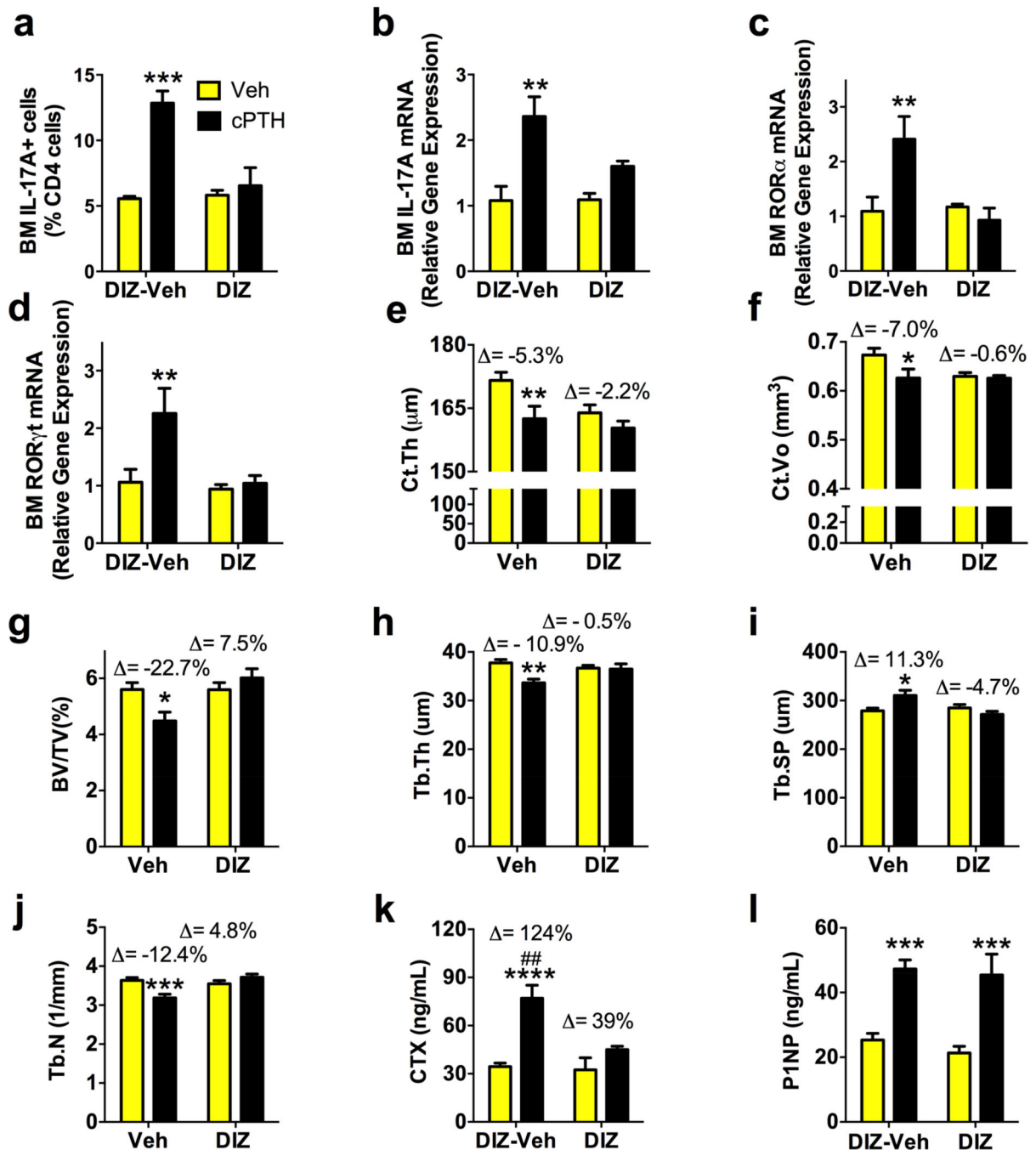


Figure 6. The L-type calcium channel blocker diltiazem (DIZ) prevents the effects of cPTH
a relative frequency of BM Th17 cells, **b** IL-17A mRNA levels in BM CD4+ cells **c-d**
 expression of ROR α and ROR γ t mRNA in BM CD4+ cells, **e-j** μ CT indices of bone volume
 and structure. **k,l** Serum levels of CTX and P1NP. Data are shown as mean \pm SEM. n = 12
 mice per group. All data passed the Shapiro-Wilk normality test and were analyzed by 2-
 Way ANOVA. *= $p < 0.05$, **= $p < 0.01$, ***= $p < 0.001$ and ****= $p < 0.0001$ compared to the
 corresponding vehicle group. ## = $p < 0.01$ compared to the DIZcPTH group.

Table 1

Demographic and clinical data of healthy controls and PHPT patients before and after surgery. Data are shown as Mean \pm SEM for normally distributed variables (serum P and demographic data) and median with interquartile range for non-normally distributed variables (serum Ca, PTH, and 25OH Vitamin D). Values in squared parenthesis denote normal range.

	Healthy Controls	PHPT before surgery	PHPT after surgery
Study Participants (n)	57	20	20
Age (years)	60.1 \pm 2.3	57.3 \pm 3.4 ^a	57.3 \pm 3.4 ^a
Males (n)	25	4	4
Males Age (years)	66.5 \pm 3.6	67.5 \pm 7.2 ^a	67.5 \pm 7.2 ^a
Females (n)	32	16	16
Female Age (years)	56.7 \pm 2.9	54.5 \pm 3.7 ^a	54.5 \pm 3.7 ^a
Postmenopausal females (n)	23	8 ^a	8 ^a
Years since menopause	15.5 \pm 2.3	15.7 \pm 3.5 ^a	15.7 \pm 3.5 ^a
Serum Ca (mg/dL) [8.8–10.4 mg/dL]	9.4 (9.1–9.7)	10.8 (10.5–12.0) ^b	8.8 (8.7–9.1) ^{d,b}
Serum P (mg/dL) [2.5–4.5 mg/dL]	3.3 \pm 0.07	2.7 \pm 0.3 ^c	3.5 \pm 0.4 ^{e,a}
PTH (pg/mL) [10–65 pg/mL]	53 (32–63)	102 (79–161) ^b	56.5 (41.8–75.8) ^{d,a}
25OH vitamin D [30–100 ng/mL]	19.6 (5.7–27.2)	17.8 (15.1–22.4) ^a	23.6 (21.9–30.4) ^{f,a}

p values:

^a ns,

^b <0.0001 and

^c 0.005 compared to Healthy Controls;

^d <0.0001,

^e <0.05 and

^f <0.01 compared to PHPT.

Simvastatin and downstream inhibitors circumvent constitutive and stromal cell-induced resistance to doxorubicin in IGHV unmutated CLL cells

Micol Rigoni^{1,2,*}, Chiara Riganti^{3,*}, Candida Vitale^{1,2}, Valentina Griggio^{1,2}, Ivana Campia³, Marta Robino¹, Myriam Foglietta^{1,2}, Barbara Castella², Patrizia Sciancalepore^{1,2}, Iliaria Buondonno³, Daniela Drandi¹, Marco Ladetto¹, Mario Boccardo¹, Massimo Massaia^{2,4,*}, Marta Coscia^{1,2,*}

¹Division of Hematology, Azienda Ospedaliero Universitaria Città della Salute e della Scienza di Torino, University of Torino, Torino, Italy

²Center for Experimental Research and Medical Studies, Azienda Ospedaliero Universitaria Città della Salute e della Scienza di Torino, Torino, Italy

³Department of Oncology, University of Torino, Torino, Italy

⁴S.C. Ematologia e Terapie Cellulari, Azienda Ospedaliera Ordine Mauriziano di Torino, Torino, Italy

*These authors have contributed equally to this work

Correspondence to:

Marta Coscia, e-mail: marta.coscia@unito.it

Keywords: chronic lymphocytic leukemia, multidrug resistance, mevalonate pathway, statins

Received: August 28, 2014

Accepted: May 15, 2015

Published: May 27, 2015

ABSTRACT

The immunoglobulin heavy-chain variable region (IGHV) mutational status is a strong determinant of remission duration in chronic lymphocytic leukemia (CLL). The aim of this work was to compare the multidrug resistance (MDR) signature of IGHV mutated and unmutated CLL cells, identifying biochemical and molecular targets potentially amenable to therapeutic intervention.

We found that the mevalonate pathway-dependent Ras/ERK1–2 and RhoA/RhoA kinase signaling cascades, and the downstream HIF-1 α /P-glycoprotein axis were more active in IGHV unmutated than in mutated cells, leading to a constitutive protection from doxorubicin-induced cytotoxicity. The constitutive MDR phenotype of IGHV unmutated cells was partially dependent on B cell receptor signaling, as shown by the inhibitory effect exerted by ibrutinib. Stromal cells further protected IGHV unmutated cells from doxorubicin by upregulating Ras/ERK1–2, RhoA/RhoA kinase, Akt, HIF-1 α and P-glycoprotein activities. Mevalonate pathway inhibition with simvastatin abrogated these signaling pathways and reversed the resistance of IGHV unmutated cells to doxorubicin, also counteracting the protective effect exerted by stromal cells. Similar results were obtained via the targeted inhibition of the downstream molecules ERK1–2, RhoA kinase and HIF-1 α .

Therefore, targeting the mevalonate pathway and its downstream signaling cascades is a promising strategy to circumvent the MDR signature of IGHV unmutated CLL cells.

INTRODUCTION

Chronic lymphocytic leukemia (CLL) is characterized by a highly heterogeneous clinical course and a poor curability with conventional chemotherapy treatment approaches. The immunoglobulin heavy-chain variable region (IGHV) mutational status has emerged as a powerful

prognosticator: patients with IGHV unmutated (UM) CLL cells display inferior survival rates [1, 2] and shorter complete remission duration than IGHV mutated (M) patients [3].

Stromal cells (SCs) are known to protect CLL cells from spontaneous apoptosis and drug-induced cytotoxicity. We previously reported that IGHV UM cells are more dependent than M cells on microenvironment-mediated

signals for their survival [4]. However, whether IGHV M and UM CLL cells differ for their *ex vivo* susceptibility to chemotherapy is controversial [5, 6].

Results from clinical trials have shown that fludarabine, even when used as a single agent, induced higher remission rates than other chemotherapies, such as CAP (cyclophosphamide, doxorubicin, prednisone) or CHOP (cyclophosphamide, doxorubicin, vincristine, prednisone), in previously untreated CLL patients [7, 8]. However, the reasons accounting for the lower effectiveness of anthracycline-containing regimens in CLL remain largely unexplored.

One of the main mechanisms of chemoresistance is the overexpression of membrane transporters which actively extrude chemotherapy drugs, a process called multidrug resistance (MDR). Anthracyclines, such as doxorubicin (Doxo), are substrates of one of the best characterized drug efflux pump, the P-glycoprotein (Pgp/ABCB1), which is encoded by the MDR1 gene [9].

Pgp activity is directly related to the amount of cell cholesterol in the plasma membrane [10], and its expression is regulated by the transcription factor hypoxia-inducible factor-1 alpha (HIF-1 α), whose activation is dependent on Ras/ERK1–2 and RhoA/RhoA kinase signaling pathways [11].

All these pathways are under the control of the mevalonate (Mev) pathway, a highly conserved metabolic cascade which produces sterols, such as cholesterol, and isoprenoids, such as farnesyl pyrophosphate (FPP) and geranylgeranyl pyrophosphate (GGPP). The latter are necessary for the isoprenylation of Ras and RhoA GTPases, and for the activation of their downstream signaling pathways [12].

The Mev pathway can be pharmacologically inhibited using statins (e.g. simvastatin, SIM) or amino-bisphosphonates (e.g. zoledronic acid, ZA) [13], and we have already shown that ZA can restore the sensitivity of MDR positive (MDR+) solid tumor cell lines to Doxo [14].

CLL cells carrying IGHV UM genes have significantly higher levels of Mev pathway activity, which are thought amenable to pharmacological manipulation by SIM and ZA [15]. It is currently unknown whether the higher activity of the Mev pathway in IGHV UM cells translates into a MDR+ phenotype, and whether the targeted inhibition of the Mev pathway or downstream signaling can eventually counteract the MDR+ signature of CLL cells.

The aim of this study was twofold: 1) to characterize the MDR status of IGHV M and UM cells, by evaluating the activity of Ras/ERK1–2, RhoA/RhoA kinases, and HIF-1 α /Pgp axis under basal conditions and after exposure to SCs; 2) to determine whether targeting the Mev pathway and its downstream signaling eventually restores the sensitivity of MDR+ CLL cells to Doxo.

RESULTS

The Ras/ERK1–2 and RhoA/RhoA kinase signaling pathways and the HIF-1 α /Pgp axis are more active in IGHV UM than M CLL cells

The activity of Ras- and RhoA-dependent signaling pathways was analyzed in IGHV M and UM CLL cells (>90% pure as described below) after *ex vivo* culture for 24 hours. Both type of cells exhibited detectable amounts of non-isoprenylated cytosolic Ras and unphosphorylated ERK1–2, but only IGHV UM cells showed high intracellular levels of the Ras GTP-bound active form and the Ras-downstream effector kinase phospho-ERK1–2 (Figure 1A, left), in keeping with their accelerated Mev pathway activity [15]. Similarly, the amount of active GTP-bound RhoA and the activity of the downstream RhoA kinase were significantly higher in IGHV UM than M cells (p always = 0.001) (Figure 1A, right).

Both ERK1–2 and RhoA kinase phosphorylate and activate the transcription factor HIF-1 α [16, 17]. Accordingly, the activation of Ras/ERK1–2 and RhoA/RhoA kinase signalling pathways in IGHV UM cells led to the phosphorylation of HIF-1 α (Supplementary Figure S1) and to the increase of its transcriptional activity, as shown by the significantly higher amounts of nuclear HIF-1 α bound to its specific DNA target sequence (p = 0.002) (Figure 1B, left). As a consequence, IGHV UM cells showed higher MDR1 mRNA expression (Figure 1B, right) and lower Doxo accumulation than IGHV M cells (p always = 0.001) (Figure 1C).

In agreement with our previous data [4], both untreated IGHV M and UM cells showed high levels of viability after *ex vivo* culture for 48 hours, whereas Doxo treatment induced a significant decrease of viability in IGHV M compared to UM CLL cells (p = 0.001) (Figure 1D and Supplementary Figure S2).

The constitutive MDR phenotype of IGHV UM cells depends on BCR signaling and is further upregulated by SC-mediated extrinsic signals

IGHV UM cells display an increased signaling through the B cell receptor (BCR) compared to IGHV M cells [18]. To study the effect of BCR signaling on Mev-regulated pathways and MDR phenotype we incubated IGHV M and UM cells with anti-IgM antibody, in the presence or absence of the Bruton tyrosine kinase (BTK) inhibitor ibrutinib. Anti-IgM-mediated BCR stimulation did not increase the baseline production of cholesterol and FPP (Figure 2A), the amount of GTP-bound RhoA and the activity of RhoA kinase (Figure 2B), the transcriptional activity of HIF-1 α and the expression of its target gene MDR1 (Figure 2C) in both IGHV M and UM cells. Of note, ibrutinib-mediated BCR inhibition

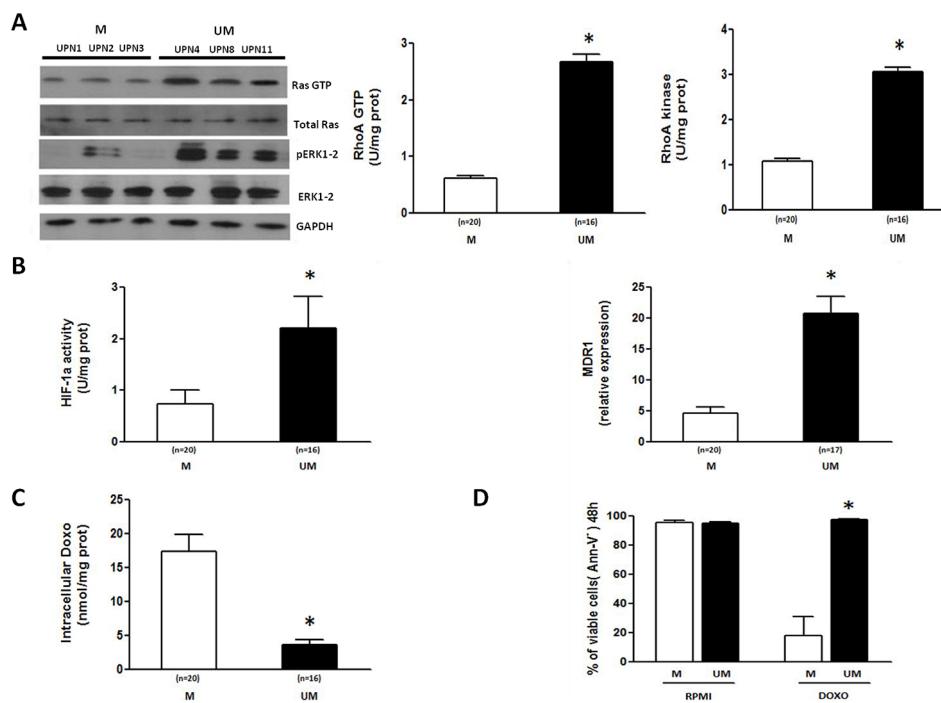


Figure 1: The Ras/ERK1–2 and RhoA/RhoA kinase signaling pathways and the HIF-1 α /Pgp axis are more active in IGHV UM than M CLL cells. The activity of the Ras/ERK1–2 and RhoA/RhoA kinase signaling cascades and the HIF-1 α /Pgp axis were measured in CLL cells isolated from the peripheral blood of IGHV M and UM patients after 24-hour *ex vivo* culture. **A.** Ras and ERK1–2 kinase activities were measured by Western Blot (WB) (left side). IGHV UM cells have a higher expression of the active forms of Ras (Ras GTP) and ERK1–2 (pERK1–2), than IGHV M cells. Results are from 3 representative experiments for both M and UM patients (UPN, unique patient number). RhoA GTP and RhoA Kinase activities were measured by ELISA assays (right side). IGHV UM cells have higher activities of RhoA GTP and RhoA Kinase compared to M cells ($*p = 0.001$). **B.** HIF-1 α activity and MDR1 mRNA expression. IGHV UM cells have higher HIF-1 α activity compared to M cells ($*p = 0.002$) after 24 hours of culture. At the same time-point, significantly higher MDR1 levels were observed in IGHV UM cells than in M cells ($*p = 0.001$). **C.** Intracellular Doxo accumulation. Significantly lower concentrations of Doxo were detected after 48-hour *ex vivo* exposure in IGHV UM than in M cells ($*p = 0.001$). **D.** Viability of CD19+/CD5+ cells was determined by Annexin-V (Ann-V) staining and cytofluorimetric analysis after 48-hour Doxo exposure. IGHV UM cells showed higher levels of viability than M cells ($*p = 0.001$). Results are from 7 experiments for both M and UM patients. In all panels, bars represent mean values \pm SEM.

significantly decreased the constitutively higher levels of cholesterol and FPP production, RhoA and RhoA kinase activity, HIF-1 α transcriptional activity and MDR1 expression in IGHV UM cells (p always ≤ 0.05), whereas it did not affect the Mev pathway and Mev-regulated signaling in IGHV M cells.

SCs are known to confer a chemoresistant phenotype to CLL cells [19–21]. Therefore, we also sought whether IGHV M and UM cells co-cultured with the murine stromal cell line M2–10B4 upregulated the Mev pathway and the RhoA/RhoA kinase signaling pathways. IGHV M and UM cells showed high and comparable levels of cell viability after 24-hour *ex vivo* culture, both in the presence and in the absence of SCs (data not shown). After exposure to M2–10B4 SCs, the production of cholesterol and FPP (Figure 3A), the amount of GTP-bound RhoA and the activity of RhoA kinase (Figure 3B), the transcriptional activity of HIF-1 α , and the expression of its target gene MDR1 (Figure 3C) were significantly increased in IGHV UM but not in M CLL cells (p always ≤ 0.03).

SIM effectively reverses the MDR phenotype of IGHV UM cells and restores Doxo-induced cytotoxicity

We next examined whether SIM, which switches off the Mev pathway downstream to the rate-controlling enzyme 3-hydroxy-3-methyl-glutaryl-CoA reductase, was effective in reversing the MDR phenotype of IGHV UM cells.

In IGHV UM cells, SIM significantly reduced cholesterol and FPP production (p always ≤ 0.05) (Figure 4A), the amounts of GTP-bound Ras and phospho-ERK1–2 kinases (Figure 4B), the amounts of GTP-bound RhoA and the activity of RhoA kinase (Figure 4C), also abrogating the upregulating effect exerted by M2–10B4 SCs (p always ≤ 0.0005).

This SIM-mediated inhibition of the Mev pathway and downstream signaling pathways was paralleled by a lower HIF-1 α phosphorylation (Supplementary Figure S3) and a statistically significant decrease in HIF-1 α activity and MDR1 expression in IGHV UM cells, both in the presence or absence of SCs (p always < 0.003) (Figure 5A, 5B). Thus,

SIM significantly increased the accumulation of intracellular Doxo, even in the presence of SCs (p always ≤ 0.002) (Figure 5C). The SIM-induced increase in Doxo accumulation determined an enhanced cytotoxic death of IGHV UM cells after exposure to the combination SIM+Doxo for 48 hours ($p \leq 0.0001$). Interestingly, SIM was also effective in reversing the protective effect exerted by M2–10B4 SCs ($p \leq 0.0001$) (Figure 5D and Supplementary Figure S4).

SIM effectively abrogates SC-induced Akt upregulation in IGHV UM cells

We next examined the effect of another Mev pathway inhibitor, ZA, which switches off the pathway downstream to FPP-synthase. ZA significantly abrogated cholesterol and FPP synthesis in IGHV UM cells cultured alone ($p \leq 0.05$),

and also in IGHV UM cells cultured with M2–10B4 SCs ($p \leq 0.03$) (Supplementary Figure S5A, S5B). Moreover, ZA was effective in reducing the amount of the active GTP-bound form of Ras and phospho-ERK1–2, even in the presence of the M2–10B4 SCs (Supplementary Figure S5C, S5D). Similarly, the exposure of IGHV UM cells to ZA significantly reduced the amount of the active GTP-bound form of RhoA and the activity of the downstream RhoA kinase, irrespective of the presence or absence of SCs (p always ≤ 0.01) (Supplementary Figure S5E, S5F).

The inhibition of Ras/ERK1–2 and RhoA/RhoA kinase signaling was paralleled by a reduction of HIF-1 α phosphorylation (Supplementary Figure S6), and a significant decrease in HIF-1 α activity and MDR1 expression in the presence or absence of SCs (p always ≤ 0.05) (Supplementary Figure S7A, S7B).

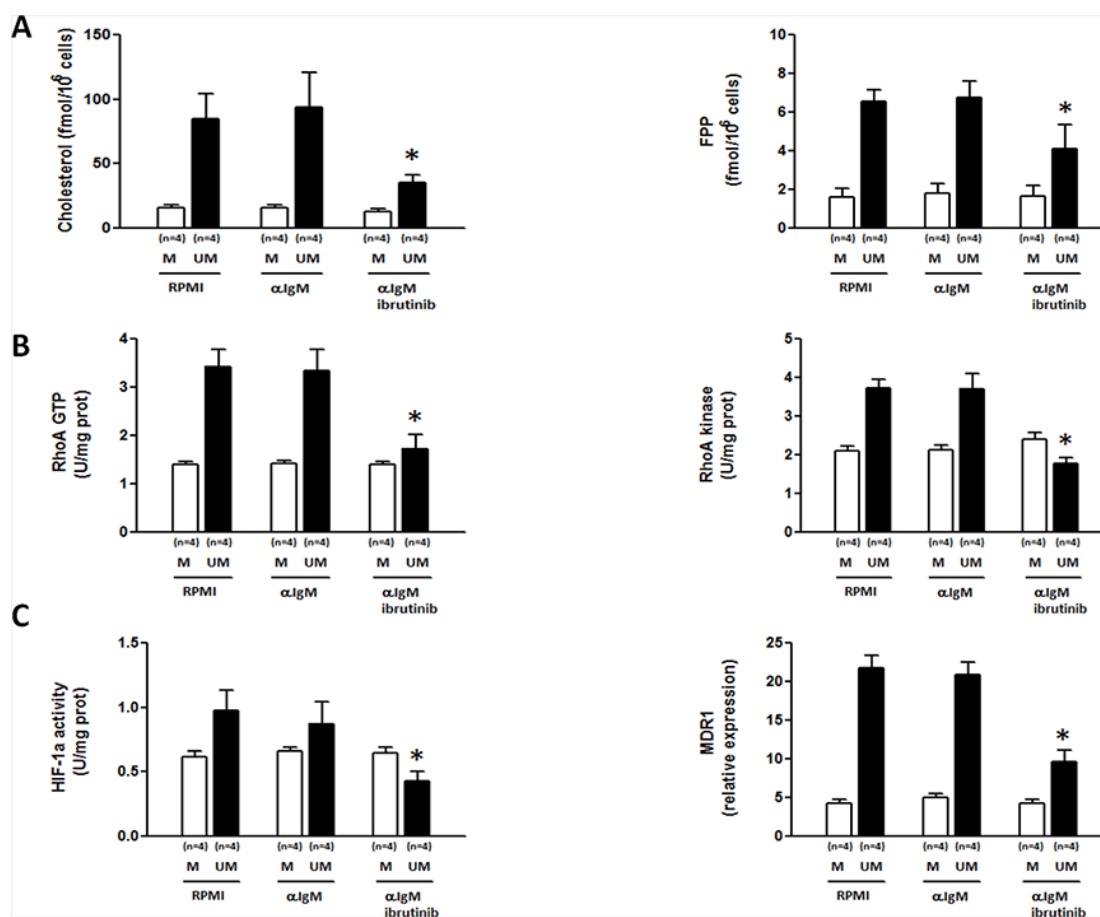


Figure 2: Ibrutinib inhibits the Mev pathway activity, the RhoA/RhoA kinase cascade and the HIF-1 α /Pgp axis in IGHV UM but not in IGHV M cells. IGHV M and UM cells were stimulated for 24 hours with anti-IgM (10 μ g/well) in the absence or presence of 30-minute pre-incubation with ibrutinib (1 μ M). **A.** Cholesterol and FPP production. Anti-IgM stimulation did not increase cholesterol and FPP production in IGHV M and UM cells. IgM+ibrutinib significantly reduced the levels of cholesterol and FPP in IGHV UM cells (* $p = 0.04$ and * $p = 0.05$, respectively). **B.** RhoA and RhoA kinase activity. Anti-IgM stimulation had no effect on RhoA-GTP expression and RhoA kinase activity in IGHV M and UM cells. The amount of GTP-bound RhoA and the activity of the RhoA kinase were significantly reduced by IgM+ibrutinib in IGHV UM cells (* $p = 0.0015$ and * $p = 0.0021$, respectively), but not in IGHV M cells. **C.** HIF-1 α activity and MDR1 expression. Anti-IgM stimulation did not increase HIF-1 α activity and MDR1 expression in IGHV M and UM cells. The activity of HIF-1 α and MDR1 expression were significantly reduced by IgM+ibrutinib in IGHV UM cells (* $p = 0.01$ and * $p = 0.0012$, respectively), but not in IGHV M cells. In all panels, bars represent mean values \pm SEM of side-by-side experiments performed in replicates.

Unlike SIM, ZA was unable to increase Doxo accumulation and Doxo-induced cytotoxicity in IGHV UM cells cultured in the presence or in the absence of M2-10B4 SCs (Supplementary Figure S7C, S7D).

To further elucidate the difference between ZA and SIM, we also evaluated the effects on Akt and NF- κ B, which are well-known pro-survival factors for CLL cells [22]. The baseline activity of Akt, but not that of NF- κ B, was significantly higher in IGHV UM than M cells ($p \leq 0.001$) (Figure 6A, 6B). The same results were confirmed by evaluating the expression of the active phosphorylated form of Akt and the nuclear translocation of the NF- κ B components p50 and p65 by western blot analyses (Supplementary Figure S8A, S8B).

Akt activity was further upregulated by the presence of M2-10B4 SCs (Figure 5C and Supplementary Figure S9A), whereas NF- κ B activity was not, as previously reported [4]. ZA significantly increased Akt activity in IGHV UM cells ($p \leq 0.009$), and this effect was particularly evident when ZA and SCs were used in combination ($p \leq 0.03$) (Supplementary Figure S9A). Of note, ZA also increased NF- κ B activity in IGHV UM cells, both in the absence and in the presence of SCs ($p \leq 0.05$ and $p \leq 0.04$, respectively) (Supplementary Figure S9B). Unlike ZA, SIM

reduced the baseline Akt and NF- κ B activities ($p \leq 0.02$), and significantly abrogated the SC-induced up-regulation of Akt and NF- κ B activity ($p \leq 0.03$; Figure 6C, 6D), Akt phosphorylation (Supplementary Figure S8C) and NF- κ B nuclear translocation (Supplementary Figure S8D).

Specific inhibitors of ERK1-2, RhoA kinase and HIF-1 α reverse the MDR phenotype of IGHV UM cells

We also tested the activity of specific inhibitors targeting ERK1-2 kinases (PD98059, PD), RhoA kinase (Y27632, Y276) and HIF-1 α (YC-1) in IGHV UM cells cultured alone or in the presence of SCs. Of note, the three inhibitors, as well as the upstream Mev pathway inhibitor SIM, had no impact on SCs viability after 48 hours of culture and did not increase the cytotoxic activity of Doxo toward SCs (Supplementary Figure S10).

In IGHV UM CLL cells, PD and Y276 markedly reduced HIF-1 α phosphorylation (Supplementary Figure S11). Moreover, PD, Y276 and YC-1 reduced HIF-1 α activity (Figure 7A) and MDR1 expression (Figure 7B), and increased intracellular Doxo accumulation (p always ≤ 0.0048) (Figure 7C) and Doxo-mediated cytotoxicity

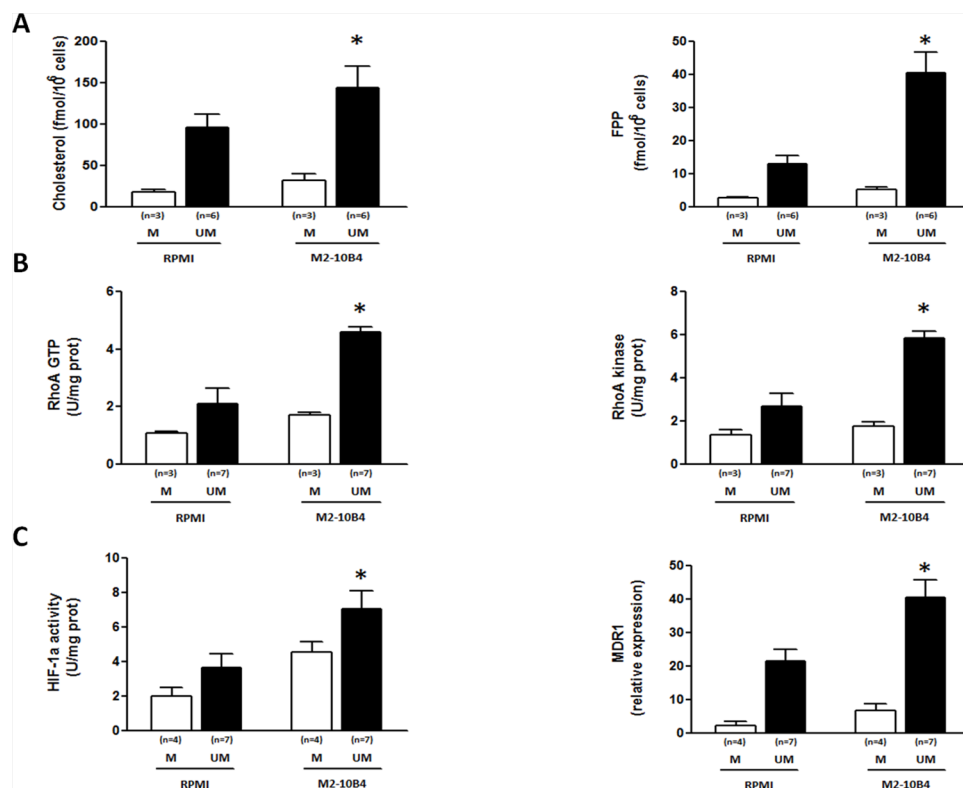


Figure 3: SCs upregulate the Mev pathway activity, the RhoA/RhoA kinase cascade and the HIF-1 α /Pgp axis in IGHV UM but not in IGHV M CLL cells. The production of cholesterol and FPP **A**, the amount of GTP-bound RhoA and the activity of the RhoA kinase **B**, the transcriptional activity of HIF-1 α and the expression of the MDR1 gene **C**, were higher in IGHV UM cells cultured for 24 hours with M2-10B4 SCs compared to IGHV UM cells cultured alone (* p always ≤ 0.002). SCs did not have a significant impact on the activity of the Mev pathway and downstream molecules in IGHV M cells. In all panels, bars represent mean values \pm SEM of side-by-side experiments performed in replicates.

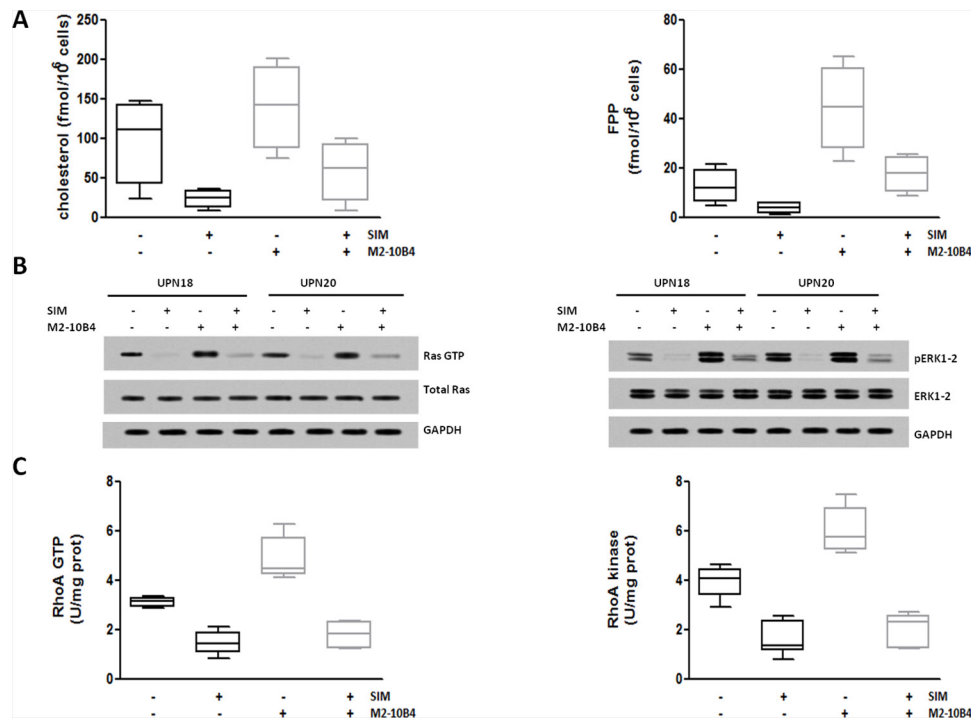


Figure 4: SIM-mediated inhibition of Ras/ERK1–2 and RhoA/RhoA kinase signaling pathways. IGHV UM cells, cultured alone or in the presence of the murine stromal cell line M2–10B4, were exposed to 1 μ M SIM. **A.** Cholesterol and FPP production. The amount of cholesterol and FPP produced by IGHV UM cells was significantly increased after 24-hour co-culture with SCs ($p = 0.007$ and $p = 0.009$, respectively). SIM significantly reduced the levels of cholesterol and FPP in IGHV UM cells both in the absence ($p = 0.04$ and $p = 0.05$, respectively) and in the presence ($p = 0.03$ and $p = 0.01$, respectively) of M2–10B4 SCs. **B.** Ras and ERK1–2 kinase activity. Co-culture with M2–10B4 SCs increased the levels of Ras-GTP and phospho-ERK1–2 kinase. SIM reduced the expression of the active forms of Ras and phospho-ERK1–2 kinase in IGHV UM cells, both in the absence and in the presence of SCs. Results are from two representative experiments (UPN, unique patient number). **C.** RhoA and RhoA kinase activity. Twenty four-hour co-culture with M2–10B4 SCs significantly increased the levels of expression of RhoA GTP and RhoA Kinase ($p = 0.0005$ and $p = 0.0024$, respectively). The expression of RhoA-GTP and RhoA kinase was significantly reduced by SIM, both in the absence ($p < 0.0001$ and $p < 0.0001$, respectively) and in the presence ($p < 0.0001$ and $p < 0.0001$, respectively) of SCs. In panels A and C results are from 8 side-by-side experiments. Box and whiskers plots represent median values, first and third quartiles, and minimum and maximum values for each dataset.

($p \leq 0.0001$) (Figure 7D and Supplementary Figure S12–S13) in IGHV UM cells, both in the absence and in the presence of SCs.

These results provided the proof-in-principle that inhibition of the Ras/ERK1–2/HIF-1 α and RhoA/RhoA kinase/HIF-1 α cascades, and the down-regulation of MDR1 gene expression and Pgp activity are mechanisms exploited by SIM to restore the chemosensitivity of MDR+ IGHV UM cells.

DISCUSSION

This study shows that IGHV UM cells are endowed with a MDR phenotype which grants them a greater resistance to Doxo-induced cytotoxicity compared with IGHV M cells. Mechanistic insights have shown that IGHV UM cells, according to their accelerated Mev pathway activity [15], had significantly higher activity of the Mev-regulated Ras/ERK1–2 and RhoA/RhoA kinase signaling cascades, increased HIF-1 α phosphorylation and activity, higher MDR1 gene expression, very effective

Doxo extrusion and enhanced survival compared with IGHV M cells. The MDR signature of IGHV UM cells is at least partially dependent on BCR signaling, as shown by the inhibitory effect exerted by ibrutinib on the Mev pathway and Mev-regulated signaling.

The constitutive MDR features of IGHV UM cells are further exacerbated by the incubation with SCs, which stimulates the Mev pathway and its downstream signaling cascades. Mev pathway manipulation with SIM, and specific ERK1–2, RhoA kinase or HIF-1 α inhibitors reset the chemosensitivity of IGHV UM cells to the same levels of IGHV M cells, and neutralize the MDR-enhancing effect operated by SCs.

A role for MDR1 in CLL chemoresistance has previously been suggested by the association of Pgp expression with IGHV UM genes and poor prognosis cytogenetics [23]. Our data confirm that the MDR1 gene, which is a primary transcriptional target of HIF-1 α [24, 25], is constitutively more expressed in IGHV UM than in M cells. HIF-1 is a heterodimeric transcription factor composed of an oxygen-induced HIF-1 α and a

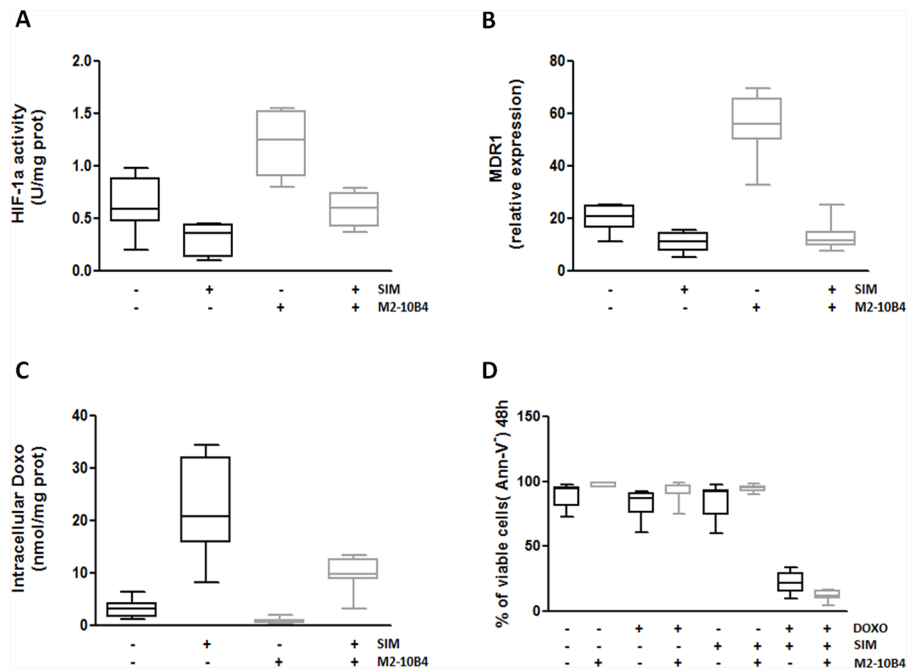


Figure 5: SIM-mediated inhibition of HIF-1 α activity and MDR1 gene expression improves Doxo-induced cytotoxicity. IGHV UM cells, cultured alone or in the presence of the murine stromal cell line M2-10B4, were exposed to 1 μ M SIM. **A.** HIF-1 α activity. The activity of HIF-1 α was significantly increased by 24-hour co-culture with M2-10B4 SCs ($p = 0.0007$). SIM significantly reduced HIF-1 α activity in IGHV UM cells, both in the absence ($p = 0.003$) and in the presence ($p < 0.0001$) of M2-10B4 SCs. **B.** MDR1 expression. Co-culture with M2-10B4 SCs significantly increased the levels of expression of MDR1 in IGHV UM cells ($p < 0.0001$). After 24-hour exposure to SIM, a significant decrease in MDR1 expression was observed in IGHV UM cells, both in the absence ($p < 0.0001$) and in the presence ($p < 0.0001$) of SCs. **C.** Doxo intracellular accumulation. The amount of intracellular Doxo in IGHV UM cells was significantly reduced by co-culture with M2-10B4 SCs ($p = 0.010$). SIM significantly increased 48-hour Doxo accumulation in IGHV UM cells cultured alone ($p = 0.0026$) or in the presence of SCs ($p = 0.0002$). **D.** Percentage of CD19+/CD5+ viable cells. IGHV UM cells were exposed to 1 μ M Doxo, 1 μ M SIM, and the combination SIM+Doxo for 48 hours, both in the absence and in the presence of M2-10B4 SCs. Cell viability was determined by Ann-V staining and cytofluorimetric analysis on CD19+/CD5+ cells. No decrease in viability was observed when IGHV UM cells were exposed to SIM and Doxo used alone ($91\% \pm 2\%$ and $90\% \pm 1\%$ of CD19+/CD5+ viable cells, respectively). By contrast, a significant reduction in cell viability was induced by the combination SIM+Doxo, both in the absence ($19, 5\% \pm 7\%$ CD19+/CD5+ viable cells, $p < 0.0001$) and in the presence ($10\% \pm 3\%$ CD19+/CD5+ viable cells, $p < 0.0001$) of SCs. In panels A-D results are from 8 side-by-side experiments. Box and whiskers plot represent median values, first and third quartiles, and minimum and maximum values for each dataset.

constitutively expressed HIF-1 β subunit. During hypoxia, HIF-1 α is positively regulated by the activation of the RhoA-dependent signaling cascade [16]. Under non-hypoxic conditions, the expression and transcriptional activity of HIF-1 α are regulated by growth factors and cytokines through the activation of kinase pathways, such as the Ras/ERK1-2 and the PI3k/Akt pathways [17]. Unlike their normal counterparts, CLL cells express HIF-1 α even under normoxia [26], and its transcriptional activity regulates CLL cells survival by inducing the expression of growth factors, such as VEGF, and the cytokines macrophage migration-inhibition factor (MIF) and midkine [26-28]. This is the first report showing that HIF-1 α activity is significantly higher in IGHV UM than in M cells, due to the higher activity of the upstream Ras/ERK1-2 and RhoA/RhoA kinase signaling cascades in these cells. The MDR signature of IGHV UM cells is partially dependent on their tonic BCR signaling, as shown

by the inhibitory effect exerted by ibrutinib but the lack of stimulatory effect exerted by anti-IgM.

Differently from anti-IgM-mediated BCR stimulation, SCs exposure further increase the activity of Ras/ERK1-2 and RhoA/RhoA kinase signaling pathways and HIF-1 α in IGHV UM cells. As a result, the target gene MDR1 is over-expressed, Doxo is more efficiently extruded and IGHV UM cells are further protected from Doxo-induced cytotoxicity. SCs are known to confer chemoresistance to CLL cells. One of the main players of the SC-induced MDR is the CXCL12/CXCR4 axis, which is known to activate the signal transducers ERK1-2 and Akt, and trigger LFA1 affinity to the integrin ICAM-1, through a RhoA-mediated mechanism [29]. It is already known that the BCR signaling modulates the activity of the CXCL12/CXCR4 axis, in fact the blockade of the BCR signaling with a BTK inhibitor decreases the migration of CXCR4-expressing CLL cells toward CXCL12 produced by SCs [30].

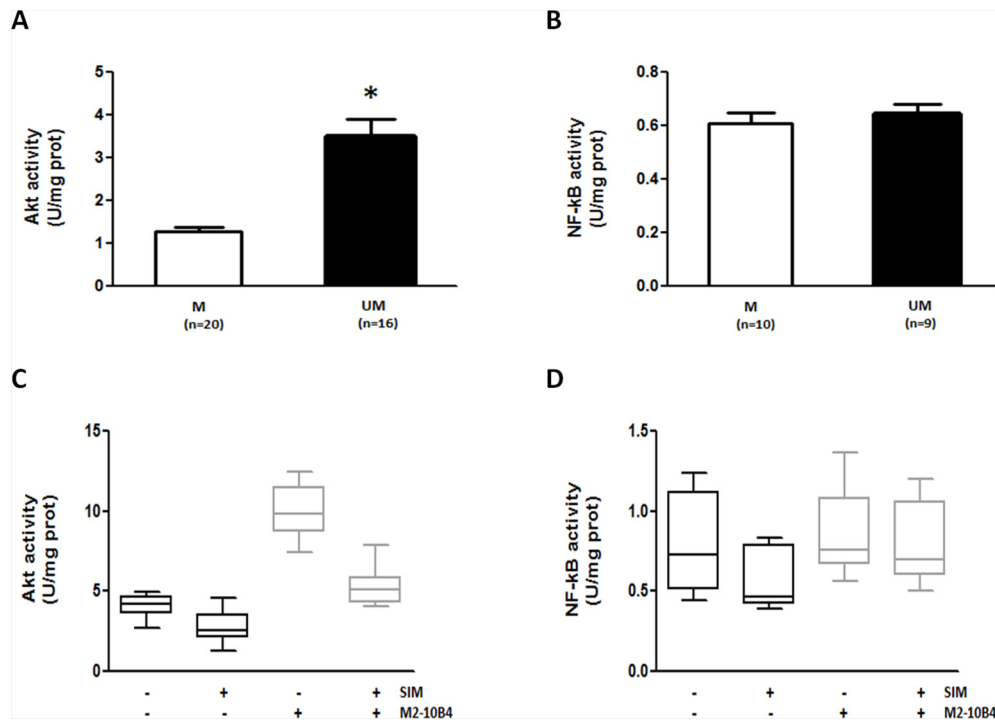


Figure 6: SIM effectively counteracts SC-induced Akt upregulation in IGHV UM cells. IGHV UM cells had constitutive higher levels of Akt activity ($p < 0.001$) compared to IGHV M cells **A**. By contrast, there was no difference in baseline NF- κ B activity between IGHV M and UM cells **B**. The Akt activity was further upregulated by the co-culture of IGHV UM cells with M2-10B4 SCs ($p = 0.0001$). SIM reduced baseline levels of Akt activity ($p = 0.0082$), and significantly counteracted SC-induced Akt upregulation ($p = 0.0004$) **C**. NF- κ B activity was not upregulated by SCs, but it was significantly reduced by SIM exposure, both in the absence ($p = 0.02$) or presence of SCs ($p = 0.034$) **D**. In panels A and B bars represent mean values \pm SEM. In panels C and D results are from 8 side-by-side experiments, and box and whiskers plot represent median values, first and third quartiles, and minimum and maximum values for each dataset.

The Mev pathway and the CXCL12/CXCR4 axis may reciprocally affect their activity, as shown by at least two observations: 1) for optimal signaling CXCR4 must be incorporated into membrane lipid rafts, whose formation require membrane cholesterol, and which orchestrate the interaction of the small GTPases Rac and Rho with their downstream transducers [31]; 2) hypercholesterolemia induces the secretion of CXCL12 and drives the migration of CD19+/CXCR4+ B lymphocytes from the bone marrow to the peripheral blood by interfering with the CXCL12/CXCR4 axis [32]. Further studies aiming at elucidating the connections between the Mev pathway and the CXCL12/CXCR4 axis in CLL are currently ongoing in our laboratory.

Statins and aminobisphosphonates, by targeting key enzymes in the Mev pathway, cause the intracellular deprivation of isoprenoid moieties such as FPP and GGPP, thus preventing Ras and RhoA prenylation and the activation of their downstream signaling pathways [33]. We have recently reported that ZA effectively interrupts Ras- and RhoA-dependent downstream signalling pathways, abrogates Pgp expression, and restores Doxo-induced cytotoxicity in MDR+ human cancer cell lines derived from solid tumors [14]. In CLL, ZA was not an ideal chemosensitizing agent since it inhibited Ras/ERK1-2 and RhoA/RhoA kinase signaling pathways, HIF-1 α

activity, and MDR1 expression, but did not increase Doxo-induced cytotoxicity. By contrast, SIM was effective in reversing the resistance of IGHV UM cells to Doxo, also in the presence of the protective effect exerted by SCs. This different efficacy was due to a stronger ability of SIM to increase the intracellular amount of Doxo, especially in the presence of SCs, but also to a differential regulatory effect exerted by the two compounds on the pro-survival factors Akt and NF- κ B. We have already reported that ZA induces the activation of NF- κ B in tumor-associated macrophages, reverting their phenotype from tumor-permissive into tumoricidal cells [34]. A similar upregulation of the Akt/NF- κ B pathway was observed in IGHV UM cells after ZA, but not after SIM exposure. This at least partially accounted for a ZA-mediated pro-survival activity which most likely prevailed on the death signals triggered by Doxo.

Among the chemo-sensitizing agents that we have tested, statins are the best candidate for clinical translation, since they are commonly used in the clinical practice as cholesterol-lowering agents. Previous data have shown that SIM, although potently effective in blocking the proliferation and inducing apoptosis of CLL cells *in vitro* [35-37], is not capable of significantly reducing the tumor burden when administered as a single agent in previously untreated

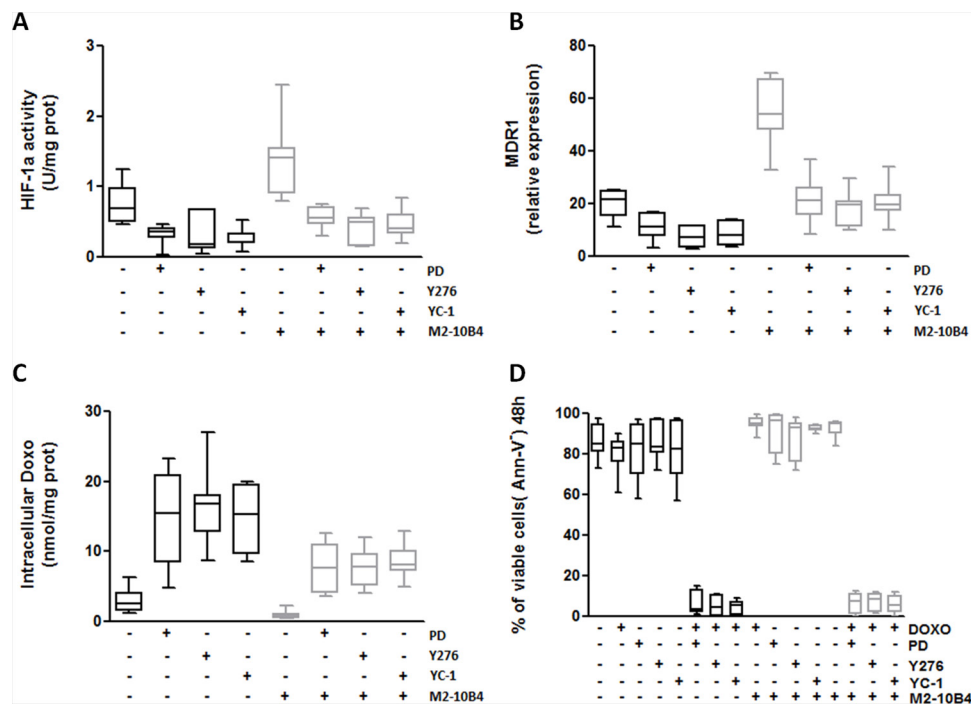


Figure 7: Specific inhibitors of RhoA, ERK1–2 and HIF-1 α effectively reverse the MDR phenotype of IGHV UM cells. IGHV UM cells were left untreated or treated with the ERK1–2 kinase inhibitor PD (10 μ M), the RhoA kinase inhibitor Y276 (10 μ M) and the HIF-1 α inhibitor YC-1 (10 μ M), both in the absence and in the presence of M2–10B4 SCs. **A.** HIF-1 α activity. Co-culture with M2–10B4 SCs significantly increased the activity of HIF-1 α ($p = 0.0014$). PD, Y276 and YC-1 significantly reduced the activity of HIF-1 α in IGHV UM cells after 24 hours of culture, both in the absence (p always ≤ 0.0048) and in the presence (p always ≤ 0.0052) of SCs. **B.** MDR1 expression. Twenty four-hour co-culture with M2–10B4 SCs significantly increased the expression of MDR1 in IGHV UM cells ($p < 0.0001$). After PD, Y276 and YC-1 treatment a significant decrease in MDR1 expression was observed in IGHV UM cells cultured alone (p always ≤ 0.001) and in the presence of SCs (p always ≤ 0.0001). **C.** Doxo intracellular accumulation. Intracellular Doxo was significantly lower in IGHV UM cells cultured with SCs than in IGHV UM cells cultured alone ($p = 0.02$). After 48-hour exposure to PD, Y276 and YC-1, Doxo accumulation was significantly increased, both in the absence (p always ≤ 0.003) and in the presence of M2–10B4 SCs (p always ≤ 0.0012). **D.** Percentage of CD19+/CD5+ viable cells. IGHV UM cells were exposed to 1 μ M Doxo, used alone and in combination with each inhibitor (i.e. PD+Doxo, Y276+Doxo, YC-1+Doxo), both in the absence and in the presence of the M2–10B4 SCs. Cell viability was determined by Ann-V staining and cytofluorimetric analysis on CD19+/CD5+ cells after 48-hours of culture. Doxo alone, as well as the three inhibitors used as single agents, did not induce a decrease in cell viability. By contrast, the combinations PD+Doxo, Y276+Doxo and YC-1+Doxo significantly reduced the viability of IGHV UM cells both in the absence and in the presence (p always < 0.0001) of SCs. In panels A–D results are from 7 side-by-side experiments. Box and whiskers plot represent median values, first and third quartiles, and minimum and maximum values for each dataset.

CLL patients [37]. By contrast, statins effectively increase the susceptibility of both drug-sensitive and drug-resistant CLL and lymphoma cells to dexamethasone and cytotoxic drugs [38], even synergizing with purine analogs to induce apoptosis of CLL cells [35]. Schmidmaier et al. have already reported that the Mev pathway and the downstream RhoA/RhoA kinase signaling pathway mediate SC-induced MDR, and that targeting of this pathway by SIM may improve the efficacy of anti-myeloma therapies by reduction of SC-induced MDR [39]. The same authors showed in a phase II clinical trial that SIM could overcome MDR in refractory myeloma receiving chemotherapy with bortezomib or bendamustine [40]. In the CLL setting, Chae et al. recently reported data on a retrospective analysis showing that the use of statin and aspirin is associated with improved outcome in CLL patients receiving salvage fludarabine, cyclophosphamide and rituximab (FCR) chemotherapy

[41], providing the rationale for a prospective study aimed at evaluating the effects of statins in CLL patients receiving chemoimmunotherapy. Since none of the drugs included in the FCR regimen are substrates of the Pgp, further studies aimed at determining the role and mechanism of action of statins in chemo-sensitizing CLL cells are warranted.

Doxo accumulation as a read-out assay to test Pgp activity could be considered a limitation of our study, due to previous data showing that the addition of anthracyclines to alkylating agents did not improve the clinical outcome of CLL patients [8]. More recently, however, the addition of mitoxantrone or epirubicine to fludarabine-based regimens has been shown to improve response rates [42–44]. Skribek et al. have reported that anthracyclines can have direct cytotoxic effects on CLL cells *in vitro* irrespectively to age, clinical stage or cytogenetic markers like del(17p) [45]. These observations and our data are strong incentives

to reconsider the therapeutic potential of anthracyclines in CLL, especially when used in combination with chemo-sensitizing agents targeting the Mev pathway such as statins, to treat specific subsets of high-risk CLL patients (e.g. IGHV UM patients). Moreover, the chemo-sensitizing effects that we observed by targeting ERK1–2 and RhoA kinase, as well as the transcription factor HIF-1 α , in addition to providing a confirmatory evidence about the mechanistic role played by these pathways in the MDR+ phenotype of IGHV UM cells, opens new perspectives on innovative targets amenable to therapeutic interventions.

Interestingly, recent data have shown that Pgp may be involved in the decreased anti-cancer efficiency and modified pharmacological properties of novel targeted agents, such as imatinib [46] and second-generation tyrosine kinase inhibitors [47]. Therefore, the study of Pgp activity and its modulation might have a broad impact in the current era of targeted therapies, providing important information on the pharmacokinetic and the anti-cancer effects of these novel agents.

MATERIALS AND METHODS

Patients

Peripheral blood (PB) samples were collected from 63 untreated CLL patients between March 2008 and November 2012 after informed consent. Patient demographics and clinical characteristics are reported in Supplementary Table S1. CLL was defined by clinical examination, PB cell count and immunophenotypic criteria. Tumor IGHV rearrangements were amplified starting from genomic DNA and sequences with deviations of < 2% or \geq 2% from the germline IGHV sequence were considered IGHV UM or M as previously reported [48].

Cell purification and cell lines

Peripheral blood mononuclear cells (PBMC) from IGHV M and UM patients were isolated from fresh samples by density gradient centrifugation (Ficoll-Histopaque, PAA Laboratories GmbH, Linz, Austria). PBMC were used without further manipulation when they contained more than 90% of CLL cells (CD19+/CD5+). When CLL cells were \leq 90% they were purified by negative selection using a Magnetic Bead-Activated Cell Sorting (MACS[®]) with a B Cell Isolation Kit II (Miltenyi Biotec, Bologna, Italy).

In selected experiments, the murine marrow-derived stromal cell line M2–10B4 (ATCC # CRL-1972) was used.

Chemicals

Electrophoresis reagents were obtained from Bio-Rad Laboratories (Hercules, CA, USA). The protein content of cell lysates was assessed with the bicinchoninic acid kit from Sigma Chemical Co (St. Louis, MO, USA). ZA was a kind gift from Novartis (Basel, Switzerland).

SIM and Y276 were purchased from Calbiochem (San Diego, CA, USA). When not otherwise specified, all the other reagents were purchased from Sigma Chemical Co.

Culture and co-culture conditions

CLL cells were cultured in 24-well plates (Costar, Cambridge, MA, USA) (10^6 cells/well) at 37°C in a 5% CO₂ humidified incubator. The standard culture medium was RPMI 1640 (Euroclone, Milano, Italy) supplemented with 10% FCS (Euroclone), 2 mM L-glutamine, 100 U/ml penicillin and 100 μ g/ml streptomycin.

For co-culture experiments, the M2–10B4 murine SCs were harvested through Trypsin-EDTA (Sigma-Aldrich, Milano, Italy) digestion and plated (150×10^3 cells/well) in complete culture medium for 24 hours. CLL cells (1×10^6 cells/well) were added to the culture the following day. In selected experiments, IGHV M and UM CLL cells were exposed to ZA 1 μ M, SIM 1 μ M, ERK1–2 kinase inhibitor PD 10 μ M, HIF-1 α inhibitor YC-1 10 μ M, RhoA kinase inhibitor Y276 10 μ M, in the absence and in the presence of Doxo 1 μ M. In selected experiments, CLL cells (5×10^6 cells/well) were pre-incubated in complete RPMI medium with or without ibrutinib (1 μ M) for 30 minutes at 37°C, and then stimulated for 24 hours with 10 μ g/well anti-IgM polyclonal goat F(ab')₂ (Southern Biotechnologies Birmingham, AL, USA) immobilized on 24-wells plates.

Mev pathway activity

After 24 hours of culture, 1×10^6 CLL cells were incubated for another 24 hours with 1 μ Ci of [³H]acetate (3600 mCi/mmol; Amersham International, Piscataway, NJ, USA) to measure the intracellular synthesis of cholesterol and FPP. Lipids were extracted in methanol/hexane, resolved by thin layer chromatography and quantified by liquid scintillation counting as reported in [15]. According to the titration curve, the results are expressed as fmol/ 1×10^6 cells.

Ras and RhoA activity

To evaluate Ras and RhoA activity, their GTP-bound fraction, taken as an index of the G-protein activation [49], was measured after 24 hours of culture. Ras-GTP was detected in a pull-down assay as previously reported [50]; RhoA-GTP binding was measured with the G-LISA RhoA Activation Assay Biochem Kit (Cytoskeleton Inc, Denver, CO, USA), according to the manufacturer's instructions. For each set of experiments a titration curve was prepared using serial dilution of the RhoA-GTP positive control of the kit. Data are expressed as U absorbance/mg cell proteins (U mg/prot).

RhoA kinase activity

RhoA kinase activity was measured after 24 hours of culture on 2×10^6 cells with the CycLex Rho Kinase Assay

Kit (CycLex Co., Nagano, Japan), as already described [50]. For each set of experiments a titration curve was set using serial dilution of recombinant RhoA kinase (Rock2, MBL Inc., Woburn, MA, USA). Data are expressed as U absorbance/mg cell proteins (U mg/prot).

Western blot (WB)

After 24 hours of culture 2×10^6 cells were lysed in MLB buffer (125 mM Tris-HCl, 750 mM NaCl, 1% v/v NP40, 10% v/v glycerol, 50 mM MgCl₂, 5 mM EDTA, 25 mM NaF, 1 mM NaVO₄, 10 µg/ml leupeptin, 10 µg/ml pepstatin, 10 µg/ml aprotinin, 1 mmol/L phenylmethylsulfonyl fluoride, pH 7.5), sonicated (with two bursts of 10 s; Labsonic sonicator, Sartorius Stedim Biotech S.A., Aubagne Cedex, France), and centrifuged at $13000 \times g$ for 10 min at 4°C. Ten µg cell lysates were subjected to SDS-PAGE, transferred to polyvinylidene fluoride membrane sheets (Immobilon-P, Millipore, Billerica, MA, USA) and probed with the following antibodies: anti phospho-(Thr202/Tyr204, Thr185/Tyr187)-ERK1-2 (Millipore); anti-ERK1-2 (Millipore); anti-phospho-(Ser473)-Akt (Millipore); anti-Akt (Millipore); anti- glyceraldehyde-3-phosphate dehydrogenase (GAPDH, used as control of equal protein loading; Santa Cruz Biotechnology Inc., Santa Cruz, CA, USA), followed by the secondary peroxidase-conjugated antibodies (Bio-Rad). Proteins were detected by enhanced chemiluminescence (PerkinElmer, Waltham, MA, USA).

HIF-1 α activity

Nuclear proteins from 2×10^6 cells were extracted after 24-hour culture using the Nuclear Extract Kit (Active Motif, Rixensart, Belgium), and quantified. The activity of HIF-1 α was assessed on 10 µg nuclear extracts using the TransAMTM HIF-1 α Transcription Factor Assay Kit (Active Motif), according to manufacturer's instructions. To assess the procedure specificity, a competition assay was performed by adding an excess (20 pmol) of HIF-1 α consensus oligonucleotide to nuclear extracts derived from CLL cells. Data are expressed as U absorbance/mg cell proteins (U mg/prot).

Real-time polymerase chain reaction (RT-PCR)

After 24 hours of *ex vivo* culture, total RNA was extracted from 1×10^6 cells and reverse-transcribed using the QuantiTect Reverse Transcription Kit (Qiagen, Hilden, Germany). RT-PCR was carried out using IQ⁻ SYBR Green Supermix (Bio-Rad), according to the manufacturer's instructions. The sequences of MDR1 primers were 5'-TGCTGGAGCGG TTCTACG-3', 5'-ATAGGCAATGTTCTCAGCAATG-3'. The sequences of GAPDH primers were 5'-GA AGGTGAAGGTCGGAGT-3', 5'-CATGGTGGAAAT CATATTGGAA-3'. The relative expression of each sample

was performed comparing the MDR1 PCR product with the *GAPDH* product, used as a housekeeping gene, with the Bio-Rad Software Gene Expression Quantitation (Bio-Rad).

NF- κ B and Akt activity

NF- κ B activity was measured on 10 µg nuclear extracts using the TransAM Flexi NF- κ B Family assay kit (Active Motif), according to the manufacturer's instructions. To assess the procedure specificity, a competition assay was performed by adding an excess (20 pmol) of the probe containing the NF- κ B consensus sequence to the positive control nuclear extracts provided by the kit.

Akt activity was measured on 2×10^6 cells with the CycLex Akt/PKB Kinase Assay/Inhibitor screening kit (CycLex Co.) in 96-well plates pre-coated with the Akt substrate AktTide-2T, according to the manufacturer's instructions. The titration curve was prepared using serial dilutions of recombinant Akt (CycLex Co.).

NF- κ B and Akt activity are expressed as U absorbance/mg cell proteins (U mg/prot).

Intracellular doxorubicin accumulation

To evaluate the activity of Pgp the intracellular accumulation of the Pgp substrate Doxo was measured. To this aim, 1×10^6 cells were incubated with 1 µM Doxo cultured alone or in presence of inhibitors for 48 hours; intracellular Doxo was measured spectrofluorimetrically, at excitation and emission wavelengths of 475 and 553 nm, as reported earlier [50]. A blank was prepared in the absence of cells in each set of experiments, and its fluorescence was subtracted from that measured in each sample. Fluorescence was converted in nmol Doxo/mg cell proteins (nmol/mg prot) using a previously prepared calibration curve.

Quantification of apoptotic and viable cells

After 48 hours of culture, cells were harvested, washed in PBS and stained with anti-CD19 PerCP (Beckman Coulter, Milano, Italy) and anti-CD5 APC (Dako SpA, Milano, Italy) monoclonal antibodies. The percentage of apoptotic cells was determined by Annexin-V (Ann-V) staining with the MEBCYTO-Apoptosis Kit (MBL Medical and Biological Laboratories, Naka-ku Nagoya, Japan). Flow cytometry was performed with a FACSCalibur and CELLQuest software (Becton Dickinson, Mountain View, CA, USA).

Statistical analysis

Statistical analysis was performed with the SigmaStat 3.5 software (Systat Software Inc., Chicago, IL, USA) and with GraphPad Prism version 5.01 for Windows (GraphPad Software, San Diego, CA, USA). All datasets were evaluated with a normality test: data with Gaussian or approximately

Gaussian distribution were compared by *t*-test, in all other cases a Mann-Whitney rank sum test was used. When experiments involved different culture conditions of the same sample a repeated-measures analysis was done.

Results are expressed as mean \pm SEM, unless otherwise specified.

Statistical significance was defined as *p* value < 0.05 .

ACKNOWLEDGMENTS AND FUNDING

Work supported by grants from Regione Piemonte (Ricerca Sanitaria Finalizzata 2008 to Marta Coscia; Progetto Immonc to Massimo Massaia); Italian Ministry of University and Research (www.miur.it; PRIN 2010–2011 to Massimo Massaia, FIRB 2012 to Chiara Riganti); Italian Association for Cancer Research (AIRC, www.airc.it; MFAG 11475 to Chiara Riganti, IG 13119 to Massimo Massaia); Compagnia SanPaolo, Torino, Italy; Fondazione Neoplasie Sangue (Fo.Ne.Sa), Torino, Italy; and local funds of the University of Turin (ex-60%). Valentina Griggio was the recipient of a “Giorgio Bissolotti e Teresina Bosio” fellowship from Fondazione “Angela Bossolasco”, Torino, Italy and currently is the recipient of a “Anna Nappa” fellowship from the Italian Association for Cancer Research (AIRC, Ref 16343); Micol Rigoni was the recipient of a fellowship from Fondazione Cassa di Risparmio di Torino (CRT) and currently is the recipient of a fellowship from Fondazione “Angela Bossolasco”, Torino, Italy.

We are grateful to Mr. Andrew Martin Garvey for editorial assistance.

Authorship

M.R. and C.R. contributed to the research design, performed the experiments, analyzed the data and wrote the paper. C.V. provided patients’ care and contributed to data analyses. V.G., I.C., M.R., M.F., P.S., B.C and I.B. assisted with the experiments. D.D. and M.L. performed IGHV mutational status analysis. M.B. reviewed the manuscript. M.M. contributed to the research design and revised the paper. M.C. contributed to the research design, supervised the study, wrote and revised the paper. All authors approved final manuscript.

CONFLICTS OF INTEREST

The authors declare no conflicts of interest.

REFERENCES

1. Damle RN, Wasil T, Fais F, Ghiotto F, Valetto A, Allen SL, Buchbinder A, Budman D, Dittmar K, Kolitz J, Lichtman SM, Schulman P, Vinciguerra VP, et al. Ig V gene mutation status and CD38 expression as novel prognostic indicators in chronic lymphocytic leukemia. *Blood*. 1999; 94:1840–7.
2. Hamblin TJ, Davis Z, Gardiner A, Oscier DG, Stevenson FK. Unmutated Ig V(H) genes are associated with a more aggressive form of chronic lymphocytic leukemia. *Blood*. 1999; 94:1848–54.
3. Lin KI, Tam CS, Keating MJ, Wierda WG, O’Brien S, Lerner S, Coombes KR, Schlette E, Ferrajoli A, Barron LL, Kipps TJ, Rassenti L, Faderl S, et al. Relevance of the immunoglobulin VH somatic mutation status in patients with chronic lymphocytic leukemia treated with fludarabine, cyclophosphamide, and rituximab (FCR) or related chemimmunotherapy regimens. *Blood*. 2009; 113:3168–71.
4. Coscia M, Pantaleoni F, Riganti C, Vitale C, Rigoni M, Peola S, Castella B, Foglietta M, Griggio V, Drandi D, Ladetto M, Bosia A, Boccadoro M, et al. IGHV unmutated CLL B cells are more prone to spontaneous apoptosis and subject to environmental prosurvival signals than mutated CLL B cells. *Leukemia*. 2011; 25:828–37.
5. Aleskog A, Tobin G, Laurell A, Thunberg U, Lindhagen E, Roos G, Nilsson K, Nygren P, Sundström C, Höglund M, Larsson R, Rosenquist R. VH gene mutation status and cellular drug resistance in chronic lymphocytic leukaemia. *European journal of haematology*. 2004; 73:407–11.
6. Lindhagen E, Norberg M, Kanduri M, Tobin G, Saisanen L, Aberg M, Gustafsson MG, Sundström C, Rosenquist R, Aleskog A. *In vitro* activity of 20 agents in different prognostic subgroups of chronic lymphocytic leukemia—rolipram and prednisolone active in cells from patients with poor prognosis. *European journal of haematology*. 2009; 83:22–34.
7. Johnson S, Smith AG, Loffler H, Osby E, Juliusson G, Emmerich B, Wyld PJ, Hiddemann W. Multicentre prospective randomised trial of fludarabine versus cyclophosphamide, doxorubicin, and prednisone (CAP) for treatment of advanced stage chronic lymphocytic leukaemia. The French Cooperative Group on CLL. *Lancet*. 1996; 347:1432–1438.
8. Leparrier M, Chevret S, Cazin B, Boudjerra N, Feugier P, Desablens B, Rapp MJ, Jaubert J, Autrand C, Divine M, Dreyfus B, Maloum K, Travade P, et al. Randomized comparison of fludarabine, CAP, and ChOP in 938 previously untreated stage B and C chronic lymphocytic leukemia patients. *Blood*. 2001; 98:2319–25.
9. Gottesman MM, Fojo T, Bates SE. Multidrug resistance in cancer: role of ATP-dependent transporters. *Nature reviews Cancer*. 2002; 2:48–58.
10. Sharma V, Dixit D, Koul N, Mehta VS, Sen E. Ras regulates interleukin-1beta-induced HIF-1alpha transcriptional activity in glioblastoma. *Journal of molecular medicine*. 2011; 89:123–36.
11. Takata K, Morishige K, Takahashi T, Hashimoto K, Tsutsumi S, Yin L, Ohta T, Kawagoe J, Takahashi K, Kurachi H. Fasudil-induced hypoxia-inducible factor-1alpha degradation disrupts a hypoxia-driven vascular endothelial growth factor autocrine mechanism in endothelial cells. *Molecular cancer therapeutics*. 2008; 7:1551–61.

12. Thurnher M, Nussbaumer O, Gruenbacher G. Novel Aspects of Mevalonate Pathway Inhibitors as Antitumor Agents. *Clinical Cancer Research*. 2012; 18:3524–31.
13. Swanson KM, Hohl RJ. Anti-cancer therapy: targeting the mevalonate pathway. *Current cancer drug targets*. 2006; 6:15–37.
14. Riganti C, Castella B, Kopecka J, Campia I, Coscia M, Pescarmona G, Bosia A, Ghigo D, Massaia M. Zoledronic acid restores doxorubicin chemosensitivity and immunogenic cell death in multidrug-resistant human cancer cells. *PloS One*. 2013; 8.
15. Coscia M, Vitale C, Peola S, Foglietta M, Rigoni M, Griggio V, Castella B, Angelini D, Chiaretti S, Riganti C, Guarini A, Drandi D, Ladetto M, et al. Dysfunctional Vgamma9Vdelta2 T cells are negative prognosticators and markers of dysregulated mevalonate pathway activity in chronic lymphocytic leukemia cells. *Blood*. 2012; 120:3271–9.
16. Turcotte S, Desrosiers RR, Beliveau R. HIF-1alpha mRNA and protein upregulation involves Rho GTPase expression during hypoxia in renal cell carcinoma. *Journal of cell science*. 2003; 116:2247–60.
17. Dimova EY, Michiels C, Kietzmann T. Kinases as upstream regulators of the HIF system: their emerging potential as anti-cancer drug targets. *Current pharmaceutical design*. 2009; 15:3867–77.
18. Allsup DJ, Kamiguti AS, Lin K, Sherrington PD, Matrai Z, Slupsky JR, Cawley JC, Zuzel M. B-cell receptor translocation to lipid rafts and associated signaling differ between prognostically important subgroups of chronic lymphocytic leukemia. *Cancer Research*. 2005; 65:7328–7337.
19. Kurtova AV, Balakrishnan K, Chen R, Ding W, Schnabl S, Quiroga MP, Sivina M, Wierda WG, Estrov Z, Keating MJ, Shehata M, Jäger U, Gandhi V, et al. Diverse marrow stromal cells protect CLL cells from spontaneous and drug-induced apoptosis: development of a reliable and reproducible system to assess stromal cell adhesion-mediated drug resistance. *Blood*. 2009; 114:4441–50.
20. Niedermeier M, Hennessy BT, Knight ZA, Henneberg M, Hu J, Kurtova AV, Wierda WG, Keating MJ, Shokat KM, Burger JA. Isoform-selective phosphoinositide 3'-kinase inhibitors inhibit CXCR4 signaling and overcome stromal cell-mediated drug resistance in chronic lymphocytic leukemia: a novel therapeutic approach. *Blood*. 2009; 113:5549–57.
21. Balakrishnan K, Burger JA, Wierda WG, Gandhi V. AT-101 induces apoptosis in CLL B cells and overcomes stromal cell-mediated Mcl-1 induction and drug resistance. *Blood*. 2009; 113:149–53.
22. Hewamana S, Alghazal S, Lin TT, Clement M, Jenkins C, Guzman ML, Jordan CT, Neelakantan S, Crooks PA, Burnett AK, Pratt G, Fegan C, Rowntree C, et al. The NF-kappaB subunit Rel A is associated with *in vitro* survival and clinical disease progression in chronic lymphocytic leukemia and represents a promising therapeutic target. *Blood*. 2008; 111:4681–9.
23. Matthews C, Catherwood MA, Larkin AM, Clynes M, Morris TC, Alexander HD. MDR-1, but not MDR-3 gene expression, is associated with unmutated IgVH genes and poor prognosis chromosomal aberrations in chronic lymphocytic leukemia. *Leukemia & lymphoma*. 2006; 47:2308–13.
24. Liu M, Li D, Aneja R, Joshi HC, Xie S, Zhang C, Zhou J. PO(2)-dependent differential regulation of multidrug resistance 1 gene expression by the c-Jun NH2-terminal kinase pathway. *The Journal of biological chemistry*. 2007; 282:17581–6.
25. Comerford KM, Wallace TJ, Karhausen J, Louis NA, Montalto MC, Colgan SP. Hypoxia-inducible factor-1-dependent regulation of the multidrug resistance (MDR1) gene. *Cancer research*. 2002; 62:3387–94.
26. Shachar I, Cohen S, Marom A, Becker-Herman S. Regulation of CLL survival by hypoxia-inducible factor and its target genes. *FEBS letters*. 2012; 586:2906–10.
27. Cohen S, Shoshana OY, Zelman-Toister E, Maharshak N, Binsky-Ehrenreich I, Gordin M, Hazan-Halevy I, Herishanu Y, Shvidel L, Haran M, Leng L, Bucala R, Harroch S, et al. The cytokine midkine and its receptor RPTPzeta regulate B cell survival in a pathway induced by CD74. *Journal of immunology*. 2012; 188:259–69.
28. Binsky I, Haran M, Starlets D, Gore Y, Lantner F, Harpaz N, Leng L, Goldenberg DM, Shvidel L, Berrebi A, Bucala R, Shachar I. IL-8 secreted in a macrophage migration-inhibitory factor- and CD74-dependent manner regulates B cell chronic lymphocytic leukemia survival. *Proceedings of the National Academy of Sciences of the United States of America*. 2007; 104:13408–13.
29. O'Hayre M, Salanga CL, Kipps TJ, Messmer D, Dorrestein PC, Handel TM. Elucidating the CXCL12/CXCR4 signaling network in chronic lymphocytic leukemia through phosphoproteomics analysis. *PLoS One*. 2010; 5:e11716.
30. Ponader S, Chen SS, Buggy JJ, Balakrishnan K, Gandhi V, Wierda WG, Keating MJ, O'Brien S, Chiorazzi N, Burger JA. The Bruton tyrosine kinase inhibitor PCI-32765 thwarts chronic lymphocytic leukemia cell survival and tissue homing *in vitro* and *in vivo*. *Blood*. 2012; 119:1182–1189.
31. Wysoczynski M, Reza R, Ratajczak J, Kucia M, Shirvaikar N, Honczarenko M, Mills M, Wanzeck J, Janowska-Wieczorek A, Ratajczak MZ. Incorporation of CXCR4 into membrane lipid rafts primes homing-related responses of hematopoietic stem/progenitor cells to an SDF-1 gradient. *Blood*. 2005; 105:40–8.
32. Gomes AL, Carvalho T, Serpa J, Torre C, Dias S. Hypercholesterolemia promotes bone marrow cell mobilization by perturbing the SDF-1: CXCR4 axis. *Blood*. 2010; 115:3886–94.

33. Thurnher M, Nussbaumer O, Gruenbacher G. Novel aspects of mevalonate pathway inhibitors as antitumor agents. *Clinical cancer research: an official journal of the American Association for Cancer Research*. 2012; 18:3524–31.
34. Coscia M, Quaglino E, Iezzi M, Curcio C, Pantaleoni F, Riganti C, Holen I, Mönkkönen H, Boccadoro M, Forni G, Musiani P, Bosia A, Cavallo F, et al. Zoledronic acid repolarizes tumour-associated macrophages and inhibits mammary carcinogenesis by targeting the mevalonate pathway. *Journal of cellular and molecular medicine*. 2010; 14:2803–15.
35. Podhorecka M, Halicka D, Klimek P, Kowal M, Chocholska S, Dmoszynska A. Simvastatin and purine analogs have a synergic effect on apoptosis of chronic lymphocytic leukemia cells. *Annals of Hematology*. 2010; 89:1115–24.
36. Chapman-Shimshoni D, Yuklea M, Radnay J, Shapiro H, Lishner M. Simvastatin induces apoptosis of B-CLL cells by activation of mitochondrial caspase 9. *Experimental Hematology*. 2003; 31:779–83.
37. Vitols S, Angelin B, Juliusson G. Simvastatin impairs mitogen-induced proliferation of malignant B-lymphocytes from humans—*in vitro* and *in vivo* studies. *Lipids*. 1997; 32:255–62.
38. van de Donk NW, Schotte D, Kamphuis MM, van Marion AM, van Kessel B, Bloem AC, Lokhorst HM. Protein geranylgeranylation is critical for the regulation of survival and proliferation of lymphoma tumor cells. *Clinical cancer research: an official journal of the American Association for Cancer Research*. 2003; 9:5735–48.
39. Schmidmaier R, Baumann P, Simsek M, Dayyani F, Emmerich B, Meinhardt G. The HMG-CoA reductase inhibitor simvastatin overcomes cell adhesion-mediated drug resistance in multiple myeloma by geranylgeranylation of Rho protein and activation of Rho kinase. *Blood*. 2004; 104:1825–32.
40. Schmidmaier R, Baumann P, Bumeder I, Meinhardt G, Straka C, Emmerich B. First clinical experience with simvastatin to overcome drug resistance in refractory multiple myeloma. *European journal of haematology*. 2007; 79:240–3.
41. Chae YK, Trinh L, Jain P, Wang X, Rozovski U, Wierda WG, Keating MJ, Estrov Z. Statin and aspirin use is associated with improved outcome of FCR therapy in relapsed/refractory chronic lymphocytic leukemia. *Blood*. 2014; 123:1424–6.
42. Bosch F, Ferrer A, Villamor N, Gonzalez M, Briones J, Gonzalez-Barca E, Abella E, Gardella S, Escoda L, Pérez-Ceballos E, Asensi A, Sayas MJ, Font L, et al. Fludarabine, cyclophosphamide, and mitoxantrone as initial therapy of chronic lymphocytic leukemia: high response rate and disease eradication. *Clinical cancer research: an official journal of the American Association for Cancer Research*. 2008; 14:155–61.
43. Bosch F, Abrisqueta P, Villamor N, Terol MJ, Gonzalez-Barca E, Ferra C, González Diaz M, Abella E, Delgado J, Carbonell F, García Marco JA, Escoda L, Ferrer S, et al. Rituximab, fludarabine, cyclophosphamide, and mitoxantrone: a new, highly active chemoimmunotherapy regimen for chronic lymphocytic leukemia. *Journal of clinical oncology: official journal of the American Society of Clinical Oncology*. 2009; 27:4578–84.
44. Chow KU, Kim SZ, von Neuhoff N, Schlegelberger B, Stilgenbauer S, Wunderle L, Cordes HJ, Bergmann L. Clinical efficacy of immunochemotherapy with fludarabine, epirubicin and rituximab in the treatment for chronic lymphocytic leukaemia and prolymphocytic leukaemia. *European journal of haematology*. 2011; 87:426–33.
45. Skribek H, Otvos R, Flaberg E, Nagy N, Markasz L, Eksborg S, Masszi T, Kozma A, Adam E, Miseta A, Klein E, Szekely L. Chronic lymphoid leukemia cells are highly sensitive to the combination of prednisolone and daunorubicin, but much less to doxorubicin or epirubicin. *Experimental hematology*. 2010; 38:1219–30.
46. Dulucq S, Bouchet S, Turcq B, Lippert E, Etienne G, Reiffers J, Molimard M, Krajcinovic M, Mahon FX. Multidrug resistance gene (MDR1) polymorphisms are associated with major molecular responses to standard-dose imatinib in chronic myeloid leukemia. *Blood*. 2008; 112:2024–7.
47. Dohse M, Scharenberg C, Shukla S, Robey RW, Volkmann T, Deeken JF, Brendel C, Ambudkar SV, Neubauer A, Bates SE. Comparison of ATP-binding cassette transporter interactions with the tyrosine kinase inhibitors imatinib, nilotinib, and dasatinib. *Drug Metabolism and Disposition*. 2010; 38:1371–80.
48. Ricca I, Rocci A, Drandi D, Francese R, Compagno M, Lobetti Bodoni C, De Marco F, Astolfi M, Monitillo L, Vallet S, Calvi R, Ficara F, Omedè P, et al. Telomere length identifies two different prognostic subgroups among VH-unmutated B-cell chronic lymphocytic leukemia patients. *Leukemia*. 2007; 21:697–705.
49. Laufs U, Liao JK. Targeting Rho in cardiovascular disease. *Circulation research*. 2000; 87:526–8.
50. Riganti C, Orecchia S, Pescarmona G, Betta PG, Ghigo D, Bosia A. Statins revert doxorubicin resistance via nitric oxide in malignant mesothelioma. *International journal of cancer. Journal international du cancer*. 2006; 119:17–27.

RESEARCH ARTICLE

An Autocrine Cytokine/JAK/STAT-Signaling Induces Kynurenine Synthesis in Multidrug Resistant Human Cancer Cells

Ivana Campia¹, Ilaria Buondonno¹, Barbara Castella^{2,3}, Barbara Rolando⁴, Joanna Kopecka¹, Elena Gazzano¹, Dario Ghigo^{1,2*}, Chiara Riganti^{1,2}

1 Department of Oncology, University of Torino, Torino, Italy, **2** Center for Experimental Research and Medical Studies (CeRMS), University of Torino, Torino, Italy, **3** Division of Hematology, University of Torino, Torino, Italy, **4** Department of Drug Science and Technology, University of Torino, Torino, Italy

* dario.ghigo@unito.it



OPEN ACCESS

Citation: Campia I, Buondonno I, Castella B, Rolando B, Kopecka J, Gazzano E, et al. (2015) An Autocrine Cytokine/JAK/STAT-Signaling Induces Kynurenine Synthesis in Multidrug Resistant Human Cancer Cells. PLoS ONE 10(5): e0126159. doi:10.1371/journal.pone.0126159

Academic Editor: Michael Platten, University Hospital of Heidelberg, GERMANY

Received: October 27, 2014

Accepted: March 29, 2015

Published: May 8, 2015

Copyright: © 2015 Campia et al. This is an open access article distributed under the terms of the [Creative Commons Attribution License](https://creativecommons.org/licenses/by/4.0/), which permits unrestricted use, distribution, and reproduction in any medium, provided the original author and source are credited.

Data Availability Statement: All relevant data are within the paper and its Supporting Information files.

Funding: This work was supported by grants from the Italian Association for Cancer Research (AIRC; grant MFAG 11475; www.airc.it), the Italian Ministry of University and Research ("Future in Research program" FIRB 2012, grant RBFR12SQ01; www.istruzione.it). JK is fellow of the Italian Foundation for Cancer Research (FIRC; www.fondazioneirc.it). The funders had no role in study design, data collection and analysis, decision to publish, or preparation of the manuscript.

Abstract

Background

Multidrug resistant cancer cells are hard to eradicate for the inefficacy of conventional anti-cancer drugs. Besides escaping the cytotoxic effects of chemotherapy, they also bypass the pro-immunogenic effects induced by anticancer drugs: indeed they are not well recognized by host dendritic cells and do not elicit a durable anti-tumor immunity. It has not yet been investigated whether multidrug resistant cells have a different ability to induce immunosuppression than chemosensitive ones. We addressed this issue in human and murine chemosensitive and multidrug resistant cancer cells.

Results

We found that the activity and expression of indoleamine 2,3-dioxygenase 1 (IDO1), which catalyzes the conversion of tryptophan into the immunosuppressive metabolite kynurenine, was higher in all the multidrug resistant cells analyzed and that IDO1 inhibition reduced the growth of drug-resistant tumors in immunocompetent animals. In chemoresistant cells the basal activity of JAK1/STAT1 and JAK1/STAT3 signaling was higher, the STAT3 inhibitor PIAS3 was down-regulated, and the autocrine production of STAT3-target and IDO1-inducers cytokines IL-6, IL-4, IL-1 β , IL-13, TNF- α and CD40L, was increased. The disruption of the JAK/STAT signaling lowered the IDO1 activity and reversed the kynurenine-induced pro-immunosuppressive effects, as revealed by the restored proliferation of T-lymphocytes in STAT-silenced chemoresistant cells.

Conclusions

Our work shows that multidrug resistant cells have a stronger immunosuppressive attitude than chemosensitive cells, due to the constitutive activation of the JAK/STAT/IDO1 axis, thus resulting chemo- and immune-evasive. Disrupting this axis may significantly improve the efficacy of chemo-immunotherapy protocols against resistant tumors.

Competing Interests: The authors have declared that no competing interests exist.

Introduction

Achieving a good chemotherapy efficacy and inducing a durable anti-tumor immune response are the main challenges of chemoimmunotherapy. Chemoresistance, in particular the simultaneous resistance towards different chemotherapeutic agents known as multidrug resistance (MDR), is one of the biggest problems encountered by chemotherapy [1]. MDR can be present at the diagnosis or induced by the selective pressure of chemotherapy; it often relies on the overexpression of ATP binding cassette (ABC) transporters responsible for the anticancer drug efflux, such as P-glycoprotein (Pgp), MDR related proteins (MRPs) and breast cancer resistance protein (BCRP). Together, they efflux both classical chemotherapeutic agents (e.g. anthracyclines, taxanes, Vinca alkaloids, epipodophyllotoxins, topotecan, methotrexate) and new targeted drugs (e.g. imatinib, dasatinib, lapatinib, gefitinib, sorafenib, erlotinib), limiting their cytotoxic effects [2].

Specific chemotherapeutic agents, such as anthracyclines and oxaliplatin, induce also pro-immunogenic effects, by inducing the translocation on the plasma membrane of specific “eat me” signals, like the chaperon calreticulin, which triggers the tumor cell phagocytosis and the subsequent activation of antitumor CD8⁺ T-lymphocytes [3]. This mechanism does not operate in cells overexpressing Pgp [4–6], which result at the same time chemo- and immune-resistant.

Moreover, tumor cells may evade the host immunosurveillance by suppressing the activity of the host immune system. A plethora of mechanisms mediate the tumor-induced immunosuppression, including: changes in tumor surface antigens; release of immunosuppressive cytokines in the tumor microenvironment; expansion of T-helper 2 lymphocytes, T-regulatory (Treg) cells, myeloid derived suppressor cells and type 2-tumor associated macrophages, which favor the tumor growth and impair the activity of anti-tumor populations, such as T-helper 1 lymphocytes, CD8⁺ T-lymphocytes, type 1-tumor associated macrophages, natural killer cells [7].

One of the strongest mediators of the tumor-induced immunosuppression is kynurenine, the product of tryptophan catabolism via tryptophan dioxygenase (TDO) [8] and indoleamine 2,3-dioxygenase enzymes (IDO1 and IDO2) [9], which are induced by interferon- γ (IFN- γ) [10, 11], nitric oxide (NO) [12] and iron [13]. Tryptophan is an essential amino acid for the proliferation and survival of CD8⁺ and CD4⁺ T-lymphocytes; moreover the increased kynurenine/tryptophan ratio severely compromises the efficiency of the host cellular immunity, because kynurenine inhibits the activation of T-lymphocytes [7, 14]. IDO1 is expressed in tumor-infiltrating dendritic cells [15] and in tumor stromal cells [16], and it has been found constitutively expressed or up-regulated in several tumor cells [14, 17]. An increased serum kynurenine/tryptophan ratio has been correlated to a faster progression of lung cancer [18] and the IDO positivity in tumor samples is usually associated with a poor clinical prognosis [19–21]. IDO1 overexpression supports tumor growth and progression of lung cancers [22], leading to hypothesize that kynurenine, besides its immunosuppressive effects, may directly enhance the tumor development.

We previously demonstrated that multidrug resistant cells are resistant to the immunogenic death operated by dendritic cells-mediated phagocytosis [4–6]. It has not been investigated whether multidrug resistant cells differ from chemosensitive ones also for the ability to induce immunosuppression: we found that multidrug resistant cells had a basally higher production of the immunosuppressive metabolite kynurenine than chemosensitive cells and we investigated the molecular basis of this phenotype.

Materials and Methods

Chemicals

The plasticware for cell cultures was from Falcon (Becton Dickinson, Franklin Lakes, NJ). The electrophoresis reagents were obtained from Bio-Rad Laboratories (Hercules, CA). The human recombinant IFN- γ was obtained from R&D Systems (Minneapolis, MN). 5-Br-brassinin was from Santa Cruz Biotechnology Inc. (Santa Cruz, CA). The protein content of cell lysates was assessed with the BCA kit from Sigma Chemicals Co (St. Louis, MO). When not otherwise specified, all the other reagents were purchased from Sigma Chemicals Co. Stock solutions of 3 mmol/L ferric nitrilotriacetate (FeNTA) were prepared by mixing 1 volume of 6 mmol/L nitrilotriacetic acid in 1 eq/L NaOH, and 1 volume of 6 mmol/L FeCl₃ in 1 eq/L HCl; the pH was adjusted to neutrality with NaOH.

Cells

The human chemosensitive non small cell lung cancer A549 cells were purchased from Istituto Zooprofilattico Sperimentale "Bruno Umbertini" (Brescia, Italy). The human chemosensitive colon cancer HT29 cells, the human chemosensitive chronic myelogenous leukemia K562 cells, the human chemosensitive mesothelial Met5A cells and the murine constitutively chemoresistant mammary JC cells were from ATCC (Manassas, VA). The resistant sublines A549/dx, HT29/dx, K562/dx were generated in our laboratory by culturing the above mentioned parental cells in a medium containing increasing concentrations of doxorubicin, used as a MDR inducer, as reported earlier [4]. The human constitutively chemoresistant malignant mesothelioma (HMM) cells were collected, after informed written consent from the patients, by the Biologic Bank of Malignant Mesothelioma (S.S. Antonio e Biagio Hospital, Alessandria, Italy), where the histological characterization was performed [23]. The experimental protocol (code: TASK3) was approved on 09/11/2011 by the Bioethics Committee ("Comitato Etico Interaziendale") of the S.S. Antonio e Biagio Hospital, Alessandria, Italy. The cells were grown in the respective culture medium supplemented with 10% v/v fetal bovine serum (FBS), 1% v/v penicillin-streptomycin, 1% v/v L-glutamine and were maintained in a humidified atmosphere at 37°C and 5% CO₂.

Kynurenine measurement

The IDO activity was determined according to [24], with minor modifications: 200 μ L of cell culture supernatants were added to 100 μ L of 30% w/v trichloroacetic acid (TCA) and incubated for 30 min at 50°C to hydrolyze N-formylkynurenine to kynurenine. After centrifugation at 10,000 x g for 10 min, 100 μ L of the supernatant were transferred into a 96-well plate, mixed with 100 μ L of 2% w/v p-dimethylamino benzaldehyde in 99.8% v/v acetic acid, and incubated for 10 min at room temperature. Kynurenine was detected by measuring the absorbance at 490 nm, using a Synergy HT Multi-Detection Microplate Reader (BioTek, Winooski, VT). The absorbance of the culture medium alone was considered as a blank and was subtracted from the values obtained in the presence of the cells. The results were expressed as nmol kynurenine/mg cell proteins, according to a titration curve previously set. Kynurenine levels in the cell culture supernatants were measured in parallel by high pressure liquid chromatography (HPLC), as reported in [25], with minor modifications: 400 μ L of the cell culture supernatants were added to 100 μ L of 30% w/v TCA, incubated for 30 min at 50°C and centrifuged at 15,000 x g for 10 min. The clear supernatant was filtered through 0.45 μ m PTFE filters (Alltech, Nicholasville, KY) and analyzed by an Agilent LC system (Palo Alto, CA), equipped with vacuum degasser (G1322A), quaternary pump (G1311A), manual-injector (Rheodyne, Cotati, CA) and multiple

wavelength detector (G1365A) integrated in the HP1200 system. The data were acquired and processed with the Agilent ChemStation software. The injection volume was 20 μ L. An Agilent Eclipse XDB-C18 column (125 mm \times 4.0 mm, 5 μ m) was used for the analysis at 30°C. The chromatographic separation was carried out using the mobile phase consisting of 15 mmol/L acetate buffer (pH 4.0) and acetonitrile (90:10, v/v) at a flow rate of 0.8 mL/min. The eluate was monitored at 365 nm, referenced against a 700 nm wavelength. The calibration samples were prepared by adding kynurenine standards (Sigma Chemical Co.) in the concentration range of 0.50–50 μ mol/L to the culture medium. The results were expressed as nmol kynurenine/mg cell proteins.

qRT-PCR and PCR arrays

The total RNA was extracted and reverse-transcribed using the iScript cDNA Synthesis Kit (Bio-Rad Laboratories). The qRT-PCR was performed with the iTaq Universal SYBR Green Supermix (Bio-Rad Laboratories). The same cDNA preparation was used to quantify the gene of interest and the housekeeping gene *β -actin*. The primer sequences, designed with the qPrimerDepot software (<http://primerdepot.nci.nih.gov/>), were: for *IDO1*: 5'- CAGGCAGATGTT TAGCAATGA -3'; 5'- GATGAAGAAGTGGGCTTTGC -3'; for *β -actin*: 5'- GCTATCCAG GCTGTGCTATC-3'; 5'- TGTCACGCACGATTTCC-3'. The amount of *IDO1* mRNA was normalized versus the amount of *β -actin* mRNA, chosen as housekeeping gene, and was expressed as *IDO1*/ *β -actin* ratio, using the Bio-Rad Software Gene Expression Quantitation (Bio-Rad Laboratories). The PCR arrays were performed on 1 μ g cDNA, using the Human JAK/STAT Signaling Pathway RT² Profiler PCR Array and the Human IL-6/STAT3 Signaling Pathway Plus RT² Profiler PCR Array (Qiagen, Hilden, Germany), following the manufacturer's instructions. The analysis of data was performed with the RT² Profiler PCR Array Data Analysis (Qiagen).

Western blotting

The cells were rinsed with the lysis buffer (125 mmol/L Tris-HCl, 750 mmol/L NaCl, 1% v/v NP40, 10% v/v glycerol, 50 mmol/L MgCl₂, 5 mmol/L EDTA, 25 mmol/L NaF, 1 mmol/L NaVO₄, 10 μ g/mL leupeptin, 10 μ g/mL pepstatin, 10 μ g/mL aprotinin, 1 mmol/L phenylmethylsulfonyl fluoride; pH 7.5), sonicated and centrifuged at 13,000 \times g for 10 min at 4°C. 20 μ g of proteins from cell lysates were subjected to Western blotting and probed with the following antibodies against: IDO1 (rabbit polyclonal, diluted 1:2,000, AG-25A-0029, Adipogen, San Diego, CA); IDO2 (mouse monoclonal, diluted 1:500, SAB3701447, Sigma Chemical Co.); TDO (rabbit polyclonal, diluted 1:1,000, SAB2102400, Sigma Chemical Co.); phospho(Tyr 1022/1023)-JAK1 (rabbit polyclonal, diluted 1:1,000, #3331, Cell Signaling Technology, Danvers, MA); JAK1 (rabbit polyclonal, diluted 1:1,000, #3344, Cell Signaling Technology); phospho(Tyr701)-STAT1 (rabbit polyclonal, diluted 1:1,000, #9167, Cell Signaling Technology); STAT1 (mouse monoclonal, diluted 1:1,000, clone 15H3, Thermo Scientific, Rockford, IL); phospho(Tyr705)-STAT3 (rabbit polyclonal, diluted 1:2,000, #9145, Cell Signaling Technology); STAT3 (mouse monoclonal, diluted 1:5,000, clone 9D8, Thermo Scientific); Pgp (rabbit polyclonal, diluted 1:250, sc-8313, Santa Cruz Biotechnology Inc.); MRP1 (mouse monoclonal, diluted 1:100, ab32574, Abcam, Cambridge, UK); MRP2 (mouse monoclonal, diluted 1:100, ab3373, Abcam); MRP3 (goat polyclonal, diluted 1:250, sc-5776, Santa Cruz Biotechnology Inc.); MRP4 (goat polyclonal, diluted 1:250, ab77184, Abcam); MRP5 (goat polyclonal, diluted 1:250, sc-5781, Santa Cruz Biotechnology Inc.); BCRP (rabbit polyclonal, diluted 1:500, sc-25882, Santa Cruz Biotechnology Inc.); β -tubulin (mouse monoclonal, diluted 1:500, sc-5274, Santa Cruz Biotechnology Inc.), followed by a secondary peroxidase-conjugated antibody (Bio-

Rad Laboratories). The proteins were detected by enhanced chemiluminescence (Bio-Rad Laboratories). Nuclear extracts were prepared with the Nuclear Extract Kit (Active Motif, Rixensart, Belgium); 10 μ g of nuclear proteins were resolved by SDS-PAGE and probed with the following antibodies against: PIAS1 (rabbit monoclonal, diluted 1:1,000, ab109388, Abcam); PIAS3 (rabbit polyclonal, diluted 1:1,000, ab22856, Abcam); phospho(Tyr701)-STAT1; STAT1; phospho(Tyr705)-STAT3; STAT3; TATA-binding protein (TBP; rabbit polyclonal, diluted 1:500, sc-273, Santa Cruz Biotechnology Inc.). To exclude any cytosolic contamination of nuclear extracts, we verified that β -tubulin was undetectable in nuclear samples (not shown).

In Vivo Tumor Growth

1 x 10⁵ human A549, A549/dx, HT29, HT29/dx cells in 20 μ L of culture medium, mixed with 20 μ L of Cultrex BME (Trevigen, Gaithersburg, MD), were implanted subcutaneously in the right flank of 6–8 weeks old female nude BALB/c mice, housed under 12 h light/dark cycle, with food and drinking provided *ad libitum*. 1 x 10⁵ murine chemoresistant JC cells, syngeneic with BALB/c mice [26], were implanted in immunocompetent animals. In a second experimental set, when A549/dx, HT29/dx and JC tumors reached the volume of 100 mm³, the animals were randomized into two groups: “Control” group (treated with 100 μ L of saline solution *per os*, 5 days/week for three weeks); “Brassinin” group (treated with 400 mg/kg of the IDO1 inhibitor 5-Br-brassinin *per os*, 5 days/week for three weeks), as described in [27]. In both experimental sets, the tumor growth was measured daily by caliper and was calculated according to the equation $(L \times W^2)/2$, where L = tumor length and W = tumor width. Mice were euthanized at day 21. The experimental procedures were approved by the Bioethics Committee (“Comitato Etico di Ateneo”) of the University of Torino, Italy.

Cytokine production

The production of cytokines was measured in the cell culture supernatant using the following commercial kits: Human interleukin-6 (IL-6) Duo Set Development Kit (R&D Systems), Human interleukin-4 (IL-4) DuoSet Development Kit (R&D Systems), Human IL1-beta (IL-1 β) platinum ELISA kit (eBioscience, San Diego, CA), Human interleukin-13 (IL-13) ELISA Development Kit (Peprotech, London, UK), Human soluble CD40 Ligand (sCD40L) ELISA Development Kit (Peprotech), Human tumor necrosis factor- α (TNF- α) DuoSet Development Kit (R&D Systems), Human IFN- γ DuoSet Development Kit (R&D Systems). Results were expressed as ng/mg cell proteins or pg/mg cell proteins, according to the calibration curve of each kit.

Cell silencing

200,000 cells were transfected with 400 nmol/L of 19–25 nucleotide non targeting scrambled siRNAs (Control siRNA-A, Santa Cruz Biotechnology Inc.), with a STAT1- or STAT3-specific siRNAs pool (Santa Cruz Biotechnology Inc.), according to the manufacturer’s instructions. To verify the silencing efficacy, the cells were lysed and checked for the expression of STAT1 and STAT3 by Western blotting, as described above.

Immunological assays

1 x 10⁶/mL of human peripheral blood mononuclear cells (PBMC), isolated from buffy coats of healthy donors (Blood Bank, A.O.U. Città della Salute e della Scienza di Torino Hospital, Torino, Italy) by centrifugation on Ficoll-Hypaque density gradient, were treated with anti-CD3 (OKT3, BioLegend, San Diego, CA) and anti-CD28 (BioLegend) antibodies, to induce the

specific proliferation of T-lymphocytes, and co-cultured with target cells (previously irradiated with 30 Gy for 15 min) for 72 h at an effector/target ratio of 10:1. The expansion of T-lymphocytes, the only PBMC population able to proliferate in these experimental conditions, was assessed by adding 1 μ Ci of [3 H]thymidine (PerkinElmer, Waltham, MA) 18 h before the end of the co-cultures, then harvesting the plates and counting the radioactivity. To analyze the lymphocyte phenotype after the incubation with tumor cells, the cells were harvested, washed and re-suspended in phosphate buffer saline (PBS) containing 5% v/v FBS. A 3- and 4-color flow cytometry analysis was performed with the appropriate combinations of fluorescein isothiocyanate-, r-phycoerythrin-, tricolor-, peridinin chlorophyll protein complex—or allophycocyanin-conjugated antibodies for CD3, CD4, CD8, CD25 (all from Miltenyi Biotec, Bergisch Gladbach, Germany), and CD127 (BioLegend). Isotype controls were run for each sample. The samples were read with a FACS Calibur flow cytometer equipped with a CELLQuestPro software (Becton Dickinson). The use of PBMC from healthy donors and the experimental protocols were approved by the Bioethics Committee (“Comitato Etico Interaziendale”) of the A.O.U. Città della Salute e della Scienza di Torino Hospital, Torino, Italy.

Cell viability assay

The neutral red staining was performed to measure the cell viability, as previously detailed [28]. The absorbance at 540 nm was read using a Synergy HT Multi-Detection Microplate Reader. The absorbance of untreated cells was considered as 100% viability; the results were expressed as percentage of viable cells versus untreated cells.

Nitrite measurement

The level of nitrite, a stable derivative of NO, in the cell culture supernatants was measured by the Griess method [29]. The results were expressed as nmol nitrite/mg cell proteins.

Iron measurement

100 x 10⁶ cells were washed with PBS, detached with trypsin/EDTA, centrifuged at 12,000 x g for 2 min, re-suspended in 1 mL PBS and sonicated. The intracellular iron was measured using a AAAnalyst 200 Atomic Absorption Spectrometer (PerkinElmer). The results were expressed as ng iron/ml cell suspension.

Statistical analysis

All data in text and figures are provided as means \pm SD. The results were analyzed by a one-way analysis of variance (ANOVA). A $p < 0.05$ was considered significant.

Results

Kynurenine synthesis is higher in multidrug resistant cells and is modulated by 5-Br-brassinin, methyl-DL-tryptophan and interferon- γ

We first analyzed the kynurenine production in a panel of chemosensitive and multidrug resistant cancer cells, showing a different pattern of ABC transporters (S1 Fig): HT29, A549, K562, Met5A were human chemosensitive cells; HT29/dx, A549/dx and K562/dx were models of acquired MDR; HMM and JC were human and murine constitutively chemoresistant cells, respectively. The multidrug resistant cell lines had higher kynurenine levels—detected by HPLC (S2 Fig) and spectrophotometric assay (Fig 1A)—and increased levels of IDO1 protein compared to chemosensitive cells (Fig 1B). IDO2 was detected at variable amounts in chemosensitive and chemoresistant cells; TDO was detected in all the cell lines analyzed, except in A549/

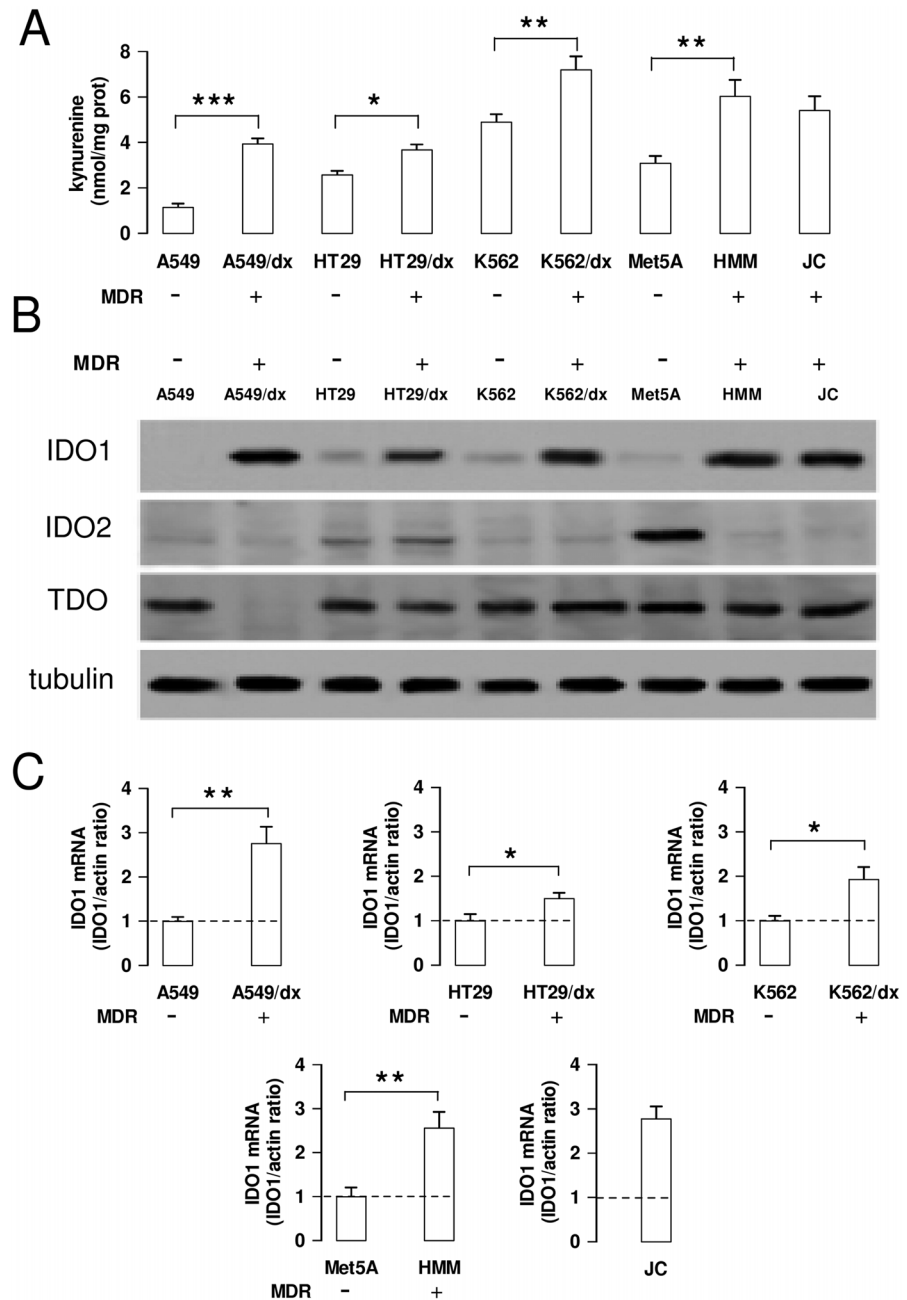


Fig 1. Kynurenine production and IDO1 expression in chemosensitive and multidrug resistant cells. Human chemosensitive lung cancer A549 cells and chemoresistant A549/dx cells, human chemosensitive colon cancer HT29 cells and chemoresistant HT29/dx cells, human chemosensitive chronic myelogenous leukemia K562 cells and chemoresistant K562/dx cells, human chemosensitive mesothelial Met5A cells and human chemoresistant malignant mesothelioma HMM cells, murine chemoresistant mammary JC cells were subjected to the following investigations. **A.** The kynurenine levels in the cell culture supernatants were measured spectrophotometrically. Data are presented as means \pm SD ($n = 4$). * $p < 0.05$, ** $p < 0.01$, *** $p < 0.001$: chemoresistant cells (MDR-positive) versus the corresponding chemosensitive (MDR-negative) cells. **B.** Western blot analysis of IDO1, IDO2 and TDO expression. The β -tubulin expression was used as control of equal protein loading. The figure is representative of 3 experiments with similar results. **C.** The expression level of *IDO1* mRNA was measured by qRT-PCR. Data are presented as means \pm SD ($n = 4$). * $p < 0.01$, ** $p < 0.002$: chemoresistant cells (MDR-positive) versus the corresponding chemosensitive (MDR-negative) cells.

doi:10.1371/journal.pone.0126159.g001

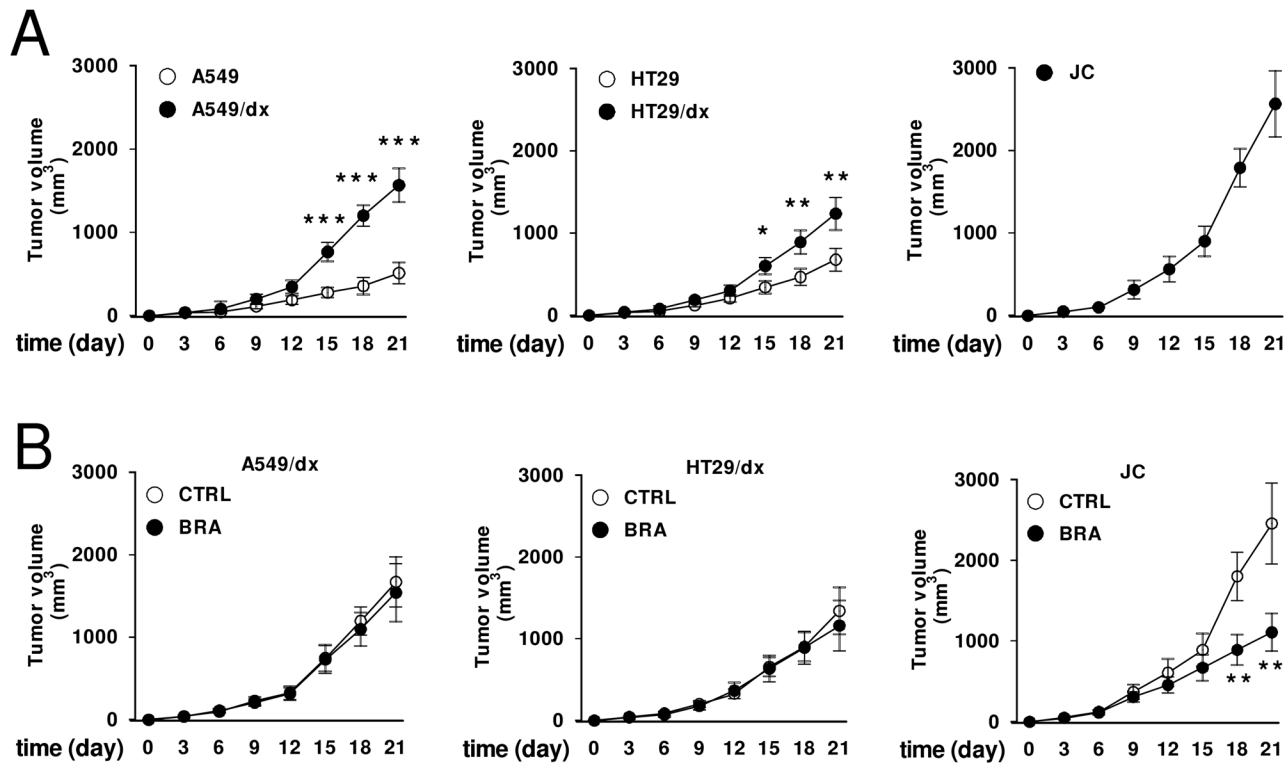


Fig 2. Effects of IDO1 inhibition on the growth of multidrug resistant tumors. A. 1×10^5 human A549, A549/dx, HT29, HT29/dx cells were implanted subcutaneously in 6–8 weeks old female nude BALB/c mice, 1×10^5 murine JC cells were implanted in immunocompetent BALB/c mice. Tumor growth was monitored daily by caliper measurement. Data are presented as means \pm SD of 10 mice/group. * $p < 0.02$, ** $p < 0.005$, *** $p < 0.001$: A549/dx or HT29/dx cells versus A549 or HT29 cells, at the corresponding time points. **B.** Animals bearing A549/dx-, HT29/dx-, JC-tumors were randomized into two groups when tumors reached the volume of 100 mm^3 : “Control” group (treated with $100 \mu\text{L}$ of saline solution *per os*, 5 days/week for three weeks; CTRL); “Brassinin” group (treated with 400 mg/kg of the IDO1 inhibitor 5-Br-brassinin *per os*, 5 days/week for three weeks; BRA). Tumor growth was monitored daily by caliper measurement. Data are presented as means \pm SD of 6 mice/group. ** $p < 0.005$: BRA-group versus CTRL-group, at the corresponding time points.

doi:10.1371/journal.pone.0126159.g002

dx cells (Fig 1B). IDO1 mRNA resulted also higher in multidrug resistant cells than in chemosensitive ones (Fig 1C).

Human chemoresistant A549/dx cells and HT29/dx cells grew faster than the chemosensitive A549 and HT29 cells implanted in nude BALB/c mice (Fig 2A). The murine chemoresistant JC cells had the highest rate of growth (Fig 2A). Interestingly, the IDO1 inhibitor 5-Br-brassinin [27] did not inhibit the growth of A549/dx and HT29/dx tumors, implanted in immunodeficient mice, but it significantly reduced the progression of JC tumors, implanted in immunocompetent animals (Fig 2B). These data suggest that IDO activity may support the fast growth of chemoresistant tumors in immunocompetent hosts.

We next investigated the reason of the difference in kynurenine production between chemosensitive and chemoresistant cells. For sake of simplicity, we focused on the A549 and A549/dx cells as models of chemosensitive and multidrug resistant cells, respectively, since in these cells the difference in kynurenine levels and IDO1 expression was very evident. Since the HPLC measurement and the spectrophotometric assay gave superimposable results for A549 and A549/dx cells (S2 Fig and Fig 1A), we used the latter assay as a reliable method to evaluate the differences in the kynurenine levels between these two cell lines.

We analyzed whether kynurenine levels varied differently in response to chemotherapeutic drugs—to which multidrug resistant cells are insensitive—to IDO1 activators, such as NO,

iron and IFN- γ , and to IDO1 inhibitors, such as 5-Br-brassinin and methyl-DL-tryptophan [30].

Doxorubicin, cisplatin, gemcitabine and mitoxantrone, used at concentrations that reduced to 50% the viability of sensitive A549 cells without affecting the viability of resistant A549/dx cells (S3A Fig), did not change the kynurenine levels, which remained significantly higher in A549/dx cells than in A549 cells, either in the absence or in the presence of the chemotherapeutic agents (S3B Fig). Similarly, the NO donors S-nitrosoglutathione and S-nitroso-N-acetylpenicillamine, which increased the levels of NO in chemosensitive and multidrug resistant cells (S4A Fig), did not modify the kynurenine synthesis compared to untreated cells in both cell populations (S4B Fig). To modulate the intracellular iron, we treated A549 and A549/dx cells with the cell permeable iron-releasing compound FeNTA and with the iron chelator desferroxamine, which respectively increased and decreased the amount of cell iron (S5A Fig): again, neither FeNTA nor desferroxamine varied the kynurenine production (S5B Fig).

IFN- γ increased the kynurenine levels in both chemosensitive and multidrug resistant cells, but the extent of such increase was greater in A549/dx cells (Fig 3A). The effect of IFN- γ , which was reduced by the inhibitors methyl-DL-tryptophan and 5-Br-brassinin (Fig 3A), was associated to the increase of *IDO1* mRNA (Fig 3B) and protein (Fig 3C). Also in this case, the increase elicited by IFN- γ was more pronounced in A549/dx than in A549 cells (Fig 3B and 3C), suggesting that the multidrug resistant cells were more responsive to the cytokine. Similar effects of IFN- γ , methyl-DL-tryptophan and 5-Br-brassinin were detected in HT29 and HT29/dx cells, K562 and K562/dx cells, Met5A and HMM cells (data not shown).

Multidrug resistant cells have a higher activity of JAK/STAT signaling and an increased autocrine production of STAT3-dependent cytokines than chemosensitive cells

Since IFN- γ activates the JAK/STAT1-3 signaling [31], and STAT1 and STAT3 are potent transcriptional activators of the *IDO1* gene in most mammalian cells [32, 33], we analyzed the expression levels of key genes of JAK/STAT pathway by a high-throughput PCR screening. As shown in S1 Table and Fig 4A, A549/dx cells did not differ from A549 cells for the expression of *JAK1-2-3*, but exhibited higher expression of *STAT1* and *STAT3*. In keeping with this trend, classical STAT1- and STAT3-target genes (*A2M*, *BCL2L1*, *CDKN1A*, *CRP*, *CXCL9*, *FAS*, *IRF1*, *JUNB*, *MMP3*, *MYC*, *NOS2*, *SOCS1*) were up-regulated in the multidrug resistant cells (S1 Table). In Western blotting validation, we found similar levels of total JAK1 protein in whole cell lysates of A549 and A549/dx cells, but higher levels of the active tyrosine-phosphorylated JAK1 in the multidrug resistant cells (Fig 4B). The amounts of STAT1, phospho(Tyr701)-STAT1, STAT3, phospho(Tyr705)-STAT3 were also higher in the chemoresistant cells (Fig 4B). The mRNA level of the STAT1 inhibitor PIAS1 was not significantly different between A549 and A549/dx cells (S1 Table and Fig 4A), and the level of PIAS1 protein was the same in the nuclear extracts (Fig 4C). By contrast, the nuclear amount of the STAT3 inhibitor PIAS3 was lower in A549/dx cells (Fig 4C); this was in line with the lower level of *PIAS3* mRNA (S2 Table). Interestingly, STAT1, phospho(Tyr701)-STAT1, STAT3, phospho(Tyr705)-STAT3 were all more translocated into the nucleus of multidrug resistant cells (Fig 4C). This pattern, which is likely due to the higher amount and phosphorylation of STAT1/STAT3 and to the lower expression of PIAS3, led us to hypothesize that STAT1- and, in particular, STAT3-target genes should be up-regulated in the multidrug resistant cells.

Indeed a global up-regulation of the STAT3-dependent genes was detected in A549/dx cells (S2 Table and Fig 5A). Of note, the mRNAs of the STAT3-target cytokines IL-6, IL-4, IL-1 β , IL-13, CD40L, TNF- α —that are IDO1 inducers [34–38]—were up-regulated more than two-

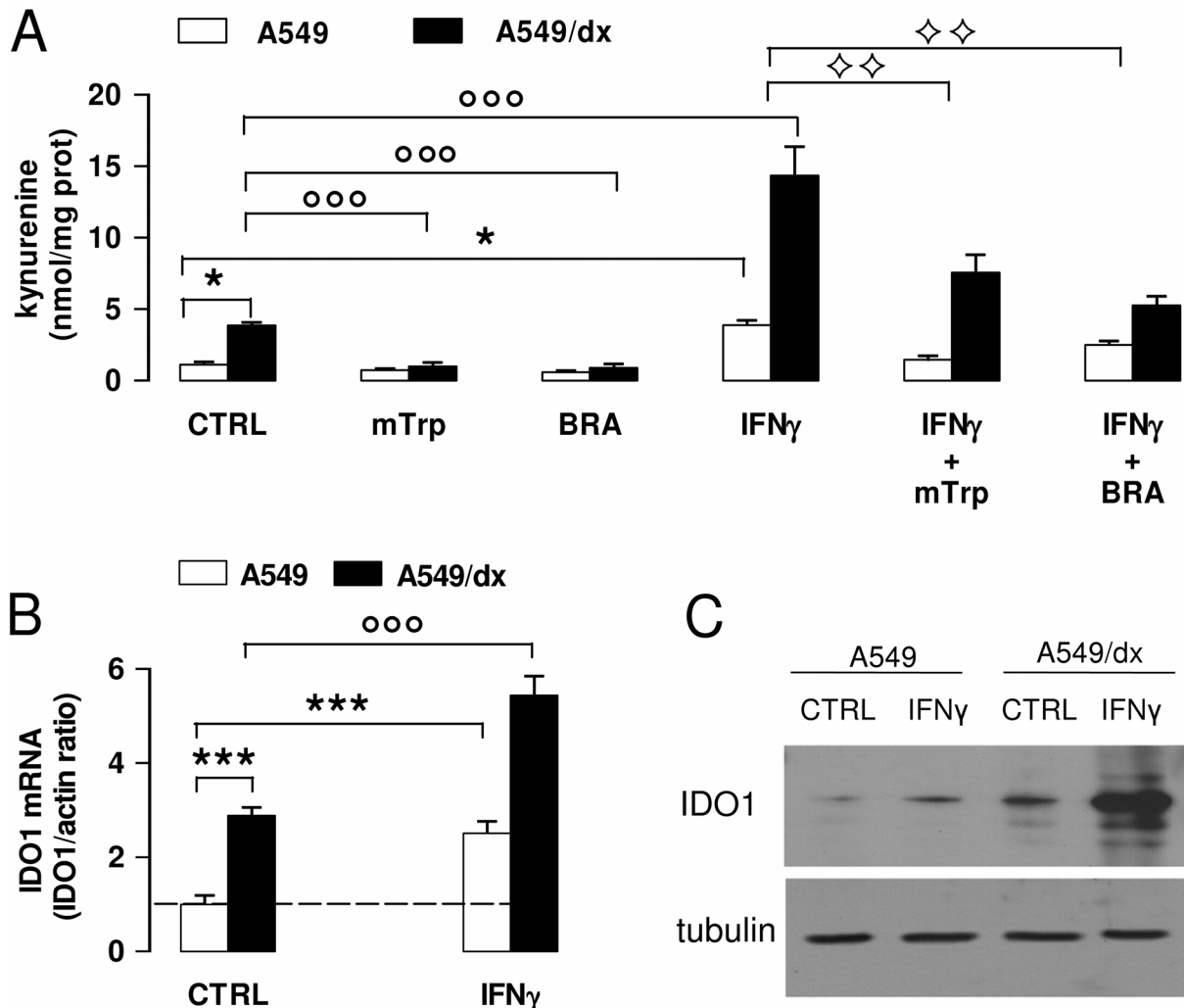


Fig 3. Effects of IFN- γ on kynurenine synthesis and IDO1 expression in chemosensitive and multidrug resistant cells. A549 and A549/dx cells were incubated for 48 h in fresh medium (CTRL) or in medium containing the IDO1 inhibitors methyl-DL-tryptophan (1 mmol/L, mTrp) or 5-Br-brassinin (100 μ mol/L, BRA), and the IDO1 inducer IFN- γ (100 ng/mL, IFN γ), alone or in combination. **A.** The kynurenine levels in the cell culture supernatants were measured spectrophotometrically. Data are presented as means \pm SD (n = 4). * p < 0.01: versus A549 CTRL cells; $^{\circ\circ}$ p < 0.001: versus A549/dx CTRL; $^{\diamond\diamond}$ p < 0.005: IFN- γ + mTrp-treated, IFN- γ + BRA-treated A549 and A549/dx cells versus the corresponding cells treated with IFN- γ alone. **B.** The expression level of IDO1 mRNA was measured by qRT-PCR. Data are presented as means \pm SD (n = 4). *** p < 0.001: versus A549 CTRL cells; $^{\circ\circ\circ}$ p < 0.001: versus A549/dx CTRL cells. **C.** Western blot analysis of IDO1 expression. The β -tubulin expression was used as control of equal protein loading. The figure is representative of 3 experiments with similar results.

doi:10.1371/journal.pone.0126159.g003

fold in A549/dx cells (S2 Table and Fig 5A). The ELISA assays confirmed the higher autocrine production of these cytokines in the multidrug resistant cells (Fig 5B), except in the case of TNF- α , whose level was below the detection limit of the kit (data not shown). Also the IFN- γ mRNA (S1 Table and Fig 4A) and protein (Fig 5B) were higher in A549/dx cells, increasing the number of the IDO-inducer cytokines produced by these cells.

STAT1/STAT3 silencing decreases the up-regulation of IDO1 and the kynurenine-induced immunosuppression in multidrug resistant cells

To validate the functional role of STAT1 and STAT3 as IDO1 inducers in multidrug resistant cells, we produced A549/dx clones transiently silenced for each protein (Fig 6A). STAT3- and,

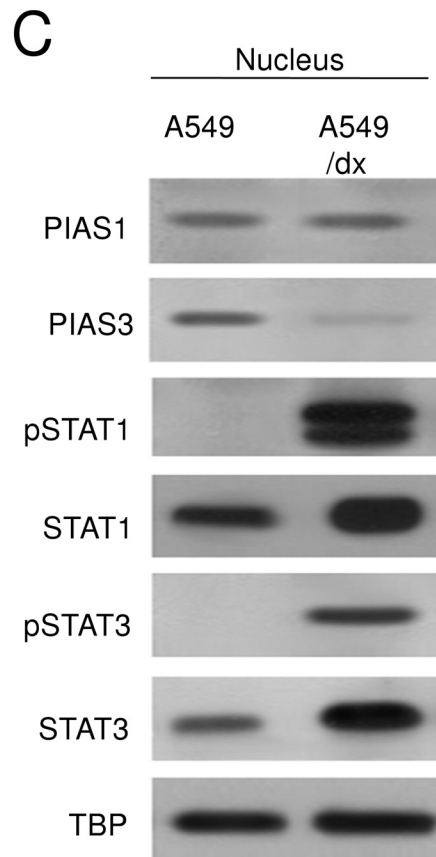
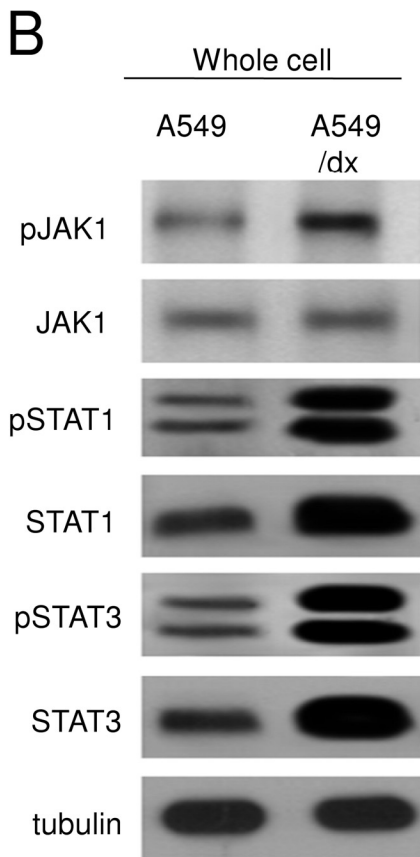
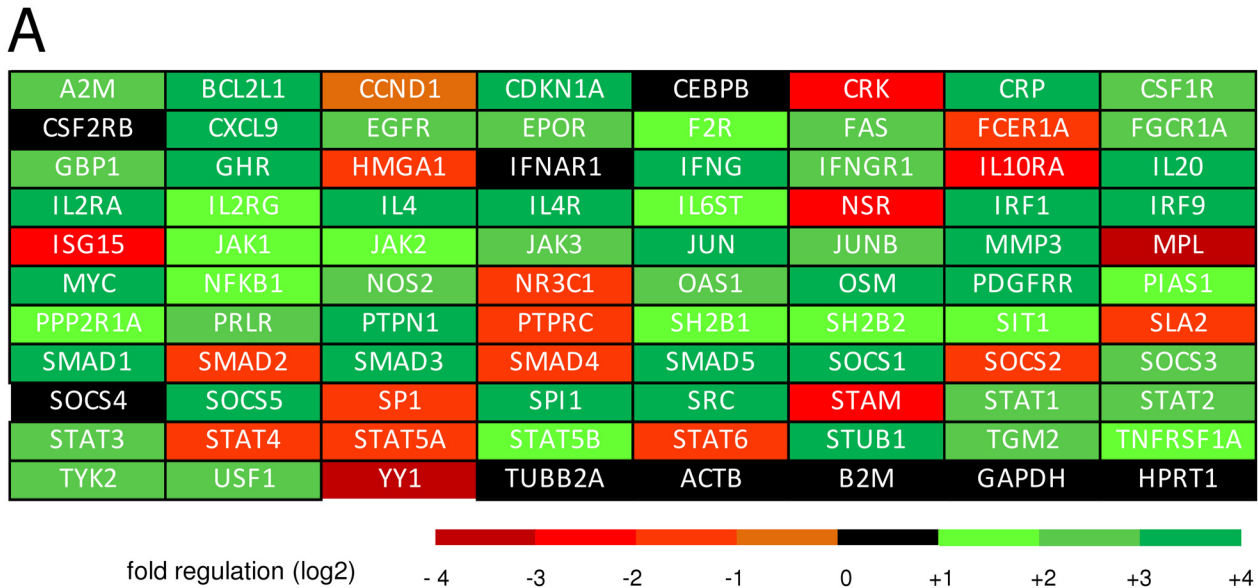
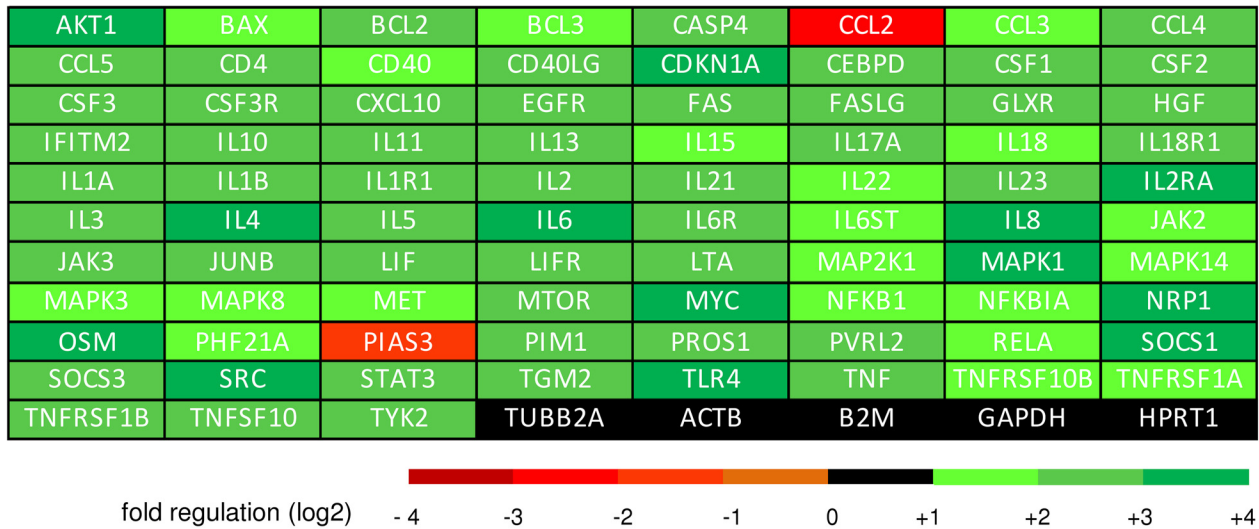


Fig 4. Multidrug resistant cells have a higher activity of JAK/STAT signaling than chemosensitive cells. A. The cDNA from A549 and A549/dx cells was analyzed by a PCR array specific for JAK/STAT signaling, as reported under Materials and methods. The fold regulation of the 83 genes analyzed, expressed in logarithmic scale, is represented in a colorimetric scale. The figure is the mean of 4 experiments. B. The cells were lysed and subjected to the Western blot analysis for phospho(Tyr 1022/1023)-JAK1, JAK1, phospho(Tyr701)-STAT1, STAT1, phospho(Tyr705)-STAT3, STAT3. The β -tubulin expression was used as control of equal protein loading. The figure is representative of 3 experiments with similar results. C. The expression of PIAS1, PIAS3, phospho(Tyr701)-STAT1, STAT1, phospho(Tyr705)-STAT3, STAT3 in nuclear extracts was measured by Western blotting. The TBP expression was used as control of equal protein loading. The figure is representative of 3 experiments with similar results.

doi:10.1371/journal.pone.0126159.g004

A



B

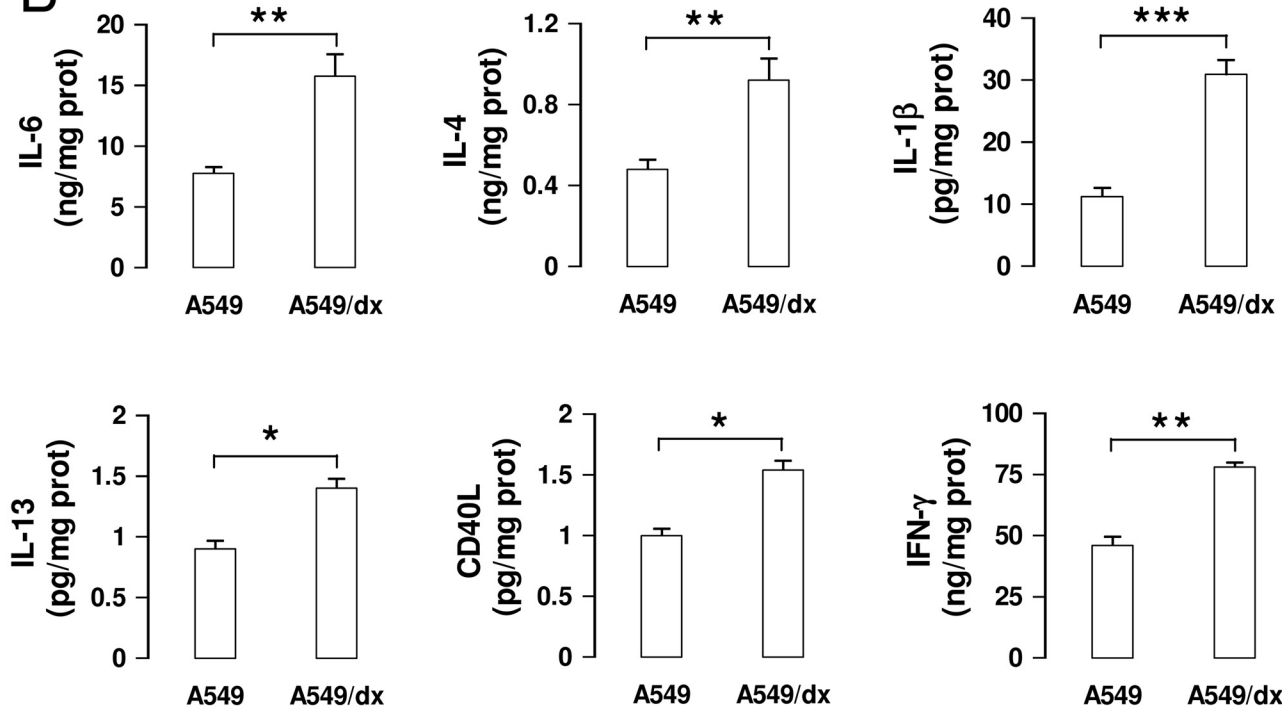


Fig 5. Multidrug resistant cells have a higher activity of IL-6/STAT3 signaling than chemosensitive cells. A. The cDNA from A549 and A549/dx cells was analyzed by a PCR array specific for IL-6/STAT3 signaling, as reported under Materials and methods. The fold regulation of the 83 genes analyzed, expressed in logarithmic scale, was represented in a colorimetric scale. The figure is the mean of 4 experiments. B. The levels of IL-6, IL-4, IL-1β, IL-13, CD40L, IFN-γ were measured in the cell culture supernatants by specific ELISAs. Data are presented as means ± SD (n = 3). * p < 0.02, ** p < 0.005, *** p < 0.001: A549/dx cells versus A549 cells.

doi:10.1371/journal.pone.0126159.g005

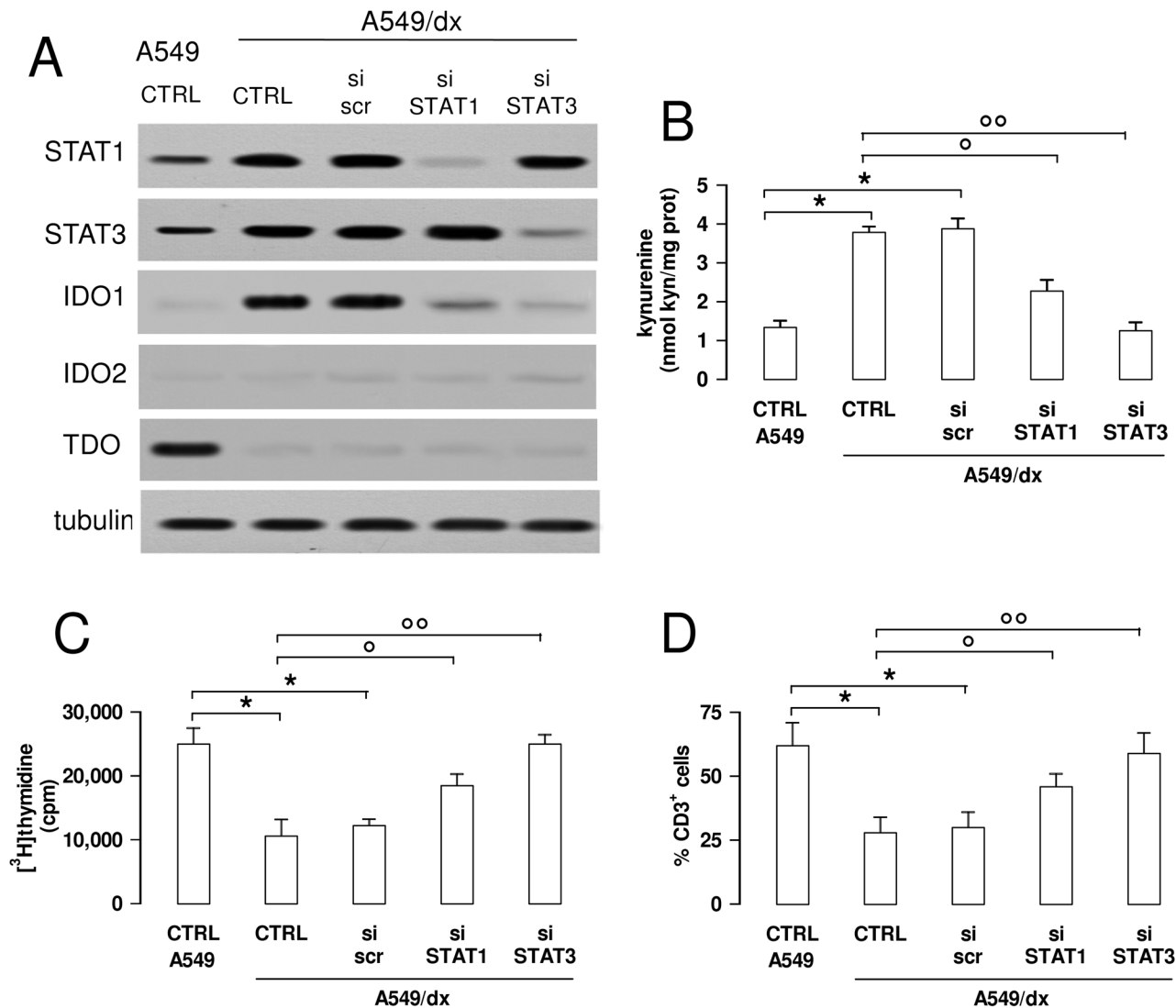


Fig 6. The inhibition of the STAT1/STAT3 signaling reverses the kynurenine-dependent immunosuppression in multidrug resistant cells. A549/dx cells were grown for 48 h in fresh medium (CTRL), treated with a non-targeting scrambled siRNA (scr) or with a specific siRNAs pool targeting STAT1 or STAT3, respectively (si STAT1, si STAT3). Untreated chemosensitive A549 cells were used as control. **A.** The expression of STAT1, STAT3, IDO1, IDO2 and TDO was measured in whole cell lysates by Western blotting, 48 h after the transfection. The β -tubulin expression was used as control of equal protein loading. The figure is representative of 3 experiments with similar results. **B.** The kynurenine levels in the cell culture supernatants were measured spectrophotometrically. Data are presented as means \pm SD (n = 4). * p < 0.01: versus A549 CTRL; ° p < 0.005, °° p < 0.001: versus A549/dx CTRL. **C.** The proliferation of activated T-lymphocytes collected from PBMC after a 72 h co-incubation with A549 and A549/dx cells was measured with the [³H]thymidine assay. In the presence of anti-CD3 and anti-CD28 stimulatory antibodies without tumor cells (positive control), the [³H]thymidine incorporation was 28,926 \pm 1,426 cpm; in the presence of RPMI medium alone (negative control), the [³H]thymidine incorporation was 4,312 \pm 529 cpm. Data are presented as means \pm SD (n = 6). * p < 0.05: versus A549 CTRL; ° p < 0.01, °° p < 0.005: versus A549/dx CTRL. **D.** The percentage of CD3⁺ T-lymphocytes collected from PBMC, co-incubated with tumor cells as reported in **C**, was measured by flow cytometry. Data are presented as means \pm SD (n = 6). * p < 0.01: versus A549 CTRL; ° p < 0.01, °° p < 0.002: versus A549/dx CTRL.

doi:10.1371/journal.pone.0126159.g006

to a lower extent, STAT1-silenced cells showed lower levels of IDO1 protein, without changes in IDO2 and TDO amount (Fig 6A). Silenced cells also had a reduced kynurenine synthesis, which in STAT3-silenced A549/dx cells was superimposable to the one of A549 cells (Fig 6B).

In keeping with the different expression of IDO1 and kynurenine levels, the chemosensitive A549 cells stimulated the proliferation of T-lymphocytes more than the multidrug resistant

A549/dx cells; the silencing of STAT1 and, in particular, of STAT3 in A549/dx cells restored the proliferation of T-cells to the same level of A549 cells (Fig 6C), which produced less kynurenine. In line with these results, the percentages of CD3⁺ cells recovered at the end of the co-incubation of PBMC with tumor cells was lower with A549/dx cells than with A549 cells, but the silencing of STAT1 and STAT3 significantly increased it (Fig 6D). No changes occurred in the proportion of CD4⁺ T-helper cells, CD8⁺ T-cytotoxic cells (S6A Fig) and Treg cells (S6B Fig), a typical subpopulation of T lymphocytes involved in immunotolerance and immunosuppression [39]. The same increase in T-lymphocyte proliferation (S7A Fig) and CD3⁺ expansion (S7B Fig) obtained after STAT-silencing was produced by treating A549/dx cells with the IDO1 inhibitor 5-Br-brassinin. These data suggest that the high kynurenine levels can be responsible for the reduced expansion of CD3⁺ T-lymphocytes induced by multidrug resistant cells.

Discussion

In this work we report for the first time that kynurenine production was higher in multidrug resistant than in chemosensitive cancer cells, independently from the type of chemoresistance (i.e. chemotherapy-induced or constitutive MDR) and the type of tumor. According to the expression pattern of IDO1, IDO2 and TDO in chemosensitive and chemoresistant cell lines, the higher synthesis of kynurenine in resistant cells was mainly due to the higher amount of IDO1.

It has been recently reported that a high intratumor amount of IDO1 favors the growth of lung cancers [22]. This observation is in keeping with our *in vivo* experiments, where the chemoresistant tumors expressing high levels of IDO1 grew faster than the chemosensitive counterparts with low levels of the enzyme. The pharmacological inhibition of IDO1 with 5-Br-brassinin significantly reduced the growth of chemoresistant tumors in immunocompetent animals, but not in immunodeficient mice. This result, which was in agreement with previous observations [27], led to the hypothesis that the antitumor effects of IDO1 inhibition require an active immune system and are mediated by the reduction of immunosuppressive cells and/or by the restoration of immune cells active against multidrug resistant tumors.

To clarify the molecular mechanisms at the basis of IDO1 overexpression in multidrug resistant cells, we focused on the model of non small cell lung cancer A549 and A549/dx cells, where the difference of IDO1 expression between sensitive and resistant cells was particularly pronounced. A recent study demonstrated that the serum kynurenine/tryptophan ratio is higher in patients affected by non small cell lung cancer compared with healthy controls and that such difference was further increased by radio-chemotherapy [40]. Differently from what it was observed in patients, we did not detect any increase of kynurenine production in cells exposed to one dose of chemotherapeutic drugs. We cannot exclude however that repeated exposures to chemotherapeutic agents, as it occurs in patients, might further increase the kynurenine synthesis also in our *in vitro* model.

The most striking difference between chemosensitive and multidrug resistant cells was the constitutive activation of the JAK/STAT axis in resistant cells. Although the expression of JAK1, a documented activator of STAT1 and STAT3 [31, 41], was not different, the multidrug resistant cells showed a higher basal amount of STAT1 and STAT3, and of the activated tyrosine-phosphorylated forms of JAK1, STAT1 and STAT3. The phosphorylation on tyrosine of STATs is necessary for their homodimerization and translocation into the nucleus [31]: indeed nuclear phospho(Tyr701)-STAT1 and phospho(Tyr705)-STAT3, which were undetectable in chemosensitive cells, were abundant in multidrug resistant ones. These results suggest that both the increased transcription of STAT1 and STAT3, as revealed by the PCR array analysis, and the increased activity of the JAK/STAT axis, as indicated by the higher phosphorylation of

STAT1/3, contribute to the increased activation of STATs in multidrug resistant cells and to the transcriptional activation of *IDO1* gene. Whereas the expression of the STAT1 inhibitor PIAS1 was equal in A549 and A549/dx cells, the amount of the STAT3 inhibitor PIAS3 was lower in A549/dx cells. According to this pattern, STAT3 more than STAT1 should have the higher transcriptional activity in our multidrug resistant cells. Indeed we found several STAT3-target genes significantly up-regulated in A549/dx cells; moreover, the selective silencing of STAT1 or STAT3 demonstrated that both factors were involved in *IDO1* transcription in multidrug resistant cells, but STAT3 had a slightly prominent role in this process.

The STAT1 and STAT3 activity is promoted by IFN- γ [31], a known *IDO1* inducer [10]. In A549/dx cells the exogenous IFN- γ elicited a strong induction of *IDO1*, more evident than in A549 cells. This result suggests that the IFN- γ -dependent signaling was more promptly activated in multidrug resistant than in chemosensitive cells: this may be explained by the higher activity of JAK/STAT axis in A549/dx cells. Interestingly, we detected an autocrine production of IFN- γ , higher in A549/dx than in A549 cells: although the amount of IFN- γ was significantly lower than the one produced by activated immune system cells [42], it might be sufficient to induce the transcription of *IDO1* in multidrug resistant cells, owing to their constitutively activated JAK/STAT axis. Therefore, an autocrine IFN- γ /JAK/STAT loop may be the driving force for the induction of *IDO1* in A549/dx cells. The maximal induction of *IDO1*, however, is often produced by the cooperation of IFN- γ with other cytokines [15]: IL-6, IL-4, IL-1 β , IL-13, TNF- α and CD40L are documented inducers of *IDO1*, alone or together with IFN- γ [34–38]. According to the PCR array analysis, these cytokines were at least two-fold up-regulated in A549/dx cells, where they may contribute to the transcription of *IDO1*. All the above-mentioned cytokines are STAT3-target genes; moreover, IL-6, IL-4 and IL-13 activate the JAK1/STAT3 axis with a feed-forward mechanism [43–45]. We might speculate that the higher basal production of these cytokines feeds multiple autocrine “cytokine/JAK/STAT3” loops, which sustain the transcription of *IDO1* in multidrug resistant cells.

The expression of *IDO1* in non small cell lung cancer cells has been already related to the constitutive activation of the IL-6/STAT3 signaling: kynurenine activates the transcription factor aryl hydrocarbon receptor, that in turn increases the autocrine synthesis of IL-6 and the subsequent activation of STAT3 [34]. Although in this work it has not been investigated whether the cells were chemosensitive or chemoresistant, it is conceivable that a similar loop works in A549/dx cells. On the other hand, with a feedback mechanism, IL-6 increases the STAT3-signaling inhibitor protein SOCS3, which induces the proteasomal degradation of *IDO1* [46]. SOCS3 mRNA was indeed up-regulated in A549/dx cells: this up-regulation may perhaps buffer the effect of IL-6 on STAT3 activity and *IDO1* transcription, limiting the maximal activation of the enzyme. We believe that the concomitant production of multiple cytokines, more than a single cytokine, contributes to the activation of STAT3 and *IDO1* in A549/dx cells.

To the best of our knowledge, only indirect evidences have correlated the activity of STAT3 and *IDO1* to the chemoresistance. For instance, the disruption of the STAT3 signaling has reduced tumor proliferation and angiogenesis [47], and has sensitized resistant breast cancer cells to doxorubicin [48]. A high production of kynurenine has been associated with resistance to olaparib, a poly(ADP-ribose) polymerase inhibitor, gamma radiations and cisplatin [49]. On the other hand, the *IDO1* inhibitor methyl-DL-tryptophan has increased the efficacy of paclitaxel in endometrial cancer xenografts [50], suggesting that the inhibition of *IDO1* may improve the chemosensitivity. Our assays suggest an additional benefit of inhibiting the STAT3/*IDO1* axis in resistant cells, i.e. the restoration of a significant expansion of T-lymphocytes that would be otherwise suppressed in the presence of multidrug resistant tumor cells.

Our work is the first demonstration that multidrug resistant cells have a higher endogenous production of kynurenine, sustained by the constitutive activation of a “cytokine/JAK/STAT3/IDO1” axis. Such phenotype is paralleled by the reduced expansion of the global population of T-lymphocytes, a feature that might favor the immune-evasion of multidrug resistant cells. Some pharmacological inhibitors of IDO1 [51] and the vaccination against IDO1 [52] are under evaluation in immunotherapy protocols to contrast the development of tumors refractory to the conventional therapies. In our multidrug resistant cells IDO1, although over-expressed, was sensitive to classical inhibitors such as methyl-DL-tryptophan and 5-Br-brassinin. This observation may be useful in a translational perspective and may represent a strong indication for the inclusion of IDO1 inhibitors in chemo-immunotherapy protocols against chemoresistant cancers, in order to limit the immunosuppressive attitude of these tumors.

Supporting Information

S1 Fig. Expression of ABC transporters in chemosensitive and multidrug resistant cells.

Human chemosensitive lung cancer A549 cells and chemoresistant A549/dx cells, human chemosensitive colon cancer HT29 cells and chemoresistant HT29/dx cells, human chemosensitive chronic myelogenous leukemia K562 cells and chemoresistant K562/dx cells, human chemosensitive mesothelial Met5A cells and human chemoresistant malignant mesothelioma HMM cells, murine chemoresistant mammary JC cells were lysed and subjected to the Western blot analysis for Pgp, MRP1, MRP2, MRP3, MRP4, MRP5, BCRP. The β -tubulin expression was used as control of equal protein loading. The figure is representative of 3 experiments with similar results. MDR-: chemosensitive cell lines; MDR+: chemoresistant cell lines. (TIF)

S2 Fig. HPLC measurement of kynurenine levels in chemosensitive and multidrug resistant cells.

The amount of kynurenine was measured by HPLC in the culture supernatants of human chemosensitive lung cancer A549 cells and chemoresistant A549/dx cells, human chemosensitive colon cancer HT29 cells and chemoresistant HT29/dx cells, human chemosensitive chronic myelogenous leukemia K562 cells and chemoresistant K562/dx cells, human chemosensitive mesothelial Met5A cells and human chemoresistant malignant mesothelioma HMM cells, murine chemoresistant mammary JC cells. Data are presented as means \pm SD (n = 3). * p < 0.05, ** p < 0.01, *** p < 0.001: chemoresistant cells (MDR-positive) versus the corresponding chemosensitive (MDR-negative) cells. (TIF)

S3 Fig. Effects of chemotherapeutic drugs on kynurenine synthesis.

A549 and A549/dx cells were incubated for 48 h in fresh medium (CTRL) or in medium containing 1 μ mol/L doxorubicin (DOX), 10 μ mol/L cisplatin (Pt), 100 nmol/L gemcitabine (GEM), 10 μ mol/L mitoxantrone (MXR). A. Cell viability was assessed by the neutral red staining, as reported under Materials and methods. Data are presented as means \pm SD (n = 4). ** p < 0.005: versus A549 CTRL cells; ° p < 0.05: A549/dx versus A549 cells. B. The kynurenine levels in the cell culture supernatants were measured spectrophotometrically. Data are presented as means \pm SD (n = 4). * p < 0.01: A549/dx cells versus A549 cells. (TIF)

S4 Fig. Effects of nitric oxide on kynurenine synthesis.

A549 and A549/dx cells were incubated for 24 h in the absence (CTRL) or in the presence of 100 μ mol/L S-nitrosoglutathione (GSNO) or S-nitroso-N-acetylpenicillamine (SNAP), chosen as NO donors. A. The amount of nitrite in the cell culture supernatants was measured spectrophotometrically by the Griess method. Data are presented as means \pm SD (n = 3). ** p < 0.005: A549- or A549/dx-treated

cells versus the respective CTRL cells. B. The kynurenine levels in the cell culture supernatants were measured spectrophotometrically. Data are presented as means \pm SD (n = 3). *** p < 0.001: A549/dx cells versus A549 cells.

(TIF)

S5 Fig. Effects of iron on kynurenine synthesis. A549 and A549/dx cells were incubated for 24 h with fresh medium (CTRL), with the cell permeable iron-releasing compound ferric nitrilotriacetate (60 μ mol/L, FeNTA) or with the iron chelator desferrioxamine (100 μ mol/L, DFX). A. The amount of intracellular iron was measured by atomic absorption spectroscopy in the cell lysate. Data are presented as means \pm SD (n = 3). *** p < 0.001: A549- or A549/dx-treated cells versus the respective CTRL cells. B. The kynurenine levels in the cell culture supernatants were measured spectrophotometrically. Data are presented as means \pm SD (n = 3). * p < 0.05: A549/dx cells versus A549 cells.

(TIF)

S6 Fig. T-lymphocytes subclasses after co-incubation with chemosensitive and multidrug resistant cells. A549/dx cells were grown for 48 h in fresh medium (CTRL), treated with a non-targeting scrambled siRNA (scr) or with a specific siRNAs pool targeting STAT1 or STAT3, respectively (si STAT1, si STAT3). Untreated chemosensitive A549 cells were used as control. The percentage of each subclass of CD3⁺ T-lymphocytes collected from PBMC, after a 72 h co-incubation with A549 and A549/dx cells, was measured by flow cytometry. A. Percentage of T-helper (CD3⁺CD4⁺) and T-cytotoxic (CD3⁺CD8⁺) lymphocytes. Data are presented as means \pm SD (n = 4). B. Percentage of Treg (CD4⁺CD25⁺CD127^{low}) lymphocytes. Data are presented as means \pm SD (n = 4).

(TIF)

S7 Fig. Effects of IDO1 inhibition in multidrug resistant cells on the proliferation of T-lymphocytes. A. The proliferation of activated T-lymphocytes collected from PBMC after a 72 h co-incubation with A549/dx cells, grown in the absence (CTRL) or in the presence of the IDO1 inhibitor 5-Br-brassinin (100 μ mol/L, BRA), was measured with the [³H]thymidine assay. In the presence of anti-CD3 and anti-CD28 stimulatory antibodies without tumor cells (positive control), the [³H]thymidine incorporation was 27,876 \pm 2,349 cpm; in the presence of RPMI medium alone (negative control), the [³H]thymidine incorporation was 3,981 \pm 705 cpm. Data are presented as means \pm SD (n = 4). *** p < 0.005: BRA-treated cells versus CTRL cells. B. The percentage of CD3⁺ T-lymphocytes collected from PBMC, co-incubated with A549/dx cells as reported in A, was measured by flow cytometry. Data are presented as means \pm SD (n = 4). *** p < 0.005: BRA-treated cells versus CTRL cells.

(TIF)

S1 Table. PCR array of JAK/STAT-signaling genes in A549 and A549-dx cells.

(DOC)

S2 Table. PCR array of IL6/STAT3-signaling genes in A549 and A549-dx cells.

(DOC)

Acknowledgments

We thank Prof. Amalia Bosia (Department of Oncology, University of Torino) for the fruitful discussion and Mr. Costanzo Costamagna (Department of Oncology, University of Torino) for the technical assistance.

Author Contributions

Conceived and designed the experiments: IC CR. Performed the experiments: IC IB BC BR JK EG. Analyzed the data: JK EG DG. Wrote the paper: DG CR.

References

1. Gottesman MM, Fojo T, Bates SE (2002). Multidrug resistance in cancer: role of ATP-dependent transporters. *Nat Rev Cancer* 2(1): 48–58. PMID: [11902585](#)
2. Agarwal S, Sane R, Oberoi R, Ohlfest JR, Elmquist WF (2011) Delivery of molecularly targeted therapy to malignant glioma, a disease of the whole brain. *Expert Rev Mol Med* 13: e17. doi: [10.1017/S1462399411001888](#) PMID: [21676290](#)
3. Obeid M, Tesniere A, Ghiringhelli F, Fimia GM, Apetoh L, Perfettini JL, et al. (2007) Calreticulin exposure dictates the immunogenicity of cancer cell death. *Nat Med* 13(1): 54–61. PMID: [17187072](#)
4. De Boo S, Kopecka J, Brusa D, Gazzano E, Matera L, Ghigo D, et al. (2009) iNOS activity is necessary for the cytotoxic and immunogenic effects of doxorubicin in human colon cancer cells. *Mol Cancer* 8: e108.
5. Kopecka J, Campia I, Brusa D, Doublier S, Matera L, Ghigo D, et al. (2011) Nitric oxide and P-glycoprotein modulate the phagocytosis of colon cancer cells. *J Cell Mol Med* 15(7): 1492–1504. doi: [10.1111/j.1582-4934.2010.01137.x](#) PMID: [20716130](#)
6. Riganti C, Castella B, Kopecka J, Campia I, Coscia M, Pescarmona G, et al. (2013) Zoledronic acid restores doxorubicin chemosensitivity and immunogenic cell death in multidrug-resistant human cancer cells. *PLoS One* 8(4): e60975. doi: [10.1371/journal.pone.0060975](#) PMID: [23593363](#)
7. Burkholder B, Huang RY, Burgess R, Luo S, Jones VS, Zhang W, et al. (2014) Tumor-induced perturbations of cytokines and immune cell networks. *Biochim Biophys Acta* 1845(2): 182–201. doi: [10.1016/j.bbcan.2014.01.004](#) PMID: [24440852](#)
8. Opitz CA, Litzenger UM, Sahm F, Ott M, Tritschler I, Trump S, et al. (2011) An endogenous tumour-promoting ligand of the human aryl hydrocarbon receptor. *Nature* 478(7368): 197–203. doi: [10.1038/nature10491](#) PMID: [21976023](#)
9. Prendergast GC (2011) Cancer: Why tumors eat tryptophan. *Nature* 478(7368): 192–194. doi: [10.1038/478192a](#) PMID: [21993754](#)
10. Ozaki Y, Edelstein MP, Duch DS (1988) Induction of indoleamine 2,3-dioxygenase: a mechanism of the antitumor activity of interferon gamma. *Proc Natl Acad Sci USA* 85(4): 1242–1246. PMID: [3124115](#)
11. Metz R, Duhadaway JB, Kamasani U, Laury-Kleintop L, Muller AJ, Prendergast GC (2007) Novel tryptophan catabolic enzyme IDO2 is the preferred biochemical target of the antitumor indoleamine 2,3-dioxygenase inhibitory compound D-1-methyl-tryptophan. *Cancer Res* 67(15): 7082–7087. PMID: [17671174](#)
12. Thomas SR, Terentis AC, Cai H, Takikawa O, Levina A, Lay PA, et al. (2007) Post-translational regulation of human indoleamine 2,3-dioxygenase activity by nitric oxide. *J Biol Chem* 282(33): 23778–23787. PMID: [17535808](#)
13. Krause-Opatz B, Wittkop U, Gutzki FM, Schmidt C, Jürgens-Saathoff B, Meier S, et al. (2009) Free iron ions decrease indoleamine 2,3-dioxygenase expression and reduce IFN γ -induced inhibition of *Chlamydia trachomatis* infection. *Microb Pathog* 46(6): 289–297. doi: [10.1016/j.micpath.2009.03.001](#) PMID: [19306922](#)
14. Lu B, Finn OJ (2008) T-cell death and cancer immune tolerance. *Cell Death Differ* 15(1): 70–79. PMID: [18007660](#)
15. Harden JL, Egilmez NK (2012) Indoleamine 2,3-dioxygenase and dendritic cell tolerogenicity. *Immunol Invest* 41(6–7): 738–764. doi: [10.3109/08820139.2012.692418](#) PMID: [22686468](#)
16. Gajewski TF, Meng Y, Blank C, Brown I, Kacha A, Kline J, et al. (2006) Immune resistance orchestrated by the tumor microenvironment. *Immunol Rev* 213: 131–145. PMID: [16972901](#)
17. Uytendhove C, Pilotte L, Théate I, Stroobant V, Colau D, Parmentier N, et al. (2003) Evidence for a tumoral immune resistance mechanism based on tryptophan degradation by indoleamine 2,3-dioxygenase. *Nat Med* 9(10): 1269–1274. PMID: [14502282](#)
18. Suzuki Y, Suda T, Furuhashi K, Suzuki M, Fujie M, Hahimoto D, et al. (2010) Increased serum kynurenine/tryptophan ratio correlates with disease progression in lung cancer. *Lung Cancer* 67(3): 361–365. doi: [10.1016/j.lungcan.2009.05.001](#) PMID: [19487045](#)
19. Okamoto A, Nikaido T, Ochiai K, Takakura S, Saito M, Aoki Y, et al. (2005) Indoleamine 2,3-dioxygenase serves as a marker of poor prognosis in gene expression profiles of serous ovarian cancer cells. *Clin Cancer Res* 11(16): 6030–6039. PMID: [16115948](#)

20. Brandacher G, Perathoner A, Ladurner R, Schneeberger S, Obrist P, Winkler C, et al. (2006) Prognostic value of indoleamine 2,3-dioxygenase expression in colorectal cancer: effect on tumour-infiltrating T cells. *Clin Cancer Res* 12(4): 1144–1151. PMID: [16489067](#)
21. Ino K, Tanizaki Y, Kobayashi A, Toujima S, Mabuchi Y, Minami S (2012) Role of the Immune Tolerance-Inducing Molecule Indoleamine 2,3-Dioxygenase in Gynecologic Cancers. *J Cancer Sci Ther* 13: e004.
22. Smith C, Chang MY, Parker KH, Beury DW, DuHadaway JB, Flick HE, et al. (2012) IDO is a nodal pathogenic driver of lung cancer and metastasis development. *Cancer Discov* 2(8): 722–735. doi: [10.1158/2159-8290.CD-12-0014](#) PMID: [22822050](#)
23. Cacciotti P, Libener R, Betta P, Martini F, Porta C, Procopio A, et al. (2001) SV40 replication in human mesothelial cells induces HGF/Met receptor activation: a model for viral-related carcinogenesis of human malignant mesothelioma. *Proc Natl Acad Sci USA* 98(21):12032–12037. PMID: [11572935](#)
24. Hou DY, Muller AJ, Sharma MD, DuHadaway J, Banerjee T, Johnson M, et al. (2007) Inhibition of indoleamine 2,3-dioxygenase in dendritic cells by stereoisomers of 1-methyl-tryptophan correlates with anti-tumor responses. *Cancer Res* 67(2): 792–801. PMID: [17234791](#)
25. Zhang X, He Y, Ding M (2009) Simultaneous determination of tryptophan and kynurenine in plasma samples of children patients with Kawasaki disease by high-performance liquid chromatography with programmed wavelength ultraviolet detection. *J Chromatogr B Analyt Technol Biomed Life Sci* 877 (16–17):1678–1682.
26. Lee B, French K, Zhuang Y, Smith C (2003) Development of a syngeneic in vivo tumor model and its use in evaluating a novel p-glycoprotein modulator, pgp-4008. *Oncol Res* 14(1): 49–60. PMID: [14552591](#)
27. Banerjee T, Duhadaway JB, Gaspari P, Sutanto-Ward E, Munn DH, Mellor AL, et al. (2008) A key in vivo antitumor mechanism of action of natural product-based brassinins is inhibition of indoleamine 2,3-dioxygenase. *Oncogene* 27(20): 2851–2857. PMID: [18026137](#)
28. Gelsomino G, Corsetto PA, Campia I, Montorfano G, Kopecka J, Castella B, et al. (2013) Omega 3 fatty acids chemosensitize multidrug resistant colon cancer cells by down-regulating cholesterol synthesis and altering detergent resistant membranes composition. *Mol Cancer* 12: e137.
29. Riganti C, Costamagna C, Doublier S, Miraglia E, Polimeni M, Bosia A, et al. (2008) The NADPH oxidase inhibitor apocynin induces nitric oxide synthesis via oxidative stress. *Toxicol Appl Pharmacol* 228 (3): 277–285. doi: [10.1016/j.taap.2007.12.013](#) PMID: [18234259](#)
30. Qian F, Vilella J, Wallace PK, Mhawech-Fauceglia P, Tario JD Jr, Andrews C, et al. (2009) Efficacy of levo-1-methyl tryptophan and dextro-1-methyl tryptophan in reversing indoleamine-2,3-dioxygenase-mediated arrest of T-cell proliferation in human epithelial ovarian cancer. *Cancer Res* 69 (13): 5498–5504. doi: [10.1158/0008-5472.CAN-08-2106](#) PMID: [19491279](#)
31. Gough DJ, Levy DE, Johnstone RW, Clarke CJ (2008) IFN γ signaling—does it mean JAK-STAT? *Cytokine Growth Factor Rev* 19(5–6): 383–394.
32. Orabona C, Grohmann U (2011) Indoleamine 2, 3-dioxygenase and regulatory function: tryptophan starvation and beyond. *Methods Mol Biol* 677: 269–280. doi: [10.1007/978-1-60761-869-0_19](#) PMID: [20941617](#)
33. Sun Y, Chin YE, Weisiger E, Malter C, Tawara I, Toubai T, et al. (2009) Cutting edge: Negative regulation of dendritic cells through acetylation of the non histone protein STAT-3. *J Immunol* 182(10): 5899–5903. doi: [10.4049/jimmunol.0804388](#) PMID: [19414739](#)
34. Litzemberger UM, Opitz CA, Sahn F, Rauschenbach KJ, Trump S, Winter M, et al. (2014) Constitutive IDO expression in human cancer is sustained by an autocrine signaling loop involving IL-6, STAT3 and the AHR. *Oncotarget* 5(4): 1038–1051. PMID: [24657910](#)
35. Yadav MC, Burudi EM, Alirezaei M, Flynn CC, Watry DD, Lanigan CM, et al. (2007) IFN- γ -induced IDO and WRS expression in microglia is differentially regulated by IL-4. *Glia* 55(13): 1385–1396. PMID: [17661345](#)
36. Zunszain PA, Anacker C, Cattaneo A, Choudhury S, Musaelyan K, Myint AM, et al. (2012) Interleukin-1 β : a new regulator of the kynurenine pathway affecting human hippocampal neurogenesis. *Neuropsychopharmacology* 37(4): 939–949. doi: [10.1038/npp.2011.277](#) PMID: [22071871](#)
37. Liu WL, Lin YH, Xiao H, Xing S, Chen H, Chi PD, et al. (2014) Epstein-Barr Virus infection induces indoleamine 2,3-dioxygenase expression in human monocyte-derived macrophages through p38/MAPK and NF- κ B pathways: impairment in T cell functions. *J Virol* 88(12): 6660–6671. doi: [10.1128/JVI.03678-13](#) PMID: [24696473](#)
38. Hwu P, Du MX, Lapointe R, Do M, Taylor MW, Young HA (2000) Indoleamine 2,3-dioxygenase production by human dendritic cells results in the inhibition of T cell proliferation. *J Immunol* 164(7): 3596–3599. PMID: [10725715](#)

39. Sakaguchi S, Yamaguchi T, Nomura T, Ono M (2008) Regulatory T cells and immune tolerance. *Cell* 133(5): 775–787. doi: [10.1016/j.cell.2008.05.009](https://doi.org/10.1016/j.cell.2008.05.009) PMID: [18510923](https://pubmed.ncbi.nlm.nih.gov/18510923/)
40. Creelan BC, Antonia S, Bepler G, Garrett TJ, Simon GR, Soliman HH (2013) Indoleamine 2,3-dioxygenase activity and clinical outcome following induction chemotherapy and concurrent chemoradiation in Stage III non-small cell lung cancer. *Oncoimmunology* 2(3): e23428. PMID: [23802083](https://pubmed.ncbi.nlm.nih.gov/23802083/)
41. Song L, Rawal B, Nemeth JA, Haura EB (2011) JAK1 activates STAT3 activity in non-small-cell lung cancer cells and IL-6 neutralizing antibodies can suppress JAK1-STAT3 signaling. *Mol Cancer Ther* 10(3): 481–494. doi: [10.1158/1535-7163.MCT-10-0502](https://doi.org/10.1158/1535-7163.MCT-10-0502) PMID: [21216930](https://pubmed.ncbi.nlm.nih.gov/21216930/)
42. Lawrence S, Reid J, Whalen M (2013) Secretion of interferon gamma from human immune cells is altered by exposure to tributyltin and dibutyltin. *Environ Toxicol* doi: [10.1002/tox.21932](https://doi.org/10.1002/tox.21932)
43. Schindler C, Levy DE, Decker T (2007) JAK-STAT signaling: from interferons to cytokines. *J Biol Chem* 282(28): 20059–20063. PMID: [17502367](https://pubmed.ncbi.nlm.nih.gov/17502367/)
44. O'Shea JJ, Murray PJ (2008) Cytokine signaling modules in inflammatory responses. *Immunity* 28(4): 477–487. doi: [10.1016/j.immuni.2008.03.002](https://doi.org/10.1016/j.immuni.2008.03.002) PMID: [18400190](https://pubmed.ncbi.nlm.nih.gov/18400190/)
45. Russell MA, Cooper AC, Dhayal S, Morgan NG (2013) Differential effects of interleukin-13 and interleukin-6 on Jak/STAT signaling and cell viability in pancreatic β -cells. *Islets* 5(2): 95–105. doi: [10.4161/isl.24249](https://doi.org/10.4161/isl.24249) PMID: [23510983](https://pubmed.ncbi.nlm.nih.gov/23510983/)
46. Orabona C, Pallotta MT, Volpi C, Fallarino F, Vacca C, Bianchi R, et al. (2008) SOCS3 drives proteasomal degradation of indoleamine 2,3-dioxygenase (IDO) and antagonizes IDO-dependent tolerogenesis. *Proc Natl Acad Sci USA* 105(52): 20828–20833. doi: [10.1073/pnas.0810278105](https://doi.org/10.1073/pnas.0810278105) PMID: [19088199](https://pubmed.ncbi.nlm.nih.gov/19088199/)
47. Yu H, Kortylewski M, Pardoll D (2007) Crosstalk between cancer and immune cells: role of STAT3 in the tumour microenvironment. *Nat Rev Immunol* 7(1): 41–51. PMID: [17186030](https://pubmed.ncbi.nlm.nih.gov/17186030/)
48. Gariboldi MB, Ravizza R, Molteni R, Osella D, Gabano E, Monti E (2007) Inhibition of Stat3 increases doxorubicin sensitivity in a human metastatic breast cancer cell line. *Cancer Lett* 258(2): 181–188. PMID: [17920763](https://pubmed.ncbi.nlm.nih.gov/17920763/)
49. Maleki Vareki S, Rytelewski M, Figueredo R, Chen D, Ferguson PJ, Vincent M, et al. (2014) Indoleamine 2,3-dioxygenase mediates immune-independent human tumor cell resistance to olaparib, gamma radiation, and cisplatin. *Oncotarget* 5(9): 2778–2791. PMID: [24784564](https://pubmed.ncbi.nlm.nih.gov/24784564/)
50. Yoshida N, Ino K, Ishida Y, Kajiyama H, Yamamoto E, Shibata K, et al. (2008) Overexpression of indoleamine 2,3-dioxygenase in human endometrial carcinoma cells induces rapid tumor growth in a mouse xenograft model. *Clin Cancer Res* 14(22): 7251–7259. doi: [10.1158/1078-0432.CCR-08-0991](https://doi.org/10.1158/1078-0432.CCR-08-0991) PMID: [19010841](https://pubmed.ncbi.nlm.nih.gov/19010841/)
51. Godin-Ethier J, Hanafi LA, Piccirillo CA, Lapointe R (2011) Indoleamine 2,3-dioxygenase expression in human cancers: clinical and immunologic perspectives. *Clin Cancer Res* 17(22): 6985–6991. doi: [10.1158/1078-0432.CCR-11-1331](https://doi.org/10.1158/1078-0432.CCR-11-1331) PMID: [22068654](https://pubmed.ncbi.nlm.nih.gov/22068654/)
52. Iversen TZ, Engell-Noerregaard L, Ellebaek E, Andersen R, Larsen SK, Bjoern J, et al. (2014) Long-lasting disease stabilization in the absence of toxicity in metastatic lung cancer patients vaccinated with an epitope derived from indoleamine 2,3 dioxygenase. *Clin Cancer Res* 20(1): 221–232. doi: [10.1158/1078-0432.CCR-13-1560](https://doi.org/10.1158/1078-0432.CCR-13-1560) PMID: [24218513](https://pubmed.ncbi.nlm.nih.gov/24218513/)

Treatment with intermittent PTH increases Wnt10b production by T cells in osteoporotic patients

P. D'Amelio¹ · F. Sassi¹ · I. Buondonno¹ · G. Fornelli¹ · E. Spertino¹ · L. D'Amico² · M. Marchetti¹ · M. Lucchiari³ · I. Roato² · G. C. Isaia¹

Received: 22 April 2015 / Accepted: 27 May 2015

© International Osteoporosis Foundation and National Osteoporosis Foundation 2015

Abstract

Summary We evaluated the effect of parathyroid hormone (PTH) on Wnt10b production by immune system cells in humans. We showed that bone anabolic effect of intermittent PTH treatment may be amplified by T cells through increased production of Wnt10b. Chronic increase in PTH as in primary hyperparathyroidism does not increase Wnt10b expression.

Introduction The aim of this study is to assess the effect of PTH on Wnt10b production by immune system cells in humans. We assessed both the effect of intermittent PTH administration (iPTH) and of chronic PTH hypersecretion in primary hyperparathyroidism (PHP).

Methods Eighty-two women affected by post-menopausal osteoporosis were randomly assigned to treatment with calcium and vitamin D alone (22) or plus 1-84 PTH (42), or intravenous ibandronate (18). Wnt10b production by unfractionated blood nucleated cells and by T, B cells and monocytes was assessed by real-time RT-PCR and ELISA at baseline, 3, 6, 12 and 18 months of treatment. The effect of chronic elevation of PTH was evaluated in 20 patients affected by PHP at diagnosis and after surgical removal of parathyroid adenoma.

WNT10b from both osteoporotic and PHP patients was compared to healthy subjects matched for age and sex.

Results iPTH increases Wnt10b production by T cells, whereas PHP does not. After surgical restoration of normal parathyroid function, WNT10b decreases, although it is still comparable with healthy subjects' level. Thus, chronic elevation of PTH does not significantly increase WNT10b production as respect to control.

Conclusions This is the first work showing the effect of both intermittent and chronic PTH increase on Wnt10b production by immune system cells. We suggest that, in humans, T cells amplified the anabolic effect of PTH on bone, by increasing Wnt10b production, which stimulates osteoblast activity.

Keywords Immune system · Osteoporosis · Primary hyperparathyroidism · PTH · T cells · Wnt10b

Introduction

Parathyroid hormone (PTH) regulates calcium and phosphate homeostasis and has profound effects on bone turnover. PTH chronic increase, as in primary or secondary hyperparathyroidism, has catabolic effects on bone, causes bone loss and increases fracture risk [1]. In contrast, intermittent PTH injection has anabolic effects on bone [2] and prevents fragility fractures; indeed, intermittent PTH is currently used for the treatment of post-menopausal osteoporosis [3, 4].

The PTH receptor (PPR) is mainly expressed in the bone and kidney, but its expression has also been reported in other tissues where it likely reflects the local paracrine role of PTH-related protein [5–7]. In the bone, PPR is expressed in osteoclasts [8] and mainly in cells of osteoblastic lineage as osteocytes [9]. A recent work by Saini et al. [9] suggests that osteocytes are necessary for intermittent PTH anabolic effects. Treatment with intermittent PTH activates Wnt signalling

✉ P. D'Amelio
patrizia.damelio@unito.it

¹ Gerontology Section, Department of Medical Science, University of Torino, Corso Bramante 88/90, 10126 Torino, Italy

² CeRMS, Città della Salute e della Scienza University Hospital of Torino-Italy, Torino, Italy

³ Clinical Biochemistry Laboratory, Città della Salute e della Scienza University Hospital of Torino-Italy, Torino, Italy

pathway in osteoblast by suppressing sclerostin production by osteocytes [10–16].

PPR is also expressed by T cells [17], which are required for intermittent PTH to exert its bone anabolic effect as recently demonstrated in mice [17–19]. The bone anabolic response to intermittent PTH is blunted in the absence of T cells and is restored by adoptive transfer of these cells [17, 18]. T cells mediate intermittent PTH anabolic effect on bone through the upregulation of Wnt10b on their surface [18]; Wnt10b interacts with osteoblasts upregulating Wnt pathway and induces bone formation.

Unlike intermittent PTH, continuous PTH infusion, a condition that mimics primary hyperparathyroidism (PHP) in humans, does not affect Wnt10b expression by T cells in mice [17, 18], whereas in humans no data are available.

Here, we show that PTH affects Wnt10b production by immune system cells in humans, potentially explaining its anabolic effect.

Materials and methods

Patients

The study was approved by the Ethical Committee of the A.O.U. Città della Salute e della Scienza - A.O. Ordine Mauriziano - A.S.L. TO1, Turin, Italy, and informed consent was obtained from all participants. The study population was recruited from the patients of A.O.U. Città della Salute e della Scienza, Turin, Italy, and healthy volunteers. The study included patients affected by post-menopausal osteoporosis and patients affected by PHP.

Post-menopausal osteoporosis

Eighty-two women affected by post-menopausal osteoporosis without fractures were randomly allocated to treatment with:

- i. intermittent PTH (PTH 1-84 100 mcg/day s.c.—Preotact®, kindly provided by Nycomed—plus calcium 1200 mg/day and colecalciferol 800 UI/day, referred to hereafter as iPTH), 42 patients,
- ii. calcium and vitamin D 1200 mg/day and colecalciferol 800 UI/day (referred to hereafter as calcium and vitamin D), 22 patients, and
- iii. intravenous ibandronate 3 mg every 3 months, plus calcium and vitamin D (referred to hereafter as IB), 18 patients.

This is a parallel, randomized controlled, open-label, trial (registered as PTH1-84 EudraCT 2009-012397-12). The randomization was done by computer-generated tables to allocate treatments. Randomization was done by the principal

investigator, patients were enrolled by participants in the study and lab measurement and statistical analyses were done in blind to treatment.

Patients affected by secondary osteoporosis or taking drugs active on bone metabolism were not considered eligible for the study.

Blood samples from patients were collected at baseline and after 3, 6, 12 and 18 months of treatment.

Primary hyperparathyroidism

We enrolled in the study 20 patients (16 women and 4 men) affected by PHP, none of them were affected by diseases affecting bone health other than PHP. Subjects with secondary hyperparathyroidism, severe vitamin D deficiency, chronic renal disease (GFR<60) and any other condition known to affect PTH levels were excluded.

The diagnosis of PHP was established on the finding of elevated circulating levels of calcium and PTH in at least two instances and the presence of normal renal function. PHP patients were subjected to parathyroidectomy and restoration of normal parathyroid function was demonstrated by the finding of normal serum PTH and calcium levels 1 month after surgery. Blood samples were collected at baseline and 1 month after parathyroidectomy.

Healthy controls

Two groups of healthy subjects were enrolled as controls for post-menopausal women (31 healthy post-menopausal women) and for PHP patients (42 healthy men and women in post-menopausal period or in fertile age). Patients and controls were matched for sex, age and years since menopause.

The study design is summarized in Fig. 1. The demographic characteristics of the study population are shown in Table 1.

Measurements of Wnt10b mRNA

Wnt10b mRNA was measured in unfractionated peripheral blood nucleated cells in osteoporotic patients, in PHP and in healthy controls. Unfractionated peripheral blood nucleated cells were obtained by red blood cells lyses, the obtained cells were frozen at -80°C until RNA extraction. In 36 osteoporotic patients (18 treated with iPTH and 18 with IB), T cells, B cells and monocytes were separated by immunomagnetic beads separation (Stemcells Technology) to evaluate which cell produces Wnt10b (Fig. 1).

Real-Time PCR (RT-PCR) was used to evaluate Wnt10b expression. RNA was isolated using TRIzol reagent (Ambion, Huntingdon, UK), chloroform extraction and subsequent isopropanol precipitation according to the manufacturer's protocol. One microgram of RNA was converted up to single-stranded cDNA by the High Capacity cDNA Reverse

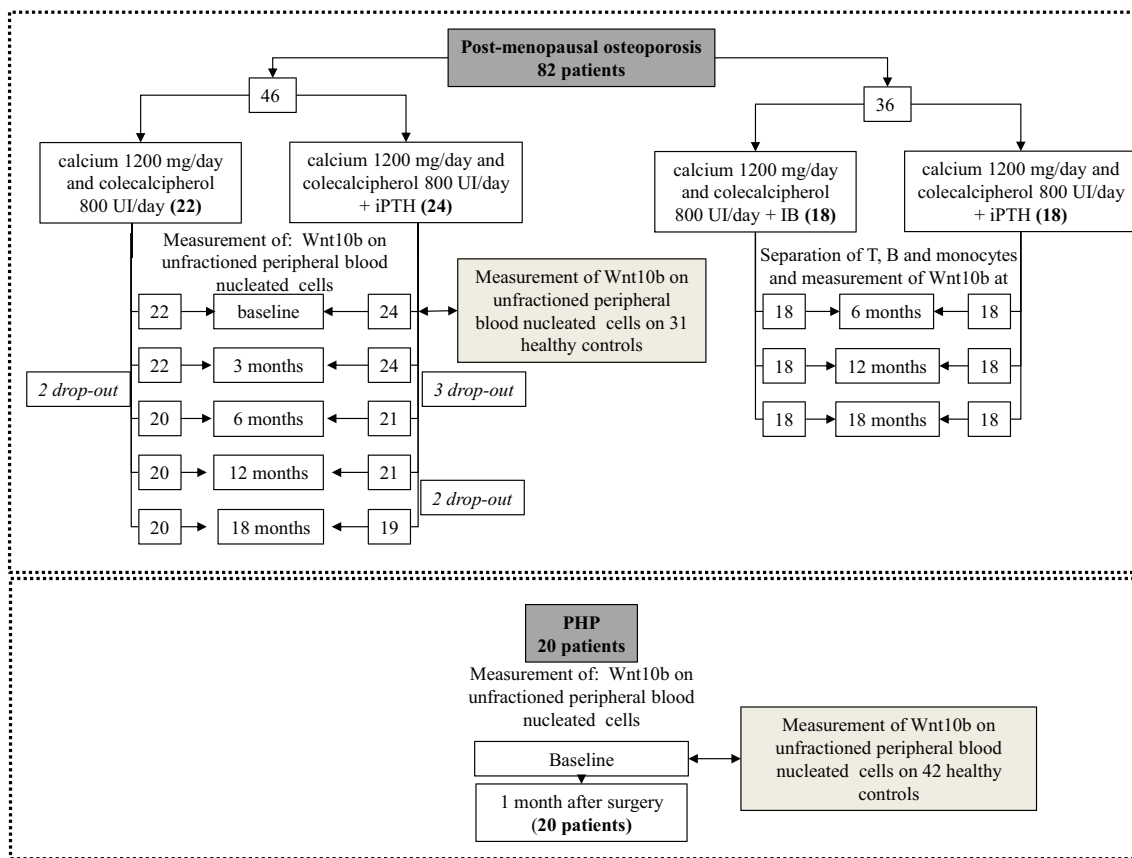


Fig. 1 The diagram shows the study design. The number of patients in each group and the experiments done in each visit are specified

Transcription Kit (Applied Biosystems). RT-PCR was performed with IQ SYBR Green Supermix (BIORAD). The housekeeping control gene was β -Actin and gene expression was quantified through $2^{-\Delta\Delta Ct}$ method. The primers used were the following:

5'- CCATGACATGGACTTTGGAGAG -3' (forward), 5'- CTGGAATCCAAGAAATCCCG -3' (reverse) for Wnt10b and 5'- CCTAAAAGCCACCCCACTTCT -3' (forward) and 5'- CACCTCCCCTGTGTGGACTT -3' (reverse) for β -Actin.

Table 1 The demographic characteristics of the study population

A. Characteristics of osteoporotic patients and healthy controls					
Treatment	Post-menopausal osteoporotic patients			Controls	<i>p</i> value
	iPTH	Calcium and vitamin D	IB	None	
Patients (<i>n</i>)	42	22	18	31	
Women (%)	100 %	100 %	100 %	100 %	
Men (%)	0 %	0 %	0 %	0 %	
Age (years)	68.1±9.5	66.6±6.2	64.7±9.2	69±15.2	0.263
Years since menopause	18.6±10	14.8±9.3	17.7±10	17.0±10.6	0.186
B. Characteristics of PHP patients and healthy controls					
	PHP patients			Controls	<i>p</i> value
Patients (<i>n</i>)	20			42	
Women (%)	80			70	0.366
Women in after menopause (%)	56			47	0.191
Men (%)	20			40	0.366
Age (years)	57.3±15.4			50.5±21.5	0.214
Years since menopause	16±9.4			20.5±14.7	0.400

Mean and standard deviations are shown for continuous variables, % for non-continuous one. *P* values were calculated by one-way ANOVA for continuous variable and by χ^2 for non-continuous one

Protein detection

Wnt10b protein was measured on cell lysates by ELISA technique (USCN Life Science) after correction for total amount of protein.

Statistical analyses

Wnt10b values were not normally distributed according to kurtosis normality test; hence, the effect of treatment on its expression was evaluated by repeated measure tests, after logarithmic transformation. Wnt10b mRNA levels were analysed by Mann-Whitney (healthy controls vs. osteoporotic or PHP) and Wilcoxon matched pairs signed-rank tests (PHP vs. PHP after surgery and different cell types).

The sample size provided an 80 % power, assuming a two-sided significance level of 0.05, to detect differences in Wnt10b of 3-fold, according with the results obtained in mice [18].

The statistical analyses were performed through SPSS 21.0 and graphs were designed through Prism Graph Pad 6.0.

Results

Osteoporosis does not affect Wnt10b production by blood nucleated cells

To evaluate whether Wnt10b expression was decreased in osteoporosis, we compared its expression in unfractionated blood nucleated cells from osteoporotic patients and healthy women, matched for age and post-menopausal period. Wnt10b was not significantly different between patients and controls (Fig. 2a), suggesting that it is not involved in the pathogenesis of post-menopausal osteoporosis.

iPTH increases Wnt10b production by T cells

Treatment with iPTH in osteoporotic women increases Wnt10b gene expression in peripheral blood nucleated cells, whereas calcium and vitamin D alone do not (Fig. 2b). In particular Wnt10b increases of approximately 21-fold after 6 months of treatment and returned to baseline values after 18 months (Fig. 2b).

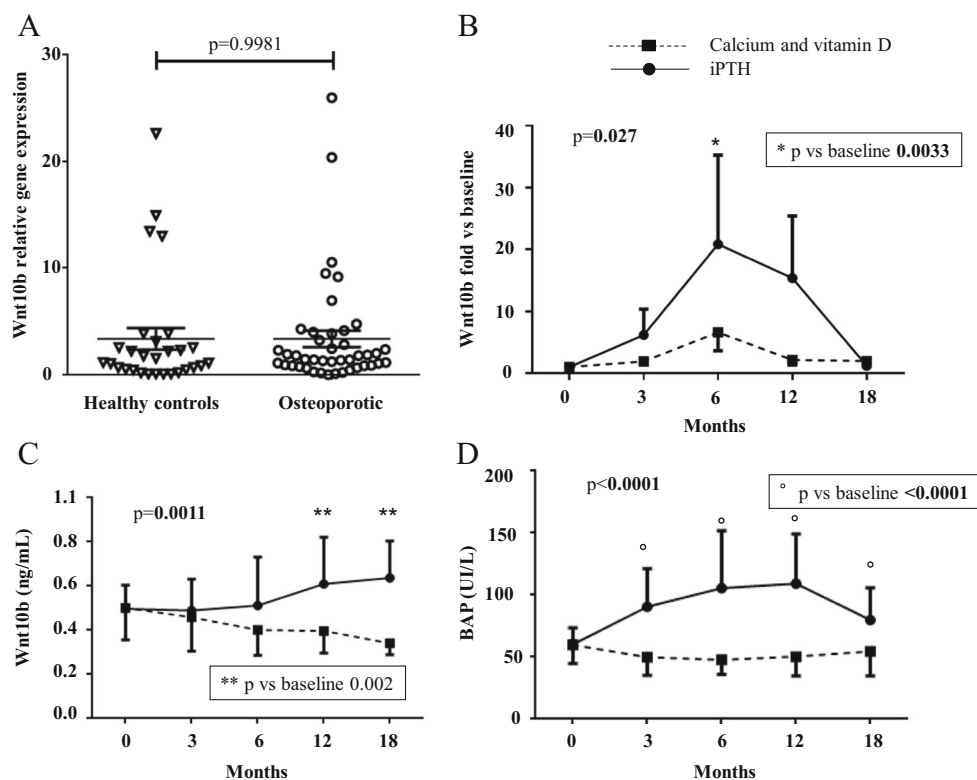


Fig. 2 Wnt 10b expression in osteoporosis and during treatment. **a** Levels (median mean \pm SE) of Wnt10b mRNA in healthy controls ($n=31$) and osteoporotic subjects ($n=46$). Data were analysed by Mann-Whitney as the data were not normally distributed according to the kurtosis normality test. **b** Wnt10b mRNA fold change versus baseline in osteoporotic patients treated with iPTH ($n=21$) or calcium and vitamin D ($n=20$). Data were analysed by multiple measurement test after logarithmic transformation, as the data were not normally

distributed according to the kurtosis normality test. **c** Wnt10b protein production by unfractionated blood nucleated cells in osteoporotic patients treated with iPTH ($n=21$) or calcium and vitamin D ($n=20$). Data were analysed by multiple measurement test after logarithmic transformation, as the data were not normally distributed according to the kurtosis normality test. **d** Serum BAP in osteoporotic patients treated with iPTH ($n=21$) or calcium and vitamin D ($n=20$). Data were analysed by multiple measurement test

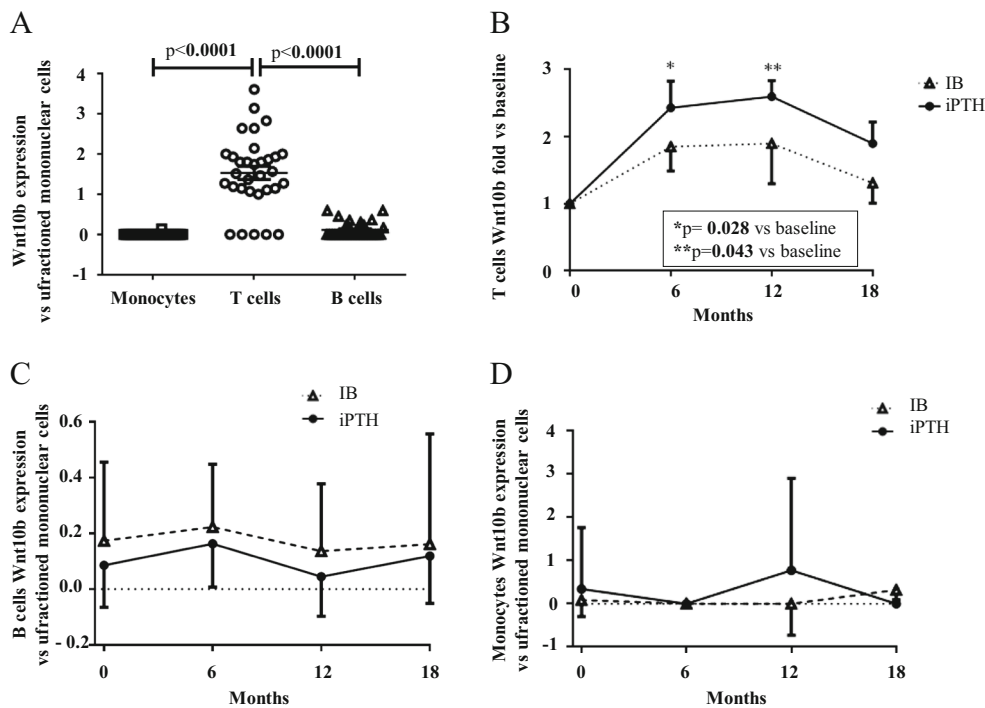


Fig. 3 Wnt 10b expression by T cells. **a** Wnt10b mRNA expression relative to unfractionated blood nucleated cells (median mean±SE) in monocytes, T and B cells from osteoporotic patients without treatment ($n=36$). Data were analysed by Wilcoxon matched pairs signed-rank test as the data were not normally distributed according to the kurtosis normality test. **b** T cells Wnt10b mRNA fold change versus baseline in osteoporotic patients treated with iPTH ($n=18$) or IB ($n=18$). Data were analysed by multiple measurement test after logarithmic transformation, as the data were not normally distributed according to the kurtosis normality test. **c** B cells Wnt10b mRNA fold change versus baseline in osteoporotic patients treated with iPTH ($n=18$) or IB ($n=18$). Data were analysed by multiple measurement test after logarithmic transformation, as the data were not normally distributed according to the kurtosis normality test. **d** Monocytes Wnt10b mRNA fold change versus baseline in osteoporotic patients treated with iPTH ($n=18$) or IB ($n=18$). Data were analysed by multiple measurement test after logarithmic transformation, as the data were not normally distributed according to the kurtosis normality test

normality test. **c** B cells Wnt10b mRNA fold change versus baseline in osteoporotic patients treated with iPTH ($n=18$) or IB ($n=18$). Data were analysed by multiple measurement test after logarithmic transformation, as the data were not normally distributed according to the kurtosis normality test. **d** Monocytes Wnt10b mRNA fold change versus baseline in osteoporotic patients treated with iPTH ($n=18$) or IB ($n=18$). Data were analysed by multiple measurement test after logarithmic transformation, as the data were not normally distributed according to the kurtosis normality test

Wnt10b protein level, detected by ELISA, confirmed an increase of Wnt10b production during treatment with iPTH (Fig. 2c), according to the RT-PCR results. The increase in Wnt10b mimics the observed rise in bone alkaline phosphatase (BAP, Fig. 2d) that is a well-known bone formation marker.

The analyses of separated T, B cells and monocytes as compared to unfractionated blood nucleated cells revealed that T cells are the main responsible for Wnt10b expression in osteoporotic patients without treatment, whereas B cells and monocytes only express a small amount of this molecule (Fig. 3a). Further evaluation of T cells during iPTH treatment compared to IB reveals that the increase of Wnt10b expression depend on iPTH; indeed, IB does not induce any significant variation (Fig. 3b). B cells and monocytes do not increase Wnt10b expression during treatment (Fig. 3c, d).

normal parathyroid function decreased Wnt10b expression of about 36 %.

Even though surgical intervention decreased Wnt10b, its expression remains not significantly different as respect to healthy controls (Fig. 4).

Chronic elevation of PTH did not increase Wnt10b expression

Wnt10b was not increased in unfractionated peripheral blood nucleated cells from patients affected by PHP compared to healthy controls (Fig. 4); nevertheless, surgical restoration of

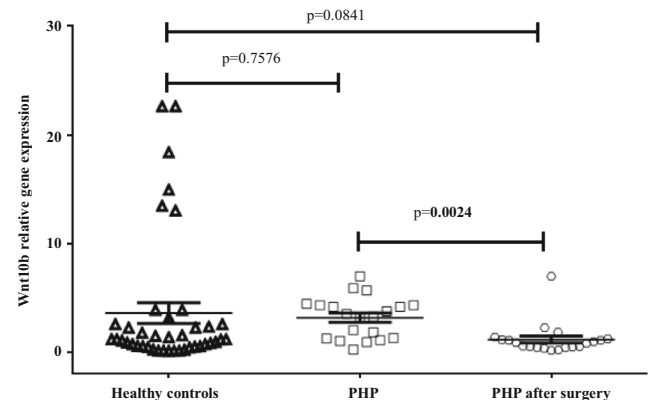


Fig. 4 Wnt 10b expression in PHP. Levels (median mean±SE) of Wnt10b mRNA in healthy controls ($n=42$) and PHP before ($n=20$) and after parathyroidectomy ($n=20$). Data were analysed by Mann-Whitney (healthy controls vs. PHP) and Wilcoxon matched pairs signed-rank tests (PHP vs. PHP after surgery) as the data were not normally distributed according to the kurtosis normality test

All the surgical intervention were completely successful as demonstrated by the fall in PTH level from 136 ± 26 to 68 ± 8 ng/mL, $p=0.008$.

Discussion

This study explores the effect of iPTH and PHP on Wnt10b production by T cells in humans, we show that T cells are the main producers of Wnt10b amongst peripheral blood nucleated cells, and Wnt10b expression increases during iPTH treatment. These data suggest that T cells may mediate the anabolic action of iPTH in humans as they do in mice [17, 18]. According to this hypothesis, literature data derived from animal models report that the anabolic activity of iPTH depends on T cells, which increase the expression of Wnt10b [17, 18]. Indeed, treatment with iPTH in mice stimulates T cell production of Wnt10b that increases osteoblastogenesis. T cell-deficient mice or mice with T cell-knock out for Wnt10b display a blunted bone anabolism after treatment with iPTH [17].

The analysis of Wnt10b expression in peripheral blood nucleated cells, at different time during iPTH treatment, allows us to create a Wnt10b curve that reveals an increase in its expression that is maximal 6 months after treatment. This increase was not observed in patients treated with calcium and vitamin D alone. The Wnt10b curve in response to iPTH mimics the well-known bone anabolic markers curve [3, 4], confirming Wnt10b role in mediating iPTH anabolic action.

Differently from iPTH, chronic elevation of PTH, as in PHP, does not increase Wnt10b expression. However, 1 month after surgical intervention, Wnt10b expression results significantly decreased, but comparable to healthy subjects. This result may depend on the small size of the cohort analysed, but we speculate a possible effect of chronic elevation in PTH on Wnt10b that is not sufficient to increase it above normal range. To support this hypothesis, literature data report that chronic elevation of PTH in PHP modulates Wnt signalling pathway also by suppressing SOST in humans [20, 21] as well as in mice [22].

This observation may explain the anabolic effect on trabecular bone of PHP; indeed, PHP preferentially involves cortical bone with preservation of cancellous areas, as demonstrated by histomorphometric analysis. In particular, the majority of patients with PHP showed reductions in cortical width, whereas the cancellous compartment of the bone biopsy specimen showed greater than average values for trabecular bone volume, trabecular number, connectivity and separation, indicating preservation of this bone compartment in most patients with PHP [23–26]. Here, we describe a decrease in Wnt10b, after surgical restoration of normal parathyroid function, which may partially explain the anabolic effect of PHP on trabecular bone.

Our study has a number of strengths: to our knowledge, this work represents the first study in humans to evaluate the effect of PTH on peripheral blood nucleated cells with particular regard to T cells. In addition, we attempted to do so without in vitro culture of the cells, which could substantially alter their gene expression and other characteristics. Patients and controls have been carefully matched for potential confounders and randomized to different treatment group. However, one major limitation of our work is the small sample size especially of PHP cohort.

In conclusion, this study reports that PTH induces an increase of Wnt10b production by T cells in humans. Thus, our data suggest that T cells amplify the anabolic effect of PTH on bone.

Acknowledgments This work was supported by an unconditioned grant from Nycomed SpA (ISAG02AP13) which also provides the PTH 1-84 and calcium and vitamin D supplements. IR was supported by a grant from Italian Ministry of Health: Ricerca Sanitaria Finalizzata e Giovani Ricercatori 2009 (GR 2009-1584485). We are grateful to Prof. G. Gasparri (University of Turin, Italy) for recruiting PHP patients.

Conflicts of interest None.

References

1. Silva BC, Costa AG, Cusano NE, Kousteni S, Bilezikian JP (2011) Catabolic and anabolic actions of parathyroid hormone on the skeleton. *J Endocrinol Invest* 34:801–810. doi:10.3275/7925
2. Chen P, Miller PD, Recker R, Resch H, Rana A, Pavo I, Sipos AA (2007) Increases in BMD correlate with improvements in bone microarchitecture with teriparatide treatment in postmenopausal women with osteoporosis. *J Bone Miner Res* 22:1173–1180
3. Neer RM, Amaud CD, Zanchetta JR et al (2001) Effect of parathyroid hormone (1-34) on fractures and bone mineral density in postmenopausal women with osteoporosis. *N Engl J Med* 344:1434–1441
4. Greenspan SL, Bone HG, Ettinger MP et al (2007) Effect of recombinant human parathyroid hormone (1-84) on vertebral fracture and bone mineral density in postmenopausal women with osteoporosis: a randomized trial. *Ann Intern Med* 146:326–339
5. Thomson M, McCarroll J, Bond J, Gordon-Thomson CD, Williams E, Moore GP (2003) Parathyroid hormone-related peptide modulates signal pathways in skin and hair follicle cells. *Exp Dermatol* 12:389–395
6. Gardella TJ, Vilaridaga JP (2015) International union of basic and clinical pharmacology. XCIII. The parathyroid hormone receptors-family B G protein-coupled receptors. *Pharmacol Rev* 67:310–337. doi:10.1124/pr.114.009464
7. Fiaschi-Taesch N, Sicari BM, Ubriani K, Bigatel T, Takane KK, Cozar-Castellano I, Bisello A, Law B, Stewart AF (2006) Cellular mechanism through which parathyroid hormone-related protein induces proliferation in arterial smooth muscle cells: definition of an arterial smooth muscle PTHrP/p27kip1 pathway. *Circ Res* 99:933–942
8. Fauchoux C, Horton MA, Price JS (2002) Nuclear localization of type I parathyroid hormone/parathyroid hormone-related protein receptors in deer antler osteoclasts: evidence for parathyroid hormone-related protein and receptor activator of NF-kappaB-dependent effects on osteoclast formation in regenerating mammalian bone. *J Bone Miner Res* 17:455–464


9. Saini V, Marengi DA, Barry KJ, Fulzele KS, Heiden E, Liu X, Dedic C, Maeda A, Lotinun S, Baron R, Pajevic PD (2013) Parathyroid hormone (PTH)/PTH-related peptide type 1 receptor (PPR) signaling in osteocytes regulates anabolic and catabolic skeletal responses to PTH. *J Biol Chem* 288:20122–20134. doi:10.1074/jbc.M112.441360
10. Leupin O, Kramer I, Collette NM, Loots GG, Natt F, Kneissel M, Keller H (2007) Control of the SOST bone enhancer by PTH using MEF2 transcription factors. *J Bone Miner Res* 22:1957–1967
11. Kramer I, Baertschi S, Halleux C, Keller H, Kneissel M (2012) Mef2c deletion in osteocytes results in increased bone mass. *J Bone Miner Res* 27:360–373. doi:10.1002/jbmr.1492
12. Genetos DC, Toupadakis CA, Raheja LF, Wong A, Papanicolaou SE, Fyhrie DP, Loots GG, Yellowley CE (2010) Hypoxia decreases sclerostin expression and increases Wnt signaling in osteoblasts. *J Cell Biochem* 110:457–467. doi:10.1002/jcb.22559
13. Collette NM, Genetos DC, Economides AN, Xie L, Shahnazari M, Yao W, Lane NE, Harland RM, Loots GG (2012) Targeted deletion of Sost distal enhancer increases bone formation and bone mass. *Proc Natl Acad Sci U S A* 109:14092–14097. doi:10.1073/pnas.1207188109
14. Drake MT, Srinivasan B, Mödder UI, Peterson JM, McCready LK, Riggs BL, Dwyer D, Stolina M, Kostenuik P, Khosla S (2010) Effects of parathyroid hormone treatment on circulating sclerostin levels in postmenopausal women. *J Clin Endocrinol Metab* 95:5056–5062. doi:10.1210/jc.2010-072
15. Piemonte S, Romagnoli E, Bratengeier C, Woloszczuk W, Tancredi A, Pepe J, Cipriani C, Minisola S (2012) Serum sclerostin levels decline in post-menopausal women with osteoporosis following treatment with intermittent parathyroid hormone. *J Endocrinol Investig* 35:866–868. doi:10.3275/8522
16. Manolagas SC (2014) Wnt signaling and osteoporosis. *Maturitas* 78:233–237. doi:10.1016/j.maturitas.2014.04.013
17. Bedi B, Li JY, Tawfeek H, Baek KH, Adams J, Vangara SS, Chang MK, Kneissel M, Weitzmann MN, Pacifici R (2012) Silencing of parathyroid hormone (PTH) receptor 1 in T cells blunts the bone anabolic activity of PTH. *Proc Natl Acad Sci U S A* 109:E725–E733. doi:10.1073/pnas.1120735109
18. Terauchi M, Li JY, Bedi B, Baek KH, Tawfeek H, Galley S, Gilbert L, Nanes MS, Zayzafoon M, Guldborg R, Lamar DL, Singer MA, Lane TF, Kronenberg HM, Weitzmann MN, Pacifici R (2009) T lymphocytes amplify the anabolic activity of parathyroid hormone through Wnt10b signaling. *Cell Metab* 10:229–240. doi:10.1016/j.cmet.2009.07.010
19. Li JY, Walker LD, Tyagi AM, Adams J, Weitzmann MN, Pacifici R (2014) The sclerostin-independent bone anabolic activity of intermittent PTH treatment is mediated by T-cell-produced Wnt10b. *J Bone Miner Res* 29:43–54. doi:10.1002/jbmr.2044
20. Viapiana O, Fracassi E, Troplini S, Idolazzi L, Rossini M, Adami S, Gatti D (2013) Sclerostin and DKK1 in primary hyperparathyroidism. *Calcif Tissue Int* 92:324–329. doi:10.1007/s00223-012-9665-7
21. Ardawi MS, Al-Sibiany AM, Bakhsh TM, Rouzi AA, Qari MH (2012) Decreased serum sclerostin levels in patients with primary hyperparathyroidism: a cross-sectional and a longitudinal study. *Osteoporos Int* 23:1789–1797. doi:10.1007/s00198-011-1806-8
22. Bellido T, Ali AA, Gubrij I, Plotkin LI, Fu Q, O'Brien CA, Manolagas SC, Jilka R (2005) Chronic elevation of parathyroid hormone in mice reduces expression of sclerostin by osteocytes: a novel mechanism for hormonal control of osteoblastogenesis. *Endocrinology* 146:4577–4583
23. Parisien M, Mellish RW, Silverberg SJ, Shane E, Lindsay R, Bilezikian JP, Dempster DW (1992) Maintenance of cancellous bone connectivity in primary hyperparathyroidism: trabecular strut analysis. *J Bone Miner Res* 7:913–919
24. Parisien M, Silverberg SJ, Shane E, de la Cruz L, Lindsay R, Bilezikian JP, Dempster DW (1990) The histomorphometry of bone in primary hyperparathyroidism: preservation of cancellous bone structure. *J Clin Endocrinol Metab* 70:930–938
25. Parisien M, Cosman F, Mellish RW et al (1995) Bone structure in postmenopausal hyperparathyroid, osteoporotic, and normal women. *J Bone Miner Res* 10:1393–1399
26. Uchiyama T, Tanizawa T, Ito A, Endo N, Takahashi HE (1999) Microstructure of the trabecula and cortex of iliac bone in primary hyperparathyroidism patients determined using histomorphometry and node-strut analysis. *J Bone Miner Metab* 17:283–288

CASE REPORT

Open Access



Ruxolitinib in steroid refractory graft-vs.-host disease: a case report

Enrico Maffini^{1,2*} , Luisa Giaccone^{1,2}, Moreno Festuccia^{1,2}, Lucia Brunello^{1,2}, Ilaria Buondonno³, Dario Ferrero^{1,2}, Mario Boccadoro², Chiara Dellacasa¹, Alessandro Busca¹, Domenico Novero⁴ and Benedetto Bruno^{1,2}

Abstract

Background: Allogeneic hematopoietic stem cell transplantation (HSCT) is potentially curative in a variety of hematological malignancies. Graft-vs.-host disease (GvHD) remains a life-threatening complication. Standard treatment is high-dose (HD) corticosteroids. Steroid-refractory (SR) GvHD is associated with poor prognosis. At present, second-line treatment is ill-defined and includes a number of agents. Novel insights into the pathophysiology of acute GvHD (aGvHD) highlight the relevant role of the host inflammatory response governed by several kinase families, including Janus kinases (JAK) 1/2. Ruxolitinib, a JAK1/2 inhibitor approved for intermediate-2/high-risk myelofibrosis, was recently employed in SR-GvHD with encouraging overall response rates. Clinical experience however remains limited.

Case presentation: A 51-year-old male with refractory anemia with excess blast type-2 underwent a myeloablative allogeneic HSCT from a 9/10 HLA-matched unrelated donor after conditioning with busulfan and cyclophosphamide. GvHD prophylaxis consisted of cyclosporine, methotrexate, and thymoglobulin. CD34⁺ cells/kg infused were 8.69 × 10⁶ kg. On day 29, the patient developed overall grade IV aGvHD with biopsy proven stage IV gastrointestinal (GI) GvHD refractory to HD corticosteroids. Patient conditions rapidly deteriorated and became critical despite the addition of mycophenolate mofetil and budesonide. On day 33, Ruxolitinib was started, and on day 39 the patient clinical conditions gradually improved. Complete resolution of aGvHD was also confirmed by histology on day 54.

Conclusions: At 5 months from HSCT, the patient is well and in continuous hematological complete remission without flare of GvHD. Ruxolitinib was discontinued on day 156. Ruxolitinib is feasible and effective in SR-aGvHD though large prospective clinical trials are warranted.

Keywords: Allogeneic hematopoietic stem cell transplant (HSCT), Steroid-refractory graft-vs.-host disease (SR-GvHD), Ruxolitinib, Regulatory T cells (Treg), Proinflammatory cytokines, Case report

Background

Allogeneic hematopoietic stem cell transplantation (HSCT) is potentially curative for several hematopoietic malignancies. Acute graft-vs.-host disease (aGvHD) remains the major cause of morbidity and mortality. High-dose corticosteroids (methylprednisolone, 1–2 mg/kg per day) are currently considered standard first-line treatment. However, a remarkable number of patients do not respond [1]. Estimated incidence of steroid-refractory aGvHD (SR-GvHD) is some 40 %, and it is associated with poor

long-term survival of 5–30 % [2–4]. At present, there are no well-defined treatment approaches although several second-line therapies aimed at inactivating alloreactive donor T cells, pro-inflammatory cytokines or their receptors have been investigated. The weighted average 6-month survival from 25 retrospective studies or phase II trials was 49 % [2]. Among others, agents used included anti-thymocyte globulin, mycophenolate mofetil, anti-CD25 monoclonal antibody (basiliximab), anti-tumor necrosis factor alpha (infliximab and etanercept), anti-interleukin 2 receptor-alpha (inolimomab), anti-CD52 (alemtuzumab), pentostatin, m-Tor inhibitors and extracorporeal photoapheresis [5–13]. Since clinical trials in SR-GvHD are difficult to design given the heterogeneity of treatment policies, direct comparisons of different agents have not been possible.

* Correspondence: shostakowitsch@libero.it

¹Department of Oncology, SSCVD Trapianto di Cellule Staminali, A.O.U. Città della Salute e della Scienza di Torino, Torino, Italy

²Department of Molecular Biotechnology and Health Sciences, University of Torino, Torino, Italy

Full list of author information is available at the end of the article



Case presentation

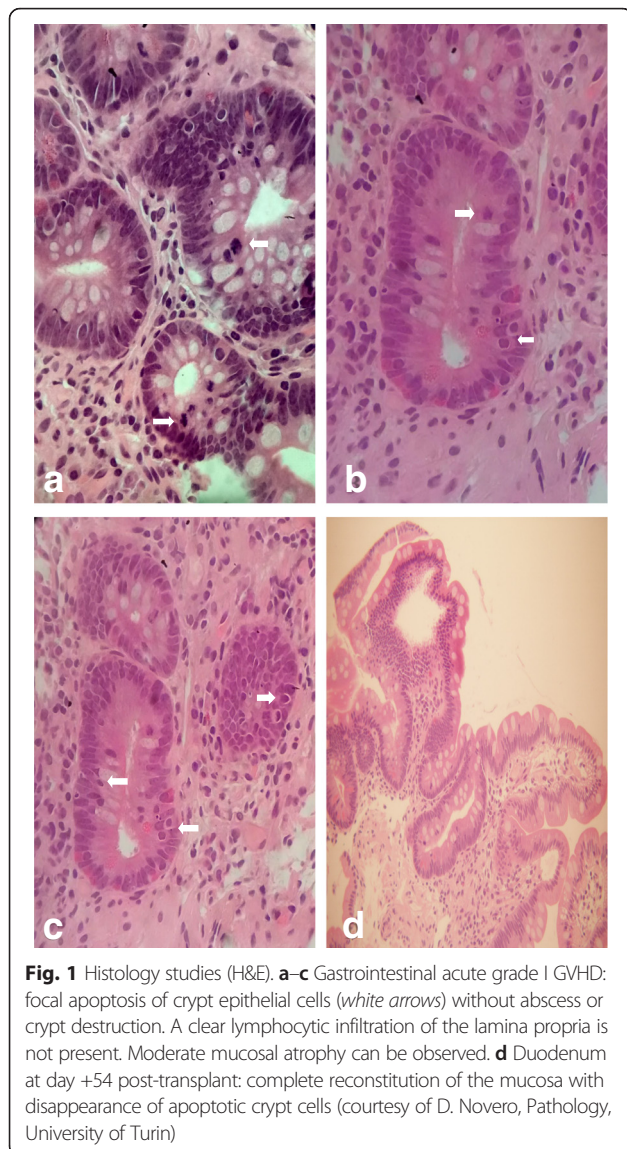
A 51-year-old male without significant comorbidities and irrelevant past medical history was diagnosed with refractory anemia with excess blast type-1 (RAEB-1) in 2013 and evolved to RAEB-2 after 24 months. Overall, the patient had a high risk score both by the International (IPSS) and by the WHO prognostic scoring systems (WPSS). Blast count was 15 % on bone marrow biopsy and 11 % on marrow aspirate. Other features included trisomy 8 by cytogenetic analysis and two cytopenias—neutropenia and thrombocytopenia—in the peripheral blood. He never required red blood cell or platelet transfusions. He was initially treated with 2 cycles of induction chemotherapy with fludarabine (30 mg/m², days 1–5), high-dose cytarabine (2000 mg/m², days 1–5), and idarubicin (10 mg/m², days 1–3). Complete remission by histology and by flow cytometry was obtained. However, FISH analysis showed persistent trisomy 8. The patient underwent an allogeneic HSCT with mobilized peripheral blood stem cells from a 9/10 HLA-matched (antigenic mismatch at HLA-A) unrelated donor. Conditioning regimen was busulfan (3.2 mg/kg/day; days –7 to –4) and cyclophosphamide (60 mg/kg/day; days –3 and –2). GvHD prophylaxis consisted of cyclosporine (CsA) (1.5 mg/kg twice daily, from day –1), methotrexate (15 mg/m², 24 h after transplant, then 10 mg/m² on days 3, 6, and 11), and thymoglobulin (2.5 mg/kg on days –3 and –2). CD34⁺ cells/kg infused were 8.69 × 10⁶. Gut decontamination with antibiotics after HSCT was not scheduled. On day 13, the patient stopped oral intake because of grade III mucositis. On day 22, he developed a maculo-papular rash on 50 % of his body surface area (stage 2) and mild (500 ml/24 h) watery diarrhea (stage 1), without fever and/or liver function tests abnormalities suggestive of aGVHD. Stool cultures ruled out gastrointestinal (GI) bacterial, viral or parasitic infections. A chest X-ray ruled out pulmonary infiltrates. Diagnosis of overall grade II aGVHD was made and intravenous (i.v.) corticosteroids at 2 mg/kg/day were promptly started on the same day. However, diarrhea worsened rapidly over the following days to stage 4 GI aGVHD with over 2500 mL/24 h of diarrhea and increasing painful abdominal cramps (Table 1). Clinical conditions did not improve despite the combination of cyclosporine, high-dose steroids and the addition of oral budesonide (3 mg three times per day) on day 28 and i.v. mycophenolate mofetil (MMF) (1 g three times per day) on day 29. An endoscopic evaluation of the upper GI tract with multiple biopsies on day 33 confirmed the diagnosis of aGVHD (Fig. 1a–c). Patient's clinical conditions rapidly deteriorated. Oral Ruxolitinib was started at 5 mg twice per day on day 33. Stools volume progressively and steadily decreased to less than 1000 mL on day 39. MMF was stopped on the same day given its unlikely clinical efficacy and to reduce immunosuppression.

Table 1 Patient timeline clinical history

Days from HSCT	Clinical condition/therapeutic intervention
0	HSCT
17	Neutrophil recovery
19	Platelet recovery
22	aGVHD onset: diarrhea (st.I) and skin (st.II). Started PDN-equivalent 2 mg/kg/iv
28	Diarrhea exceeded 1500 mL/day (st.III) and started budesonide 3 mg tid po
29	Diarrhea exceeded 2000 mL/day (st.IV) and started MMF 1 g tid iv
33	EGDS with biopsies (GvHD confirmation). Started Ruxolitinib 5 mg bid
36	Steroid taper
39	Diarrhea below 1000 mL and Ruxolitinib 5 + 10 mg/day. Stop MMF
45	Resumed oral food intake
49	Switch to oral CsA
54	EGDS with biopsies: no signs of GvHD
61	Switch PDN po
66	Reduced Ruxolitinib to 5 mg bid
70	Patient discharged
100	Reduced Ruxolitinib to 5 mg/day
135	Steroid stopped
156	Ruxolitinib stopped

abbreviations: HSCT hematopoietic stem cell transplantation, aGVHD acute graft-vs.-host disease, PDN prednisone, iv intravenously, po orally, MMF mycophenolic acid, EGDS esophagous-gastro-duodenoscopy, CsA cyclosporine A, bid twice daily, tid three times a day, st stage

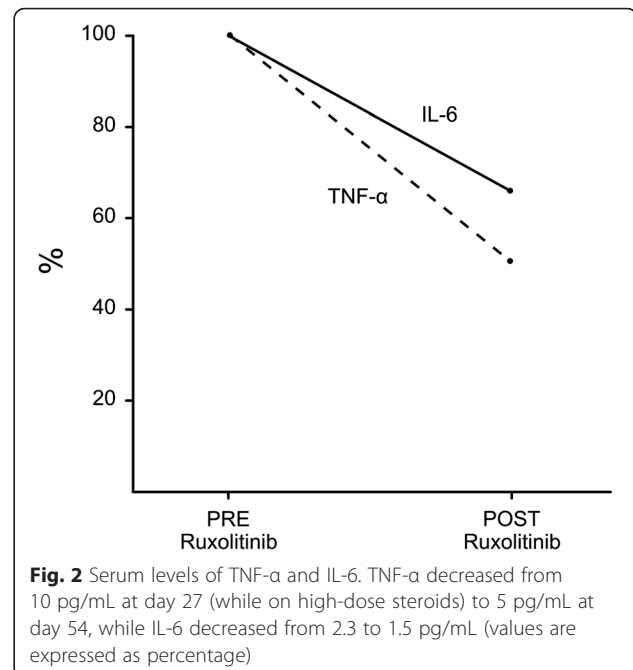
Clinical conditions gradually improved. Neutrophil and platelet engraftment (defined as the first of 3 consecutive days of neutrophils ≥500/uL and as the first of 7 consecutive days with platelet counts ≥20,000/uL without transfusion support, respectively) occurred at days 17 and 19. Platelet counts were ≥300,000/uL on day 28 and then dropped below 100,000/uL on day 49 and remained stable around 40,000–50,000/uL until discharge (with concurrent oral Ruxolitinib at 5 mg twice daily). Hemoglobin values peaked at 136 g/L on day 31 and dropped below 100 g/L on day 35. Overall, 4 units of red blood cells were required during hospitalization. Skin lesions disappeared completely by day 50. On day 45, the patient resumed oral food intake without nausea and/or vomiting and by day 61 stools were formed. A second endoscopy with multiple biopsies on day 54 revealed no residual signs of aGVHD in the GI tract (Fig. 1d). Bone marrow biopsy on day 64 showed a hypocellular marrow with normal myeloid maturation without evidence of disease recurrence and full donor engraftment by mixed-chimerism analysis. On day 70, the patient was discharged. Ruxolitinib was initially reduced because of progressive pancytopenia to 5 mg per day on day 100 and to 5 mg every other day on day 107. It was



resumed at 5 mg per day on day 113 because of soft stools and abdominal discomfort with prompt improvement of GI symptoms. Platelet counts progressively raised to $\geq 80,000/\mu\text{L}$.

Cytokine measurement

Serum levels of tumor necrosis factor alpha (TNF- α) and interleukin-6 (IL-6) were measured in serum samples from day +27 (before the start of Ruxolitinib) and day +56 (after 23 days of treatment), by Becton Dickinson Biosciences Human Inflammatory Cytokine kit. Interestingly, we observed a decrease of both these pro-inflammatory markers during Ruxolitinib treatment (Fig. 2). We cannot, however, rule out a potential effect of glucocorticoids and mycophenolic acid [14, 15].



Conclusions

Donor T cell immune response to recipient antigens represents a key mechanism of GvHD and is combined with a massive production of inflammatory cytokines such as TNF- α , IL-1, IL-6 and IL-2-R. Cytokine-induced activation of the various effector cells—including T cells, dendritic cells, and neutrophils—is mediated by the interplay between cytokine receptors and a number of specialized kinases [16]. Family members of Janus kinases (JAK) are among the most studied. Ruxolitinib is a selective oral JAK1/2 inhibitor approved for the treatment of patients with intermediate-2 or high-risk primary myelofibrosis [17, 18]. Spleen size reduction and improvement of constitutional symptoms are directly correlated with inhibition of JAK-STAT signal transducer hyperactivity and with reduction of both effector cells activity and pro-inflammatory cytokine signature [19]. Apart from its ability to depress the pro-inflammatory environment of GvHD, Ruxolitinib shapes T cell mediated immune response toward a FoxP3⁺ regulatory T cell (Treg) polarization mostly by a sparing mechanism of the JAK3-STAT5 pathway [18]. Tregs improve signs and symptoms of aGvHD and promote immunotolerance [19–23]. These mechanisms have been shown on murine models [14] and also form the rationale for the potential efficacy of Ruxolitinib in the treatment of GvHD in man.

Only a few clinical experiences have been reported so far. Spoerl et al. [24] explored JAK1/2 inhibition during aGvHD both in a major HLA-mismatched murine model and in a cohort of 6 HSCT recipients who developed

SR-aGvHD (GI in 2 and skin in 4). In the murine model, Ruxolitinib was associated with a significantly prolonged survival with reduced weight loss and GvHD severity by histology studies and suppression of the serum inflammatory cytokine profile. Moreover, a reduction of donor alloreactive T cells with a concomitant expansion of CD4⁺ FoxP3⁺ Treg in GvHD target organs demonstrated the ability of Ruxolitinib to shift T cell phenotype. In HSCT recipients, response rates were optimal with clinical regression in all and a marked reduction of pro-inflammatory cytokines such as IL-6 and soluble IL-2 receptor. Ruxolitinib was employed at a starting dose of 5 mg twice per day daily with a dose increase to 10 mg twice per day. Neither thrombocytopenia nor anemia were reported. A recent retrospective multi-center survey on 95 HSCT recipients with SR-GVHD—54 acute and 51 chronic GvHD (cGvHD), reported the most significant clinical experience so far completed [25]. Median prior lines of treatment were three (range: 1–7 for aGvHD; 1–10 for cGvHD). Overall response rate was 81.5 % in the aGvHD group (44/54) with 57 % (25/44) complete remissions and of 85.4 % (35/41) in the cGvHD group, respectively. Overall survival was 79 and 97.4 %. Among responders, GvHD flare was 6.8 % for aGvHD and 5.7 % for cGvHD patients. Side effects such as cytopenia (55.6 and 17.1 % in the aGvHD and cGvHD group, respectively) and cytomegalovirus (CMV) reactivation (33.3 and 14.6 %) were comparable to those reported with other agents including steroids, infliximab, alemtuzumab, mycophenolate mofetil, or cyclosporine. Overall, one of the concerns was the loss of a graft-vs.-leukemia effect, given the pharmacological interference with the JAK1/2 signal pathway; however, the reported rate of disease recurrence after Ruxolitinib was of 9.3 and 2.4 % of the patients in the aGvHD and cGvHD groups, respectively. Initial signs of improvement (partial response) of GVHD symptoms were observed 6 days from the start of Ruxolitinib and complete resolution after 3 weeks of treatment. These findings are similar to those reported by Zeiser et al. (median time to response 1.5 weeks, range 1–11). A possible synergistic role with budesonide and MMF cannot be completely ruled out even though these agents were administered only for a very few days. The most effective Ruxolitinib tapering schedule remains to be defined, given the limited clinical experience. Our schedule was purely based on clinical grounds in the light of GvHD signs/symptoms, worsening of cytopenias, or viral reactivation. A steroid-sparing effect in chronic GvHD has also recently been proposed [26] with encouraging results. A similar role in aGvHD has not yet been reported. Ruxolitinib dose-dependent cytopenias are usually expected during treatment [27] even though, in our patient, other factors such as GvHD itself and prolonged immunosuppressive therapy with several agents may have been

involved [28]. At 5 months from HSCT, the patient is doing well, with full donor mixed chimerism and in continuous complete remission (confirmed at bone marrow biopsy on day 148) with no signs and/or symptoms of GvHD on CsA taper. Prednisone was stopped on day 135 and Ruxolitinib on day 156. Of note, there was no CMV (though both donor and recipient were CMV seronegative)- nor Epstein Barr Virus-DNAemia breakthrough. Overall, our clinical findings suggest that Ruxolitinib played a fundamental role in the successful GvHD treatment of our patient. SR-GvHD is a challenging complication with no current standard treatment. GI tract involvement is life-threatening also in the light of the long process required for a complete repair of the intestinal mucosa. Therapeutic efficacy of Ruxolitinib is underlined by recent biological insights into the relevant role played by the JAK-STAT signaling pathway in aGvHD. However, treatment duration and possible impacts on graft-vs.-leukemia and immune-responses against infections remain a matter of debate. Thus, larger clinical phase II–III controlled trials and comparisons with best available treatments are warranted. A German multi-center phase II clinical trial on Ruxolitinib in SR-aGvHD is due to start accrual this fall (NCT02396628).

Abbreviations

aGvHD, acute graft-vs.-host disease; cGvHD, chronic GvHD; CMV, cytomegalovirus; GI, gastrointestinal; HSCT, hematopoietic stem cell transplantation; i.v., intravenous; JAK, Janus kinases; MMF, mycophenolate mofetil; RAEB-1, refractory anemia with excess blast type-1; SR-GvHD, steroid-refractory graft-vs.-host disease; Treg, regulatory T cells

Acknowledgements

Not applicable.

Funding

This work was supported by Progetti di Ricerca Finalizzata 2008, Progetto di Ricerca Sanitaria Finalizzata 2009, Fondi di Ricerca Locale, Università degli Studi di Torino, Torino, Italy, and by Fondazione Neoplasie del sangue (FO.NE.SA.), Torino, Italy.

Availability of data and materials

The authors did not use any database, software, or tools for the writing of this manuscript.

Authors' contributions

EM collected the patient's data and drafted the manuscript along with LG, MF, LB, DF, MB, CD and AB. BB revised the manuscript. DN provided the histological images. IB did the cytokine analysis. All authors read and approved the final manuscript.

Competing interests

The authors declare that they have no competing interests.

Consent for publication

The authors obtained informed consent from the patient to publish information on his disease and clinical course.

Ethics approval and consent to participate

Ethical approval is not appropriate. The authors obtained patient's consent to participate.

Author details

¹Department of Oncology, SSCVD Trapianto di Cellule Staminali, A.O.U. Città della Salute e della Scienza di Torino, Torino, Italy. ²Department of Molecular Biotechnology and Health Sciences, University of Torino, Torino, Italy. ³Department of Oncology, University of Torino, Torino, Italy. ⁴Department of Pathology, AOU Città della Salute e della Scienza di Torino, University of Torino, Torino, Italy.

Received: 7 June 2016 Accepted: 3 August 2016

Published online: 08 August 2016

References

- Deeg J. How I, treat refractory acute GVHD. *Blood*. 2007;109(10):4119–26.
- Martin PJ, Rizzo JD, Wingard JR, Ballen K, Curtin PT, Cutler C, Litzow MR, Nieto Y, Savani BN, Schriber JR, Shaughnessy PJ, Wall DA, Carpenter PA. First- and second-line systemic treatment of acute graft-versus-host disease: recommendations of the American Society of Blood and Marrow Transplantation. *Biol Blood Marrow Transplant*. 2012;18(8):1150–63.
- Xhaard A, Rocha V, Bueno B, et al. Steroid refractory acute GVHD: lack of long-term improved survival using new generation anti cytokine treatment. *Biol Blood Marrow Transplant*. 2012;18(3):406–13.
- Robin M, Porcher R, de Castro R, et al. Initial liver involvement in acute GVHD is predictive for non relapse mortality. *Transplantation*. 2009;88:1131–6.
- Inagaki J, Kodama Y, Fukano R, Noguchi M, Okamura J. Mycophenolate mofetil for treatment of steroid-refractory acute graft-versus-host disease after pediatric hematopoietic stem cell transplantation. *Pediatr Transplant*. 2015;19(6):652–8.
- Nadeau M, Perreault S, Seropian S, Foss F, Isufi I, Cooper DL. The use of basiliximab-infliximab combination for the treatment of severe gastrointestinal acute GvHD. *Bone Marrow Transplant*. 2016;51(2):273–6.
- Van Groningen LF, Liefkerink AM, de Haan AF, Schaap NP, Donnelly JP, Blijlevens NM, van der Velden WJ. Combination therapy with inolimomab and etanercept for severe steroid-refractory acute graft-versus-host disease. *Biol Blood Marrow Transplant*. 2016;22(1):179–82.
- Park JH, Lee HJ, Kim SR, Song GW, Lee SK, Park SY, Kim KC, Hwang SH, Park JS. Etanercept for steroid-refractory acute graft versus host disease following allogeneic hematopoietic stem cell transplantation. *Korean J Intern Med*. 2014;29(5):630–6.
- Meunier M, Bulabois CE, Thiebaut-Bertrand A, Itzykson R, Carre M, Carras S, Garban F, Cahn JY. Alemtuzumab for severe steroid-refractory gastrointestinal acute graft-versus-host disease. *Biol Blood Marrow Transplant*. 2014;20(9):1451–4.
- Abu-Dalle I, Reljic T, Nishihori T, Antar A, Bazarbachi A, Djulbegovic B, Kumar A, Kharfan-Dabaja MA. Extracorporeal photopheresis in steroid-refractory acute or chronic graft-versus-host disease: results of a systematic review of prospective studies. *Biol Blood Marrow Transplant*. 2014;20(11):1677–86.
- Alam N, Atenafu EG, Tse G, Viswabandya A, Gupta V, Kim D, Lipton JH, Messner HA, Kuruvilla J. Limited benefit of pentostatin salvage therapy for steroid-refractory grade III-IV acute graft-versus host disease. *Clin Transplant*. 2013;27(6):930–7.
- Hoda D, Pidala J, Salgado-Vila N, Kim J, Perkins J, Bookout R, et al. Sirolimus for treatment of steroid-refractory acute graft-versus-host disease. *Bone Marrow Transplant*. 2010;45:1347–51.
- Ghez D, Rubio MT, Maillard N, Suarez F, Chandesris MO, Delarue R, et al. Rapamycin for refractory acute graft-versus-host disease. *Transplantation*. 2009;88:1081–7.
- Brattsand R, Linden M. Cytokine modulation by glucocorticoids: mechanisms and actions in cellular studies. *Aliment Pharmacol Ther*. 1996;10(2):81–90.
- Baer PC, Wegner B, Geiger H. Effects of mycophenolic acid on IL-6 expression of human renal proximal and distal tubular cells *in vitro*. *Nephro Dial Transpl*. 2004;19:47–52.
- Teshima T, Reddy P, Zeiser R. Acute graft-versus-host disease. *Biol Blood Marrow Transpl*. 2016;22:11–6.
- Harrison C, Kiladjian JJ, Al-Ali HK, Gisslinger H, Waltzman R, Stalbovskaia V, McQuitty M, Hunter DS, Levy R, Knoops L, Cervantes F, Vannucchi AM, Barbui T, Barosi G. JAK inhibition with ruxolitinib versus best available therapy for myelofibrosis. *N Engl J Med*. 2012;366:779–87.
- Verstovsek S, Mesa RA, Gotlib J, Levy RS, Gupta V, Di Persio JF, Catalano J, Deininger M, Miller C, Silver RT, Talpaz M, Winton EF, Harvey Jr JH, Arasoy MO, Hexner E, Lyons RM, Paquette R, Raza A, Vaddi K, Erickson-Vitanen S, Koumenis IL, Sun W, Sandor V, Kantarjian HM. A double-blind, placebo-controlled trial of ruxolitinib for myelofibrosis. *N Engl J Med*. 2012;366(9):799–807.
- Hasselbach C. Chronic inflammation as a promotor of mutagenesis in essential thrombocythemia, polycythemia vera and myelofibrosis. A human inflammation model for cancer development? *Leuk Res*. 2013;2:214–20.
- Teshima T. JAK inhibitors: a home run for GVHD patients? *Blood*. 2014; 123(24):3691–3.
- Zeiser R, Negrin RS. Interleukin-2 receptor downstream events in regulatory T cells: implications for the choice of immunosuppressive drug therapy. *Cell Cycle*. 2008;7(4):458–62.
- Koreth J, Matsuoka K, Kim HT, McDonough SM, Bindra B, Alyea 3rd EP, Armand P, Cutler C, Ho VT, Treister NS, Bienfang DC, Prasad S, Tzachanis D, Joyce RM, Avigan DE, Antin JH, Ritz J, Soiffer RJ. Interleukin-2 and regulatory T cells in graft-versus-host disease. *N Engl J Med*. 2011;365(22):2055–66.
- Zeiser R, Leveson-Gower DB, Zambricki EA, Kambham N, Beilhack A, Loh J, Hou JZ, Negrin RS. Differential impact of mammalian target of rapamycin inhibition on CD4+ CD25+ FoxP3+ regulatory T cells compared with conventional CD4+ T cells. *Blood*. 2008;111(1):453–62.
- Spoerl S, Mathew NR, Bscheider M, Schmitt-Graeff A, Chen S, Mueller T, Verbeek M, Fischer J, Otten V, Schmickl M, Maas-Bauer K, Finke J, Peschel C, Duyster J, Poeck H, Zeiser R, von Bubnoff N. Activity of therapeutic JAK 1/2 blockade in graft-versus-host disease. *Blood*. 2014;123(24):3832–42.
- Zeiser R, Burchert A, Lengerke C, Verbeek M, Maas-Bauer K, Metzelder SK, Spoerl S, Ditschkowski M, Ecsedi M, Sockel K, Ayuk F, Ajib S, de Fontbrune FS, Na IK, Pentler L, Holtick U, Wolf D, Schuler E, Meyer E, Apostolova P, Bertz H, Marks R, Lübbert M, Wäsch R, Scheid C, Stölzel F, Ordemann R, Bug G, Kobbe G, Negrin R, Brune M, Spyridonidis A, Schmitt-Gräff A, van der Velden W, Huls G, Mielke S, Grigoleit GU, Kuball J, Flynn R, Ihorst G, Du J, Blazar BR, Arnold R, Kröger N, Passweg J, Halter J, Socié G, Beelen D, Peschel C, Neubauer A, Finke J, Duyster J, von Bubnoff N. Ruxolitinib in corticosteroidrefractory graft-versus-host disease after allogeneic stem cell transplantation: a multi-center survey. *Leukemia*. 2015;29(10):2062–8.
- Khoury HJ, Kota V, Arellano M et al. Ruxolitinib as sparing agent for steroid-dependent chronic graft-versus-host disease (cGVHD). Presented at: 2016 ASH Annual Meeting; December 5–8, 2015. Orlando, Florida; Abstract 1938.
- Vertovsek S, Gotlib J, Gupta V, Atallah E, Mascarehas J, Quintas-Cardama A, Sun W, Sarlis NJ, Sandor V, Levy RS, Kantarjian HM, Mesa RA. Management of cytopenias in patients with myelofibrosis treated with ruxolitinib and effect of dose modifications on efficacy outcomes. *Onco Targets Ther*. 2013;7:13–21.
- Bruno B, Gooley T, Sullivan KM, Davis C, Bensinger WI, Storb R, Nash RA. Secondary failure of platelet recovery after hematopoietic stem cell transplantation. *Biol Blood Marrow Transplant*. 2001;7(3):154–62.

Submit your next manuscript to BioMed Central and we will help you at every step:

- We accept pre-submission inquiries
- Our selector tool helps you to find the most relevant journal
- We provide round the clock customer support
- Convenient online submission
- Thorough peer review
- Inclusion in PubMed and all major indexing services
- Maximum visibility for your research

Submit your manuscript at
www.biomedcentral.com/submit



H₂S-Donating Doxorubicins may overcome Cardiotoxicity and Multidrug Resistance

Konstantin CHEGAEV, Barbara Rolando, Daniela Cortese, Elena Gazzano,
Ilaria Buondonno, Loretta Lazzarato, Marilu Fanelli, Claudia Maria Hattinger,
Massimo Serra, Chiara Riganti, Roberta Fruttero, Dario Ghigo, and Alberto Gasco

J. Med. Chem., **Just Accepted Manuscript** • DOI: 10.1021/acs.jmedchem.6b00184 • Publication Date (Web): 27 Apr 2016

Downloaded from <http://pubs.acs.org> on May 2, 2016

Just Accepted

“Just Accepted” manuscripts have been peer-reviewed and accepted for publication. They are posted online prior to technical editing, formatting for publication and author proofing. The American Chemical Society provides “Just Accepted” as a free service to the research community to expedite the dissemination of scientific material as soon as possible after acceptance. “Just Accepted” manuscripts appear in full in PDF format accompanied by an HTML abstract. “Just Accepted” manuscripts have been fully peer reviewed, but should not be considered the official version of record. They are accessible to all readers and citable by the Digital Object Identifier (DOI®). “Just Accepted” is an optional service offered to authors. Therefore, the “Just Accepted” Web site may not include all articles that will be published in the journal. After a manuscript is technically edited and formatted, it will be removed from the “Just Accepted” Web site and published as an ASAP article. Note that technical editing may introduce minor changes to the manuscript text and/or graphics which could affect content, and all legal disclaimers and ethical guidelines that apply to the journal pertain. ACS cannot be held responsible for errors or consequences arising from the use of information contained in these “Just Accepted” manuscripts.

H₂S-Donating Doxorubicins may overcome Cardiotoxicity and Multidrug Resistance

*Konstantin Chegaev,[§] Barbara Rolando,[§] Daniela Cortese,[§] Elena Gazzano,[#] Ilaria Buondonno,[#]
Loretta Lazzarato,[§] Marilù Fanelli,[†] Claudia M. Hattinger,[†] Massimo Serra,[†] Chiara Riganti,^{#,*}
Roberta Fruttero,^{§,*} Dario Ghigo,[#] Alberto Gasco.[§]*

[§]Department of Science and Drug Technology, University of Torino, via Pietro Giuria 9, 10125,
Torino, Italy

[#]Department of Oncology and Center for Experimental Research and Medical Studies (CeRMS),
University of Torino, via Santena, 5/bis, 10126, Torino, Italy

[†]Orthopaedic Rizzoli Institute, Laboratory of Experimental Oncology, Pharmacogenomics and
Pharmacogenetics Research Unit, via G. C. Pupilli 1, 40136, Bologna, Italy

ABSTRACT. Doxorubicin (DOXO) is one of the most effective antineoplastic agents in clinical practice. Its use is limited by acute and chronic side effects, in particular by its cardiotoxicity and by the rapid development of resistance to it. As part of a program aimed at developing new DOXO derivatives endowed with reduced cardiotoxicity, and active against DOXO-resistant tumor cells, a series of H₂S-releasing DOXOs (H₂S-DOXOs) were obtained by combining DOXO with appropriate H₂S-donor substructures. The resulting compounds were studied on H9c2 cardiomyocytes and in DOXO-sensitive U-2OS osteosarcoma cells, as well as in related

1
2
3 cell variants with increasing degrees of DOXO-resistance. Differently from DOXO, most of the
4
5 products were not toxic at 5 μ M concentration on H9c2 cells. A few of them triggered high
6
7 activity on the cancer cells. H₂S-DOXOs **10** and **11** emerged as the most interesting members of
8
9 the series. The capacity of **10** to impair Pgp transporter is also discussed.
10
11

12 13 14 **Introduction**

15
16 Doxorubicin (DOXO) **1** (Chart 1), known also as Adriamicin, is a potent broad-spectrum
17
18 antineoplastic antibiotic, isolated from *Streptomyces* species, widely used as single agent or in
19
20 combination with other anticancer drugs in treating of hematological cancers and solid tumors,
21
22 lymphomas and sarcomas.¹ Its use is accompanied by a number of clinical toxicities, of which
23
24 cardiomyopathy is the most important. Clinically, there are two kinds of cardiomyopathy: an
25
26 acute form, with rapid onset after the administration of a single dose of antibiotic, and a chronic,
27
28 cumulative, dose-related form.^{2,3} The former is characterized by abnormal electrocardiographic
29
30 changes, and is rarely a serious problem; the latter can lead to congestive heart failure that is
31
32 unresponsive to digitalis. The mortality rate in patients with congestive heart failure is close to
33
34 50%. The production of high levels of reactive oxygen species (ROS), including peroxide anion
35
36 (O₂⁻), hydrogen peroxide (H₂O₂), and hydroxyl radical (OH[•]), by induction of the antibiotic's
37
38 redox cycle at complex I of the mitochondrial electron transport chain, is the most likely of the
39
40 mechanisms proposed to explain this cardiotoxicity.^{4,5} The heart is very sensitive to oxidative
41
42 stress because of its poor antioxidant defenses compared to other organs.^{6,7} The cardiomyocyte
43
44 damage appears to be principally due to impairment of mitochondrial functioning.^{4,7,8}
45
46
47
48
49
50
51

52
53 Several synthetic DOXOs characterized by lower cardiotoxicity have been described. For
54
55 instance, the DOXO's analogs N-trifluoroacetyladiamycin-14-valerate (AD32), N-
56
57 trifluoroacetyladiamycin-14-O-hemiadipate (AD143) and N-benzyladiamycin-14-valerate
58
59
60

1
2
3 (AD198), induce lower toxicity in rat hearts thanks to their different effects on mitochondrial
4 energy metabolism.⁹ Semi-synthetic DOXOs conjugated with the antioxidant ferulic or caffeic
5 acids were less cardiotoxic but still retain their antitumor efficacy.¹⁰ Similarly, a synthetic
6 doxorubicin targeting mitochondria, which is effective against ovarian cancer cells, induces at
7 the same time a lower mitochondria-dependent cardiac damage.¹¹ A critical issue in the
8 production of DOXO analogs with lower cardiotoxicity is to prevent the loss of their cytotoxicity
9 against tumors with low sensitivity to the drug. Indeed, DOXO's efficacy in cancer therapy is
10 also hampered by the ease with which resistance to it develops. This occurs through a number of
11 mechanisms, principally the increased capacity of the cancer cells to efflux the drug, thus
12 limiting its cellular accumulation and reducing its toxicity.¹² Interestingly, DOXO resistance is
13 decreased by nitric oxide (NO)-donors, namely compounds able to increase the intracellular NO
14 concentration.¹³⁻¹⁷

15
16
17
18
19
20
21
22
23
24
25
26
27
28
29
30
31
32
33
34
35
36
37
38
39
40
41
42
43
44
45
46
47
48
49
50
51
52
53
54
55
56
57
58
59
60
Hydrogen sulfide (H₂S) is a colorless gas with a characteristic smell of rotten eggs that, as a
biochemical agent, has long only been considered as a poisonous and toxic pollutant. It is a weak
acid ($pK_{a1} \approx 6.9$, $pK_{a2} > 12$ at 25 °C) and at physiological pH (7.4) the two species present in
equilibrium are HS⁻ and H₂S, in a ratio of about 3:1. At 37 °C its water solubility is about 80
mM.¹⁸ It is able to cross lipid membranes by simple diffusion, and does not require facilitation by
membrane channels.¹⁹ A huge amount of experimental evidence has accumulated in the past
fifteen years to show that hydrogen sulfide is an endogenous gasotransmitter produced from L-
cysteine by the action of two pyridoxal-5'-phosphate (PLP)-dependent enzymes: cystathionine β-
synthase (CBS), and cystathionine γ-lyase, also called cystathionase (CSE).²⁰

Like the other two gasotransmitters, NO and carbon monoxide (CO), H₂S performs a variety of
homeostatic functions, especially in the nervous and cardiovascular systems.²⁰⁻²⁵ Several reports

1
2
3 indicate that there is cross-talk between H₂S and NO. This relation is complex, and requires
4
5 further investigation. It has been suggested that these two species may interact producing an
6
7 unidentified nitrosothiol, which triggers a weak vasorelaxing effect, if any.^{26,27} In addition, H₂S
8
9 plays roles in modulating the cellular S-nitrosothiol profile, probably through the formation of
10
11 thionitrous acid (HSNO), which is a source of nitrosonium ion (NO⁺), NO, and nitroxyl
12
13 (HNO).^{28,29} H₂S exhibits strong cytoprotective effects through a combination of antioxidant and
14
15 antiapoptotic signals.³⁰⁻³³ It is able to scavenge ROS and reactive nitrogen species (RNS).³³ In
16
17 particular it is able to suppress peroxynitrite (HOONO) induced cell damage, owing to its ability
18
19 to react with HOONO, giving rise to sulfinyl nitrite (HSNO₂), a new NO-donor.³⁴ A number of
20
21 recent reports show that sodium hydrosulfide (NaSH), which at physiological pH is in
22
23 equilibrium with H₂S, attenuates doxorubicin-induced cardiotoxicity in H9c2 embryonic rat
24
25 cardiac cells, by inhibiting endoplasmatic reticulum (ER) stress and oxidative stress.³⁵ Inhibition
26
27 of the p38 MAPK pathway, activated by DOXO, seems to be an important mechanism
28
29 underlying this protection.³⁶ Exogenous H₂S has also recently been shown to attenuate DOXO-
30
31 induced cardiotoxicity in H9c2 cells, by inhibiting calreticulin (CRT) expression.³⁷ On the basis
32
33 of this rationale, DOXO linked to H₂S donors (H₂S-DOXO), namely compounds capable of
34
35 releasing H₂S in physiological conditions,³⁸⁻⁴⁰ might be expected to give rise to chimeras
36
37 endowed with improved biochemical profiles than the antibiotic lead.
38
39
40
41
42
43
44

45
46 This paper describes a number of such compounds (Scheme 1) obtained by combining DOXO
47
48 with H₂S donors through an ester linkage at C-14. They are shown to be less cardiotoxic than the
49
50 lead, and maintain high levels of activity against DOXO-resistant cancer cell lines.
51
52

53 **Results and Discussion**

54
55
56
57
58
59
60

1
2
3 **Synthesis.** The H₂S-DOXOs **10-16** were obtained by the reaction of 14-bromo/chloro
4 daunomicin hydrobromide **2** with the appropriate H₂S-donor acids **3-9** (Scheme 1). The reaction
5 was performed in dry DMF in the presence of KF at room temperature. The resulting products
6 were purified by flash chromatography, successively suspended/dissolved in dry THF, and
7 treated with 1 eq. of HCl in dry dioxane to obtain the corresponding hydrochlorides. The purity
8 of the compounds was evaluated by RP-HPLC techniques.

9
10
11 **Stability of the H₂S-DOXOs.** Stability of all the new DOXO derivatives was evaluated by
12 high-performance liquid chromatography (HPLC) in Dulbecco's Modified Eagle Medium
13 (DMEM), in Iscove's Modified Dulbecco's Medium (IMDM) as well as in human serum. The
14 products hydrolyzed following pseudo-first-order kinetics. The half-lives ($t_{1/2}$), determined by
15 fitting the data to one-phase exponential decay equation, are reported in Table 1.

16
17
18 In DMEM, the compounds may be separated into four clusters: compounds possessing high
19 (**10, 11**, $t_{1/2} > 20$ h), medium (**15, 16**, $t_{1/2} = 3-6$ h), low (**12, 13**, $t_{1/2} = 16-17$ min) and very low
20 (**14**, $t_{1/2} < 1$ min) stability (Table 1).

21
22
23 Similar results (data not shown) were obtained in IMDM. In human serum, the products **12-14**
24 and **16** showed $t_{1/2} < 38$ min, while more stable **10, 11** and **15** showed $t_{1/2}$ values in the range 2.8-
25 4.6 h. The $t_{1/2}$ values measured in the different media principally reflect the presence of two
26 vulnerable moieties in the H₂S-DOXOs: the ester group, and the H₂S donor substructure. HPLC
27 analysis (see Supplementary) showed that both these moieties contribute to determining this
28 parameter, in different degrees depending on the specific product.

29
30
31 **Hydrogen sulfide release from the H₂S-DOXOs.** H₂S release was assessed using a
32 fluorometric assay based upon the reaction of H₂S with dansyl azide (DNS-Az) to give the
33 fluorescent related amide, which was detected with a HPLC system equipped with a fluorimetric
34

1
2
3 detector.⁴¹ The results of H₂S release in DMEM are reported in Figure 1. The most potent H₂S
4
5 donor was **11**, a derivative of benzoic acid bearing, in *para*-position, the 3-thioxo-3*H*-1,2-dithiol-
6
7 5-yl group. Introduction into **11** of a phenyl substituent at the 4-position of the thione ring (**10**)
8
9 reduced this capacity. Substitution of the thione ring with a thiocarbamoyl group (**16**), and in
10
11 particular manipulation of the ester bridge (**13**), but also transformation of 2-thioxo-1,3-dithiole-
12
13 4-carboxylic acid into the ester (**12**), decreased H₂S release. Compounds **14** and **15**, two aliphatic
14
15 esters, were markedly less potent H₂S-donors than **11**. Very similar results were obtained when
16
17 the experiments were performed in IMDM (data not shown). In human serum, H₂S release was
18
19 increased, except in the case of compound **14** (Supplementary Figure 1).
20
21
22
23

24 **Biological assays**

25
26
27 *Accumulation of H₂S-DOXOs and their cytotoxic effects in H9c2 cardiomyocytes.* We
28
29 compared the effect of DOXO and H₂S-DOXOs at 5 μM concentration, that we previously found
30
31 to be cytotoxic in H9c2 cardiomyocytes^{10,16,17} and in DOXO-sensitive cancer cells, but not in
32
33 DOXO-resistant ones.^{13,16,42,43} The accumulation of H₂S-DOXOs within H9c2-cardiomyocytes
34
35 was measured by a fluorimetric assay, and their cytotoxic effects were assayed by detecting the
36
37 activity of lactic dehydrogenase (LDH) in the extracellular medium, considered as an index of
38
39 doxorubicin-induced damage.^{13,15} As shown in Figure 2A, H₂S DOXOs were retained within
40
41 H9c2 cells at similar concentrations as DOXO was. However, while DOXO induced significant
42
43 cytotoxicity, the hybrid antibiotics **10-14** were significantly less toxic than the lead, and did not
44
45 produce significantly higher toxicity compared to the untreated cells Figure 2B.
46
47
48
49

50
51 Compound **3**, the H₂S releasing moiety present in **10**, did not modify the intracellular retention
52
53 of DOXO within H9c2 cells when co-incubated at an equimolar concentration (Supplementary,
54
55 Figure 2A), and it was not toxic when used alone. Conversely, co-incubation significantly
56
57
58
59
60

1
2
3 reduced DOXO's toxicity, suggesting that the H₂S-DOXOs' lack of cardiotoxicity is due to the
4 presence of the H₂S releasing moieties (Supplementary, Figure 2B). The case is different with
5
6 presence of the H₂S releasing moieties (Supplementary, Figure 2B). The case is different with
7
8 compounds **15** and **16**, which are significantly more cardiotoxic than the lead (Figure 2B). To
9
10 shed light on this difference, the ethyl ester of acid **8** and the methyl ester of acid **9** (**17** and **18**
11
12 respectively, see Supplementary), the H₂S-donor substructures present in **15** and **16**, were tested
13
14 for their toxicity on H9c2 cells. The results clearly indicate that these two products are more
15
16 toxic than the lead (Supplementary, Figure 3). It may thus reasonably be supposed that the
17
18 cardiotoxicity of H₂S-DOXOs **15**, **16** is due to the presence in their structure of these two
19
20 moieties.
21
22
23

24 *Effect of H₂S-DOXOs on ROS intracellular levels.* Intracellular levels of ROS, which are
25
26 critical mediators of DOXO-induced cardiotoxicity,⁷ were measured by a fluorimetric assay.
27
28 DOXO significantly increased ROS levels in H9c2 cardiomyocytes; by contrast, intracellular
29
30 ROS measured in the same cells treated with H₂S DOXO were significantly lower than those
31
32 produced by the parent antibiotic and did not differ from untreated cells (Figure 3A). To
33
34 determine whether the reduced ROS levels were caused by release of H₂S, ROS were again
35
36 measured in the presence of hydroxocobalamin (OHCbl), a well-known H₂S scavenger.⁴⁴ The
37
38 product did not affect ROS levels in cells treated with DOXO, but markedly increased them in
39
40 those exposed to H₂S-DOXO, producing the same range of ROS measured in DOXO-treated
41
42 cells (Figure 3A). In line with this data, OHCbl was not toxic in untreated cardiomyocytes, and
43
44 did not modify the cytotoxicity of DOXO; conversely, it significantly increased the cytotoxic
45
46 effects induced by all H₂S-DOXOs except for **15** and **16**, which showed the opposed trend
47
48 (Figure 3B). Compound **3** alone was sufficient to reduce basal ROS levels in H9c2 cells, an
49
50 event that was reversed by OHCbl (Supplementary, Figure 4A). Similarly, the presence of
51
52
53
54
55
56
57
58
59
60

1
2
3
4
5
6
7
8
9
10
11
12
13
14
15
16
17
18
19
20
21
22
23
24
25
26
27
28
29
30
31
32
33
34
35
36
37
38
39
40
41
42
43
44
45
46
47
48
49
50
51
52
53
54
55
56
57
58
59
60

OHCbl increased the cytotoxicity of **3**, alone or co-incubated with DOXO (Supplementary, Figure 4B). Similarly, the antioxidant N-acetyl-L-cysteine (NAC), used at a concentration that significantly reduced the amount of ROS produced by DOXO (Supplementary, Figure 5A), strongly reduced the release of LDH (Supplementary, Figure 5B), as compounds **10-14** did. By contrast, the co-incubation of DOXO with dexrazoxane, which achieves significant cardioprotection acting through ROS-independent mechanism,⁴⁵ failed to reduce DOXO's cytotoxicity in H9c2 cells (Supplementary Figure 6).

As demonstrated by the experiments with OHCbl and NAC, the presence of appropriate H₂S-releasing moieties linked to DOXO or the presence of an excess of an antioxidant molecule play a pivotal role in lowering ROS levels and preventing toxicity in cardiomyocytes. These results strongly support the hypothesis that the reduced cardiotoxicity of compounds **10-14** was due to the decreased intracellular level of ROS.

H₂S-DOXOs as effective anti-cancer agents. Since oxidative stress is one of the main mechanisms involved in DOXO's anti-tumor-activity,⁷ the next point to clarify was whether the H₂S-releasing DOXOs still retained their activity on cancer cells. The attention was focused on human osteosarcoma cells, since DOXO is the first-line drug in this kind of tumor;⁴⁶ however, its efficacy is limited in osteosarcoma expressing P-glycoprotein (Pgp/ABCB1),⁴⁷ a membrane transporter that effluxes DOXO and limits its anti-cancer efficacy.¹² The effects of H₂S-DOXOs in DOXO-sensitive U-2OS osteosarcoma cells, and in the related cell variants with increasing degrees of DOXO-resistance, namely U-2OS/DX30, U-2OS/DX100, and U-2OS/DX580, were investigated. The DOXO IC₅₀ of these variants shows a progressive increase (Supplementary Table 1), according to the increasing expression of Pgp.⁴⁸ As expected, DOXO was accumulated in progressively less amounts in the resistant cells (Figure 4A), where it progressively lost its

1
2
3 toxicity (Figure 4B). By screening the intracellular retention of the H₂S-releasing DOXOs, **10**,
4
5 **11**, **15** and **16** were identified as being accumulated to a significantly greater extent than DOXO
6
7
8 itself, in both sensitive and resistant cells (Figure 4A).
9

10
11 In line with their higher intracellular retention, these compounds were significantly more
12
13 cytotoxic than DOXO in both drug-sensitive and drug-resistant cells (Figure 4B). Co-incubation
14
15 of **3** with DOXO increased drug retention and cytotoxicity in U-2OS/DX30 and U-2OS/DX100
16
17 cells; however, this combination did not show superior efficacy than DOXO in U-2OS/DX580
18
19 cells (Supplementary Figure 7A, B). These data suggest that the sole presence of a H₂S-releasing
20
21 group may be sufficient to improve DOXO's efficacy in mildly-chemoresistant cells, but not in
22
23 strongly-resistant ones. Interestingly, while DOXO increased ROS levels in U-2OS cells but not
24
25 in resistant cells, in sensitive cells the H₂S-DOXOs produced significantly less ROS than DOXO
26
27 did (Figure 5A). Of note, **10** and **11**, which exerted high cytotoxicity, also significantly reduced
28
29 the ROS amount compared with untreated osteosarcoma cells (Figure 5A). This reduction of
30
31 ROS levels is likely due to the presence of the H₂S-releasing groups, since ROS levels were
32
33 decreased in osteosarcoma cells exposed to DOXO plus **3** to a significantly greater extent than
34
35 they were in cells exposed to DOXO alone (Supplementary Figure 7C). The observed increase in
36
37 ROS production in cells treated with **10** in the presence of OHCbl is in line with this result
38
39 (Figure 5B).
40
41
42
43
44

45
46 Similar data were obtained with **11** (not shown). These results indicate that **10** and **11** are
47
48 cytotoxic in both drug-sensitive and drug-resistant cells notwithstanding the lower ROS
49
50 production, leading to the hypothesis that they may exert their anti-cancer effects through an
51
52 oxidative-stress-independent mechanism. Several works highlight that part of the anticancer
53
54 efficacy of anthracyclines is due to the inhibition of topoisomerase II.⁴⁹ By contrast, all H₂S-
55
56
57
58
59
60

1
2
3 DOXOs were unable to inhibit this enzyme (Supplementary Figure 8), leading to exclude that
4
5 their anticancer effects were mediated by this mechanism.
6
7

8 ***H₂S-DOXOs are less effluxed by Pgp in osteosarcoma-resistant cells.*** To shed light on how
9
10 the presence of H₂S-releasing groups improves the efficacy of doxorubicin in resistant cells, the
11
12 efflux kinetics of parental DOXO, DOXO co-incubated with **3**, and with **10**, were measured in
13
14 the Pgp over-expressing U-2OS/DX580 cells. As shown in Figure 6, the presence of **3** reduced
15
16 the V_{max} of DOXO efflux, without affecting the K_m ; by contrast, **10** had a lower V_{max} and a higher
17
18 K_m than DOXO.
19
20
21

22 These results suggest that the release of H₂S by an appropriate H₂S donor impairs the catalytic
23
24 efficacy of Pgp, thus explaining the increased intracellular accumulation of doxorubicin in the
25
26 presence of **3**. In the case of **10**, the presence of an H₂S donor linked to the anthracycline moiety
27
28 not only impairs the catalytic activity Pgp, but also reduces the compound's affinity for the
29
30 protein, producing maximal benefit in terms of drug accumulation and toxicity.
31
32
33

34 **Conclusion**

35
36 A series of H₂S-releasing moieties were linked through an ester bridge to C-14 of DOXO to
37
38 improve its pharmaceutical profile, in view of their ability to release H₂S. All products were
39
40 tested on cardiac H9c2 cells, and on U-2OS osteosarcoma cells and related cell variants with
41
42 increasing degrees of DOXO-resistance. The specific H₂S-releasing moiety strongly influenced
43
44 the products' biological behavior. All H₂S-DOXOs were able to reduce the oxidative stress
45
46 induced by the antibiotic on the cardiomyocytes, and most of them were significantly less toxic
47
48 on the cardiomyocytes than the lead. Compounds **15**, **16** reduced the oxidative stress but not the
49
50 cardiotoxicity, paralleling the intrinsic toxicity of the two H₂S-releasing moieties **7**, **8** present in
51
52 their structures. Compounds **10**, **11** emerged as the most interesting members of the series. When
53
54
55
56
57
58
59
60

1
2
3 tested on H9c2 cells, they did not produce a significantly higher toxicity than the control. In
4
5 addition, when tested on sarcoma cell lines they displayed significantly more potent cytotoxic
6
7 effects than those of the lead. Preliminary studies carried out on **10**, taken as a representative
8
9 member of the class, suggest that the increased cytotoxicity is likely due to a reduced efflux of
10
11 the product by Pgp. Dedicated investigations to shed light on the action mechanisms of this new
12
13 class of modified doxorubicins, as well as in *in vivo* studies of **10**, **11**, are now in progress.
14
15

16 17 **Experimental Section**

18
19 **Chemistry.** ^1H and ^{13}C NMR spectra were recorded on a BrukerAvance 300, at 300 and 75
20
21 MHz, respectively, using SiMe_4 as internal standard. The following abbreviations indicate peak
22
23 multiplicity: *s* = singlet, *d* = doublet, *t* = triplet, *m* = multiplet, *bs* = broad singlet. ESI MS spectra
24
25 were recorded on a Micromass Quattro API micro (Waters Corporation, Milford, MA, USA)
26
27 mass spectrometer. Data were processed using a MassLynxSystem (Waters). High resolution MS
28
29 spectra were recorded on a Bruker Bio Apex Fourier transform ion cyclotron resonance (FT-
30
31 ICR) mass spectrometer equipped with an Apollo I ESI source, a 4.7 T superconducting magnet,
32
33 and a cylindrical infinity cell (Bruker Daltonics, Billerica, MA, USA). Melting points were
34
35 determined with a capillary apparatus (Büchi 540) in open capillary. Flash column
36
37 chromatography was performed on silica gel (Merck Kieselgel 60, 230–400 mesh ASTM). The
38
39 progress of the reactions was followed by thin-layer chromatography (TLC) on 5×20 cm plates
40
41 Merck Kieselgel 60 F254, with a layer thickness of 0.20 mm. Anhydrous sodium sulfate
42
43 (Na_2SO_4) was used as drying agent for the organic phases. Organic solvents were removed under
44
45 reduced pressure at 30 °C. Synthetic-purity solvents dichloromethane (DCM), acetonitrile
46
47 (CH_3CN), methanol (MeOH), diethyl ether (Et_2O), diisopropyl ether (*i*-Pr $_2\text{O}$),
48
49 dimethylformamide (DMF) and 40–60 petroleum ether (PE) were used. Dry tetrahydrofuran
50
51
52
53
54
55
56
57
58
59
60

1
2
3 (THF) was distilled immediately before use from Na and benzophenone under positive N₂
4
5 pressure. Dry DMF was obtained through storage on 4Å molecular sieves. Commercial starting
6
7 materials were purchased from Sigma-Aldrich, Alfa Aesar, and TCI Europe. For the synthesis of
8
9 **2-9** see supporting material.
10
11

12 **The purity determination of compounds.** RP-HPLC analyses were run with a HP 1100
13
14 chromatograph system (Agilent Technologies, Palo Alto, CA, USA) equipped with a quaternary
15
16 pump (model G1311A), a membrane degasser (G1379A), and a diode-array detector (DAD)
17
18 (model G1315B) integrated into the HP1100 system. Data were processed using a HP
19
20 ChemStation system (Agilent Technologies). The analytical column was a Tracer Excel 120
21
22 ODS-B (250×4.6mm, 5 μm; Teknokroma, Barcelona). Compounds were dissolved in the mobile
23
24 phase and injected through a 20 μL loop (Rheodyne, Cotati, CA). The mobile phase consisted of
25
26 0.1% aqueous HCOOH (solvent A) and CH₃CN (solvent B) and elution was in gradient mode:
27
28 initially 35% of solvent B until 5 min, from 35 to 80% of solvent B between 5 and 10 min, 80%
29
30 of solvent B until 20 min, and from 80 to 35% of solvent B between 20 and 25 min. HPLC
31
32 retention times (*t_R*) were obtained at flow rates of 1.0 mL·min⁻¹, and the column effluent was
33
34 monitored at 234 nm and 480 nm referenced against a 700 nm wavelength. All products
35
36 displayed purity ≥ 95% with the exception of **10** and **12** (93% purity).
37
38
39
40
41
42

43 **General procedure for the synthesis of H₂S donor doxorubicins 10-16.** To a solution of the
44
45 appropriate acid (1.35 mmol) in dry DMF, KF (155 mg, 2.70 mmol) was added in one portion,
46
47 and the reaction was vigorously stirred for 15 min. 14-Bromo/chloro daunorubicin hydrobromide
48
49 (**2**) (300 mg, 0.45 mmol) was added and the reaction was stirred at r.t. until completed (LC
50
51 control). Solvent was removed under reduced pressure at 30 °C and the resulting mixture was
52
53 separated by flash chromatography (eluent: gradient from 98/2 to 80/20 CH₂Cl₂/MeOH) to give a
54
55
56
57
58
59
60

red solid. The resulting compound was dissolved/suspended in dry THF, and 2 equivalents of HCl solution in dry dioxane were added. The resulting mixture was stirred for 2 h at r.t., then diluted with Et₂O and the precipitate was filtered, washed with Et₂O and dried in desiccators to give a title compound as a red powder.

Doxorubicin 14-[4-(4-phenyl-5-thioxo-5H-[1,2]dithiol-3-yl)]benzoate (10). Yield: 52%; pHPLC 93% ($t_R = 12.2$ min); m.p. 166 – 170 °C (dec.); ¹H-NMR (CD₃OD + CDCl₃) δ ppm: 1.36 (d, $J_{HH}^3 = 6.22$ Hz, 3H, ⁶CH₃); 1.91 (m, 1H), 2.06 (m, 1H) (^{2'}CH₂); 2.19 (m, 1H), 2.51 (m, 1H) (⁸CH₂); 3.05 (m, 1H), 3.28 (m, 1H) (¹⁰CH₂); 3.35 (m, 1H, ^{3'}CH); 3.56 (m, 1H, ^{4'}CHOH); 3.79 (br. s, 1H, ^{4'}CHOH); 4.08 (s, 3H, OCH₃); 4.28 (m, 1H, ^{5'}CH); 5.23 (m, 1H, ⁷CH); 5.42 (m, 1H), 5.57 (m, 2H, (^{1'}CH and ¹⁴CH₂)); 7.15 (m, 1H, ²CH); 7.36 (m, 2H), 7.51 (m, 5H), 7.83 (m, 2H), (m, 1H.), 8.01 (m, 2H) (CH Ar.); MS (ESI⁺) m/z 856 (M+H)⁺. HRMS (ESI⁺) m/z calcd for C₄₃H₃₇NO₁₂S₃ (M+H)⁺ 856.1551, found 856.1551.

Doxorubicin 14-[4-(3-thioxo-3H-1,2-dithiol-4-yl)]benzoate (11). Yield: 20%; pHPLC 97% ($t_R = 11.9$ min); m.p. 159 – 163 °C (dec.); ¹H-NMR (DMSO-*d*₆) δ ppm: 1.21 (d, $J_{HH}^3 = 6,22$ Hz, 3H, ⁶CH₃); 1.71 (m, 1H), 1.92 (m, 1H) (^{2'}CH₂); 2.12 (m, 1H), 2.38 (m, 1H) (⁸CH₂); 2.89 (d, $J_{HH}^2 = 18.3$ Hz, 1H), 3.12 (d, $J_{HH}^2 = 18.3$ Hz, 1H) (¹⁰CH₂); 3.62 (m, 1H, ^{4'}CHOH); 3.98 (s, 3H, OCH₃); 4.29 (m, 1H, ^{5'}CH); 4.97 (m, 1H, ⁷CH); 5.32 (br. s, 1H, ^{4'}CHOH); 5.54 (m, 3H, ^{1'}CH and ¹⁴CH₂); 5.77 (s, 1H, ⁹COH); 7.64 (m, 1H, ²CH); 7.69 (d, 2H), 7.90 (m, 2H), 8.08 (d, 2H) (6CH Ar.); 9.30 (s, 1H, SCH), 13.24 (s, 1H), 14.02 (s, 1H) (2ArOH); MS (ESI⁺) m/z 780 (M+H)⁺. HRMS (ESI⁺) m/z calcd for C₃₇H₃₃NO₁₂S₃ (M+H)⁺ 780.1238, found 780.1237.

Doxorubicin 14-[2-thioxo-1,3-dithiole-4]carboxylate (12). Yield: 43%; pHPLC 93% ($t_R = 13.0$ min); m.p. 190 – 195 °C (dec.); ¹H-NMR (DMSO-*d*₆) δ ppm: 1.17 (d, $J_{HH}^3 = 6.31$ Hz, 3H, ⁶CH₃); 1.70 (m, 1H), 1.90 (m, 1H) (^{2'}CH₂); 2.09 (m, 1H), 2.30 (m, 1H) (⁸CH₂); 2.88 (d, $J_{HH}^2 =$

1
2
3 18.0 Hz, 1H), 3.12 (d, $J_{HH}^2 = 18.4$ Hz, 1H) ($^{10}\text{CH}_2$); 3.60 (m, 1H, $^4\text{CHOH}$); 3.99 (s, 3H, OCH_3);
4 4.24 (m, 1H, ^5CH); 4.95 (m, 1H, ^7CH); 5.30 (br. s, 1H, $^4\text{CHOH}$); 5.50 (m, 3H, ^1CH and $^{14}\text{CH}_2$);
5 5.88 (br. s, 1H, ^9COH); 7.67 (m, 1H, ^2CH); 7.93 (m, 2H, 2CH Ar.); 8.60 (s, 1H, CHS); 13.25 (s,
6 1H, ArOH); MS (ESI⁺) m/z 704 (M+H)⁺; HRMS (ESI⁺) m/z calcd for $\text{C}_{31}\text{H}_{29}\text{NO}_{12}\text{S}_3$ (M+H)⁺
7 704.0925, found 704.0929.

14
15 **Doxorubicin 14-[4-(5-Thioxo-5H-[1,2]dithiol-3-yl)phenoxy]acetate (13).** Yield: 45%;
16 pHPLC 95% ($t_R = 14.2$ min); m.p. 159 – 162 °C (dec.); $^1\text{H-NMR}$ (DMSO- d_6) δ ppm: 1.16 (d,
17 $J_{HH}^3 = 6,59$ Hz, 3H, $^6\text{CH}_3$); 1.71 (m, 1H), 1.89 (m, 1H) ($^2\text{CH}_2$); 2.08 (m, 1H), 2.29 (m, 1H)
18 ($^8\text{CH}_2$); 2.87 (d, $J_{HH}^2 = 17.9$ Hz, 1H), 3.09 (d, $J_{HH}^2 = 18.0$ Hz, 1H) ($^{10}\text{CH}_2$); 3.60 (m, 1H,
19 $^4\text{CHOH}$); 3.98 (s, 3H, OCH_3); 4.23 (m, 1H, ^5CH); 4.95 (m, 1H, ^7CH); 5.09 (s, 2H, CH_2COO);
20 5.29 (br. s, 1H, $^4\text{CHOH}$); 5.44 (m, 3H, ^1CH and $^{14}\text{CH}_2$); 5.76 (s, 1H, ^9COH); 7.13 (d, 2H, 2CH
21 Ar.); 7.65 (m, 1H, ^2CH); 7.78 (s, 1H, SCH); 7.90 (m, 4H, 4CH Ar.); 13.23 (s, 1H), 14.02 (s, 1H)
22 (2ArOH); MS (ESI⁺) m/z 810 (M+H)⁺. HRMS (ESI⁺) m/z calcd for $\text{C}_{38}\text{H}_{35}\text{NO}_{13}\text{S}_3$ (M+H)⁺
23 810.1343, found 810.1342.

24
25
26
27
28
29
30
31
32
33
34
35
36 **Doxorubicin 14-[2(S)-2-acetylamino-3-allylsulfanyl]propionate (14).** Yield: 44%; pHPLC
37 97% ($t_R = 10.3$ min); m.p. 143 – 146 °C (dec.); $^1\text{H-NMR}$ (DMSO- d_6) δ ppm: 1.16 (d, $J_{HH}^3 = 6,59$
38 Hz, 3H, $^6\text{CH}_3$); 1.71 (m, 1H), 1.89 (m, 4H) ($^2\text{CH}_2$ and CH_3CONH); 2.08 (m, 1H), 2.27 (m, 1H)
39 ($^8\text{CH}_2$); 2.71 (dd, 1H), 2.83 (d, $J_{HH}^2 = 18.0$ Hz, 1H), 2.94 (dd, 1H), 3.07 (d, $J_{HH}^2 = 18.3$ Hz, 1H)
40 ($^{10}\text{CH}_2$ and $\text{SCH}_2\text{CH}(\text{NHAc})\text{COO}$); 3.19 (d, 2H, $\text{SCH}_2\text{CHCH}_2$); 3.60 (m, 1H, $^4\text{CHOH}$); 3.98 (s,
41 3H, OCH_3); 4.24 (m, 1H, ^5CH); 4.57 (m, 1H, CHCOO); 4.94 (m, 1H, ^7CH); 5.13 (m, 2H,
42 $\text{CH}=\text{CH}_2$); 5.29 (br. s, 3H, $^4\text{CHOH}$ and $^{14}\text{CH}_2$); 5.47 (m, 1H, ^1CH); 5.74 (m, 2H, $\text{CH}=\text{CH}_2$ and
43 ^9COH); 7.65 (m, 1H, ^2CH); 7.91 (m, 2H, 2CH Ar.); 8.48 (d, 1H, NH); 13.22 (s, 1H, ArOH); MS
44
45
46
47
48
49
50
51
52
53
54
55
56
57
58
59
60

(ESI⁺) *m/z* 729 (M+H)⁺. HRMS (ESI⁺) *m/z* calcd for C₃₅H₄₀N₂O₁₃S (M+H)⁺ 729.2324, found 729.2326.

Doxorubicin 14-(3-Allyldisulfanyl)propionate (15). Yield: 42%; pHPLC 98% (*t_R* = 12.4 min); m.p. 135 – 138 °C (dec.); ¹H-NMR (DMSO-*d*₆) δ ppm: 1.15 (d, *J*_{HH}³ = 6.31 Hz, 3H, ⁶CH₃); 1.56 (m, 1H), 1.74 (m, 1H) (²CH₂); 2.05 (m, 1H), 2.29 (m, 1H) (⁸CH₂); 2.71 (d, *J*_{HH}² = 12.4 Hz, 1H) (¹⁰CHH), 2.88 (m, 4H, CH₂CH₂), 3.06 (m, 1H) (¹⁰CHH); 3.40 (d, 2H, SCH₂CH); 3.57 (m, 1H, ⁴CHOH); 3.98 (s, 3H, OCH₃); 4.16 (m, 1H, ⁵CH); 4.94 (br. s, 1H, ⁷CH); 5.21 (m, 4H, ¹⁴CH₂, CH=CH₂); 5.60 (br. s, 1H, ¹CH); 5.81 (m, 1H, CH=CH₂) 7.64 (m, 1H, ²CH); 7.92 (m, 2H, 2CH Ar.); MS (ESI⁺) *m/z* 704 (M+H)⁺. HRMS (ESI⁺) *m/z* calcd for C₃₃H₃₇NO₁₂S₂ (M+H)⁺ 704.1830, found 704.1829.

Doxorubicin 14-(4-thiocarbamoyl)benzoate (16). Yield: 51%; pHPLC 99% (*t_R* = 10.5 min); m.p. 179 – 183 °C (dec.); ¹H-NMR (DMSO-*d*₆) δ ppm: 1.20 (d, *J*_{HH}³ = 6,31 Hz, 3H, ⁶CH₃); 1.72 (m, 1H), 1.91 (m, 1H) (²CH₂); 2.12 (m, 1H), 2.37 (m, 1H) (⁸CH₂); 2.89 (d, *J*_{HH}² = 18.9 Hz, 1H), 3.13 (d, *J*_{HH}² = 18.9 Hz, 1H) (¹⁰CH₂); 3.62 (m, 1H, ⁴CHOH); 3.98 (s, 3H, OCH₃); 4.28 (m, 1H, ⁵CH); 4.96 (m, 1H, ⁷CH); 5.31 (br. s, 1H, ⁴CHOH); 5.50 (m, 3H, ¹CH and ¹⁴CH₂); 5.82 (s, 1H, ⁹COH); 7.65 (m, 1H, ²CH); 7.96 (m, 6H, 6CH Ar.); 9.75 (s, 1H), 10.12 (s, 1H) (NH₂); MS (ESI⁺) *m/z* 707 (M+H)⁺. HRMS (ESI⁺) *m/z* calcd for C₃₅H₃₄N₂O₁₂S (M+H)⁺ 707.1905, found 707.1906.

Chemicals. Fetal bovine serum (FBS) and culture medium were supplied by Invitrogen Life Technologies (Carlsbad, CA); human serum (sterile filtered from human male AB plasma) was supplied by Sigma-Aldrich; plasticware for cell cultures was from Falcon (Becton Dickinson, Franklin Lakes, NJ). Electrophoresis reagents were from Bio-Rad Laboratories (Hercules, CA); the protein content of cell monolayers and lysates was assessed with the BCA kit from Sigma

1
2
3 Chemical Co (St. Louis, MO). Doxorubicin and reagents not specified were from Sigma
4
5 Chemical Co.
6

7
8 **Stability in culture medium and in human serum.** Before addition of the compound, culture
9
10 medium (DMEM or IMDM) was pre-heated at 37 °C. 10 mM solution of each H₂S-DOXO in
11
12 DMSO was added to culture medium to have a final concentration of compound 200 μM. The
13
14 obtained solution was incubated at 37 ± 0.5 °C, and at appropriate time intervals, an aliquot of
15
16 200 μL of sample were collected and diluted with the same amount of acetonitrile containing
17
18 0.1% HCOOH to final concentration of 100 μM. The obtained mixture was vortexed, filtrated
19
20 (PTFE filters, 0.45 μM) and immediately analysed by RP-HPLC. All experiments were
21
22 performed at least in triplicate.
23
24
25

26
27 The stability of the H₂S-DOXOs to the esterase was evaluated by incubating the compounds in
28
29 human serum; the solution of compound (10 mM in DMSO) was added to human serum pre-
30
31 heated at 37 °C; the final concentration of the compound was 100 μM. The solution was
32
33 incubated at 37 ± 0.5 °C, and at appropriate time intervals, an aliquot of 300 μL of reaction
34
35 mixture was withdrawn and added to 300 μL of acetonitrile containing 0.1% HCOOH, in order
36
37 to deproteinize the serum. The sample was sonicated, vortexed, and centrifuged for 10 min at
38
39 2150 g. The clear supernatant was filtered through 0.45 μm PTFE filters and analysed by RP-
40
41 HPLC. All experiments were performed at least in triplicate.
42
43
44

45
46 In both the assays the HPLC analyses were performed with a HP 1100 chromatograph system
47
48 (Agilent Technologies, Palo Alto, CA, USA) in the experimental conditions previously
49
50 described. The reverse-phase HPLC procedure allowed separation and quantitation of H₂S-
51
52 DOXOs and of degradation products (DOXO, H₂S donor substructure); quantitation of H₂S-
53
54
55
56
57
58
59
60

1
2
3 DOXOs and of DOXO was done using calibration curve obtained with standards solutions
4
5 chromatographed in the same conditions in a concentration range of 1–200 μM ($r^2 > 0.99$).
6
7

8 The half-lives ($t_{1/2}$) of all the H₂S-DOXOs were determined by fitting the data with one phase
9
10 exponential decay equation using Prism software vers. 5 (Graph Pad, San Diego, CA, USA).
11
12

13
14 **H₂S release in culture medium and human serum.** To 1900 μL of culture medium (DMEM
15
16 or IMDM) or human serum pre-heated at 37 °C, 60 μL of dansylazide solution (10 mM in
17
18 Ethanol) and 40 μL of H₂S-DOXO stock solution (10 mM in DMSO) were added to have an
19
20 initial H₂S-DOXO concentration of 200 μM . Compounds **10** and **11** were incubated at half
21
22 concentration due to their low solubility. The solution was incubated at 37 ± 0.5 °C, and at fixed
23
24 time (1 h, 4 h and 24 h) 200 μL of reaction mixture was withdrawn and diluted with 200 μL of
25
26 CH₃CN to have a final concentration of compound 100 μM . The mixture was vortexed,
27
28 centrifuged for 10 min at $2150 \times g$. The clear supernatant was filtered through 0.45 μm PTFE
29
30 filters and analysed by RP-HPLC. All experiments were performed at least in triplicate. HPLC
31
32 analyses were performed with a HP 1200 chromatograph system (Agilent Technologies, Palo
33
34 Alto, CA, USA) equipped with a quaternary pump (model G1311A), a membrane degasser
35
36 (G1322A), a UV detector, MWD (model G1365D) and a fluorescence detector (model G1321A)
37
38 integrated in the HP1200 system. Data analysis was done using a HP ChemStation system
39
40 (Agilent Technologies). The sample was eluted on Tracer Excel 120 ODSB C18 (250 \times 4.6mm, 5
41
42 μm ; Teknokroma); injection volume was 20 μL . The mobile phase consisted of 0.1% aqueous
43
44 HCOOH and CH₃CN 20/80 v/v; elution was in isocratic mode at a flow rate of 0.8 ml/min. The
45
46 signals were obtained on fluorescence using an excitation and emission wavelength of 340 and
47
48 535 nm, respectively (gain factor =10). Data manipulation was performed by Agilent
49
50
51
52
53
54
55
56
57
58
59
60

1
2
3 ChemStation. The values obtained from integration of the peak of dansyl amide were
4
5 interpolated in a calibration line, prepared using NaHS as a standard, so the concentration of
6
7 dansyl amide in each sample is an index of H₂S amount.
8
9

10 **Cell lines.** Rat H9c2 cardiomyocytes and human doxorubicin-sensitive U-2OS cells were
11
12 purchased from ATCC (Manassas, VA) and cultured in DMEM medium. The corresponding
13
14 variants with increasing resistance to doxorubicin (U-2OS/DX30, U-2OS/DX100, U-
15
16 2OS/DX580), selected by culturing parental cells in a medium with 30, 100, 580 ng/mL
17
18 doxorubicin, were generated as described elsewhere.⁵⁰ Culture media were supplemented with
19
20 10% FBS, 1% penicillin-streptomycin, and 1% L-glutamine. Cell cultures were maintained in a
21
22 humidified atmosphere at 37 °C and 5% CO₂.
23
24
25
26

27 **Intracellular DOXOs accumulation.** The amount of DOXOs in cell lysates was measured
28
29 spectrofluorimetrically, as described elsewhere,¹³ using a Synergy HT Multi-Detection
30
31 Microplate Reader (Bio-Tek Instruments, Winooski, VT). Excitation and emission wavelengths
32
33 were 475 and 553 nm, respectively. A cell-free blank was prepared for each set of experiments,
34
35 and its fluorescence was subtracted from that measured in the presence of cells. Fluorescence
36
37 was converted to nmol DOXOs/mg cell proteins using a previously-prepared calibration curve.
38
39
40

41 **Cytotoxicity assays.** To verify the cytotoxic effect of DOXOs, the extracellular medium was
42
43 centrifuged at 12,000 × g for 5 min to pellet cellular debris, while cells were washed with fresh
44
45 medium, detached with trypsin/EDTA, re-suspended in 0.2 mL of 82.3 mM triethanolamine
46
47 phosphate-HCl (pH 7.6) and sonicated on ice with two 10 s bursts. Lactic dehydrogenase (LDH)
48
49 activity was measured in extracellular medium and cell lysate, as reported elsewhere.¹⁶ The
50
51 reaction was monitored for 6 min, measuring absorbance at 340 nm with a Synergy HT Multi-
52
53 Detection Microplate Reader, and was linear throughout the measurement time. Both
54
55
56
57
58
59
60

1
2
3 intracellular and extracellular enzyme activities were expressed in $\mu\text{mol NADH}$
4 oxidized/min/dish. Extracellular LDH activity was calculated as the percentage of the total LDH
5 activity occurring in the dish.
6
7
8

9
10 To determine the IC_{50} of doxorubicin, the cell viability was measured by the neutral red
11 staining method, as reported elsewhere.⁴² The absorbance of untreated cells was considered as
12 100% viability; the results are expressed as percentages of viable cells versus untreated cells.
13
14
15 IC_{50} was considered as the concentration of each drug that reduces to 50% the cell viability
16 versus untreated cells.
17
18
19

20
21 **Reactive oxygen species (ROS) measurement.** The amount of intracellular ROS was
22 measured fluorimetrically as described elsewhere.⁴³ 1×10^6 cells were re-suspended in a final
23 volume of 0.5 mL PBS, incubated for 30 min at 37 °C with 5 μM of the fluorescent probe 5-
24 (and-6)-chloromethyl-2',7'-dichlorodihydro-fluorescein diacetate-acetoxymethyl ester (DCFDA-
25 AM), centrifuged at $13,000 \times g$ at 37 °C and re-suspended in 0.5 mL PBS. The fluorescence of
26 each sample, an indicator of ROS levels, was read at 492 nm (λ excitation) and 517 nm (λ
27 emission). The results were expressed as nmol ROS/mg cell proteins.
28
29
30
31
32
33
34
35
36
37

38
39 **Doxorubicin efflux.** DOXOs efflux kinetics was measured as described elsewhere.⁵¹ Cells
40 were incubated for 20 min with increasing (0-50 μM) concentrations of parent or synthetic
41 doxorubicins, then washed and analyzed for intracellular doxorubicin concentration. A second
42 series of dishes, incubated in the same experimental conditions, were left for a further 10 min at
43 37 °C, then washed and tested for intracellular drug content. The difference of doxorubicin
44 concentration between the two series, expressed as nmol DOXOs extruded/min/mg cell proteins,
45 was plotted versus initial drug concentration. Values were fitted to the Michaelis-Menten
46
47
48
49
50
51
52
53
54
55
56
57
58
59
60

1
2
3 equation to calculate V_{max} and K_m , using the Enzfitter software (Biosoft Corporation, Cambridge,
4
5
6 United Kingdom).

7
8 **Statistical analysis.** All data in text and figures are given as means \pm SD. The results were
9
10 analyzed by one-way analysis of variance (ANOVA) and Tukey's test. $p < 0.05$ was considered
11
12 significant.
13

14 15 16 ASSOCIATED CONTENT

17
18
19 Supporting Information (synthesis of intermediate compounds, supplementary biological tests,
20
21 HPLC chromatograms of final compounds, ^1H - and ^{13}C -NMR spectra and hydrolytic profile of
22
23 H_2S -DOXOs) is available free of charge via the Internet at <http://pubs.acs.org>.
24
25
26

27 28 AUTHOR INFORMATION

29 30 31 **Corresponding Authors**

32
33 *Address: Department of Science and Drug Technology, University of Torino, via Pietro Giuria
34
35 9, 10125, Torino, Italy. Tel: +39-011-6707850. E-mail: roberta.fruttero@unito.it; Department of
36
37 Oncology and Center for Experimental Research and Medical Studies (CeRMS), University of
38
39 Torino, via Santena, 5/bis, 10126, Torino, Italy. Tel: +39-011-6705857. E-mail:
40
41
42 chiara.riganti@unito.it.
43
44
45

46 47 **Author Contributions**

48
49 The manuscript was written through contributions of all authors. All authors have given approval
50
51 to the final version of the manuscript.
52

53 54 55 **Notes**

56
57 The authors declare no competing financial interest.
58
59
60

ACKNOWLEDGMENT

This work was supported by grants from Italian Ministry of University and Research; Future in Research Program (FIRB 2011; grant: RBFR12SOQ1), Italian Association for Cancer Research (AIRC IG grants) and University of Turin (ricerca locale 2014), 5% contributions to Orthopaedic Rizzoli Institute.

ABBREVIATIONS

DOXO, doxorubicin; Pgp, P-glycoprotein; ROS, reactive oxygen species; PLP, pyridoxal-5'-phosphate; CBS, cystathionine β -synthase; CSE, cystathionine γ -lyase; RSN, reactive nitrogen species; ER, endoplasmatic reticulum; MAPK, Mitogen-activated protein kinase; CRT, calreticulin; DMEM, Dulbecco's Modified Eagle Medium; IMDM, Iscove's Modified Dulbecco's Medium; DNS-Az, dansyl azide; LDH, lactic dehydrogenase; OHCbl, hydroxocobalamin; ABCB1, ATP binding cassette B1; FBS, fetal bovine serum; BCA, bicinchoninic acid; DCFDA-AM, 5-(and-6)-chloromethyl-2',7'-dichlorodihydro-fluorescein diacetate-acetoxymethyl ester; BSA, bovine serum albumin.

REFERENCES

- 1) Minotti, G.; Menna, P.; Salvatorelli, E.; Cairo, G.; Gianni, L. Anthracyclines: molecular advances and pharmacologic developments in antitumor activity and cardiotoxicity. *Pharmacol. Rev.* **2004**, *56*, 185-229.
- 2) Chabner, A.; Amrein, P. C.; Druker, B. J.; Michaelson, M. D.; Mitsiades, C. S.; Goss, P. E.; Ryan, D. P.; Ramachandra, S.; Richardson, P. G.; Supko, J. G.; Wilson, W. H. Antineoplastic Agents. In *Goodman & Gilman's, The Pharmacological Basis of Therapeutic*, Brunton, L.; Lazo, J. S.; Parker, K. L., New York, Chicago: McGraw-Hill, **2006**; 1315-1403.

1
2
3 3) Buzdar, A. U.; Marcus, C.; Smith, T. L.; Blumenschein, G. R. Early and delayed clinical
4 cardiotoxicity of doxorubicin. *Cancer* **1985**, *55*, 2761-2765.
5
6

7
8 4) Doroshow J. H.; Davies, K. J. A. Redox cycling of anthracyclines by cardiac mitochondria.
9 II. Formation of superoxide anion, hydrogen-peroxide, and hydroxyl radical. *J. Biol. Chem.*
10 **1986**, *261*, 3068-3074.
11
12

13
14 5) Simunek, T.; Sterba, M.; Popelova, O.; Adamcova, M.; Hrdina, R.; Gersl, V. Anthracycline-
15 induced cardiotoxicity: overview of studies examining the roles of oxidative stress and free
16 cellular iron. *Pharmacol. Rep.* **2009**, *61*, 154-171.
17
18

19
20 6) Doroshow, J. H.; Locker, G. Y.; Myers, C. E. Enzymatic defenses of the mouse heart
21 against reactive oxygen metabolites: alterations produced by doxorubicin. *J. Clin. Invest.* **1980**,
22 *65*, 128-135.
23
24

25
26 7) Granados-Principal, S.; Quiles, J.L.; Ramirez-Tortosa, C. L.; Sanchez-Rovira, P.; Ramirez-
27 Tortosa, M. C. New advances in molecular mechanisms and the prevention of adriamycin
28 toxicity by antioxidant nutrients. *Food Chem. Toxicol.* **2010**, *48*, 1425-1438.
29
30

31
32 8) Berthiaume, J. M.; Wallace, K. B. Adriamycin-induced oxidative mitochondrial
33 cardiotoxicity. *Cell Biol.Toxicol.* **2007**, *23*, 15-25.
34
35

36
37 9) Kashfi, K.; Israel, M.; Sweatman, T.W.; Seshadri, R.; Cook, G.A. Inhibition of
38 mitochondrial carnitine palmitoyltransferases by adriamycin and adriamycin analogues.
39 *Biochem. Pharmacol.* **1990**, *40*, 1441-1448.
40
41

42
43 10) Chegaev, K.; Riganti, C.; Rolando, B.; Lazzarato, L.; Gazzano, E.; Guglielmo, S.; Ghigo,
44 D.; Fruttero, R.; Gasco, A. Doxorubicin-antioxidant co-drugs. *Bioorg. Med. Chem. Lett.* **2013**,
45 *23*, 5307-5310.
46
47

48
49 11) Jean, J.R.; Tulumello, D.V.; Riganti, C.; Liyanage, S.U.; Schimmer, A.D.; Kelley, S.O.
50 Mitochondrial targeting of doxorubicin eliminates nuclear effects associated with cardiotoxicity.
51 *ACS Chem. Biol.* **2015**, *10*, 2007-2015.
52
53
54
55
56
57
58
59
60

1
2
3 12) Gottesman, M. M. Mechanisms of cancer drug resistance. *Annu. Rev. Med.* **2002**, *53*, 615-
4 627.

5
6
7
8 13) Riganti, C.; Miraglia, E.; Viarisio, D.; Costamagna, C.; Pescarmona, G.; Ghigo, D.; Bosia,
9 A. Nitric oxide reverts the resistance to doxorubicin in human colon cancer cells by inhibiting
10 the drug efflux. *Cancer Res.* **2005**, *65*, 516–525.

11
12
13
14 14) Fruttero, R.; Crosetti, M.; Chegaev, K.; Guglielmo, S.; Gasco, A.; Berardi, F.; Niso, M.;
15 Perrone, R.; Panaro, M. A.; Colabufo, N. A. Phenylsulfonylfuroxans as modulators of multidrug-
16 resistance associated protein-1 and P-glycoprotein. *J. Med. Chem.* **2010**, *53*, 5467–5475.

17
18
19
20 15) Chegaev, K.; Riganti, C.; Lazzarato, L.; Rolando, B.; Guglielmo, S.; Campia, I.; Fruttero,
21 R.; Bosia, A.; and Gasco, A. Nitric oxide donor doxorubicins accumulate into doxorubicin-
22 resistant human colon cancer cells inducing cytotoxicity. *ACS Med. Chem. Lett.* **2011**, *2*, 494-
23 497.

24
25
26
27
28 16) Riganti, C.; Rolando, B.; Kopecka, J.; Campia, I.; Chegaev, K.; Lazzarato, L.; Federico,
29 A.; Fruttero, R.; Ghigo, D. Mitochondrial-targeting nitrooxy-doxorubicin: a new approach to
30 overcome drug resistance. *Mol. Pharmaceut.* **2013**, *10*, 161-174.

31
32
33
34 17) Gazzano, E.; Chegaev, K.; Rolando, B.; Blangetti, M.; Annaratone, L.; Ghigo, D.; Fruttero,
35 R.; Riganti, C. Overcoming multidrug resistance by targeting mitochondria with NO-donating
36 doxorubicins. *Bioorg. Med. Chem.* **2016**, *24*, 967-975.

37
38
39
40 18) Kabil, O.; Banerjee, R. Redox Biochemistry of hydrogen sulfide. *J. Biol. Chem.* **285**, *29*,
41 21903-21907.

42
43
44
45 19) Mathai, J. C.; Missner, Kuegler, A.P.; Saporov, S. M.; Zeidel, M. L.; Lee, J. K.; Pohl, P.
46 No facilitator required for membrane transport of hydrogen sulphide. *Proc. Natl. Acad. Sci.*
47 *U.S.A.* **2009**, *106*, 16633-16638.

48
49
50
51 20) Szabo, C. Hydrogen sulphide and its therapeutic potential. *Nat. Rev. Drug Discov.* **2007**, *6*,
52 917-935.
53
54
55
56
57
58
59
60

- 1
2
3 21) Wang, R. Two's company, three's a crowd: can H₂S be the third endogenous gaseous
4 transmitter. *Faseb J.* **2002**, *16*, 1792-1798.
5
6
7
8 22) Caliendo, G.; Cirino, G.; Santagata, V.; Wallace, J. L. Synthesis and biological effects of
9 hydrogen sulfide (H₂S): development of H₂S releasing drugs as pharmaceuticals. *J. Med. Chem.*
10 **2010**, *53*, 6275–6286.
11
12
13
14 23) Tan, B. H. Wong, P. T. H.; Bian, J.-S. Hydrogen sulfide: a novel signaling molecule in the
15 central nervous system. *Neurochem. Int.* **2010**, *56*, 3-10.
16
17
18
19 24) Liu, Y-H.; Yan, C-D.; Bian, J-S. Hydrogen sulphide: a novel signalling molecule in the
20 vascular system. *J. Cardiovasc. Pharmacol.* **2011**, *58*, 560-569.
21
22
23
24 25) R. Wang, R. Hydrogen sulfide: a new EDRF. *Kidney Int.* **2009**, *76*, 700-704.
25
26
27 26) Ali, M. Y.; Ping, C. Y.; Mok, Y. Y. P.; Ling, L.; Whiteman, M.; Bhatia, M.; Moore, P. K.
28 Regulation of vascular nitric oxide in vitro and in vivo; a new role for endogenous hydrogen
29 sulphide. *Br. J. Pharmacol.* **2006**, *149*, 625-634.
30
31
32
33 27) Whiteman, M.; Li, L.; Kostetski, I.; Chu, S. H.; Siau, J. L.; Bhatia, M.; Moore, P. K.
34 Evidence for the formation of a novel nitrosothiol from the gaseous mediators nitric oxide and
35 hydrogen sulphide. *Biochem. Biophys. Res. Commun.* **2006**, *343*, 303-310.
36
37
38
39 28) Bertova, A.; Cacanyiova, S.; Kristek, F.; Krizanova, O.; Ondrias, K.; Tomaskova, Z. The
40 hypothesis of the main role of H₂S in coupled sulphide-nitroso signalling pathway. *Gen. Physiol.*
41 *Biophys.* **2010**, *29*, 402-410.
42
43
44
45 29) Filipovic, M. R.; Miljkovic, J. L.; Nauser, T.; Royzen, M.; Klos, K.; Shubina, T.;
46 Koppenol, W. H.; Lippard, S. J.; Ivanovic-Burmazovic, I. Chemical characterization of the
47 smallest S-nitrosothiol, HSNO; cellular cross-talk of H₂S and S-nitrosothiols. *J. Am. Chem. Soc.*
48 **2012**, *134*, 12016-12027.
49
50
51
52
53 30) Elrod, J. W.; Calvert, J. W.; Morrison, J.; Doeller, J. E.; Kraus, D. W.; Tao, L.; Jiao, X.;
54 Scalia, R.; Kiss, L.; Szabo, C.; Kimura, H.; Chow, C.-W.; Lefter, D. J. Hydrogen sulfide
55
56
57
58
59
60

1
2
3 attenuates myocardial ischemia-reperfusion injury by preservation of mitochondrial function.
4
5 *Proc. Natl. Acad. Sci. U.S.A.* **2007**, *104*, 15560-15565.

6
7
8 31) Calvert, J. W.; Jha, S.; Gundewar, S.; Elrod, J. W.; Ramachandran, A.; Pattillo, C. B.;
9
10 Kevil, C. G.; Lefer, D. J. Hydrogen sulfide mediates cardioprotection through Nrf2 signaling.
11
12 *Circ.Res.* **2009**, *105*, 365-374.

13
14 32) Guo, W.; Kan, J.-T.; Cheng, Z.-y.; Chen, J.-F.; Shen, Y.-Q.; Xu, J.; Wu, D.; Zhu, Y.-Z.
15
16 Hydrogen sulfide as an endogenous modulator in mitochondria and mitochondria dysfunction.
17
18 *Oxidative Med. Cell. Longev.* **2012**, *2012*, 9 pages.

19
20
21 33) Lowicka, E.; Beltowski, J. Hydrogen sulfide (H₂S): the third gas of interest for
22
23 pharmacologists. *Pharmacol. Rep.* **2007**, *59*, 4–24.

24
25 34) Filipovic, M. R.; Miljkovic, J.; Allgaeuer, A.; Chaurio, R.; Shubina, T.; Herrmann, M.;
26
27 Ivanovic-Burmazovic, I. Biochemical insight into physiological effects of H₂S: reaction with
28
29 peroxynitrite and formation of a new nitric oxide donor, sulfinyl nitrite. *Biochem. J.* **2012**, *441*,
30
31 609-621.

32
33 35) Wang, X.-Y.; Yang, C.-T.; Zheng, D.-D.; Mo, L.-Q.; Lan, A.-P.; Yang, Z.-L.; Hu, F.;
34
35 Chen, P.-X.; Liao, X.-X.; Feng, J.-Q. Hydrogen sulphide protects H9c2 cells against
36
37 doxorubicin-induced cardiotoxicity through inhibition of endoplasmatic reticulum stress. *Mol.*
38
39 *Cell Biochem.* **2012**, *363*, 419-426.

40
41 36) Guo, R.; Lin, J.; Xu, W.; Shen, N.; Mo, L.; Zhang, C.; Feng, J. Hydrogen sulphide
42
43 attenuates doxorubicin-induced cardiotoxicity by inhibition of the p38 MAPK pathway in H9c2
44
45 cells. *Int. J. Mol. Med.* **2013**, *31*, 644-650.

46
47 37) Liu, M.-H.; Zhang, Y.; Lin, X.-L.; He, J.; Tan, T.-P.; Wu, S.-J.; Yu, S.; Chen, L.; Chen, Y.-
48
49 D.; Fu, H.-Y.; Yuan, C.; Li, J. E. Hydrogen sulphide attenuates doxorubicin-induced
50
51 cardiotoxicity by inhibiting calreticulin expression in H9c2 cells. *Mol. Med. Rep.* **2015**, *12*,
52
53 5197-5202.

54
55
56 38) Jacob, C. Perspective on recent developments on sulphur-containing agents and hydrogen
57
58 sulphide signalling. *Planta Med.* **2008**, *74*, 1580-1592.

1
2
3 39) Zhao, Y.; Biggs, T. D.; Xian, M. Hydrofen sulphide (H₂S) releasing agents: chemistry and
4 biological applications. *Chem. Commun.* **2014**, *50*, 11788-11805.
5
6

7
8 40) Kashfi, K.; Olson, K. R. Biology and therapeutic potential of hydrogen sulphide and
9 hydrogen sulphide-releasing chimeras. *Biochem. Pharmacol.* **2013**, *85*, 689-703.
10
11

12 41) Peng, H.; Cheng, Y.; Dai, C.; King, A. L.; Predmore, B. L.; Lefer, D. J.; Wang, B. A
13 fluorescent probe for fast and quantitative detection of hydrogen sulphide in blood. *Angew.*
14 *Chem.-Int. Edit.* **2011**, *50*, 9672-9675.
15
16
17

18 42) Riganti, C.; Kopecka, J.; Panada, E.; Barak, S.; Rubinstein, M. The role of C/EBP- β LIP in
19 multidrug resistance. *J. Natl. Cancer Inst.* **2015**, *107*, 46-59.
20
21
22

23 43) Riganti, C.; Gazzano, E.; Gulino, G. R.; Volante, M.; Ghigo, D.; Kopecka, J. Two repeated
24 low doses of doxorubicin are more effective than a single high dose against tumors
25 overexpressing P-glycoprotein. *Cancer Lett.* **2015**, *360*, 219-226.
26
27
28

29 44) Truong, D.; Hindmarsh, W.; O'Brien, P.J. The molecular mechanisms of diallyl disulphide
30 and diallyl sulphide induced hepatocyte cytotoxicity. *Chem.-Biol. Interact.* **2009**, *180*, 79-88.
31
32
33

34 45) Rharass, T.; Gbankoto, A.; Canal, C.; Kursunluoglu, G.; Bijoux, A.; Panakova, D.; Ribou,
35 A.-C. Oxidative stress does not play a primary role in the toxicity induced with clinical doses of
36 doxorubicin in myocardial H9c2 cells. *Mol. Cell. Biochem.* **2016**, *413*, 199-215.
37
38
39

40 46) Hattinger, C.M.; Fanelli, M.; Tavanti, E.; Vella, S.; Ferrari, S.; Picci, P.; Serra, M.
41 Advance in emerging drugs for osteosarcoma. *Expert Opin Emerg. Drugs.* **2015**, *28*, 1-20.
42
43
44

45 47) Baldini, N.; Scotlandi, K.; Barbanti-Bròdano, G.; Manara, M. C.; Maurici, D.; Bacci, G.;
46 Bertoni, F.; Picci, P.; Sottili, S.; Campanacci, M.; Serra, M. Expression of P-glycoprotein in
47 high-grade osteosarcomas in relation to clinical outcome. *N. Engl. J. Med.* **1995**, *333*, 1380-
48 1385.
49
50
51
52

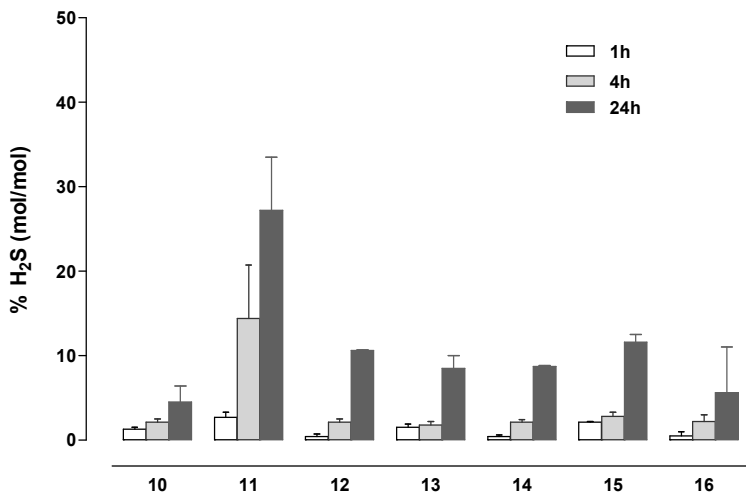
53 48) Fanelli, M.; Hattinger, C.M.; Vella, S.; Tavanti, E.; Michelacci, F.; Gudeman, B.; Barnett,
54 D.; Picci, P.; Serra, M. Targeting ABCB1 and ABCC1 with their specific inhibitor CBT-1® can
55 overcome drug resistance in osteosarcoma. *Curr. Cancer Drug Targets*, **2016**, *16*, 261-274.
56
57
58
59
60

1
2
3 49) Apetoh, L.; Mignot, G.; Panaretakis, T.; Kroemer, G.; Zitvogel, L. Immunogenicity of
4 anthracyclines: moving towards more personalized medicine. *Trends Mol. Med.* **2008**, *14*, 141–
5 151.
6
7

8
9 50) Serra, M.; Scotlandi, K.; Manara, M. C.; Maurici, D.; Lollini, P. L.; De Giovanni, C.;
10 Toffoli, G.; Baldini, N. Establishment and characterization of multidrug-resistant human
11 osteosarcoma cell lines. *Anticancer Res.* **1993**, *13*, 323-329.
12
13

14
15 51) Kopecka, J.; Salzano, G.; Campia, I.; Lusa, S.; Ghigo, D.; De Rosa, G.; Riganti, C. Insights
16 in the chemical components of liposomes responsible for P-glycoprotein inhibition.
17
18
19 *Nanomedicine* **2014**, *10*, 77-87.
20
21
22
23
24
25
26
27
28
29
30
31
32
33
34
35
36
37
38
39
40
41
42
43
44
45
46
47
48
49
50
51
52
53
54
55
56
57
58
59
60

Figure 1. H₂S release assessment from the H₂S-DOXOs at 1, 4 and 24 hours incubation time in DMEM. Data are presented as mean \pm SEM (SEM \leq 3; number of determinations = 3-5).



1
2
3
4 **Figure 2.** Intracellular accumulation and cytotoxicity of H₂S-DOXOs in cardiomyocytes. H9c2
5
6 cardiomyocytes were incubated for 24 h in fresh medium (CTRL) or in medium containing 5 μM
7
8 doxorubicin (DOXO) or H₂S-DOXOs (**10-16**). **A.** The amount of intracellular DOXOs was
9
10 measured fluorimetrically in cell lysates in duplicate (n = 3). Data are presented as means ± SD.
11
12 *Vs* DOXO: * p < 0.002. **B.** The release of extracellular LDH in the culture medium was
13
14 measured spectrophotometrically in duplicate (n = 3). *Vs* CTRL: * p < 0.001; *vs* DOXO: ° p <
15
16 0.05.
17
18
19
20

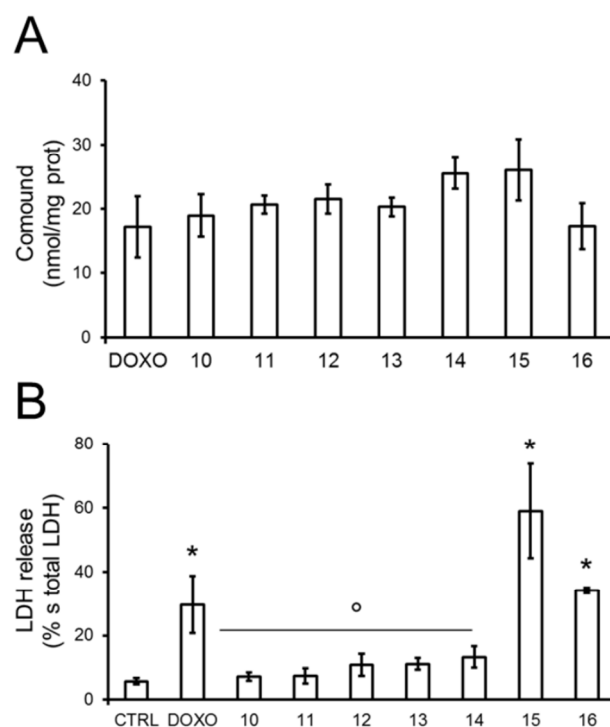


Figure 3. Intracellular ROS and cytotoxicity of H₂S-DOXOs in cardiomyocytes treated with the H₂S scavenger hydroxocobalamin. H9c2 cardiomyocytes were incubated for 24 h in fresh medium (CTRL) or in medium containing 5 μM DOXO or H₂S- DOXOs (**10-16**), in the absence (-) or in the presence (+) of 100 μM OHCbl, chosen as H₂S scavenger. **A.** The amount of intracellular ROS was measured fluorimetrically in cell lysates in duplicate (n = 3). Data are presented as means ± SD. *Vs* respective CTRL: * p < 0.01; vs DOXO: ° p < 0.002; - OHCbl *vs* + OHCbl: p < 0.01 for all compounds (not shown). **B.** The release of extracellular LDH in the culture medium was measured spectrophotometrically in duplicate (n = 3). *Vs* respective CTRL: * p < 0.05; vs DOXO: ° p < 0.05; - OHCbl *vs* + OHCbl: p < 0.05 for all compounds (not shown).

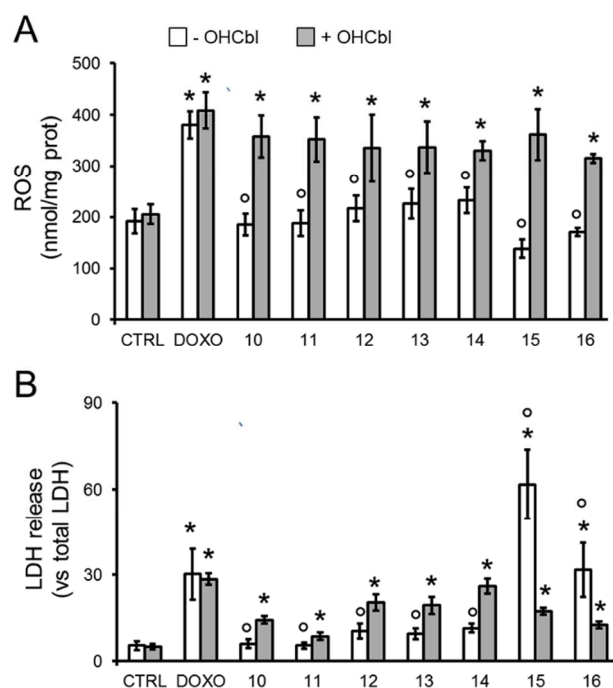


Figure 4. Intracellular accumulation and cytotoxicity of H₂S-DOXOs in osteosarcoma cells. Doxorubicin-sensitive U-2OS cells and the doxorubicin-resistant variants (U-2OS/DX30, U-2OS/DX100, U-2OS/DX580) were incubated for 24 h in fresh medium (CTRL) or in medium containing 5 μM DOXO or H₂S-DOXOs (**10-16**). **A.** The amount of intracellular DOXOs was measured fluorimetrically in cell lysates in duplicate (n = 3). Data are presented as means ± SD. For DOXO, resistant cells vs U-2OS cells: * p < 0.05; for all compounds, vs DOXO: * p < 0.05. **B.** Release of extracellular LDH into the culture medium was measured spectrophotometrically in duplicate (n = 3). Data are presented as means ± SD. Vs respective CTRL: * p < 0.01; vs DOXO: ° p < 0.05.

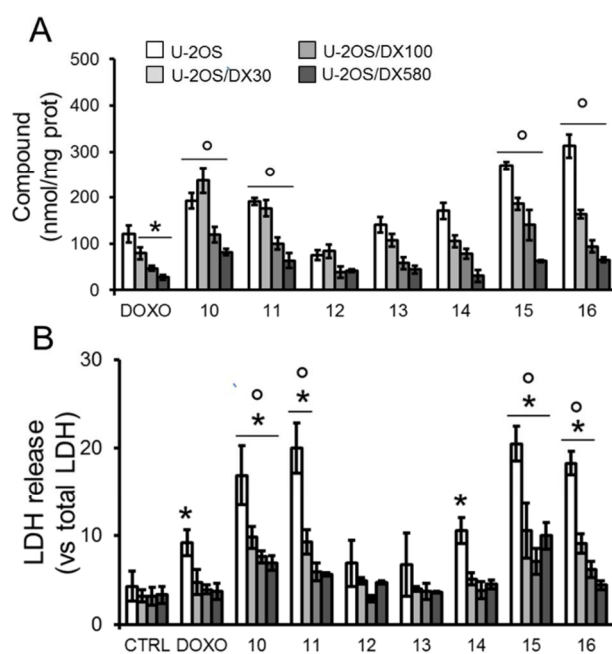


Figure 5. Intracellular ROS and cytotoxicity of H₂S-DOXOs in osteosarcoma cells treated with OHCbl. Doxorubicin-sensitive U-2OS cells and the doxorubicin-resistant variants (U-2OS/DX30, U-2OS/DX100, U-2OS/DX580) were incubated for 24 h in fresh medium (CTRL) or in medium containing 5 μM DOXO or H₂S-DOXOs (**10-16**), in the absence (-) or in the presence (+) of 100 μM OHCbl. **A-B.** The amount of intracellular ROS was measured fluorimetrically in cell lysates in duplicate (n = 3). Data are presented as means ± SD. For panel **A:** vs respective CTRL: * p < 0.001; vs DOXO: ° p < 0.05. For panel **B:** vs respective CTRL: * p < 0.001; - OHCbl vs + OHCbl: p < 0.001.

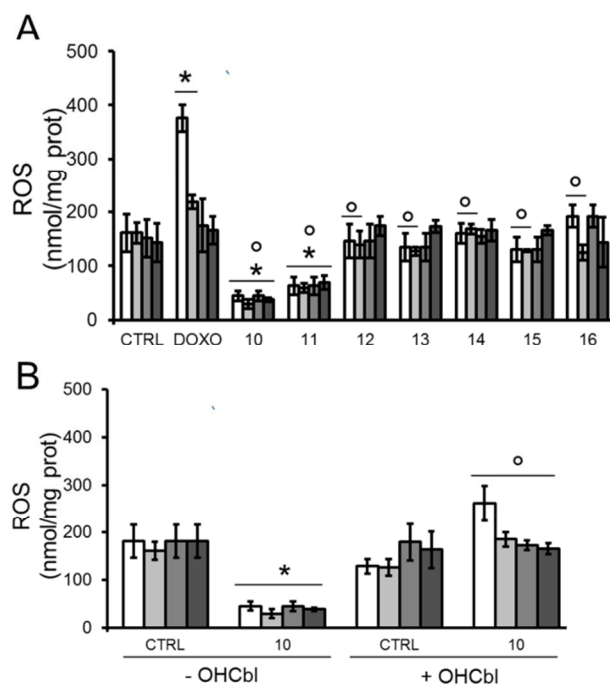
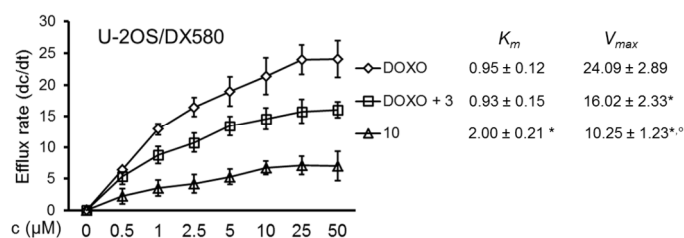
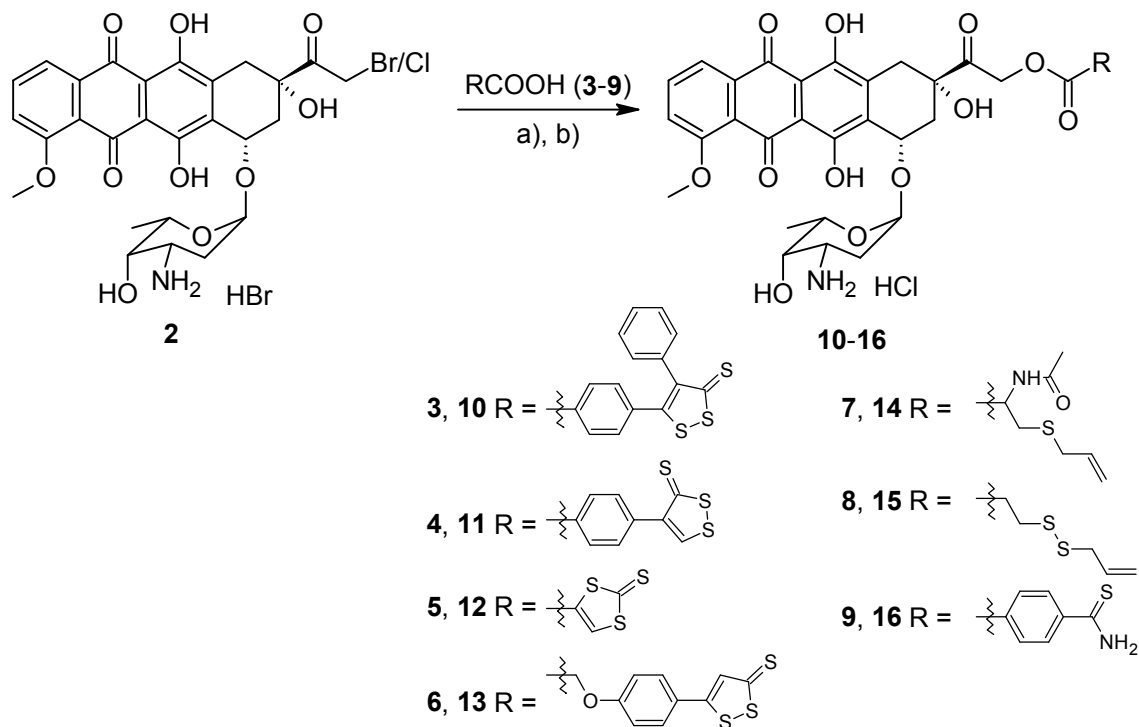


Figure 6. Efflux kinetics of DOXO, DOXO + **3** and **10**, from drug-resistant osteosarcoma cells.

Doxorubicin-resistant U-2OS/DX580 cells were incubated for 20 min with increasing concentrations (0-50 μM) of DOXO, DOXO with the H₂S-releasing compound **3**, or the H₂S-DOXO **10**. Cells were washed and tested fluorimetrically for their intracellular drug content. The procedure was repeated on a second series of dishes, incubated in the same experimental conditions and analyzed after 10 min. Data are presented as means \pm SD (n = 3). The rate of DOXOs efflux (dc/dt) was plotted versus the initial concentration of the drug. V_{max} (nmol/min/mg proteins) and K_m (nmol/mg proteins) were calculated with the Enzfitter software. DOXO + **3** vs DOXO: p \leq 0.001, for concentrations 1-50 μM ; **10** vs DOXO: p \leq 0.001, for concentrations 0.5-50 μM ; **10** vs DOXO + **3**: p \leq 0.01, concentrations 0.5-50 μM (not shown). For K_m , vs DOXO: * p 0.01; for V_{max} , vs DOXO: * p < 0.001; vs DOXO + **3**: ° p < 0.05.



Scheme 1.^a

a) Reagents and conditions: a) KF, DMF, rt; b) dry THF, HCl in dry dioxane.

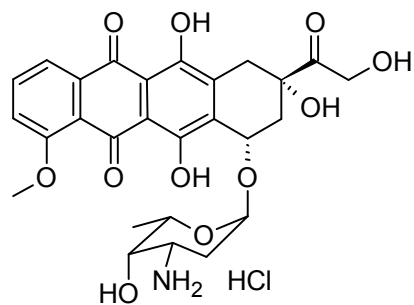


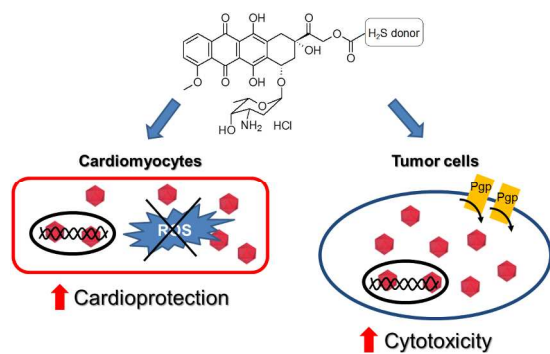
Chart 1. Doxorubicin (DOXO).

Table 1. Stability ($t_{1/2}$) of H₂S-DOXOs in cell culture medium (DMEM) and in human serum.

Data derived from 3-5 independent experiments.

Compound	DMEM	Human serum
	$t_{1/2}$	$t_{1/2}$
10	> 24 h	2.8 h
11	21.5 h	4.6 h
12	17 min	17 min
13	16 min	3 min
14	< 1 min	11 min
15	5.6 h	3.8 h
16	3.4 h	38 min

Table of Contents graphic.



Supporting Information

H₂S-Donating Doxorubicins may overcome Cardiotoxicity and Multidrug Resistance

*Konstantin Chegaev,[§] Barbara Rolando,[§] Daniela Cortese,[§] Elena Gazzano,[#] Ilaria Buondonno,[#]
Loretta Lazzarato,[§] Marilù Fanelli,[†] Claudia M. Hattinger,[†] Massimo Serra,[†] Chiara Riganti,^{#,*} Roberta
Fruttero,^{§,*} Dario Ghigo,[#] Alberto Gasco.[§]*

[§]Department of Science and Drug Technology, University of Torino, via Pietro Giuria 9, 10125, Torino,
Italy

[#]Department of Oncology and Center for Experimental Research and Medical Studies (CeRMS),
University of Torino, via Santena, 5/bis, 10126, Torino, Italy

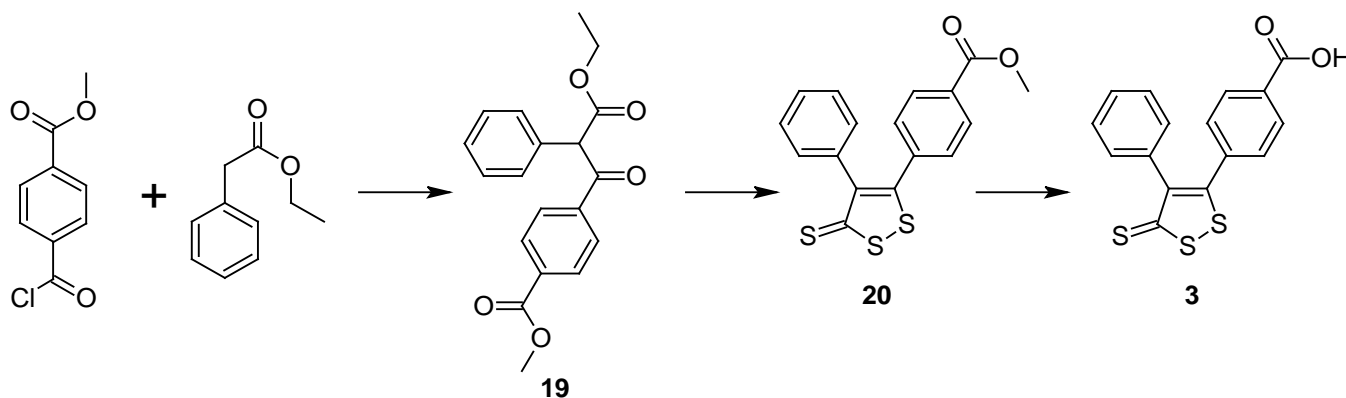
[†]Orthopaedic Rizzoli Institute, Laboratory of Experimental Oncology, Pharmacogenomics and
Pharmacogenetics Research Unit, via G. C. Pupilli 1, 40136, Bologna, Italy

- Table of contents (total of 55 pages),	page S1
- Supplementary experimental section,	pages S2-S8
- Supplementary Table,	page S9
- Supplementary Figures,	pages S10-S15
- Supplementary References,	pages S16-S17
- ¹H-NMR spectra,	pages S18-S37
- ¹³C-NMR spectra of compounds,	pages S38-S47
- HPLC chromatograms of compounds 10-16,	pages S48-S51
- Degradation profile of compounds 10-16 in human serum,	pages S52-S55

Supplementary experimental section

^1H and ^{13}C NMR spectra were recorded on a BrukerAvance 300, at 300 and 75 MHz, respectively, using SiMe_4 as internal standard. The following abbreviations indicate peak multiplicity: s = singlet, d = doublet, t = triplet, m = multiplet, bs = broad singlet. ESI spectra were recorded on Micromass Quattro API micro (Waters Corporation, Milford, MA, USA) mass spectrometer. Data were processed using a MassLynxSystem (Waters). Melting points were determined with a capillary apparatus (Büchi 540) in open capillary. Flash column chromatography was performed on silica gel (Merck Kieselgel 60, 230–400 mesh ASTM). The progress of the reactions was followed by thin-layer chromatography (TLC) on 5×20 cm plates Merck Kieselgel 60 F₂₅₄, with a layer thickness of 0.20 mm. Anhydrous sodium sulfate (Na_2SO_4) was used as drying agent for the organic phases. Organic solvents were removed under reduced pressure at 30°C . Synthetic-purity solvents ethyl acetate (EtOAc), acetone, hexane, dichloromethane (DCM), acetonitrile (CH_3CN), methanol (MeOH), diethyl ether (Et_2O), dimethylformamide (DMF) and 40–60 petroleum ether (PE) were used. Dry tetrahydrofuran (THF), was distilled immediately before use from Na and benzophenone under positive N_2 pressure. Dry DMF was obtained through storage on molecular sieves 4Å. Commercial starting materials were purchased from Sigma-Aldrich, Alfa Aesar, and TCI Europe. Compounds **2**,¹ **4**,² **5**,³ **8**² and **21**⁴ were prepared as described elsewhere.

4-(4-Phenyl-3-thioxo-3H-1,2-dithiol-5-yl)benzoic acid (**3**)



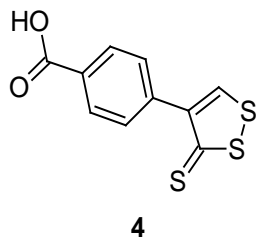
Methyl 4-(3-ethoxy-3-oxo-2-phenylpropanoyl)benzoate (19). To the solution of ethyl phenylacetate (4.64 g, 28.4 mmol) in dry THF (57 mL), 57 mL of 1.0 M LiHMDS solution in THF were added dropwise at -70°C (dry-ice/acetone bath). Then the solution of methyl 4-(chlorocarbonyl)benzoate (6.1 g, 28.4 mmol) in THF (50 mL) was added dropwise and the reaction was stirred at -70°C for 15 min. The cooling bath was removed and the reaction was allowed to reach 0°C. Then NH₄Cl sat. sol. (20 mL) was added and the solution was concentrated to the volume of 40 mL approx. Afterwards H₂O (20 mL) were added and the product was extracted with EtOAc (3 × 20 mL). The organic extracts were washed with brine and dried and evaporated. Obtained oil was purified by flash chromatography (eluent gradient from 95/5 to 90/10 PE/acetone) to give the title compound as a white solid. Analytically pure sample was obtained by the crystallization from *i*-Pr₂O. Yield 88%, m.p. 69-71°C (*i*-Pr₂O). The compound exists as a mixture of keto- and eno- tautomers: ¹H-NMR (CDCl₃) δ ppm: 1.22-1.30 (t, 3H, CH₂CH₃), 3.88 (s, COOCH₃ eno), 3.94 (s, COOCH₃, keto) (3H), 4.17-4.35 (m, 2H, CH₂), 5.61 (s, CH keto), 7.05-7.45 (m, C₆H₅ + 2CH of C₆H₄, eno), 7.83 (d, 2CH of C₆H₄, eno), 8.01 (d, 2CH of C₆H₄, keto), 8.09 (d, 2CH of C₆H₄, keto) (9H), 13.62 (s, OH eno). ¹³C-NMR (CDCl₃) δ ppm: 14.2, 14.3, 52.3, 52.6, 61.0, 61.5, 62.0, 105.6, 127.2, 128.2, 128.4, 128.9, 128.9, 129.1, 129.4, 129.7, 130.0, 130.8, 132.0, 132.6, 134.3, 134.5, 139.0, 139.4, 166.1, 166.6, 168.6, 169.8, 173.3, 193.0. MS (ESI⁺) *m/z* 327 [M+H]⁺.

Methyl 4-(4-phenyl-3-thioxo-3H-1,2-dithiol-5-yl)benzoate (20). To the solution of **19** (3.82 g, 11.71 mmol) in toluene (40 mL), P₂S₅ 7.80 g (35.1 mmol) was added and reaction was heated at reflux overnight. Next day the reaction was cooled down to room temperature and a 10% solution of NH₃ was added until all the precipitate was solubilized. H₂O (20 mL) was then added and obtained mixture was extracted with EtOAc (3 × 20 mL). The organic extracts were joined together, washed with brine, dried and the organic solvent was evaporated. Obtained brown oil was only partially purified by flash chromatography (eluent 30/70 CH₂Cl₂/PE) to give a brown oil that became a brown foam during desiccation. ¹H-NMR (CDCl₃) δ ppm: 3.90 (s, 3H, CH₃), 7.05-7.15 (m, 2H, 2CH), 7.28-7.36 (m, 5H,

5CH), 7.95 (d, 2H, 2CH) ($C_6H_5 + C_6H_4$); ^{13}C -NMR ($CDCl_3$) δ ppm: 52.6, 128.8, 128.8, 129.1, 130.2, 130.9, 132.0, 133.8, 137.5, 146.4, 166.1, 168.7, 215.0. MS (ESI⁺) m/z 345 [M+H]⁺.

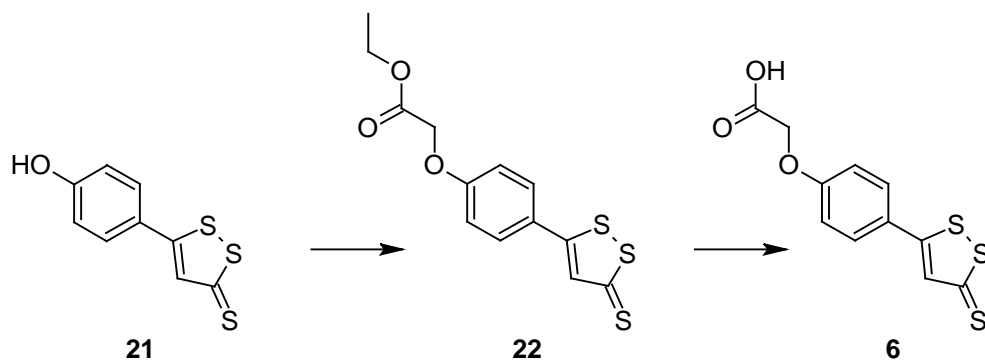
4-(4-Phenyl-3-thioxo-3H-1,2-dithiol-5-yl)benzoic acid (3). The solution of **20** in dioxane (20 mL) and HCl 6 N (20 mL) was heated at reflux overnight. The mixture was cooled down to room temperature and the precipitate was filtered off. The solid was dissolved in EtOAc (45 mL) and washed with H₂O (20 mL). The organic extracts was washed with brine, dried and evaporated. The crude product was crystallized twice from toluene to give the title compound as dark red crystals. The compound crystallized from toluene as a solvate ($\cdot 1/3 C_7H_8$). Yield 47% (for two steps), mp 220-222°C dec. (C_7H_8). Analytically pure sample was obtained by crystallization from $ClCH_2CH_2Cl$. 1H -NMR (DMSO-*d*₆) δ ppm: 7.07-7.14 (m, 2H, 2CH), 7.27-7.35 (m, 3H, 3CH), 7.42 (d, 2H, 2CH), 7.87 (d, 2H, 2CH) ($C_6H_5 + C_6H_4$); ^{13}C -NMR (DMSO-*d*₆) δ ppm: 128.3 (2 peaks), 129.3, 129.7, 130.8, 132.4, 133.9, 136.8, 146.2, 166.5, 170.1, 214.7. MS (ESI) m/z 329 [M-H]⁻.

4-(3-Thioxo-3H-1,2-dithiol-4-yl)benzoic acid (4).



M.p. 255-256°C dec. 1H -NMR (DMSO-*d*₆) δ ppm: 7.63-7.78 (m, 2H), 7.95-8.02 (m, 2H) (C_6H_4), 9.25 (s, 1H, CHS), 13.07 (br.s., 1H, OH). ^{13}C -NMR (DMSO-*d*₆) δ ppm: 129.1, 129.2, 130.6, 137.8, 147.0, 160.3, 167.0, 213.5. MS (ES⁻) m/z 253.2 [M-H]⁻.

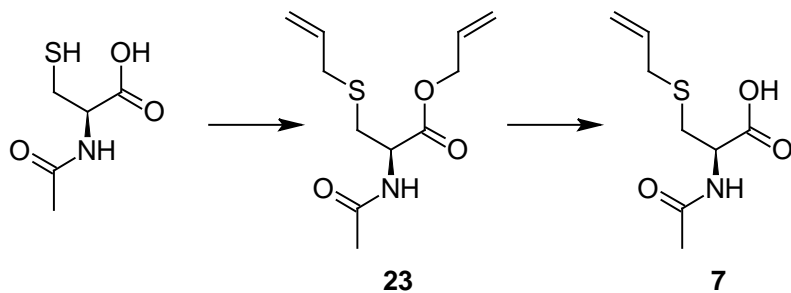
[4-(3-Thioxo-3H-1,2-dithiol-5-yl)phenoxy]acetic acid (6).



Ethyl [4-(3-thioxo-3H-1,2-dithiol-5-yl)phenoxy]acetate (22). To the solution of PPh_3 (470 mg, 1.79 mmol) in dry THF (15 mL) diisopropylazodicarboxylate (335 μL ; 346 mg, 1.80 mmol) was added in one portion at -15°C and reaction was stirred for 30 min (abundant white precipitated formed after 10-15 min of stirring). Then **21** (340 mg, 1.50 mmol) was added followed by ethyl glycolate (170 μL , 188 mg, 1.80 mmol). The ice-salt bath was removed and the reaction was stirred at room temperature overnight. The mixture was diluted with EtOAc, organic phase was washed with water, brine, dried and evaporated. Obtained oil was purified by flash chromatography (eluent 90/10 PE/Acetone) to give **22** as a red solid. Yield 56 %, mp $99\text{-}100^\circ\text{C}$. $^1\text{H-NMR}$ (CDCl_3) δ ppm: 1.30 (t, 3H, CH_3), 4.28 (q, 2H, CH_2CH_3), 4.69 (s, 2H, OCH_2COO), 6.97 (d, 2H, 2CH Ar), 7.37 (s, 1H, $\text{C}=\text{CH}$), 7.61 (d, 2H, 2CH Ar); $^{13}\text{C-NMR}$ (CDCl_3) δ ppm: 14.3, 61.8, 65.3, 115.7, 125.2, 128.8, 135.0, 161.1, 168.2, 172.8, 215.0. MS (ES^+) m/z 313 $[\text{M}+\text{H}]^+$.

[4-(3-Thioxo-3H-1,2-dithiol-5-yl)phenoxy]acetic acid (6). To the solution of **22** (0,90 g, 2.88 mmol) in dioxane (15 mL), HCl 37% (5 mL) was added and the reaction was heated at reflux overnight. Next day the reaction was cooled to the rt and H_2O (40 mL) was added. The precipitate was filtered off, washed with water and dried. The red solid obtained was crystallized from MeOH to give **6** as a brown solid. Yield 63 %, mp $230\text{-}233^\circ\text{C}$ dec. (MeOH). $^1\text{H-NMR}$ ($\text{DMSO-}d_6$) δ ppm: 4.82 (s, 2H, CH_2), 7.06 (d, 2H, 2CH Ar), 7.77 (s, 1H, $\text{C}=\text{CH}$), 7.87 (d, 2H, 2CH Ar), 13.11 (br. s, 1H, COOH); $^{13}\text{C-NMR}$ ($\text{DMSO-}d_6$) δ ppm: 48.6, 64.6, 115.6, 124.1, 129.0, 134.4, 161.2, 169.8, 173.7, 214.9. MS (ES^-) m/z 283 $[\text{M}-\text{H}]^-$.

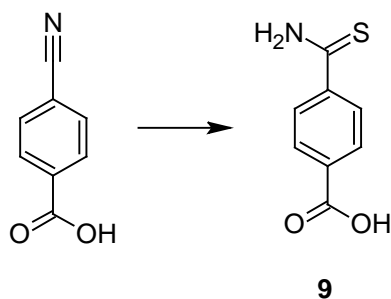
(2R)-2-(Acetylamino)-3-(prop-2-en-1-ylsulfanyl)propanoic acid (7)



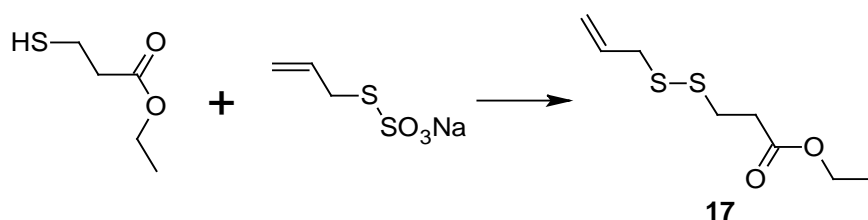
Prop-2-en-1-yl (2R)-2-(acetylamino)-3-(prop-2-en-1-ylsulfanyl)propanoate (21). To the solution of PPh_3 (3.9 g, 14.9 mmol) in dry THF (30 mL) diisopropylazodicarboxylate (3.0 mL, 3.10 g, 15.3 mmol) was added in one portion at -15°C and reaction was stirred for 30 min (abundant white precipitated formed after 10-15 min of stirring). Then N-acetyl-L-cysteine (1.0 g, 6.10 mmol) was added followed by the allyl alcohol (1.05 mL, 890 mg, 15.3 mmol). The ice-salt bath was removed and the reaction was stirred at room temperature overnight. Solvent was evaporated and the crude was purified by flash chromatography (eluent gradient from 30/70 to 40/60 PE / AcOEt) to give **23** as a yellow oil. Yield 47%. $^1\text{H-NMR}$ (DMSO-*d*₆) δ ppm: 1.86 (s, 3H, OCCH_3), 2.61-2.74 (m, 1H), 2.75-2.88 (m, 1H, CH_2CHCOO), 3.16 (d, 2H, $\text{SCH}_2\text{CH}=\text{CH}_2$), 4.38-4.51 (m, 1H, CHCOO), 4.59 (d, 2H, $\text{OCH}_2\text{CH}=\text{CH}_2$), 4.97-5.39 (m, 4H, $\text{SCH}_2\text{CH}=\text{CH}_2 + \text{OCH}_2\text{CH}=\text{CH}_2$), 5.65-5.81 (m, 1H, $\text{SCH}_2\text{CH}=\text{CH}_2$), 5.82-5.98 (m, 1H, $\text{OCH}_2\text{CH}=\text{CH}_2$), 8.42 (d, 1H, NH); $^{13}\text{C-NMR}$ (DMSO-*d*₆) δ ppm: 22.3, 31.2, 34.0, 51.8, 65.0, 117.6, 117.7, 132.3, 134.1, 169.4, 170.5. MS (ESI⁺) m/z 236 $[\text{M}+\text{H}]^+$.

(2R)-2-(Acetylamino)-3-(prop-2-en-1-ylsulfanyl)propanoic acid (7). To the solution of **23** (680 mg, 2.80 mmol) in dry THF (70 mL) a 0.1 M solution of LiOH (56 mL) was added at 0°C . The ice bath was removed and reaction was stirred at rt for 1h. The HCl 1 M (6 mL) was added and the solution was concentrated, then brine (20 mL) was added and the product was extracted with EtOAc (3×30 mL). The organic phase was dried and evaporated. Obtained solid was crystallized from toluene to give the title compound as a white solid. Yield 80%, mp $121\text{-}123^\circ\text{C}$ (C_7H_8). $[\alpha]_{\text{D}}^{21} = -27.920^\circ \pm 0.036^\circ$ (MeOH, $c = 1.0$); lit.⁵ $[\alpha]_{\text{D}}^{21} = -34.0^\circ$ (MeOH, $c = 1.0$). $^1\text{H-NMR}$ (CDCl_3) δ ppm: 2.10 (s, 3H, CH_3), 2.86-3.05 (m, 2H, CH_2CHCOOH), 3.14 (d, 2H, $\text{SCH}_2\text{CH}=\text{CH}_2$), 4.71-4.81 (m, 1H, CHCOOH), 5.08-5.18 (m, 2H,

CH=CH₂), 5.65-5.82 (m, 1H, CH=CH₂), 6.84 (d, 1H, NH), 10.48 (br. s, 1H, COOH). ¹³C-NMR (CDCl₃) δ ppm: 22.9, 32.3, 35.3, 52.1, 118.3, 133.6, 172, 1, 173.5. MS (ES⁻) *m/z* 202 [M-H]⁻.

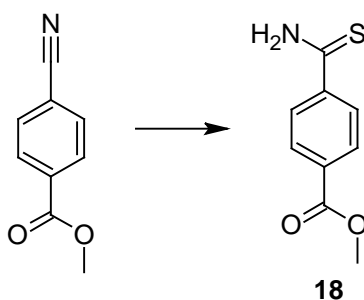


4-Carbamothioylbenzoic acid (9). A solution of P₄S₁₀ (1.5 g, 6.79 mmol) in EtOH (10 mL) was stirred for 1 h at rt. After that 4-cyanobenzoic acid (500 mg, 3.40 mmol) was added in one portion and the resulting mixture was heated under reflux for 5 h. Reaction mixture was poured into ice-water and the precipitated was filtered off. Obtained solid was crystallised from EtOH to give the title compound as a yellow solid. Yield 61%; mp 256-257°C (dec. EtOH), lit. mp 296-298°C (dec.)⁶; 238-240°C (MeOH)⁷. ¹H-NMR (DMSO-*d*₆) δ ppm: 7.89-7.99 (m, 4H, C₆H₄), 9.65 (s, 1H), 10.04 (s, 1H) (NH₂), 13.18 (br.s., 1H, COOH). ¹³C-NMR (DMSO-*d*₆) δ ppm: 127.4, 129.0, 132.7, 143.3, 166.8, 199.6. MS (ES⁻) *m/z* 180 [M-H]⁻.



Ethyl 3-(allyldisulfanyl)propanoate (17). To a solution of sodium S-allyl sulfathioate (3.12 g, 17.7 mmol) in MeOH (20 mL), ethyl 3-mercaptopropanoate (2.00 mL, 2.08 g, 15.4 mmol) followed by Et₃N (3.02 mL, 2.19 g, 21.6 mmol) were added and the reaction mixture was stirred at room temperature for 3h. Reaction was concentrated, poured into H₂O and extracted with EtOAc (3 × 30 mL). The organic phase was washed with brine, dried and solvent was removed under reduced pressure. The crude product was purified by flash chromatography (eluent: gradient from 10/90 to 50/50 CH₂Cl₂/PE) to give the title compound as a yellow oil. Yield 43%. ¹H-NMR (DMSO-*d*₆) δ ppm: 1.26 (3H, t, CH₃), 2.72

(2H, t, SCH₂CH₂), 2.92 (2H, CH₂CH₂CO), 3.32 (2H, SCH₂CH), 4.15 (2H, OCH₂CH₃), 5.11-5.25 (2H, m, CH₂=CH), 5.74-5.93 (1H, m, CH); ¹³C-NMR (DMSO-*d*₆) δ ppm: 14.27, 33.35, 34.31, 42.18, 60.78, 118.73, 133.33, 171.80. MS (CI) *m/z* 207 [M+H]⁺.



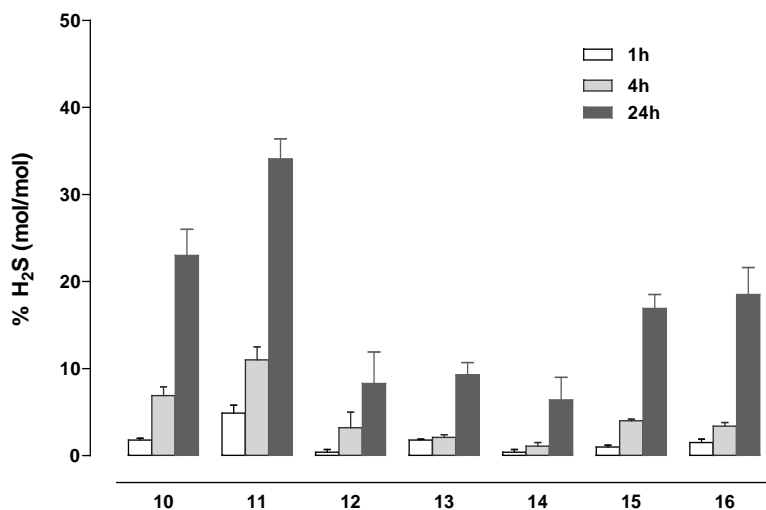
Methyl 4-carbamothioylbenzoate (18). A solution of P₂S₅ (1.4 g, 6.20 mmol) in EtOH (10 mL) was stirred for 1 h, at room temperature. After that, methyl 4-cyanobenzoate (500 mg, 3.10 mmol) was added in one portion and the resulting mixture was heated under reflux for 5 h. Reaction mixture was cooled to r.t. and the precipitated was filtered. The solid was crystallised from EtOH. A second crystallization from toluene gave the title compound as a yellow solid. Yield 51%; mp 192-193°C (C₇H₈); lit.⁸ mp 189–191°C (EtOH); lit.⁹ mp 145–147°C. ¹H-NMR (DMSO-*d*₆) δ ppm: 3.87 (3H, s, CH₃), 7.92-7.99 (4H, m, CH arom.), 9.69 (1H, s, NH₂), 10.09 (1H, s, NH₂); ¹³C-NMR (DMSO-*d*₆) δ ppm: 52.42, 127.14, 128.84, 131.38, 143.60, 165.74, 199.32. MS (CI) *m/z* 196 [M+H]⁺.

Topoisomerase II activity. The in vitro activity of topoisomerase II was measured using the Topoisomerase II Drug Screening Kit (Topogen Inc., Port Orange, FL), as previously detailed.¹⁰

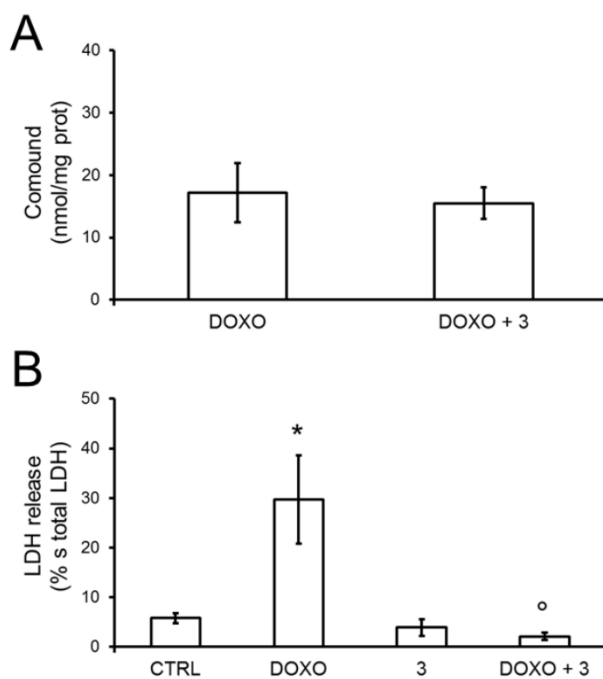
Supplementary Table 1. IC₅₀ (μM) of DOXO in osteosarcoma cells

Cell line	IC ₅₀ (μM)
U-2OS	2.50 ± 0.23
U-2OS/DX30	25.61 ± 1.16 *
U-2OS/DX100	79.66 ± 6.17 *
U-2OS/DX580	> 100 *

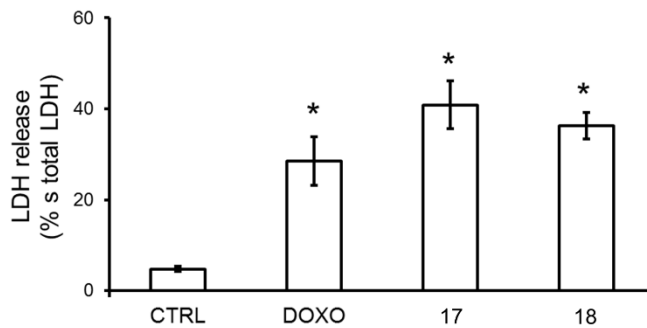
Cells were incubated for 72 h with increasing concentrations (1 nM - 1 μM) of DOXO, then stained in quadruplicate with neutral red. Data are presented as means ±SD (n = 3). Doxorubicin-resistant variants vs U-2OS cells: * p < 0.001.



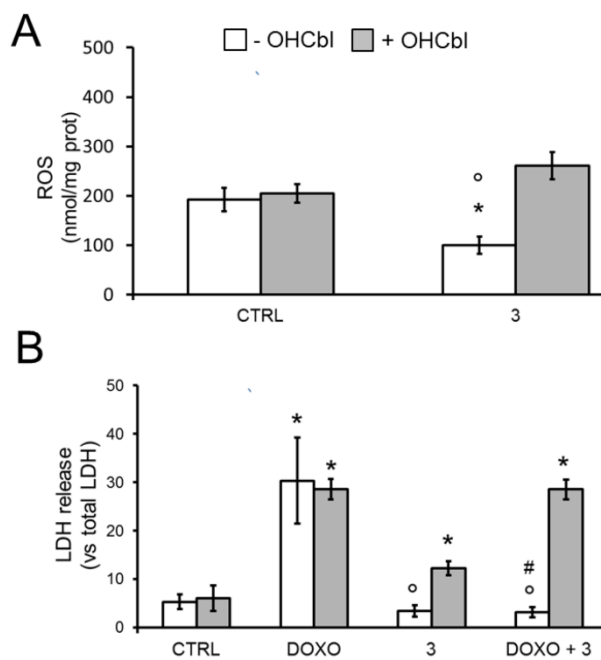
Supplementary Figure 1. H₂S release assessment from the H₂S DOXOs in human serum.



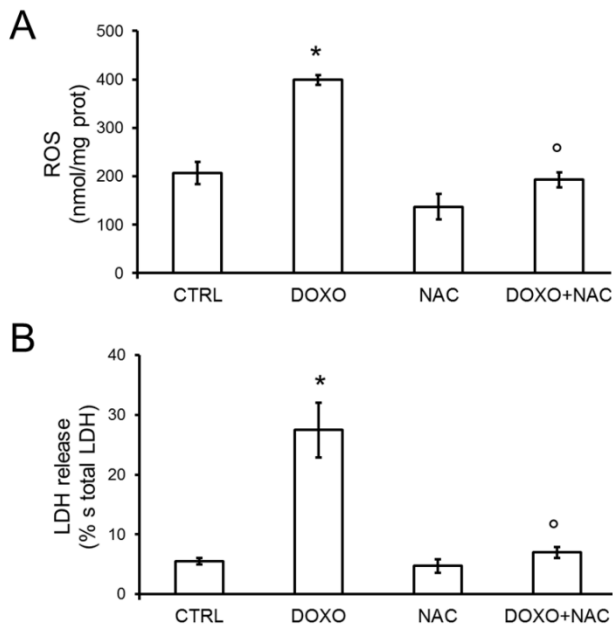
Supplementary Figure 2. Intracellular accumulation and toxicity of DOXO in the presence of 3 in cardiomyocytes. H9c2 cardiomyocytes were incubated for 24 h in fresh medium (CTRL) or in medium containing 5 μ M doxorubicin (DOXO), the H₂S-releasing compound 3 or both. **A.** The amount of intracellular DOXO was measured fluorimetrically in cell lysates in duplicate (n = 3). Data are presented as means \pm SD. **B.** The release of extracellular LDH in the culture medium was measured spectrophotometrically in duplicate (n = 3). Data are presented as means \pm SD. Vs CTRL: * p < 0.001; vs DOXO: ° p < 0.001.



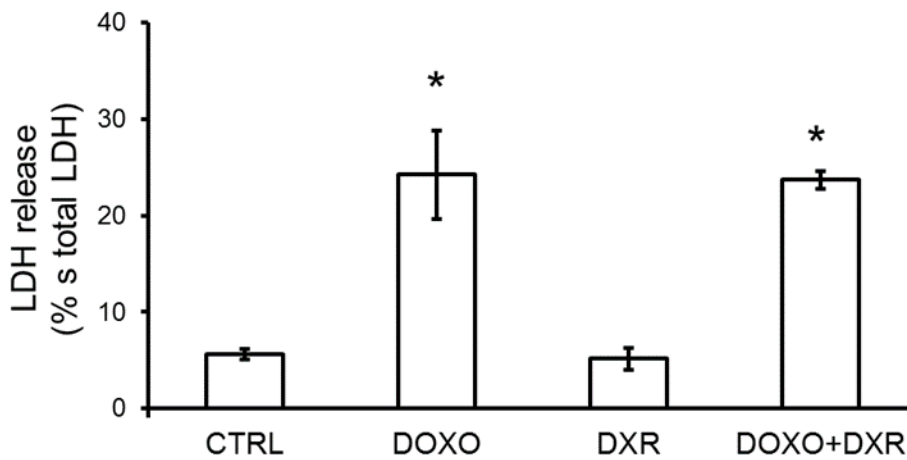
Supplementary Figure 3. Toxicity of **17** and **18** in cardiomyocytes. H9c2 cardiomyocytes were incubated for 24h in fresh medium (CTRL) or in medium containing 5 μ M doxorubicin (DOXO), **17** or **18**. The release of extracellular LDH in the culture medium was measured spectrophotometrically in duplicate (n = 3). Data are presented as means \pm SD. Vs CTRL: * p < 0.001.



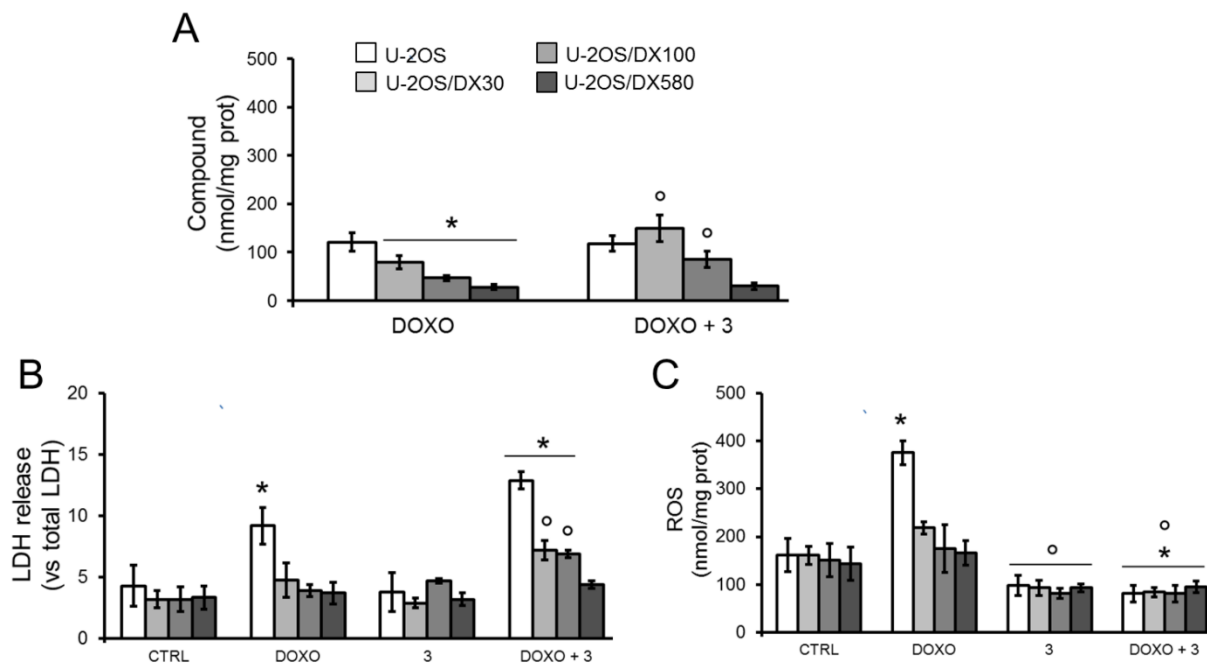
Supplementary Figure 4. Effects of **3** and HOCbl on intracellular ROS and cytotoxicity in cardiomyocytes. H9c2 cardiomyocytes were incubated for 24 h in fresh medium (CTRL) or in medium containing 5 μ M of **3**, in the absence (-) or in the presence (+) of 100 μ M HOCbl. **A.** The amount of intracellular ROS was measured fluorimetrically in cell lysates in duplicate (n= 3). Data are presented as means \pm SD. Vs CTRL: * p < 0.01; - OHCbl vs +OHCbl: \circ p < 0.005. **B.** The release of extracellular LDH in the culture medium was measured spectrophotometrically in duplicate (n = 3). Data are presented as means \pm SD. Vs CTRL * p < 0.005; -OHCbl vs +OHCbl: \circ p < 0.001; vs DOXO: # p < 0.01.



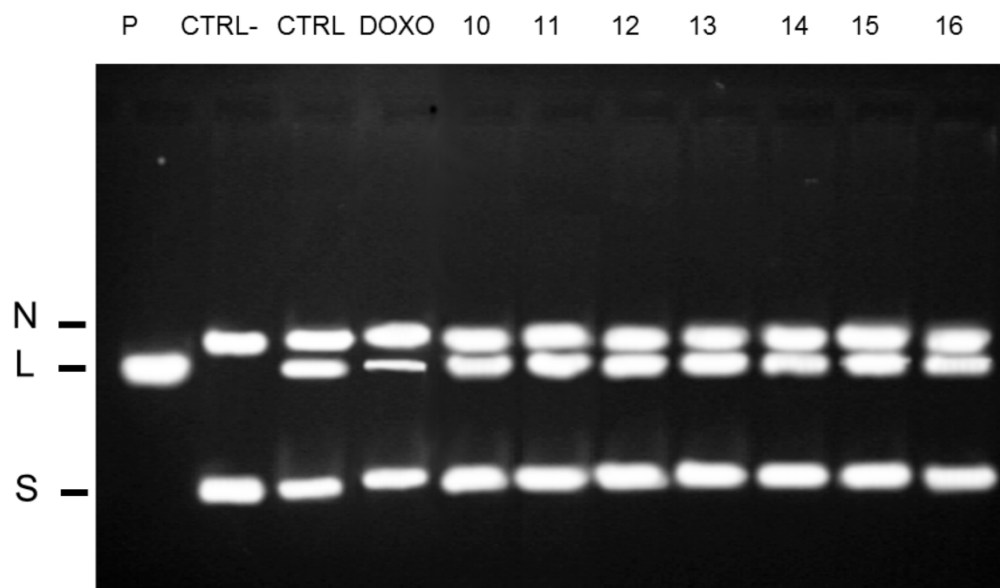
Supplementary Figure 5. Effect of N-acetyl-L-cysteine on DOXO's cardiotoxicity. H9c2 cells were incubated 24 h in fresh medium (CTRL) or in medium containing 5 μ M DOXO or 1 mM N-acetyl-L-cysteine (NAC), alone or in combination. **A.** The amount of intracellular ROS was measured fluorimetrically in cell lysates in duplicate (n = 3). Data are presented as means \pm SD. Vs CTRL: * p < 0.01; vs DOXO: ^o p < 0.002. **B.** The release of extracellular LDH in the culture medium was measured spectrophotometrically in duplicate (n = 3). Vs CTRL: * p < 0.005; vs DOXO: ^o p < 0.005.



Supplementary Figure 6. Effect of dexrazoxane on DOXO's cardiotoxicity. H9c2 cells were incubated 24 h in fresh medium (CTRL) or in medium containing 5 μ M doxorubicin (DOXO) or 50 μ M dexrazoxane (DXR), alone or in combination. The release of extracellular LDH in the culture medium was measured spectrophotometrically in duplicate (n = 3). Vs CTRL: * p < 0.005.



Supplementary Figure 7. Effects of **3** on DOXO accumulation, cytotoxicity and intracellular ROS in osteosarcoma cells. Doxorubicin-sensitive U-2OS cells and the doxorubicin-resistant variants (U-2OS/DX30, U-2OS/DX100, U-2OS/DX580) were incubated for 24h in fresh medium (CTRL) or in medium containing 5 μ M DOXO or **3**, alone or in combination. **A.** The amount of intracellular doxorubicin was measured fluorimetrically in cell lysates in duplicate (n = 3). Data are presented as means \pm SD. Resistant cells vs U-2OS cells: * p < 0.05; vs DOXO: \circ p < 0.001. **B.** The release of extracellular LDH in the culture medium was measured spectrophotometrically in duplicate (n = 3). Data are presented as means \pm SD. Vs respective CTRL: * p < 0.05; vs DOXO: \circ p < 0.05. **C.** The amount of intracellular ROS was measured fluorimetrically in cell lysates in duplicate (n = 3). Data are presented as means \pm SD. Vs respective CTRL: * p < 0.05; vs DOXO: \circ p < 0.05.



Supplementary Figure 8. Activity of purified topoisomerase II. The activity of human purified topoisomerase II was measured after incubating the enzyme with the supercoiled pHOT1 plasmid, in the absence (CTRL) or presence of 5 μ M doxorubicin (DOXO) or compounds **10-16**. The reaction products were resolved on agarose gel. Linear pHOT1 (P) was used as a marker. As a blank, supercoiled pHOT1 was incubated in the absence of topoisomerase II (CTRL-). N: nicked plasmid; L: linear plasmid; S: supercoiled plasmid

Supplementary References

- 1) Fernandez, A.-M.; Dubios, V. Method for synthesis of antracycline-peptide conjugates, WO2004/011033, **2004**.
- 2) Lee, M.; Tazzari, V.; Giustarini, D.; Rossi, R.; Sparatore, A.; Del Soldato, P.; McGeer, E.; McGeer, P.L. Effects of hydrogen sulfide-releasing L-DOPA derivatives on glial activation. *J. Biol. Chem.* **2010**, *23*, 17318-17328.
- 3) Dartigues, B.; Cambar, J.; Trebaul, C.; Brelivet J.; Guglielmetti, R. Proprietes diuretiques de derives des dithiole-thiones. Recherche d'une relation structure-activite. *Eur. J. Med. Chem.* **1980**, *15*, 405-412.
- 4) Wallace, J. L; Cirino, G.; Caliendo, G.; Sparatore, A.; Santagada, V.; Fiorucci, S. Derivatives of 4- or 5-aminosalicylic acid. WO2006125293, **2006**.
- 5) Stoll, A.; Seebeck, E. Allium compounds. I. Alliine, the true mother compound of garlic oil. *Helvetica Chimica Acta* **1948**, *31*, 189-210.
- 6) Wallace, J.L.; Cirino, G.; Santagada, V.; Caliendo, G.; Wallace, J., Salts of trimebutine and n-desmethyl trimebutine. US2007275905 (A1), **2007**.
- 7) Lamei, N.; Foroumadi, A.; Emami, S.; Amini, M.; Shafiee, A. Heterocycle-bridged and conformationally constrained retinoids: synthesis of 4-(7,8,9,10-tetrahydro-7,7,10,10-tetramethyl-4H-benzo[6,7]chromeno[4,3-d]thiazole-2-yl)benzoic acid. *Chinese J. Chem.* **2010**, *28*, 1951-1956.
- 8) Sakai, T.T.; Krishna, N.R. Synthesis and properties of some novel anti-calmodulin drugs. *Bioorg. Med. Chem.* **1999**, *7(8)*, 1559-1565.

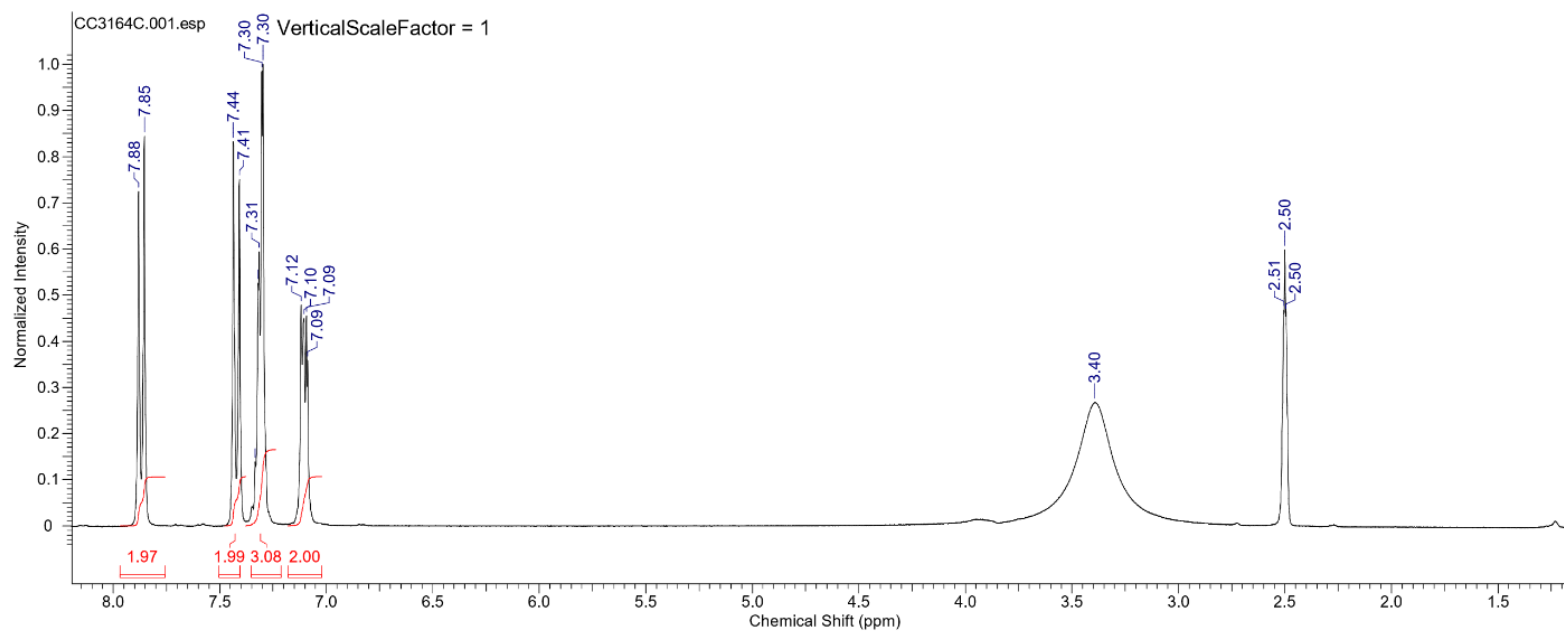
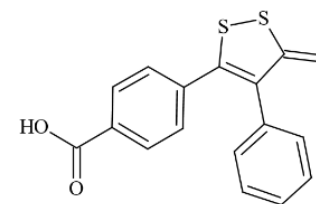
- 9) Yadav, A.K.; Srivastava, V.P.; Yadav, L.D.S. Metal-Free, One-Pot Oxidative Conversion of Aldehydes to Primary Thioamides in Aqueous Media. *Synth. Comm.* **2014**, *44*(3), 408-416.
- 10) Riganti, C.; Rolando, B.; Kopecka, J.; Campia, I.; Chegaev, K.; Lazzarato, L.; Federico, A.; Fruttero, R.; Ghigo, D. Mitochondrial-targeting nitrooxy-doxorubicin: a new approach to overcome drug resistance. *Molecular Pharmaceutics*, **2013**, *10*, 161–174.

¹H-NMR spectrum of compounds 3-23.

This report was created by ACD/NMR Processor Academic Edition. For more information go to www.acdlabs.com/nmrproc/

11/03/2016 15:11:05

Formula	C ₁₈ H ₁₀ O ₂ S ₃	FW	330.4444		
Acquisition Time (sec)	3.6438	Comment	CC3164C_1H_DMSO-d6_091014_23011_RG=100	Date	09 Oct 2014 13:12:00
Date Stamp	09 Oct 2014 13:12:00	File Name	\\NMR2\Farmaceutica 2014\data\CC\nmr\CC3164C\1\fid		
Frequency (MHz)	300.13	Nucleus	1H	Number of Transients	16
Original Points Count	16384	Owner	root	Points Count	16384
Receiver Gain	101.60	SW(cyclical) (Hz)	4496.40	Solvent	CHLOROFORM-d
Spectrum Offset (Hz)	1949.2102	Spectrum Type	STANDARD	Sweep Width (Hz)	4496.13
				Temperature (degree C)	22.360

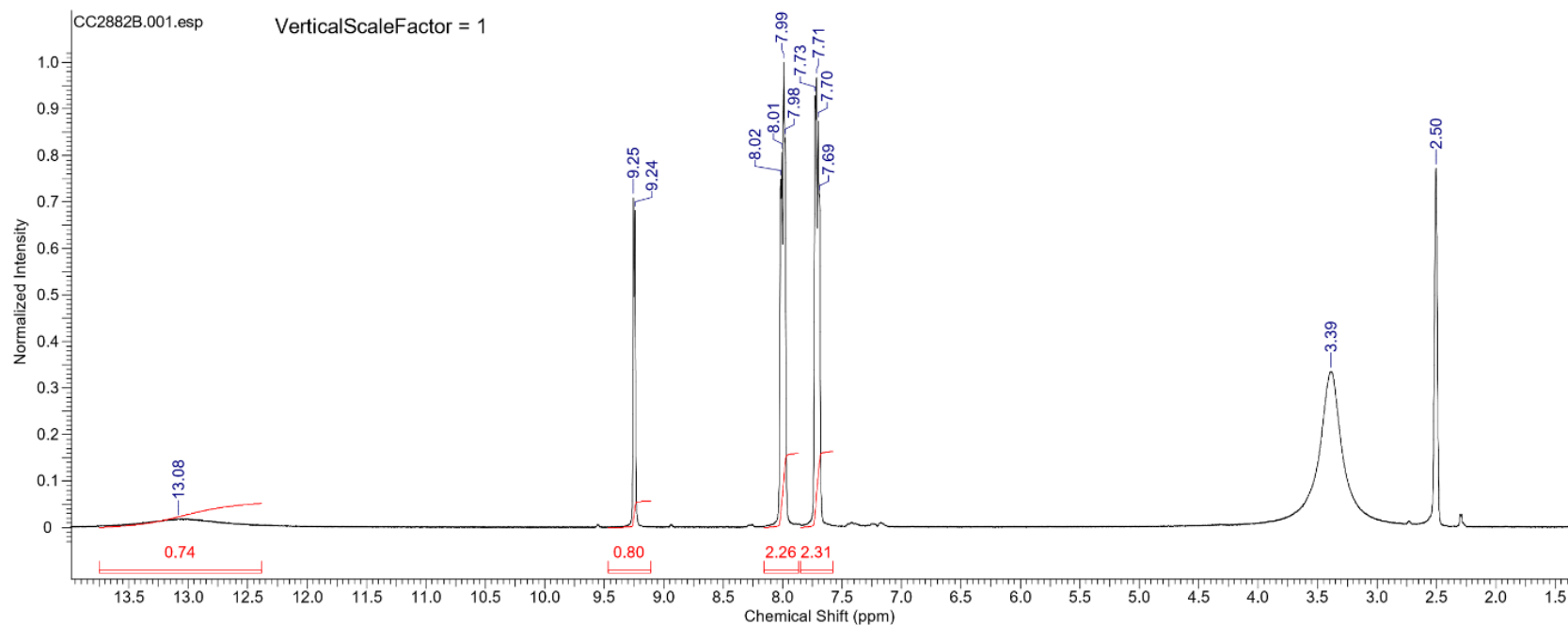
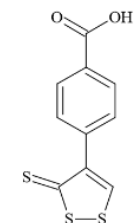


This report was created by ACD/NMR Processor Academic Edition. For more information go to www.acdlabs.com/nmrproc/

10/03/2016 11:24:07

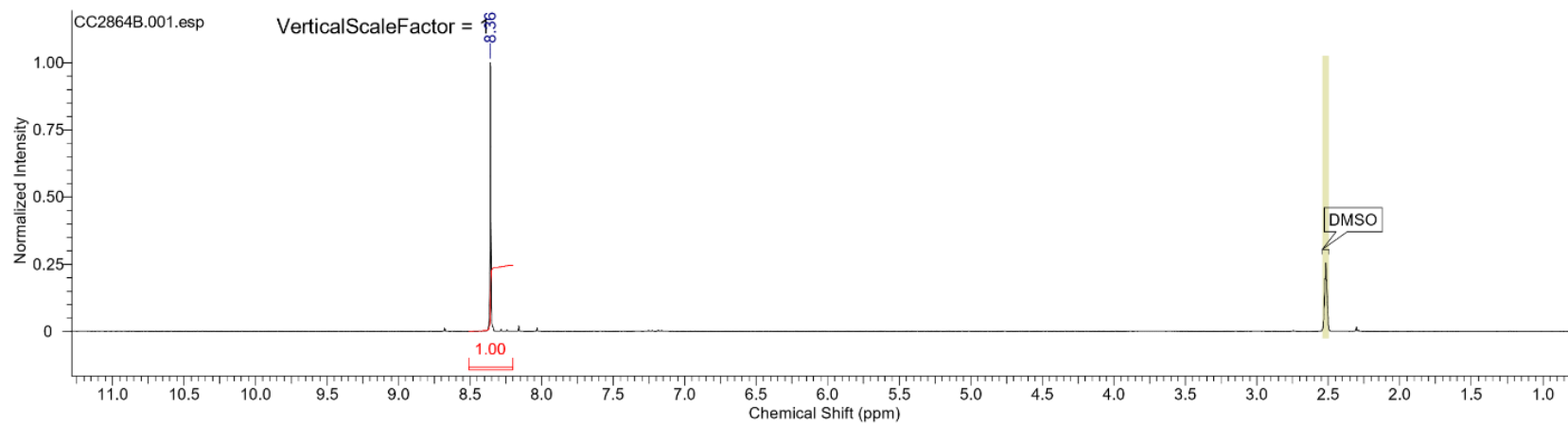
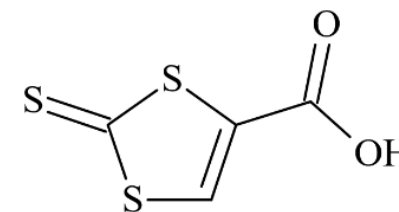
Formula C₁₀H₈O₂S₃ FW 254.3484

Acquisition Time (sec)	2.7329	Comment	CC2882B_H_DMSO-d6_040413_21553_RG=161	Date	04 Apr 2013 08:30:24
Date Stamp	04 Apr 2013 08:30:24	File Name	\NMR2\Farmaceutica 2013\data\CC\nmr\CC2882B\1\fid		
Frequency (MHz)	300.13	Nucleus	1H	Number of Transients	32
Original Points Count	16384	Owner	root	Points Count	16384
Receiver Gain	161.30	SW(cyclical) (Hz)	5995.20	Solvent	CHLOROFORM-d
Spectrum Offset (Hz)	1951.4429	Spectrum Type	STANDARD	Sweep Width (Hz)	5994.84
				Temperature (degree C)	21.760



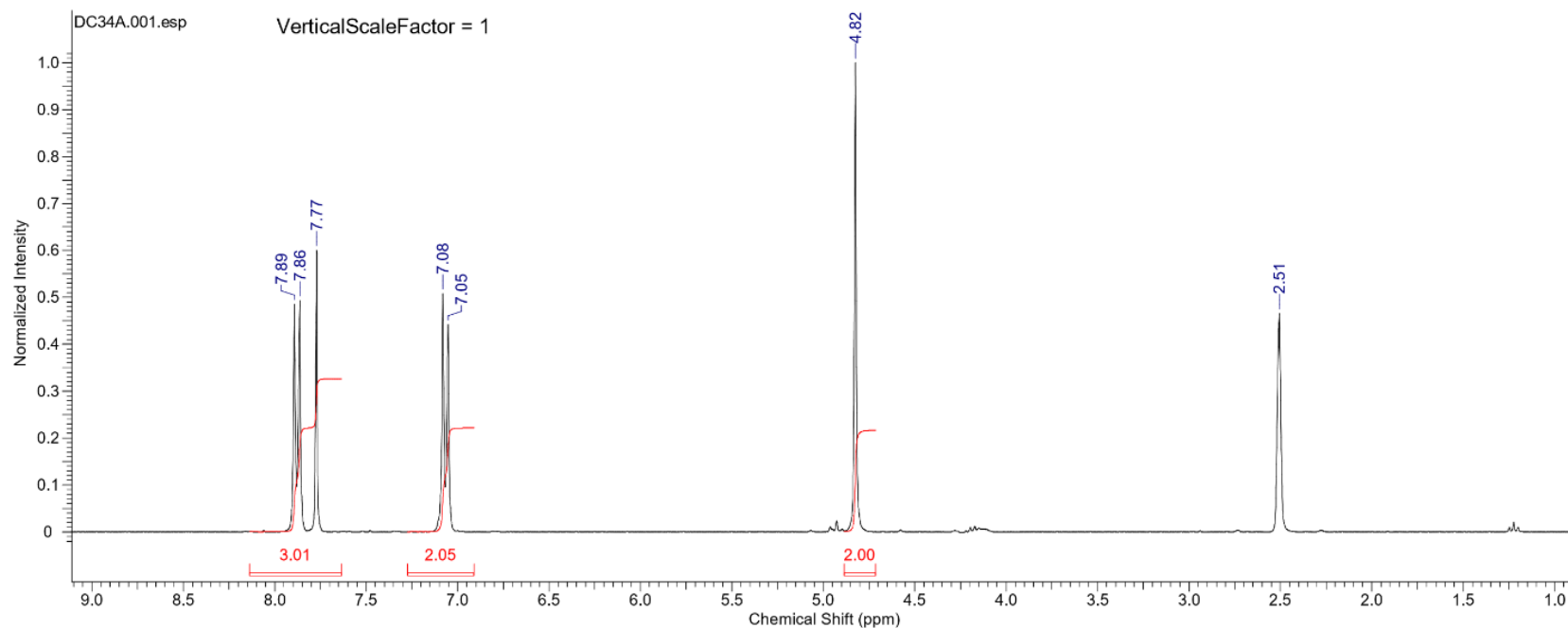
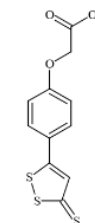
Formula C₄H₇O₂S₃ FW 178.2525

Acquisition Time (sec)	2.7329	Comment	CC2864B H DMSO-d6 120213 21433 RG=256	Date	12 Feb 2013 08:51:28
Date Stamp	12 Feb 2013 08:51:28	File Name	\\NMR2\Farmaceutica 2013\data\CC\nmr\CC2864B\1\fid		
Frequency (MHz)	300.13	Nucleus	1H	Number of Transients	32
Original Points Count	16384	Owner	root	Points Count	16384
Receiver Gain	256.00	SW(cyclical) (Hz)	5995.20	Solvent	DMSO-d6
Spectrum Type	STANDARD	Sweep Width (Hz)	5994.84	Temperature (degree C)	18.560
				Spectrum Offset (Hz)	1955.1014



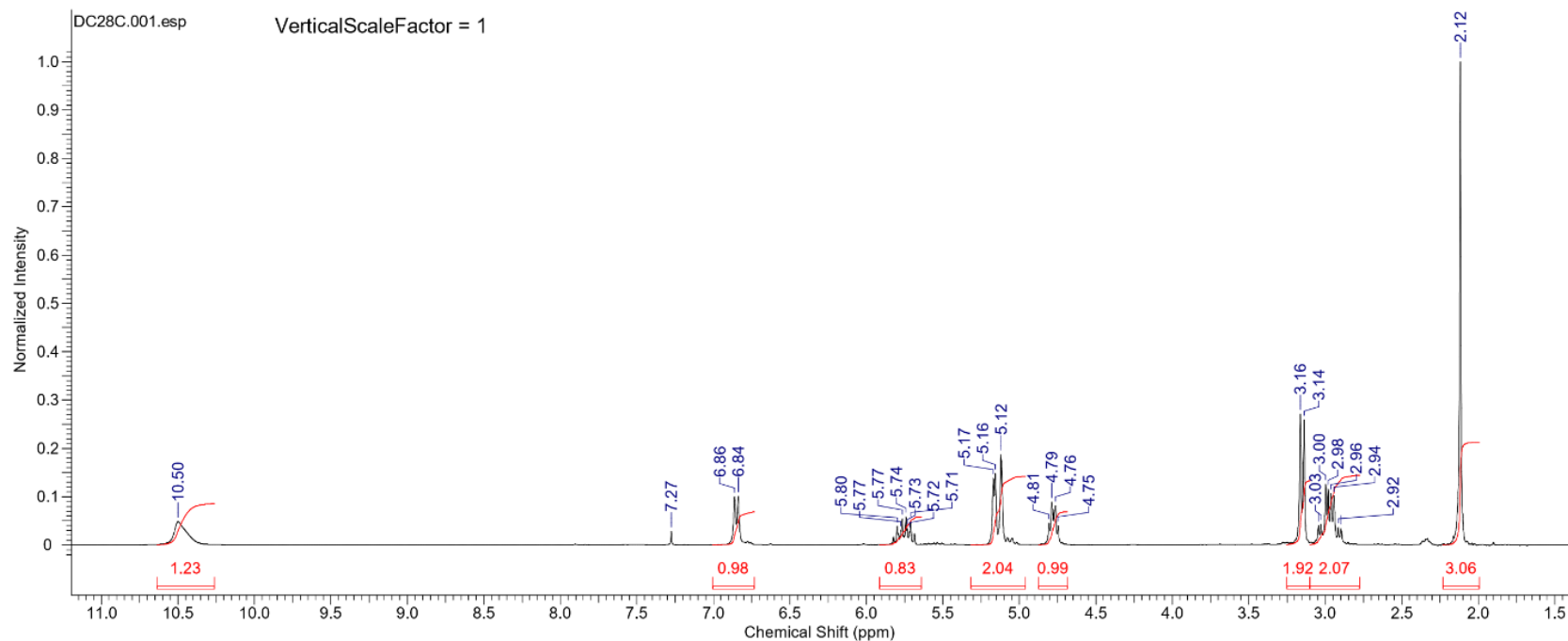
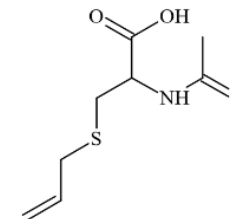
Formula C₁₁H₈O₃S₃ FW 284.3744

Acquisition Time (sec)	2.7329	Comment	DC34A_H_DMSO-d6_130513_21646_RG=200		Date	13 May 2013 10:51:12	
Date Stamp	13 May 2013 10:51:12	File Name	\NMR2\Farmaceutica_2013\data\DC\nmr\DC34A\1.fid				
Frequency (MHz)	300.13	Nucleus	1H	Number of Transients	32	Origin	spect
Original Points Count	16384	Owner	root	Points Count	16384	Pulse Sequence	zg
Receiver Gain	203.20	SW(cyclical) (Hz)	5995.20	Solvent	CHLOROFORM-d		
Spectrum Offset (Hz)	1951.9906	Spectrum Type	STANDARD	Sweep Width (Hz)	5994.84	Temperature (degree C)	21.460



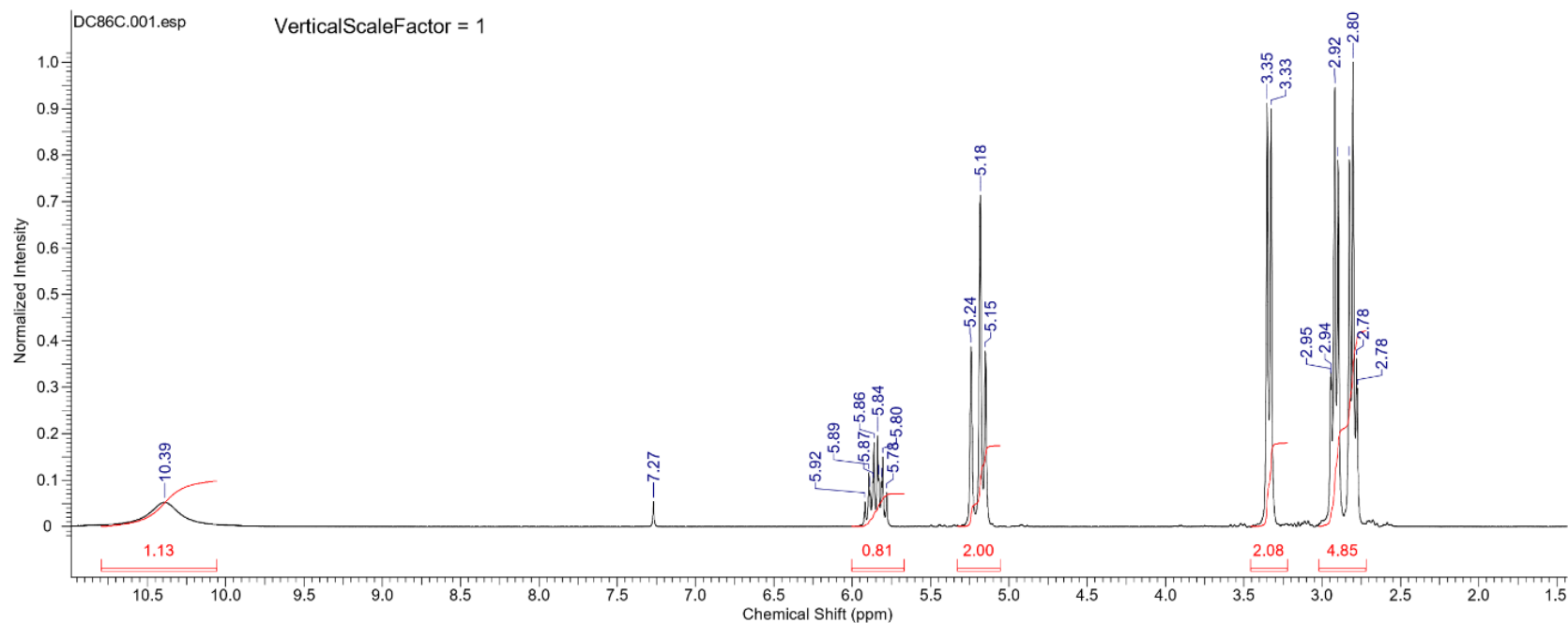
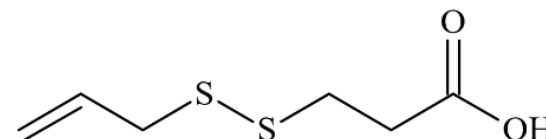
Formula C₈H₁₃NO₃S FW 203.2587

Acquisition Time (sec)	2.7329	Comment	DC28C_H CDCI3 150513 21659 RG=71	Date	15 May 2013 10:46:56
Date Stamp	15 May 2013 10:46:56	File Name	\\NMR2\Farmaceutica 2013\data\DC\nmr\DC28C\1\fid	Frequency (MHz)	300.13
Nucleus	1H	Number of Transients	32	Origin	spect
Points Count	16384	Pulse Sequence	zg	Receiver Gain	71.80
Spectrum Offset (Hz)	1948.8800	Spectrum Type	STANDARD	SW(cyclical) (Hz)	5995.20
				Temperature (degree C)	20.460



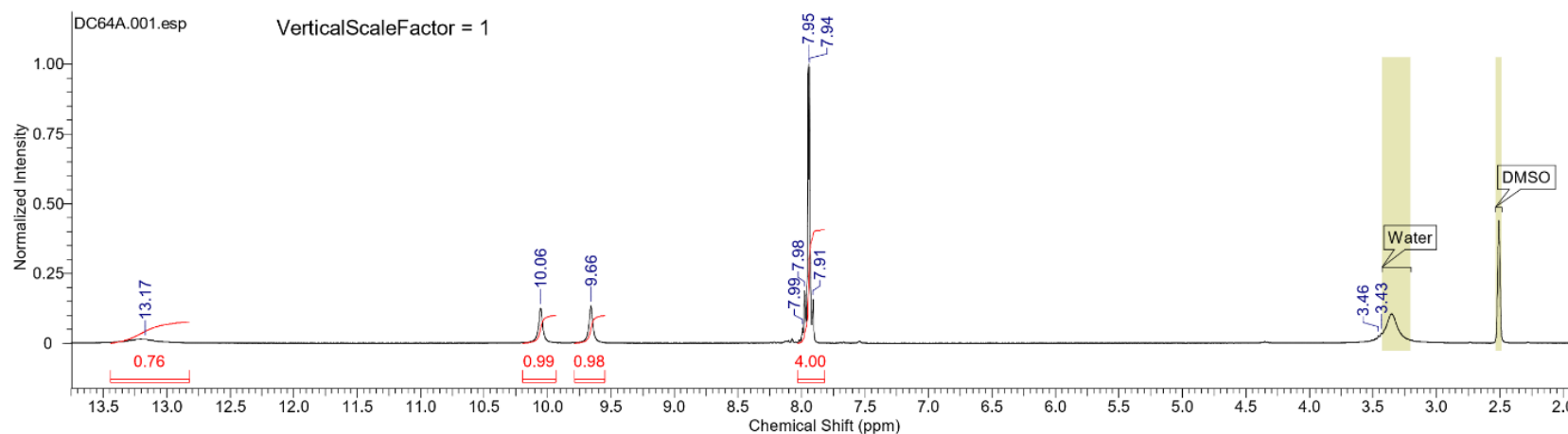
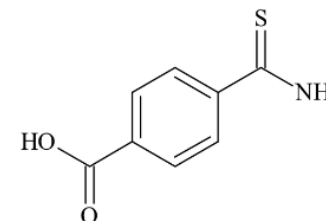
Formula C₆H₁₀O₂S₂ FW 178.2724

Acquisition Time (sec)	3.6438	Comment	DC86C_1H_CDCI3_251013_21962_RG=300	Date	25 Oct 2013 09:13:04
Date Stamp	25 Oct 2013 09:13:04	File Name	\\NMR2\Farmaceutica 2013\data\DC\nmr\DC86C\1\fid		
Frequency (MHz)	300.13	Nucleus	1H	Number of Transients	16
Original Points Count	16384	Owner	root	Points Count	16384
Receiver Gain	90.50	SW(cyclical) (Hz)	4496.40	Solvent	CHLOROFORM-d
Spectrum Offset (Hz)	1947.1420	Spectrum Type	STANDARD	Sweep Width (Hz)	4496.13
				Temperature (degree C)	21.160



Formula C₈H₇NO₂S FW 181.2117

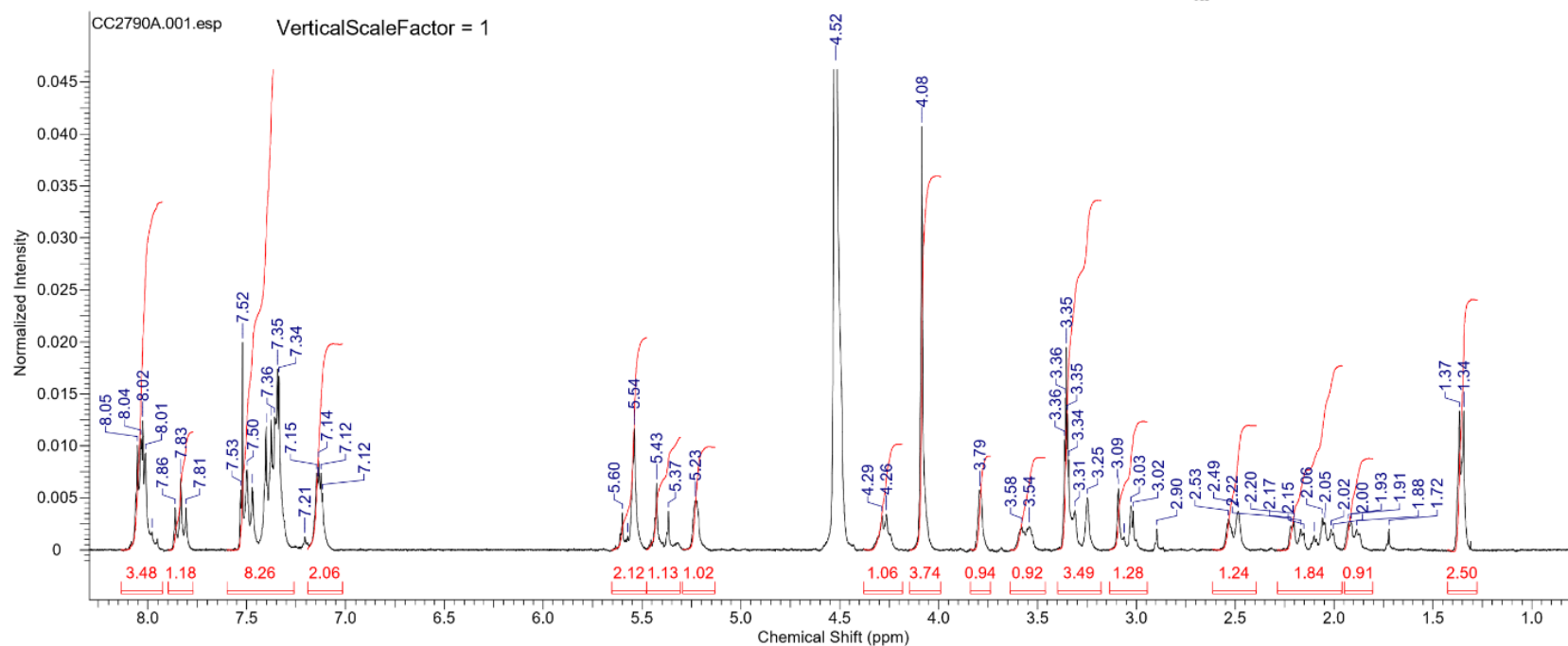
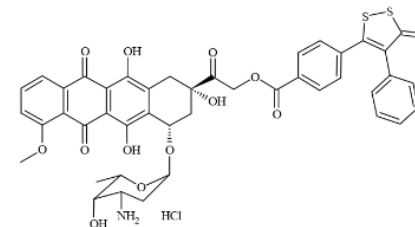
Acquisition Time (sec)	2.7329	Comment	DC64A_H CDCI3_020813_21809_RG=160	Date	02 Aug 2013 10:36:16	
Date Stamp	02 Aug 2013 10:36:16	File Name	\\NMR2\Farmaceutica 2013\data\DC\nmr\DC64A\1\fid	Frequency (MHz)	300.13	
Nucleus	1H	Number of Transients	32	Origin	spect	
Points Count	16384	Pulse Sequence	zg	Receiver Gain	161.30	
Spectrum Offset (Hz)	1952.1750	Spectrum Type	STANDARD	SW(cyclical) (Hz)	5995.20	
			Sweep Width (Hz)	5994.84	Temperature (degree C)	23.760



This report was created by ACD/NMR Processor Academic Edition. For more information go to www.acdlabs.com/nmrproc/

11/03/2016 15:30:36

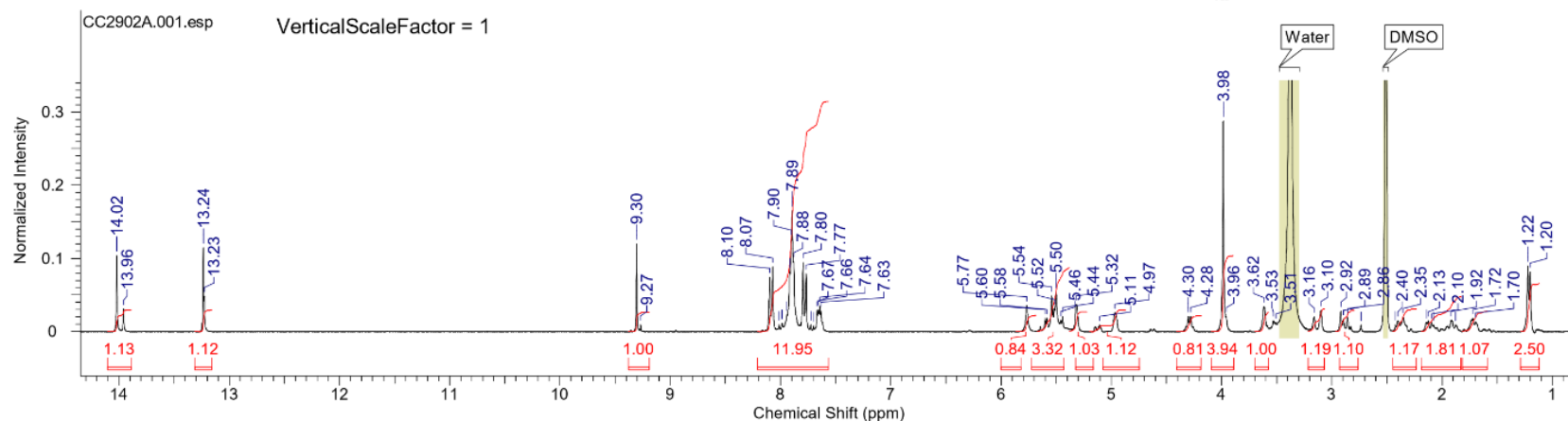
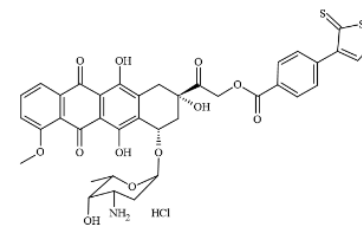
Formula C ₄₃ H ₃₈ ClNO ₁₂ S ₃		FW 892.4093 (36.4609+855.9484)				
Acquisition Time (sec)	2.7329	Comment	CC2790A_H_CD3OD_300712_21229	Date	30 Jul 2012 08:56:00	
Date Stamp	30 Jul 2012 08:56:00	File Name	\\NMR2\Farmaceutica 2013\data\CC\nmr\CC2790A\1\fid	Frequency (MHz)	300.13	
Nucleus	1H	Number of Transients	32	Origin	spect	
Points Count	16384	Pulse Sequence	zg	Receiver Gain	181.00	
Spectrum Offset (Hz)	1958.5771	Spectrum Type	STANDARD	SW(cyclical) (Hz)	5995.20	
			Sweep Width (Hz)	5994.84	Temperature (degree C)	23.860
				Original Points Count	16384	
				Owner	root	
				Solvent	METHANOL-d4	



This report was created by ACD/NMR Processor Academic Edition. For more information go to www.acdlabs.com/nmrproc/

10/03/2016 10:47:36

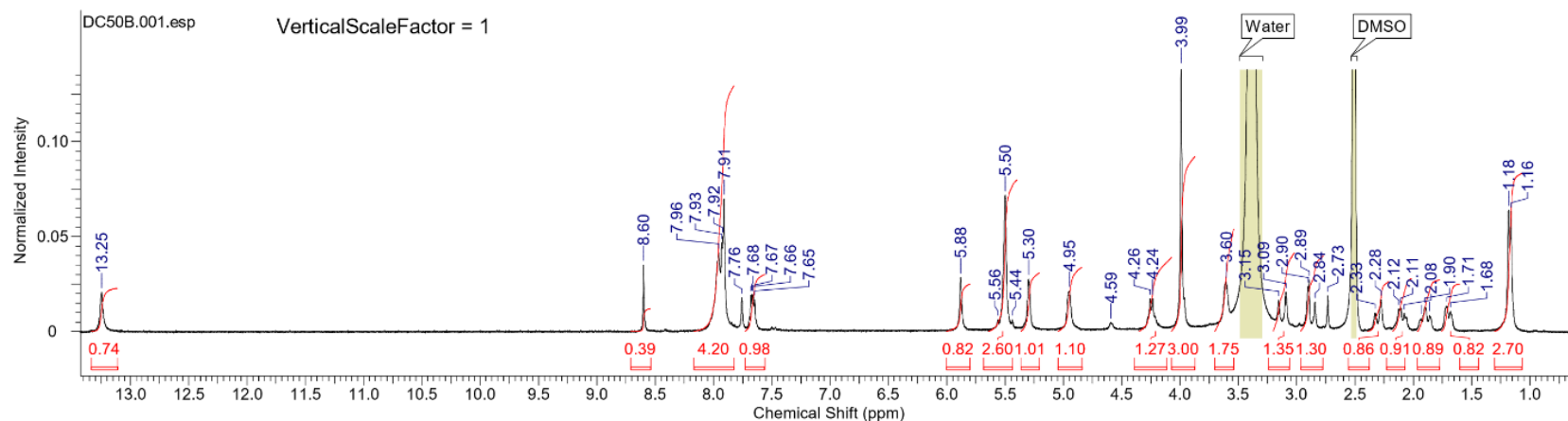
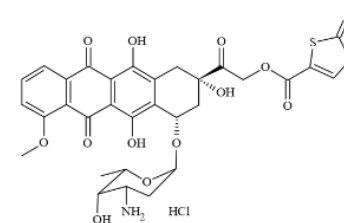
Formula C ₃₇ H ₃₄ ClNO ₁₂ S ₃		FW 816.3134 (36.4609+779.8524)			
Acquisition Time (sec)	2.7329	Comment	CC2902A_1H DMSO-d6 181013 21943 RG=180	Date	18 Oct 2013 07:56:16
Date Stamp	18 Oct 2013 07:56:16	File Name	\\NMR2\Farmaceutica 2013\data\CC\nmr\CC2902A\1\fid		
Frequency (MHz)	300.13	Nucleus	1H	Number of Transients	32
Original Points Count	16384	Owner	root	Points Count	16384
Receiver Gain	181.00	SW(cyclical) (Hz)	5995.20	Solvent	DMSO-d6
Spectrum Type	STANDARD	Sweep Width (Hz)	5994.84	Temperature (degree C)	21.160
				Spectrum Offset (Hz)	1952.9043



This report was created by ACD/NMR Processor Academic Edition. For more information go to www.acdlabs.com/nmrproc/

10/03/2016 11:11:38

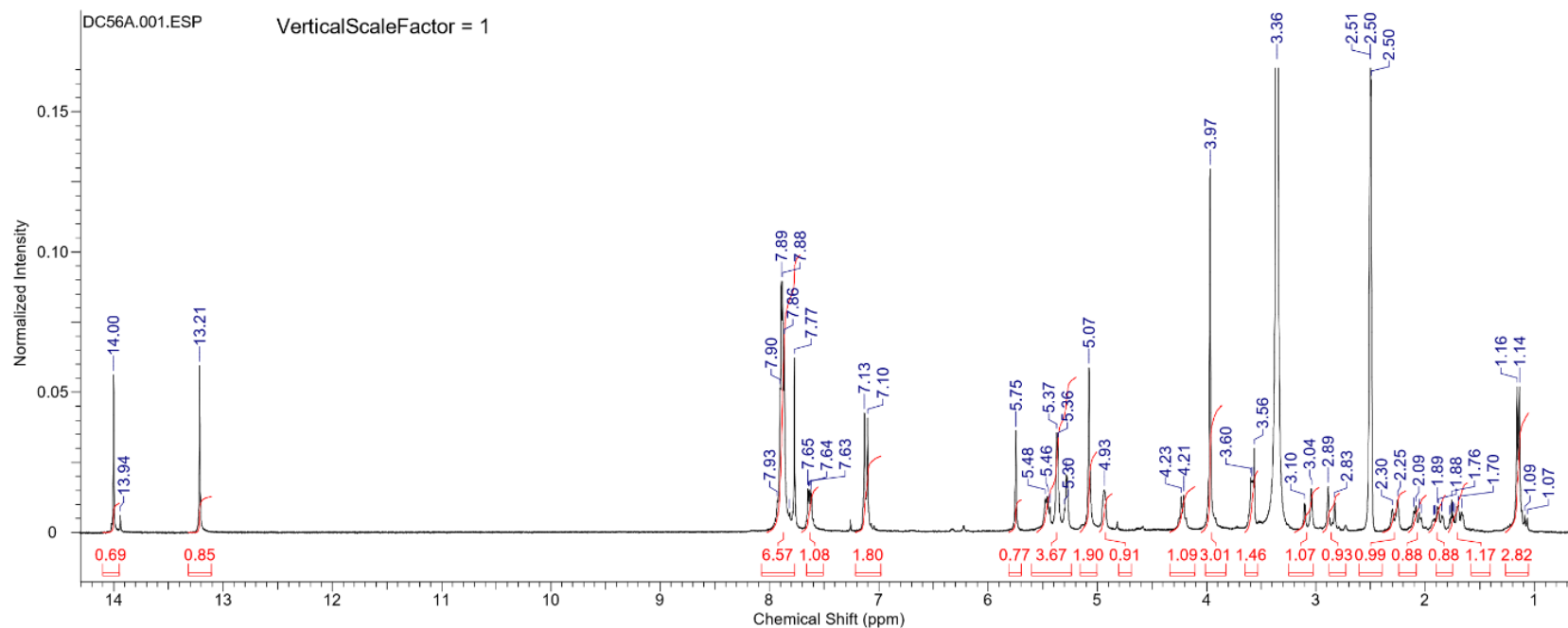
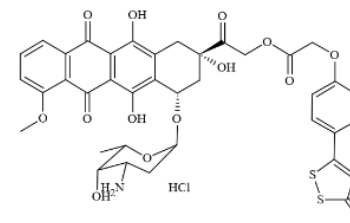
Formula C ₃₁ H ₃₀ ClNO ₁₂ S ₃		FW 740.2174 (36.4609+703.7565)	
Acquisition Time (sec)	3.6438	Comment	DC50B_1H_DMSO-d6_21954_221013_RG=160
Date Stamp	22 Oct 2013 14:11:44	Date	22 Oct 2013 14:11:44
Frequency (MHz)	300.13	File Name	\\NMR2\Farmaceutica 2013\data\DC\nmr\DC50B\1\fid
Original Points Count	16384	Nucleus	1H
Receiver Gain	161.30	Number of Transients	32
Spectrum Type	STANDARD	Owner	root
		Points Count	16384
		Solvent	DMSO-d6
		Sweep Width (Hz)	4496.13
		Temperature (degree C)	21.260
		Pulse Sequence	zg
		Spectrum Offset (Hz)	1952.0819



This report was created by ACD/NMR Processor Academic Edition. For more information go to www.acdlabs.com/nmrproc/

10/03/2016 10:34:50

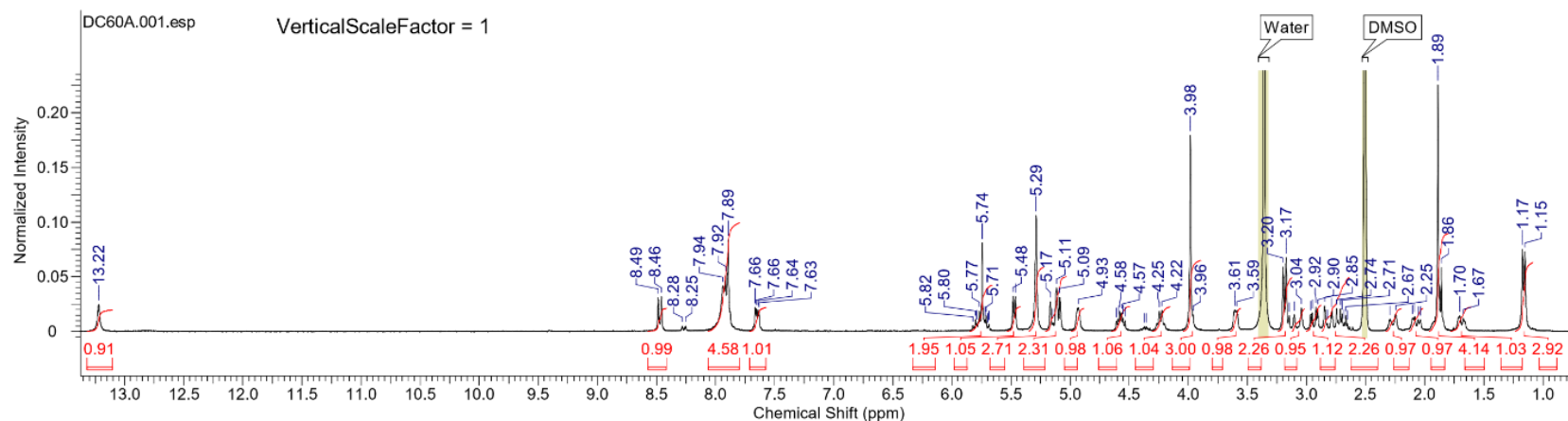
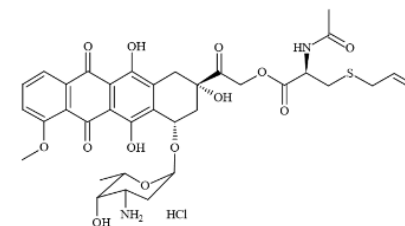
Formula C ₃₈ H ₃₆ ClNO ₁₃ S ₃		FW 846.3393 (809.8784+36.4609)	
Acquisition Time (sec)	2.7329	Comment	DC56A_1H_DMSO-d6_181013_21944_RG=200
Date Stamp	18 Oct 2013 08:06:56	File Name	\\NMR2\Farmaceutica_2013\data\DC\nmr\DC56A\1\fid
Frequency (MHz)	300.13	Nucleus	1H
Original Points Count	16384	Number of Transients	32
Receiver Gain	203.20	Owner	root
Spectrum Offset (Hz)	1949.9878	Points Count	16384
		Pulse Sequence	zg
		Solvent	CHLOROFORM-d
		Sweep Width (Hz)	5994.84
		Temperature (degree C)	21.160



This report was created by ACD/NMR Processor Academic Edition. For more information go to www.acdlabs.com/nmrproc/

10/03/2016 11:04:06

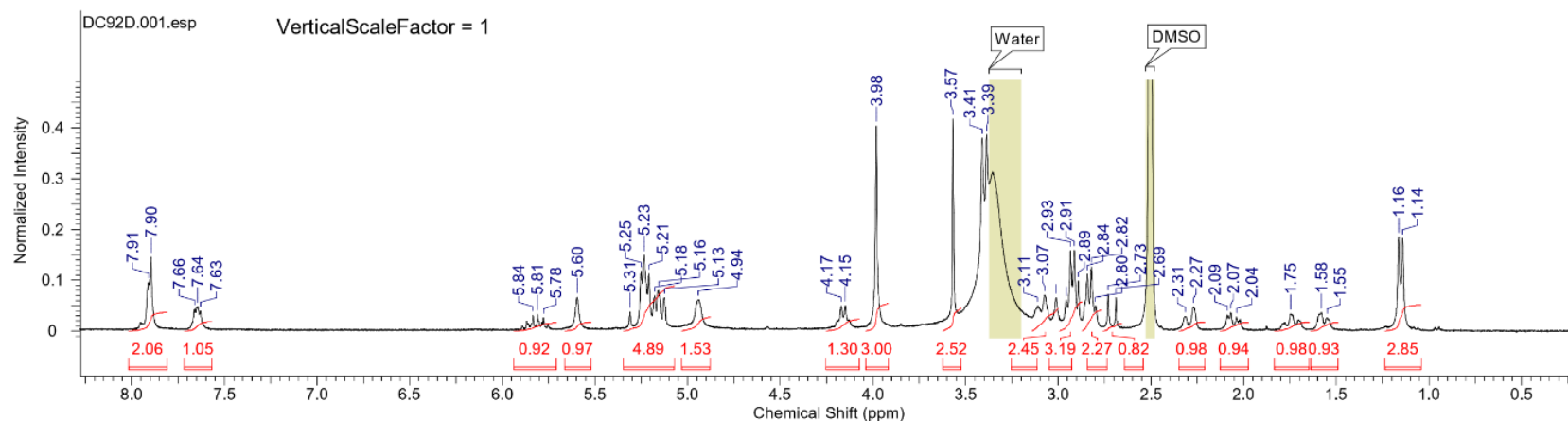
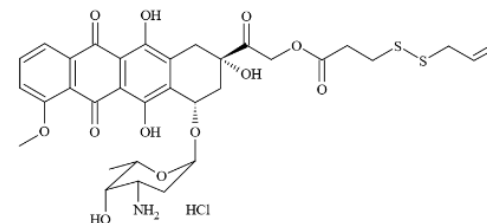
Formula C ₃₅ H ₄₁ ClN ₂ O ₁₃ S		FW 765.2236 (36.4609+728.7627)	
Acquisition Time (sec)	3.6438	Comment	DC60A_1H_DMSO-d6_141013_21930_RG=180
Date Stamp	14 Oct 2013 10:46:56	Date	14 Oct 2013 10:46:56
File Name	\\NMR2\Farmaceutica 2013\data\DC\nmr\DC60A\1\fid		
Frequency (MHz)	300.13	Nucleus	1H
Number of Transients	16	Origin	spect
Original Points Count	16384	Points Count	16384
Pulse Sequence	zg		
Receiver Gain	181.00	Spectrum Offset (Hz)	1951.5326
SW(cyclical) (Hz)	4496.40	Solvent	DMSO-d6
Sweep Width (Hz)	4496.13	Temperature (degree C)	21.160



This report was created by ACD/NMR Processor Academic Edition. For more information go to www.acdlabs.com/nmrproc/

10/03/2016 10:57:51

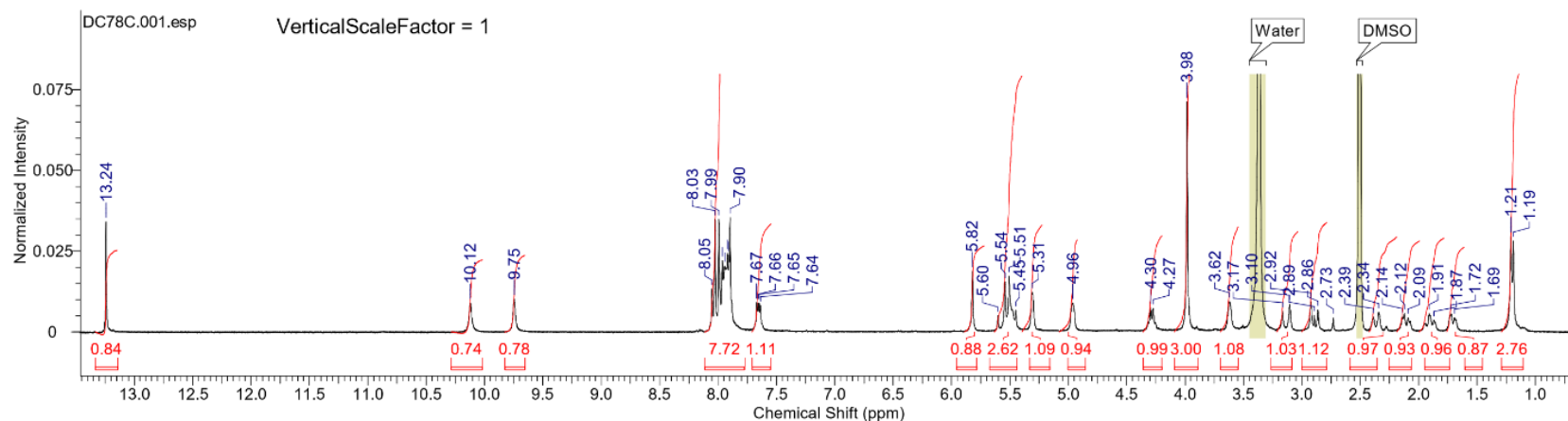
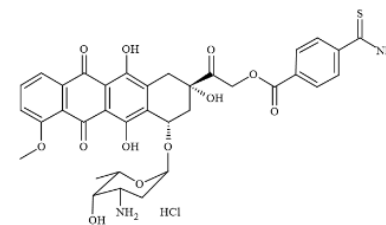
Formula C ₃₃ H ₃₈ ClNO ₁₂ S ₂		FW 740.2373 (36.4609+703.7764)	
Acquisition Time (sec)	3.6438	Comment	DC92D_1H_DMSO-d6_21995_11112013_RG=140
Date Stamp	11 Nov 2013 10:57:20	Date	11 Nov 2013 10:57:20
Frequency (MHz)	300.13	File Name	\\NMR2\Farmaceutica_2013\data\DC\nmr\DC92D\1\fid
Original Points Count	16384	Nucleus	1H
Receiver Gain	143.70	Number of Transients	16
Spectrum Type	STANDARD	Owner	root
		Points Count	16384
		Solvent	DMSO-d6
		Sweep Width (Hz)	4496.13
		Temperature (degree C)	21.160
		Pulse Sequence	zg
		Spectrum Offset (Hz)	1950.9836



This report was created by ACD/NMR Processor Academic Edition. For more information go to www.acdlabs.com/nmrproc/

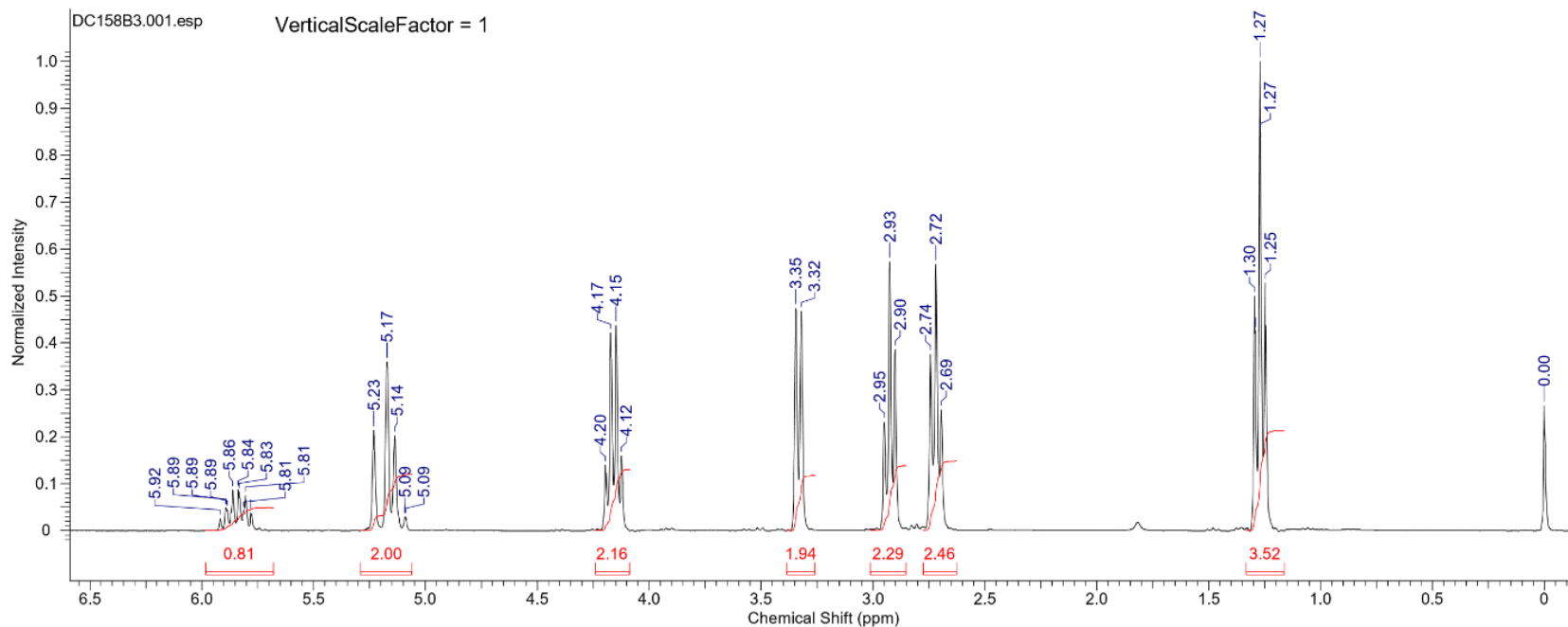
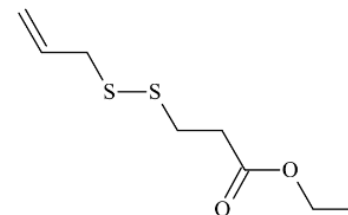
10/03/2016 11:14:56

Formula C ₃₅ H ₃₅ ClN ₂ O ₁₂ S		FW 743.1766 (36.4609+706.7157)	
Acquisition Time (sec)	3.6438	Comment	DC78C_1H_DMSO-d6_141013_21931_RG=160
Date Stamp	14 Oct 2013 11:01:52	Date	14 Oct 2013 11:01:52
Frequency (MHz)	300.13	File Name	\\NMR2\Farmaceutica 2013\data\DC\nmr\DC78C\1\fid
Original Points Count	16384	Nucleus	1H
Receiver Gain	161.30	Number of Transients	16
Spectrum Type	STANDARD	Owner	root
		Points Count	16384
		Solvent	DMSO-d6
		Spectrum Offset (Hz)	1951.5358
		Temperature (degree C)	21.160



Formula C₈H₁₄O₂S₂ FW 206.3256

Acquisition Time (sec)	1.8219	Comment	DC158B3_1H.CDCI3_280715_24232_RG=50	Date	28 Jul 2015 11:33:52
Date Stamp	28 Jul 2015 11:33:52	File Name	\\NMR2\farmaceutica_2015\data\DC\nmr\DC158B3\1\fid		
Frequency (MHz)	300.13	Nucleus	1H	Number of Transients	16
Original Points Count	8192	Owner	root	Points Count	8192
Receiver Gain	50.80	SW(cyclical) (Hz)	4496.40	Solvent	CHLOROFORM-d
Spectrum Offset (Hz)	1951.2595	Spectrum Type	STANDARD	Sweep Width (Hz)	4495.85
				Temperature (degree C)	24.360

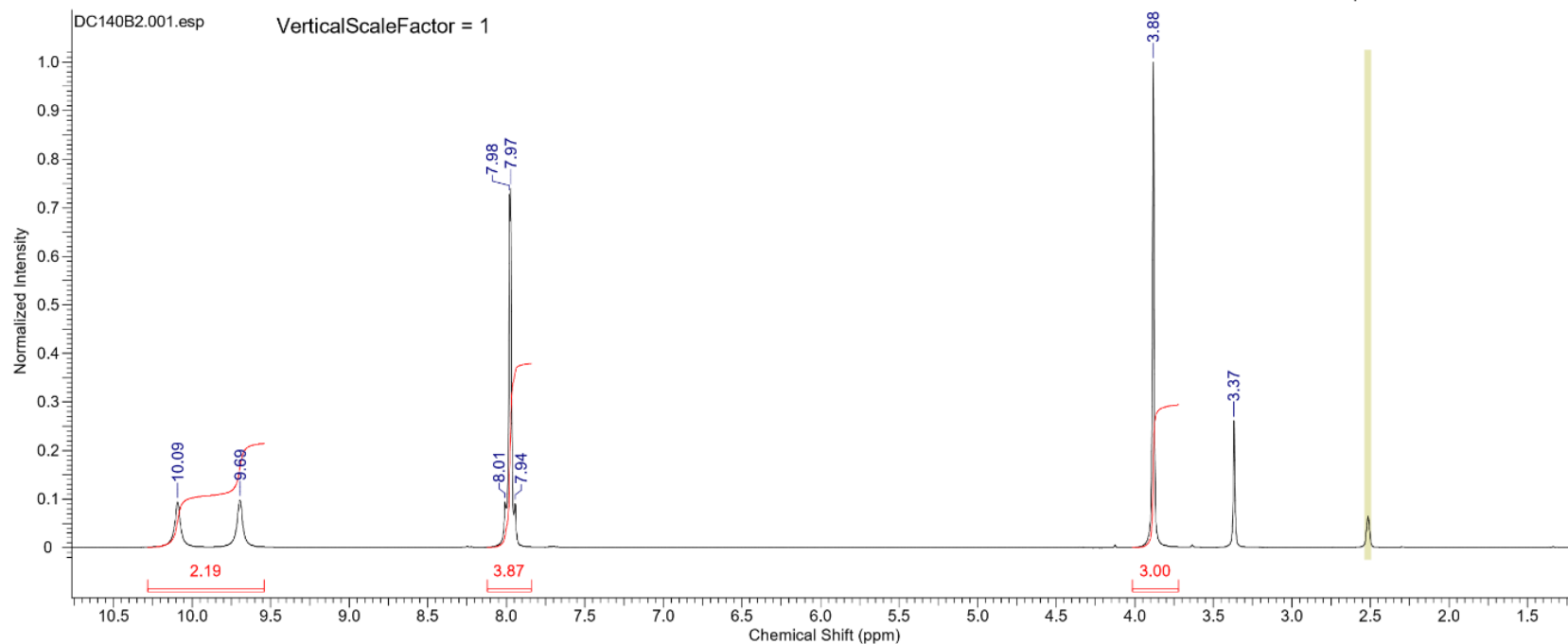
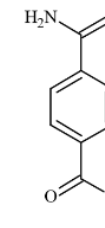


This report was created by ACD/NMR Processor Academic Edition. For more information go to www.acdlabs.com/nmrproc/

10/03/2016 16:21:28

Formula C₉H₉NO₂S FW 195.2383

Acquisition Time (sec)	1.8219	Comment	DC140B2_1H_DMSO-d6_280715_24230_RG=80	Date	28 Jul 2015 10:17:04				
Date Stamp	28 Jul 2015 10:17:04	File Name	\\NMR2\farmaceutica 2015\data\DC\nmr\DC140B2\1\fid	Frequency (MHz)	300.13				
Nucleus	1H	Number of Transients	16	Origin	spect	Original Points Count	8192	Owner	root
Points Count	8192	Pulse Sequence	zg	Receiver Gain	80.60	SW(cyclical) (Hz)	4496.40	Solvent	DMSO-d6
Spectrum Offset (Hz)	1953.7288	Spectrum Type	STANDARD	Sweep Width (Hz)	4495.85	Temperature (degree C)	23.660		

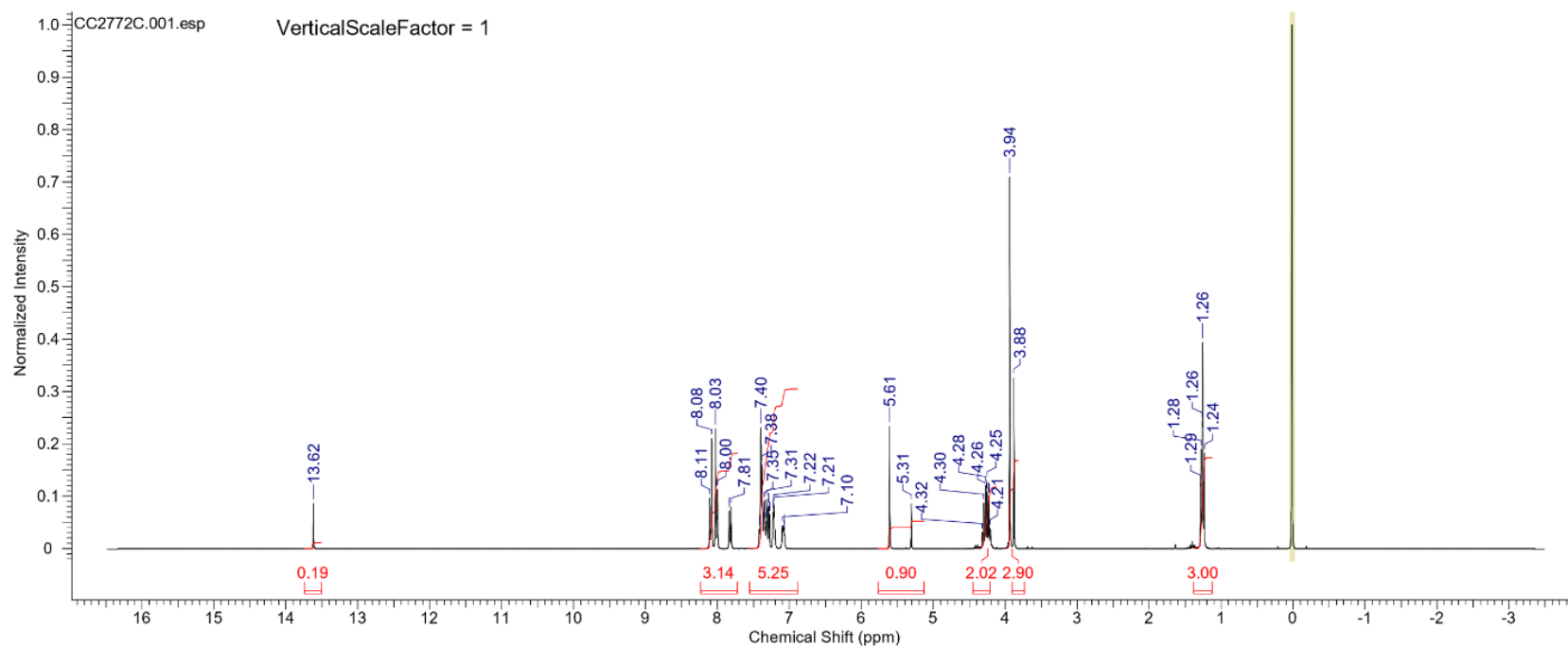
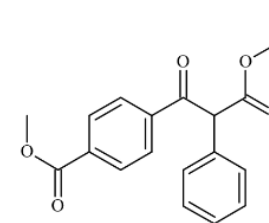


This report was created by ACD/NMR Processor Academic Edition. For more information go to www.acdlabs.com/nmrproc/

11/03/2016 15:16:54

Formula C₁₈H₁₈O₅ FW 326.3432

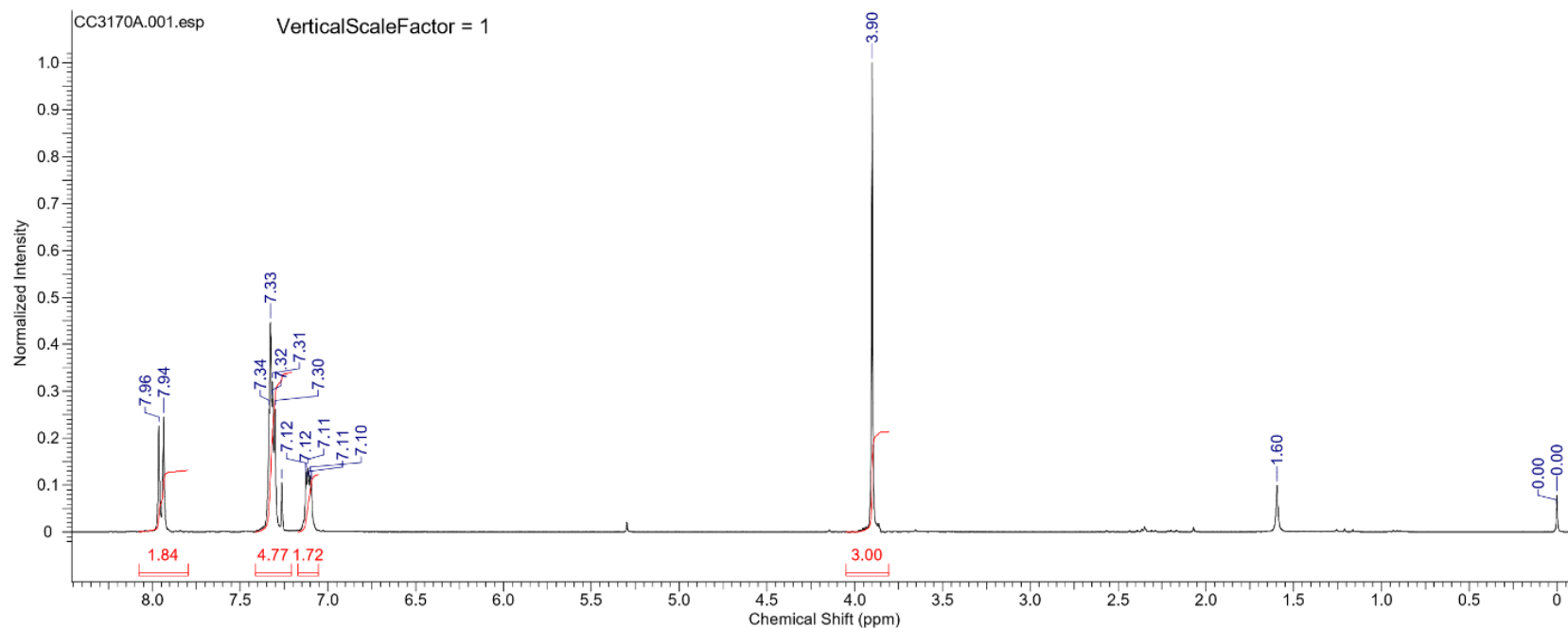
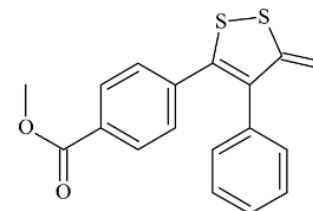
Acquisition Time (sec)	2.7329	Comment	CC2772C_H CDCl3 160512 21089	Date	16 May 2012 11:21:04
Date Stamp	16 May 2012 11:21:04	File Name	\\NMR2\Farmaceutica 2013\data\CC\nmr\CC2772C\1\fid	Frequency (MHz)	300.13
Nucleus	1H	Number of Transients	64	Origin	spect
Points Count	16384	Pulse Sequence	zg	Receiver Gain	101.60
Spectrum Offset (Hz)	1949.6122	Spectrum Type	STANDARD	SW(cyclical) (Hz)	5995.20
				Temperature (degree C)	20.960



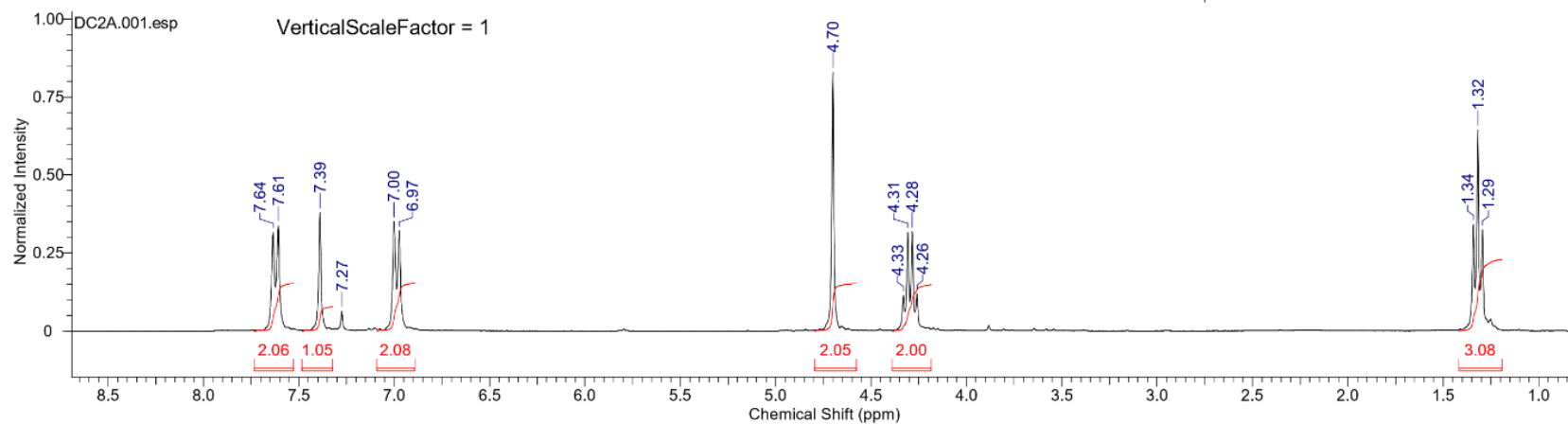
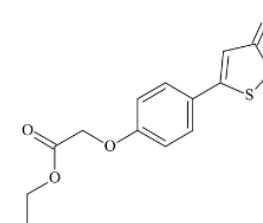
This report was created by ACD/NMR Processor Academic Edition. For more information go to www.acdlabs.com/nmrproc/

10/03/2016 13:41:11

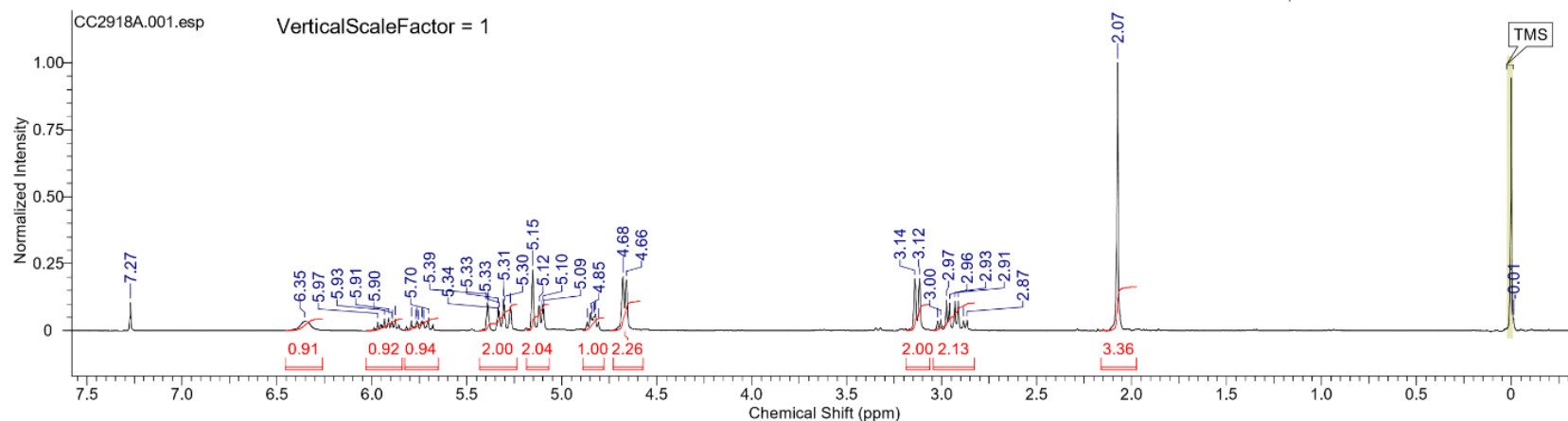
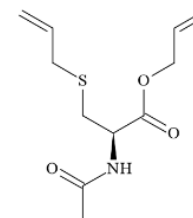
Formula	C ₁₇ H ₁₂ O ₂ S ₃	FW	344.4710		
Acquisition Time (sec)	3.6438	Comment	CC3170A_1H_CDCl3_091014_23013_RG=180	Date	09 Oct 2014 14:41:36
Date Stamp	09 Oct 2014 14:41:36	File Name	\\NMR2\Farmaceutica 2014\data\CC\inmr\CC3170A\1fid		
Frequency (MHz)	300.13	Nucleus	1H	Number of Transients	16
Original Points Count	16384	Owner	root	Points Count	16384
Receiver Gain	181.00	SW(cyclical) (Hz)	4496.40	Solvent	CHLOROFORM-d
Spectrum Offset (Hz)	1944.6718	Spectrum Type	STANDARD	Sweep Width (Hz)	4496.13
				Temperature (degree C)	22.560



Formula	C ₁₃ H ₁₂ O ₃ S ₃	FW	312.4276
Acquisition Time (sec)	2.7329	Comment	DC2A_H_CDCI3_090113_21358
Date Stamp	09 Jan 2013 10:42:24	Date	09 Jan 2013 10:42:24
Nucleus	1H	File Name	\\NMR2\Farmaceutica 2013\data\DC\inmr\DC2A\1\fid
Points Count	16384	Frequency (MHz)	300.13
Solvent	CHLOROFORM-d	Number of Transients	32
Temperature (degree C)	20.660	Origin	spect
		Original Points Count	16384
		Receiver Gain	101.60
		SW(cyclical) (Hz)	5995.20
		Spectrum Offset (Hz)	1948.8800
		Spectrum Type	STANDARD
		Sweep Width (Hz)	5994.84



Formula	C ₁₁ H ₁₇ NO ₃ S	FW	243.3226
Acquisition Time (sec)	2.3462	Comment	CC2918A_H_CDCl3_140613_21704_RG=140
Date Stamp	14 Jun 2013 09:40:48	File Name	\\NMR2\Farmaceutica 2013\data\CC\inmr\CC2918A\1\fid
Frequency (MHz)	300.13	Nucleus	1H
Original Points Count	16384	Number of Transients	16
Receiver Gain	143.70	Owner	root
Spectrum Offset (Hz)	1947.8401	Points Count	16384
		Pulse Sequence	zg
		Solvent	CHLOROFORM-d
		Spectrum Type	STANDARD
		Sweep Width (Hz)	6982.81
		Temperature (degree C)	20.960

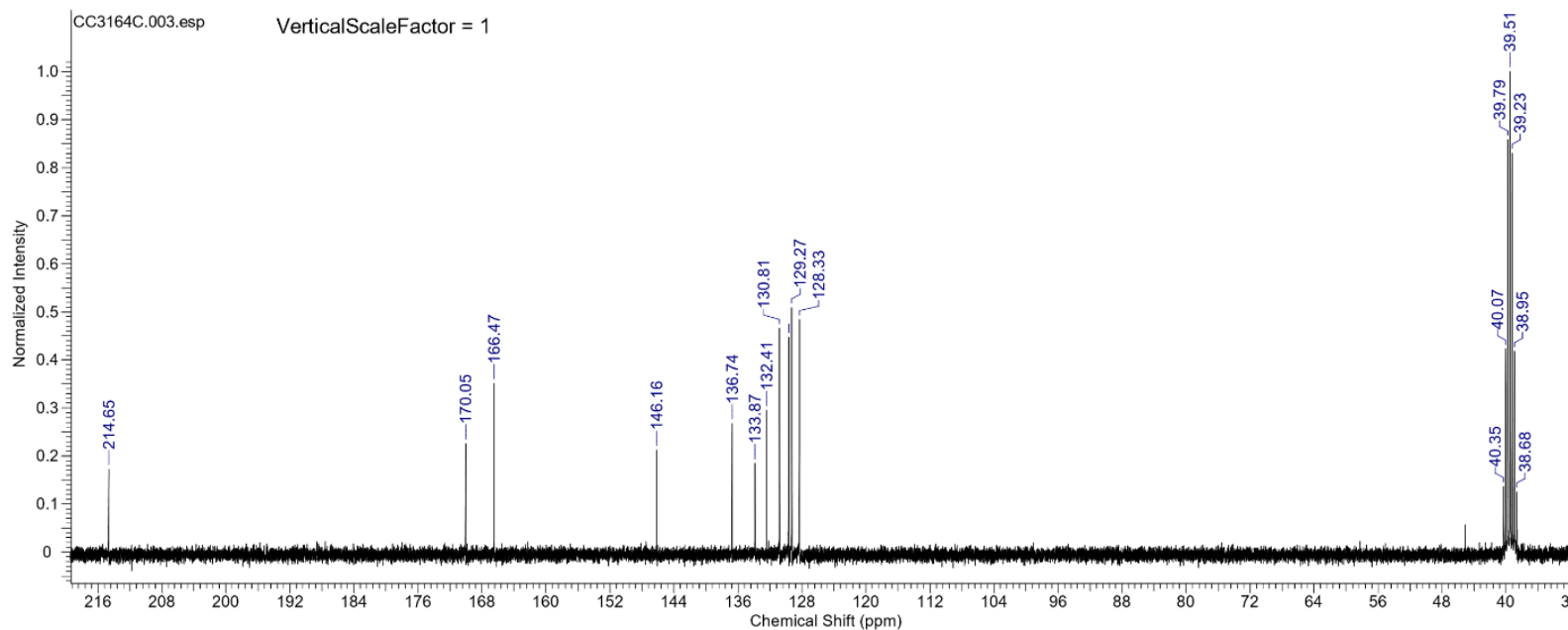
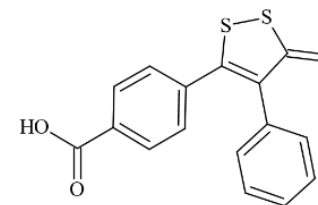


¹³C-NMR spectrum of compounds 3-9 and 17-22.

This report was created by ACD/NMR Processor Academic Edition. For more information go to www.acdlabs.com/nmrproc/

11/03/2016 15:12:19

Formula	C ₁₆ H ₁₀ O ₂ S ₃	FW	330.4444				
Acquisition Time (sec)	1.8088	Comment	CC3164C_13C DMSO-d6 091014 23011 RG=100	Date	09 Oct 2014 13:50:24		
Date Stamp	09 Oct 2014 13:50:24	File Name	\NMR2\Farmaceutica 2014\data\CC\nmr\CC3164C\3\fid				
Frequency (MHz)	75.47	Nucleus	13C	Number of Transients	165	Origin	spect
Original Points Count	32768	Owner	root	Points Count	32768	Pulse Sequence	zgpg.save.txt
Receiver Gain	4597.60	SW(cyclical) (Hz)	18115.94	Solvent	CHLOROFORM-d		
Spectrum Offset (Hz)	8238.5479	Spectrum Type	STANDARD	Sweep Width (Hz)	18115.39	Temperature (degree C)	22.760

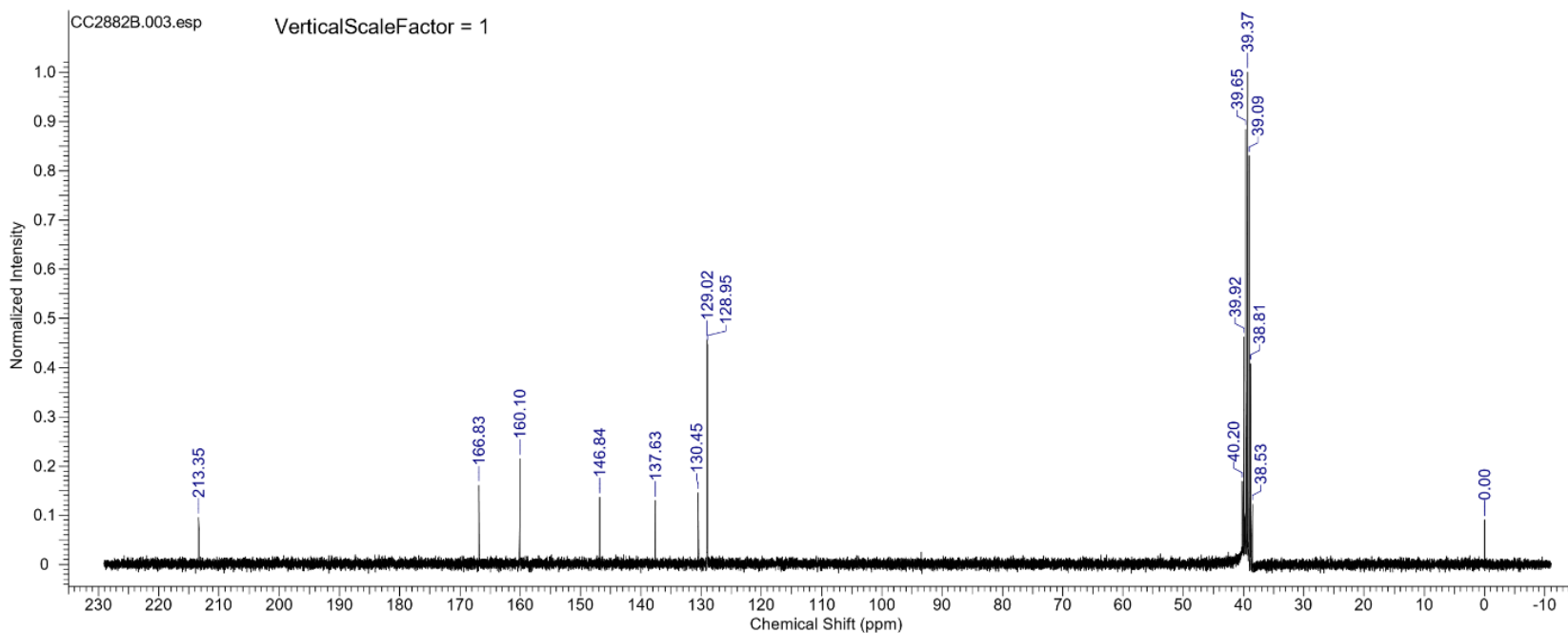
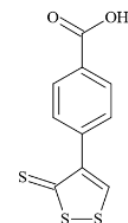


This report was created by ACD/NMR Processor Academic Edition. For more information go to www.acdlabs.com/nmrproc/

10/03/2016 11:27:40

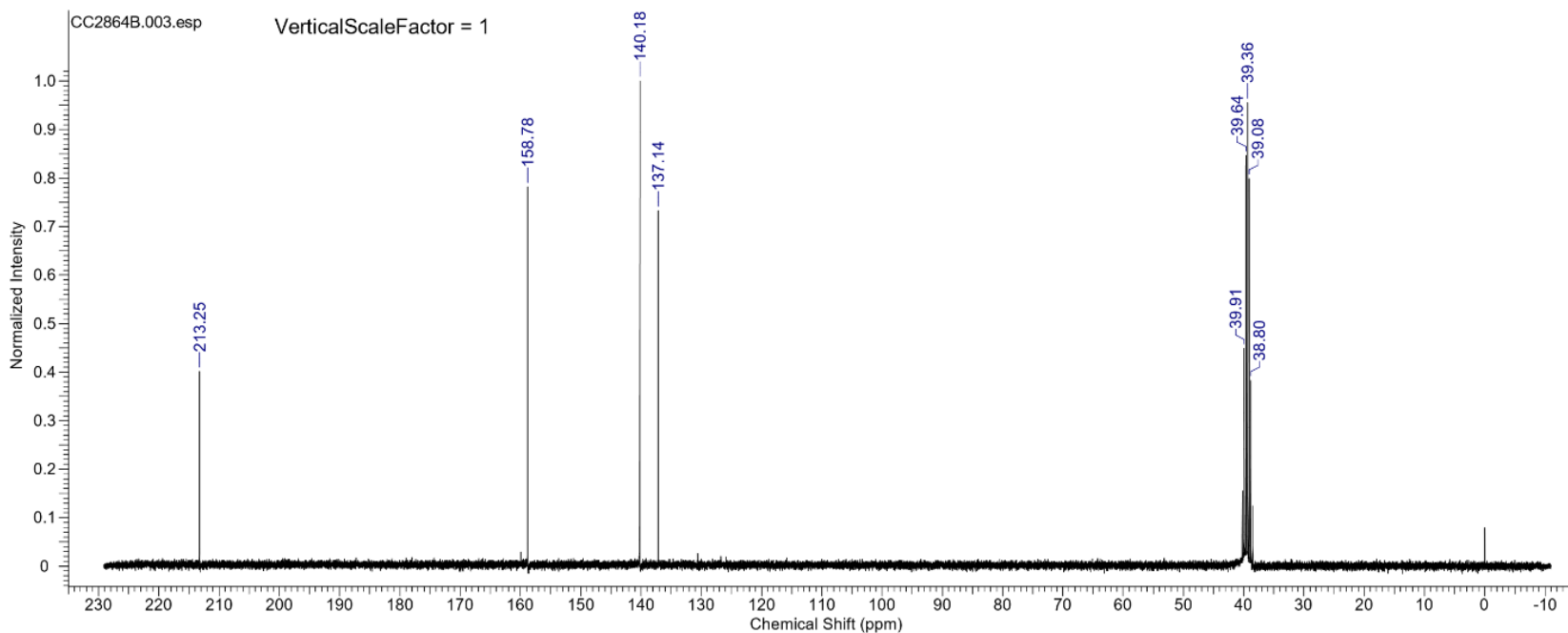
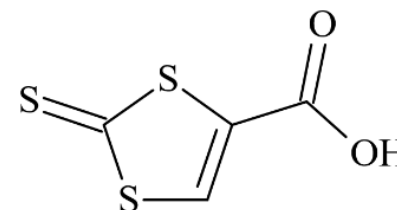
Formula C₁₀H₆O₂S₃ FW 254.3484

Acquisition Time (sec)	1.8088	Comment	CC2882B_C DMSO-d6 040413 21553 RG=161	Date	04 Apr 2013 09:08:48
Date Stamp	04 Apr 2013 09:08:48	File Name	\\NMR2\Farmaceutica 2013\data\CC\nmr\CC2882B\3\fid		
Frequency (MHz)	75.47	Nucleus	13C	Number of Transients	441
Original Points Count	32768	Owner	root	Points Count	32768
Receiver Gain	4597.60	SW(cyclical) (Hz)	18115.94	Solvent	CHLOROFORM-d
Spectrum Offset (Hz)	8227.8594	Spectrum Type	STANDARD	Sweep Width (Hz)	18115.39
				Temperature (degree C)	21.260



Formula C₄H₂O₂S₃ FW 178.2525

Acquisition Time (sec)	1.8088	Comment	CC2864B_13C_DMSO-d6_120213_21435_RG=256	Date	12 Feb 2013 11:59:12
Date Stamp	12 Feb 2013 11:59:12	File Name	\NMR2\Farmaceutica 2013\data\CC\nmr\CC2864B\3\fid		
Frequency (MHz)	75.47	Nucleus	13C	Number of Transients	568
Original Points Count	32768	Owner	root	Points Count	32768
Receiver Gain	4597.60	SW(cyclical) (Hz)	18115.94	Solvent	DMSO-d6
Spectrum Type	STANDARD	Sweep Width (Hz)	18115.39	Temperature (degree C)	20.760
				Spectrum Offset (Hz)	8229.7979

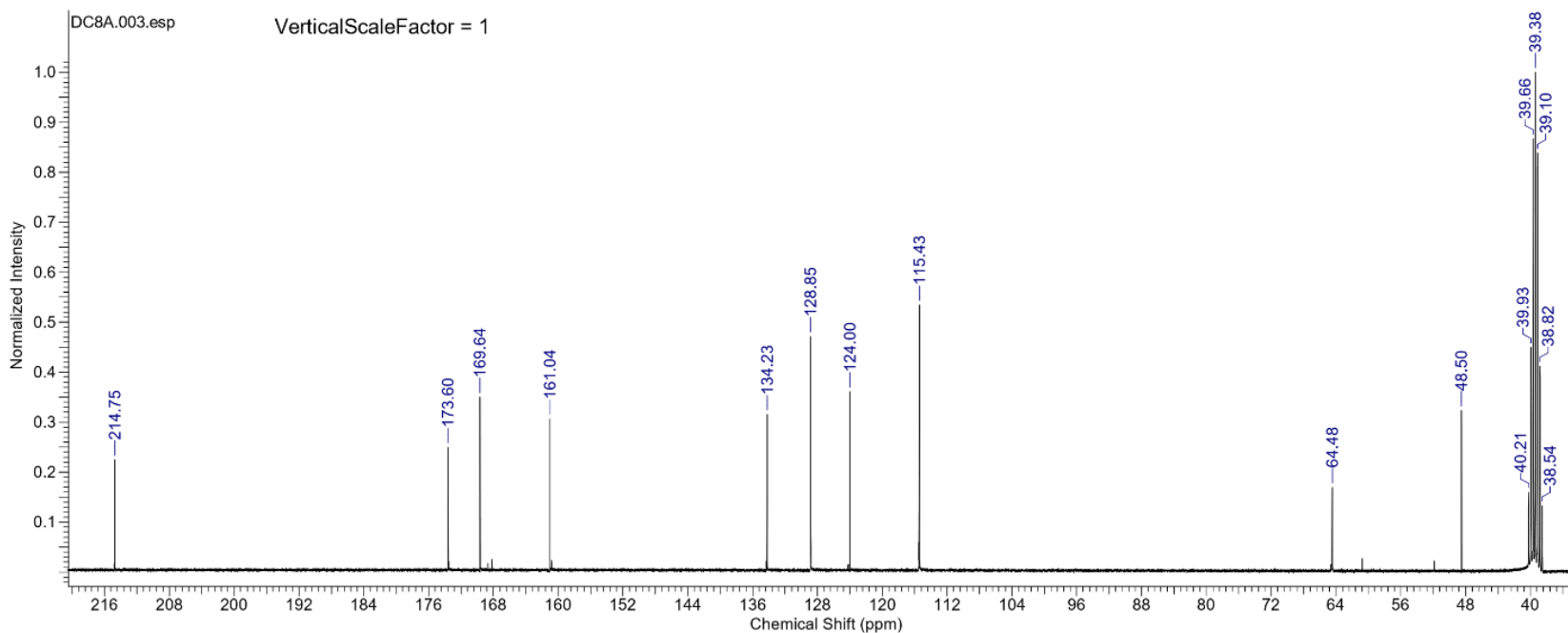
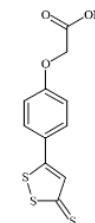


This report was created by ACD/NMR Processor Academic Edition. For more information go to www.acdlabs.com/nmrproc/

10/03/2016 11:35:21

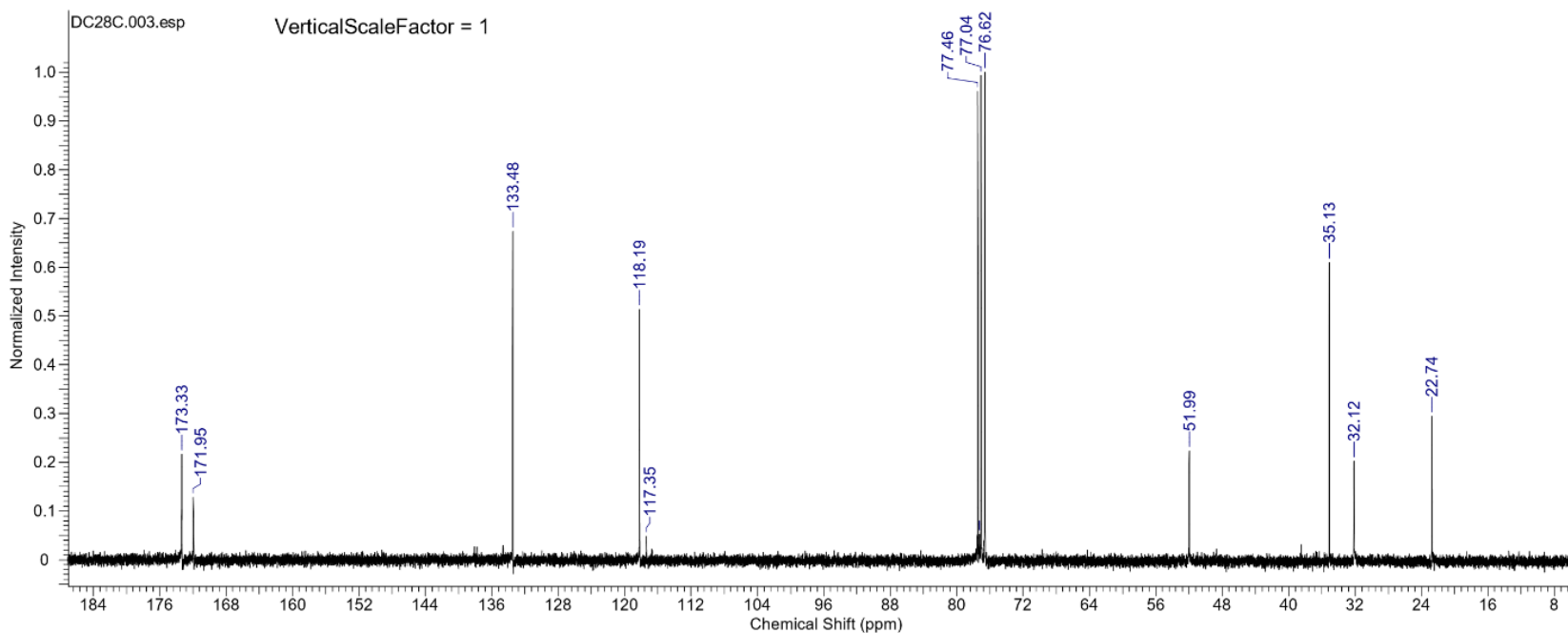
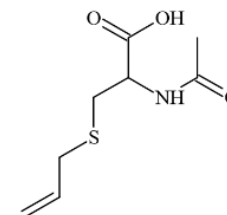
Formula C₁₁H₈O₃S₃ FW 284.3744

Acquisition Time (sec)	1.8088	Comment	DC8A_C_DMSO-d6_310113_21411_RG=128	Date	31 Jan 2013 12:12:00		
Date Stamp	31 Jan 2013 12:12:00	File Name	\\NMR2\Farmaceutica 2013\data\DC\nmr\DC8A\3\fid				
Frequency (MHz)	75.47	Nucleus	13C	Number of Transients	6352	Origin	spect
Original Points Count	32768	Owner	root	Points Count	32768	Pulse Sequence	zgpg.save.txt
Receiver Gain	4597.60	SW(cyclical) (Hz)	18115.94	Solvent	CHLOROFORM-d		
Spectrum Offset (Hz)	8228.6885	Spectrum Type	STANDARD	Sweep Width (Hz)	18115.39	Temperature (degree C)	21.460



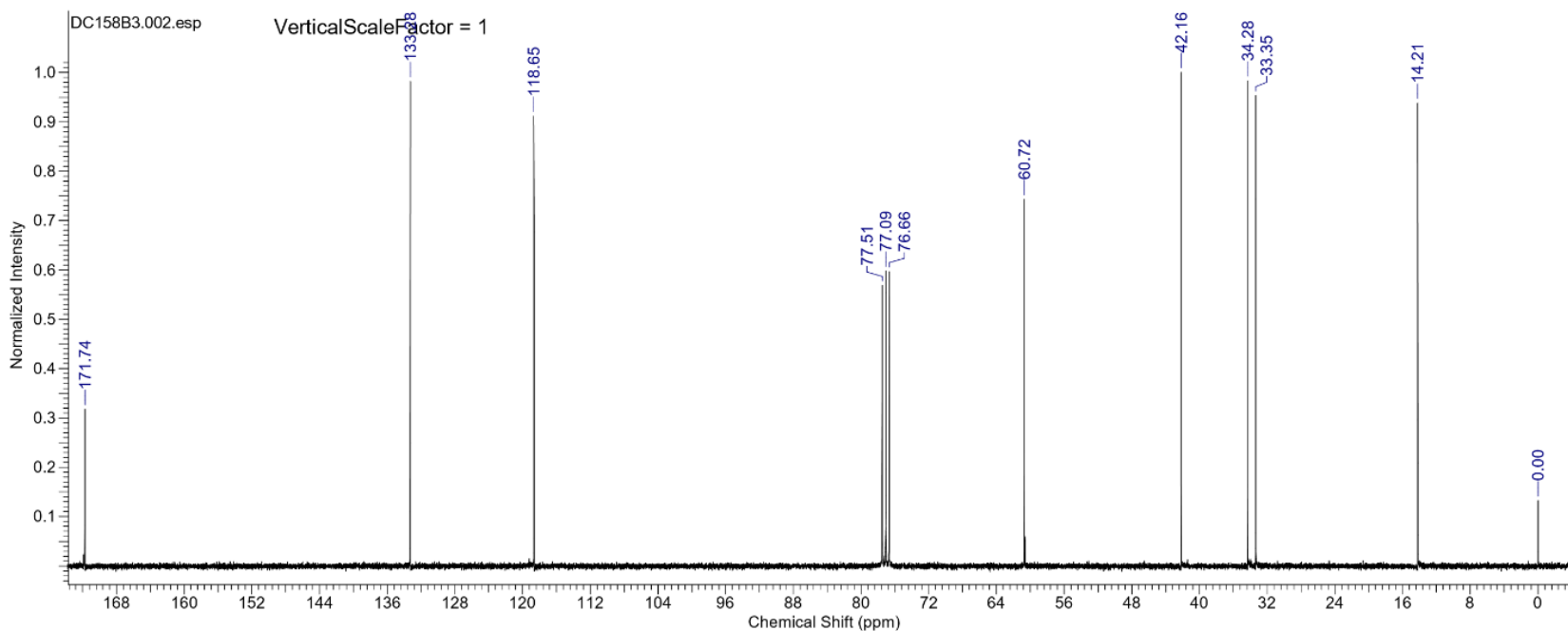
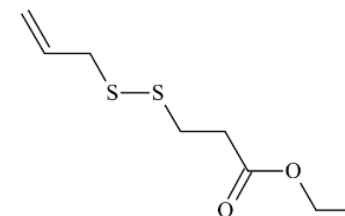
Formula C₈H₁₃NO₃S FW 203.2587

Acquisition Time (sec)	1.8088	Comment	DC28C_C_CDCI3_150513_21659_RG=71	Date	15 May 2013 11:38:08
Date Stamp	15 May 2013 11:38:08	File Name	\\NMR2\Farmaceutica 2013\data\DC\nm\DC28C\3\fid		
Frequency (MHz)	75.47	Nucleus	13C	Number of Transients	1080
Original Points Count	32768	Owner	root	Points Count	32768
Receiver Gain	4597.60	SW(cyclical) (Hz)	18115.94	Solvent	CHLOROFORM-d
Spectrum Offset (Hz)	8270.7080	Spectrum Type	STANDARD	Sweep Width (Hz)	18115.39
				Temperature (degree C)	20.960



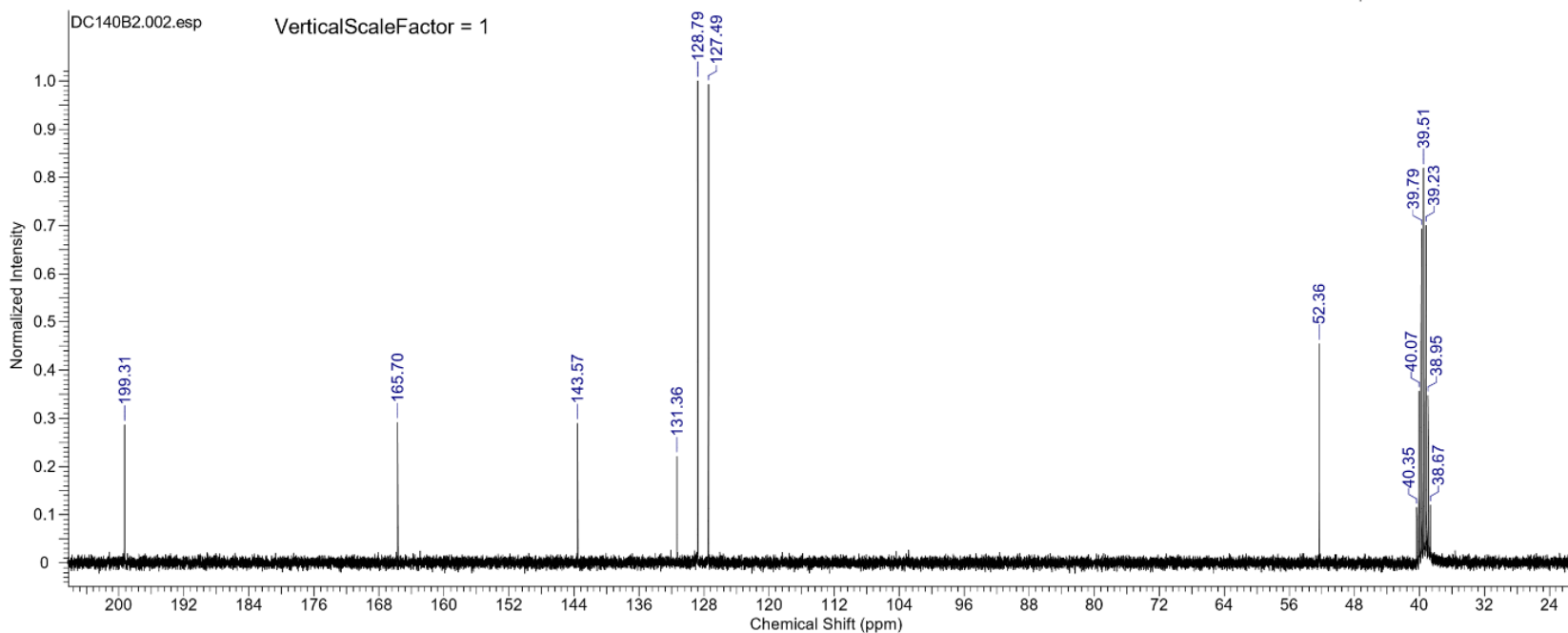
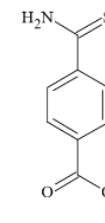
Formula C₈H₁₄O₂S₂ FW 206.3256

Acquisition Time (sec)	1.8088	Comment	DC158B3_13C CDCl3 280715_24232 RG=50	Date	28 Jul 2015 11:59:28
Date Stamp	28 Jul 2015 11:59:28	File Name	\NMR2\farmaceutica 2015\data\DC\nmr\DC158B3\2\fid		
Frequency (MHz)	75.47	Nucleus	13C	Number of Transients	1041
Original Points Count	32768	Owner	root	Points Count	32768
Receiver Gain	4597.60	SW(cyclical) (Hz)	18115.94	Solvent	CHLOROFORM-d
Spectrum Offset (Hz)	8272.0879	Spectrum Type	STANDARD	Sweep Width (Hz)	18115.39
				Temperature (degree C)	24.960



Formula C₉H₉NO₂S FW 195.2383

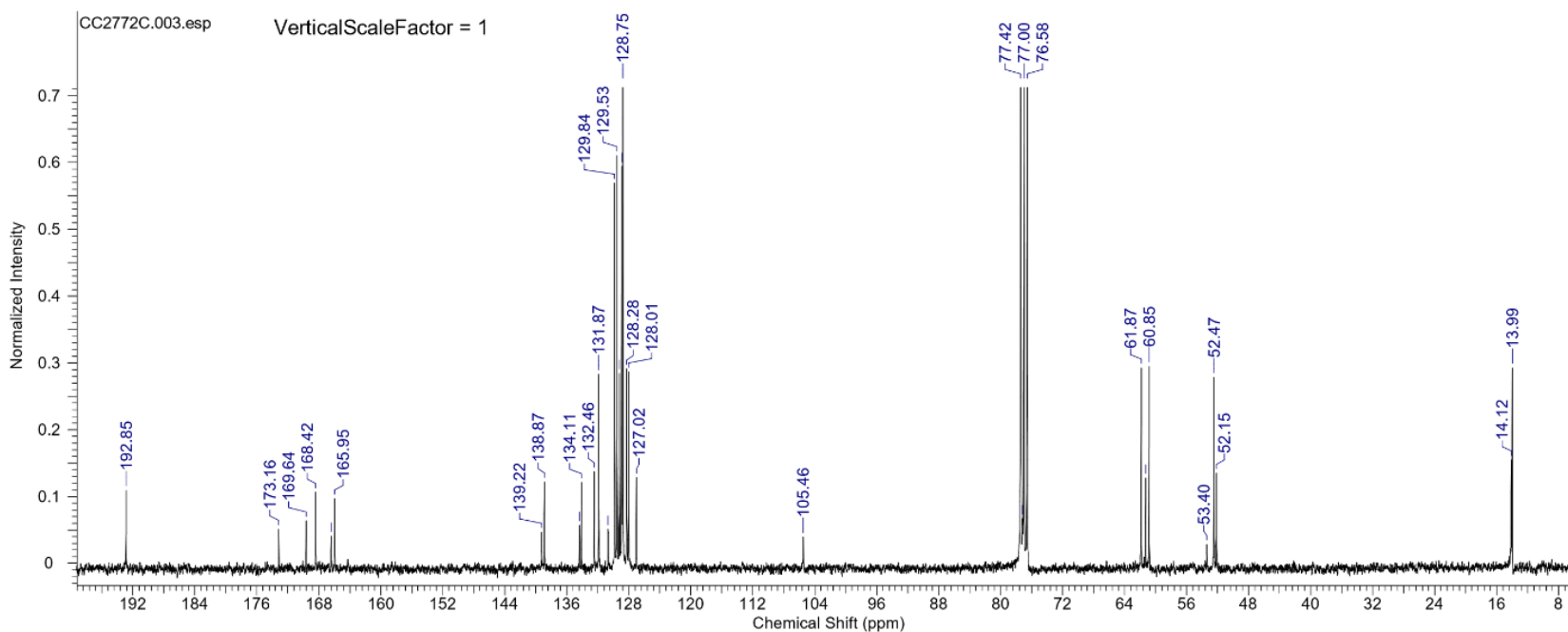
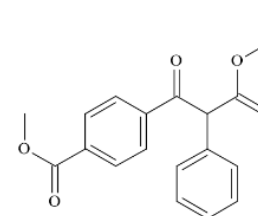
Acquisition Time (sec)	1.8088	Comment	DC140B2_13C DMSO-d6 280715_24230 RG=80	Date	28 Jul 2015 10:42:40
Date Stamp	28 Jul 2015 10:42:40	File Name	\NMR2\farmaceutica 2015\data\DC\nmr\DC140B2\2\fid		
Frequency (MHz)	75.47	Nucleus	13C	Number of Transients	146
Original Points Count	32768	Owner	root	Points Count	32768
Receiver Gain	4597.60	SW(cyclical) (Hz)	18115.94	Solvent	DMSO-d6
Spectrum Type	STANDARD	Sweep Width (Hz)	18115.39	Temperature (degree C)	24.260
				Spectrum Offset (Hz)	8236.8896



This report was created by ACD/NMR Processor Academic Edition. For more information go to www.acdlabs.com/nmrproc/

11/03/2016 15:18:19

Formula	C ₁₉ H ₁₈ O ₅	FW	326.3432		
Acquisition Time (sec)	1.8088	Comment	CC2772C.C.CDCI3_160512_21089	Date	16 May 2012 12:22:56
Date Stamp	16 May 2012 12:22:56	File Name	\\NMR2\Farmaceutica 2013\data\CC\nmr\CC2772C\3\fid		
Frequency (MHz)	75.47	Nucleus	13C	Number of Transients	265
Original Points Count	32768	Owner	root	Points Count	32768
Receiver Gain	4597.60	SW(cyclical) (Hz)	18115.94	Solvent	CHLOROFORM-d
Spectrum Offset (Hz)	8267.6270	Spectrum Type	STANDARD	Sweep Width (Hz)	18115.39
				Temperature (degree C)	21.960

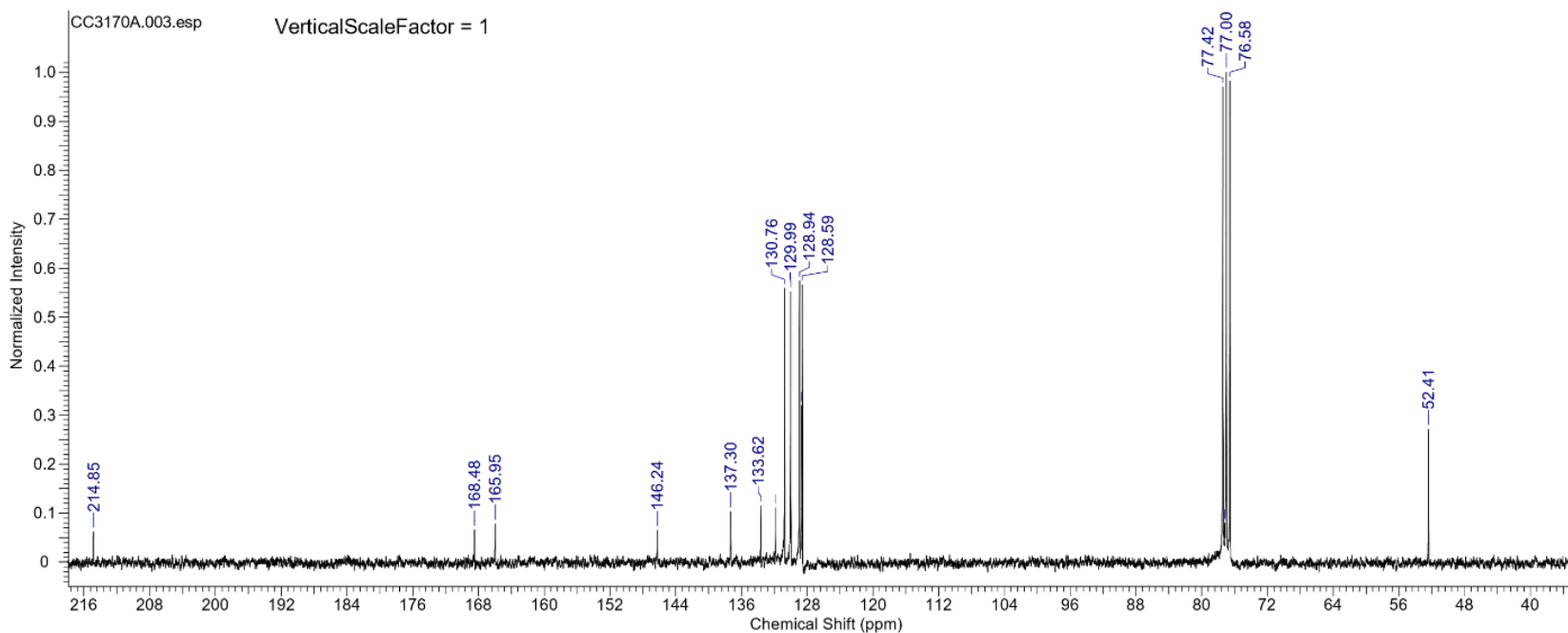
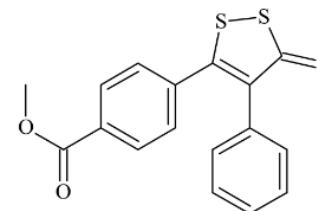


This report was created by ACD/NMR Processor Academic Edition. For more information go to www.acdlabs.com/nmrproc/

10/03/2016 13:43:10

Formula C₁₇H₁₂O₂S₃ FW 344.4710

Acquisition Time (sec)	1.8088	Comment	CC3170A_13C_CDCl3_091014_23013_RG=180	Date	09 Oct 2014 15:15:44
Date Stamp	09 Oct 2014 15:15:44	File Name	\NMR2\Farmaceutica 2014\data\CC\nmr\CC3170A\3\fid		
Frequency (MHz)	75.47	Nucleus	13C	Number of Transients	156
Original Points Count	32768	Owner	root	Points Count	32768
Receiver Gain	4597.60	SW(cyclical) (Hz)	18115.94	Solvent	DMSO-d6
Spectrum Type	STANDARD	Sweep Width (Hz)	18115.39	Temperature (degree C)	22.860
				Spectrum Offset (Hz)	8267.0713

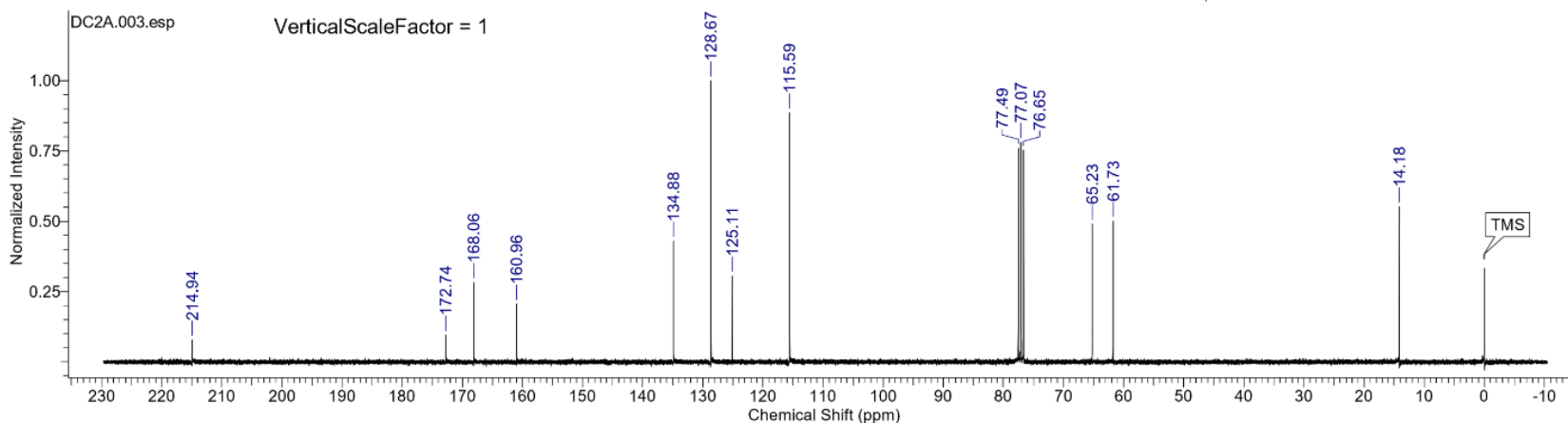
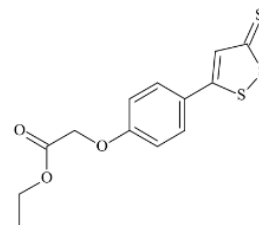


This report was created by ACD/NMR Processor Academic Edition. For more information go to www.acdlabs.com/nmrproc/

10/03/2016 13:47:50

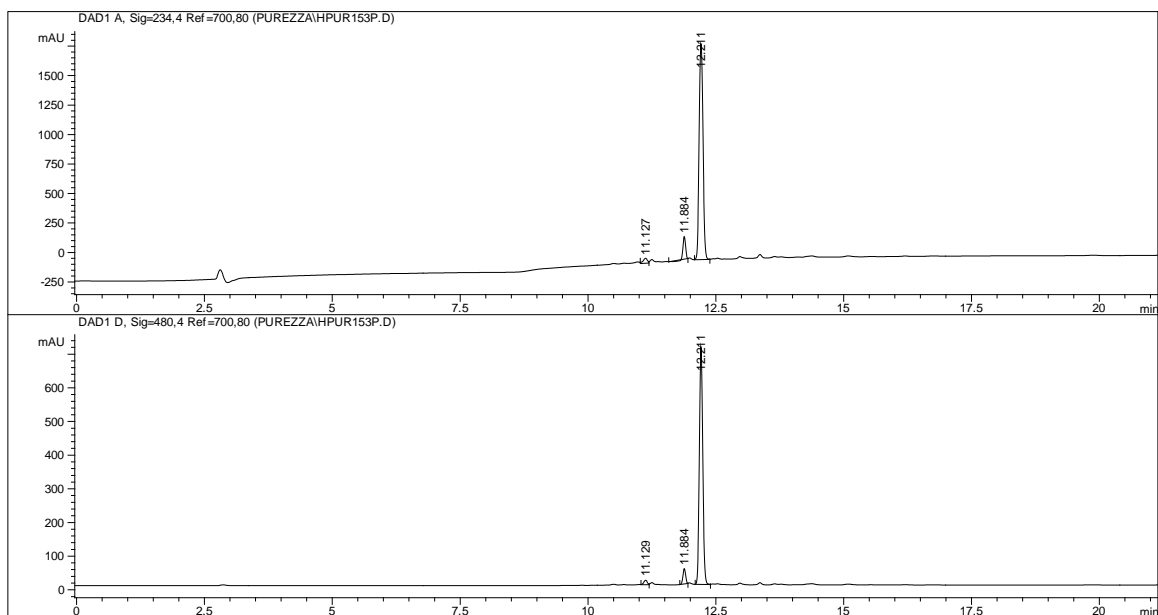
Formula C₁₃H₁₂O₃S₃ FW 312.4276

Acquisition Time (sec)	1.8088	Comment	DC2A_DEPT_CDCI3_090113_21358	Date	09 Jan 2013 11:22:56
Date Stamp	09 Jan 2013 11:22:56	File Name	\\NMR2\Farmaceutica 2013\data\DC\nmr\DC2A\3\fid		
Frequency (MHz)	75.47	Nucleus	13C	Number of Transients	756
Original Points Count	32768	Owner	root	Points Count	32768
Receiver Gain	4597.60	SW(cyclical) (Hz)	18115.94	Solvent	CHLOROFORM-d
Spectrum Offset (Hz)	8270.1494	Spectrum Type	STANDARD	Sweep Width (Hz)	18115.39
				Temperature (degree C)	21.060

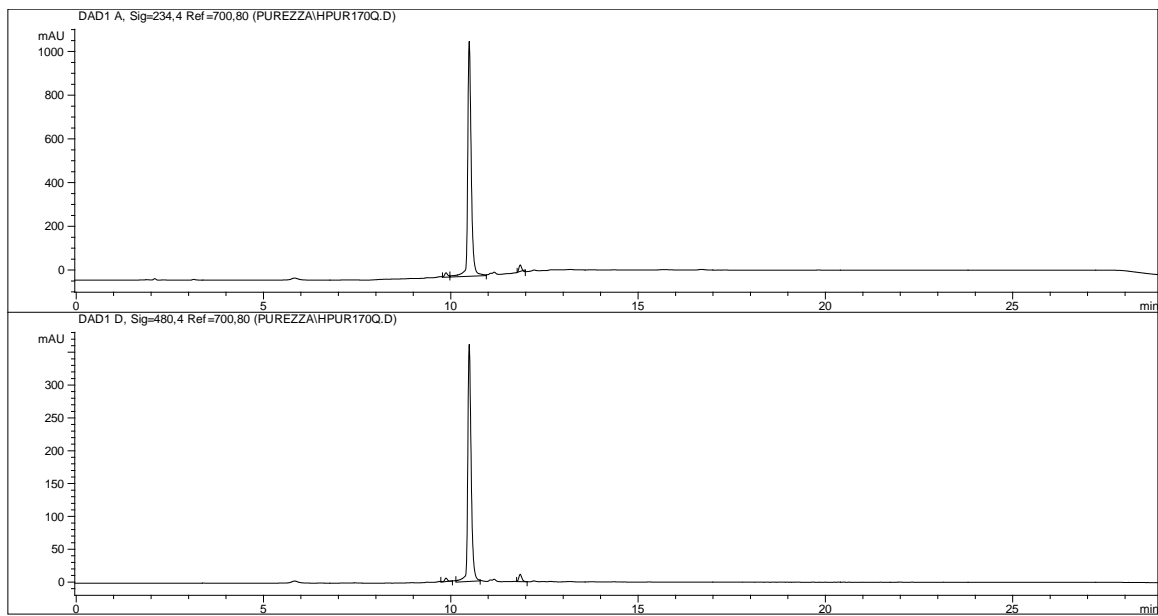


HPLC chromatogram of compounds 10-27. HPLC analysis

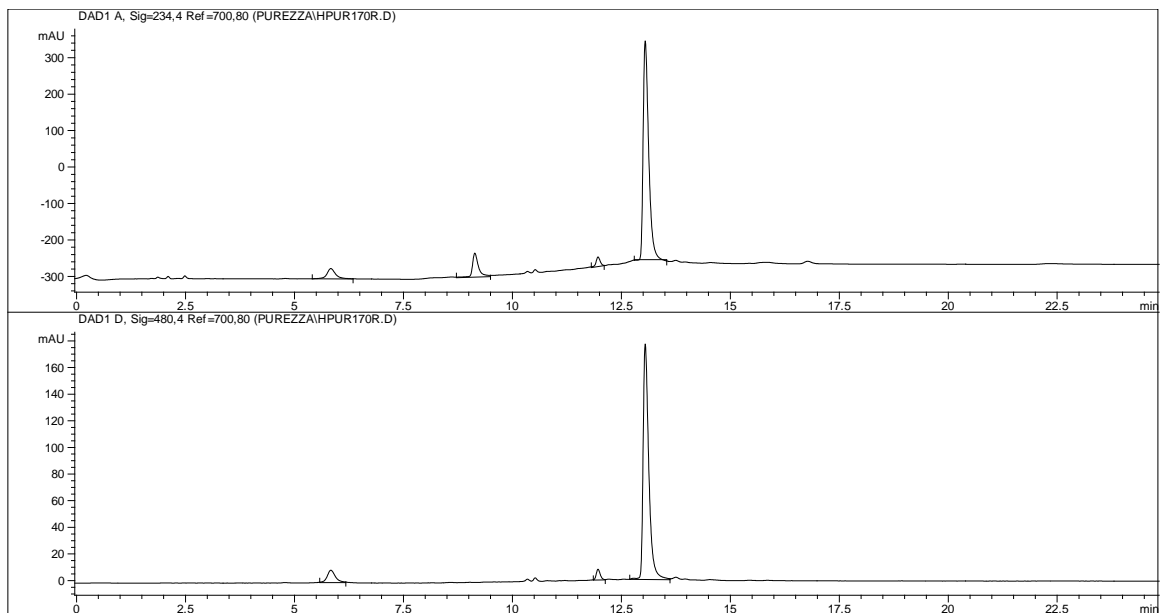
Compound 10. pHPLC 93% t_r 12.2 min.



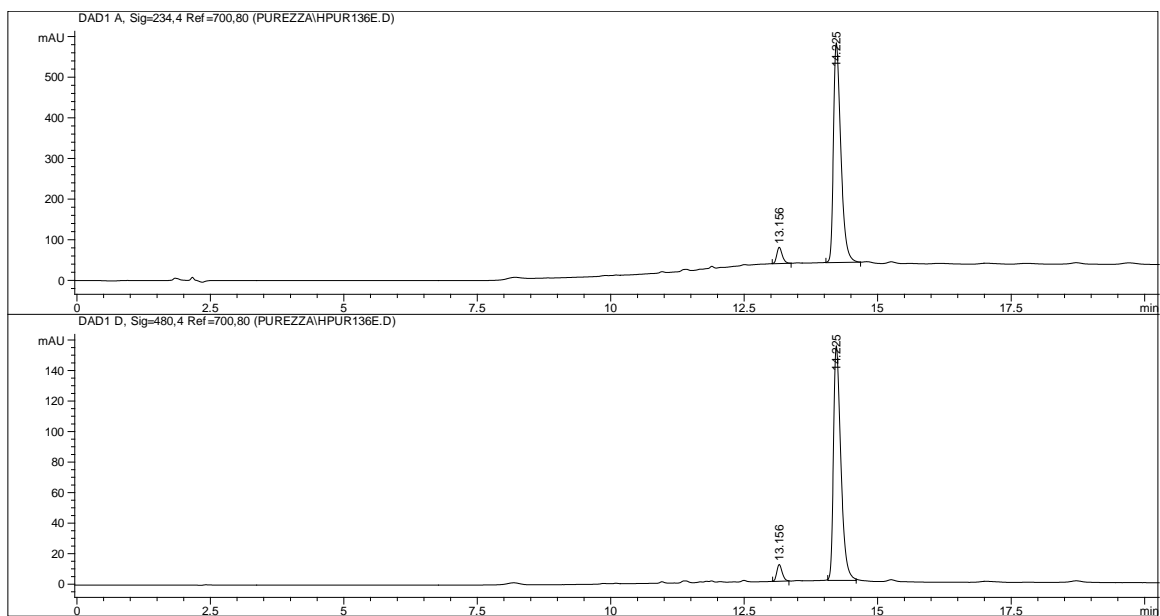
Compound 11. pHPLC 97% t_r 11.9 min.



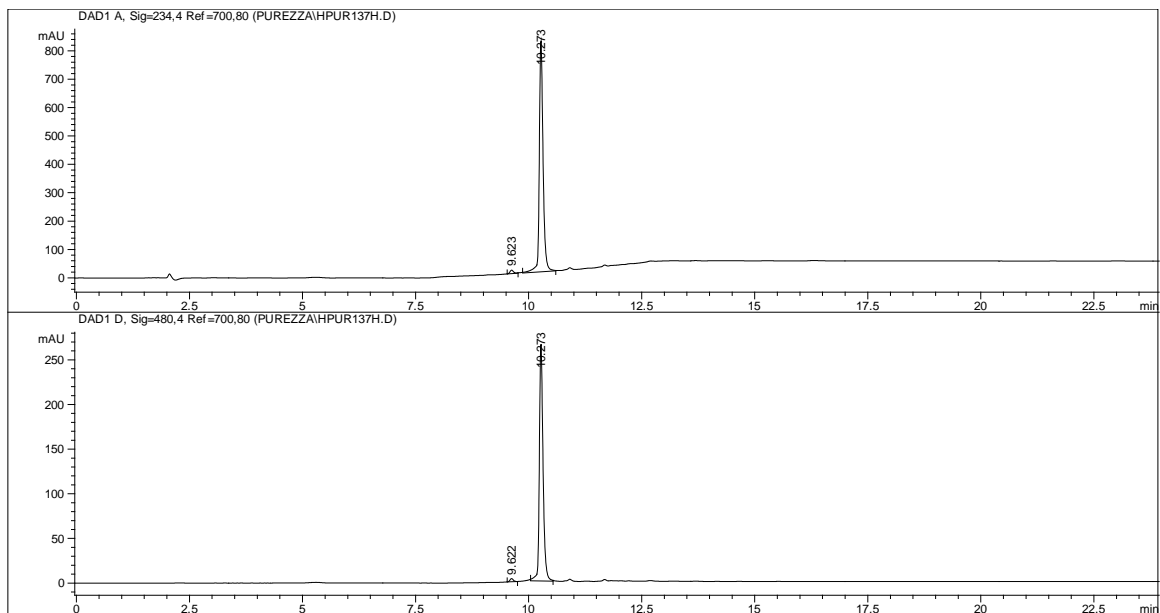
Compound 12. pHPLC 93% t_r 13.0 min.



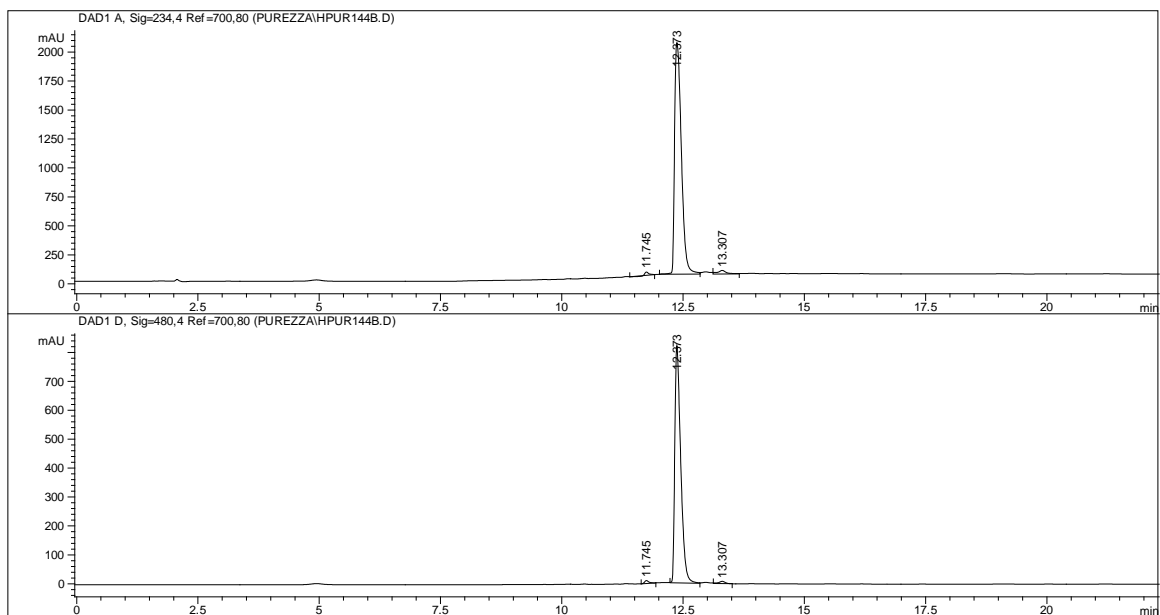
Compound 13. pHPLC 95% t_r 14.2 min.



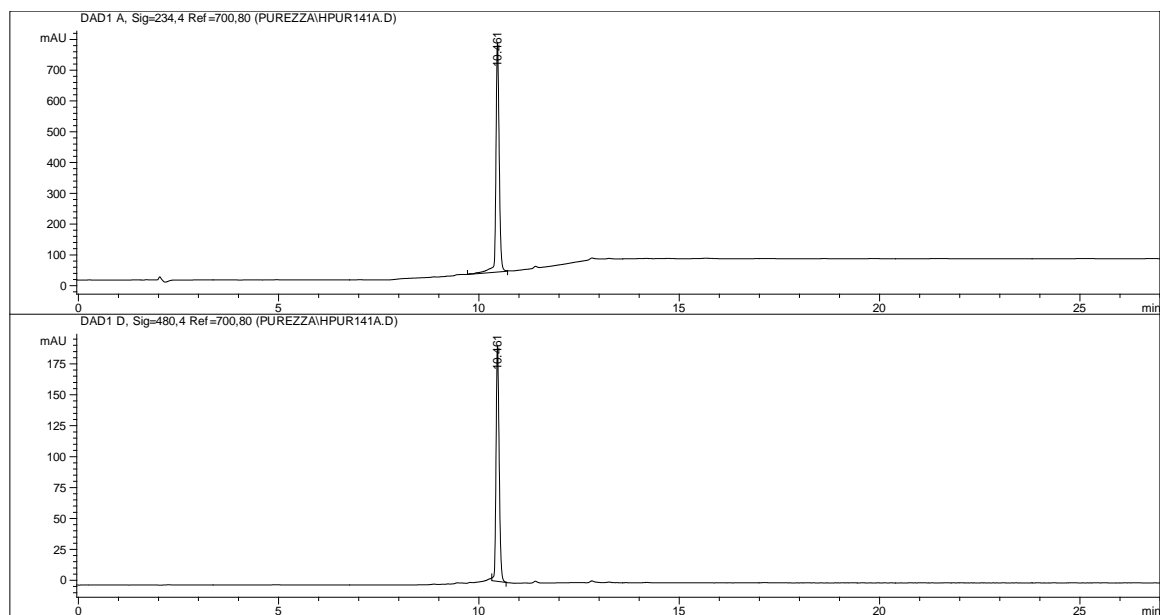
Compound 14. pHPLC 97% t_r 10.3 min.



Compound 15. pHPLC 98% t_r 12.4 min.



Compound 16. pHPLC 99%; t_r 10.5 min.

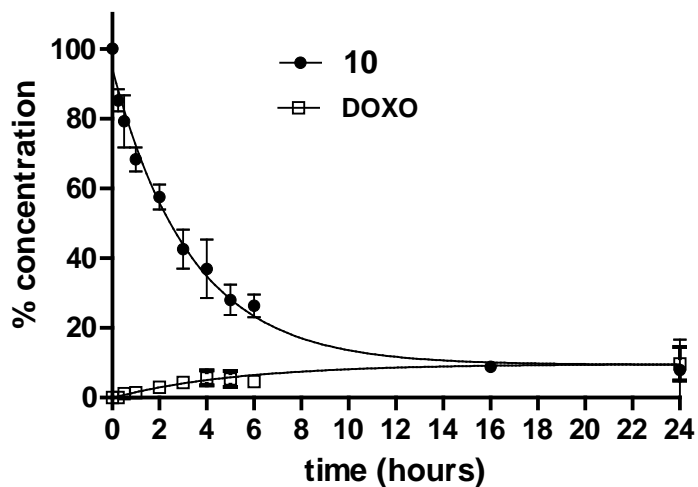


Degradation profile of compounds 10-16 in human serum.

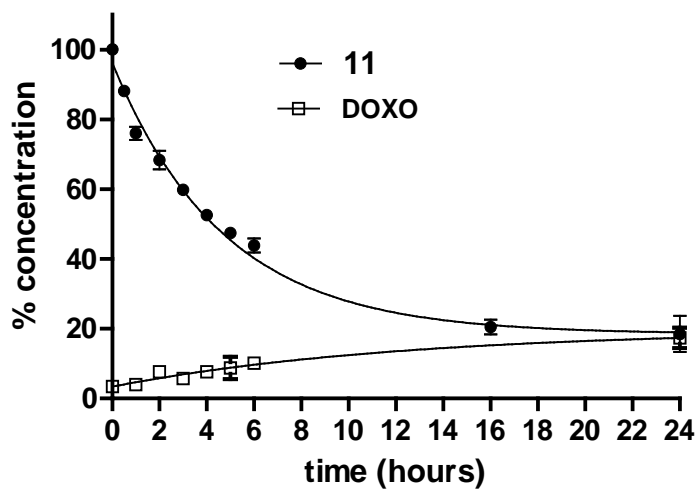
Concentration over time of the H₂S-DOXOs and DOXO in human serum during 24 hours' incubation.

Values are means \pm SEM (SEM < 1; n=3-5).

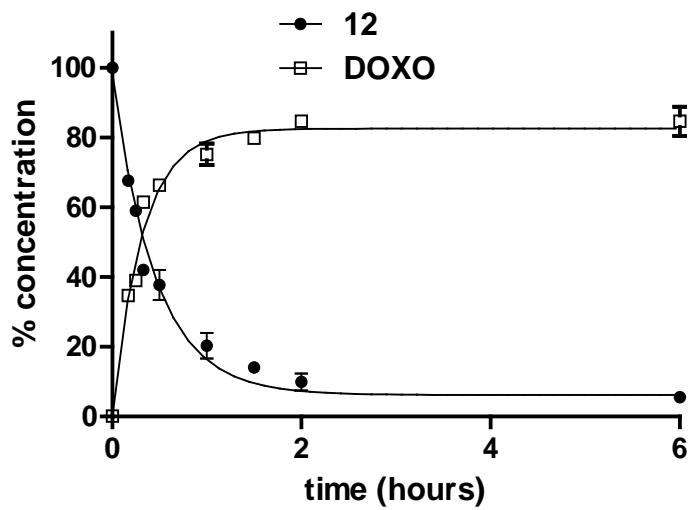
Compound 10



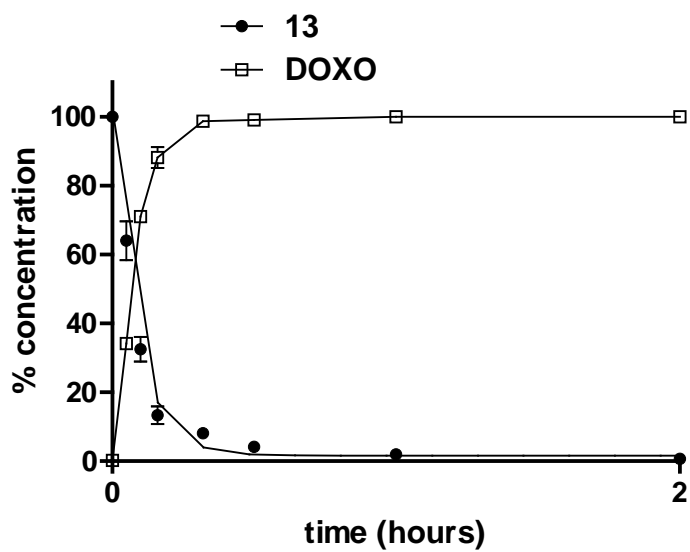
Compound 11



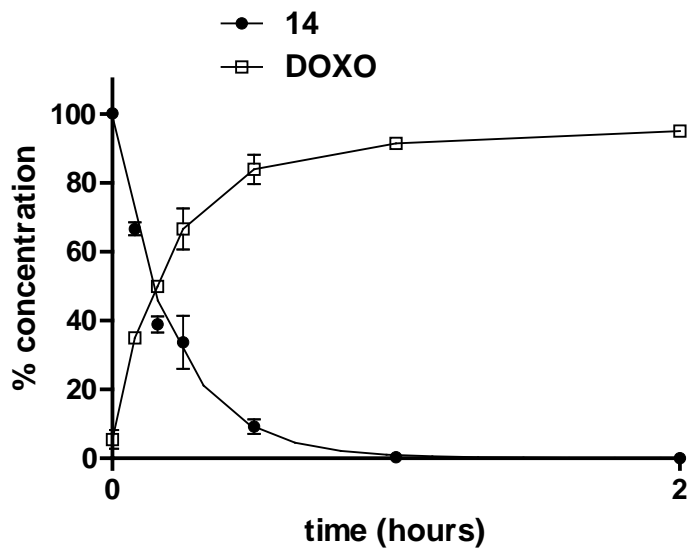
Compound 12



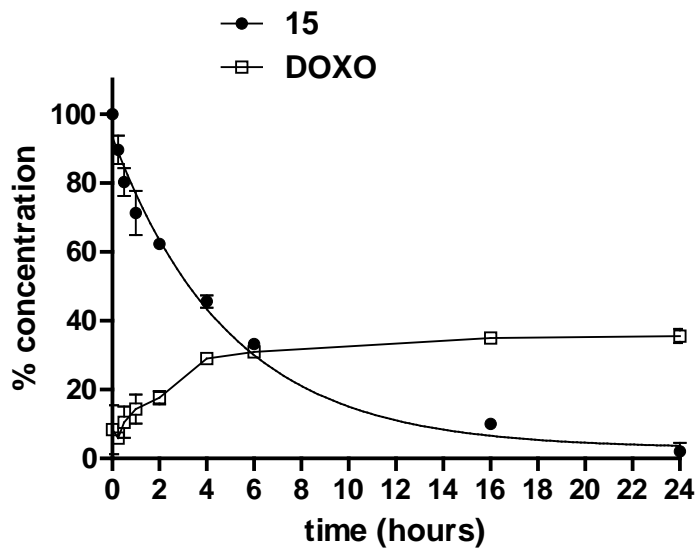
Compound 13



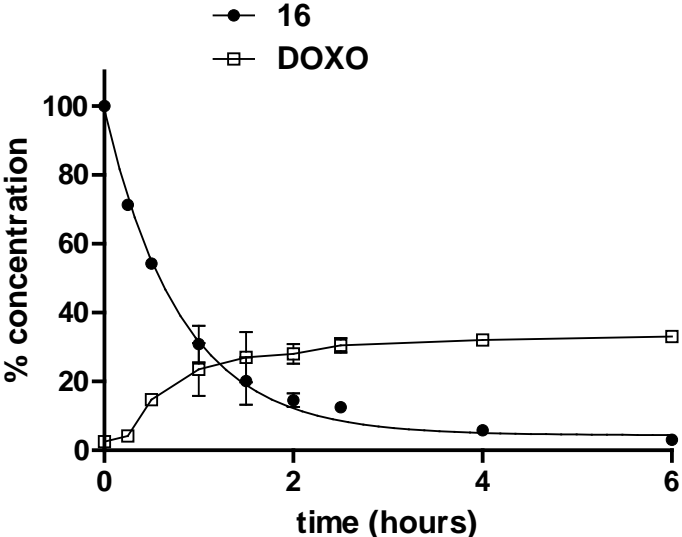
Compound 14



Compound 15



Compound 16



Mitochondria-Targeted Doxorubicin: A New Therapeutic Strategy against Doxorubicin-Resistant Osteosarcoma

Ilaria Buondonno¹, Elena Gazzano¹, Sae Rin Jean^{2,3}, Valentina Audrito^{4,5}, Joanna Kopecka¹, Marilù Fanelli⁶, Iris C. Salaroglio¹, Costanzo Costamagna¹, Ilaria Roato⁷, Eleonora Mungo¹, Claudia M. Hattinger⁶, Silvia Deaglio^{4,5}, Shana O. Kelley^{2,3}, Massimo Serra⁶, and Chiara Riganti¹

Abstract

Doxorubicin is one of the leading drugs for osteosarcoma standard chemotherapy. A total of 40% to 45% of high-grade osteosarcoma patients are unresponsive, or only partially responsive, to doxorubicin (Dox), due to the overexpression of the drug efflux transporter ABCB1/P-glycoprotein (Pgp). The aim of this work is to improve Dox regimens in resistant osteosarcomas. We used a chemically modified mitochondria-targeted Dox (mtDox) against Pgp-overexpressing osteosarcomas with increased resistance to Dox. Unlike Dox, mtDox accumulated at significant levels intracellularly, exerted cytotoxic activity, and induced necrotic and immunogenic cell death in Dox-resistant/Pgp-overexpressing cells, fully reproducing the activities exerted by anthracyclines in drug-sensitive tumors. mtDox reduced tumor growth and cell proliferation, increased apoptosis, primed tumor cells for recognition by the host immune system, and was less

cardiotoxic than Dox in preclinical models of drug-resistant osteosarcoma. The increase in Dox resistance was paralleled by a progressive upregulation of mitochondrial metabolism. By widely modulating the expression of mitochondria-related genes, mtDox decreased mitochondrial biogenesis, the import of proteins and metabolites within mitochondria, mitochondrial metabolism, and the synthesis of ATP. These events were paralleled by increased reactive oxygen species production, mitochondrial depolarization, and mitochondria-dependent apoptosis in resistant osteosarcoma cells, where Dox was completely ineffective. We propose mtDox as a new effective agent with a safer toxicity profile compared with Dox that may be effective for the treatment of Dox-resistant/Pgp-positive osteosarcoma patients, who strongly need alternative and innovative treatment strategies. *Mol Cancer Ther*; 15(11); 2640–52. ©2016 AACR.

Introduction

Osteosarcoma is the most frequent bone tumor observed clinically. The standard treatment for conventional osteosarcoma (tumors, which are not metastatic at clinical onset, with high-grade malignancy, located at the extremities in patients younger than 40 years) is based on pre- and postoperative chemotherapy, including doxorubicin (Dox), cisplatin, and methotrexate. This treatment is successful in about 55% to 60% of patients. Despite

numerous attempts to find new therapeutic approaches for osteosarcoma, the patients' prognosis has not improved in the last decades (1, 2, and references therein). The main drawbacks of Dox are the onset of drug resistance that makes chemotherapy progressively ineffective (2) and the onset of cardiotoxicity (3).

Dox is a substrate of ATP-binding cassette (ABC) transporters, such as ABCB1/P-glycoprotein (Pgp) and ABCC1/multidrug resistance related protein 1 (MRP1), which efflux the drug outside the tumor cell and limit its cytotoxicity (4). The presence of Pgp in osteosarcoma patients is a negative prognostic factor and is predictive of poor response to treatment (5–8). Both natural (9, 10) and synthetic (11, 12) inhibitors of Pgp have been tested to reverse Dox resistance in osteosarcoma cell lines *in vitro*. The specific silencing of Pgp (13) or the inhibition of pathways involved in drug resistance—such as the hypoxia inducible factor-1 α (14) or polo-like kinase 1-dependent signaling (15)—appears to be promising strategies, but the translation of these approaches to clinical settings is still under investigation.

Recently, targeting mitochondria of osteosarcoma cells has been proposed as an effective therapeutic strategy (16). On the other hand, because the heart has an aerobic mitochondria-based metabolism, mitochondria-targeting drugs—while effective on tumor cells—may produce serious cardiotoxicity.

We recently developed chemically modified Dox derivatives with mitochondrial tropism that are effective against drug-resistant tumor cells overexpressing Pgp (17, 18). One of these

¹Department of Oncology, University of Torino, Torino, Italy. ²Department of Pharmaceutical Sciences, Leslie Dan Faculty of Pharmacy, University of Toronto, Toronto, Ontario, Canada. ³Department of Chemistry, Faculty of Arts and Science, University of Toronto, Toronto, Ontario, Canada. ⁴Human Genetics Foundation (HuGeF), Torino, Italy. ⁵Department of Medical Sciences, University of Torino, Torino, Italy. ⁶Orthopaedic Rizzoli Institute, Laboratory of Experimental Oncology, Pharmacogenomics and Pharmacogenetics Research Unit, Bologna, Italy. ⁷Center for Research and Experimental Medicine (Ce.R.M.S.), San Giovanni Battista Hospital, Torino, Italy.

Note: Supplementary data for this article are available at Molecular Cancer Therapeutics Online (<http://mct.aacrjournals.org/>).

Corresponding Author: Chiara Riganti, University of Torino, via Santena 5/bis, 10126 Torino, Italy. Phone: 390116705857; Fax: 390116745845; E-mail: chiara.riganti@unito.it

doi: 10.1158/1535-7163.MCT-16-0048

©2016 American Association for Cancer Research.

mitochondria-targeted Dox compounds (mtDox; 18) did not elicit cardiotoxicity in animals, showing a safer toxicity profile compared with Dox (19).

In this work, we used mtDox against Pgp-overexpressing osteosarcomas *in vitro* and *in vivo* and found that it was significantly more effective and less cardiotoxic than Dox, and that it overcame drug resistance by exploiting the metabolic signature typical of drug-resistant osteosarcoma cells. Our data indicate mtDox as a very promising new chemotherapeutic drug for a possible clinical application in Dox-unresponsive patients.

Materials and Methods

Chemicals

FBS and culture medium were from Invitrogen Life Technologies. Plasticware for cell cultures was from Falcon (Becton Dickinson). The protein content in cell monolayers, mitochondrial, and nuclear extracts was assessed with the BCA Kit from Sigma Chemical Co. Electrophoresis reagents were obtained from Bio-Rad Laboratories. Dox was purchased by Sigma Chemical Co. mtDox (Supplementary Fig. S1) was synthesized as described in ref. 18. Unless otherwise specified, all the other reagents were purchased from Sigma Chemical Co.

Cell lines

Murine osteosarcoma K7M2 cells, human Dox-sensitive osteosarcoma U-2OS and Saos-2 cells, and rat neonatal H9c2 cardiomyocytes were purchased from the ATCC in 2012. The corresponding variants with increasing resistance to Dox (U-2OS/DX30, U-2OS/DX100, U-2OS/DX580, Saos-2/DX30, Saos-2/DX100, and Saos-2/DX580), selected by culturing parental cells in a medium with 30, 100, and 580 ng/mL Dox, were generated as reported in ref. 20. All cell lines were authenticated by microsatellite analysis, using the PowerPlex Kit (Promega Corporation; last authentication: September 2015). Mesenchymal stem cells, derived by discarded lipoaspirates of healthy subjects, were cultured in osteogenic condition to obtain primary nontransformed osteoblasts (21, 22). Fourteen days after culture, Bone Alkaline Phosphatase (BAP staining Kit; Sigma Chemicals Co.) was performed as authentication test for osteoblasts (last authentication: April 2016). Cells were maintained in medium supplemented with 10% v/v FBS, 1% v/v penicillin–streptomycin, and 1% v/v L-glutamine. Drug-resistant variants were continuously cultured in presence of Dox.

Cell viability and proliferation

Cell viability was measured by the neutral red staining method, as previously reported (23). The absorbance of untreated cells was considered as 100% viability; the results were expressed as a percentage of viable cells versus untreated cells. To determine IC_{50} , reported in Supplementary Table S1, 1×10^5 cells were incubated for 72 hours with increasing concentrations of Dox or mtDox (from 1 nmol/L to 1 mmol/L). IC_{50} was considered the concentration of the drug that reduced cell viability to 50%. Cell-cycle analysis was measured by flow cytometry, after propidium iodide staining (24).

ABCB1/Pgp and ABCC1/MRP1 expression

For flow cytometry assays, cells were harvested, washed once in PBS, twice with 10 mmol/L Hepes in Hank's balanced salt solution, and fixed with 4% paraformaldehyde in PBS for 5 minutes.

After a wash in Hepes, cells were permeabilized in 0.1% w/v saponin and incubated with an anti-ABCB1/Pgp (clone MRK16; Kamiya) or anti-ABCC1/MRP1 (clone MRPm5; Abcam) antibodies. After washing with saponin, cells were incubated with a secondary anti-mouse FITC-conjugated antibody (Sigma Chemical Co.), washed twice with saponin and once with Hepes. In the negative control, primary antibody was replaced by 0.1% saponin. Samples were analyzed by flow cytometry (FACSCalibur; Becton Dickinson). For Western blot analysis, 20 μ g of proteins from cell lysates were probed with anti-Pgp (clone 17F9; BD Biosciences) or anti- β -tubulin (clone D-10; Santa Cruz Biotechnology Inc.) antibodies.

Confocal microscope analysis

Cells (5×10^5) were grown on sterile glass coverslips and transfected with the GFP-E1 α pyruvate dehydrogenase expression vector (Cell Light BacMan 2.0; Invitrogen Life Technologies) to label mitochondria. After 24 hours, cells were incubated with 5 μ mol/L Dox or mtDox for 6 hours. Samples were rinsed with PBS, fixed with 4% w/v paraformaldehyde for 15 minutes, washed 3 times with PBS and once with water, and mounted with 4 μ L of Gel Mount Aqueous Mounting. Slides were analyzed using an Olympus FV300 laser scanning confocal microscope (Olympus Biosystems; ocular lens: 10X; objective: 60X). For each experimental condition, a minimum of 5 microscopic fields were examined.

Isolation of mitochondria and nuclei

Mitochondria were isolated as reported in ref. 25. A 50 μ L aliquot was sonicated and used for the measurement of protein content or Western blotting; the remaining part was stored at -80°C until use. To confirm the presence of mitochondrial proteins in the extracts, 10 μ g of each sonicated sample were subjected to SDS-PAGE and probed with an anti-porin antibody (clone 20B12AF2; Abcam). To exclude any mitochondrial contamination in the cytosolic extracts, the absence of porin in the latter was analyzed by Western blotting. Nuclear proteins were extracted using the Nuclear Extract Kit (Active Motif). To exclude any cytosolic contamination in the nuclear extracts, the absence of actin (#A2066; Sigma Chemical Co.) in the latter was analyzed by Western blotting.

Dox accumulation

Cellular, nuclear, or mitochondrial extracts were resuspended in 0.5 mL ethanol/0.3 N HCl. The amount of Dox was measured fluorimetrically (17). Fluorescence was converted into nmol/mg cellular, nuclear, or mitochondrial proteins, using a previously set calibration curve.

Necrotic and immunogenic death assays

The activity of lactate dehydrogenase (LDH) released in the extracellular medium, taken as index of necrotic cell death, was measured spectrophotometrically (26). The results were expressed as the percentage of extracellular LDH activity versus total (intracellular + extracellular) LDH activity. To evaluate the immunogenic cell death induced by Dox, the extracellular release of ATP was measured by a chemiluminescence-based assay, the extracellular release of high mobility group box 1 (HMGB1) protein was measured by Western blotting. Following a procedure commonly used in the immunoblotting of extracellular proteins (27), we stained the blot with Red Ponceau and reported a band at

the same level of the HMGB1 band, as the control of equal protein loading. Surface translocation of calreticulin, detected by flow cytometry, was measured (27). The mean fluorescence intensity was calculated using Cell Quest software (Becton Dickinson).

Tumor cell phagocytosis

Murine dendritic cells (DC) were obtained as reported by Obeid and colleagues (28). Tumor cell phagocytosis was performed by flow cytometry (28). In each set of experiments, a phagocytosis assay was performed by coincubating DCs and tumor cells at 4°C, instead of 37°C, and the percentage of phagocytized cells at 4°C was subtracted from values observed at 37°C. The phagocytosis rate was expressed as a phagocytic index, calculated as previously reported (28).

In vivo tumor growth, hematochemical parameters, and immunohistochemical analysis

1×10^6 K7M2 cells, stably transfected with the pGL4.51[luc2/CMV/Neo] Vector (Promega Corporation), mixed with 100 μ L Matrigel, were injected s.c. in 6-week-old female BALB/c mice (weight: 20 g \pm 1.3; Charles River Laboratories Italia); 1×10^7 U-2OS cells, mixed with 100 μ L Matrigel, were injected s.c. in 6-week-old female NOD SCID BALB/c mice (weight: 19.6 g \pm 1.6; Charles River Laboratories Italia). Animals were housed (5 per cage) under 12-hour light/dark cycles, with food and drinking provided *ad libitum*. Tumor growth was measured daily by caliper and calculated according to the equation $(L \times W^2)/2$, where L = tumor length and W = tumor width. When the tumor reached a volume of 50 mm³ (day 7 after injection), the mice were randomized into 3 groups: (1) Control group, treated with 0.1 mL saline solution i.v. on days 7, 14, 21, and 28; (2) Dox group, treated with Dox i.v. on days 7, 14, 21, and 28; (3) mtDox group, treated with mitochondria-targeting Dox i.v. on days 7, 14, 21, and 28. *In vivo* bioluminescence imaging was performed on days 7, 21, and 35 with a Xenogen IVIS Spectrum (PerkinElmer). Tumor volumes were monitored daily by caliper, and animals were euthanized by injecting zolazepam (0.2 mL/kg) and xylazine (16 mg/kg) i.m. at day 35. The inhibition rate was calculated as a percentage (i.e., the tumor weight of the control group minus that of the tumor weight of the test group) divided by the tumor weight of the control group. The hematochemical parameters LDH, aspartate aminotransferase (AST), alanine aminotransferase (ALT), alkaline phosphatase (AP), creatinine, creatine phosphokinase (CPK) were measured on 0.5 mL of blood collected immediately after mice sacrifice, using the respective kits from Beckman Coulter Inc. For immunohistochemical analysis, tumors were resected and fixed in 4% v/v paraformaldehyde. The paraffin sections were stained with hematoxylin/eosin or immunostained for Ki67 (AB9260; Millipore), cleaved caspase 3 (#9661, Asp175; Cell Signaling Technology Inc.), calreticulin (#PA3900; Affinity Bioreagents), CD11c (clone HL3; BD Biosciences), followed by a peroxidase-conjugated secondary antibody (Dako). Nuclei were counterstained with hematoxylin. Sections were examined with a Leica DC100 microscope (Leica Microsystems GmbH; 10 \times ocular lens, 20 \times objective).

All animal care and experimental procedures were approved by the Bio-Ethical Committee of the University of Torino, Italy.

PCR arrays and qRT-PCR

Total RNA was extracted and reverse-transcribed using the iScript cDNA Synthesis Kit (Bio-Rad Laboratories). The PCR arrays

were performed on 1 μ g cDNA, using Mitochondria and Mitochondria Energy Metabolism Arrays (Bio-Rad Laboratories). The expression levels of specific mitochondria-related genes, representative of the main biological categories screened by PCR arrays, were validated by qRT-PCR. Primer sequences were designed using qPrimerDepot software (<https://primerdepot.nci.nih.gov/>). *S14* was used as the housekeeping gene. Data analysis was performed with PrimePCR Analysis Software (Bio-Rad Laboratories).

Mitochondrial DNA quantification

Mitochondrial DNA was extracted, amplified, and quantified by PicoGreen (Invitrogen Life Technologies) staining as reported in ref. 19. The results are expressed as ng DNA/10⁵ cells.

Mitochondria biogenesis

The expression of peroxisome proliferator-activated receptor gamma coactivator-1 α (PGC-1 α), measured on 30 μ g of nuclear proteins and considered an index of increased mitochondria biogenesis (29), was evaluated by Western blotting, using an anti-PGC-1 α (#ab54481; Abcam) antibody. An anti-TATA-box binding protein (TBP; clone 58C9; Santa Cruz Biotechnology Inc.) was used to check equal protein loading. Mitochondria biogenesis was also evaluated by measuring the expressions of subunit I of complex IV (COX-I), which is encoded by mitochondrial DNA, and succinate dehydrogenase-A of complex II (SDH-A), which is encoded by nuclear DNA, using the MitoBiogenesis In-Cell ELISA Kit (Abcam). The results are expressed as units (U) of each protein/mg mitochondrial proteins.

Tricarboxylic acid cycle

The glucose flux through tricarboxylic acid (TCA) cycle was measured by radiolabeling cells with 2 μ Ci/mL [6-¹⁴C]-glucose (55 mCi/mmol; PerkinElmer). Cell suspensions were incubated for 1 hour in a closed experimental system to trap the ¹⁴CO₂ developed from [¹⁴C]-glucose. The reaction was stopped by injecting 0.8 N HClO₄. The amount of glucose transformed into CO₂ through the TCA cycle was calculated as described by Riganti and colleagues (30) and expressed as pmol CO₂/h/mg cellular proteins.

Fatty acids β -oxidation

Long-chain fatty acids β -oxidation was measured as detailed in ref. 31. The precipitates, containing ¹⁴C-acid soluble metabolites (ASM), were collected. The radioactivity of each sample was counted by liquid scintillation. Results are expressed as nmol/min/mg cellular proteins. In each experimental set, cells were preincubated for 30 minutes with the carnitine palmitoyltransferase inhibitor etomoxir (1 μ mol/L) or with the AMP-kinase activator 5-aminoimidazole-4-carboxamide ribonucleotide (AICAR; 1 mmol/L), as negative and positive controls, respectively. In the presence of etomoxir, the rate of β -oxidation was less than 10% than in its absence; in the presence of AICAR, the rate of β -oxidation was increased 2-fold.

Mitochondrial energy metabolism

The oxygen consumption rate (OCR) was measured on 20,000 cells with the XFp Mito Stress Test Kit, using a Seahorse XFp Extracellular Flux Analyzer (Seahorse Bioscience, M&M Biotech). Carbonyl cyanide 4-(trifluoromethoxy) phenylhydrazone (FCCP) was used at a concentration of 0.3 μ mol/L to uncouple mitochondrial oxidative phosphorylation and induce maximal

respiration. The data were analyzed using Wave Seahorse software. The amount of ATP produced by oxidative phosphorylation was measured on 20 μg mitochondrial proteins with the ATP Bioluminescent Assay Kit (FL-AA; Sigma Chemical Co.). Data were converted into nmol/mg mitochondrial proteins, using a previously set calibration curve.

Intramitochondrial reactive oxygen species levels

After extraction, mitochondria were incubated with the reactive oxygen species (ROS)-sensitive probe 5-(and-6)-chloromethyl-2',7'-dichlorodihydro-fluorescein diacetate-acetoxymethyl ester (5 $\mu\text{mol/L}$; DCFDA-AM), as described (32). The results are expressed as nmol/mg mitochondrial proteins.

Mitochondrial electric potential ($\Delta\psi$) measurement

Staining with JC-1 fluorescent probe (Biotium Inc.) was performed (32). The fluorescence units were used to calculate the percentage of green-fluorescent (i.e., depolarized) mitochondria versus red-fluorescent (i.e., polarized) mitochondria.

Apoptosis measurement

20 μg proteins of whole cell, cytosolic, or mitochondrial extracts were subjected to the Western blot analysis with the following antibodies (all from Cell Signaling Technology): anti-BAD (clone 11E3); anti-BAK (clone D4E4); anti-BAX (#2772); anti-BID (#2002); anti-BIM (clone C34C5); anti-PUMA (clone D30C10); anti-BCL-2 (#2872); anti-BCL-xL (clone #2762); anti-cytochrome c (#4272). Images were acquired by Image Lab software (Bio-Rad Laboratories). Caspase 9 and caspase 3 activity was measured fluorimetrically in the cytosolic extracts (17). The results are expressed as nmol of the hydrolyzed substrate of each caspase/mg cellular proteins, according to a previously set titration curve.

Statistical analysis

All data in the text and figures are provided as mean \pm SD. The results were analyzed by a one-way ANOVA and Tukey test. $P < 0.05$ was considered significant.

Results

Mitochondria-targeted Dox is effective against Dox-resistant osteosarcoma

We compared the antitumor efficacy of Dox and mtDox in the Dox-sensitive human osteosarcoma U-2OS cells and in the corresponding Dox-resistant variants U-2OS/DX30, U-2OS/DX100, U-2OS/DX580, with increasing expression of Pgp and MRP1 (Supplementary Fig. S2). Dox exhibited typical nuclear localization in U-2OS cells (Fig. 1A). There was a high accumulation of the drug in the nuclear extracts (Fig. 1B) and a low accumulation in mitochondria (Fig. 1C) in U-2OS cells, whereas both nuclear and mitochondrial accumulation progressively decreased in U-2OS/DX30, U-2OS/DX100, and U-2OS/DX580 cells. By contrast, mtDox had a distinct mitochondrial localization profile in U-2OS cells (Fig. 1A): intranuclear accumulation was very low in both sensitive and resistant cells (Fig. 1B); intramitochondrial accumulation was significantly higher than Dox and progressively increased in the resistant cells (Fig. 1C). At a concentration (5 $\mu\text{mol/L}$) corresponding to the IC_{50} in chemosensitive osteosarcoma (Supplementary Table S1), Dox retention in the whole cell was progressively lower (Fig. 1D), and the inhibition of cell

survival was lost (Fig. 1E) in the resistant variants. However, at the same concentration, mtDox exhibited lower intracellular accumulation in the most resistant variants (Fig. 1D), but it still reduced cell survival (Fig. 1E).

Dox is one of the few chemotherapeutic drugs able to induce direct cytotoxicity on tumor cells, as indicated by the extracellular release of LDH (26), and to elicit tumor immunogenic cell death, typically followed by tracking the extracellular release of ATP and HMGB1, and by monitoring cell surface levels of the immune-activating protein calreticulin (33). In U-2OS cells, Dox increased the extracellular release of LDH (Fig. 1F), ATP (Fig. 1G) and HMGB1 (Fig. 1H), and surface expression of calreticulin (Fig. 1I), but it progressively lost these properties in the resistant variants. By contrast, mtDox increased all these parameters in sensitive and resistant cells (Fig. 1F-I).

The effects of mtDox were not cell- or species-specific. Indeed, mtDox exhibited greater intracellular accumulation and was more cytotoxic than Dox in human Saos-2 cells and the corresponding resistant variants Saos-2/DX30, Saos-2/DX100, and Saos-2/DX580 cells (Supplementary Fig. S3A and S3B; Supplementary Table S1), as well as in murine Pgp-expressing K7M2 cells (Supplementary Fig. S3C-S3E; Supplementary Table S1). However, mtDox exhibited lower intracellular accumulation (Supplementary Fig. S4A and S4D) and was less toxic (Supplementary Fig. S4B, S4C, S4E, and S4F), in nontransformed osteoblasts and H9c2 cardiomyocytes, where it had a higher IC_{50} than Dox (Supplementary Table S1).

K7M2 tumors implanted in immunocompetent BALB/c mice did not respond to the MTD (5 mg/kg) of Dox (Fig. 2A-C). Dox neither reduced K7M2 cell proliferation (Fig. 2D), nor increased the activity of caspase 3 (Fig. 2E), the amount of surface calreticulin (Fig. 2F), the tumor cell phagocytosis by DCs (Fig. 2G). On the contrary, mtDox elicited all these effects (Fig. 2). Immunohistochemical staining of K7M2 tumor sections confirmed that mtDox reduced tumor cell proliferation, increased apoptotic and calreticulin-positive cells, and increased intratumor infiltration of DCs (Supplementary Fig. S5). According to the hematological parameters of the animals at the time of sacrifice, mtDox was significantly less cardiotoxic than Dox and did not elicit liver or kidney toxicity (Table 1). Dose-response experiments revealed that the antitumor effect of mtDox was dose-dependent and that the drug was still effective against resistant osteosarcoma at 1 of 5 of Dox MTD (Supplementary Fig. S6). By contrast, mtDox did not produce any significant advantage compared with Dox against drug-sensitive tumors (Supplementary Fig. S7).

Mitochondria-targeting Dox deeply alters the expression of mitochondria-related genes in Dox-resistant osteosarcoma cells

We next analyzed the expression of genes involved in mitochondria functions and mitochondria-dependent apoptosis. As shown in Fig. 3A and Supplementary Table S2, the progressive increase in Dox resistance was paralleled by the upregulation of genes controlling processing, import, and folding of mitochondrial proteins; mitochondrial fusion, fission, and trafficking; transport of metabolites and cofactors across the mitochondrial membranes; mitochondrial metabolic pathways, such as TCA cycle, fatty acids β -oxidation, and electron transport; ATP synthesis; and ROS protection, such as superoxide dismutase (SOD) 1

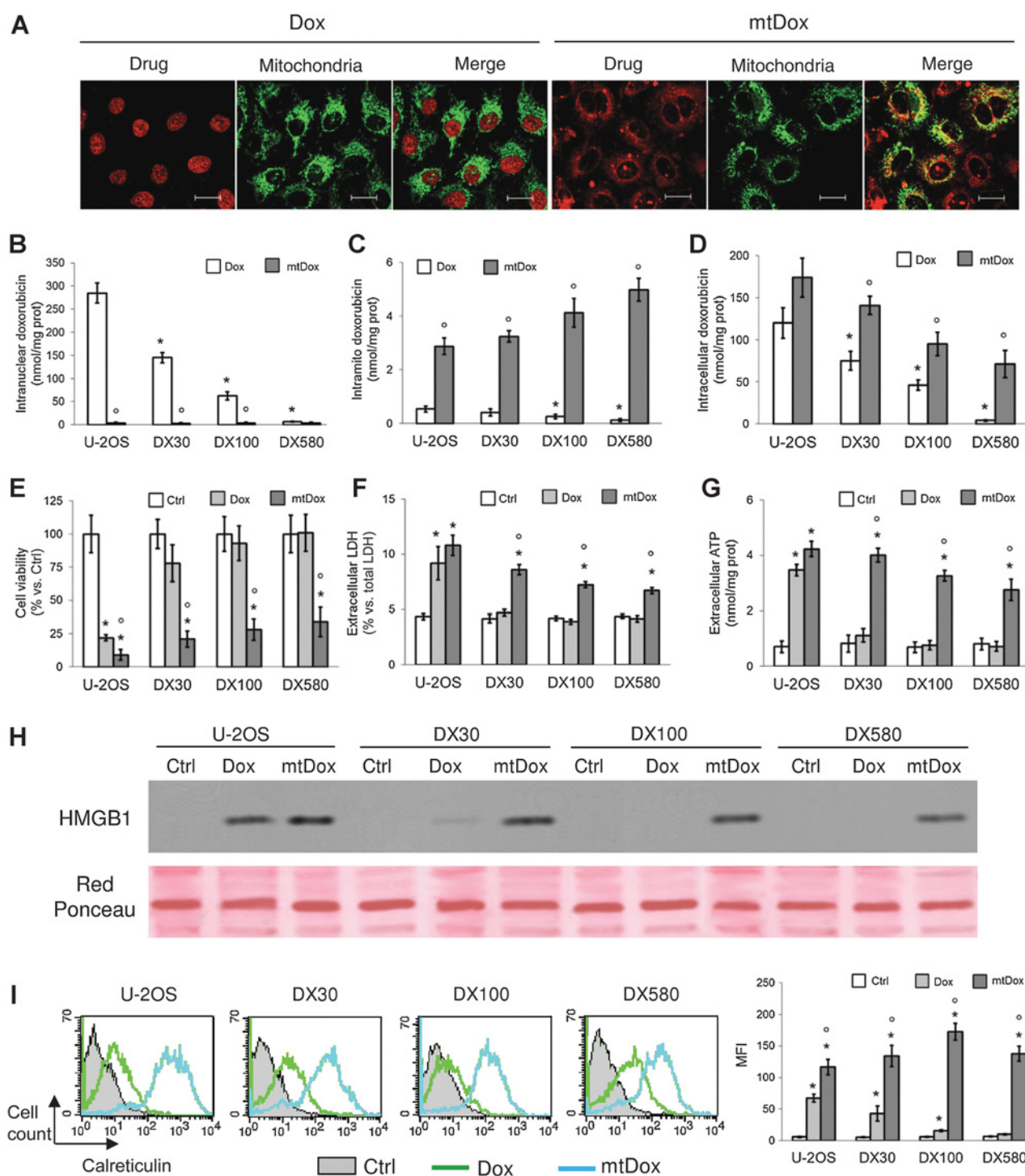


Figure 1. Mitochondria-targeted Dox is more accumulated and more cytotoxic than Dox in drug-resistant osteosarcoma cells. Dox-sensitive U-2OS cells and Dox-resistant variants (U-2OS/DX30, U-2OS/DX100, U-2OS/DX580) were incubated in the absence (Ctrl) or in the presence of 5 μ mol/L Dox or mtDox for 6 hours (**A-D**), 24 hours (**F-I**), or 72 hours (**E**). **A**, U-2OS cells were incubated for 24 hours with the GFP-E1 α pyruvate dehydrogenase expression vector to label mitochondria, then treated with Dox or mtDox. The intracellular localization of the drugs was analyzed by confocal microscopy. Bar, 10 μ m. The micrographs are representative of 3 experiments with similar results. **B**, the amount of Dox was measured spectrofluorimetrically in nuclear extracts in duplicate. Data are presented as mean \pm SD ($n = 3$). Versus U-2OS cells: *, $P < 0.001$; mtDox versus Dox: $^{\circ}$, $P < 0.001$. **C**, the amount of Dox was measured spectrofluorimetrically in isolated mitochondria in duplicate. Data are presented as mean \pm SD ($n = 3$). Versus U-2OS cells: *, $P < 0.02$; mtDox versus Dox: $^{\circ}$, $P < 0.001$. **D**, the content of Dox in whole cell lysates was measured spectrofluorimetrically in duplicate. Data are presented as mean \pm SD ($n = 4$). Versus U-2OS cells: *, $P < 0.05$; mtDox versus Dox: $^{\circ}$, $P < 0.002$. **E**, cells were stained with neutral red solution in quadruplicate. (Continued on the following page.)

and 2. However, genes encoding for proteins uncoupling oxidative phosphorylation and ATP synthesis, such as *SLC25A27* and *UCP1*, were progressively downregulated.

In drug-sensitive U-2OS cells, both Dox and mtDox downregulated at least 2-fold 25 genes encoding for metabolite transporters, subunits of respiratory chain complexes and ATP synthase, antioxidant genes such as *SOD1* and *SOD2*, and anti-apoptotic genes such as *BCL2* and *BCL2L1* (also known as *Bcl-xL*). They both upregulated genes encoding for the uncoupling proteins *SLC25A27*, *UCP1*, *UCP2*, *UCP3* as well as the pro-apoptotic genes *BAK1*, *BBC3* (also known as *PUMA*), and *BNIP3* (Fig. 3B; Supplementary Table S3). In U-2OS/DX580 cells, Dox up- or downregulated most of these genes less than 1-fold, consistently with the low-drug accumulation and efficacy. MtDox, by contrast, downregulated at least 2-fold the vast majority of genes involved in protein import and processing, mitochondrial fusion and fission, metabolite and electron transport, ATP synthesis, ROS protection, and apoptosis inhibition. In parallel, mtDox upregulated genes encoding for uncoupling proteins (e.g., *SLC25A27*, *UCP1*, and *UCP3*) and proapoptotic factors (e.g., *BAK1*, *BBC3*, *BID*, *BNIP3*; Fig. 3C; Supplementary Table S4).

Given the distinct signatures of drug-sensitive versus drug-resistant variants and the diverse effects of Dox versus mtDox in resistant cells, we then investigated the impact of mtDox on mitochondria biogenesis and energy metabolism in our osteosarcoma models. Up- or downregulation of key mitochondria-related genes was validated by qRT-PCR (Supplementary Tables S5–S7). For the sake of simplicity, we only show the results obtained in U-2OS and U-2OS/DX580 cells. The effects of Dox and mtDox on gene expression and mitochondrial functions of U-2OS/DX30 and U-2OS/DX100 variants were intermediate relative to those produced in U-2OS and U-2OS/DX580 cells.

Mitochondria-targeted Dox reduces mitochondrial biogenesis, protein import, and energy metabolism in Dox-resistant osteosarcoma cells

Compared with U-2OS cells, U-2OS/DX580 cells had higher mitochondrial DNA (Fig. 4A) and protein content (Fig. 4B), a higher level of nuclear translocation of PGC-1 α (Fig. 4C), and higher expression of COX-I (Fig. 4D), which is encoded by mitochondrial DNA. These observations are consistent with increased mitochondria biogenesis in the resistant variant. SDH-A, which is encoded by nuclear DNA, was also higher (Fig. 4E), likely in consequence of the higher expression of mitochondrial protein importers in U-2OS/DX580 cells. Consistent with the gene expression signature, U-2OS/DX580 cells had elevated: TCA cycle (Fig. 4F); fatty acids β -oxidation rate (Fig. 4G); ATP-linked OCR (Fig. 4H and I); maximal respiration capacity (Fig. 4H and J), and ATP synthesis by oxidative phosphorylation (Fig. 4K). Dox and mtDox decreased all these parameters in drug-

sensitive cells. Only mtDox affected these pathways in drug-resistant cells (Fig. 4).

Mitochondria-targeting Dox triggers a mitochondria-dependent apoptosis in drug-resistant osteosarcoma cells

We did not detect any significant differences in intramitochondrial ROS levels in U-2OS and U-2OS/DX580 cells (Fig. 5A). Dox increased ROS in drug-sensitive cells but not in drug-resistant ones; mtDox significantly increased intramitochondrial ROS in both cell populations (Fig. 5A). The higher levels of ROS were paralleled by mitochondrial depolarization (Fig. 5B). Dox increased proapoptotic proteins such as BAK, active BID (tBID), and PUMA, and decreased antiapoptotic proteins such as BCL-2 and BCL-xL only in U-2OS cells. mtDox elicited these effects in both variants (Fig. 5C), in line with its effects on gene expression. Consistent with the change in mitochondria polarization, Dox increased mitochondria-associated Bad, Bak, Bax, tBid, Bim_L, and Puma, the release of cytochrome c into the cytosol (Fig. 5D), the activity of caspase 9 (Fig. 5E) and caspase 3 (Fig. 5F) only in drug-sensitive cells, whereas mtDox produced these effects in both U-2OS and U-2OS/DX580 cells (Fig. 5D–F).

Discussion

Because targeting mitochondria is an effective therapeutic strategy in osteosarcoma (16), we used chemically modified Dox with a mitochondrial tropism against Dox-sensitive and Dox-resistant osteosarcoma cells. This modified mtDox was effective against osteosarcoma cells overexpressing Pgp and showing resistance to Dox.

The selective delivery into the mitochondria, due to the conjugation of the anthracycline moiety with a peptide containing cationic and hydrophobic residues that deliver cargoes into mitochondria (34), may limit the availability of Dox for the Pgp on the plasma membrane, reducing the efflux of the drug from tumor cells (18). Our work supports this hypothesis. Unlike Dox, mtDox was well retained within mitochondria in both drug-sensitive and drug-resistant/Pgp-overexpressing osteosarcoma cells. Although Dox accumulation and cytotoxic efficacy dramatically decreased in the Pgp-overexpressing variants, mtDox accumulation within resistant cells was only slightly lower, and its cytotoxicity remained high in Pgp-overexpressing cells. Although these data might suggest that Pgp effluxes both mtDox and Dox, the preferential intramitochondrial delivery of the former preserves its high intracellular retention.

The higher the intracellular accumulation of Dox, the higher the ability of the drug to kill cancer cells due to the induction of necro-apoptotic death and activation of the host immune system against the tumor (35): Dox promotes the exposure on the plasma membrane of calreticulin, which activates the local DCs to phagocytize tumor cells, stimulating a subsequent

(Continued.) The results were expressed as a percentage of viable cells versus untreated cells. Data are presented as mean \pm SD ($n = 3$). Versus respective Ctrl: *, $P < 0.001$; mtDox versus Dox: \circ , $P < 0.01$. **F**, the release of LDH in the extracellular medium was measured spectrophotometrically in duplicate. Data are presented as mean \pm SD ($n = 4$). Versus respective Ctrl: *, $P < 0.005$; mtDox versus Dox: \circ , $P < 0.001$. **G**, the extracellular release of ATP was measured in duplicate by a chemiluminescence-based assay. Data are presented as mean \pm SD ($n = 3$). Versus respective Ctrl: *, $P < 0.001$; mtDox versus Dox: \circ , $P < 0.001$. **H**, the release of HMGB1 in the cell supernatants was analyzed by Western blotting. Red Ponceau staining was used to check the equal loading of proteins. The figure is representative of 1 of 3 experiments. **I**, the amount of surface calreticulin was measured by flow cytometry in duplicate. Left, histograms representative of 3 experiments with similar results; right: mean fluorescence intensity (MFI) of calreticulin-positive cells. Data are presented as mean \pm SD ($n = 3$). Versus respective Ctrl: *, $P < 0.01$; mtDox versus Dox: \circ , $P < 0.001$.

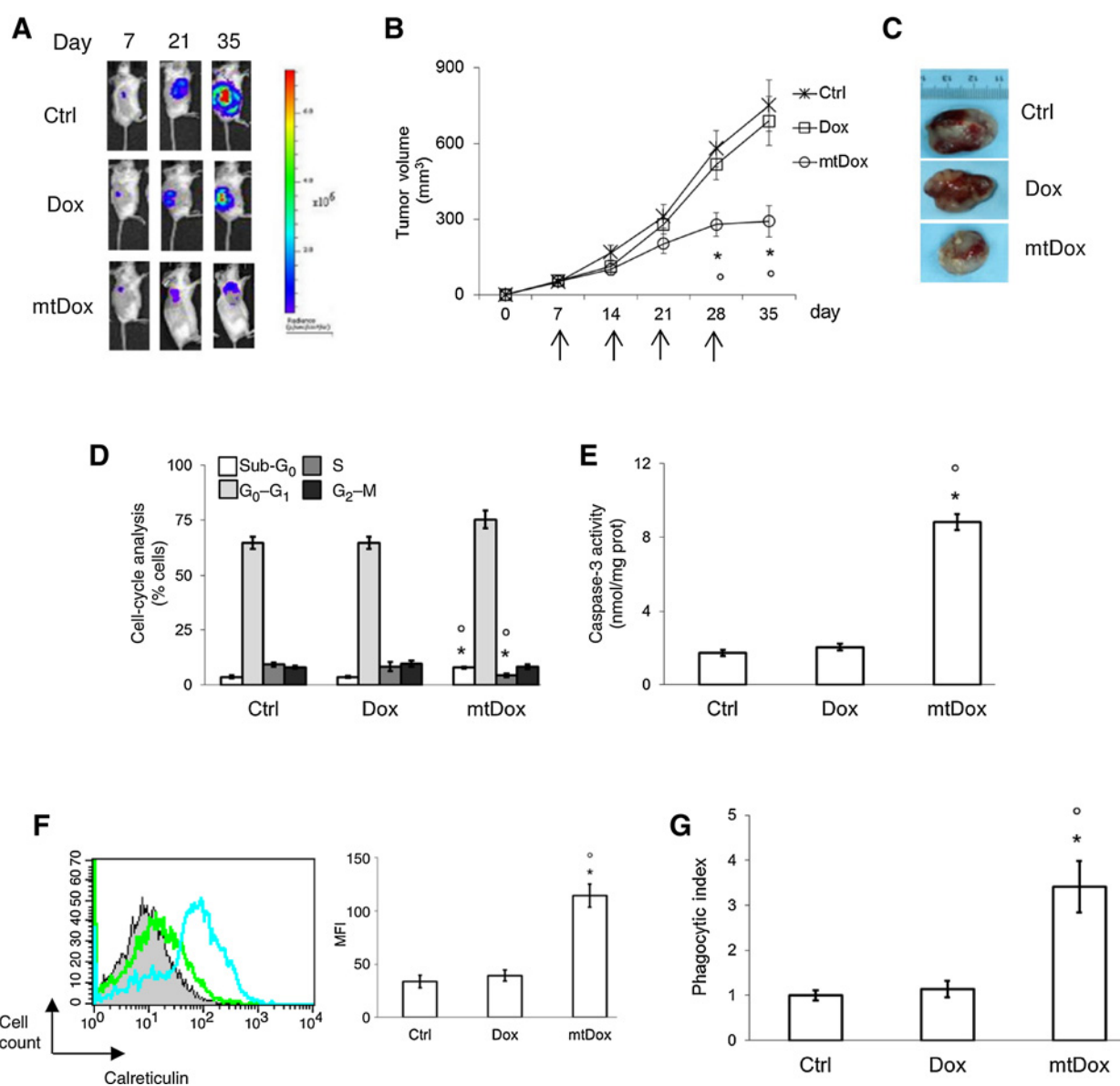


Figure 2. Mitochondria-targeted Dox is effective against drug-resistant osteosarcoma *in vivo*. Six-week-old female BALB/c mice were inoculated s.c. with 1×10^6 K7M2 cells. When the tumor reached the volume of 50 mm^3 (day 7), the animals (10 mice/group) were randomized and treated on days 7, 14, 21, and 28 as follows: (1) Ctrl group, treated with 0.1 mL saline solution i.v.; (2) Dox group, treated with 5 mg/kg Dox i.v.; (3) mtDox group, treated with 5 mg/kg mitochondria-targeted Dox i.v. **A**, representative *in vivo* bioluminescence imaging, performed on days 7, 21, and 35 after implant. **B**, tumor growth monitored by caliper measurements. Arrows represent saline, Dox, or mtDox injections. Data are presented as mean \pm SD. Versus Ctrl group: *, $P < 0.001$; mtDox group versus Dox group: °, $P < 0.001$. The inhibition rate in Dox-treated animals was 16.86%, in mtDox-treated animals, it was 45.49%. **C**, photographs of representative tumors from each treatment group after mice sacrifice. **D-G**, K7M2 cells were left untreated (Ctrl) or treated for 24 hours with $5 \mu\text{mol/L}$ Dox or mtDox. **D**, cell-cycle analysis was measured by flow cytometry. Data are presented as mean \pm SD ($n = 3$). Versus Ctrl: *, $P < 0.01$; mtDox versus Dox: °, $P < 0.001$. **E**, the activity of caspase 3 was measured fluorimetrically in duplicate in the cytosolic extracts. Data are presented as mean \pm SD ($n = 4$). Versus Ctrl: *, $P < 0.001$; mtDox versus Dox: °, $P < 0.001$. **F**, the amount of surface calreticulin was measured by flow cytometry in duplicate. Left, histograms are representative of 1 of 3 experiments; right, mean fluorescence intensity (MFI) of calreticulin-positive cells. Data are presented as mean \pm SD ($n = 3$). Versus Ctrl: *, $P < 0.001$; mtDox versus Dox: °, $P < 0.001$. **G**, DC-mediated phagocytosis of K7M2 cells was measured by flow cytometry. Data are presented as mean \pm SD ($n = 4$). The phagocytic index of untreated cells was considered as 1. Versus Ctrl: *, $P < 0.002$; mtDox versus Dox: °, $P < 0.005$.

expansion of antitumor CD8^+ T lymphocytes and eliciting a durable antitumor response (36). These mechanisms do not work in drug-resistant tumors (35). Neither cytotoxic nor proimmunogenic effects were exerted by Dox in Pgp-overex-

pressing osteosarcoma cells. MtDox, however, exerted all the canonical effects of anthracyclines in drug-resistant cells as well, as suggested by the extracellular release of LDH and by the increase of immunogenic cell death biomarkers

Table 1. Hematochemical parameters of animals

	Ctrl	Dox	mtDox
LDH (U/L)	6,231 ± 1,098	6,234 ± 724	6,198 ± 821
AST (U/L)	187 ± 52	234 ± 27	212 ± 82
ALT (U/L)	38 ± 9	41 ± 5	43 ± 10
AP (U/L)	87 ± 13	94 ± 15	91 ± 13
Creatinine (mg/L)	0.041 ± 0.006	0.039 ± 0.008	0.037 ± 0.009
CPK (U/L)	321 ± 93	850 ± 150*	453 ± 83

NOTE: Animals ($n = 10/\text{group}$) were treated as reported under Materials and Methods. Blood was collected immediately after mice euthanasia and analyzed for LDH, AST, ALT, AP, creatinine, and CPK. Ctrl, mice treated with saline solution; Dox, mice treated with Dox; mtDox, mice treated with mitochondria-targeting Dox. Versus Ctrl group: * $P < 0.005$.

(extracellular ATP and HMGB1 release, surface calreticulin). Mitochondrial depolarization, changes in calcium homeostasis, and increased ROS levels have been correlated with calreticulin upregulation and translocation from endoplasmic reticulum (ER) to the plasma membrane (37, 38): indeed, changes in intramitochondrial calcium and ROS are "sensed" by the ER membrane-associated to mitochondria (MAM) compartment, which is rich in calreticulin and controls the protein trafficking to the plasma membrane (39). Because mtDox depolarized mitochondria and increased ROS in both drug-sensitive and drug-resistant osteosarcoma cells, these events likely trigger the upregulation of calreticulin and/or its translocation from ER/MAM to the plasma membrane.

The efficacy of mtDox was validated in a preclinical model of Dox-resistant osteosarcoma implanted in immunocompetent animals, i.e., the Pgp-expressing K7M2 cells that are syngeneic with BALB/c mice. In both *in vitro* and *in vivo* assays, mtDox exerted direct cytotoxicity on tumor cells (as indicated by the reduced tumor growth and cell proliferation, and by the increased apoptosis) and primed tumor cells for the recognition by the host immune system (as suggested by the increased percentage of calreticulin-positive tumor cells, tumor cell phagocytosis, and intratumor DC infiltration). Moreover, mtDox still retained antitumor efficacy at 1/2 to 1/5 of Dox MTD. Importantly, unlike the mice treated with Dox, those treated with mtDox did not show any increase in CPK. These results are in accordance with previous observations, showing that mtDox did not exert systemic and cardio-specific toxicity *in vivo* (19), and with the reduced toxicity observed in cultured cardiomyocytes. In preclinical models, mtDox was more advantageous than Dox in drug-resistant tumors, not in drug-sensitive ones, leading to hypothesize that the greater efficacy of mtDox was due to the targeting of pathways which are crucial for the survival of drug-resistant cells.

The increase of Dox resistance was associated with the upregulation of genes controlling mitochondrial biogenesis, the import of proteins, metabolites and cofactors, and energy metabolism, and with the downregulation of genes encoding for uncoupling proteins. This signature made the mitochondrial metabolism of Dox-resistant osteosarcoma cells more efficient, as confirmed by the higher content of mitochondrial DNA and proteins, and by the higher metabolic flux through the main energy pathways in U-2OS/DX580 cells. It is noteworthy that genes encoded by both nuclear and mitochondrial DNA were upregulated in drug-resistant cells. These results suggest that the higher mitochondrial metabolism of drug-resistant cells was supported partly by the increased mitochondria biogenesis and

partly by the increased import of cytosolic proteins and metabolites within mitochondria. This process may favor a more efficient assembly of mitochondrial complexes involved in the TCA cycle, fatty acids β -oxidation, electron transport, and ATP synthesis, and may supply all these pathways with anaplerotic metabolites and essential cofactors. Contrarily to most tumor cells, which obtain energy from anaerobic glycolysis, chemoresistant cells often simultaneously activate glycolysis and oxidative phosphorylation to meet their energy requirements (40). The higher ATP level produced by mitochondrial oxidative phosphorylation may support the ATP-dependent efflux activity of ABC transporters, contributing to the chemoresistant phenotype. On the other hand, a high proton motive force induces a high production of ROS from mitochondria (41). We did not detect any differences in intramitochondrial ROS between U-2OS and U-2OS/DX580 cells, which was most likely due to the upregulation of mitochondrial SOD2 in the latter: this feature may also contribute to chemoresistance.

Dox acts through pleiotropic mechanisms on tumor cells, including mitochondrial-dependent mechanisms. For example, it reduces the activity of complexes I, II, and III (42) and the synthesis of ATP (43), and increases intramitochondrial ROS through iron-catalyzed redox cycles within complex I (44). In sensitive osteosarcoma cells, Dox downregulated specific metabolite transporters, subunits of mitochondrial respiratory complexes and ATP synthase, cytosolic and mitochondrial isoforms of SOD, and upregulated uncoupling proteins and proapoptotic factors. The consequent reduction of mitochondria biogenesis and ATP synthesis, coupled with the increase in intramitochondrial ROS, triggered a mitotoxicity-dependent apoptosis. None of these events occurred in the drug-resistant U-2OS/DX580 variant, where Dox did not reach an intracellular concentration sufficient to elicit effects at genomic and metabolic levels.

By contrast, mtDox produced genomic and metabolic signatures that were similar in drug-sensitive and drug-resistant osteosarcoma cells. By downregulating genes involved in mitochondria biogenesis and mitochondrial protein import, it significantly reduced mitochondrial DNA and protein contents. Previously, it was reported that in cardiomyocytes, mtDox decreased mitochondrial DNA after 6 hours and increased it after 24 hours: This trend suggests a recovery from the initial damage due to mitochondrial biogenesis. On the contrary, in ovarian cancer cells, mitochondrial DNA levels remained significantly lower after 24 hours of treatment with mtDox, indicating that tumor cells are not able to increase mitochondria biogenesis in response to mtDox (19). These findings are in line with the results obtained in osteosarcoma cells. The different response of cardiomyocytes and tumor cells to the mitochondrial damage elicited by mtDox may explain the key properties of mtDox, i.e., its antitumor efficacy and its cardiac safety.

By decreasing the expression of several transporters and subunits of oxidative phosphorylation complexes, mtDox strongly reduced the mitochondrial energy metabolism. It is noteworthy that it upregulated the expression of uncoupling proteins and proapoptotic factors, and markedly decreased the expression of mitochondrial SOD2. These events uncoupled oxidative phosphorylation from ATP synthesis and increased the intramitochondrial levels of ROS, which were not buffered by SOD2. This metabolic dysfunction causes the opening of the mitochondrial permeability transition pore and triggers a

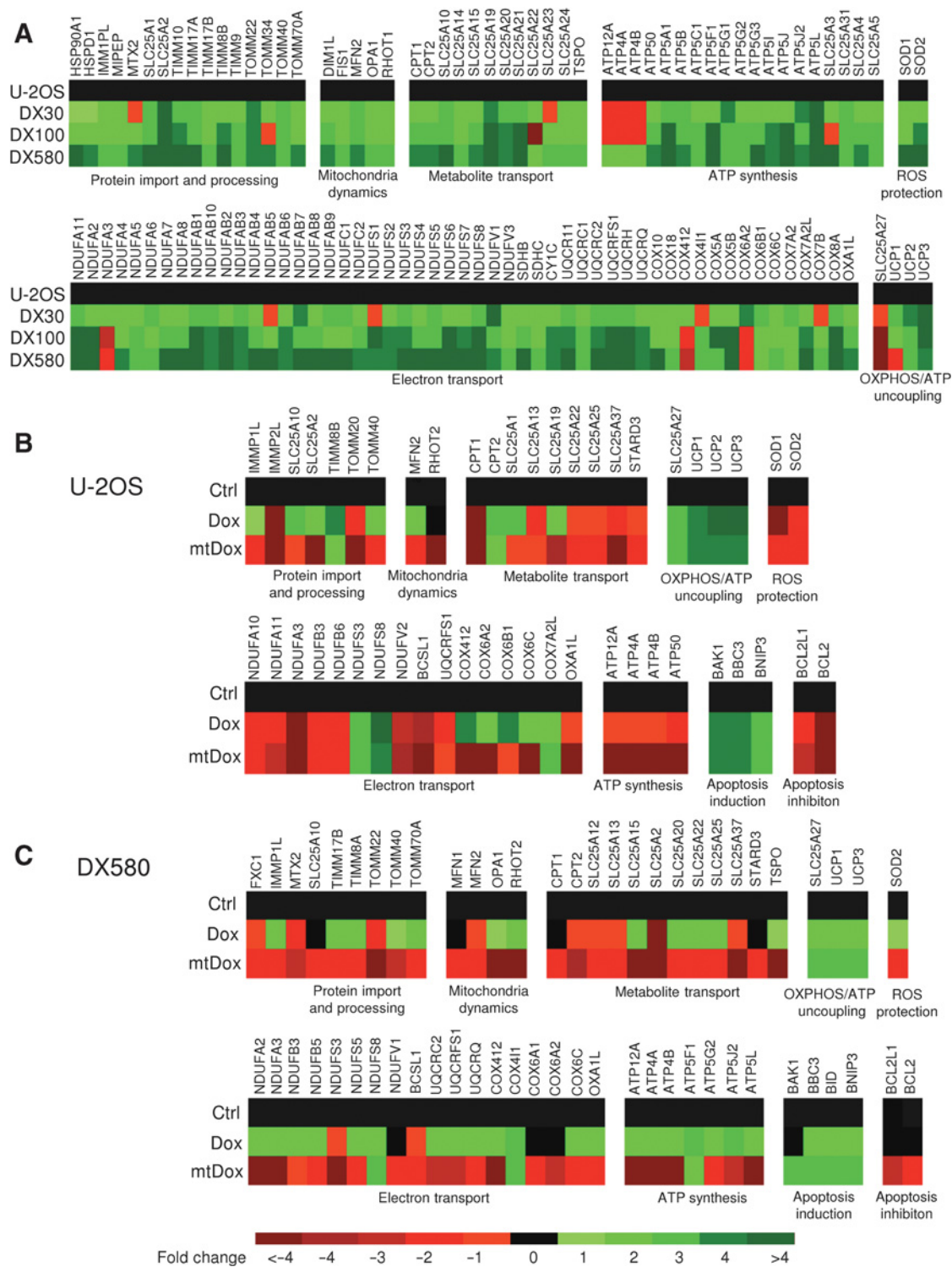


Figure 3. Modulation of mitochondria-related genes by Dox and mitochondria-targeted Dox in drug-sensitive and drug-resistant osteosarcoma cells. **A**, the cDNA from Dox-sensitive U-2OS cells and Dox-resistant variants (U-2OS/DX30, U-2OS/DX100, and U-2OS/DX580) was analyzed by PCR arrays specific for mitochondria-related genes, as reported under Materials and Methods. The figure reports the genes up- or downregulated 2-fold or more in at least one cell line, in a colorimetric scale ($n = 4$). **B** and **C**, U-2OS cells (**B**) or U-2OS/DX580 cells (**C**) were grown for 24 hours in fresh medium (Ctrl), in medium containing 5 $\mu\text{mol/L}$ Dox, or mtDox. The cDNA was analyzed by the same PCR arrays in **A**. The figures report the genes up- or downregulated 2-fold or more in at least one experimental condition, in a colorimetric scale ($n = 4$). OXPHOS, oxidative phosphorylation.

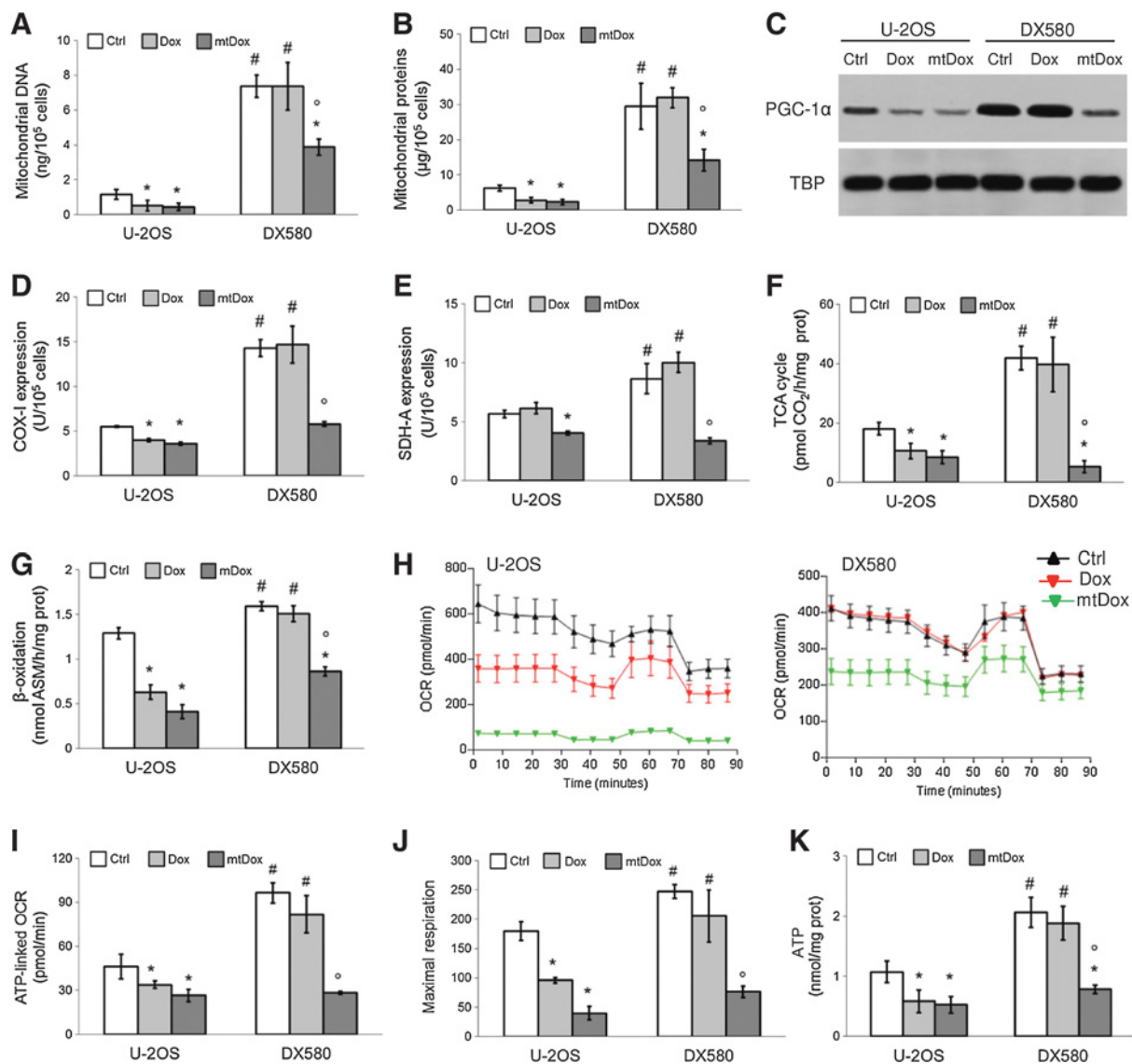


Figure 4.

Mitochondria biogenesis and energy metabolism in cells treated with Dox or mitochondria-targeted Dox. Dox-sensitive U-2OS cells and Dox-resistant U-2OS/DX580 cells were incubated in the absence (Ctrl) or in the presence of 5 $\mu\text{mol/L}$ Dox or mtDox for 24 hours. Data are presented as mean \pm SD ($n = 4$). **A** and **B**, the amount of mitochondrial DNA (**A**) and proteins (**B**) was measured in duplicate after mitochondria isolation, as described under Materials and Methods. For both panels, versus U-2OS Ctrl cells: *, $P < 0.05$; versus U-2OS/DX580 Ctrl cells: \circ , $P < 0.02$; U-2OS/DX580 versus U-2OS cells: #, $P < 0.001$. **C**, nuclear extracts were analyzed for the levels of PGC-1 α by Western blotting. The TBP expression was used as the control of equal protein loading. The figure is representative of 1 of 3 experiments. **D** and **E**, the expression of subunit I of complex IV (COX-I, **D**) and succinic acid dehydrogenase-A of complex II (SDH-A, **E**) was measured by quantitative immunocytochemistry in duplicate. For both panels, versus U-2OS Ctrl cells: *, $P < 0.05$; versus U-2OS/DX580 Ctrl cells: \circ , $P < 0.001$; U-2OS/DX580 versus U-2OS cells: #, $P < 0.05$. **F**, the glucose flux through the TCA cycle was measured in duplicate in cells radiolabeled with [6-¹⁴C]-glucose. Versus U-2OS Ctrl cells: *, $P < 0.05$; versus U-2OS/DX580 Ctrl cells: \circ , $P < 0.001$; U-2OS/DX580 versus U-2OS cells: #, $P < 0.002$. **G**, the amount of ¹⁴C-ASM derived from fatty acids β -oxidation was measured in duplicate in cells labeled with [1-¹⁴C]-palmitoyl coenzyme A. Versus U-2OS Ctrl cells: *, $P < 0.001$; versus U-2OS/DX580 Ctrl cells: \circ , $P < 0.001$; U-2OS/DX580 versus U-2OS cells: #, $P < 0.05$. **H**, mitochondrial bioenergetic profiles generated using the Seahorse XFP Analyzer, in U-2OS cells (left) and U-2OS/DX580 cells (right). The figures are representative of 1 of 4 experiments, each performed in triplicate. **I** and **J**, ATP-linked OCR rates (**I**) and maximal respiration (**J**) were determined from the bioenergetic profiles in **H**. ATP-linked OCR represents the difference between basal and oligomycin-treated OCR, whereas maximal respiration represents the difference between FCCP- and rotenone/antimycin-treated OCR. Versus U-2OS Ctrl cells: *, $P < 0.05$; versus U-2OS/DX580 Ctrl cells: \circ , $P < 0.001$; U-2OS/DX580 versus U-2OS cells: #, $P < 0.05$. **K**, ATP levels in isolated mitochondria were measured in duplicate by a chemiluminescence-based assay. Versus U-2OS Ctrl cells: *, $P < 0.05$; versus U-2OS/DX580 Ctrl cells: \circ , $P < 0.005$; U-2OS/DX580 versus U-2OS cells: #, $P < 0.01$.

mitochondria-dependent apoptosis. The simultaneous down-regulation of antiapoptotic genes further supported the apoptotic process.

The events described above were more pronounced in Dox-resistant cells than in Dox-sensitive ones, in accordance with the higher mitochondrial metabolic activity of the former. Of note,

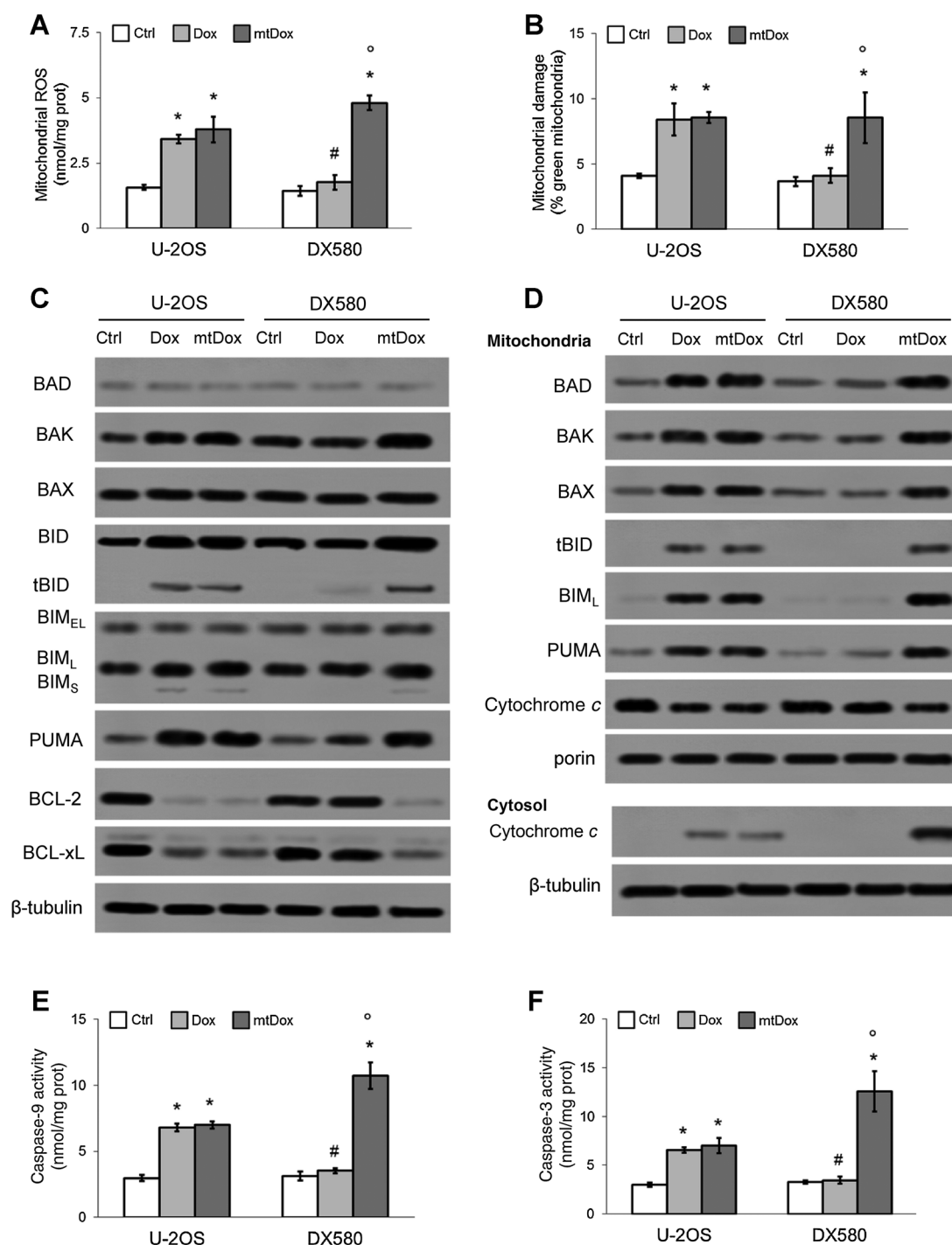


Figure 5.

Effects of Dox and mitochondria-targeted Dox on mitochondria integrity and mitochondria-dependent apoptosis. Dox-sensitive U-2OS cells and Dox-resistant U-2OS/DX580 cells were incubated in the absence (Ctrl) or in the presence of 5 μmol/L Dox or mtDox for 24 hours. **A**, intramitochondrial ROS levels were measured fluorimetrically in triplicate using the DCFDA-AM probe. Data are presented as mean ± SD ($n = 4$). Versus U-2OS Ctrl cells: *, $P < 0.001$; versus U-2OS/DX580 Ctrl cells: °, $P < 0.001$; U-2OS/DX580 versus U-2OS cells: #, $P < 0.001$. **B**, the mitochondrial membrane potential was assessed in duplicate by the JC-1 staining method. The percentage of green versus red mitochondria was considered an index of mitochondrial depolarization and permeability transition. Data are presented as mean ± SD ($n = 4$). Versus U-2OS Ctrl cells: *, $P < 0.005$; versus U-2OS/DX580 Ctrl cells: °, $P < 0.005$; U-2OS/DX580 versus U-2OS cells: #, $P < 0.002$. **C**, whole cell lysates were probed with the indicated antibodies. BID full-length and truncated (tBID) protein, BIM isoforms BIM_{EL}, BIM_L, BIM_S are shown. The β-tubulin expression was used as the control of equal protein loading. The figure is representative of 1 of 3 experiments. **D**, mitochondrial and cytosolic extracts were subjected to Western blotting and probed with the indicated antibodies. tBID and BIM_L isoforms are shown. Porin and β-tubulin expression were used as the control of equal protein loading in the respective extracts. The figure is representative of 1 of 3 experiments. **E** and **F**, the activity of caspase 9 (**E**) and caspase 3 (**F**) was measured fluorimetrically in duplicate in the cytosolic extracts. Data are presented as mean ± SD ($n = 4$). For both panels, versus U-2OS Ctrl cells: *, $P < 0.001$; versus U-2OS/DX580 Ctrl cells: °, $P < 0.001$; U-2OS/DX580 versus U-2OS cells: #, $P < 0.001$.

mtDox was relatively nontoxic in nontransformed osteoblasts. On the one hand, the lower uptake of mtDox by nontransformed cells may explain the reduced toxicity; on the other hand, osteoblasts are more dependent on anaerobic glycolysis than on mitochondrial metabolism for their growth and differentiation (45, 46). These factors may explain the relatively selective cytotoxicity of mtDox for tumor cells over nontransformed cells.

Despite their resistance to chemotherapy, drug-resistant tumors are more susceptible than drug-sensitive ones to the depletion of ATP and to the increase of ROS, an event known as "collateral sensitivity" (CS; ref. 47). Agents that lower intracellular ATP and/or increase ROS levels are effective against chemoresistant cells *in vitro*. Unfortunately, the intrinsic toxicity of these agents limits their use *in vivo* (48). However, thanks to its ability to lower the levels of ATP produced by oxidative phosphorylation and increase ROS levels within drug-resistant cells, mtDox is an excellent inducer of CS. Unlike the other compounds exerting CS, it did not produce appreciable toxicity for the liver, kidneys, or heart in our preclinical model of resistant osteosarcoma, thus appearing suitable for being used *in vivo*.

The novelty of the therapeutic strategy proposed in this work relates to two factors. First, we used a derivative of the first-line drug Dox, the efficacy of which is limited by the expression of Pgp in osteosarcoma cells and by the development of cardiotoxicity: by chemically modifying Dox to achieve its selective delivery into mitochondria, we overcame a key limitation frequently encountered in patients treated with Dox-based regimens. Second, mtDox exploited a metabolic signature typical of chemoresistant cells—i.e., the hyperactive mitochondrial metabolism—and hit energy pathways that are crucial for drug-resistant tumors. This drug conjugate produced promising results that may be applied to the treatment of Pgp-expressing osteosarcomas. These results may pave the way for the potential use of mtDox in clinical settings, in particular for patients with Pgp-positive osteosarcomas or as a possible second-line treatment for relapsed patients.

Disclosure of Potential Conflicts of Interest

No potential conflicts of interest were disclosed.

References

- Rivera-Valentin RK, Zhu L, Hughes DP. Bone sarcomas in pediatrics: Progress in our understanding of tumor biology and implications for therapy. *Paediatr Drugs* 2015;17:257–71.
- Hattinger CM, Fanelli M, Tavanti E, Vella S, Ferrari S, Picci P, et al. Advances in emerging drugs for osteosarcoma. *Expert Opin Emerg Drugs* 2015; 20:495–514.
- Lipshultz SE, Karnik R, Sambatakos P, Franco VI, Ross SW, Miller TL. Anthracycline-related cardiotoxicity in childhood cancer survivors. *Curr Opin Cardiol* 2014;29:103–12.
- Gottesman MM, Fojo T, Bates SE. Multidrug resistance in cancer: Role of ATP-dependent transporters. *Nat Rev Cancer* 2002;2:48–58.
- Baldini N, Scotlandi K, Barbanti-Bròdano G, Manara MC, Maurici D, Bacci G, et al. Expression of P-glycoprotein in high-grade osteosarcomas in relation to clinical outcome. *N Engl J Med* 1995;333: 1380–5.
- Serra M, Scotlandi K, Reverter-Branchat G, Ferrari S, Manara MC, Benini S, et al. Value of P-glycoprotein and clinicopathologic factors as the basis for new treatment strategies in high-grade osteosarcoma of the extremities. *J Clin Oncol* 2003;21:536–42.
- Serra M, Pasello M, Manara MC, Scotlandi K, Ferrari S, Bertoni F, et al. May P-glycoprotein status be used to stratify high-grade osteosarcoma patients? Results from the Italian/Scandinavian Sarcoma Group 1 treatment protocol. *Int J Oncol* 2006;29:1459–68.
- Bramer JA, van Linge JH, Grimer RJ, Scholten RJ. Prognostic factors in localized extremity osteosarcoma: A systematic review. *Eur J Surg Oncol* 2009;35:1030–6.
- Condello M, Cosentino D, Corinti S, Di Felice G, Multari G, Gallo FR, et al. Voacamine modulates the sensitivity to doxorubicin of resistant osteosarcoma and melanoma cells and does not induce toxicity in normal fibroblasts. *J Nat Prod* 2014;77:855–62.
- Xia YZ, Ni K, Guo C, Zhang C, Geng YD, Wang ZD, et al. Alopecurone B reverses doxorubicin-resistant human osteosarcoma cell line by inhibiting P-glycoprotein and NF-kappa B signaling. *Phytomedicine* 2015;22: 344–51.
- Duan Z, Zhang J, Ye S, Shen J, Choy E, Cote G, et al. A-770041 reverses paclitaxel and doxorubicin resistance in osteosarcoma cells. *BMC Cancer* 2014;14:e681.
- Yang X, Yang P, Shen J, Osaka E, Choy E, Cote G, et al. Prevention of multidrug resistance (MDR) in osteosarcoma by NSC23925. *Br J Cancer* 2014;110:2896–904.
- Susa M, Iyer AK, Ryu K, Choy E, Hornicek FJ, Mankin H, et al. Inhibition of ABCB1 (MDR1) expression by an siRNA nanoparticulate delivery

Authors' Contributions

Conception and design: S.R. Jean, C. Riganti
Development of methodology: I. Buondonno, V. Audrito, J. Kopecka, C. Costamagna, I. Roato, E. Mungo, S. Deaglio
Acquisition of data (provided animals, acquired and managed patients, provided facilities, etc.): I. Buondonno, E. Gazzano, I.C. Salaroglio, E. Mungo
Analysis and interpretation of data (e.g., statistical analysis, biostatistics, computational analysis): I. Buondonno, E. Gazzano, V. Audrito, J. Kopecka, I.C. Salaroglio, C. Costamagna, S. Deaglio, S.O. Kelley, C. Riganti
Writing, review, and/or revision of the manuscript: I. Buondonno, E. Gazzano, S.R. Jean, M. Fanelli, C.M. Hattinger, S.O. Kelley, M. Serra, C. Riganti
Administrative, technical, or material support (i.e., reporting or organizing data, constructing databases): M. Fanelli, C.M. Hattinger, M. Serra
Study supervision: C. Riganti
Other (synthesized and characterized mitochondria-targeted doxorubicin for the study): S.R. Jean
Other (bioenergetic studies): V. Audrito

Acknowledgments

The authors are grateful to Professor Amalia Bosia, Department of Oncology, University of Torino, for the fruitful discussion, and to Dr. Erika Ortolan, Department of Medical Sciences, University of Torino, for technical assistance. We are also grateful to Mr. Andrew Martin Garvey, BA(Hons) LTCL(TESOL) PGDip MA, for editorial assistance.

Grant Support

This work was supported with funds from Italian Association for Cancer Research (IG15232 to C. Riganti) and Italian Ministry of University and Research (FIRB 2012, grant RBF12SQ1 to C. Riganti); Canadian Institutes for Health Research Operating Grant (to S.O. Kelley); 5% contributions to Rizzoli Institute (to M. Serra). I. Buondonno and I.C. Salaroglio are recipients of PhD scholarships from the Italian Institute for Social Security (INPS). E. Gazzano is recipient of a postdoctoral fellowship from the Italian Ministry of University and Research. V. Audrito is recipient of the #15047 fellowship from the Italian Association for Cancer Research/Italian Foundation for Cancer Research (FIRC). J. Kopecka is recipient of a fellowship from "Fondazione Umberto Veronesi." The costs of publication of this article were defrayed in part by the payment of page charges. This article must therefore be hereby marked *advertisement* in accordance with 18 U.S.C. Section 1734 solely to indicate this fact.

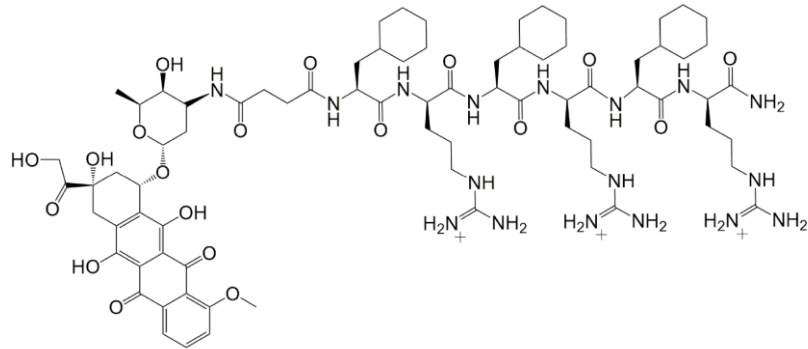
Received February 1, 2016; revised June 10, 2016; accepted June 23, 2016; published OnlineFirst July 27, 2016.

- system to overcome drug resistance in osteosarcoma. *PLoS One* 2010;5:e10764.
14. Roncuzzi L, Pancotti F, Baldini N. Involvement of HIF-1 α activation in the doxorubicin resistance of human osteosarcoma cells. *Oncol Rep* 2014;32:389–94.
 15. Sero V, Tavanti E, Vella S, Hattinger CM, Fanelli M, Michelacci F, et al. Targeting polo-like kinase 1 by NMS-P937 in osteosarcoma cell lines inhibits tumor cell growth and partially overcomes drug resistance. *Invest New Drugs* 2014;32:1167–80.
 16. Armstrong J, Dass CR. Doxorubicin action on mitochondria: relevance to osteosarcoma therapy? *Curr Drug Targets* 2015 Apr 16. [Epub ahead of print].
 17. Riganti C, Rolando B, Kopecka J, Campia I, Chegaev K, Lazzarato L, et al. Mitochondrial-targeting nitrooxy-doxorubicin: A new approach to overcome drug resistance. *Mol Pharm* 2013;10:161–74.
 18. Chamberlain GR, Tulumello DV, Kelley SO. Targeted delivery of doxorubicin to mitochondria. *ACS Chem Biol* 2013;8:1389–95.
 19. Jean SR, Tulumello DV, Riganti C, Liyanage SU, Schimmer AD, Kelley SO. Mitochondrial targeting of doxorubicin eliminates nuclear effects associated with cardiotoxicity. *ACS Chem Biol* 2015;10:2007–15.
 20. Serra M, Scotlandi K, Manara MC, Maurici D, Lollini PL, De Giovanni C, et al. Establishment and characterization of multidrug-resistant human osteosarcoma cell lines. *Anticancer Res* 1993;13:323–9.
 21. Gronthos S, Zannettino AC, Hay SJ, Shi S, Graves SE, Kortessidis A, et al. Molecular and cellular characterisation of highly purified stromal stem cells derived from human bone marrow. *J Cell Sci* 2003;116:1827–35.
 22. Brunetti G, Rizzi R, Oranger A, Gigante I, Mori G, Taurino G, et al. LIGHT/TNFSF14 increases osteoclastogenesis and decreases osteoblastogenesis in multiple myeloma-bone disease. *Oncotarget* 2014;5:12950–67.
 23. Gelsomino G, Corsetto PA, Campia I, Montorfano G, Kopecka J, Castella B, et al. Omega 3 fatty acids chemosensitize multidrug resistant colon cancer cells by downregulating cholesterol synthesis and altering detergent resistant membranes composition. *Mol Cancer* 2013;12:e137.
 24. Riganti C, Salaroglio IC, Caldera V, Campia I, Kopecka J, Mellai M, et al. Temozolomide downregulates P-glycoprotein expression in glioblastoma stem cells by interfering with the Wnt3a/GSK3/ β -catenin pathway. *Neuro-Oncol* 2013;15:1502–17.
 25. Campia I, Lussiana C, Pescarmona G, Ghigo D, Bosia A, Riganti C. Geranylgeraniol prevents the cytotoxic effects of mevastatin in THP-1 cells, without decreasing the beneficial effects on cholesterol synthesis. *Br J Pharmacol* 2009;158:1777–86.
 26. Riganti C, Miraglia E, Viarisio D, Costamagna C, Pescarmona G, Ghigo D, et al. Nitric oxide reverts the resistance to doxorubicin in human colon cancer cells by inhibiting the drug efflux. *Cancer Res* 2005;65:516–25.
 27. Riganti C, Castella B, Kopecka J, Campia I, Coscia M, Pescarmona G, et al. Zoledronic acid restores doxorubicin chemosensitivity and immunogenic cell death in multidrug-resistant human cancer cells. *PLoS One* 2013;8:e60975.
 28. Obeid M, Tesniere A, Ghiringhelli F, Fimia GM, Apetoh L, Perfettini JL, et al. Calreticulin exposure dictates the immunogenicity of cancer cell death. *Nat Med* 2007;13:54–61.
 29. LeBleu VS, O'Connell JT, Gonzalez Herrera KN, Wikman H, Pantel K, Haigis MC, et al. PGC-1 α mediates mitochondrial biogenesis and oxidative phosphorylation in cancer cells to promote metastasis. *Nat Cell Biol* 2014;16:992–1003.
 30. Riganti C, Gazzano E, Polimeni M, Costamagna C, Bosia A, Ghigo D. Diphenylethylidonium inhibits the cell redox metabolism and induces oxidative stress. *J Biol Chem* 2004;279:47726–31.
 31. Gaster M, Rustan AC, Aas V, Beck-Nielsen H. Reduced lipid oxidation in skeletal muscle from type 2 diabetic subjects may be of genetic origin evidence from cultured myotubes. *Diabetes* 2004;53:542–8.
 32. Riganti C, Gazzano E, Gulino GR, Volante M, Ghigo D, Kopecka J. Two repeated low doses of doxorubicin are more effective than a single high dose against tumors overexpressing P-glycoprotein. *Cancer Lett* 2015;360:219–26.
 33. Kepp O, Senovilla L, Vitale I, Vacchelli E, Adjemian S, Agostinis P, et al. Consensus guidelines for the detection of immunogenic cell death. *Oncoimmunology* 2014;3:e955691.
 34. Horton KL, Stewart KM, Foseca SB, Guo Q, Kelley SO. Mitochondria-penetrating peptides. *Chem Biol* 2008;15:375–82.
 35. De Boo S, Kopecka J, Brusa D, Gazzano E, Matera L, Ghigo D, et al. iNOS activity is necessary for the cytotoxic and immunogenic effects of doxorubicin in human colon cancer cells. *Mol Cancer* 2009;8:e108.
 36. Apetoh L, Mignot G, Panaretakis T, Kroemer G, Zitvogel L. Immunogenicity of anthracyclines: Moving towards more personalized medicine. *Trends Mol Med* 2008;14:141–51.
 37. Biswas G, Guha M, Avadhani NG. Mitochondria-to-nucleus stress signaling in mammalian cells: Nature of nuclear gene targets, transcription regulation, and induced resistance to apoptosis. *Gene* 2005;354:132–9.
 38. Zhang Y, Liu L, Jin L, Yi X, Dang E, Yang Y, et al. Oxidative stress-induced calreticulin expression and translocation: New insights into the destruction of melanocytes. *J Invest Dermatol* 2014;134:183–91.
 39. Poston CN, Krishnan SC, Bazemore-Walker CR. In-depth proteomic analysis of mammalian mitochondria-associated membranes (MAM). *J Proteomics* 2013;79:219–30.
 40. Martinez-Outschoorn UE, Pestell RG, Howell A, Tykocinski ML, Nagarajothi F, Machado FS, et al. Energy transfer in "parasitic" cancer metabolism: mitochondria are the powerhouse and Achilles' heel of tumor cells. *Cell Cycle* 2011;10:4208–16.
 41. Mailloux RJ, Harper ME. Mitochondrial proticity and ROS signaling: Lessons from the uncoupling proteins. *Trends Endocrinol Metab* 2012;23:451–8.
 42. Marcillat O, Zhang Y, Davies KJ. Oxidative and non-oxidative mechanisms in the inactivation of cardiac mitochondrial electron transport chain components by doxorubicin. *Biochem J* 1989;259:181–9.
 43. Strigun A, Wahrheit J, Niklas J, Heinzle E, Noor F. Doxorubicin increases oxidative metabolism in HL-1 cardiomyocytes as shown by ¹³C metabolic flux analysis. *Toxicol Sci* 2012;125:595–606.
 44. Simunek T, Sterba M, Popelova O, Adamcova M, Hrdina R, Gersl V. Anthracycline-induced cardiotoxicity: overview of studies examining the roles of oxidative stress and free cellular iron. *Pharmacol Rep* 2009;61:154–71.
 45. Esen E, Chen J, Karner CM, Okunade AL, Patterson BW, Long F. WNT-LRP5 signaling induces Warburg effect through mTORC2 activation during osteoblast differentiation. *Cell Metab* 2013;17:745–55.
 46. Regan JN, Lim J, Shi Y, Joeng KS, Arbeit JM, Shohet RV, et al. Upregulation of glycolytic metabolism is required for HIF1 α -driven bone formation. *Proc Natl Acad Sci U S A* 2014;111:8673–8.
 47. Pluchino KM, Hall MD, Goldsborough AS, Callaghan R, Gottesman MM. Collateral sensitivity as a strategy against cancer multidrug resistance. *Drug Resist Updat* 2012;15:98–105.
 48. Callaghan R, Luk F, Bebawy M. Inhibition of the multidrug resistance P-glycoprotein: time for a change of strategy? *Drug Metab Dispos* 2014;42:623–31.

Supplementary materials

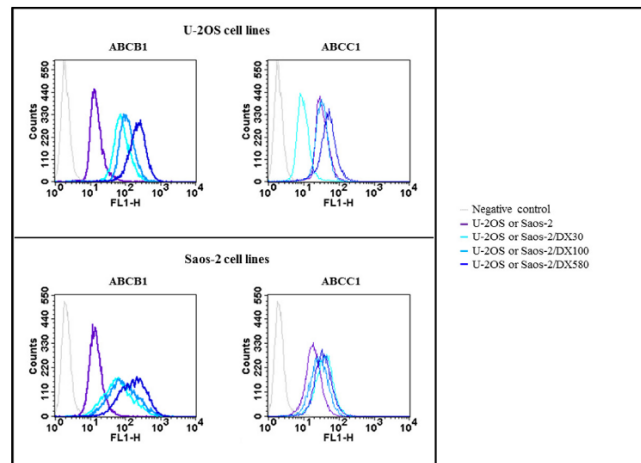
Supplementary Figures

Supplementary Figure 1



Supplementary Figure S1. Chemical structure of mitochondria-targeted doxorubicin.

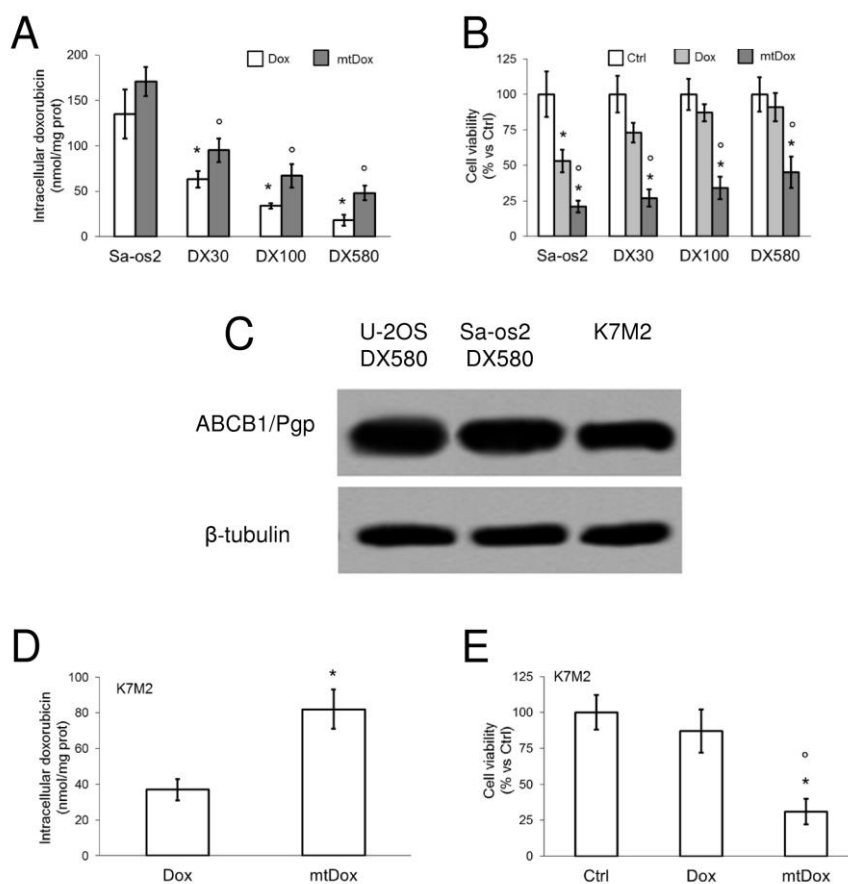
Supplementary Figure 2



Supplementary Figure S2. Expression of Pgp and MRP1 in doxorubicin-sensitive and doxorubicin-resistant osteosarcoma cells

Human Dox-sensitive U-2OS cells and Dox-resistant variants (U-2OS/DX30, U-2OS/DX100, U-2OS/DX580), human Dox-sensitive Saos-2 cells and Dox-resistant variants (Saos-2/DX30, Saos-2/DX100, Saos-2/DX580) were analyzed for the surface expression of ABCB1/Pgp and ABCC1/MRP1 by flow cytometry in duplicate. The figure is representative of 1 out of 3 experiments.

Supplementary Figure 3



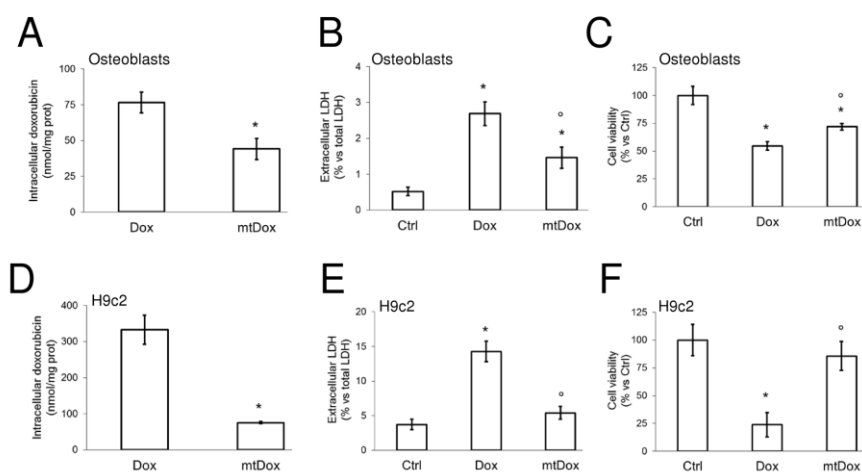
Supplementary Figure S3. Intracellular accumulation and cytotoxicity of mitochondria-targeted doxorubicin in drug-sensitive Saos-2 cells and in their resistant variants, and in K7M2 cells

A. Dox-sensitive Saos-2 cells and Dox-resistant variants (Saos-2/DX30, Saos-2/DX100, Saos-2/DX580) were incubated with 5 μ mol/L Dox or mtDox for 24 h. The amount of Dox in whole cell lysates was measured spectrofluorimetrically in duplicate. Data are presented as means \pm SD (n= 3). Versus Saos-2 cells: * p < 0.01; mtDox versus Dox: $^{\circ}$ p < 0.05. **B.** Cells were grown for 72 h in fresh medium (Ctrl), in medium containing 5 μ mol/L Dox or mtDox, then stained with neutral red solution in quadruplicate. The results were expressed as a percentage of viable cells versus untreated cells. Data are presented as means \pm SD (n= 3). Versus respective Ctrl: * p < 0.005; mtDox versus Dox: $^{\circ}$ p < 0.005. **C.** Murine osteosarcoma K7M2 cells were lysed and subjected to the Western blot analysis of ABCB1/Pgp. The resistant U-2OS/DX580 and Saos-2/DX580 variants

Targeting mitochondria to overcome drug resistance in osteosarcoma

were included as control of Pgp-overexpressing cells. The β -tubulin expression was used as a control of equal protein loading. The figure is representative of 1 out of 2 experiments. **D.** K7M2 cells were incubated for 24 h with 5 $\mu\text{mol/L}$ Dox or mtDox. The amount of Dox was measured spectrofluorimetrically in duplicate. Data are presented as means \pm SD (n= 3). mtDox versus Dox: * $p < 0.01$. **E.** Cells were grown for 72 h in fresh medium (Ctrl), in medium containing 5 $\mu\text{mol/L}$ Dox or mtDox, then stained with neutral red solution in quadruplicate. The results were expressed as a percentage of viable cells versus untreated cells. Data are presented as means \pm SD (n= 3). Versus Ctrl: * $p < 0.002$; mtDox versus Dox: ° $p < 0.002$.

Supplementary Figure 4



Supplementary Figure S4. Intracellular accumulation and cytotoxicity of mitochondria-targeted doxorubicin in non-transformed osteoblasts and cardiomyocytes

Human non-transformed osteoblasts and rat neonatal H9c2 cardiomyocytes were cultured for 24 h (panels **A, B, D, E**) or 72 h (panels **C, F**) in fresh medium (Ctrl), in medium containing 5 $\mu\text{mol/L}$ Dox or mtDox.

A and D. The amount of Dox in whole cell lysates was measured

spectrofluorimetrically in duplicate. Data are presented as means \pm SD (n= 3). mtDox versus Dox: *

p < 0.02. **B and E.** The release of LDH in the extracellular medium was measured

spectrophotometrically in duplicate. Data are presented as means \pm SD (n= 3). Versus respective

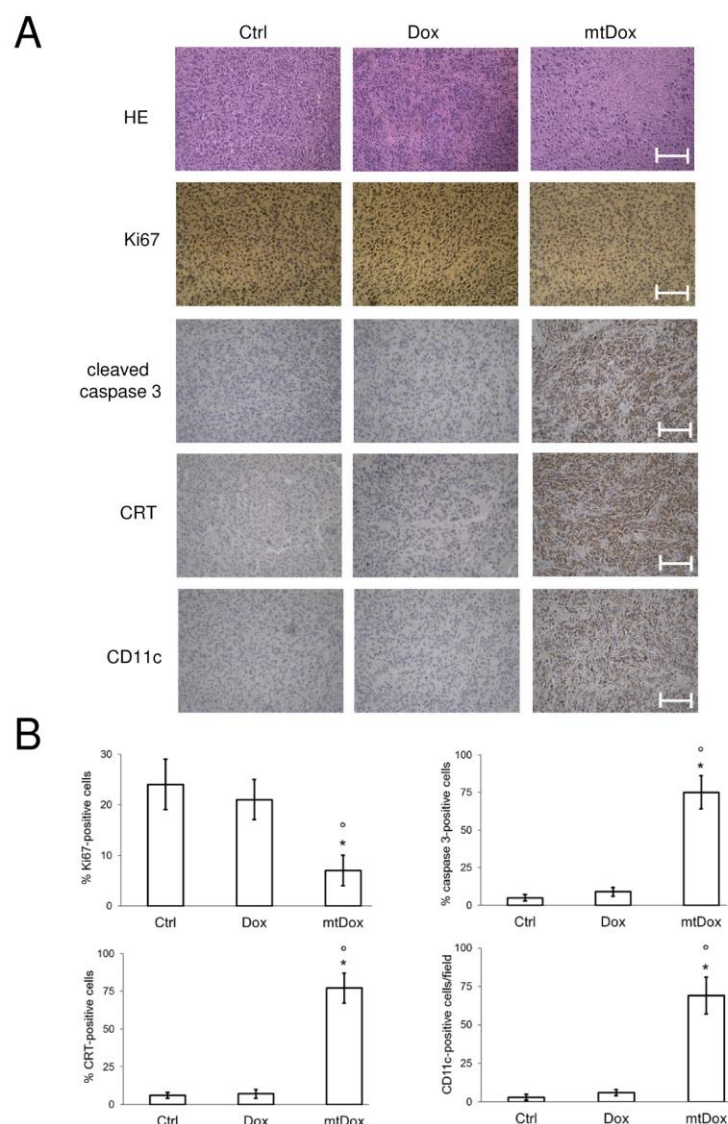
Ctrl: * p < 0.005; mtDox versus Dox: ° p < 0.01. **C and F.** Cells were stained with neutral red

solution in quadruplicate. The results were expressed as a percentage of viable cells versus

untreated cells. Data are presented as means \pm SD (n= 4). Versus respective Ctrl: * p < 0.01; mtDox

versus Dox: ° p < 0.02.

Supplementary Figure 5



Supplementary Figure S5. Immunohistochemical analysis of drug-resistant osteosarcoma treated with mitochondria-targeted doxorubicin

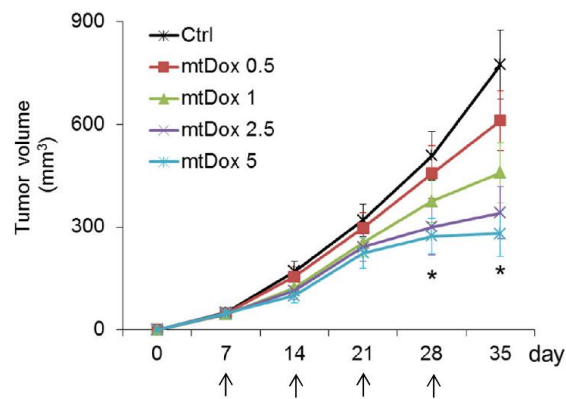
Six week-old female NOD SCID BALB/c mice were inoculated s.c. with 1×10^7 U-2OS cells.

When the tumor reached the volume of 50 mm^3 (day 7), the animals were randomized and treated on days 7, 14, 21, 28 as follows: 1) Ctrl group, treated with 0.1 mL saline solution i.v.; 2) Dox group, treated with 5 mg/kg Dox i.v.; 3) mtDox group, treated with 5 mg/kg mitochondria-targeted Dox i.v. Animals were sacrificed on day 35. **A.** Sections of tumors from each group of animals were stained with hematoxylin and eosin (HE) or immunostained for the proliferation marker Ki67, the apoptotic marker cleaved caspase 3, the immunogenic death marker calreticulin (CRT), the DC

Targeting mitochondria to overcome drug resistance in osteosarcoma

marker CD11c. Nuclei were counterstained with hematoxylin. Bar = 10 μ m. The photographs are representative of sections from 5 tumors/group. **B. Quantification of immunohistochemical images,** performed on sections from 5 animals of each group (105-83 nuclei/field). The percentage of proliferating cells was determined by the ratio Ki67-positive nuclei/total number (hematoxylin-positive) of nuclei using ImageJ software (<http://imagej.nih.gov/ij/>). The ctrl group percentage was considered 100%. The percentage of caspase 3-positive and CRT-positive cells was determined by Photoshop program. The number of CD11c-positive cells/field was calculated by ImageJ software. Data are presented as means \pm SD. Versus Ctrl group: * $p < 0.02$; mtDox group versus Dox group: $^{\circ} p < 0.01$.

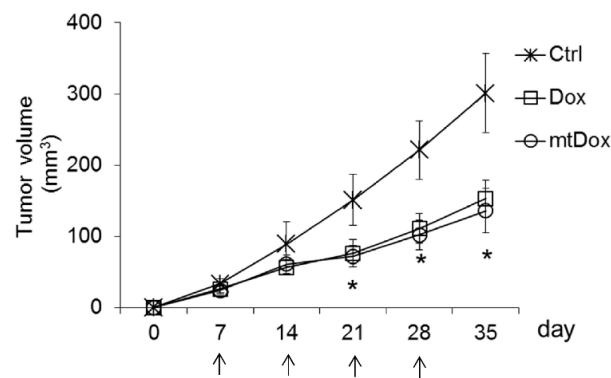
Supplementary Figure 6



Supplementary Figure S6. Dose-response effects of mitochondria-targeted doxorubicin on drug-resistant osteosarcoma *in vivo*

Six week-old female BALB/c mice were inoculated s.c. with 1×10^6 K7M2 cells. When the tumor reached the volume of 50 mm^3 (day 7), the animals (10 mice/group) were randomized and treated on days 7, 14, 21, 28 with 0.1 mL saline solution i.v. (Ctrl group) or with 0.5, 1, 2.5, 5 mg/kg mtDox. Tumor growth monitored by caliper measurements. Arrows represent saline or mtDox injections. Data are presented as means \pm SD. 1, 2.5, 5 mg/kg mtDox group versus Ctrl group: * $p < 0.01$.

Supplementary Figure 7



Supplementary Figure S7. Effects of mitochondria-targeted doxorubicin on drug-sensitive osteosarcoma *in vivo*

Six week-old female NOD SCID BALB/c mice were inoculated s.c. with 1×10^7 U-2OS cells.

When the tumor reached the volume of 50 mm^3 (day 7), the animals were randomized and treated on days 7, 14, 21, 28 as it follows: 1) Ctrl group, treated with 0.1 mL saline solution i.v.; 2) Dox group, treated with 5 mg/kg Dox i.v.; 3) mtDox group, treated with 5 mg/kg mitochondria-targeted Dox i.v. Arrows represent saline or drug injections. Data are presented as means \pm SD. Dox/mtDox group versus Ctrl group: * $p < 0.001$.

Supplementary Tables

Supplementary Table S1. IC₅₀ (μmol/L) of doxorubicin and mitochondria-targeted doxorubicin

Cell line	Dox	mtDox
U-2OS	3.91 ± 0.43	1.09 ± 0.12 °
U-2OS/DX30	25.62 ± 1.16 *	2.35 ± 0.28 °
U-2OS/DX100	79.67 ± 6.17 *	4.68 ± 0.99 °
U-2OS/DX580	124.18 ± 11.07 *	10.71 ± 0.87 °
Saos-2	4.55 ± 0.71	2.31 ± 0.23 °
Saos-2/DX30	18.78 ± 2.37 *	3.81 ± 0.42 °
Saos-2/DX100	53.29 ± 8.93 *	6.17 ± 0.52 °
Saos-2/DX580	109.82 ± 21.09 *	9.71 ± 0.87 °
K7M2	75.71 ± 4.77	8.54 ± 0.41 °
Primary osteoblasts	4.93 ± 0.29	27.52 ± 4.11 °
H9c2	0.72 ± 0.08	12.39 ± 5.27 °

Cells were incubated for 72 h with increasing concentrations (1 nmol/L-1 mmol/L) of Dox or mtDox, then stained in quadruplicate with neutral red. Data are presented as means ± SD (n = 3). Dox-resistant variants versus their parental cells: * p < 0.001; mtDox versus Dox: °p < 0.001.

Targeting mitochondria to overcome drug resistance in osteosarcoma

Supplementary Table S2. Expression of mitochondria-related genes in U-2OS cells and resistant variants

Gene	Fold change DX30 versus U-2OS	p value	Fold change DX100 versus U-2OS	p value	Fold change DX580 versus U-2OS	p value	Biological function
<i>AIFM2</i>	1.66	0.02	1.42	0.005	1.04	Ns	Apoptosis induction
<i>ATP12A</i>	0.34	0.005	0.45	0.02	1.70	Ns	H ⁺ /ATP exchange
<i>ATP4A</i>	0.33	0.005	0.45	0.02	1.70	Ns	H ⁺ /ATP exchange
<i>ATP4B</i>	0.34	0.005	0.45	0.02	1.67	Ns	H ⁺ /ATP exchange
<i>ATP50</i>	1.29	Ns	2.40	0.001	3.71	0.001	ATP synthase subunit
<i>ATP5A1</i>	2.24	0.002	5.82	0.001	6.38	0.001	ATP synthase subunit
<i>ATP5B</i>	2.09	0.005	2.96	0.001	3.93	0.001	ATP synthase subunit
<i>ATP5C1</i>	1.38	0.05	2.91	0.001	2.26	0.001	ATP synthase subunit
<i>ATP5F1</i>	1.70	0.01	4.62	0.001	4.91	0.001	ATP synthase subunit
<i>ATP5G1</i>	3.40	0.001	2.53	0.001	2.42	0.001	ATP synthase subunit
<i>ATP5G2</i>	1.72	0.01	2.24	0.001	2.42	0.001	ATP synthase subunit
<i>ATP5G3</i>	1.80	0.01	2.29	0.001	5.41	0.001	ATP synthase subunit
<i>ATP5I</i>	1.82	0.005	3.4	0.001	3.93	0.001	ATP synthase subunit
<i>ATP5J</i>	1.59	0.001	5.92	0.001	6.38	0.001	ATP synthase subunit
<i>ATP5J2</i>	3.17	0.001	2.06	0.001	3.93	0.001	ATP synthase subunit
<i>ATP5L</i>	4.41	0.001	4.49	0.001	10.38	0.001	ATP synthase subunit
<i>BAK1</i>	1.55	0.02	1.10	Ns	1.42	Ns	Apoptosis induction
<i>BBC3</i>	1.44	Ns	1.52	Ns	0.88	Ns	Apoptosis induction
<i>BCL2</i>	1.35	0.05	0.88	Ns	1.13	Ns	Apoptosis inhibition
<i>BCL2L1</i>	1.78	0.001	0.73	Ns	1.17	Ns	Apoptosis induction
<i>BCS1L</i>	1.82	0.005	1.82	0.001	1.39	0.01	Ubiquinol-cytochrome c reductase assembly
<i>BID</i>	1.55	0.02	1.19	Ns	1.59	Ns	Apoptosis induction
<i>BNIP3</i>	1.18	Ns	1.99	Ns	1.90	Ns	Apoptosis induction
<i>COX10</i>	1.66	0.01	1.41	Ns	4.02	0.05	Cytochrome c oxidase assembly
<i>COX18</i>	1.78	0.02	1.40	Ns	2.05	0.02	Cytochrome c oxidase assembly
<i>COX4I2</i>	1.70	Ns	0.45	0.02	0.34	0.01	Cytochrome c oxidase subunit
<i>COX4I1</i>	0.79	Ns	2.40	0.001	2.39	0.01	Cytochrome c oxidase assembly
<i>COX5A</i>	1.95	0.005	4.16	0.001	2.59	0.001	Cytochrome c oxidase subunit
<i>COX5B</i>	1.95	0.005	4.16	0.001	5.81	0.001	Cytochrome c oxidase subunit
<i>COX6A1</i>	1.70	0.01	0.81	0.001	0.71	0.02	Cytochrome c oxidase subunit
<i>COX6A2</i>	3.32	0.01	0.41	0.001	0.34	0.001	Cytochrome c oxidase subunit
<i>COX6B1</i>	2.41	0.005	1.16	0.001	1.71	0.001	Cytochrome c oxidase assembly/regulation
<i>COX6C</i>	1.38	0.05	1.49	0.05	2.26	0.001	Cytochrome c oxidase assembly/regulation
<i>COX7A2</i>	2.24	0.005	1.86	0.001	1.71	0.001	Cytochrome c oxidase assembly/regulation
<i>COX7A2L</i>	1.29	Ns	3.81	0.001	4.21	0.001	Cytochrome c oxidase assembly/regulation
<i>COX7B</i>	0.85	0.002	1.96	0.001	2.11	0.001	Cytochrome c oxidase subunit

Targeting mitochondria to overcome drug resistance in osteosarcoma

<i>COX8A</i>	2.09	0.001	4.53	0.001	4.51	0.001	Cytochrome c oxidase regulation
<i>CPT1</i>	1.66	0.01	2.05	0.05	3.30	0.05	Long chain fatty acylCoA import/ β -oxidation
<i>CPT2</i>	1.55	0.02	2.04	0.05	3.42	0.01	Long chain fatty acylCoA import/ β -oxidation
<i>CYCI</i>	1.95	0.005	3.24	0.001	3.98	0.001	Electron transport
<i>DMMIL</i>	1.91	0.01	2.16	0.02	3.18	0.05	Control of mitochondria morphology
<i>FIS1</i>	1.35	0.05	1.52	Ns	2.71	0.05	Control of mitochondria fission
<i>FXC1</i>	1.45	0.05	0.78	Ns	1.05	Ns	Mitochondrial proteins import
<i>HSP90A1</i>	1.26	Ns	2.26	0.05	4.40	0.05	Proteins chaperon
<i>HSPD1</i>	1.26	Ns	2.16	0.05	3.33	0.05	Mitochondrial proteins chaperon
<i>IMMP1L</i>	1.45	0.05	1.24	0.05	2.01	0.05	Mitochondrial proteins processing/import
<i>IMMP2L</i>	0.59	0.001	0.80	Ns	1.56	Ns	Mitochondrial proteins processing/import
<i>LRPPRC</i>	1.10	Ns	1.42	Ns	1.59	Ns	Mitochondrial transcription factor
<i>MFN1</i>	0.63	0.02	0.86	Ns	1.15	Ns	Control of mitochondria fusion
<i>MFN2</i>	2.19	0.002	2.43	0.05	3.49	0.05	Control of mitochondria fusion
<i>MIPEP</i>	1.78	0.01	1.39	Ns	2.47	0.05	Mitochondrial proteins processing
<i>MPV17</i>	1.66	0.01	1.18	Ns	1.45	0.005	Metabolism of mitochondrial ROS
<i>MTX2</i>	0.72	0.05	1.18	Ns	3.11	0.001	Mitochondrial proteins import
<i>NDUFA1</i>	1.82	0.005	1.40	0.001	1.71	0.001	NADH:ubiquinone oxidoreductase subunit
<i>NDUFA10</i>	1.70	0.01	1.38	0.001	1.70	0.002	NADH:ubiquinone oxidoreductase subunit
<i>NDUFA11</i>	2.58	0.001	5.29	0.001	6.84	0.001	NADH:ubiquinone oxidoreductase subunit
<i>NDUFA2</i>	1.70	0.01	5.16	0.001	6.41	0.001	NADH:ubiquinone oxidoreductase assembly
<i>NDUFA3</i>	1.95	0.005	0.29	0.001	0.40	0.05	NADH:ubiquinone oxidoreductase subunit
<i>NDUFA4</i>	1.82	0.005	1.91	0.001	3.96	0.001	NADH:ubiquinone oxidoreductase subunit
<i>NDUFA5</i>	1.70	0.01	2.19	0.001	2.26	0.001	NADH:ubiquinone oxidoreductase subunit
<i>NDUFA6</i>	2.09	0.005	1.91	0.001	2.11	0.001	NADH:ubiquinone oxidoreductase subunit
<i>NDUFA7</i>	1.48	0.02	2.24	0.001	4.21	0.001	NADH:ubiquinone oxidoreductase subunit
<i>NDUFA8</i>	1.70	0.01	2.78	0.001	8.38	0.001	NADH:ubiquinone oxidoreductase subunit
<i>NDUFAB1</i>	2.76	0.001	4.12	0.001	6.35	0.001	NADH:ubiquinone oxidoreductase subunit
<i>NDUFAB10</i>	2.76	0.001	3.91	0.001	3.93	0.001	NADH:ubiquinone oxidoreductase subunit
<i>NDUFB2</i>	1.95	0.005	5.92	0.001	6.38	0.001	NADH:ubiquinone oxidoreductase subunit
<i>NDUFB3</i>	2.09	0.005	3.81	0.001	3.97	0.001	NADH:ubiquinone oxidoreductase subunit
<i>NDUFB4</i>	1.82	0.005	2.59	0.001	5.16	0.001	NADH:ubiquinone oxidoreductase subunit
<i>NDUFB5</i>	0.79	Ns	1.71	0.001	4.19	0.001	NADH:ubiquinone oxidoreductase subunit
<i>NDUFB6</i>	1.59	0.01	3.67	0.001	3.91	0.001	NADH:ubiquinone oxidoreductase subunit
<i>NDUFB7</i>	3.65	0.005	2.24	0.001	7.86	0.001	NADH:ubiquinone oxidoreductase subunit
<i>NDUFB8</i>	1.82	0.005	2.42	0.001	8.38	0.001	NADH:ubiquinone oxidoreductase subunit
<i>NDUFB9</i>	2.96	0.001	1.83	0.001	6.35	0.001	NADH:ubiquinone oxidoreductase subunit
<i>NDUFC1</i>	2.24	0.002	1.26	0.001	4.19	0.001	NADH:ubiquinone oxidoreductase subunit
<i>NDUFC2</i>	1.38	0.05	2.26	0.001	3.40	0.001	NADH:ubiquinone oxidoreductase subunit
<i>NDUFS1</i>	0.85	Ns	4.81	0.001	3.67	0.001	NADH:ubiquinone oxidoreductase subunit
<i>NDUFS2</i>	1.29	Ns	3.65	0.001	3.19	0.001	NADH:ubiquinone oxidoreductase subunit
<i>NDUFS3</i>	2.41	0.002	3.19	0.001	5.53	0.001	NADH:ubiquinone oxidoreductase subunit

Targeting mitochondria to overcome drug resistance in osteosarcoma

<i>NDUFS4</i>	1.59	0.01	2.59	0.001	4.49	0.001	NADH:ubiquinone oxidoreductase subunit
<i>NDUFS5</i>	2.24	0.002	2.78	0.001	5.16	0.001	NADH:ubiquinone oxidoreductase subunit
<i>NDUFS6</i>	2.24	0.005	4.81	0.001	4.84	0.001	NADH:ubiquinone oxidoreductase subunit
<i>NDUFS7</i>	1.82	0.001	3.93	0.001	4.49	0.001	NADH:ubiquinone oxidoreductase subunit
<i>NDUFS8</i>	2.76	0.001	14.49	0.001	16.76	0.001	NADH:ubiquinone oxidoreductase subunit
<i>NDUFV1</i>	4.19	0.001	2.98	0.001	3.65	0.001	NADH:ubiquinone oxidoreductase subunit
<i>NDUFV2</i>	1.59	0.01	1.29	0.001	1.05	Ns	NADH:ubiquinone oxidoreductase subunit
<i>NDUFV3</i>	1.20	Ns	1.49	0.002	2.24	0.001	NADH:ubiquinone oxidoreductase subunit
<i>OPA1</i>	1.45	0.05	1.79	0.05	2.01	0.05	Control of mitochondria network
<i>OXA1L</i>	1.59	0.005	2.11	0.001	3.65	0.001	Cytochrome c oxidase assembly
<i>RHOT1</i>	1.55	0.02	1.39	Ns	2.71	0.05	Control of mitochondria fission and fusion
<i>RHOT2</i>	1.91	0.005	0.62	Ns	1.15	Ns	Control of mitochondria fission and fusion
<i>SDHA</i>	1.17	Ns	1.48	0.005	1.83	0.001	Succinate dehydrogenase subunit
<i>SDHB</i>	1.59	0.01	2.29	0.001	4.21	0.001	Succinate dehydrogenase subunit
<i>SDHC</i>	1.38	0.05	1.58	0.001	1.83	0.001	Succinate dehydrogenase subunit
<i>SDHD</i>	1.29	Ns	1.35	0.001	2.98	0.001	Succinate dehydrogenase subunit
<i>SH3SGLB1</i>	1.45	0.05	1.84	Ns	1.53	Ns	Apoptosis induction
<i>SLC25A1</i>	2.52	0.002	2.74	0.02	5.29	0.05	Tricarboxylic acids import
<i>SLC25A10</i>	2.35	0.005	2.66	0.02	6.22	0.05	Mitochondrial proteins import
<i>SLC25A12</i>	1.78	0.01	1.39	0.02	1.96	0.02	Dicarboxylic acids import
<i>SLC25A13</i>	1.02	Ns	1.50	Ns	1.87	Ns	Aspartic acid/glutamic acid exchange
<i>SLC25A14</i>	1.91	0.01	1.42	Ns	2.30	0.02	Aspartic acid/glutamic acid exchange
<i>SLC25A15</i>	1.55	0.02	2.01	0.05	3.57	0.05	Ornithine import
<i>SLC25A19</i>	3.10	0.002	4.01	0.05	6.93	0.05	Thiamine pyrophosphate import
<i>SLC25A2</i>	4.09	0.001	4.53	0.05	4.70	0.05	Mitochondrial proteins import
<i>SLC25A20</i>	2.46	0.002	3.10	0.05	3.74	0.001	Carnitine/acylcarnitine translocation
<i>SLC25A21</i>	2.76	0.01	5.07	0.05	5.77	0.05	Oxodicarboxylic acids import
<i>SLC25A22</i>	1.35	0.05	0.14	0.05	1.29	0.05	Glutamate import
<i>SLC25A23</i>	0.72	0.05	1.39	Ns	2.01	0.05	Phosphate import
<i>SLC25A24</i>	1.66	0.01	1.71	0.01	2.77	0.05	Phosphate import
<i>SLC25A25</i>	1.35	0.05	0.96	0.01	1.07	Ns	Phosphate import
<i>SLC25A27</i>	0.59	0.01	0.16	0.01	0.13	0.001	OXPPOS/ATP synthesis uncoupling
<i>SLC25A3</i>	1.78	0.01	0.82	Ns	4.30	0.05	Phosphate/hydroxyl ions exchange
<i>SLC25A31</i>	2.44	0.01	2.52	0.05	2.41	0.005	Adenine nucleotide translocation
<i>SLC25A37</i>	1.55	0.02	0.92	Ns	0.74	Ns	Iron import
<i>SLC25A4</i>	1.10	Ns	2.98	0.05	3.18	0.05	Adenine nucleotide translocation
<i>SLC25A5</i>	1.26	Ns	2.72	0.05	2.65	0.05	Adenine nucleotide translocation
<i>SOD1</i>	1.26	Ns	1.09	Ns	4.01	0.05	ROS protection (cytosol)
<i>SOD2</i>	1.48	0.005	3.39	0.001	4.30	0.001	ROS protection (mitochondria)
<i>STARD3</i>	1.02	Ns	0.94	Ns	1.07	Ns	Cholesterol import
<i>TIMM10</i>	2.05	0.005	3.34	0.05	4.30	0.05	Protein insertion in the inner membrane
<i>TIMM17A</i>	2.35	0.005	2.78	0.02	4.72	0.05	Protein insertion in the inner membrane

Targeting mitochondria to overcome drug resistance in osteosarcoma

<i>TIMM17B</i>	1.10	Ns	1.45	Ns	2.01	0.05	Protein insertion in the inner membrane
<i>TIMM8A</i>	1.91	0.01	1.88	Ns	3.66	0.05	Protein insertion in the inner membrane
<i>TIMM8B</i>	1.66	0.01	3.58	0.02	5.54	0.05	Protein insertion in the inner membrane
<i>TIMM9</i>	1.26	Ns	2.84	0.05	2.30	0.05	Protein insertion in the inner membrane
<i>TOMM20</i>	1.35	0.05	1.46	Ns	1.35	0.05	Mitochondrial proteins import
<i>TOMM22</i>	3.35	0.01	3.13	0.05	3.01	0.05	Mitochondrial proteins import
<i>TOMM34</i>	1.45	0.05	0.90	Ns	3.66	0.05	Mitochondrial proteins import
<i>TOMM40</i>	2.19	0.005	2.48	0.02	2.65	0.01	Mitochondrial proteins import
<i>TOMM70A</i>	1.78	0.01	1.75	0.01	3.74	0.002	Mitochondrial proteins import
<i>TSPO</i>	1.18	Ns	1.42	Ns	2.25	0.05	Cholesterol import
<i>UCP1</i>	2.44	0.05	1.34	Ns	0.42	0.05	OXPHOS/ATP synthesis uncoupling
<i>UCP2</i>	3.34	0.005	2.12	0.05	2.10	0.05	OXPHOS/ATP synthesis uncoupling
<i>UCP3</i>	9.19	0.001	9.01	0.05	3.12	0.05	OXPHOS/ATP synthesis uncoupling
<i>UQCRI1</i>	2.58	0.001	3.42	0.001	4.81	0.001	Ubiquinol-cytochrome c reductase subunit
<i>UQCRC1</i>	1.29	Ns	2.22	0.001	2.96	0.001	Ubiquinol-cytochrome c reductase subunit
<i>UQCRC2</i>	2.41	0.002	3.67	0.001	5.53	0.001	Ubiquinol-cytochrome c reductase subunit
<i>UQRCFS1</i>	2.09	0.002	8.42	0.001	15.63	0.001	Ubiquinol-cytochrome c reductase subunit
<i>UQCRH</i>	2.41	0.002	5.56	0.001	10.31	0.001	Ubiquinol-cytochrome c reductase subunit
<i>UQCRQ</i>	1.95	0.005	1.71	0.001	3.40	0.001	Ubiquinol-cytochrome c reductase subunit

OXPHOS: oxidative phosphorylation.

Fold-Change ($2^{(-\Delta\Delta Ct)}$) is the normalized gene expression ($2^{(-\Delta Ct)}$) in U-2OS/DX30, U-2OS/DX100 or U-2OS/DX580 cells, divided the normalized gene expression ($2^{(-\Delta Ct)}$) in U-2OS cells (n= 4), where Ct is the threshold cycle in qRT-PCR; when the fold-change is less than 1, the value is the negative inverse of the fold-change. Ns: not significant. Bold characters: up- or down-regulation more than two-fold.

Targeting mitochondria to overcome drug resistance in osteosarcoma

Supplementary Table S3. Expression of mitochondria-related genes in U-2OS cells untreated and treated with doxorubicin or mitochondria-targeted doxorubicin

Gene	Fold change Dox versus Ctrl	p value	Fold change mtDox versus Ctrl	p value	Biological function
<i>AIFM2</i>	1.83	0.05	0.71	0.02	Apoptosis induction
<i>ATP12A</i>	0.80	0.001	0.21	0.001	H ⁺ /ATP exchange
<i>ATP4A</i>	0.71	0.001	0.22	0.001	H ⁺ /ATP exchange
<i>ATP4B</i>	0.80	0.001	0.21	0.001	H ⁺ /ATP exchange
<i>ATP50</i>	0.35	0.001	0.06	0.001	ATP synthase subunit
<i>ATP5A1</i>	1.29	0.005	1.99	0.005	ATP synthase subunit
<i>ATP5B</i>	1.21	0.02	1.39	0.002	ATP synthase subunit
<i>ATP5C1</i>	0.86	0.05	1.13	Ns	ATP synthase subunit
<i>ATP5F1</i>	1.39	0.005	1.26	0.01	ATP synthase subunit
<i>ATP5G1</i>	1.30	0.01	1.06	Ns	ATP synthase subunit
<i>ATP5G2</i>	0.65	0.001	1.39	0.02	ATP synthase subunit
<i>ATP5G3</i>	0.99	0.05	1.21	0.05	ATP synthase subunit
<i>ATP5I</i>	0.70	0.002	0.68	0.01	ATP synthase subunit
<i>ATP5J</i>	1.49	0.002	1.11	0.01	ATP synthase subunit
<i>ATP5J2</i>	1.06	Ns	1.97	0.001	ATP synthase subunit
<i>ATP5L</i>	1.84	0.001	1.21	0.02	ATP synthase subunit
<i>BAK1</i>	3.42	0.05	3.72	0.001	Apoptosis induction
<i>BBC3</i>	3.46	0.05	3.17	0.001	Apoptosis induction
<i>BCL2</i>	0.20	0.05	0.10	0.001	Apoptosis inhibition
<i>BCL2L1</i>	0.48	0.05	0.31	0.005	Apoptosis inhibition
<i>BCS1L</i>	0.28	0.001	0.21	0.001	Ubiquinol-cytochrome c reductase assembly
<i>BID</i>	1.65	0.05	2.76	0.05	Apoptosis induction
<i>BNIP3</i>	2.48	0.05	2.06	0.05	Apoptosis induction
<i>COX10</i>	1.01	Ns	1	Ns	Cytochrome c oxidase assembly
<i>COX18</i>	0.54	0.05	0.66	0.005	Cytochrome c oxidase assembly
<i>COX4I2</i>	3.20	0.001	0.21	0.001	Cytochrome c oxidase subunit
<i>COX4I1</i>	0.92	Ns	1.97	0.001	Cytochrome c oxidase assembly
<i>COX5A</i>	1.30	0.01	0.99	0.005	Cytochrome c oxidase subunit
<i>COX5B</i>	1.06	Ns	1.60	0.001	Cytochrome c oxidase subunit
<i>COX6A1</i>	0.70	0.002	0.57	0.001	Cytochrome c oxidase subunit
<i>COX6A2</i>	1.13	0.005	0.10	0.001	Cytochrome c oxidase subunit
<i>COX6B1</i>	3.20	0.001	0.92	Ns	Cytochrome c oxidase assembly/regulation
<i>COX6C</i>	1.21	0.02	0.21	0.001	Cytochrome c oxidase assembly/regulation
<i>COX7A2</i>	0.75	0.005	1.21	0.02	Cytochrome c oxidase assembly/regulation
<i>COX7A2L</i>	1.81	0.001	2.26	0.002	Cytochrome c oxidase assembly/regulation
<i>COX7B</i>	0.80	0.01	1.30	0.01	Cytochrome c oxidase subunit

Targeting mitochondria to overcome drug resistance in osteosarcoma

<i>COX8A</i>	1.71	0.001	1.30	0.01	Cytochrome c oxidase regulation
<i>CPT1</i>	0.18	0.001	0.18	0.001	Long chain fatty acylcoA import/ β -oxidation
<i>CPT2</i>	2.06	0.05	0.54	0.005	Long chain fatty acylcoA import/ β -oxidation
<i>CYCI</i>	0.98	Ns	1.06	Ns	Electron transport
<i>DMMIL</i>	0.96	Ns	1.06	Ns	Control of mitochondria morphology
<i>FIS1</i>	1.42	0.05	1.24	Ns	Control of mitochondria fission
<i>FXC1</i>	0.56	0.05	0.60	0.05	Mitochondrial proteins import
<i>HSP90A1</i>	0.92	Ns	1.20	Ns	Proteins chaperon
<i>HSPD1</i>	0.58	Ns	1.09	Ns	Mitochondrial proteins chaperon
<i>IMMP1L</i>	0.66	0.05	0.41	0.001	Mitochondrial proteins processing/import
<i>IMMP2L</i>	0.16	0.001	0.24	0.001	Mitochondrial proteins processing/import
<i>LRPPRC</i>	0.58	Ns	0.95	Ns	Mitochondrial transcription factor
<i>MFN1</i>	0.55	0.05	1.09	Ns	Control of mitochondria fusion
<i>MFN2</i>	1.39	0.05	0.36	0.001	Control of mitochondria fusion
<i>MIPEP</i>	1.13	Ns	0.79	0.01	Mitochondrial proteins processing
<i>MPV17</i>	1.33	Ns	0.83	0.05	Metabolism of mitochondrial ROS
<i>MTX2</i>	1.63	0.005	1.15	Ns	Mitochondrial proteins import
<i>NDUFA1</i>	0.75	0.005	1.30	0.01	NADH:ubiquinone oxidoreductase subunit
<i>NDUFA10</i>	0.46	0.001	0.35	0.005	NADH:ubiquinone oxidoreductase subunit
<i>NDUFA11</i>	0.43	0.001	0.27	0.001	NADH:ubiquinone oxidoreductase subunit
<i>NDUFA2</i>	1.71	0.001	1.91	0.005	NADH:ubiquinone oxidoreductase assembly
<i>NDUFA3</i>	0.24	0.001	0.10	0.001	NADH:ubiquinone oxidoreductase subunit
<i>NDUFA4</i>	0.70	0.002	1.13	Ns	NADH:ubiquinone oxidoreductase subunit
<i>NDUFA5</i>	0.75	0.005	1.06	Ns	NADH:ubiquinone oxidoreductase subunit
<i>NDUFA6</i>	1.06	Ns	1.30	0.01	NADH:ubiquinone oxidoreductase subunit
<i>NDUFA7</i>	0.86	0.05	1.30	0.01	NADH:ubiquinone oxidoreductase subunit
<i>NDUFA8</i>	1.26	0.002	1.42	0.001	NADH:ubiquinone oxidoreductase subunit
<i>NDUFAB1</i>	1.39	0.005	1.71	0.001	NADH:ubiquinone oxidoreductase subunit
<i>NDUFAB10</i>	0.86	0.05	1.13	Ns	NADH:ubiquinone oxidoreductase subunit
<i>NDUFB2</i>	0.79	0.001	1.46	0.005	NADH:ubiquinone oxidoreductase subunit
<i>NDUFB3</i>	0.42	0.001	0.36	0.001	NADH:ubiquinone oxidoreductase subunit
<i>NDUFB4</i>	0.98	Ns	1.84	0.005	NADH:ubiquinone oxidoreductase subunit
<i>NDUFB5</i>	1.06	Ns	1.26	0.01	NADH:ubiquinone oxidoreductase subunit
<i>NDUFB6</i>	0.36	Ns	0.37	0.001	NADH:ubiquinone oxidoreductase subunit
<i>NDUFB7</i>	3.20	0.001	1.97	0.001	NADH:ubiquinone oxidoreductase subunit
<i>NDUFB8</i>	1.13	Ns	1.30	0.005	NADH:ubiquinone oxidoreductase subunit
<i>NDUFB9</i>	1.20	0.05	0.75	0.005	NADH:ubiquinone oxidoreductase subunit
<i>NDUFC1</i>	1.06	Ns	1.49	0.002	NADH:ubiquinone oxidoreductase subunit
<i>NDUFC2</i>	1.30	0.01	1.60	0.001	NADH:ubiquinone oxidoreductase subunit
<i>NDUFS1</i>	0.86	0.05	1.11	Ns	NADH:ubiquinone oxidoreductase subunit
<i>NDUFS2</i>	0.92	Ns	1.60	0.001	NADH:ubiquinone oxidoreductase subunit
<i>NDUFS3</i>	2.11	0.001	2.11	0.001	NADH:ubiquinone oxidoreductase subunit

Targeting mitochondria to overcome drug resistance in osteosarcoma

<i>NDUFS4</i>	0.70	0.002	0.97	0.001	NADH:ubiquinone oxidoreductase subunit
<i>NDUFS5</i>	1.30	0.01	1.39	0.02	NADH:ubiquinone oxidoreductase subunit
<i>NDUFS6</i>	1.84	0.005	1.84	0.001	NADH:ubiquinone oxidoreductase subunit
<i>NDUFS7</i>	1.60	0.001	1.84	0.001	NADH:ubiquinone oxidoreductase subunit
<i>NDUFS8</i>	4.22	0.001	3.43	0.001	NADH:ubiquinone oxidoreductase subunit
<i>NDUFV1</i>	0.98	Ns	0.70	0.02	NADH:ubiquinone oxidoreductase subunit
<i>NDUFV2</i>	0.30	0.001	0.25	0.001	NADH:ubiquinone oxidoreductase subunit
<i>NDUFV3</i>	0.92	Ns	1.49	0.002	NADH:ubiquinone oxidoreductase subunit
<i>OPA1</i>	0.84	Ns	0.60	0.005	Control of mitochondria network
<i>OXA1L</i>	0.80	0.001	0.21	0.001	Cytochrome c oxidase assembly
<i>RHOT1</i>	0.56	0.05	1	Ns	Control of mitochondria fission and fusion
<i>RHOT2</i>	1.03	Ns	0.22	0.02	Control of mitochondria fission and fusion
<i>SDHA</i>	0.65	0.001	0.94	Ns	Succinate dehydrogenase subunit
<i>SDHB</i>	1.49	0.002	1.65	0.01	Succinate dehydrogenase subunit
<i>SDHC</i>	0.91	Ns	1.71	0.02	Succinate dehydrogenase subunit
<i>SDHD</i>	1.71	0.001	1.42	0.01	Succinate dehydrogenase subunit
<i>SH3SGLB1</i>	1.27	0.005	1.51	Ns	Apoptosis induction
<i>SLC25A1</i>	2.42	0.001	0.76	0.005	Tricarboxylic acids import
<i>SLC25A10</i>	2.98	0.001	0.69	0.005	Mitochondrial proteins import
<i>SLC25A12</i>	0.59	0.05	0.62	0.005	Dicarboxylic acids import
<i>SLC25A13</i>	0.41	0.01	0.52	0.02	Aspartic acid/glutamic acid exchange
<i>SLC25A14</i>	1.15	Ns	0.66	0.05	Aspartic acid/glutamic acid exchange
<i>SLC25A15</i>	1.48	0.05	1.06	Ns	Ornithine import
<i>SLC25A19</i>	1.88	0.05	0.29	0.01	Thiamine pyrophosphate import
<i>SLC25A2</i>	1.88	0.02	0.19	0.001	Mitochondrial proteins import
<i>SLC25A20</i>	0.98	Ns	0.55	0.01	Carnitine/acylcarnitine translocation
<i>SLC25A21</i>	0.91	Ns	0.76	0.005	Oxodicarboxylic acids import
<i>SLC25A22</i>	0.82	Ns	0.40	0.001	Glutamate import
<i>SLC25A23</i>	0.96	Ns	1.26	Ns	Phosphate import
<i>SLC25A24</i>	1.10	Ns	0.91	Ns	Phosphate import
<i>SLC25A25</i>	0.56	0.05	0.41	0.02	Phosphate import
<i>SLC25A27</i>	2.10	0.001	2.55	0.05	OXPPOS/ATP synthesis uncoupling
<i>SLC25A3</i>	1.49	0.05	1.51	Ns	Phosphate/hydroxyl ions exchange
<i>SLC25A31</i>	1.01	Ns	1.09	Ns	Adenine nucleotide translocation
<i>SLC25A37</i>	0.41	0.01	0.19	0.001	Iron import
<i>SLC25A4</i>	1.60	0.05	1.58	Ns	Adenine nucleotide translocation
<i>SLC25A5</i>	1.05	Ns	1.34	Ns	Adenine nucleotide translocation
<i>SOD1</i>	0.20	0.001	0.38	0.02	ROS protection (cytosol)
<i>SOD2</i>	0.42	0.001	0.40	0.05	ROS protection (mitochondria)
<i>STARD3</i>	0.86	0.02	0.45	0.02	Cholesterol import
<i>TIMM10</i>	1.56	0.01	1.20	Ns	Protein insertion in the inner membrane
<i>TIMM17A</i>	1.71	0.001	0.95	Ns	Protein insertion in the inner membrane

Targeting mitochondria to overcome drug resistance in osteosarcoma

<i>TIMM17B</i>	1.63	0.02	0.79	0.01	Protein insertion in the inner membrane
<i>TIMM8A</i>	1.67	0.02	1.00	Ns	Protein insertion in the inner membrane
<i>TIMM8B</i>	3.63	0.001	1.74	0.05	Protein insertion in the inner membrane
<i>TIMM9</i>	0.60	Ns	1.20	Ns	Protein insertion in the inner membrane
<i>TOMM20</i>	0.41	0.01	0.20	0.001	Mitochondrial proteins import
<i>TOMM22</i>	1.67	0.01	1.20	Ns	Mitochondrial proteins import
<i>TOMM34</i>	1.21	Ns	1.51	Ns	Mitochondrial proteins import
<i>TOMM40</i>	1.67	0.02	0.40	0.02	Mitochondrial proteins import
<i>TOMM70A</i>	1.21	Ns	1.09	Ns	Mitochondrial proteins import
<i>TSPO</i>	1.13	Ns	1.15	Ns	Cholesterol import
<i>UCP1</i>	3.46	0.001	3.17	0.002	OXPPOS/ATP synthesis uncoupling
<i>UCP2</i>	4.12	0.001	3.44	0.001	OXPPOS/ATP synthesis uncoupling
<i>UCP3</i>	4.12	0.001	3.18	0.005	OXPPOS/ATP synthesis uncoupling
<i>UQCRI1</i>	1.39	0.005	1.60	0.001	Ubiquinol-cytochrome c reductase subunit
<i>UQCRC1</i>	1.49	0.002	1.30	0.01	Ubiquinol-cytochrome c reductase subunit
<i>UQCRC2</i>	1.06	Ns	1.60	0.001	Ubiquinol-cytochrome c reductase subunit
<i>UQRCFS1</i>	0.42	0.001	0.68	0.001	Ubiquinol-cytochrome c reductase subunit
<i>UQCRH</i>	1.60	0.001	1.11	0.05	Ubiquinol-cytochrome c reductase subunit
<i>UQCRQ</i>	1.13	Ns	0.92	Ns	Ubiquinol-cytochrome c reductase subunit

Ctrl: untreated cells; Dox: cells treated with 5 $\mu\text{mol/L}$ Dox for 24 h; mtDox: cells treated with 5 $\mu\text{mol/L}$ mtDox for 24 h; OXPPOS: oxidative phosphorylation.

Fold-Change ($2^{(-\Delta\Delta Ct)}$) is the normalized gene expression ($2^{(-\Delta Ct)}$) in Dox- or mtDox-treated U-2OS cells, divided the normalized gene expression ($2^{(-\Delta Ct)}$) in untreated cells ($n=4$), where Ct is the threshold cycle in qRT-PCR; when the fold-change is less than 1, the value was the negative inverse of the fold-change. Ns: not significant. Bold characters: up- or down-regulation more than two-fold.

Targeting mitochondria to overcome drug resistance in osteosarcoma

Supplementary Table S4. Expression of mitochondria-related genes in U-2OS/DX580 cells untreated and treated with doxorubicin or mitochondria-targeted doxorubicin

Gene	Fold change Dox versus Ctrl	p value	Fold change mtDox versus Ctrl	p value	Biological function
<i>AIFM2</i>	1.58	Ns	0.71	0.002	Apoptosis induction
<i>ATP12A</i>	1.22	Ns	0.23	0.001	H ⁺ /ATP exchange
<i>ATP4A</i>	1.26	Ns	0.21	0.001	H ⁺ /ATP exchange
<i>ATP4B</i>	1.28	Ns	0.21	0.001	H ⁺ /ATP exchange
<i>ATP50</i>	1.66	0.05	1.62	0.001	ATP synthase subunit
<i>ATP5A1</i>	1.67	0.01	1.46	0.001	ATP synthase subunit
<i>ATP5B</i>	1.34	0.02	1.31	0.01	ATP synthase subunit
<i>ATP5C1</i>	1.22	Ns	1.44	0.001	ATP synthase subunit
<i>ATP5F1</i>	2.01	0.02	1.76	0.002	ATP synthase subunit
<i>ATP5G1</i>	1.26	Ns	0.76	0.005	ATP synthase subunit
<i>ATP5G2</i>	1.37	Ns	0.41	0.001	ATP synthase subunit
<i>ATP5G3</i>	0.89	Ns	0.51	0.001	ATP synthase subunit
<i>ATP5I</i>	1.11	Ns	1.23	Ns	ATP synthase subunit
<i>ATP5J</i>	1.26	0.05	1.62	0.005	ATP synthase subunit
<i>ATP5J2</i>	2.07	0.01	0.22	0.001	ATP synthase subunit
<i>ATP5L</i>	1.21	0.02	0.33	0.001	ATP synthase subunit
<i>BAK1</i>	1.00	Ns	2.72	0.001	Apoptosis induction
<i>BBC3</i>	1.23	Ns	2.19	0.001	Apoptosis induction
<i>BCL2</i>	1.03	0.05	0.43	0.001	Apoptosis inhibition
<i>BCL2L1</i>	0.93	Ns	0.29	0.005	Apoptosis inhibition
<i>BCS1L</i>	0.66	0.05	0.41	0.001	Ubiquinol-cytochrome c reductase assembly
<i>BID</i>	1.89	0.05	2.76	0.01	Apoptosis induction
<i>BNIP3</i>	1.26	Ns	2.09	0.05	Apoptosis induction
<i>COX10</i>	1.44	Ns	1	Ns	Cytochrome c oxidase assembly
<i>COX18</i>	0.72	0.02	0.66	0.05	Cytochrome c oxidase assembly
<i>COX4I2</i>	1.21	Ns	0.20	0.001	Cytochrome c oxidase subunit
<i>COX4I1</i>	2.11	0.01	2.14	0.001	Cytochrome c oxidase assembly
<i>COX5A</i>	1.78	0.005	1.86	0.001	Cytochrome c oxidase subunit
<i>COX5B</i>	1.09	Ns	1.11	Ns	Cytochrome c oxidase subunit
<i>COX6A1</i>	0.98	Ns	0.41	0.001	Cytochrome c oxidase subunit
<i>COX6A2</i>	1.00	Ns	0.29	0.001	Cytochrome c oxidase subunit
<i>COX6B1</i>	0.92	Ns	1.20	0.05	Cytochrome c oxidase assembly/regulation
<i>COX6C</i>	1.21	Ns	0.43	0.001	Cytochrome c oxidase assembly/regulation
<i>COX7A2</i>	1.23	Ns	1.23	Ns	Cytochrome c oxidase assembly/regulation
<i>COX7A2L</i>	1.26	Ns	1.28	0.02	Cytochrome c oxidase assembly/regulation
<i>COX7B</i>	1.39	Ns	1.41	0.02	Cytochrome c oxidase subunit

Targeting mitochondria to overcome drug resistance in osteosarcoma

<i>COX8A</i>	1.30	Ns	1.51	0.02	Cytochrome c oxidase regulation
<i>CPT1</i>	1.04	0.05	0.24	0.05	Long chain fatty acylcoA import/ β -oxidation
<i>CPT2</i>	0.81	Ns	0.37	0.02	Long chain fatty acylcoA import/ β -oxidation
<i>CYCI</i>	1.51	0.002	1.23	Ns	Electron transport
<i>DMMIL</i>	1.04	Ns	1.24	Ns	Control of mitochondria morphology
<i>FIS1</i>	1.44	Ns	1.06	Ns	Control of mitochondria fission
<i>FXC1</i>	1.55	0.02	0.40	0.05	Mitochondrial proteins import
<i>HSP90A1</i>	1.44	Ns	1.20	Ns	Proteins chaperon
<i>HSPD1</i>	1.15	Ns	1.09	Ns	Mitochondrial proteins chaperon
<i>IMMP1L</i>	1.79	0.01	0.41	0.005	Mitochondrial proteins processing/import
<i>IMMP2L</i>	1.81	Ns	1.82	Ns	Mitochondrial proteins processing/import
<i>LRPPRC</i>	0.91	Ns	0.95	Ns	Mitochondrial transcription factor
<i>MFN1</i>	0.95	Ns	0.36	0.05	Control of mitochondria fusion
<i>MFN2</i>	0.83	0.05	0.39	0.02	Control of mitochondria fusion
<i>MIPEP</i>	1.05	Ns	0.79	Ns	Mitochondrial proteins processing
<i>MPV17</i>	0.79	0.01	1.15	Ns	Metabolism of mitochondrial ROS
<i>MTX2</i>	0.45	0.02	0.31	0.02	Mitochondrial proteins import
<i>NDUFA1</i>	0.77	0.01	1.23	0.005	NADH:ubiquinone oxidoreductase subunit
<i>NDUFA10</i>	0.97	Ns	0.76	0.005	NADH:ubiquinone oxidoreductase subunit
<i>NDUFA11</i>	1.56	0.005	1.62	0.001	NADH:ubiquinone oxidoreductase subunit
<i>NDUFA2</i>	1.34	0.01	0.29	0.001	NADH:ubiquinone oxidoreductase assembly
<i>NDUFA3</i>	1.51	0.01	0.08	0.001	NADH:ubiquinone oxidoreductase subunit
<i>NDUFA4</i>	1.13	Ns	1.29	Ns	NADH:ubiquinone oxidoreductase subunit
<i>NDUFA5</i>	1.78	0.02	1.63	0.001	NADH:ubiquinone oxidoreductase subunit
<i>NDUFA6</i>	1.30	0.05	1.51	0.001	NADH:ubiquinone oxidoreductase subunit
<i>NDUFA7</i>	1.24	Ns	1.17	0.05	NADH:ubiquinone oxidoreductase subunit
<i>NDUFA8</i>	1.61	0.001	1.02	Ns	NADH:ubiquinone oxidoreductase subunit
<i>NDUFAB1</i>	1.23	Ns	1.41	0.001	NADH:ubiquinone oxidoreductase subunit
<i>NDUFAB10</i>	1.45	0.05	1.15	Ns	NADH:ubiquinone oxidoreductase subunit
<i>NDUFB2</i>	1.42	0.05	1.71	0.05	NADH:ubiquinone oxidoreductase subunit
<i>NDUFB3</i>	1.26	0.05	0.50	0.02	NADH:ubiquinone oxidoreductase subunit
<i>NDUFB4</i>	1.84	0.02	0.63	0.05	NADH:ubiquinone oxidoreductase subunit
<i>NDUFB5</i>	1.23	Ns	0.40	0.01	NADH:ubiquinone oxidoreductase subunit
<i>NDUFB6</i>	1.56	Ns	1.14	Ns	NADH:ubiquinone oxidoreductase subunit
<i>NDUFB7</i>	1.56	0.05	1.41	0.01	NADH:ubiquinone oxidoreductase subunit
<i>NDUFB8</i>	1.29	0.05	1.99	0.005	NADH:ubiquinone oxidoreductase subunit
<i>NDUFB9</i>	0.78	0.05	0.81	0.02	NADH:ubiquinone oxidoreductase subunit
<i>NDUFC1</i>	1.42	0.01	1.41	0.001	NADH:ubiquinone oxidoreductase subunit
<i>NDUFC2</i>	1.60	0.01	1.23	0.005	NADH:ubiquinone oxidoreductase subunit
<i>NDUFS1</i>	1.72	0.002	1.46	0.001	NADH:ubiquinone oxidoreductase subunit
<i>NDUFS2</i>	1.11	Ns	1.74	0.001	NADH:ubiquinone oxidoreductase subunit
<i>NDUFS3</i>	0.78	Ns	0.24	0.001	NADH:ubiquinone oxidoreductase subunit

Targeting mitochondria to overcome drug resistance in osteosarcoma

<i>NDUFS4</i>	1.62	0.001	1.13	Ns	NADH:ubiquinone oxidoreductase subunit
<i>NDUFS5</i>	1.28	0.05	0.38	0.005	NADH:ubiquinone oxidoreductase subunit
<i>NDUFS6</i>	1.36	Ns	1.46	0.001	NADH:ubiquinone oxidoreductase subunit
<i>NDUFS7</i>	1.17	Ns	1.51	0.002	NADH:ubiquinone oxidoreductase subunit
<i>NDUFS8</i>	2.11	0.05	3.46	0.001	NADH:ubiquinone oxidoreductase subunit
<i>NDUFV1</i>	1.01	Ns	0.37	0.001	NADH:ubiquinone oxidoreductase subunit
<i>NDUFV2</i>	1.32	Ns	1.12	Ns	NADH:ubiquinone oxidoreductase subunit
<i>NDUFV3</i>	0.71	Ns	0.81	Ns	NADH:ubiquinone oxidoreductase subunit
<i>OPA1</i>	1.02	0.002	0.16	0.001	Control of mitochondria network
<i>OXA1L</i>	1.56	0.02	0.46	0.005	Cytochrome c oxidase assembly
<i>RHOT1</i>	0.63	0.01	0.52	0.05	Control of mitochondria fission and fusion
<i>RHOT2</i>	1.16	0.001	0.22	0.05	Control of mitochondria fission and fusion
<i>SDHA</i>	1.32	Ns	0.61	0.001	Succinate dehydrogenase subunit
<i>SDHB</i>	1.89	0.001	1.34	0.001	Succinate dehydrogenase subunit
<i>SDHC</i>	1.42	0.002	0.87	0.05	Succinate dehydrogenase subunit
<i>SDHD</i>	1.70	0.002	1.99	0.001	Succinate dehydrogenase subunit
<i>SH3SGLB1</i>	1.32	Ns	1.51	0.05	Apoptosis induction
<i>SLC25A1</i>	0.79	0.005	0.56	0.01	Tricarboxylic acids import
<i>SLC25A10</i>	1	Ns	0.46	0.005	Mitochondrial proteins import
<i>SLC25A12</i>	0.83	0.05	0.49	0.005	Dicarboxylic acids import
<i>SLC25A13</i>	0.76	0.01	0.42	0.01	Aspartic acid/glutamic acid exchange
<i>SLC25A14</i>	1.91	0.005	0.56	0.005	Aspartic acid/glutamic acid exchange
<i>SLC25A15</i>	1.71	Ns	0.29	0.001	Ornithine import
<i>SLC25A19</i>	1.32	Ns	1.09	Ns	Thiamine pyrophosphate import
<i>SLC25A2</i>	0.10	0.05	0.19	0.05	Mitochondrial proteins import
<i>SLC25A20</i>	1.07	Ns	0.45	0.05	Carnitine/acylcarnitine translocation
<i>SLC25A21</i>	0.72	0.01	0.76	0.05	Oxodicarboxylic acids import
<i>SLC25A22</i>	1.69	0.01	0.40	0.05	Glutamate import
<i>SLC25A23</i>	1.32	Ns	1.26	Ns	Phosphate import
<i>SLC25A24</i>	1.15	Ns	0.70	Ns	Phosphate import
<i>SLC25A25</i>	1.45	0.002	0.41	0.05	Phosphate import
<i>SLC25A27</i>	1.18	Ns	2.45	0.02	OXPPOS/ATP synthesis uncoupling
<i>SLC25A3</i>	1.38	Ns	1.51	Ns	Phosphate/hydroxyl ions exchange
<i>SLC25A31</i>	0.72	0.005	1.09	Ns	Adenine nucleotide translocation
<i>SLC25A37</i>	0.81	0.05	0.21	0.002	Iron import
<i>SLC25A4</i>	1.74	0.05	1.32	Ns	Adenine nucleotide translocation
<i>SLC25A5</i>	1.26	Ns	1.58	Ns	Adenine nucleotide translocation
<i>SOD1</i>	1.38	Ns	0.38	Ns	ROS protection (cytosol)
<i>SOD2</i>	1.09	Ns	0.40	0.05	ROS protection (mitochondria)
<i>STARD3</i>	1.00	0.02	0.45	0.02	Cholesterol import
<i>TIMM10</i>	1.26	Ns	1.20	Ns	Protein insertion in the inner membrane
<i>TIMM17A</i>	1.04	Ns	0.75	Ns	Protein insertion in the inner membrane

Targeting mitochondria to overcome drug resistance in osteosarcoma

<i>TIMM17B</i>	1.26	Ns	0.49	0.01	Protein insertion in the inner membrane
<i>TIMM8A</i>	1.15	Ns	0.41	0.005	Protein insertion in the inner membrane
<i>TIMM8B</i>	1.58	Ns	1.74	0.05	Protein insertion in the inner membrane
<i>TIMM9</i>	1.32	Ns	1.20	Ns	Protein insertion in the inner membrane
<i>TOMM20</i>	0.87	Ns	1.20	Ns	Mitochondrial proteins import
<i>TOMM22</i>	0.40	0.02	0.21	0.001	Mitochondrial proteins import
<i>TOMM34</i>	1.51	Ns	1.51	Ns	Mitochondrial proteins import
<i>TOMM40</i>	1.06	0.005	0.33	0.05	Mitochondrial proteins import
<i>TOMM70A</i>	1.20	Ns	0.47	0.02	Mitochondrial proteins import
<i>TSPO</i>	1.09	Ns	0.17	0.005	Cholesterol import
<i>UCP1</i>	1.21	Ns	2.19	0.05	OXPPOS/ATP synthesis uncoupling
<i>UCP2</i>	1.66	0.05	1.44	Ns	OXPPOS/ATP synthesis uncoupling
<i>UCP3</i>	1.21	Ns	2.18	0.05	OXPPOS/ATP synthesis uncoupling
<i>UQCRI1</i>	1.34	Ns	0.93	Ns	Ubiquinol-cytochrome c reductase subunit
<i>UQCRC1</i>	1.65	0.005	1.62	0.001	Ubiquinol-cytochrome c reductase subunit
<i>UQCRC2</i>	1.32	0.05	0.32	0.001	Ubiquinol-cytochrome c reductase subunit
<i>UQRCFS1</i>	1.72	0.05	0.30	0.001	Ubiquinol-cytochrome c reductase subunit
<i>UQCRH</i>	1.19	Ns	1.15	Ns	Ubiquinol-cytochrome c reductase subunit
<i>UQCRQ</i>	0.89	Ns	0.46	0.01	Ubiquinol-cytochrome c reductase subunit

Ctrl: untreated cells; Dox: cells treated with 5 $\mu\text{mol/L}$ Dox for 24 h; mtDox: cells treated with 5 $\mu\text{mol/L}$ mtDox for 24 h; OXPPOS: oxidative phosphorylation.

Fold-Change ($2^{(-\Delta\Delta Ct)}$) is the normalized gene expression ($2^{(-\Delta Ct)}$) in Dox- or mtDox-treated U-2OS/DX580 cells, divided the normalized gene expression ($2^{(-\Delta Ct)}$) in untreated cells ($n=4$), where Ct is the threshold cycle in qRT-PCR; when the fold-change is less than 1, the value is the negative inverse of the fold-change. Ns: not significant. Bold characters: up- or down-regulation more than two-fold.

Supplementary Tables S5. qRT-PCR validation of PCR-arrays results in U-2OS, U-2OS/DX30, U-2OS/DX100, U-2OS/DX580 cells

Gene name	Relative expression U-2OS/DX30 vs U-2OS	Relative expression U-2OS/DX30 vs U-2OS	Relative expression U-2OS/DX30 vs U-2OS	Biological function
<i>TIMM8B</i>	1.92 ± 0.32 *	2.89 ± 0.34 *	5.01 ± 0.47 *	Protein insertion in the inner membrane
<i>TOMM70A</i>	1.72 ± 0.21 *	1.81 ± 0.29 *	3.34 ± 0.27 *	Mitochondrial proteins import
<i>MFN2</i>	2.92 ± 0.37 *	2.82 ± 0.71 *	3.72 ± 0.52 *	Control of mitochondria fusion
<i>OPA1</i>	1.26 ± 0.12	1.54 ± 0.12 *	2.91 ± 0.43 *	Control of mitochondria network
<i>SLC25A10</i>	2.12 ± 0.61 *	2.73 ± 0.37 *	5.88 ± 0.34 *	Dicarboxylic acids import
<i>CPT1</i>	1.52 ± 0.26	2.44 ± 0.23 *	3.17 ± 0.28 *	Long chain fatty acylCoA import/ β -oxidation
<i>NDUFA2</i>	1.43 ± 0.21	5.03 ± 0.47 *	5.99 ± 0.71 *	NADH:ubiquinone oxidoreductase assembly
<i>NDUFS5</i>	2.35 ± 0.36 *	2.67 ± 0.11 *	5.56 ± 0.43 *	NADH:ubiquinone oxidoreductase subunit
<i>UQRQCQ</i>	1.76 ± 0.33 *	1.82 ± 0.32 *	2.47 ± 0.55 *	Ubiquinol-cytochrome c reductase subunit
<i>UQRCS1</i>	2.21 ± 0.65 *	7.13 ± 1.29 *	13.09 ± 2.24 *	Ubiquinol-cytochrome c reductase subunit
<i>OXA1L</i>	1.26 ± 0.21	2.53 ± 0.12 *	4.82 ± 0.33 *	Cytochrome c oxidase assembly
<i>ATP5L</i>	3.67 ± 0.56 *	4.45 ± 0.87 *	8.33 ± 1.21 *	ATP synthase subunit
<i>UCP1</i>	2.02 ± 0.35 *	1.18 ± 0.21	0.19 ± 0.05 *	OXPPOS/ATP synthesis uncoupling
<i>SLC25A27</i>	0.62 ± 0.12 *	0.26 ± 0.11 *	0.13 ± 0.06 *	OXPPOS/ATP synthesis uncoupling
<i>SOD2</i>	1.54 ± 0.31	2.28 ± 0.54 *	3.66 ± 0.29 *	ROS protection (mitochondria)
<i>BAK1</i>	1.23 ± 0.22	1.09 ± 0.03	0.98 ± 0.15	Apoptosis induction
<i>BCL2</i>	0.93 ± 0.21	1.22 ± 0.11	1.32 ± 0.09	Apoptosis inhibition

The expression levels of specific mitochondria-related genes, representative of the main biological categories screened by PCR arrays (Supplementary Table S2), were validated by qRT-PCR (n = 3). The expression level of each gene in U-2OS cells was considered as 1. The relative expression of the other genes was calculated with PrimePCR™ Analysis Software. *S14* gene was used as the housekeeping gene. Versus U-2OS cells: * p < 0.05.

Supplementary Tables S6. qRT-PCR validation of PCR-arrays results in U-2OS cells treated with doxorubicin or mitochondria-targeted doxorubicin

Gene name	Relative expression Dox vs Ctrl	Relative expression mtDox vs Ctrl	Biological function
<i>TIMM8B</i>	3.56 ± 0.34 *	1.65 ± 0.41	Protein insertion in the inner membrane
<i>TOMM70A</i>	1.12 ± 0.11	1.34 ± 0.26	Mitochondrial proteins import
<i>MFN2</i>	1.11 ± 0.19	0.27 ± 0.11 *	Control of mitochondria fusion
<i>OPA1</i>	0.79 ± 0.27	0.51 ± 0.09 *	Control of mitochondria network
<i>SLC25A10</i>	3.09 ± 0.45 *	0.62 ± 0.20 *	Dicarboxylic acids import
<i>CPT1</i>	0.32 ± 0.11 *	0.19 ± 0.08 *	Long chain fatty acylCoA import/ β -oxidation
<i>NDUFA2</i>	1.83 ± 0.14 *	1.89 ± 0.25 *	NADH:ubiquinone oxidoreductase assembly
<i>NDUFS5</i>	1.27 ± 0.06	1.35 ± 0.09	NADH:ubiquinone oxidoreductase subunit
<i>UQRQCQ</i>	1.01 ± 0.28	1.14 ± 0.28	Ubiquinol-cytochrome c reductase subunit
<i>UQRDFS1</i>	0.59 ± 0.18 *	0.63 ± 0.12 *	Ubiquinol-cytochrome c reductase subunit
<i>OXA1L</i>	0.92 ± 0.31	0.42 ± 0.11 *	Cytochrome c oxidase assembly
<i>ATP5L</i>	1.57 ± 0.33	1.26 ± 0.05	ATP synthase subunit
<i>UCP1</i>	3.01 ± 0.72 *	3.35 ± 0.61 *	OXPHOS/ATP synthesis uncoupling
<i>SLC25A27</i>	2.13 ± 0.27 *	2.61 ± 0.64 *	OXPHOS/ATP synthesis uncoupling
<i>SOD2</i>	0.61 ± 0.18 *	0.42 ± 0.19 *	ROS protection (mitochondria)
<i>BAK1</i>	2.93 ± 0.34 *	3.37 ± 0.71 *	Apoptosis induction
<i>BCL2</i>	0.39 ± 0.12 *	0.18 ± 0.08 *	Apoptosis inhibition

The expression levels of specific mitochondria-related genes, representative of the main biological categories screened by PCR arrays (Supplementary Table S3), were validated by qRT-PCR (n = 3). The expression level of each gene in untreated U-2OS cells was considered as 1. The relative expression of the other genes was calculated with PrimePCR™ Analysis Software. *S14* gene was used as the housekeeping gene. Versus untreated U-2OS cells: * p < 0.05.

Supplementary Tables S7. qRT-PCR validation of PCR-arrays results in U-2OS/DX580 cells treated with doxorubicin or mitochondria-targeted doxorubicin

Gene name	Relative expression Dox vs Ctrl	Relative expression mtDox vs Ctrl	Biological function
<i>TIMM8B</i>	1.28 ± 0.21	1.54 ± 0.33	Protein insertion in the inner membrane
<i>TOMM70A</i>	1.07 ± 0.21	0.52 ± 0.13 *	Mitochondrial proteins import
<i>MFN2</i>	0.95 ± 0.13	0.43 ± 0.18 *	Control of mitochondria fusion
<i>OPA1</i>	0.91 ± 0.08	0.21 ± 0.10 *	Control of mitochondria network
<i>SLC25A10</i>	1.14 ± 0.21	0.33 ± 0.06 *	Dicarboxylic acids import
<i>CPT1</i>	0.95 ± 0.18	0.26 ± 0.05 *	Long chain fatty acylcoA import/ β -oxidation
<i>NDUFA2</i>	1.04 ± 0.12	0.21 ± 0.03 *	NADH:ubiquinone oxidoreductase assembly
<i>NDUFS5</i>	1.04 ± 0.19	0.41 ± 0.23 *	NADH:ubiquinone oxidoreductase subunit
<i>UQRQCQ</i>	1.08 ± 0.11	0.61 ± 0.15 *	Ubiquinol-cytochrome c reductase subunit
<i>UQRDFS1</i>	1.52 ± 0.13	0.33 ± 0.07 *	Ubiquinol-cytochrome c reductase subunit
<i>OXA1L</i>	1.24 ± 0.11	0.61 ± 0.17 *	Cytochrome c oxidase assembly
<i>ATP5L</i>	1.06 ± 0.14	0.41 ± 0.19 *	ATP synthase subunit
<i>UCP1</i>	1.17 ± 0.25	2.49 ± 0.36 *	OXPHOS/ATP synthesis uncoupling
<i>SLC25A27</i>	0.97 ± 0.21	2.27 ± 0.31 *	OXPHOS/ATP synthesis uncoupling
<i>SOD2</i>	0.87 ± 0.11	0.36 ± 0.14 *	ROS protection (mitochondria)
<i>BAK1</i>	1.32 ± 0.22	3.11 ± 0.39 *	Apoptosis induction
<i>BCL2</i>	1.059 ± 0.19	0.37 ± 0.13 *	Apoptosis inhibition


The expression levels of specific mitochondria-related genes, representative of the main biological categories screened by PCR arrays (Supplementary Table S4), were validated in qRT-PCR (n = 3). The expression level of each gene in untreated U-2OS/DX580 cells was considered as 1. The relative expression of the other genes was calculated with PrimePCR™ Analysis Software. *S14* gene was used as the housekeeping gene. Versus untreated U-2OS/DX580 cells: * p < 0.05.

RESEARCH

Open Access



PERK induces resistance to cell death elicited by endoplasmic reticulum stress and chemotherapy

Iris C. Salaroglio^{1†}, Elisa Panada^{1,2†}, Enrico Moiso³, Ilaria Buondonno¹, Paolo Provero³, Menachem Rubinstein⁴, Joanna Kopecka^{1*†}  and Chiara Riganti^{1*†}

Abstract

Background: Nutrient deprivation, hypoxia, radiotherapy and chemotherapy induce endoplasmic reticulum (ER) stress, which activates the so-called unfolded protein response (UPR). Extensive and acute ER stress directs the UPR towards activation of death-triggering pathways. Cancer cells are selected to resist mild and prolonged ER stress by activating pro-survival UPR. We recently found that drug-resistant tumor cells are simultaneously resistant to ER stress-triggered cell death. It is not known if cancer cells adapted to ER stressing conditions acquire a chemoresistant phenotype.

Methods: To investigate this issue, we generated human cancer cells clones with acquired resistance to ER stress from ER stress-sensitive and chemosensitive cells.

Results: ER stress-resistant cells were cross-resistant to multiple chemotherapeutic drugs: such multidrug resistance (MDR) was due to the overexpression of the plasma-membrane transporter MDR related protein 1 (MRP1). Gene profiling analysis unveiled that cells with acquired resistance to ER stress and chemotherapy share higher expression of the UPR sensor protein kinase RNA-like endoplasmic reticulum kinase (PERK), which mediated the erythroid-derived 2-like 2 (Nrf2)-driven transcription of MRP1. Disrupting PERK/Nrf2 axis reversed at the same time resistance to ER stress and chemotherapy. The inducible silencing of *PERK* reduced tumor growth and restored chemosensitivity in resistant tumor xenografts.

Conclusions: Our work demonstrates for the first time that the adaptation to ER stress in cancer cells produces a MDR phenotype. The PERK/Nrf2/MRP1 axis is responsible for the resistance to ER stress and chemotherapy, and may represent a good therapeutic target in aggressive and resistant tumors.

Keywords: Eukaryotic translation initiation factor-2 α kinase 3/protein kinase RNA-like endoplasmic reticulum kinase, Multidrug resistance related protein 1, Endoplasmic reticulum stress, Unfolded protein response, Chemoresistance

Background

Cancer cells often face conditions of nutrient deprivation, hypoxia, alterations in glycosylation status and calcium flux [1, 2], leading to the accumulation of unfolded or misfolded proteins in the endoplasmic reticulum (ER) lumen. These conditions activate the so-called unfolded protein response (UPR; [3, 4]). In the early phase, UPR mediates

the adaptation to stress by modifying the transcriptional and translational programs responsible for protein folding, and/or by promoting ER-associated degradation (ERAD) pathways to remove misfolded proteins. If the attempt to adapt to ER stress fails, the UPR activates cell death programs to eliminate the damaged cells [5, 6]. Recently, we demonstrated that cancer cells with constitutive or acquired resistance to chemotherapy are also resistant to ER stress-triggered cell death. This resistance was due to ubiquitination and subsequent degradation of the ER stress-activated transcription factor CAAT/enhancer- β liver-enriched

* Correspondence: joanna.kopecka@unito.it; chiara.riganti@unito.it

Iris C Salaroglio and Elisa Panada were co-first authors.

Joanna Kopecka and Chiara Riganti were co-last authors

[†]Equal contributors

¹Department of Oncology, University of Torino, via Santena 5/bis, 10126 Torino, Italy

Full list of author information is available at the end of the article



inhibitory protein (C/EBP- β LIP). Consequently, the proapoptotic axis C/EBP homologous protein (CHOP)/caspase 3 was down-regulated in the resistant cells. Moreover, LIP elimination in the chemoresistant cells up-regulates the transcription of P-glycoprotein (Pgp) [7]. Pgp prevents the accumulation of chemotherapeutic drugs and targeted therapy-agents, determining multidrug resistance (MDR) [8]. Since many chemotherapeutic drugs – such as anthracyclines [9], cisplatin [10], oxaliplatin [9], 5-fluorouracil [11] and paclitaxel [12] – induce a massive ER-stress mediated cell death, the lack of ER stress-dependent apoptotic response coupled with the increased drug efflux strongly reduces the efficacy of these drugs in MDR cells.

Three sensors of ER stress - activating transcription factor 6 (ATF6), inositol-requiring enzyme 1 (IRE1) and protein kinase RNA-like endoplasmic reticulum kinase/eukaryotic translation initiation factor-2 α kinase 3 (PERK) - initiate the UPR in cancer cells [3, 13]. Activated PERK phosphorylates eukaryotic translation initiation factor-2 α (EIF2 α) and nuclear factor erythroid-derived 2-like 2 (Nrf2), thereby attenuating protein translation and inducing genes controlling redox homeostasis [13, 14]. The activation of PERK may determine resistance to ER stress-induced cell death in a EIF2 α -dependent manner [6, 13] and resistance to chemotherapy-induced cell death in a Nrf2-dependent manner [15–18]. By binding antioxidant response elements (AREs) in promoter regions, Nrf2 up-regulates antioxidant genes, metal-binding proteins, stress response proteins, drug-metabolizing enzyme and drug efflux transporters such as MDR-related protein 1 (MRP1) [16, 19].

While our previous findings suggest that cells with acquired resistance to chemotherapy are also resistant to ER stress-dependent cell death, it is not known whether chemosensitive cancer cells adapted to ER stress acquire resistance to chemotherapy as well. To address this issue, we exposed ER stress-sensitive/chemosensitive cancer cells to 3 different ER stress inducers developing the corresponding ER stress-resistant clones. We demonstrated that the activation of PERK/Nrf2/MRP1 axis determines the resistance to ER stress and also resistance to chemotherapy. Inhibiting this axis is an effective anti-proliferative and chemosensitizing strategy.

Methods

Chemicals and supplies

Cell culture plasticware were obtained from Falcon (Becton Dickinson, Franklin Lakes, NJ). Gel electrophoresis reagents were obtained from Bio-Rad Laboratories (Hercules, CA). The protein content of cell lysates was measured with the BCA kit from Sigma Chemicals Co. (St. Louis, MO) using bovine serum albumin as a standard. Unless specified otherwise, all other reagents were purchased from Sigma Chemical Co.

Cells

Human chemosensitive colon cancer HT29 cells (ATCC, Manassas, VA) were cultured in RPMI-1640 medium supplemented with 10% fetal bovine serum (FBS, Invitrogen Life Technologies, Carlsbad, CA) and 100 U/ml penicillin, 100 μ g/ml streptomycin. HT29/MDR cells, a subpopulation of HT29 cells displaying resistance to chemotherapy and ER stress inducers (Additional file 1: Table S1), were obtained as reported [7]. ER stress-resistant subpopulations, termed HT29/Tg, HT29/Tun and HT29/Bfa, were created by stepwise selection of parental HT29 cells in RPMI-1640 medium containing increasing concentrations of thapsigargin, tunicamycin and brefeldin A, respectively. Resistant subclones were then maintained at a concentration of each ER stress inducer that allowed > 95% cell viability (500 nM thapsigargin, 250 nM tunicamycin and 250 nM brefeldin A). ER stress-resistant clones were similarly derived from human chemosensitive breast cancer MCF7 cells and human chemosensitive osteosarcoma U-2OS cells (ATCC). MCF7/Tun and U-2OS/Tun were maintained in DMEM/F12 and IMDM medium (Invitrogen Life Technologies), supplemented with 10% FBS, 100 U/ml penicillin, 100 μ g/ml streptomycin, containing 500 nM tunicamycin. When cultured in 3D-systems, 1×10^5 cells were seeded in 96-well plate coated with Biomimesys™ matrix (Celenys, Rouen, France). After 7 days, 3D-cultures were treated and analyzed by contrast phase Leica DC100 microscope (Leica Microsystems GmbH, Wetzlar, Germany; 10X ocular lens, 4X objective). Cell lines were authenticated by microsatellite analysis using the PowerPlex kit (Promega Corporation, Madison, WI; last authentication: September 2016).

Measurement of cell necrosis and cell viability

Cells were incubated for 24 h (for the High Mobility Group Protein 1, HMGB1, assay) or 48 h (for Neutral red and crystal violet staining) in fresh medium, or in medium containing thapsigargin (10 μ M), tunicamycin (1 μ M), brefeldin A (1 μ M), or the chemotherapeutic drugs oxaliplatin or cisplatin (10 μ M), 5-fluorouracil (5 μ M), doxorubicin (5 μ M). Acute cell toxicity was measured by evaluating the release of HMGB1 in the cell culture supernatant, using the High Mobility Group Protein 1 ELISA kit (Cloud-Clone Corp., Houston, Texas). Results were expressed in pg/mg total cellular protein, employing a pre-made titration curve. Cell viability was measured using Neutral red staining assay [7]. The viability of untreated cells was considered 100%; the results were expressed as percentage of viable cells in each experimental condition versus untreated cells. IC₅₀ was calculated by incubating cells with increasing concentrations of the drugs (from 10^{-10} to 10^{-3} M), then staining cells with Neutral red. To evaluate morphology, cells were stained with 5% w/v crystal violet solution in 66% v/v

methanol, washed and analyzed under bright field microscope (10X objective; 10X ocular lens).

Immunoblotting

Cells were rinsed with ice-cold lysis RIPA buffer (50 mM Tris, 10 mM EDTA, 1% v/v Triton-X100; pH 7.5), supplemented with the protease inhibitor cocktail set III (80 μ M aprotinin, 5 mM bestatin, 1.5 mM leupeptin, 1 mM pepstatin; Calbiochem, San Diego, CA), 2 mM phenylmethylsulfonyl fluoride and 1 mM Na_3VO_4 . The cells were then sonicated (10 bursts of 10 s, 4 °C, 100 W, using a Labsonic sonicator, Hielscher, Teltow, Germany) and centrifuged at 13,000 \times g for 10 min at 4 °C. 20 μ g protein extracts were subjected to 4-20% gradient SDS-PAGE and probed with the following antibodies: anti-Pgp (1:500; Calbiochem); anti-MRP1 (1:500; Abcam, Cambridge, UK); anti-MRP2 (1:250; Abcam); anti-MRP3 (1:500; Santa Cruz Biotechnology Inc., Santa Cruz, CA); anti-MRP4 (1:250; Santa Cruz Biotechnology Inc.); anti-MRP5 (1:500; Abcam); anti-BCRP (1:1000; Santa Cruz Biotechnology Inc.), anti-PERK (1:500; Santa Cruz Biotechnology Inc.), anti-IRE1 (1:500; Thermo Scientific Inc., Rockford, IL), anti-ATF6 (1:500; Santa Cruz Biotechnology Inc.), anti-eIF2 α (1:1000; Abcam), anti-phospho(Ser51)eIF2 α (1:500; Abcam), anti- β -tubulin (1:1000; Santa Cruz Biotechnology Inc.). The membranes were then incubated with peroxidase-conjugated secondary antibody (1:3000; Bio-Rad Laboratories) and washed with Tris-buffered saline-Tween 0.1% v/v solutions. Protein bands were detected by enhanced chemiluminescence (Bio-Rad Laboratories). Nuclear extracts were prepared using the Nuclear Extract kit (Active Motif, La Hulpe, Belgium). Nuclear proteins were separated by SDS-PAGE and probed with anti-Nrf2 (1:500; Abcam) or anti-TATA box binding protein antibodies (TBP, 1:500; Santa Cruz Biotechnology Inc.).

Quantitative Real Time-PCR (qRT-PCR) and PCR expression arrays

Total RNA was extracted and reverse-transcribed using the iScript™ cDNA Synthesis Kit (Bio-Rad Laboratories). qRT-PCR was performed using IQ™ SYBR Green Supermix (Bio-Rad Laboratories). The same cDNA preparation was used for measuring genes of interest and the house-keeping gene *SI4*. The primer sequences, designed with qPrimerDepot software (<https://primerdepot.nci.nih.gov/>), are reported in the Additional File 2. Relative gene expression levels were calculated using Gene Expression Quantitation software (Bio-Rad Laboratories). PCR arrays were generated using 1 μ g cDNA and Human Unfolded Protein Response Plus RT² Profiler™ PCR Array (Bio-Rad Laboratories) according to the manufacturer's instructions. Data analysis was performed using the PrimePCR™ Analysis Software (Bio-Rad Laboratories).

Flow cytometry

Cells (1×10^6) were rinsed and fixed with 2% w/v paraformaldehyde for 2 min, permeabilized using 0.1% v/v Triton-X100 for 2 min on ice, washed three times with PBS and stained with an anti-MRP1 antibody (1:250, Abcam) for 1 h on ice. The cells were then incubated with an AlexaFluor 488-conjugated secondary antibody (1:100, Millipore, Billerica, MA) for 30 min and washed again. Samples were analyzed with a FACS-Calibur flow cytometer (Becton Dickinson). For each analysis 10000 events were collected. Control experiments included incubation with non immune isotype antibody followed by the secondary antibody. The results were expressed as mean fluorescence value of MRP1 expression, calculated with the Cell Quest software (Becton Dickinson).

Intracellular doxorubicin accumulation

Doxorubicin content was measured by fluorimetry as detailed elsewhere [20]. The results were expressed as nmol doxorubicin/mg cell proteins, according to a preformed titration curve.

Chromatin immunoprecipitation (ChIP)

ChIP experiments were performed for determining binding of Nrf2 to the ARE1 site of the *MRP1* promoter [21]. The PCR primers used were: 5'-CGGCTCGAGT TATCATGTCTCCAGGCTTCA-3'; 5'-CGGAAGCTTG CCGGTGGCGCGGG-3'.

PERK silencing

Cells (2×10^6 in 0.25 mL FBS/antibiotic-free medium) were transduced with 6×10^5 lentiviral particles (Thermo Scientific Open Biosystems, Waltham, MA). 6 h after the transfection, 0.25 mL complete medium was added. Medium was fully replaced 24 h after the transfection. Transfection efficiency was checked by evaluating the percentage of green fluorescent protein (GFP)-positive cells by fluorescence microscopy, 48 h after the transfection: in each experiment, GFP-positive cells were $\geq 90\%$. Stably transduced clones were selected by culturing cells in medium containing 2 μ g/mL puromycin, for 3 weeks. *PERK* shRNA was induced by adding 1 μ g/mL doxycycline to the culture medium for 72 h. To verify the silencing efficacy, cells were lysed and PERK was visualized by immunoblotting, as described above.

In vivo tumor growth

HT29 cells or HT29/MDR cells (1×10^6) transduced with the inducible silencing vector for *PERK*, were re-suspended in 100 μ L culture medium, mixed with 100 μ L Matrigel and injected s.c. into 6–8 weeks old NOD SCID BALB/c female mice (weight: 20.82 ± 2.34 g), housed under 12 h light/dark cycle, with food and drinking provided ad libitum. Tumor growth was

measured daily by caliper, and was calculated according to the equation $(L \times W^2)/2$, where L = tumor length and W = tumor width. When tumor reached the volume of 100 mm³, mice were randomized and treated on day 3, 9, 15 as it follows: 1) Ctrl group was treated with 200 μ L saline solution i.v.; 2) oxaliplatin (oPt) group was treated with 5 mg/Kg oPt i.p. Intratumor *PERK* silencing was activated by doxycycline (2 mg/mL) in the drinking water. Animals were euthanized at day 21. Tumors were resected, photographed and fixed in 4% v/v paraformaldehyde. The paraffin sections were stained with hematoxylin/eosin or immunostained for PERK (1:50), MRP1 (1:50), cleaved caspase 3 (Asp175, 1:50; Cell Signaling Technology Inc., Danvers, MA), followed by a peroxidase-conjugated secondary antibody (1:100, Dako, Glostrup, Denmark). Sections were examined with a Leica DC100 microscope (Leica Microsystems GmbH, Wetzlar, Germany; 10X ocular lens, 63X objective).

Cell migration

In vitro migration was evaluated by the scratch wound healing assay over a period of 24 h, as reported [22]. Results were expressed as μ m/h, by performing ≥ 100 measurement per each condition.

Statistical analysis

All data in text and figures are provided as means \pm SD. The results were analyzed by a one-way Analysis of Variance (ANOVA). $p < 0.05$ was considered significant.

Gene expression profiles and clinical data were obtained from The Cancer Genome Atlas (TCGA; <https://cancergenome.nih.gov/>) and analysed using R (<https://www.R-project.org>). Survival association analyses were performed using Cox's proportional hazard model in univariate setting and Kaplan-Meier method, applying false discovery rate (FDR) and Bonferroni correction for multiple testing.

Results

Cells adapted to ER stress acquire resistance to chemotherapy

Chemosensitive human colon cancer HT29 and its chemoresistant clone HT29/MDR were incubated with the ER stress inducers thapsigargin, tunicamycin or brefeldin A, or with the chemotherapeutic agents oxaliplatin (a substrate of MRP1 and MRP4), 5-fluorouracil (a substrate of MRP1, MRP3, MRP4 and MRP5) or doxorubicin (a substrate of Pgp, MRP1, MRP2, MRP3 and BCRP), at concentrations that were cytotoxic in chemosensitive cells but not in chemoresistant ones ([7]; Additional file 1). Cytotoxicity was characterized by release of HMGB1 to the culture media and by reduced cell viability (Fig. 1a-f). To verify whether cells resistant to ER stress were also cross-resistant to chemotherapy, we generated the ER stress resistant clones

HT29/Tg, HT29/Tun, HT29/Bfa from the ER stress-sensitive/chemosensitive HT29 cells. In these clones neither ER stress inducers nor chemotherapeutic agents increased the release of HMGB1 (Fig. 1a, b) or reduced cell viability (Fig. 1c-f). Resistance to oxaliplatin, chosen as a paradigmatic first-line treatment in colon cancer, was preserved in 3D-cultures of HT29/MDR and HT29/Tun cells (Additional file 3). Overall, these data suggest that the acquisition of resistance to ER stress is associated to the acquisition of resistance to chemotherapy.

ER stress- and chemotherapy-resistant cells up-regulate MRP1

Chemoresistance is often mediated by increased expression of ABC transporters [8]. Therefore, we analyzed their expression level in chemosensitive/ER stress-sensitive HT29 cells and in the HT29/Tg, HT29/Tun and HT29/Bfa clones. HT29/MDR were used as control of chemoresistant/ER-stress resistant cells overexpressing Pgp, MRP1, MRP2, MRP3, MRP5 and BCRP. Compared to HT29 cells, all the ER stress-resistant clones showed higher expression of MRP1 at the protein (Fig. 2a) and mRNA (Fig. 2b) levels, associated with a higher amount of MRP1 on the cell surface (Fig. 2c-d). In line with this trend, the intracellular accumulation of doxorubicin, which is inversely related to MRP1 activity, was lower in the ER-stress resistant clones, as well as in HT29/MDR cells (Fig. 2e).

To verify whether the cross resistance to ER stress inducers and to chemotherapeutic drugs was limited to HT29 cells or not, we generated two other ER stress-resistant clones, MCF7/Tun and U-2OS/Tun, from ER stress-sensitive/chemosensitive breast cancer MCF7 cells and osteosarcoma U-2OS cells. As for HT29 subclones, MCF7/Tun and U-2OS/Tun cells were resistant to both ER stress inducers and to chemotherapeutic drugs. These cells exhibited higher expression of MRP1 protein and mRNA, higher amount of MRP1 on cell surface, and lower retention of doxorubicin (Additional files 4 and 5). These data suggested that up-regulation of MRP1 is associated with the dual resistance to ER stress and to chemotherapy and is exhibited by a variety of cancer cells of different histological origin.

The PERK/Nrf2 axis up-regulates MRP1 and controls the resistance to ER stress and to chemotherapy

To investigate whether there is a common gene signature between chemoresistant cells and ER stress-resistant cells, we compared the expression of 83 genes involved in UPR in HT29/Tun, HT29/MDR and HT29 cells.

As expected, several genes involved in protein synthesis, ER quality control and ERAD were significantly up-regulated in HT29/Tun cells (Fig. 3a; Additional file 6). By contrast, only *PERK* was significantly increased in HT29/MDR cells (Fig. 3b; Additional file 6). Interestingly, the fold-

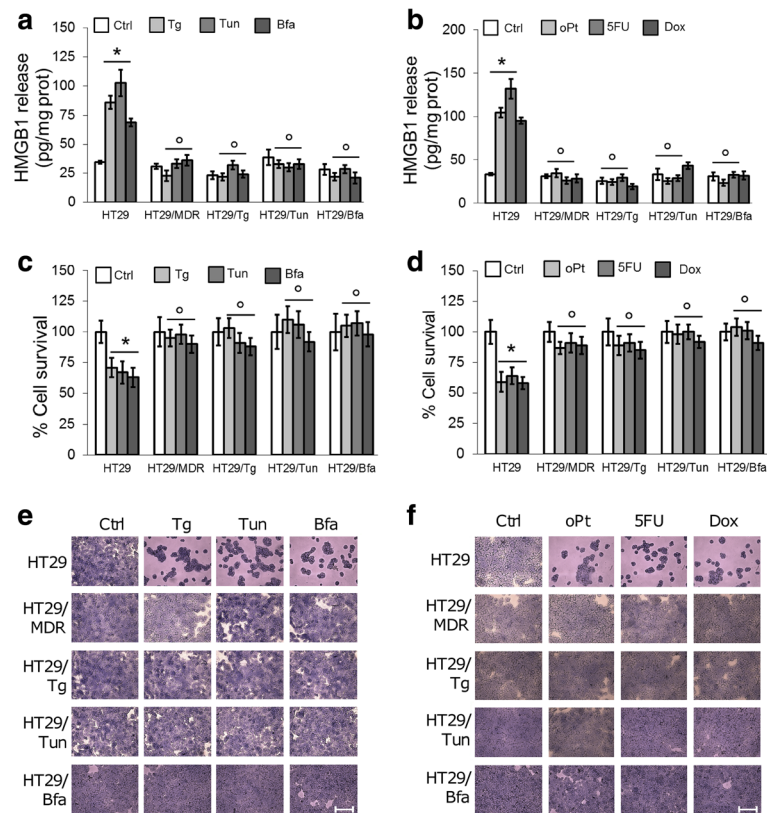


Fig. 1 Drug resistance of human colon cancer cells adapted to ER stress. **a, b.** Release of the necrosis marker HMGB1 to culture media of the indicated cells (human chemosensitive HT29 cells, chemoresistant HT29/MDR cells, ER stress-resistant clones HT29/Tg, HT29/Tun, HT29/Bfa), following incubation in fresh medium (Ctrl), or in media containing: thapsigargin (Tg), tunicamycin (Tun), brefeldin A (Bfa), oxaliplatin (oPt), 5-fluorouracil (5FU), doxorubicin (Dox), as indicated in Methods. Data are mean \pm SD. ($n = 3$). * $p < 0.001$ for treated cells vs. Ctrl HT29 cells. $^{\circ}p < 0.001$ for HT29/MDR, HT29/Tg, HT29/Tun/HT29/Bfa cells vs. the corresponding condition in HT29 cells. **c, d.** Viability of cells measured by Neutral red staining. Data are mean \pm SD ($n = 4$). * $p < 0.02$ for treated cells vs. Ctrl HT29 cells; $^{\circ}p < 0.05$ for HT29/MDR, HT29/Tg, HT29/Tun/HT29/Bfa cells vs. the corresponding condition in HT29 cells. **e, f.** Crystal violet staining of cells grown in 96-well plates and treated as in **a** and **b**. The images are representatives of at least 5 microscopic fields showing similar cell density. Bars = 500 μ M

increase of *PERK* mRNA in HT29/Tun and HT29/MDR cells was very similar (Fig. 3a, b; Additional file 6) and was associated with increased *PERK* protein levels (Fig. 3c). No appreciable change in the expression of the other ER stress sensors IRE1 and ATF6 was observed (Fig. 3c).

In line with previous findings [13, 14], the highly *PERK*-expressing HT29/MDR, HT29/Tg, HT29/Tun and HT29/Bfa cells had higher mRNA levels of the *PERK*-target/redox-sensitive factor *Nrf2* (Fig. 3d). *Nrf2* protein was also more translocated in the nucleus (Fig. 3e) and it was bound to the *ABCC1/MRP1* promoter (Fig. 3e). Overall, these data suggest that the increase of *MRP1* expression in cells resistant to ER stress and to chemotherapy is associated to up-regulation of *PERK* and *Nrf2*.

Targeting the *PERK/Nrf2/MRP1* axis abrogates the dual resistance to ER stress and chemotherapy

We next generated HT29/MDR, HT29/Tg, HT29/Tun, HT29/Bfa clones transduced with a doxycycline-inducible

shRNA for *PERK*. In parallel, we treated these clones with the MEK/ERK inhibitor PD98059, which prevents the phosphorylation and transcriptional activity of *Nrf2* in colon cancer [23]. As expected, the silencing of *PERK* reduced the phosphorylation on serine 51 of *eIF2 α* (Fig. 4a), a typical *PERK* substrate [13]. Both *PERK*-silenced cells and PD98059-treated cells showed decreased nuclear translocation of *Nrf2* (Fig. 4b), *MRP1* mRNA level (Fig. 4c) and *MRP1* amount on the cell surface (Fig. 4d; Additional file. 7a, b), coupled with increased doxorubicin accumulation (Fig. 4e).

Direct downstream targets of *PERK*, selected using GeneOntology database (www.geneontology.org/), such as eukaryotic translation initiation factor 2 subunit 1 (*EIF2S1*), activating transcription factor 4 (*ATF4*), and *Nrf2* [13, 14; Additional file 8a), were up-regulated in HT29/MDR and HT29/Tun cells (Additional file 8b), in accord with the increased amount of *PERK* in these cells. *PERK*-silencing significantly reduced the expression

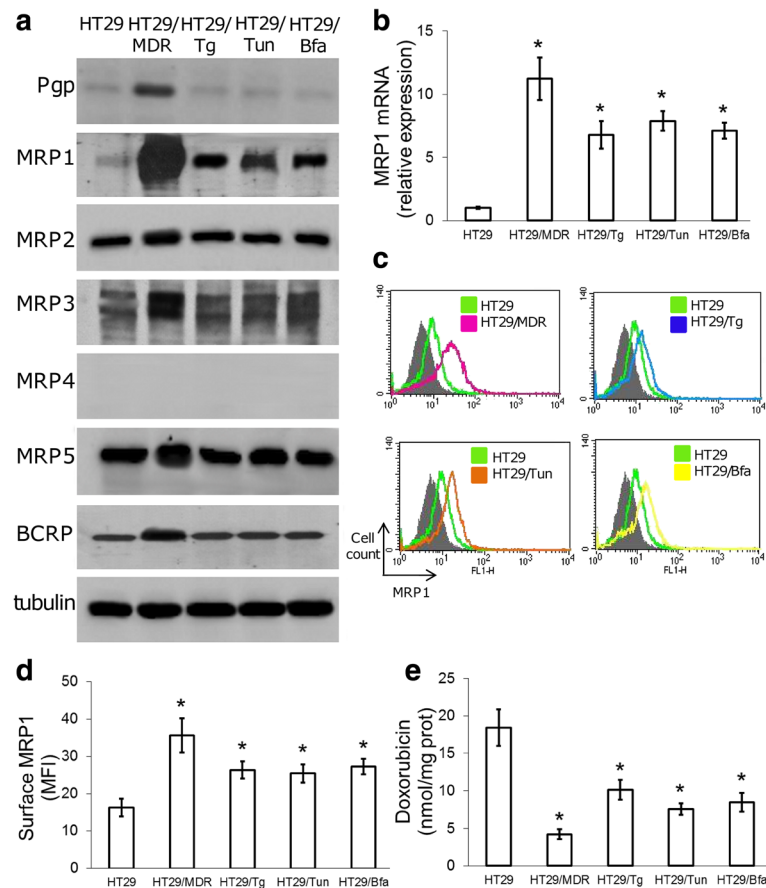


Fig. 2 Expression of MRP1 in cells resistant to chemotherapy and to ER stress. **a.** Immunoblots of the indicated proteins in extracts of untreated cells. β -tubulin was used as a loading control. The figure is representative of 3 experiments with similar results. **b.** *MRP1* mRNA level as measured by qRT-PCR. Data are mean \pm SD ($n = 4$). * $p < 0.001$ vs. HT29 cells. **c.** Representative flow cytometry histograms of MRP1 protein. Grey peaks: non immune isotypic antibody. **d.** Cell surface MRP1 was determined by flow cytometry. Data are mean fluorescence intensity (MFI) \pm SD ($n = 3$). * $p < 0.02$ vs. HT29 cells. **e.** Intracellular doxorubicin content, an index of MRP1 activity, measured by fluorimetry. Data are mean \pm SD ($n = 3$). * $p < 0.001$ vs. HT29 cells

levels of all these genes (Additional file 8b). Other upstream controllers of Nrf2 such as glycogen synthase kinase 3 β (*GSK3 β*), c-Jun N-terminal kinase 1 (*JNK1*), mitogen activated kinase 1 (*MAPK1*), phosphatidylinositol-4,5-bisphosphate 3-kinase catalytic subunit δ (*PI3KCD*), protein kinase C α (*PRKCA*), were increased in HT29/MDR and HT29/Tun cells, but variably modulated by *PERK*-silencing, likely because multiple pathways control the transcription of these genes. We also analyzed the expression of Nrf2-target genes (www.geneontology.org/), divided into two main categories: 1) genes encoding for anti-oxidant/detoxifying enzymes and chaperones, such as glutathione-disulfide reductase (*GSR*), glucose-6-phosphate dehydrogenase (*G6PD*), thioredoxin reductase 1 (*TXNRD1*), superoxide dismutase 1 (*SOD1*), heme oxygenase 1 (*HMOX1*), NAD(P)H quinone dehydrogenase 1 (*NQO1*), stress induced phosphoprotein 1 (*STIP1*); 2) genes encoding for membrane efflux transporters like *MRP1* (Additional file 8a). All these genes were significantly up-regulated in HT29/MDR cells and

HT29/Tun cells and significantly down-regulated in both populations by either *PERK*-silencing or Nrf2-inhibition (Additional file 8b).

The inducible silencing of *PERK* increased the release of HMGB1 (Fig. 5a, b) and reduced cell survival (Fig. 5c-e). ER stress inducers and chemotherapeutic drugs enhanced the effect of *PERK* silencing in all the resistant clones (Fig. 5). Similar effects were observed upon inhibition of Nrf2 (Additional file 9a-d).

Since the expression of *PERK* and *NRF2* is variably related to patient clinical outcome (Additional file 10), to better clarify the impact of *PERK* on tumor progression and response to therapy in a preclinical model, we implanted HT29/MDR cells transduced with inducible shRNA for *PERK* in NOD SCID BALB/c mice, treated with oxaliplatin, with or without doxycycline. HT29 cells were implanted to establish a control oxaliplatin-sensitive tumor. HT29/MDR cells generated tumors faster than HT29 cells (Fig. 6a; Additional file 11). Although we did not detect significant differences in the proliferation rate

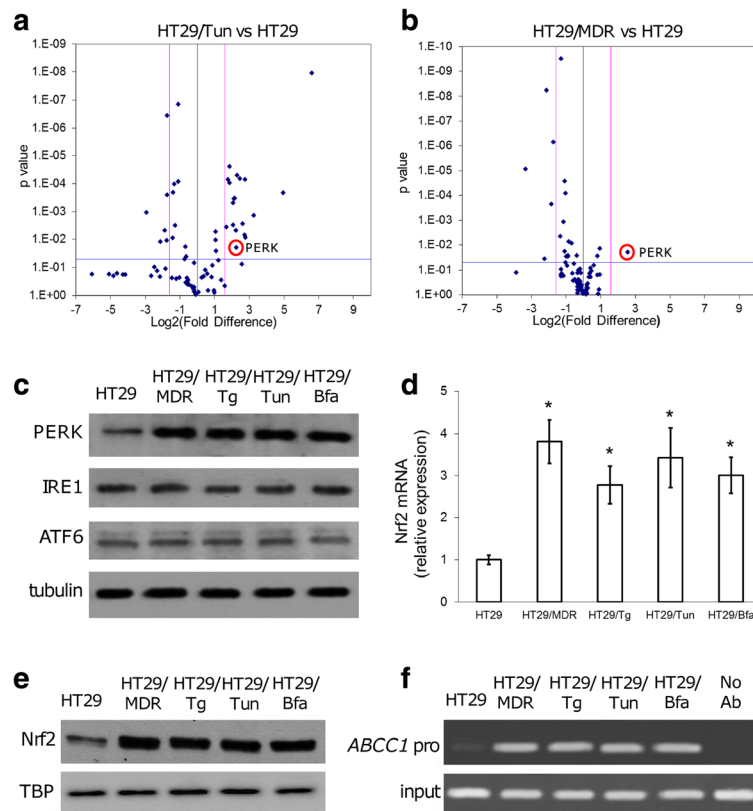


Fig. 3 PERK expression in cells resistant to chemotherapy and to ER stress. **a, b.** Relative expression of 83 UPR genes in untreated HT29/Tun vs. HT29 cells (**a**), and in untreated HT29/MDR vs. HT29 cells (**b**). The Volcano plots are representative of 4 independent experiments. The spots corresponding to PERK are encircled. **c.** Immunoblots of the indicated proteins in extracts of untreated cells. β -tubulin was used as a loading control. The figure is representative of 3 experiments with similar results. **d.** Nrf2 mRNA levels in extracts of untreated cells. Data are mean \pm SD ($n = 4$). * $p < 0.005$ vs. HT29 cells. **e.** Immunoblot of Nrf2 in nuclear extracts of the indicated cells. TATA-box binding protein (TBP) served as a loading control. The figure is representative of 3 experiments with similar results. **f.** Binding of Nrf2 to the *ABCC1/MRP1* promoter (*ABCC1* pro) as measured by CHIP. The figure is representative of 3 experiments with similar results. Amplification of *ABCC1* promoter from genomic DNA (input) was used as control of equal DNA loading. No Ab: HT29/MDR DNA fragments were immunoprecipitated without the anti-Nrf2 antibody and used as a negative control

between sensitive and resistant clones in vitro [7], HT29/MDR cells displayed higher migration (Additional file 12), indicating a higher aggressive phenotype. This may explain the faster growth of tumors derived from HT29/MDR cells. Oxaliplatin treatment alone reduced tumor growth and increased the percentage of apoptotic cells in the HT29-derived tumors but not in the HT29/MDR tumors, which were strongly positive for PERK and MRP1 (Fig. 6a-d).

Administration of doxycycline decreased HT29/MDR tumor growth (Fig. 6a, b), reduced the percentage of cells positive for PERK and MRP1 and increased the number of cells positive for cleaved caspase 3 (Fig. 6c, d). The antitumor effect of oxaliplatin against HT29/MDR tumors was fully restored in doxycycline-treated animals, showing a significant decrease in tumor growth, in line with that of oxaliplatin-treated HT29 tumors (Fig. 6a, b), a decrease in the expression of PERK and MRP1, an increase in intratumor apoptosis (Fig. 6c, d).

Discussion

Chemotherapeutic agents act at least in part by triggering ER stress [3, 4]. We have recently demonstrated that cells with an acquired resistance to chemotherapy are also resistant to ER stress-triggered cell death [7]. Here we demonstrated that also the inverse sequence of events occurs in cancer cells: the progressive adaptation of chemosensitive cells to ER stress inducers selects cells that are resistant to multiple chemotherapeutic drugs. The acquisition of this double-resistant phenotype, regardless of the ER stress inducer used or the tumor type, was paralleled by the up-regulation of MRP1.

The correlation between acute exposure to ER stress inducers and MRP1 is matter of debate. For instance, thapsigargin did not change MRP1 level in prostate cancer cells [24], but increased MRP1 in colon and lung cancer [25]. Acute exposure to tunicamycin alters the glycosylation of MRP1 and MRP4 and increases the resistance to oxaliplatin in ovarian cancer cells, but under these conditions MRP4 is

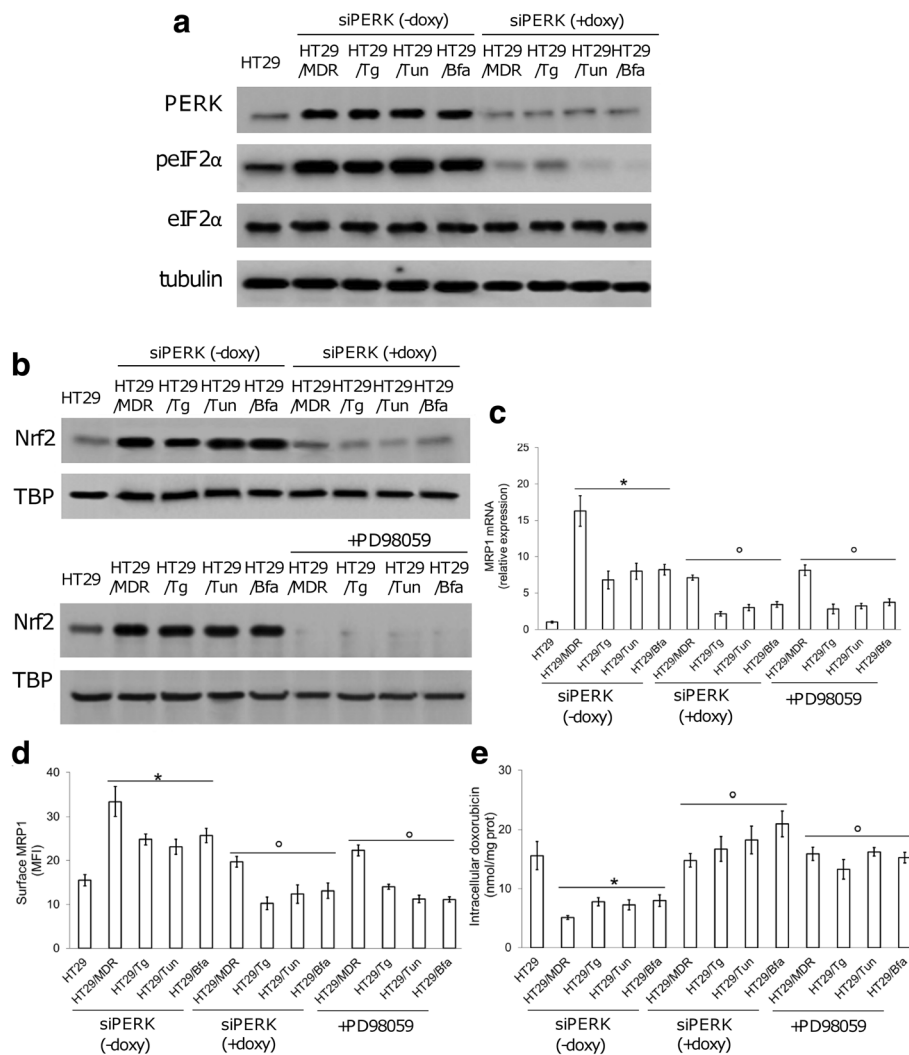


Fig. 4 Role of the PERK/Nrf2 axis in MRP1 expression and activity. Human chemoresistant colon cancer HT29/MDR cells and ER stress-resistant clones (HT29/Tg, HT29/Tun, HT29/Bfa) were stably and inducibly silenced for *PERK* (siPERK). Silencing was induced by doxycycline (doxy, 1 μ g/mL, 72 h). HT29 cells were used as control of chemosensitive/ER stress-sensitive cells. **a**. Immunoblots of protein extracts from the indicated cells stably and inducibly silenced for *PERK* (siPERK). β -tubulin was used as a loading control. The figure is representative of 3 experiments with similar results. **b**. Immunoblots of Nrf2 in nuclear extracts of cells stably and inducibly silenced for *PERK*, or treated with PD98059 (10 μ M, 72 h), which prevents Nrf2 nuclear translocation. TBP was used as a loading control. The figure is a representative of 3 experiments with similar results. **c**. Total *MRP1* mRNA in extracts of the indicated cells. Data are mean \pm SD ($n = 4$). * $p < 0.001$ for siPERK-treated cells vs. untreated HT29 cells; * $p < 0.001$ for siPERK + doxy-treated cells/PD98059-treated cells, vs. the corresponding condition in siPERK - doxy cells. **d**. Cell surface MRP1 as measured by flow cytometry. Data are mean fluorescence intensity (MFI) \pm SD. ($n = 3$). * $p < 0.002$ for siPERK(- doxy)-treated cells vs. untreated HT29 cells; * $p < 0.005$ for siPERK(+ doxy)-treated cells and PD98059-treated cells vs. the corresponding cell type in siPERK(-doxy) cells. **e**. Doxorubicin uptake in cells treated as above and measured by fluorimetry. Data are mean \pm SD ($n = 3$). * $p < 0.001$ for siPERK(- doxy)-cells vs. untreated HT29 cells; * $p < 0.001$ for siPERK(+ doxy)-treated cells and PD98059-treated cells vs. the corresponding cell type in siPERK(-doxy) cells

apparently the prominent player in chemoresistance [26]. Acute exposure to brefeldin A prevents MRP1 translocation from Golgi apparatus to plasma-membrane [27]. Our study differs from the previous ones because it was aimed at selecting clones adapted to survive in prolonged conditions of mild ER stress. This approach simulates the process that occurs in solid tumors constantly facing several conditions inducing ER stress, such as nutrient deprivation, hypoxia, radiotherapy or chemotherapy [1–4].

By comparing of the expression of UPR-related genes we noticed that PERK was the only gene significantly up-regulated in both cells selected for chemoresistance and cells selected for ER stress resistance. This analysis led us to investigate whether the activation of PERK was responsible for the resistance to either ER stress or chemotherapy.

Depending on tumor type and activation kinetics, PERK may promote cell death or survival [28, 29]. Such

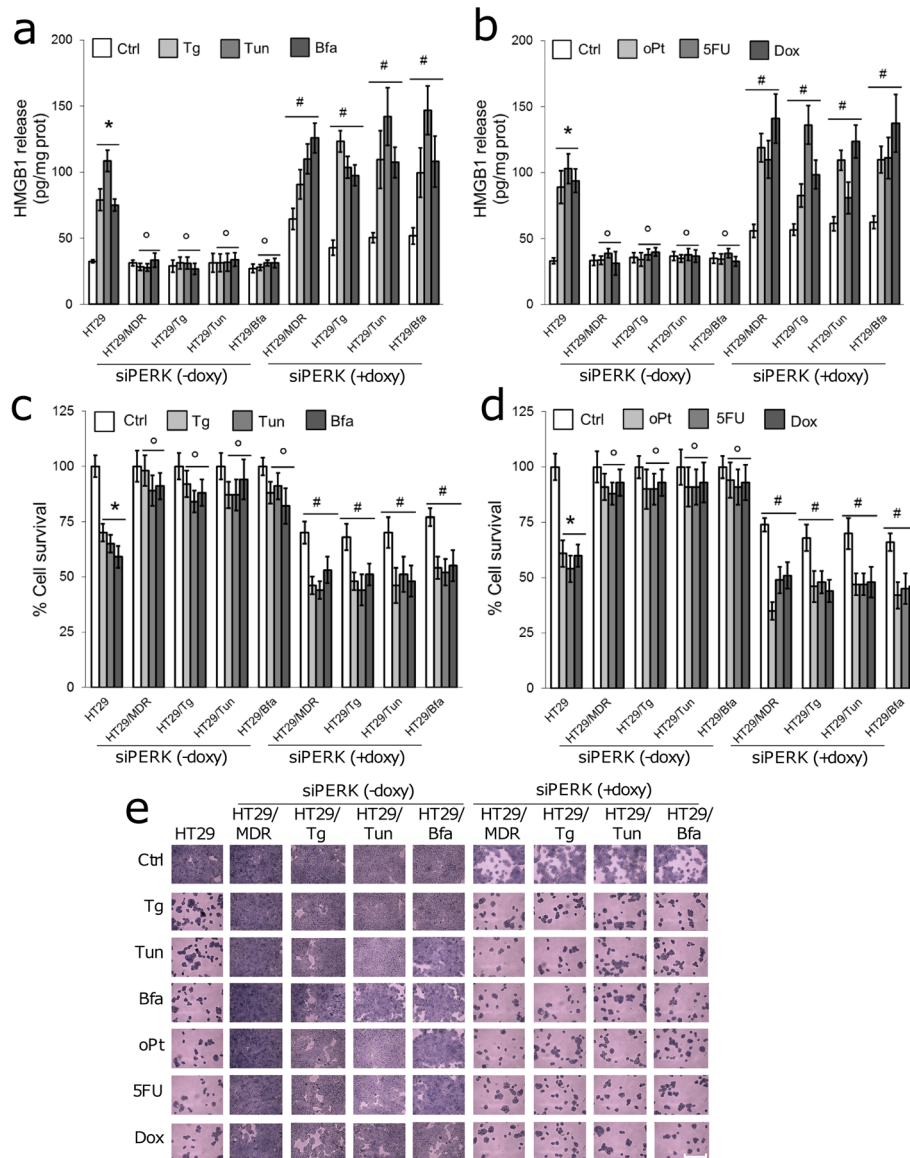


Fig. 5 Role of the PERK/Nrf2 axis in resistance to chemotherapy and to ER stress. Human chemoresistant colon cancer HT29/MDR cells and ER stress-resistant clones (HT29/Tg, HT29/Tun, HT29/Bfa) were stably and inducibly silenced for *PERK* (siPERK). Silencing was induced by doxycycline (doxy, 1 μg/mL, 72 h). HT29 cells were used as control of chemosensitive/ER stress-sensitive cells. **a, b.** Release of the necrosis marker HMGB1 to culture media of the indicated cells following incubation in fresh medium (Ctrl), or in media containing: thapsigargin (Tg), tunicamycin (Tun), brefeldin A (Bfa), oxaliplatin (oPt), 5-fluorouracil (5FU), doxorubicin (Dox), as indicated in Methods. Data are mean ± SD (n = 3). *p < 0.001 for treated cells vs. Ctrl HT29 cells; °p < 0.001 for siPERK – doxy cells vs. HT29 cells treated with the same agent; #p < 0.05 for siPERK + doxy cells vs. siPERK – doxy cells treated with the same agent. **c, d.** Viability of cells measured by Neutral red staining. Data are mean ± SD (n = 4). *p < 0.001 for treated cells vs. Ctrl HT29 cells; °p < 0.01 for siPERK – doxy cells vs. HT29 cells treated with the same agent; #p < 0.001 for siPERK + doxy cells vs. siPERK – doxy cells treated with the same agent. **e.** Crystal violet staining of cells grown in 96-well plates and treated as in **a** and **b**. The images are representatives of at least 5 microscopic fields showing similar cell density. Bar = 500 μM

pleiotropism is reflected by the highly variable and tumor-dependent prognostic role of PERK and Nrf2 in human tumors: mutations in specific oncogenes or oncosuppressor genes, factors related to the tumor micro-environment and immune-system anti-tumor activity, different treatments used in patients likely explain the great variability linking *PERK/Nrf2* expression and clinical outcome.

Contrasting findings have been reported also on the role of PERK in response to anti-cancer treatments. For instance, acute activation of PERK is required for colon cancer cell death mediated by sulindac [30], mesalamine derivatives [31] and histone deacetylase inhibitors [32], suggesting a chemosensitizing role for PERK. In contrast, the prolonged activation of PERK and consequent

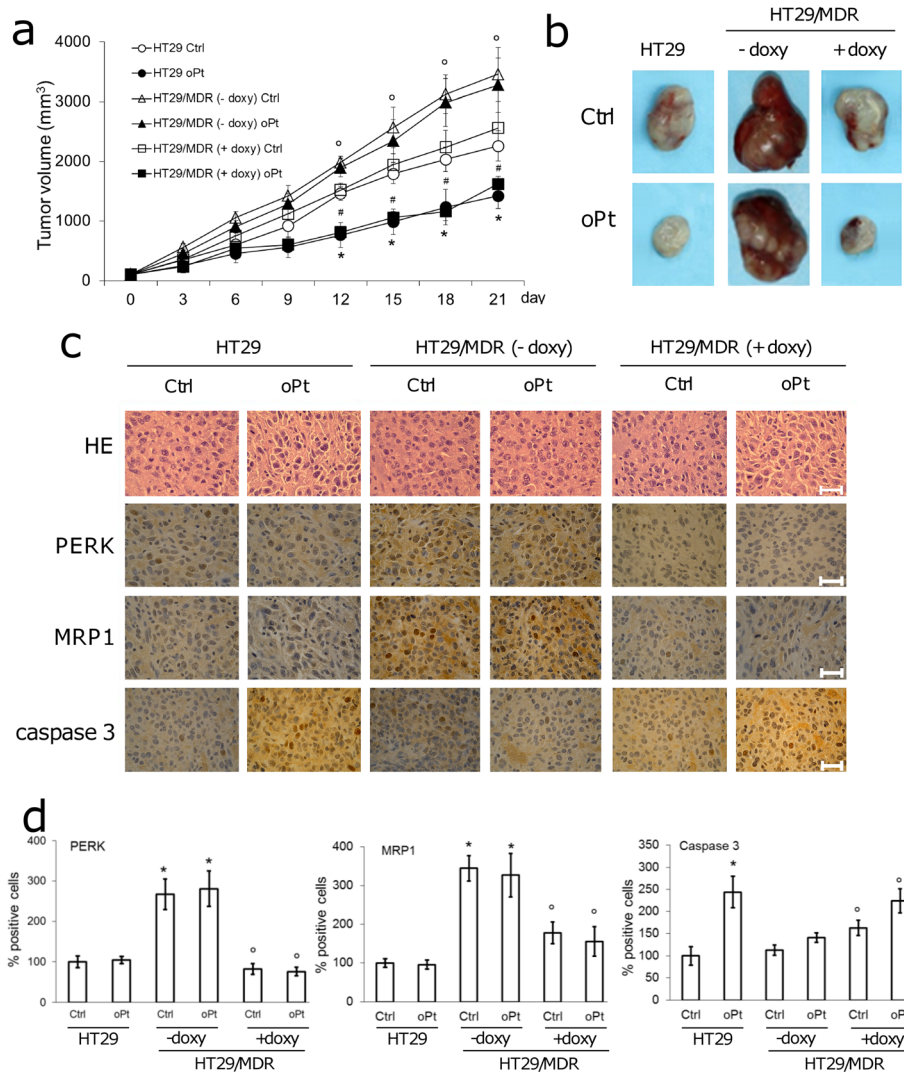


Fig. 6 The role of PERK in chemosensitivity in vivo. **a** Tumor growth of HT29 and HT29/MDR, inducibly silenced for PERK, untreated (Ctrl) or treated with oxaliplatin (oPt), as indicated in Methods. Data are mean \pm SD (15 mice/group). * $p < 0.01$ for HT29 oPt vs. HT29 Ctrl group; * $p < 0.005$ for HT29/MDR Ctrl - doxy vs. HT29 Ctrl, HT29/MDR oPt - doxy vs. HT29 oPt group; # $p < 0.005$ for HT29/MDR Ctrl + doxy vs. HT29/MDR Ctrl - doxy, HT29/MDR oPt + doxy vs. HT29/MDR oPt - doxy. **b** Photographs of representative tumors of each group. **c** Sections of tumors from each group of animals stained with hematoxylin and eosin (HE) or with the indicated antibodies. Nuclei were counter-stained with hematoxylin. Bar = 10 μ m. The photographs are representative of sections from 5 tumors. **d** Immunostaining quantification. Percentage of PERK, MRP1 and cleaved caspase 3-positive cells was determined in sections from 5 animals of each group (91–109 cells/field), using Photoshop program. * $p < 0.002$ for HT29/MDR Ctrl - doxy vs HT29 Ctrl, HT29/MDR oPt - doxy vs HT29 oPt, * $p < 0.02$ for HT29/MDR Ctrl + doxy vs HT29/MDR Ctrl - doxy, HT29/MDR oPt + doxy vs HT29/MDR oPt - doxy

phosphorylation of EIF2 α counteract the cytotoxic effects of tumor necrosis factor- α (TNF- α) and bortezomib [33], docosahexaenoic acid and TNF-related apoptosis inducing ligand [34], thereby preventing the UPR-mediated cell death. These findings are in line with our observations: indeed, clones exhibiting constitutively active PERK were more resistant to cell death triggered either by ER stress or by chemotherapy. The constant challenge with ER stress inducers selected clones with a constitutive up-regulation of PERK and MRP1. Our finding that the PERK-induced

Nrf2 activation up-regulates MRP1 expression provides the mechanism by which ER stress induces MRP1 and subsequent MRP1-dependent chemoresistance.

The correlation between Nrf2 and chemoresistance is well known, in particular in colon cancer, where Nrf2 even serves as a marker of chemoresistance [35, 36]. The resistance to platinum-derivatives in Nrf2 expressing cells is usually attributed to the simultaneous up-regulation of antioxidant enzymes, phase II metabolizing enzymes and drug efflux transporters, including MRP1

[37, 38]. Both antioxidant enzymes and MRP1 were indeed up-regulated in ER stress-resistant cancer cells, explaining the refractoriness of these clones to oxaliplatin and cisplatin. The strong up-regulation of MRP1 may explain the simultaneous resistance of ER stress-resistant clones to 5-fluorouracil and doxorubicin, two other substrates of MRP1.

Of note, we also detected a similar activation of PERK/Nrf2/MRP1 axis in the HT29/MDR clone, i.e. a clone with an acquired resistance to chemotherapy and ER stress [7]. It is known that stepwise selection with doxorubicin led to increased Nrf2 expression in ovary cancer cells [39]. It is likely that the same process occurred in HT29/MDR cells, selected with increasing concentration of doxorubicin [20]. Indeed, the analysis of upstream and downstream targets of PERK and Nrf2 in *PERK*-silenced and Nrf2-inhibited cells revealed a strong parallelism between chemoresistant and ER stress-resistant cells: in both populations PERK and its downstream targets are up-regulated, and PERK controls Nrf2 expression. The PERK/Nrf2 axis in turn finely controls the expression of specific gene sets, involved in the protection from oxidant and xenobiotic agents like chemotherapeutic drugs. We thus propose that PERK/Nrf2-controlled genes, including MRP1, may be critical for the acquisition and maintenance of the dual resistance to chemotherapy and ER stress.

Disrupting PERK/Nrf2 axis re-sensitized both ER stress-resistant clones and chemoresistant clones to ER stress-triggered and chemotherapy-triggered cell death, overcoming the double- and cross-resistant phenotype. In preclinical models of colon cancer, PERK-inhibition made ER stress-resistant/MDR tumors as responsive to oxaliplatin as ER stress-sensitive/chemosensitive tumors: this chemosensitizing effects was likely due to the decreased expression of MRP1 that restored the proapoptotic effects of oxaliplatin in resistant tumors.

Conclusions

We demonstrated for the first time that adaptation to ER stress leads to the acquisition of a MDR phenotype in different tumor types, as a consequence of the constitutive activation of PERK/Nrf2/MRP1 axis. Disrupting this axis may overcome MRP1-dependent chemoresistance, opening new perspectives for the treatment of aggressive and resistant solid tumors.

Additional files

Additional file 1: IC₅₀ (μM) of chemotherapeutic agents and ER stress inducers in HT29 and HT29/MDR cells. Data are mean ± SD (*n* = 3). **p* < 0.02 for HT29/MDR vs. HT29 cells. (XLSX 12 kb)

Additional file 2: Primers used in qRT-PCR experiments. (XLSX 12 kb)

Additional file 3: Effect of oxaliplatin in 3D-cultures of colon cancer cells. Human chemosensitive HT29 cells, chemoresistant HT29/MDR cells

and ER stress-resistant HT29/Tun cells were cultured 7 days embedded in Biomimesys™ matrix to generate 3D-systems. Medium was replaced with fresh medium (Ctrl) or with medium containing 10 μM oxaliplatin (oPt) for 48 h, then cells were analysed by contrast phase microscope. The images are representative of 3 independent experiments. Bar = 50 μM. (TIF 1680 kb)

Additional file 4: Effects of chemotherapeutic drugs in human chemosensitive breast cancer cells with acquired resistance to ER stress. **a.** Release of the necrosis marker HMGB1 to culture media of human chemosensitive breast cancer MCF7 cells and the ER stress-resistant clone MCF7/Tun, grown in fresh medium (Ctrl) or in media containing: thapsigargin (Tg), tunicamycin (Tun), brefeldin A (Bfa), doxorubicin (Dox), cisplatin (Pt), as indicated in Methods. Data are mean ± SD (*n* = 3). **p* < 0.001 vs MCF7 Ctrl cells; **p* < 0.001 for MCF7/Tun treated cells vs MCF7 treated cells. **b.** Viability of cells measured by Neutral red staining. Data are mean ± SD (*n* = 3). **p* < 0.05 vs MCF7 Ctrl cells; **p* < 0.02 for MCF7/Tun treated cells vs MCF7 treated cells. **c.** Whole cell lysates were analyzed for the expression of MRP1. β-tubulin expression was used as control of equal protein loading. The figure is representative of 3 experiments with similar results. **d.** MRP1 mRNA levels were measured by qRT-PCR. Data are mean ± SD (*n* = 3). **p* < 0.01 vs MCF7 cells. **e.** MRP1 protein on cell surface was measured by flow cytometry. *Left panel:* data are presented as mean fluorescence intensity (MFI) ± SD (*n* = 3). **p* < 0.02 vs MCF7 cells. *Right panel:* representative flow cytometry histograms. Grey peak: non immune isotypic antibody. **f.** Intracellular doxorubicin content, an index of MRP1 activity, measured by fluorimetry. Data are mean ± SD (*n* = 3). **p* < 0.005 vs MCF7 cells. (TIF 1434 kb)

Additional file 5: Effects of chemotherapeutic drugs in human chemosensitive osteosarcoma cells with acquired resistance to ER stress. **a.** Release of the necrosis marker HMGB1 to culture media of human chemosensitive osteosarcoma U-2OS cells and the ER stress-resistant clone U-2OS/Tun, grown in fresh medium (Ctrl) or in media containing: thapsigargin (Tg), tunicamycin (Tun), brefeldin A (Bfa), doxorubicin (Dox), cisplatin (Pt), as indicated in Methods. Data are mean ± SD (*n* = 3). **p* < 0.005 vs U-2OS Ctrl cells; **p* < 0.005 for U-2OS/Tun treated cells vs U-2OS treated cells. **b.** Viability of cells measured by Neutral red staining. Data are mean ± SD (*n* = 3). **p* < 0.02 vs U-2OS Ctrl cells; **p* < 0.05 for U-2OS/Tun treated cells vs U-2OS treated cells. **c.** Whole cell lysates were analyzed for the expression of MRP1. β-tubulin expression was used as control of equal protein loading. The figure is representative of 3 experiments with similar results. **d.** MRP1 mRNA levels were measured by qRT-PCR. Data are mean ± SD (*n* = 3). **p* < 0.005 vs U-2OS cells. **e.** MRP1 protein on cell surface was measured by flow cytometry. *Left panel:* data are presented as mean fluorescence intensity (MFI) ± SD (*n* = 3). **p* < 0.02 vs U-2OS cells. *Right panel:* representative flow cytometry histograms. Grey peak: non immune isotypic antibody. **f.** Intracellular doxorubicin content, an index of MRP1 activity, measured by fluorimetry. Data are mean ± SD (*n* = 3). **p* < 0.05 vs U-2OS cells. (TIF 1533 kb)

Additional file 6: Expression of genes involved in the UPR in HT29, HT29/Tun and HT29/MDR cells. ERAD: ER-associated degradation; UPR: unfolded protein response; ERQC: ER-quality control. Fold-Change ($2^{\Delta(-\Delta Ct)}$) is the normalized gene expression ($2^{\Delta(-\Delta Ct)}$) in HT29/Tun or HT29/MDR cells, divided the normalized gene expression ($2^{\Delta(-\Delta Ct)}$) in HT29 cells (*n* = 4), where Ct is the threshold cycle in qRT-PCR. Fold-change values greater than 1 indicate up-regulation, fold-change values less than 1 indicate down-regulation. The *p* values are calculated based on a Student's *t*-test of the replicate $2^{\Delta(-\Delta Ct)}$ values for each gene. *p* < 0.05 was considered significant. Genes significantly up- or down-regulated more than 2-fold either in HT29/Tun or HT29/MDR cells are in bold characters. (XLSX 16 kb)

Additional file 7: MRP1 expression on cell surface of sensitive and resistant colon cancer cells upon PERK/Nrf2 inhibition. **a, b.** Representative flow cytometry histograms of MRP1 protein in human chemoresistant colon cancer HT29/MDR cells and ER stress-resistant clones (HT29/Tg, HT29/Tun, HT29/Bfa), stably and inducibly transduced with a silencing vector for *PERK*, or treated with PD98059 (10 μM, 72 h), which blocks Nrf2 nuclear translocation. HT29 were included as control of chemosensitive/ER stress-sensitive cells. Grey peaks: non immune isotypic antibody. (TIF 1205 kb)

Additional file 8: Expression of PERK- and Nrf2-upstream and downstream genes in chemoresistant and ER stress-resistant cells. **a.** Schematic representation of upstream and downstream targets of PERK

and Nrf2. Blue box: genes upstream PERK; red boxes: genes downstream PERK; orange boxes: genes upstream Nrf2; green boxes: genes downstream Nrf2. **b.** Relative expression, indicated in a colorimetric scale, of the indicated PERK- and Nrf2-upstream and downstream genes, in HT29/MDR and HT29/Tun cells, grown in fresh medium (Ctrl), transduced with a silencing vector for PERK, or treated with PD98059 (PD; 10 μ M, 72 h), measured by RT-PCR. The expression of each gene in HT29 cells, used as internal control, was considered equal to 1. Data are mean \pm SD ($n = 4$). * $p < 0.05$ for untreated (Ctrl) HT29/MDR or HT29/Tun cells vs. HT29 cells; $^{\circ}p < 0.05$ for significantly reduced genes in siPERK- and PD-treated cells vs. respective untreated (Ctrl) HT29/MDR or HT29/Tun cells. *GRP78*: glucose-regulated protein 78; *EIF2S1*: eukaryotic translation initiation factor 2 subunit 1; *ATF4*: activating transcription factor 4; *GSK3 β* : glycogen synthase kinase 3 β ; *JNK1*: c-Jun N-terminal kinase 1; *MAPK1*: mitogen activated kinase 1; *PI3KCD*: phosphatidylinositol-4,5-bisphosphate 3-kinase catalytic subunit δ ; *PRKCA*: protein kinase Ca; *NFKB*: nuclear factor-kB; *GSR*: glutathione-disulfide reductase; *G6PD*: glucose-6-phosphate dehydrogenase; *TXNRD1*: thioredoxin reductase 1; *SOD1*: superoxide dismutase 1; *HMOX1*: heme oxygenase 1; *NQO1*: NAD(P)H quinone dehydrogenase 1; *STIP1*: stress induced phosphoprotein 1. (TIF 836 kb)

Additional file 9: Nrf2 inhibition reverses the resistance to chemotherapy and ER stress. Human chemoresistant colon cancer HT29/MDR cells and ER stress-resistant clones (HT29/Tg, HT29/Tun, HT29/Bfa) were grown in the absence or in the presence of PD98059 (10 μ M, 72 h), which blocks Nrf2 nuclear translocation. **a, b.** Release of the necrosis marker HMGB1 to culture media of the indicated cells following incubation in fresh medium (Ctrl), or in media containing: thapsigargin (Tg), tunicamycin (Tun), brefeldin A (Bfa), oxaliplatin (oPt), 5-fluorouracil (5FU), doxorubicin (Dox), as indicated in Methods. Data are mean \pm SD ($n = 3$). * $p < 0.001$ vs HT29 Ctrl cells; $^{\circ}p < 0.001$ for HT29/MDR, HT29/Tg, HT29/Tun, HT29/Bfa vs HT29 cells; $^{\#}p < 0.001$ for PD98059-treated cells vs PD98059-untreated cells. **c, d.** Viability of cells measured by Neutral red staining. * $p < 0.005$ vs HT29 Ctrl cells; $^{\circ}p < 0.01$ for HT29/MDR, HT29/Tg, HT29/Tun, HT29/Bfa vs HT29 cells; $^{\#}p < 0.02$ for PD98059-treated cells vs PD98059-untreated cells. (TIF 3494 kb)

Additional file 10: Correlation between PERK or NRF2 expression and patient clinical outcome in different tumors. Patient overall survival was calculated by Cox's proportional hazard model and Kaplan-Meier method using the GSEA software. Z score: correlation score between gene expression and survival. FDR: false discovery rate. ACC: adrenocortical carcinoma; BRCA: breast invasive carcinoma; BLCA: bladder urothelial carcinoma; CESC: cervical squamous cell carcinoma and endocervical adenocarcinoma; CHOL: cholangiocarcinoma; COAD: colon adenocarcinoma; COADREAD: colorectal adenocarcinoma; DLBC: diffuse large B-cell lymphoma; GBM: glioblastoma multiforme; HNSC: head and neck squamous cell carcinoma; KICH: chromophobe renal cell carcinoma; KIRC: kidney renal clear cell carcinoma; KIRP: kidney renal papillary cell carcinoma; LGG: lower grade glioma; LIHC: liver hepatocellular carcinoma; LUAD: lung adenocarcinoma; LUSC: lung squamous cell carcinoma; MESO: mesothelioma; OV: ovarian serous cystadenocarcinoma; PAAD: pancreatic adenocarcinoma; PCPG: pheochromocytoma and paraganglioma; PRAD: prostate adenocarcinoma; READ: rectum adenocarcinoma; SARC: sarcoma; SKCM: skin cutaneous melanoma; TGCT: testicular germ cell tumor; THCA: thyroid carcinoma; THYM: thymoma; UCEC: uterine corpus endometrial carcinoma; UCS: uterine carcinosarcoma; UVM: uveal melanoma. Significant p values are in bold characters. (XLSX 17 kb)

Additional file 11: Tumor growth in mice bearing HT29 and HT29/MDR tumors. Tumor volume (reported in mm³) of HT29 and HT29/MDR, inducibly silenced for PERK, untreated (Ctrl) or treated with oxaliplatin (oPt), as indicated in Methods and in the main Figure 6, at different time points for each animal. (XLSX 24 kb)

Additional file 12: Migration of sensitive and resistant colon cancer cells. Migration ability of HT29, HT29/MDR and HT29/Tun cells was evaluated as capacity to close the wound over a period of 24 h. **a.** Representative images of 1 out of 3 experiments. Bar: 200 μ m. **b.** Quantification of migration rate. Data are mean \pm SD ($n = 3$). * $p < 0.002$ vs HT29 cells; $^{\circ}p < 0.001$ vs HT29/MDR cells. (TIF 2275 kb)

Abbreviations

ANOVA: Analysis of variance; ATF4: Activating transcription factor 4; ATF6: activating transcription factor 6; C/EBP- β LIP: CAAT/enhancer- β liver-enriched inhibitory protein; CHIP: Chromatin immunoprecipitation; CHOP: C/EBP homologous protein; EIF2AK3: Eukaryotic translation initiation factor-2 α kinase 3; EIF2S1: Eukaryotic translation initiation factor 2 subunit 1; ER: Endoplasmic reticulum; ERAD: ER-associated degradation; FBS: Foetal bovine serum; G6PD: Glucose-6-phosphate dehydrogenase; GRP78: Glucose-regulated protein 78; GSK3 β : Glycogen synthase kinase 3 β ; GSR: Glutathione-disulfide reductase; HMGB1: High Mobility Group Protein 1; HMOX1: Heme oxygenase 1; IRE1: Inositol-requiring enzyme 1; JNK1: c-Jun N-terminal kinase 1; MAPK1: Mitogen activated kinase 1; MDR: Multidrug resistance; MRP1, 2, 3, 4: MDR related protein 1, 2, 3, 4; NQO1: NAD(P)H quinone dehydrogenase 1; Nrf2: Erythroid-derived 2-like 2; PERK: Protein kinase RNA-like endoplasmic reticulum kinase; Pgp: P-glycoprotein; PI3KCD: Phosphatidylinositol-4,5-bisphosphate 3-kinase catalytic subunit δ ; PRKCA: Protein kinase Ca; qRT-PCR: Quantitative real-time polymerase chain reaction; RIPA: Radioimmunoprecipitation assay; shRNA: Short hairpin RNA; SOD1: Superoxide dismutase 1; STIP1: Stress induced phosphoprotein 1; TNF- α : Tumor necrosis factor- α ; TRB3: Tribbles-related protein 3; TXNRD1: Thioredoxin reductase 1; UPR: Unfolded protein response

Acknowledgements

We are grateful to Prof. Amalia Bosia, Department of Oncology, University of Torino, for the fruitful discussion, and to Mr. Costanzo Costamagna, Department of Oncology, University of Torino, for technical assistance.

Funding

This work was supported with funds from Italian Association for Cancer Research (IG15232 to CR) and Italian Ministry of University and Research (FIRB 2012, grant RBF12SQO1; EX60% Funding 2015 to CR); De Benedetti-Cherasco Foundation (Torino-Weizmann Collaborative Program: Scientific Cooperation and Exchange to MR and CR). JK is a fellow of "Fondazione Umberto Veronesi". ICS and IB are recipients of PhD scholarships from the Italian Institute for Social Security (INPS). The funding institutions had no role in the study design, in the data collection and analysis, or in writing the manuscript.

Availability of data and materials

All datasets on which the conclusions of the manuscript rely are presented in the paper.

Authors' contributions

CR, JK and MR developed the original hypothesis and supervised the experimental design. ICS, EP, IB performed in vitro and in vivo experiments. EM, PP analyzed data and performed statistical analysis. MR, CR and JK wrote and revise the manuscript. All authors read and approved the final manuscript.

Competing interests

The authors declare that they have no competing interests.

Consent for publication

Not applicable.

Ethics approval

Animal care and experimental procedures were approved by the Bio-Ethical Committee of the Italian Ministry of Health (#122/2015-PR).

Publisher's Note

Springer Nature remains neutral with regard to jurisdictional claims in published maps and institutional affiliations.

Author details

¹Department of Oncology, University of Torino, via Santena 5/bis, 10126 Torino, Italy. ²System Biology Ireland, University College Dublin, Dublin 4, Ireland. ³Department of Molecular Biotechnology and Health Sciences, University of Torino, via Nizza 52, 10126 Torino, Italy. ⁴Department of Molecular Genetics, The Weizmann Institute of Science, 234 Herzl Street, 7610001 Rehovot, Israel.

Received: 12 December 2016 Accepted: 3 May 2017

Published online: 12 May 2017

References

- Koppenol WH, Bounds PL, Dang CV. Otto Warburg's contributions to current concepts of cancer metabolism. *Nat Rev Cancer*. 2011;11:325–37.
- Cairns RA, Harris IS, Mak TW. Regulation of cancer cell metabolism. *Nat Rev Cancer*. 2011;11:85–95.
- Kim I, Xu W, Reed JC. Cell death and endoplasmic reticulum stress: disease relevance and therapeutic opportunities. *Nat Rev Drug Discov*. 2008;7:1013–30.
- Schwarz DS, Blower MD. The endoplasmic reticulum: structure, function and response to cellular signaling. *Cell Mol Life Sci*. 2016;73:79–94.
- Ohoka N, Yoshii S, Hattori T, Onozaki K, Hayashi H. TRB3, a novel ER stress-inducible gene, is induced via ATF4-CHOP pathway and is involved in cell death. *EMBO J*. 2005;24:1243–55.
- Hetz C. The unfolded protein response: controlling cell fate decisions under ER stress and beyond. *Nat Rev Mol Cell Biol*. 2012;13:89–102.
- Riganti C, Kopecka J, Panada E, Barak S, Rubinstein M. The role of C/EBP- β LIP in multidrug resistance. *J Natl Cancer Inst*. 2015;107(5). doi:10.1093/jnci/djv046.
- Gottesman MM, Fojo T, Bates SE. Multidrug resistance in cancer: role of ATP-dependent transporters. *Nat Rev Cancer*. 2002;2:48–58.
- Panaretakis T, Kepp O, Brockmeier U, Tesniere A, Bjorklund AC, Chapman DC, et al. Mechanisms of pre-apoptotic calreticulin exposure in immunogenic cell death. *EMBO J*. 2009;28:578–90.
- Mandic A, Hansson J, Linder S, Shoshan MC. Cisplatin induces endoplasmic reticulum stress and nucleus-independent apoptotic signaling. *J Biol Chem*. 2003;278:9100–06.
- Yadunandam AK, Yoon JS, Seong YA, Oh CW, Kim GD. Prospective impact of 5-FU in the induction of endoplasmic reticulum stress, modulation of GRP78 expression and autophagy in Sk-Hep1 cells. *Int J Oncol*. 2012;41:1036–42.
- Mhaidat NM, Alali FQ, Matalqah SM, Matalka II, Jaradat SA, Al-Sawalha NA, et al. Inhibition of MEK sensitizes paclitaxel-induced apoptosis of human colorectal cancer cells by downregulation of GRP78. *Anticancer Drugs*. 2009;20:601–06.
- Chevet E, Hetz C, Samali A. Endoplasmic reticulum stress-activated cell reprogramming in oncogenesis. *Cancer Discov*. 2015;5:586–97.
- Cullinan SB, Zhang D, Hannink M, Arvais E, Kaufman RJ, Diehl JA. Nrf2 is a direct PERK substrate and effector of PERK-dependent cell survival. *Mol Cell Biol*. 2003;23:7198–209.
- Tao S, Wang S, Moghaddam SJ, Ooi A, Chapman E, Wong PK, et al. Oncogenic KRAS confers chemoresistance by upregulating NRF2. *Cancer Res*. 2014;74:7430–41.
- Xu X, Zhang Y, Li W, Miao H, Zhang H, Zhou Y, et al. Wogonin reverses multi-drug resistance of human myelogenous leukemia K562/A02 cells via downregulation of MRP1 expression by inhibiting Nrf2/ARE signaling pathway. *Biochem Pharmacol*. 2014;92:220–34.
- Sukumari-Ramesh S, Prasad N, Alleyne CH, Vender JR, Dhandapani KM. Overexpression of Nrf2 attenuates Carmustine-induced cytotoxicity in U87MG human glioma cells. *BMC Cancer*. 2015;15:e118.
- Palam LR, Gore J, Craven KE, Wilson JL, Korc M. Integrated stress response is critical for gemcitabine resistance in pancreatic ductal adenocarcinoma. *Cell Death Dis*. 2015;6:e1913.
- Ji L, Li H, Gao P, Shang G, Zhang DD, Zhang N, et al. Nrf2 pathway regulates multidrug-resistance-associated protein 1 in small cell lung cancer. *PLoS One*. 2013;8:e63404.
- Riganti C, Miraglia E, Viarisio D, Costamagna C, Pescarmona G, Ghigo D, et al. Nitric oxide reverts the resistance to doxorubicin in human colon cancer cells by inhibiting the drug efflux. *Cancer Res*. 2005;65:516–25.
- Doublier S, Belisario DC, Polimeni M, Annaratone L, Riganti C, Allia E, et al. HIF-1 activation induces doxorubicin resistance in MCF7 3-D spheroids via P-glycoprotein expression: a potential model of the chemo-resistance of invasive micropapillary carcinoma of the breast. *BMC Cancer*. 2012;4:12–4.
- Principe M, Borgoni S, Cascione M, Chattaragada MS, Ferri-Borgogno S, Capello M, et al. Alpha-enolase (ENO1) controls alpha v/beta 3 integrin expression and regulates pancreatic cancer adhesion, invasion, and metastasis. *J Hematol Oncol*. 2017;10:e16.
- Ebert B, Kisiela M, Malátková P, El-Hawari Y, Maser E. Regulation of human carbonyl reductase 3 (CBR3; SDR21C2) expression by Nrf2 in cultured cancer cells. *Biochemistry*. 2010;49:8499–511.
- Lee DJ, Sumbilla C, Lee M, Natesavelalar C, Klein MG, Ross DD, et al. Mechanisms of resistance and adaptation to thapsigargin in androgen-independent prostate cancer PC3 and DU145 cells. *Arch Biochem Biophys*. 2007;464:19–27.
- Filipeanu CM, Nelemans A, Veldman RJ, de Zeeuw D, Kok JW. Regulation of [Ca²⁺]_i homeostasis in MRP1 overexpressing cells. *FEBS Lett*. 2000;474:107–10.
- Beretta GL, Benedetti V, Cossa G, Assaraf YG, Bram E, Gatti L, et al. Increased levels and defective glycosylation of MRPs in ovarian carcinoma cells resistant to oxaliplatin. *Biochem Pharmacol*. 2010;79:1108–17.
- Van Luyn MJ, Müller M, Renes J, Meijer C, Scheper RJ, Nienhuis EF, et al. Transport of glutathione conjugates into secretory vesicles is mediated by the multidrug-resistance protein 1. *Int J Cancer*. 1998;76:55–62.
- Ranganathan AC, Ojha S, Kourtidis A, Conklin DS, Aguirre-Ghiso JA. Dual function of pancreatic endoplasmic reticulum kinase in tumor cell growth arrest and survival. *Cancer Res*. 2008;68:3260–68.
- Hamanaka RB, Bobrovnikova-Marjon E, Ji X, Lieberhaber SA, Diehl JA. PERK-dependent regulation of IAP translation during ER stress. *Oncogene*. 2009;28:910–20.
- Yang H, Park SH, Choi HJ, Moon Y. The integrated stress response-associated signals modulates intestinal tumor cell growth by NSAID-activated gene 1 (NAG-1/MIC-1/PTGF-beta). *Carcinogenesis*. 2010;31:703–11.
- Stolfi C, Sarra M, Caruso R, Fantini MC, Fina D, Pellegrini R, et al. Inhibition of colon carcinogenesis by 2-methoxy-5-amino-N-hydroxybenzamide, a novel derivative of mesalamine. *Gastroenterology*. 2010;138:221–30.
- Liu J, Edagawa M, Goshima H, Inoue M, Yagita H, Liu Z, et al. Role of ATF3 in synergistic cancer cell killing by a combination of HDAC inhibitors and agonistic anti-DR5 antibody through ER stress in human colon cancer cells. *Biochem Biophys Res Commun*. 2014;445:320–26.
- Nowis D, McConnell EJ, Dierlam L, Palamarchuk A, Lass A, Wójcik C. TNF potentiates anticancer activity of bortezomib (Velcade) through reduced expression of proteasome subunits and dysregulation of unfolded protein response. *Int J Cancer*. 2007;121:431–41.
- Skender B, Hofmanová J, Slavik J, Jelinková I, Machala M, Moyer MP, et al. DHA-mediated enhancement of TRAIL-induced apoptosis in colon cancer cells is associated with engagement of mitochondria and specific alterations in sphingolipid metabolism. *Biochim Biophys Acta*. 1841;2014:1308–17.
- Zhao XQ, Zhang YF, Xia YF, Zhou ZM, Cao YQ. Promoter demethylation of nuclear factor-erythroid 2-related factor 2 gene in drug-resistant colon cancer cells. *Oncol Lett*. 2015;10:1287–92.
- Wang XJ, Li Y, Luo L, Wang H, Chi Z, Xin A, et al. Oxaliplatin activates the Keap1/Nrf2 antioxidant system conferring protection against the cytotoxicity of anticancer drugs. *Free Radic Biol Med*. 2014;70:68–77.
- Homma S, Ishii Y, Morishima Y, Yamadori T, Matsuno Y, Haraguchi N, et al. Nrf2 enhances cell proliferation and resistance to anticancer drugs in human lung cancer. *Clin Cancer Res*. 2009;15:3423–32.
- Hayes JD, McMahon M. NRF2 and KEAP1 mutations: permanent activation of an adaptive response in cancer. *Trends Biochem Sci*. 2009;34:176–88.
- Shim GS, Manandhar S, Shin DH, Kim TH, Kwak MK. Acquisition of doxorubicin resistance in ovarian carcinoma cells accompanies activation of the NRF2 pathway. *Free Radic Biol Med*. 2009;47:1619–31.

Submit your next manuscript to BioMed Central and we will help you at every step:

- We accept pre-submission inquiries
- Our selector tool helps you to find the most relevant journal
- We provide round the clock customer support
- Convenient online submission
- Thorough peer review
- Inclusion in PubMed and all major indexing services
- Maximum visibility for your research

Submit your manuscript at
www.biomedcentral.com/submit



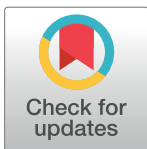
RESEARCH ARTICLE

Vitamin D and immunomodulation in early rheumatoid arthritis: A randomized double-blind placebo-controlled study

Ilaria Buondonno¹, Guido Rovera², Francesca Sassi¹, Micol Maria Rigoni¹, Claudia Lomater², Simone Parisi³, Raffaele Pellerito², Giovanni Carlo Isaia¹, Patrizia D'Amelio^{1*}

1 Department of Medical Science, Gerontology and Bone Metabolic Disease Section, University of Torino, Torino, Italy, **2** Rheumatology Unit, Ospedale Mauriziano, Torino, Italy, **3** Rheumatology Department, AOU Città della Salute e della Scienza di Torino, Torino, Italy

* patrizia.damelio@unito.it



OPEN ACCESS

Citation: Buondonno I, Rovera G, Sassi F, Rigoni MM, Lomater C, Parisi S, et al. (2017) Vitamin D and immunomodulation in early rheumatoid arthritis: A randomized double-blind placebo-controlled study. *PLoS ONE* 12(6): e0178463. <https://doi.org/10.1371/journal.pone.0178463>

Editor: Michael Nurmohamed, VU University Medical Center, NETHERLANDS

Received: December 10, 2016

Accepted: May 12, 2017

Published: June 5, 2017

Copyright: © 2017 Buondonno et al. This is an open access article distributed under the terms of the [Creative Commons Attribution License](https://creativecommons.org/licenses/by/4.0/), which permits unrestricted use, distribution, and reproduction in any medium, provided the original author and source are credited.

Data Availability Statement: All relevant data are within the paper and its Supporting Information files.

Funding: Unconditional grant was provided by the Fondazione San Paolo (Torino), grant number pratica 2009.1337 (<http://www.compagniadisanpaolo.it/>).

Competing interests: The authors have declared that no competing interests exist.

Abstract

The aim of this study was to evaluate differences in T helper cell sub-types and osteoclast (OCs) precursors in peripheral blood between patients affected by early rheumatoid arthritis (eRA) and healthy controls. The effect of administration of cholecalciferol on clinical and laboratory parameters was subsequently evaluated, by a parallel, randomized double blind, placebo controlled trial. Thirty nine eRA patients and 31 age-matched controls were enrolled and compared for levels of 25OH vitamin D, T helper cell sub-types, OCs precursors including both classical and non-classical and pro-inflammatory cytokines at baseline. Eligible patients were female ≥ 18 years of age with a diagnosis of RA, as defined by the American College of Rheumatology 2010 criteria for <6 months prior to inclusion in the study. Patients with auto-immune or inflammatory diseases other than RA were excluded. Patients treated with glucocorticoids (GCs), disease modifying activity drugs and biologic agents within the past 6 months were also excluded. In the second phase of the study, eRA patients were randomly assigned to standard treatment with methotrexate (MTX) and GCs with (21) or without (18) cholecalciferol (300,000 IU) and followed for 3 months; the randomization was done by computer generated tables to allocate treatments. Three patients didn't come back to the follow up visit for personal reasons. None of the patients experienced adverse events. The main outcome measures were T cells phenotypes, OCs precursors and inflammatory cytokines. Secondary outcome measure were clinical parameters. In eRA, 25OH vitamin D levels were significantly lower. CD4+/IFN γ +, CD4+/IL4+, CD4+/IL17A+ and CD4+IL17A+IFN γ +, cells were increased in eRA as well as non-classical OCs precursors, whereas T regulatory cells were not altered. TNF α , TGF β 1, RANKL, IL-23 and IL-6 were increased in eRA. Non-classical OCs, IL-23 and IL-6 correlated with disease severity and activity. Standard treatment with MTX and GC ameliorated clinical symptoms and reduced IL-23, whereas it did not affect CD4+ cells sub-sets nor OCs precursors. After 3 months, the combined use of cholecalciferol significantly ameliorated the effect of treatment on global health. In eRA, a significant imbalance in T CD4+ sub-types accompanied by increased levels of non-classical OCs precursors and pro-inflammatory cytokines was observed. A single

dose of cholecalciferol (300,000 IU) combined with standard treatment significantly ameliorates patients general health.

Introduction

Recent studies have focused on the role of hypovitaminosis D in the pathogenesis of rheumatoid arthritis (RA) [1] and an inverse relationship between serum levels of 25-hydroxyvitamin D and disease activity or functional impairment has been observed [2,3].

Recently, a pilot exploratory study demonstrated that supplementation of vitamin D is effective in ameliorating clinical outcomes in RA patients affected by hypovitaminosis D [4].

Despite these recent efforts, there are no intervention studies that have specifically evaluated the effect of vitamin D treatment on T helper (CD4+, Th) cell phenotypes, cytokine production and osteoclast (OCs) precursor cells in RA patients.

It is well known that RA is an immune-mediated disease characterized by T cell activation and bone erosions with articular inflammation and progressive joint destruction that severely reduces patients quality of life; nevertheless a clear role for different Th cells has not yet been established [5].

An imbalance in Th cell activation has been suggested as the main pathogenic features of RA, nevertheless, studies on the role for different Th phenotypes such as T regulatory cells (Tregs), Th1, Th2 and Th17, have obtained contradictory results [5].

Different studies on Treg phenotype and function in RA patients have obtained conflicting results [6–11], these cells may have a role in the control of bone erosions in RA as, in experimental models, are able to inhibit OCs formation and activity [12–13].

Some recent studies also suggest a role for increased Th1 cells in the pathogenesis of RA, in particular these cells being frequently observed in the synovial fluid of RA patients [14].

Th1 produces IFN γ that have controversial effects on OCs formation and activity [15–16], and TNF α that induces OCs formation in the presence of adequate levels of RANKL [17], RANKL being the cytokine mainly responsible for OCs formation and activity.

Th17 have also been investigated in RA and these cells have been shown to play an important role in experimental models of arthritis [5,18,19].

In RA patients, Th17 are recruited within the synovium where they exert pro-inflammatory and pro-osteoclastogenic effects [20,21].

Another Th subtype has been described in RA patients; this is a transitional cell that expresses both IFN γ and IL-17, and correlates with disease activity [22].

Taken together, these data suggest that both an increase in levels of Th1 and Th17 cells may be responsible for increased OCs formation and bone erosions in RA, whereas a role for reduced Tregs still remains controversial.

OCs have a critical role in RA and are required for bone erosions to occur [23].

OCs precursors circulate in the peripheral blood and express the following cell surface antigenic markers: CD14+/CD11b+ and CD51/61+ (classical OCs precursors) and CD14 and high levels of CD16 (CD14+/CD16^{bright}, non-classical OCs precursors). Classical OCs precursors have been found to be increased in conditions characterized by increased bone resorption such as post-menopausal osteoporosis, bone metastases and other conditions; whereas non-classical OCs precursors has been observed during inflammatory diseases characterized by increased bone resorption [24–26].

How chronic inflammation affects bone resorption and different OCs precursors in RA is still largely unclear.

Despite the fact that studies have shown an immunomodulatory effect of vitamin D in animal models of RA [27], this is the first double-blind placebo-controlled pilot study that specifically examines the effect of vitamin D administration on Th phenotype, and OCs precursor cells in patients affected by early RA (eRA), moreover we evaluated the effect of cholecalciferol on clinical signs and symptoms of eRA.

Materials and methods

Trial design

This is a parallel, randomized, placebo-controlled, double blind, trial (registered on 2010-03-29 in the European Clinical Trials Database (EudraCT) as OM-2009-01 EudraCT 2009-015835-34, available at <https://www.clinicaltrialsregister.eu/ctr-search/trial/2009-015835-34/IT>). The authors confirm that all ongoing and related trials for this drug/intervention are registered.

The randomization was done by computer generated tables to allocate treatments. The study was approved by the Ethical Committee of the A.O.U. Città della Salute e della Scienza—A.O. Ordine Mauriziano—A.S.L. TO1, Turin Italy (protocol number: OM-2009-001, on 2010-01-12) and informed consent was obtained from all participants.

Patients and controls were enrolled in the Rheumatology Unit, Ospedale Mauriziano, and in the Rheumatology Department, AOU Città della Salute e della Scienza di Torino, Torino, Italy. Lab experiments were performed in the bone biology lab of the Department of Medical Science, Gerontology and Bone Metabolic Disease Section, University of Torino, Torino, Italy, researcher were in blind as respect to diagnosis (healthy control or eRA) and to treatment allocation.

The study was divided into two phases: in the first phase, we compared T CD4+ phenotypes, OCs precursor cells and cytokines in the peripheral blood of women affected by eRA compared to healthy age-matched women.

The second phase of the study was a parallel, double-blind placebo-controlled randomized trial on the effect of 300,000 IU of cholecalciferol on clinical features and experimental parameters of eRA patients.

First phase: Baseline evaluation of patients and control subjects

Thirty nine women affected by eRA not previously treated with glucocorticoid (GC) or disease modifying activity drugs (DMARDs) and 31 healthy age-matched women were enrolled in the present study between 2010-07-05 and 2014-25-11.

Eligible patients were female ≥ 18 years of age with a diagnosis of RA, as defined by the American College of Rheumatology (ACR; formerly, the American Rheumatism Association) 2010 [28] criteria for < 6 months prior to inclusion in the study.

Patients with a history of auto-immune or inflammatory diseases other than RA, tuberculosis, malignancy, renal, hepatic, hematologic, gastrointestinal, endocrine, pulmonary, cardiac, neurologic, or cerebral disease were excluded. Patients treated with GCs, DMARDs, biologic agents within the past 6 months were also excluded. Renal insufficiency was ruled out on the basis of clinical history and previous creatinine measure.

Clinical evaluation of eRA

Disease activity and progression was evaluated using the Disease Activity Score 28 (DAS 28) [17]. This score assesses the number of swollen and tender joints and includes measurement of erythrocyte sedimentation rate (ESR).

Joint pain was evaluated by the Visual Analog Scale for Pain (VAS Pain) and the Health Assessment Questionnaire (HAQ) was used to evaluate the functional status (disability) [29]. Global Health (GH) was evaluated on a numeric scale (0–100, 0 worst, 100 best status). Basal levels of 25-OH vitamin D, ESR and C reactive protein (CRP) were measured in all subjects. ESR and CRP were not measured in healthy controls as their increase is not sensitive nor specific in healthy subject.

Enumeration of T helper and osteoclast precursor cells by flow cytometry

Peripheral blood mononuclear cells (PBMCs) were obtained from all the surveyed groups with the Ficoll-Paque method from 40 ml peripheral blood in lithium heparin as previously described [17].

Flow cytometry was used to quantify osteoclast precursors and Th cell subsets in peripheral blood. We measured classical OC precursors identified by staining PBMCs (1×10^6) with fluorescein isothiocyanate-conjugated (FITC)-conjugated anti-VNR, phycoerythrin-conjugated (PE)-conjugated anti-CD14 and allophycocyanin-conjugated (APC)-conjugated anti-CD11b mAb, or with the corresponding isotype control followed by incubation at 4°C for 30 min. Triple-positive (CD14+/CD11b+/VNR+) cells were considered as osteoclast precursors according to previous literature [17].

We also measured non-classical OC precursors stained with anti-CD14 (PE) and CD16 peridinin-chlorophyll protein-conjugated (PerCP) antibodies or with the corresponding isotype control followed by incubation at 4°C for 30 min. Cells positive for CD14 and expressing high levels of CD16 (CD16^{bright}) were considered non-classical osteoclast precursors according to previous literature [25].

T helper cells were identified by T helper 1/2/17 phenotyping kit (BD Biosciences, Franklin Lakes, NJ, USA), according to manufacturer's instructions. PBMCs (1×10^6) were incubated in 6-well plates, with the cell cytokine secretion inhibitor, ionomycin (50ng/ml) and phorbol 12-myristate 13-acetate (1μg/ml) (as aspecific stimulus). After 5 hours, cells were collected and fixed with 1 ml Cytofix Buffer for 20 min at room temperature, then washed and re-incubated with 1 ml BD Perm/Wash Buffer for 20 min at room temperature.

T-helper lymphocytes were identified by incubating with monoclonal labelled antibodies cocktail (and corresponding isotype controls): anti-IL4 (APC-conjugated), anti-IL17 (PE-conjugated), anti-CD4 (PerCP) and anti-IFN γ (FITC-conjugated). Cells were washed and collected in 300 μl 1% PAF.

T regulatory (Treg) cells were identified by the "Human Regulatory T-cell Staining Kit" (eBioscience Inc. San Diego, CA, USA) in accordance with manufacturer's instructions. Briefly, the following labelled monoclonal antibodies and corresponding isotype controls were used: anti-CD4 (FITC-conjugated); anti-CD25 (APC-conjugated); and anti-FOXP3 (PE-conjugated). After surface staining for CD4 and CD25 for 20 min at room temperature, cells were washed and fixed with the fixative and permeability solution (Fix-Perm Buffer) and incubated with rat serum to remove aspecific binding sites. Cells were then incubated with anti-FoxP3 (PE-conjugated), as intra-nuclear staining, and collected in 300 μl 1% PAF. Flow cytometry was performed by FACS Calibur flow cytometer and Cell Quest Software (BD Biosciences) and each analysis consisted of at least 100,000 events recorded within the lymphocyte gate.

Measurement of cytokine production

In order to evaluate the activity of various T cell subtypes and to study cytokines involved in OCs formation we measured the levels of TNF α , IFN γ , TGF β 1, IL-4, IL-17, IL-23, IL-6, OPG (R&D Duoset, Minneapolis, MN, USA), and total RANKL (BioVendor R&D, Brno, Czech Republic) by the ELISA technique in serum.

Second phase: Therapeutic intervention

After baseline evaluation, eRA patients were randomly allocated to treatment with: methotrexate (MTX) 15 mg/week (im or sc) and methylprednisolone (GC) per os 2–4 mg/day plus cholecalciferol 300,000 IU (N = 21) or placebo (N = 18) in single administration at the baseline evaluation (cholecalciferol was kindly provided by Abiogen Pharma S.p.A, Pisa Italy), healthy controls do not participate in this phase of the study. Levels of 25-OH vitamin D were measured at the end of the study, the use of 300000 UI of cholecalciferol was decided regardless to basal level of 25-OH vitamin D and starting from the hypothesis of the presence of vitamin D insufficiency in eRA patients, according to previous literature [1–3]. The use of 300000 UI was chosen according with Premaor MO and coll. [30], they showed that, in the short term, a single 300 000 IU oral dose of vitamin D was more effective than 800 IU per day to increase serum 25(OH)D levels. Randomization was done by the principal investigator, patients were enrolled by participants in the study, lab measurement and statistical analyses were done in blind to treatment.

The use of nonsteroidal anti-inflammatory drugs (NSAID) and paracetamol for pain relief was allowed and recorded at the control visit as “less than 7 day a week” or “daily”. After three months of therapy, patients were recalled to the centre and baseline evaluations were repeated, 3 patients did not come back to the follow up visit due to personal problems (Fig 1), physician were asked to register any adverse event, and to judge if such event may be related to cholecalciferol. None of the patients experienced adverse events. Data from patients dropped out were considered for the comparison with healthy controls, but not on the second part of the study.

The primary outcome measures of the first phase of the study were differences in Th subtypes and OCs precursors between patients and healthy controls.

The primary outcome measures of the second phase of the study were changes in number of Tregs, secondary outcome measures were changes in number of other CD4+ cells, OCs precursors and clinical parameters.

Statistical analysis

Patients at baseline and controls were compared for the analysed variables by one-way ANOVA for Gaussian variables and by Mann Whitney test for non-Gaussian variables. T cell sub-sets, OCs precursors and cytokines were correlated with clinical parameters by means of Spearman coefficient correlation. To evaluate a possible effect of cholecalciferol on clinical parameters and on laboratory variables significantly affected by eRA a multivariate analysis of variance (MANOVA) for repeated measures was used after logarithmically transforming non-Gaussian variables. The sample size of the second phase of the study provided an 80% power, assuming a two-sided significance level of 0.05, to detect differences greater than 1.5% in Tregs (t-test). Tregs were chosen as key variables on the basis of previous intervention trial in healthy volunteers [28].

Statistical analysis was performed using SPSS 21.0 for windows. Graphs were drawn using Graph Pad 7.0 for windows and a p-value <0.05 was considered statistically significant.

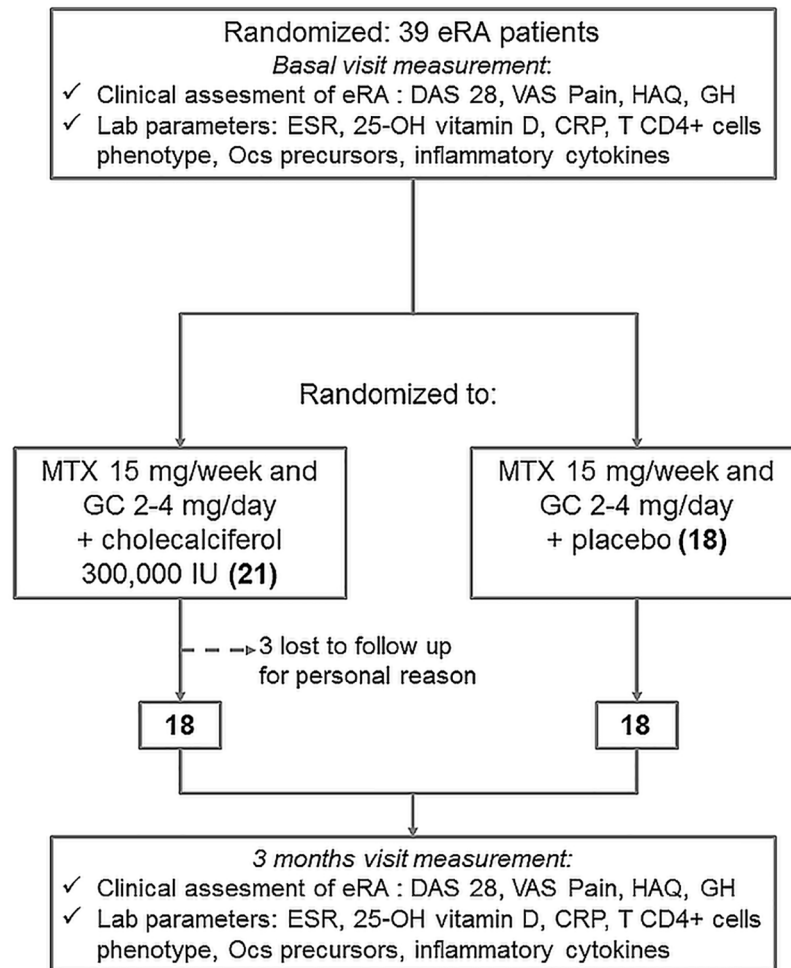


Fig 1. The diagram shows the study design and the number of patients at each visit in bold, the tests performed at each visits are specified.

<https://doi.org/10.1371/journal.pone.0178463.g001>

Results and discussion

Clinical characteristics of patients and controls

Patients and control subjects were not significantly different for age, post-menopausal period and body mass index (BMI), whereas levels of 25-OH vitamin D were significantly lower in patients compared to controls (Table 1).

T helper cell subsets in eRA

In patients affected by eRA, T helper subsets were significantly altered. In particular, we found an increase in the number of CD4+/IL17A+, CD4+/IFN γ +, CD4+/IL4+ and CD4+/IL17A+/IFN γ + lymphocytes, whereas Tregs were not significantly affected (Fig 2). CD4+/IL17A+ cells were the only T h cells correlated with a clinical parameter: CRP ($r = 0.35$, $p = 0.04$).

OCs precursor cells in eRA

In order to evaluate the role of OCs precursor cells in bone damage, we measured both classical and non-classical OCs precursors in PBMCs from eRA and controls. Classical OCs were not

Table 1. Clinical characteristics of patients and controls. Mean \pm SD is shown for Gaussian variables, for non-Gaussian variables (indicated by *) median (25–75 percentiles) are indicated. P values were calculated by means of ANOVA one-way for Gaussian variables and by means of Mann-Whitney test for non-Gaussian ones.

	eRA (39)	Controls (31)	p
Age (yrs)	54 \pm 8	55 \pm 13	0.743
post-menopausal period (yrs)	5 \pm 9	6 \pm 9	0.076
BMI	26.4 \pm 6.1	25.7 \pm 5.3	0.602
25OH-vitamin D (ng/mL)	16 \pm 2.1	26 \pm 2.23	0.002
PTH (pg/mL)*	38.15 (25.9–61.8)	32.9 (25.9–50.5)	0.545
Creatinine (mg/dL)	0.60 \pm 0.4	0.59 \pm 0.35	0.958
DAS 28	5.7 \pm 0.9	ND	
HAQ	1.3 \pm 0.8	ND	
NRS	62.9 \pm 20.2	ND	
ESR*	38 (22.3–57.8)	ND	
CRP (mg/L)*	10.0 (4.0–25.0)	ND	
GH	50.1 \pm 17.1	ND	

<https://doi.org/10.1371/journal.pone.0178463.t001>

increased in eRA patients whereas non-classical OCs were significantly increased (Fig 3A and 3B). Interestingly, non-classical OCs precursors, but not classical were directly correlated with DAS28 score ($r = 0.36$, $p = 0.033$) and with CRP ($r = 0.37$, $p = 0.033$).

Inflammatory cytokines in eRA

Levels of RANKL were significantly increased in eRA vs controls while OPG was not affected and, as a consequence, the RANKL/OPG ratio was significantly increased (Fig 3C and 3D). Furthermore, RANKL/OPG ratio was directly correlated with levels of non-classical OCs precursor cells ($r = 0.36$, $p = 0.04$).

Analysis of other inflammatory cytokines in the peripheral blood of patients revealed a significant increase in TNF α , TGF β , IL-23 and IL-6, whereas IL-17 and IFN γ levels were not significantly different in patients compared to controls (Fig 4). IL-23 and IL 6 were significantly correlated with clinical parameters. In particular, IL-23 was positively correlated with ESR ($r = 0.36$, $p = 0.04$), IL-6 with CRP ($r = 0.39$, $p = 0.03$) and DAS28 ($r = 0.4$, $p = 0.02$).

Effect of vitamin D on GH in eRA patients

To evaluate the possible effect of vitamin D treatment on clinical signs and symptoms of eRA, on T cells differentiation and function, on inflammation and osteoclastogenesis, we randomly assigned eRA patients to receive 300,000 IU of cholecalciferol or placebo, in addition to standard treatment. Three months after treatment levels of 25-OH vitamin D were significantly increased in patients treated with cholecalciferol ($p = 0.015$), whereas remained stable in patients treated with placebo ($p = 0.08$, Table 2) as expected. Patients receiving standard treatment plus colecalciferol or placebo had similar clinical characteristics (Table 2).

For clinical parameters, standard treatment significantly reduced DAS28, CRP, ESR and VAS pain and improved GH and HAQ. Furthermore, the association of vitamin D to standard treatment was more effective in ameliorating GH, whereas it had no effect on the other parameters (Fig 5). As regards the use of NSAID and paracetamol it was equally distributed in the two groups, in the placebo group 3 patients (17%) used NSAID or paracetamol less than 7day a week, whereas 15 (83%) used NSAID or paracetamol daily. In the group treated with

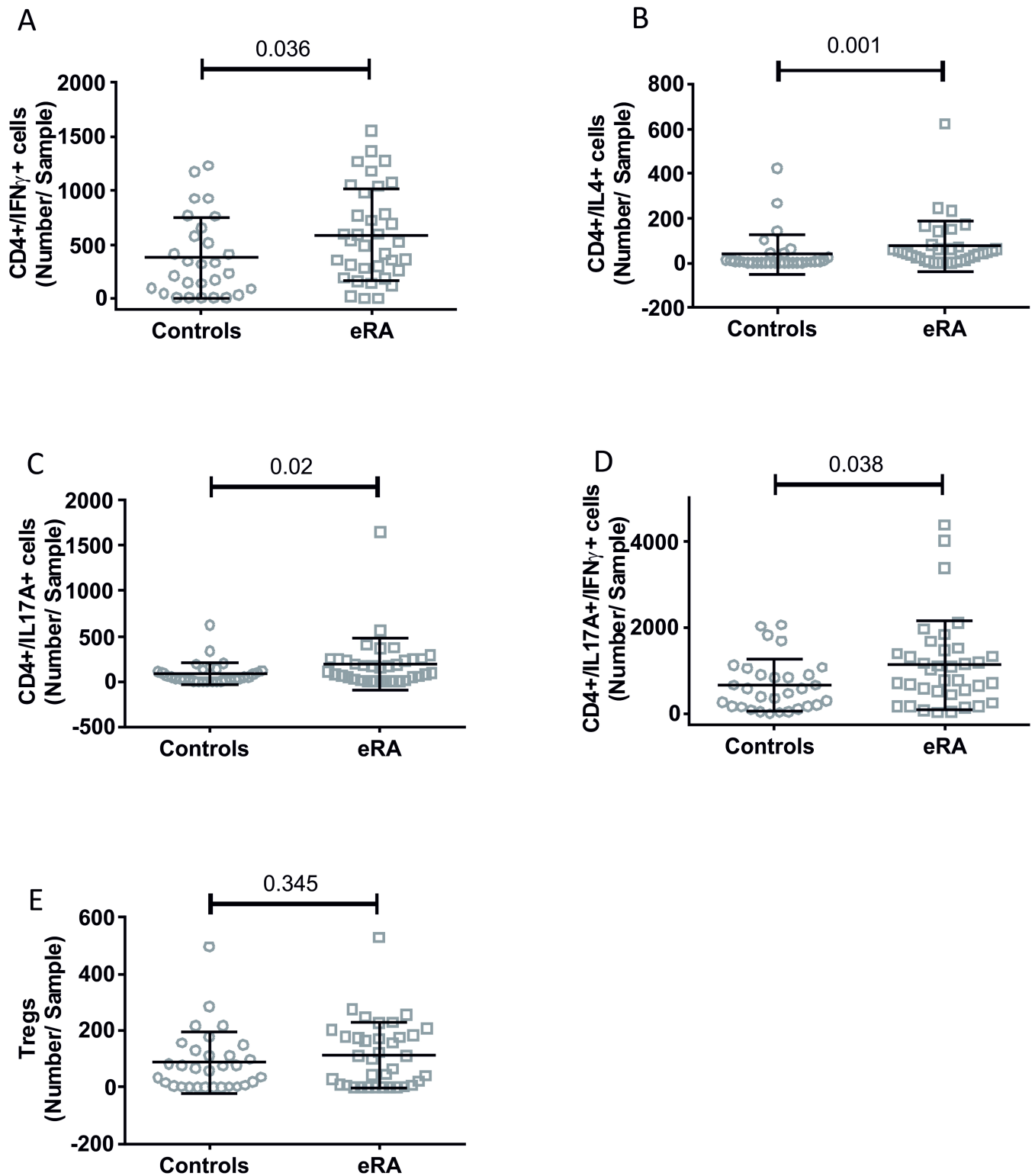


Fig 2. T helper subsets in eRA patients and healthy controls. Dot plots show CD4+/IFN γ + (panel A), CD4+/IL4+ (panel B), CD4+/IL17A+ (panel C), CD4+/IL17A+/IFN γ + (panel D) and Tregs (panel E); mean and SD are shown, p values were calculated by Mann-Whitney test and are displayed.

<https://doi.org/10.1371/journal.pone.0178463.g002>

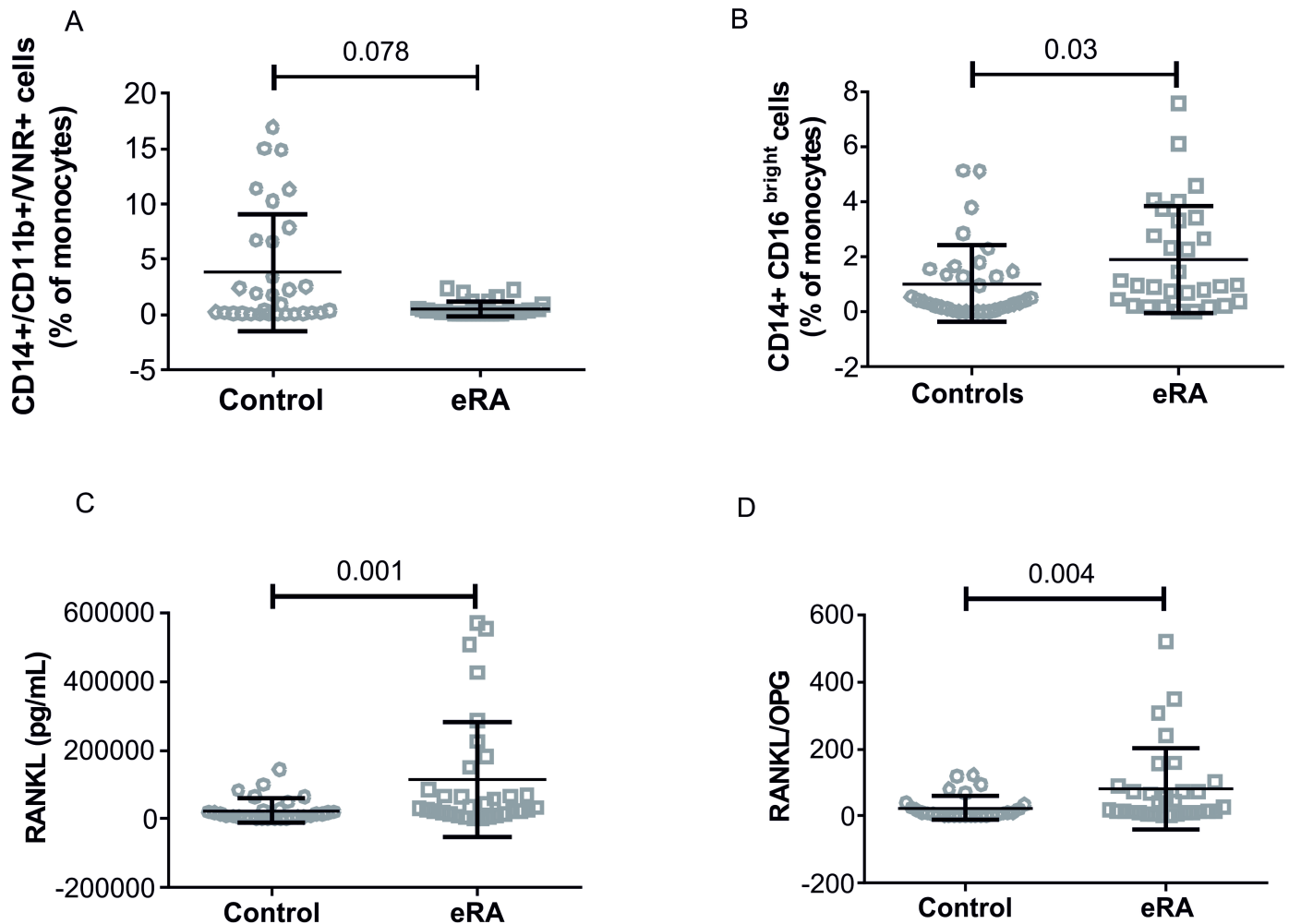


Fig 3. OCs precursors in eRA patients and healthy controls. Dot plots show classical OCs precursor (panel A), non-classical OCs precursor (panel B), RANKL (panel C) and RANKL/OPG (panel D); mean and SD are shown, p values were calculated by Mann-Whitney test and are displayed.

<https://doi.org/10.1371/journal.pone.0178463.g003>

cholecalciferol 6 patients (33%) used NSAID or paracetamol less than 7day a week, whereas 12 (67%) used NSAID or paracetamol daily ($\chi^2 = 2.62, p = 0.270$).

Standard treatment with or without the addition of vitamin D had no significant effect on T helper subset and on OCs precursor cells (Table 3). T helper cells and OCs were not significantly different between eRA treated with standard treatment or with standard treatment plus cholecalciferol (data not shown).

Regarding inflammatory and pro-osteoclastogenic cytokines, standard treatment had a significant effect in reducing IL-23, whereas the addition of vitamin D had no significant effect (Fig 6).

Data on treatment were obtained in 18 eRA patients per group (standard treatment with or without cholecalciferol).

In this paper, we evaluated RA patients at the very beginning of their disease, therefore permitting us to investigate early immunological alterations in RA. Our data revealed a significant increase in levels of CD4+/IFN γ + and CD4+/IL17A cells in the peripheral blood of eRA patients compared to age- and gender-matched control subjects. This finding supports previous literature on more advanced RA showing increased homing of CD4+/IFN γ + and

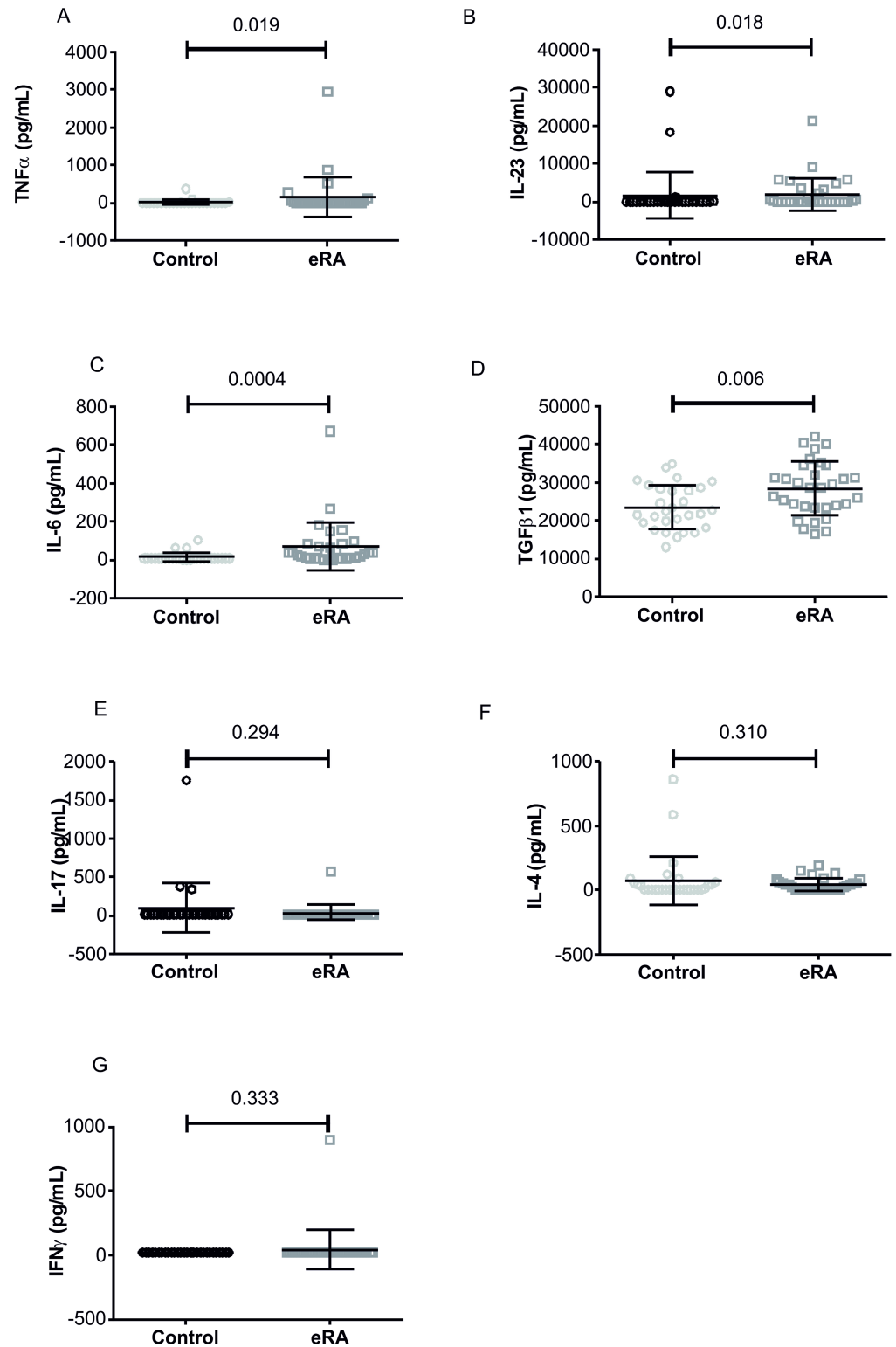


Fig 4. Inflammatory cytokines in eRA patients and healthy controls. Dot plots show classical IL-23 (panel A), IL-17 (panel B), IL-4 (panel C), IL-6 (panel D), TGF β 1 (panel E), TNF α (panel F) and IFN γ (panel G); mean and SD are shown, p values were calculated by Mann-Whitney test and are displayed.

<https://doi.org/10.1371/journal.pone.0178463.g004>

Table 2. Clinical characteristics of patients treated with standard treatment with or without cholecalciferol 300000 IU. Mean \pm SD is shown for Gaussian variables, for non-Gaussian variables (indicated by *) median (25–75 percentiles) are indicated. Comparison between the two groups after intervention were calculated by means of ANOVA one-way after Bonferroni correction, p values are shown where appropriate.

	Placebo (18)	Cholecalciferol 300000 IU (18)	p
Age (yrs)	54 \pm 12	56 \pm 14	
post-menopausal period (yrs)	6 \pm 9	5 \pm 9	
BMI	25.5 \pm 5.6	26.0 \pm 5.0	
Basal 25OH-vitamin D (ng/mL)	16 \pm 2.1	16 \pm 4	
Three month 25-OH vitamin D (ng/mL)	18 \pm 3.4	28.7 \pm 4.3	0.01
Basal PTH (pg/mL)	37.1 (24.2–71.15)	43.5 (32.9–52)	
Three months PTH (pg/mL)	47.2 (41.5–60.0)	32.6 (21.1–50.5)	0.200
Basal creatinine (mg/dL)	0.35 \pm 0.24	0.7 \pm 0.4	
Three months creatinine (mg/dL)	0.3 \pm 0.2	0.45 \pm 0.3	0.288
DAS 28	5.8 \pm 0.9	5.6 \pm 0.9	
HAQ	1.4 \pm 0.7	1.3 \pm 1.0	
VAS pain	68.3 \pm 18.9	57.5 \pm 20.6	
ESR*	38 (23.5–59)	38 (17.5–60.0)	
CRP (mg/L)*	12.35 (5.5–23.5)	10.0 (2.5–31.0)	
GH	50.0 \pm 16.5	50.3 \pm 18.2	

<https://doi.org/10.1371/journal.pone.0178463.t002>

CD4+/IL17A cells in the inflamed synovium [31,32] and suggests that, during the early phase, levels of these cells are increased in the peripheral blood and may migrate to the synovium only in the more advanced phase. Moreover, CD4+/IL17A cells detected in the peripheral blood are directly correlated to severity of inflammation, as measured by CRP levels, thus confirming their involvement in the pathogenesis of the disease.

We did not find a significant imbalance in Tregs, on this regard, previous studies have found conflicting results as some papers described a decrease in Tregs [6–8], whereas others did not observe this decrease [9,10] or found an increase [11]. This discrepancy largely depends on differences in the study design [5]. In our study, we found no significant difference in levels of Tregs in the peripheral blood of eRA patients suggesting that the *primum movens* of RA is not due to a decreased ability of the immune system to control inflammation, but to an increase in T cell activation *per se*. This observation is also reinforced by the increased levels of TGF β 1, suggesting an increased reaction of Tregs against auto immunity in these patients. In addition, CD4+/IL4+ cells were modestly increased in our patients thus suggesting an early imbalance also in these Th cells; other studies suggested a decrease of Th2 in more advanced forms of RA, our data suggest that this decrease may be more a consequence of the treatment rather than a cause of the disease. According to this hypothesis a recent paper on untreated eRA showed an increase in Th2 cells in peripheral blood [11].

A transitional cell type CD4+/IL17A-IFN γ has been previously described in RA [21] in particular at the level of the synovium. We found a significant increase in the number of these cells in the peripheral blood of eRA patients, that may later migrate within the inflamed synovium.

We also observed a significant increase in levels of non-classical OCs in eRA, whereas classical ones were not significantly different in patients and controls. Non-classical OCs precursors correlates with the grade of inflammation and the severity of the disease, suggesting that these cells, more than classical OCs, may be responsible for articular erosions in eRA patients. Moreover RANKL is increased in eRA and significantly correlates with these cells confirming a direct involvement of these precursors in RA bone damage.

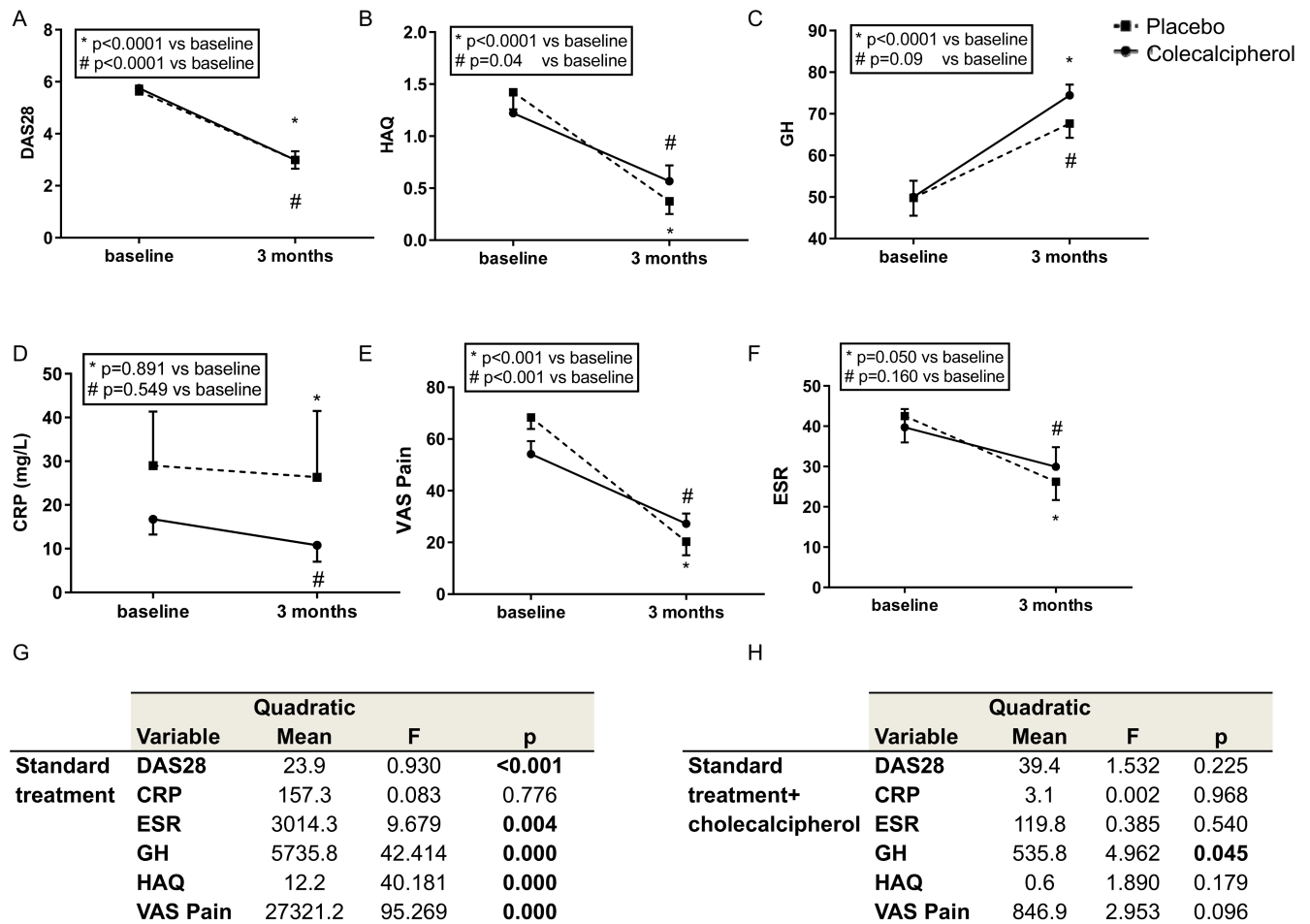


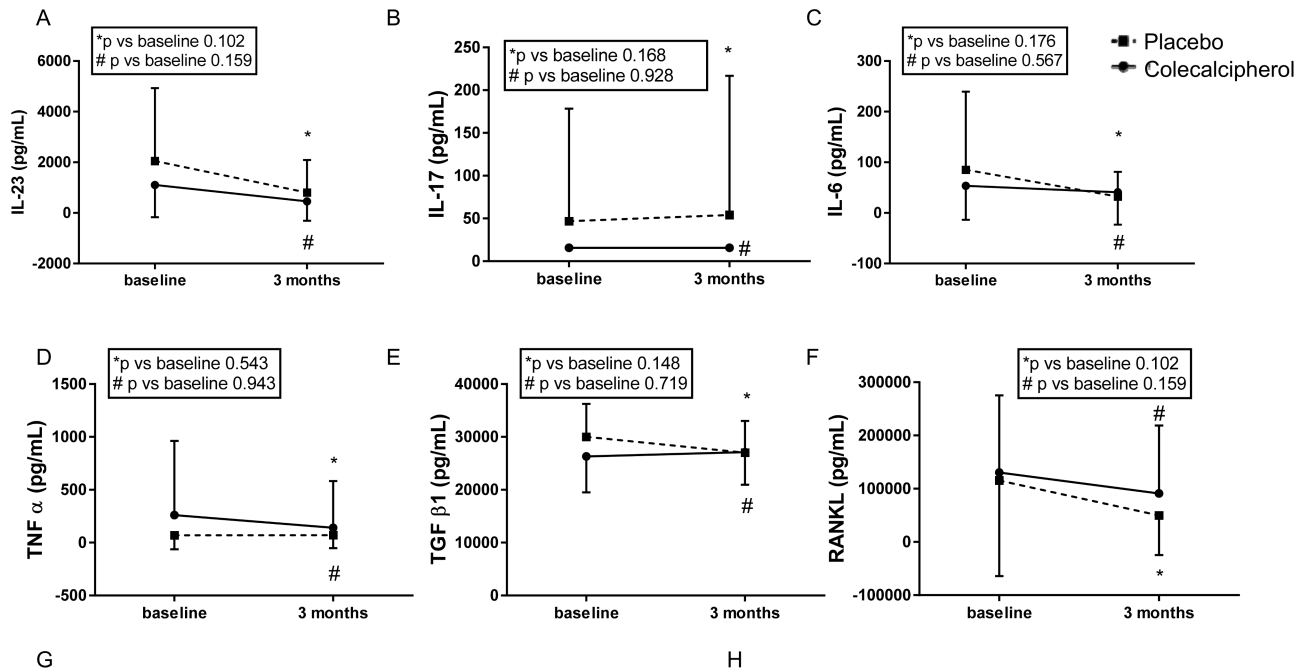
Fig 5. Effect of treatment with and without cholecalciferol on clinical parameters in eRA patients. Graphs show DAS28 (panel A), HAQ (panel B), GH (panel C), CRP (panel D), VAS pain (panel E) and ERS (panel F); mean and SD are shown, p values were calculated by Student paired t-test and are displayed. Tables (panels G and H) show the MANOVA for repeated measures for DAS28, HAQ, GH, CRP, VAS pain and ESR and the effect of standard treatment with or without the addition of cholecalciferol, quadratic mean, F and p value are shown. All the analyses were done in 18 patients per group. P values were corrected for multiple comparisons.

<https://doi.org/10.1371/journal.pone.0178463.g005>

Table 3. The table shows the effect of standard treatment compared with standard treatment plus cholecalciferol 300000 IU on CD4+/IFN γ +, CD4+/IL17A+, CD4+/IL4+, CD4+/IL17A+/IFN γ + and non-classical OCs precursors (these variables were significantly different between patients and controls). The variables were transformed in logarithm as they were distributed according to a non-Gaussian curve. Mean \pm SE, quadratic mean (Q), F and p values were calculated by MANOVA for repeated measures. P values were corrected for multiple comparisons. P values are shown for comparison between different treatment (*) and within treatment (baseline vs 3 months **).

	Variable	Mean \pm SE basal	Mean \pm SE 3 months	p**	Q	F	p*
Treatment (18)	CD4+/IFN γ	1.3 \pm 0.3	2.6 \pm 0.7	0.095	31.41	3.5	0.071
	CD4+/IL4+	0.3 \pm 0.1	0.2 \pm 0.06	0.917	0.021	0.166	0.687
	CD4+/IL17A+	0.6 \pm 0.3	1.2 \pm 0.5	0.391	1.933	1.112	0.301
	CD4+/IL17A+/IFN γ +	0.8 \pm 0.3	2.2 \pm 0.5	0.238	8.041	0.256	0.617
	Non-classical OCs	0.1 \pm 0.04	0.1 \pm 0.04	0.168	39.84	2.071	0.161
Treatment* Colecalciferol (18)	CD4+/IFN γ	2.0 \pm 0.4	2.3 \pm 0.7	0.403	3.600	0.403	0.531
	CD4+/IL4+	0.2 \pm 0.1	0.2 \pm 0.1	0.552	0.004	0.030	0.863
	CD4+/IL17A+	0.6 \pm 0.3	0.4 \pm 0.5	0.472	5.346	3.077	0.090
	CD4+/IL17A+/IFN γ +	1.2 \pm 0.3	0.7 \pm 0.5	0.324	82.34	2.622	0.117
	Non-classical OCs	0.1 \pm 0.04	0.1 \pm 0.04	0.928	26.63	1.384	0.249

<https://doi.org/10.1371/journal.pone.0178463.t003>



		Quadratic						Quadratic			
		Variable	Mean	F	p			Variable	Mean	F	p
Standard treatment	IL17		209.2	0.772	0.387	Standard treatment+ Cholecalciferol	IL17		209.2	0.772	0.387
	IL23		34236675.7	4.317	0.046		IL23		809017.8	0.102	0.752
	IL6		17715.9	2.480	0.126		IL6		5822.4	0.815	0.374
	TGFβ1		86560226.9	3.044	0.091		TGFβ1		83450078.1	2.934	0.097
	TNFα		71026.8	2.427	0.130		TNFα		77673.5	2.654	0.114
	RANKL		29465763126	2.504	0.124		RANKL		7826673554	0.665	0.421

Fig 6. Effect of treatment with and without cholecalciferol on inflammatory cytokines in eRA patients. Graphs show IL-23 (panel A), IL-17 (panel B), IL-6 (panel C), TNFα (panel D), TGFβ1 (panel E) and RANKL (panel F); mean and SD are shown, p values were calculated by Mann-Whitney test and are displayed. Tables (panels G and H) show the MANOVA for repeated measures for IL-23, IL-17, IL-6, TNFα, TGFβ1 and RANKL and the effect of standard treatment with or without the addition of cholecalciferol, quadratic mean, F and p value are shown. The linear model was carried out after logarithmic transformation of non-Gaussian variables. All the analyses were done in 18 patients per group. P values were corrected for multiple comparisons.

<https://doi.org/10.1371/journal.pone.0178463.g006>

With regard to inflammatory cytokines, our results confirmed previous studies showing increased levels of IL-6, TNFα and RANKL [33] also in the early phase of RA. Interestingly, we also observed increased levels of IL-23 and TGFβ1.

IL-23 is required for the amplification and stabilization of CD4+/IL17A+ cells and an increase in levels of IL-23 may explain the increased formation of CD4+/IL17A+ [31]. Previous studies have demonstrated that levels of IL-23 are elevated in the serum and synovial fluid of patients with established RA, and these levels positively correlated with levels of disease severity [34,35]. In our study, we observed an increase in IL-23, recognised as occurring earlier than that the described increase in IL-17 [36].

TGFβ1 modulates anti-inflammatory and immunosuppressive responses and plays a key role in self-tolerance [37]. TGFβ1 also plays a complex role in the regulation of bone turnover and has been shown to cause both bone loss and gain in mice [38].

A recent study conducted in RA patients showed a non-significant increase in this molecule in the serum of patients compared to healthy controls [39], however our study is the first to

evaluate levels of TGF β 1 in the early RA phase. We showed a significant increase in TGF β 1 that may have a compensatory effect in response to increased inflammatory state.

Regarding the possible role of vitamin D status in the development of RA, we confirmed findings from previous studies on the association between RA and lower levels of 25-OH vitamin D. The administration of standard treatment plus 300,000 IU of cholecalciferol in this population was able to ameliorate their global health, but had no significant effect on specific signs and symptoms of RA, CRP, VAS pain and DAS 28, that were decreased following standard treatment. A previous open-label study in patients affected by RA showed that the administration of cholecalciferol over a period of 3 months in patients with active disease and hypovitaminosis contributed to a significant improvement in disease activity [4]. In our study we did not observe any significant effect of cholecalciferol on DAS28. This may be due to the different study setting since we used different doses of cholecalciferol: we administered 300,000 IU of cholecalciferol as a single dose and evaluated the effect after three months. In contrast, the study by Chandrashekhara and Patted, patients with active RA and hypovitaminosis were enrolled and treated with 60,000 IU/week for 6 weeks, followed by 60,000 IU/month for a total duration of 3 months [4].

Vitamin D receptor (VDR) gene is widely expressed in a variety of human cell types suggesting that vitamin D has, via the VDR, a far wider physiological function than the control of calcium homeostasis and bone remodeling. As regards immune system cells of the innate and adaptive immune system, such as monocytes, T and B cells and monocytes express VDR and are responsive to vitamin D (see for a review [40]). Here we focused on T cells due to their important role in the pathogenesis of RA [5] and considering experimental evidence that points towards an effect of vitamin D in regulating T cell proliferation, differentiation in different subsets and cytokine production (see for a review [40]). In our study, we found no significant effect of cholecalciferol administration on T helper subsets, nor on cytokines production. Previous studies have shown that 1,25OH cholecalciferol inhibits Th1 cytokines production [41], and promotes Th2 cytokines [42]. More recently it has been shown that 1,25OH cholecalciferol reduces the differentiation of Th towards CD4+/IL17A+ markers and their secretion of pro-inflammatory cytokines (IL-17A, IFN γ) and induces differentiation towards Tregs [43].

Nonetheless, we found no significant effect of cholecalciferol on T helper cells in eRA in our study. A recent study in humans affected by chronic autoimmune thyroiditis showed that oral cholecalciferol is able to reduce IFN γ + and IL-17+ Th cells [44] and to increase the expression Tregs [45]; in patients with type 1 diabetes mellitus the administration of oral cholecalciferol was able to increase the suppressive capacity of Tregs within 12 months of treatment [46]. The majority of previous studies on the effect of vitamin D on T cells has been performed in vitro and using 1,25-OH cholecalciferol. Human studies have been undertaken in different disease states using different doses of vitamin D, therefore, it is very difficult to compare the results. Corroborating our findings, a recent double-blind placebo-controlled study performed in hemodialysis patients showed no effect of oral cholecalciferol on Th cell subsets [47]. The present report is the first human study evaluating the effect of cholecalciferol administration in eRA patients. Also standard treatment with MTX has no effect of Th cells subsets, previous studies showed an effect of MTX on activated T cells in vitro [48, 49], whereas in a recent paper patients treated with MTX administered orally in a dose ranging from 7 to 25 mg has no decrease in peripheral T cells count [50]. Our data confirm no effect of MTX in combination with GCs of different T cells sub-types. As regards the effect of MTX on OCs it has been recently demonstrated that it inhibits osteoclastogenesis by reducing RANKL-induced calcium influx into OC precursors [51], however these data were obtained in vitro, whereas no data on humans in vivo are available. Here we show no effect of cholecalciferol

on classical and non-classical OCs precursors, although it has previously been shown that 1,25OH cholecalciferol is effective in reducing CD16 expression in monocytes from asthmatic patients in vitro [52], whereas in hemodialysis patients, no effect on CD16+ cells was observed following treatment with oral cholecalciferol [47].

We enrolled only women in this study as RA is more frequent in this gender, however this could be a limitation of the study, also the inclusion of patients regardless their basal 25-OH vitamin D levels could be a limitation of the study as the effect of cholecalciferol may be greater in patients affected by more severe forms of hypovitaminosis D. Nevertheless the result of our study may be generalized to women with eRA especially considering the absence of adverse events, probably the administration of cholecalciferol may be more effective in patients with lower levels of 25OH vitamin D as also shown by Chandrashekara and Patted [4].

Conclusion

In conclusion, we show that eRA patients significantly differ from age and sex matched controls for 25-OH vitamin D levels, Th cell subsets with increased CD4+/IFN γ +, CD4+/IL4+, CD4+/IL17A+ and CD4+/IL17A+/ IFN γ + cells, and increased non classical OCs precursors. We also observed an increase in TNF α , TGF β 1, RANKL, IL23 and IL-6. Among experimental parameters non-classical OCs, IL-23 and IL-6 correlated with disease severity and disease activity.

Since it is known that standard treatment with MTX and GC is able to ameliorate clinical symptoms, here we show that standard treatment is effective in reducing IL-23, whereas it does not affect Th subset nor OCs precursors. However, the combined use of 300,000 IU of cholecalciferol significantly ameliorates the effect of treatment on global health in eRA patients.

Supporting information

S1 File. Consort check list 2010. Consort check list for the study.
(PDF)

S2 File. Study protocol approved by Ethical committee (Italian). Protocol of the study approved by the Ethical committee in original language (Italian).
(PDF)

S3 File. Study protocol approved by Ethical committee (English). Protocol of the study approved by the Ethical committee in English language.
(PDF)

Acknowledgments

Cholecalciferol was kindly provided by Abiogen Pharma S.p.A.

Author Contributions

Conceptualization: PD RP GCI.

Data curation: MMR.

Formal analysis: PD.

Funding acquisition: PD RP.

Investigation: IB FS GR CL SP.

Methodology: PD IB.

Project administration: PD IB.

Resources: GR CL SP RP GCI.

Supervision: PD.

Validation: PD IB.

Visualization: PD IB MMR SP.

Writing – original draft: PD IB GR SP MMR CL.

Writing – review & editing: PD RP GCI.


References

1. Souberbielle JC, Body JJ, Lappe JM, Plebani M, Shoenfeld Y, Wang TJ, et al. Vitamin D and musculoskeletal health, cardiovascular disease, autoimmunity and cancer: Recommendations for clinical practice. *Autoimmun Rev* 2010; 9:709–15 <https://doi.org/10.1016/j.autrev.2010.06.009> PMID: 20601202
2. Craig SM, Yu F, Curtis JR, Alarcon GS, Conn DL, Jonas B, et al. Vitamin D status and its associations with disease activity and severity in African Americans with recent-onset rheumatoid arthritis. *J Rheumatol* 2010; 37:275–81 <https://doi.org/10.3899/jrheum.090705> PMID: 20032100
3. Haque UJ, Bartlett SJ. Relationships among vitamin D, disease activity, pain and disability in rheumatoid arthritis. *Clin Exp Rheumatol* 2010; 28:745–7 PMID: 20883640
4. Chandrashekhara S, Patted A. Role of vitamin D supplementation in improving disease activity in rheumatoid arthritis: An exploratory study. *Int J Rheum Dis* 2015 Oct 20. <https://doi.org/10.1111/1756-185X.12770> PMID: 26481198
5. Komatsu N, Takayanagi H. Arthritogenic T cells in autoimmune arthritis. *Int J Biochem Cell Biol* 2015; 58:92–6 <https://doi.org/10.1016/j.biocel.2014.11.008> PMID: 25450406
6. Sempere-Ortells JM, Pérez-García V, Marín-Alberca G, Peris-Pertusa A, Benito JM, Marco FM, et al. Quantification and phenotype of regulatory T cells in rheumatoid arthritis according to disease activity score-28. *Autoimmunity* 2009; 42:636–45 <https://doi.org/10.3109/08916930903061491> PMID: 19886735
7. Raghavan S, Cao D, Widhe M, Roth K, Herrath J, Engstrom M, et al. FOXP3 expression in blood, synovial fluid and synovial tissue during inflammatory arthritis and intra-articular corticosteroid treatment. *Ann Rheum Dis* 2009; 68:1908–15 <https://doi.org/10.1136/ard.2008.100768> PMID: 19066178
8. Zare HR, Habibagahi M, Vahdati A, Habibagahi Z. Patients with Active Rheumatoid Arthritis Have Lower Frequency of nTregs in Peripheral Blood. *Iran J Immunol* 2015; 12:166–75 PMID: 26412635
9. Basdeo SA, Moran B, Cluxton D, Canavan M, McCormick J, Connolly M, et al. Polyfunctional, Pathogenic CD161+ Th17 Lineage Cells Are Resistant to Regulatory T Cell-Mediated Suppression in the Context of Autoimmunity. *J Immunol* 2015; 195:528–40 <https://doi.org/10.4049/jimmunol.1402990> PMID: 26062995
10. Walter GJ, Fleskens V, Frederiksen KS, Rajasekhar M, Menon B, Gerwien JG, et al. Phenotypic, functional and gene expression profiling of peripheral CD45RA+ and CD45RO+ CD4+CD25+CD127low regulatory T cells in rheumatoid arthritis. *Arthritis Rheumatol* 2016; 68:103–16 <https://doi.org/10.1002/art.39408> PMID: 26314565
11. Pandya JM, Lundell AC, Hallström M, Andersson K, Nordström I, Rudin A. Circulating T helper and T regulatory subsets in untreated early rheumatoid arthritis and healthy control subjects. *J Leukoc Biol* 2016; 100:823–833 <https://doi.org/10.1189/jlb.5A0116-025R> PMID: 27190305
12. Buchwald ZS, Kiesel JR, DiPaolo R, Pagadala MS, Aurora R. Osteoclast activated FoxP3+ CD8+ T-cells suppress bone resorption in vitro. *PLoS One* 2012; 7:e38199 <https://doi.org/10.1371/journal.pone.0038199> PMID: 22701612
13. Roato I, Caldo D, D'Amico L, D'Amelio P, Godio L, Patanè S, et al. Osteoclastogenesis in peripheral blood mononuclear cell cultures of periprosthetic osteolysis patients and the phenotype of T cells localized in periprosthetic tissues. *Biomaterials* 2010; 31:7519–25 <https://doi.org/10.1016/j.biomaterials.2010.06.027> PMID: 20638717

14. Ito Y, Hashimoto M, Hirota K, Ohkura N, Morikawa H, Nishikawa H, et al. Detection of T cell responses to a ubiquitous cellular protein in autoimmune disease. *Science* 2014; 346:363–8 <https://doi.org/10.1126/science.1259077> PMID: 25324392
15. Takayanagi H, Ogasawara K, Hida S, Chiba T, Murata S, Sato K, et al. T-cell-mediated regulation of osteoclastogenesis by signalling cross-talk between RANKL and IFN-gamma. *Nature* 2000; 408:600–5 <https://doi.org/10.1038/35046102> PMID: 11117749
16. Gao Y, Grassi F, Ryan MR, Terauchi M, Page K, Yang X, et al. IFN-gamma stimulates osteoclast formation and bone loss in vivo via antigen-driven T cell activation. *Clin Invest* 2007; 117:122–32
17. D'Amelio P, Grimaldi A, Di Bella S, Brianza SZ, Cristofaro MA, Tamone C, et al. Estrogen deficiency increases osteoclastogenesis up-regulating T cells activity: a key mechanism in osteoporosis. *Bone* 2008; 43:92–100 <https://doi.org/10.1016/j.bone.2008.02.017> PMID: 18407820
18. Lubberts E, Koenders MI, Oppers-Walgreen B, van den Bersselaar L, Coenen-deRoo CJ, Joosten LA, et al. Treatment with a neutralizing anti-murine interleukin-17 anti-body after the onset of collagen-induced arthritis reduces joint inflammation, cartilage destruction, and bone erosion. *Arthritis Rheum* 2004; 50:650–9 <https://doi.org/10.1002/art.20001> PMID: 14872510
19. Nakae S, Nambu A, Sudo K, Iwakura Y. Suppression of immune induction of collagen-induced arthritis in IL-17-deficient mice. *J Immunol* 2003; 171:6173–7 PMID: 14634133
20. Shahrara S, Huang Q, Mandelin AM, Pope RM. TH-17 cells in rheumatoid arthritis. *Arthritis Res Ther* 2008; 10:R93. <https://doi.org/10.1186/ar2477> PMID: 18710567
21. Tyagi AM, Srivastava K, Mansoori MN, Trivedi R, Chattopadhyay N, Singh D. Estrogen deficiency induces the differentiation of IL-17 secreting Th17 cells: a new candidate in the pathogenesis of osteoporosis. *PLoS One* 2012; 7:e44552. <https://doi.org/10.1371/journal.pone.0044552> PMID: 22970248
22. Cosmi L, Cimaz R, Maggi L, Santarlasci V, Capone M, Borriello F, et al. Evidence of the transient nature of the Th17 phenotype of CD4+CD161+T cells in the synovial fluid of patients with juvenile idiopathic arthritis. *Arthritis Rheum* 2011; 63:2504–15 <https://doi.org/10.1002/art.30332> PMID: 21381000
23. Schett G. Cells of the synovium in rheumatoid arthritis. Osteoclasts. *Arthritis Research & Therapy* 2007; 9:203
24. Everts V, de Vries TJ. Osteoclast Formation from Peripheral Blood of Patients with Bone-lytic Diseases. *Clinic Rev Bone Miner Metab* 2009; 7:285–92
25. Chiu YG, Shao T, Feng C, Mensah KA, Thullen M, Schwarz EM et al. CD16 (FcRgammaIII) as a potential marker of osteoclast precursors in psoriatic arthritis. *Arthritis Research & Therapy* 2010; 12:1–14
26. Zhang JY, Zou ZS, Huang A, Zhang Z, Fu JL, Xu XS, et al. Hyper-activated pro-inflammatory CD16 monocytes correlate with the severity of liver injury and fibrosis in patients with chronic hepatitis B. *PLoS one* 2011; 6:e17484. <https://doi.org/10.1371/journal.pone.0017484> PMID: 21390263
27. Daniel C, Sartory NA, Zahn N, Radeke HH, Stein JM. Immune modulatory treatment of trinitrobenzene sulfonic acid colitis is associated with a change of a T helper (Th) 1/Th17 to a Th2 and regulatory T cell profile. *J Pharmacol Exp Ther* 2008; 324:23–33 <https://doi.org/10.1124/jpet.107.127209> PMID: 17911375
28. Aletaha D, Neogi T, Silman AJ, Funovits J, Felson DT, Bingham CO, et al. Rheumatoid arthritis classification criteria: an American College of Rheumatology/European League Against Rheumatism collaborative initiative. *Arthritis Rheum* 2010; 62:2569–81 <https://doi.org/10.1002/art.27584> PMID: 20872595
29. Roato I, D'Amelio P, Gorassini E, Grimaldi A, Bonello L, Fiori C, et al. Osteoclasts are active in bone forming metastases of prostate cancer patients. *PLoS ONE* 2008; 3:e3627 <https://doi.org/10.1371/journal.pone.0003627> PMID: 18978943
30. Premaor MO, Scalco R, da Silva MJ, Froehlich PE, Furlanetto TW. The effect of a single dose versus a daily dose of cholecalciferol on the serum 25-hydroxycholecalciferol and parathyroid hormone levels in the elderly with secondary hyperparathyroidism living in a low-income housing unit. *J Bone Miner Metab*. 2008; 26:603–8. <https://doi.org/10.1007/s00774-008-0858-0> PMID: 18979160
31. Astry B, Venkatesha SH, Moudgil KD. Involvement of the IL-23/IL-17 axis and the Th17/Treg balance in the pathogenesis and control of autoimmune arthritis. *Cytokine* 2015; 74:54–61 <https://doi.org/10.1016/j.cyt.2014.11.020> PMID: 25595306
32. Ito Y, Hashimoto M, Hirota K, Ohkura N, Morikawa H, Nishikawa H, et al. Detection of T cell responses to a ubiquitous cellular protein in autoimmune disease. *Science* 2014; 346:363–8 <https://doi.org/10.1126/science.1259077> PMID: 25324392
33. Liu W, Zhang X. Receptor activator of nuclear factor- κ B ligand (RANKL)/RANK/osteoprotegerin system in bone and other tissues (review). *Mol Med Rep* 2015; 11:3212–8 <https://doi.org/10.3892/mmr.2015.3152> PMID: 25572286
34. Abu Al Fadl E.M, Fattouh M, Allam AA. High IL-23 level is a marker of disease activity in rheumatoid arthritis. *Egypt J Immunol* 2013; 20:85–92 PMID: 24617049

35. Guo YY, Wang NZ, Zhao S, Hou LX, Xu YB, Zhang N. Increased interleukin-23 is associated with increased disease activity in patients with rheumatoid arthritis. *Chin Med J* 2013; 126:850–54 PMID: [23489789](https://pubmed.ncbi.nlm.nih.gov/23489789/)
36. Metawi SA, Abbas D, Kamal MM, Ibrahim MK. Serum and synovial fluid levels of interleukin-17 in correlation with disease activity in patients with RA. *Clin Rheumatol* 2011; 30:1201–7 <https://doi.org/10.1007/s10067-011-1737-y> PMID: [21874405](https://pubmed.ncbi.nlm.nih.gov/21874405/)
37. Li MO, Wan YY, Sanjabi S, Robertson AK, Flavell RA. Transforming growth factor-beta regulation of immune responses. *Annu Rev Immunol* 2006; 24:99–146 <https://doi.org/10.1146/annurev.immunol.24.021605.090737> PMID: [16551245](https://pubmed.ncbi.nlm.nih.gov/16551245/)
38. Swallow CJ, Partridge EA, Macmillan JC, Tajirian T, DiGuglielmo GM, Hay K, et al. Alpha2HS-glycoprotein, an antagonist of transforming growth factor beta in vivo, inhibits intestinal tumor progression. *Cancer Res* 2004; 64:6402–9 <https://doi.org/10.1158/0008-5472.CAN-04-1117> PMID: [15374947](https://pubmed.ncbi.nlm.nih.gov/15374947/)
39. Harman H, Tekeoğlu İ, Gürol G, Sağ MS, Karakeçe E, Çiftçi İH, et al. Comparison of fetuin-A and transforming growth factor beta 1 levels in patients with spondyloarthropathies and rheumatoid arthritis. *Int J Rheum Dis* 2016 Jan 22. <https://doi.org/10.1111/1756-185X.12791> PMID: [26799059](https://pubmed.ncbi.nlm.nih.gov/26799059/)
40. Chun RF, Liu PT, Modlin RL, Adams JS, Hewison M. Impact of vitamin D on immune function: lessons learned from genome-wide analysis. *Front Physiol* 2014; 5:151 <https://doi.org/10.3389/fphys.2014.00151> PMID: [24795646](https://pubmed.ncbi.nlm.nih.gov/24795646/)
41. Lemire JM, Archer DC, Beck L, Spiegelberg HL. Immunosuppressive actions of 1,25-dihydroxyvitamin D3: preferential inhibition of Th1 functions. *J Nutr* 1995; 125:1704S–8S PMID: [7782931](https://pubmed.ncbi.nlm.nih.gov/7782931/)
42. Boonstra A, Barrat FJ, Crain C, Heath VL, Savelkoul HF, O'Garra A. 1alpha,25-Dihydroxyvitamin d3 has a direct effect on naive CD4(+) T cells to enhance the development of Th2 cells. *J Immunol* 2001; 167:4974–80 PMID: [11673504](https://pubmed.ncbi.nlm.nih.gov/11673504/)
43. Fawaz L, Mrad MF, Kazan JM, Sayegh S, Akika R, Khoury SJ. Comparative effect of 25(OH)D3 and 1,25(OH)2D3 on Th17 cell differentiation. *Clin Immunol* 2016; 166–167:59–71 <https://doi.org/10.1016/j.clim.2016.02.011> PMID: [27041081](https://pubmed.ncbi.nlm.nih.gov/27041081/)
44. Drozdenko G, Heine G, Worm M. Oral vitamin D increases the frequencies of CD38+ human B cells and ameliorates IL-17-producing T cells. *Exp Dermatol* 2014; 23:107–12 <https://doi.org/10.1111/exd.12300> PMID: [24313624](https://pubmed.ncbi.nlm.nih.gov/24313624/)
45. Şıklar Z, Karataş D, Doğu F, Hacıhamdioğlu B, İkinçioğulları A, Berberoğlu M. Regulatory T Cells and Vitamin D status in children with Chronic Autoimmune Thyroiditis. *J Clin Res Pediatr Endocrinol* 2016; 8:276–81. <https://doi.org/10.4274/jcrpe.2766> PMID: [27086659](https://pubmed.ncbi.nlm.nih.gov/27086659/)
46. Treiber G, Prietl B, Fröhlich-Reiterer E, Lechner E, Ribitsch A, Fritsch M, et al. Cholecalciferol supplementation improves suppressive capacity of regulatory T-cells in young patients with new-onset type 1 diabetes mellitus—A randomized clinical trial. *Clin Immunol* 2015; 161:217–24 <https://doi.org/10.1016/j.clim.2015.08.002> PMID: [26277548](https://pubmed.ncbi.nlm.nih.gov/26277548/)
47. Seibert E, Heine GH, Ulrich C, Seiler S, Köhler H, Girmdt M. Influence of cholecalciferol supplementation in hemodialysis patients on monocyte subsets: a randomized, double-blind, placebo-controlled clinical trial. *Nephron Clin Pract* 2013; 123:209–19
48. Genestier L, Paillet R, Fournel S, Ferraro C, Miossec P, Revillard JP. Immunosuppressive properties of methotrexate: apoptosis and clonal deletion of activated peripheral T cells. *J Clin Invest*. 1998; 102:322–8 <https://doi.org/10.1172/JCI2676> PMID: [9664073](https://pubmed.ncbi.nlm.nih.gov/9664073/)
49. Strauss G, Osen W, Debatin KM. Induction of apoptosis and modulation of activation and effector function in T cells by immunosuppressive drugs. *Clin Exp Immunol*. 2002; 128:255–66 <https://doi.org/10.1046/j.1365-2249.2002.01777.x> PMID: [11985515](https://pubmed.ncbi.nlm.nih.gov/11985515/)
50. Aira LE, Hernández P, Prada D, Chico A, Gómez JA, González Z, et al. Immunological evaluation of rheumatoid arthritis patients treated with itolizumab. *MAbs*. 2016; 8:187–95 <https://doi.org/10.1080/19420862.2015.1105416> PMID: [26466969](https://pubmed.ncbi.nlm.nih.gov/26466969/)
51. Kanagawa H, Masuyama R, Morita M, Sato Y, Niki Y, Kobayashi T, et al. Methotrexate inhibits osteoclastogenesis by decreasing RANKL-induced calcium influx into osteoclast progenitors. *J Bone Miner Metab*. 2016; 34:526–31. <https://doi.org/10.1007/s00774-015-0702-2> PMID: [26202855](https://pubmed.ncbi.nlm.nih.gov/26202855/)
52. Grubczak K, Lipinska D, Eljaszewicz A, Singh P, Radzikowska U, Miklasz P, et al. Vitamin D3 Treatment Decreases Frequencies of CD16-Positive and TNF- α -Secreting Monocytes in Asthmatic Patients. *Int Arch Allergy Immunol* 2015; 166:170–6 <https://doi.org/10.1159/000380882> PMID: [25872112](https://pubmed.ncbi.nlm.nih.gov/25872112/)

Regulatory T cells are expanded by Teriparatide treatment in humans and mediate intermittent PTH-induced bone anabolism in mice

Mingcan Yu¹, Patrizia D'Amelio², Abdul Malik Tyagi¹, Chiara Vaccaro¹, Jau-Yi Li¹, Emory Hsu¹, Ilaria Buondonno², Francesca Sassi², Jonathan Adams¹, M Neale Weitzmann^{1,3}, Richard DiPaolo⁴ & Roberto Pacifici^{1,5,*} 

Abstract

Teriparatide is a bone anabolic treatment for osteoporosis, modeled in animals by intermittent PTH (iPTH) administration, but the cellular and molecular mechanisms of action of iPTH are largely unknown. Here, we show that Teriparatide and iPTH cause a ~two–threefold increase in the number of regulatory T cells (Tregs) in humans and mice. Attesting *in vivo* relevance, blockade of the Treg increase in mice prevents the increase in bone formation and trabecular bone volume and structure induced by iPTH. Therefore, increasing the number of Tregs is a pivotal mechanism by which iPTH exerts its bone anabolic activity. Increasing Tregs pharmacologically may represent a novel bone anabolic therapy, while iPTH-induced Treg increase may find applications in inflammatory conditions and transplant medicine.

Keywords bone; bone formation; parathyroid hormone; regulatory T cells

Subject Categories Immunology; Molecular Biology of Disease

DOI 10.15252/embr.201744421 | Received 27 April 2017 | Revised 3 October 2017 | Accepted 17 October 2017

Introduction

Primary hyperparathyroidism is a common cause of bone loss and fractures due to the continuous production of high levels of parathyroid hormone (PTH) by the parathyroid glands [1,2]. By contrast, when PTH is injected daily, a regimen known as intermittent PTH (iPTH) treatment, the hormone increases bone volume and strength due to a stimulation of bone formation tempered by a more moderate increase in resorption [3,4]. As a result, intermittent treatment with the 1–34 fragment of PTH is an FDA-approved treatment modality for postmenopausal osteoporosis (PMO) [5].

PTH acts by binding to the PTH/PTHrP receptor PPR, which is expressed in all osteoblastic cells, including stromal cells (SCs), osteoblasts, and osteocytes [6–10]. Moreover, PPR is expressed in conventional CD4⁺ and CD8⁺ T cells [11] and macrophages [12]. iPTH stimulates bone formation by increasing osteoblast formation and life span. Activation of Wnt signaling in osteocytes and osteoblasts is one of the proposed mechanisms by which iPTH stimulates bone formation [4,13,14]. Wnt signaling activation is achieved through multiple mechanisms including Wnt ligand-independent activation of Wnt coreceptors [15], blunted osteocytic production of the Wnt inhibitor sclerostin [16–18], and decreased production by osteoblasts of the Wnt inhibitor Dkk1 [19].

While osteocytes and their production of sclerostin are critical for the activity of iPTH, part of this hormone activity is sclerostin independent [20] and mediated by T cells [21], a cell lineage that potentiates the anabolic activity of iPTH in trabecular bone [11,20,22]. Accordingly, iPTH fails to stimulate bone formation and increase bone mass in T-cell null mice [11]. By contrast, the effects of iPTH in cortical bone are completely T cell independent [11,20,22], likely due to the fact that T cells have no contacts with periosteal surfaces and have limited capacity to communicate with osteocytes. Among the T cells required for iPTH to exert its full anabolic activity are bone marrow (BM) CD8⁺ T cells [11]. CD8⁺ T cells express higher levels of the receptor PPR than CD4⁺ T cells [11,20,22]. Moreover, BM CD8⁺ T cells, but not CD4⁺ T cells, respond to iPTH by releasing Wnt10b [11,20,22], an osteogenic Wnt ligand that activates Wnt signaling in osteoblastic cells [23].

Regulatory T cells (Tregs) are a suppressive population of predominantly CD4⁺ T cells that play a critical role in maintaining immune tolerance and immune homeostasis. Tregs are comprised of thymus-derived Tregs (tTregs, also known as nTregs) and peripherally derived Tregs (pTregs, also known as iTregs) [24]. Tregs are defined by the expression of the transcription factor Foxp3 and the ability to block inflammatory diseases and maintain immune

1 Division of Endocrinology, Metabolism and Lipids, Department of Medicine, Emory University, Atlanta, GA, USA

2 Gerontology Section, Department of Medical Sciences, University of Torino, Torino, Italy

3 Atlanta Department of Veterans Affairs Medical Center, Decatur, GA, USA

4 Department of Molecular Microbiology & Immunology, Saint Louis University School of Medicine, St. Louis, MO, USA

5 Immunology and Molecular Pathogenesis Program, Emory University, Atlanta, GA, USA

*Corresponding author. Tel: +1 404 712 8420; Fax: +1 404 727 1300; E-mail: roberto.pacifici@emory.edu

homeostasis and tolerance [25]. Accordingly, defects in Treg numbers and/or activity have been implicated in several chronic inflammatory diseases. Moreover, Tregs have furthermore been found blunt bone resorption [26,27], prevent ovariectomy-induced bone loss [28], and regulate osteoclast formation [26,29,30].

In vitro, conventional CD4⁺ T cells differentiate into Tregs by TCR stimulation under the influence of TGFβ and IL-2 [31–33]. Recently, IGF-1 has been recognized as an additional inducer of Tregs [34,35]. Since iPTH increases TGFβ and IGF-1 production in bone [36–38], it is likely that iPTH may induce and/or expand BM Tregs.

This study was designed to investigate the effects of iPTH on Treg formation and activity in humans and mice, and to determine whether Tregs play a role in the bone anabolic activity of iPTH in mice. We report that treatment with iPTH increases the number of Tregs in humans and mice. In rodents, an increase in the number of Tregs is required for iPTH to exert its bone anabolic activity.

Results

Teriparatide treatment increases the number of Tregs in human peripheral blood

The PTH fragment Teriparatide is the only approved bone anabolic treatment for osteoporosis but its intricate mechanism of action remains largely unknown. Among the pleiotropic effects of PTH is the capacity to increase the production of TGFβ1 and IGF-1 by human osteoblasts [39–41], factors which induce Treg differentiation. To investigate whether Teriparatide regulates the number of Tregs in humans, 40 Italian women afflicted by PMO of similar age and years since menopause were enrolled in a 6-month-long prospective clinical trial. Twenty of the 40 women were treated with calcium and vitamin D (control treatment), while the remaining 20 women were treated with calcium, vitamin D, and human PTH 1-34 (Teriparatide), a treatment modality referred to hereafter as Teriparatide treatment. The baseline demographic characteristics of the study population and the serum levels of calcium, PTH, and 25-hydroxy vitamin D are shown in Table 1. Peripheral blood mononuclear cells (PBMCs) were obtained at baseline and 3 and 6 months of treatment. Analysis by flow cytometry revealed that Teriparatide treatment increased the absolute and relative number of Tregs (CD4⁺CD25⁺Foxp3⁺ cells) in human PBMC at 3 and 6 months of treatment, compared to baseline (Fig 1A and B). By contrast, treatment with calcium and vitamin D did not alter the number of Tregs during the 6 months of the study. As a result, both at 3 and 6 months the absolute and relative number of Tregs in PBMC was higher in women treated with Teriparatide than in those in the calcium and vitamin D control group.

TGFβ1 not only is a critical inducer of Treg differentiation, but is also an important product of Tregs that contributes to suppress effector T cells *in vivo* [25,42]. Production of TGFβ1 by Tregs is therefore an indicator of Treg function. To determine if Teriparatide regulates the function of Tregs, we measured the level of TGFβ1 mRNA in sorted peripheral blood CD4⁺CD25⁺ T cells from the last 18 women enrolled in the trial. We selected this cell population because most CD4⁺CD25⁺ T cells are Foxp3⁺ Tregs, while measurements of TGFβ1 mRNA in Tregs sorted by Foxp3 staining is

Table 1. Demographic and clinical data of patients with postmenopausal osteoporosis treated with calcium and vitamin D, or calcium and vitamin D and teriparatide.

	Control	Teriparatide	P
n	20	20	
Age	68.5 ± 1.8	69.7 ± 1.6	0.535
Years since menopause	18.4 ± 2.1	20.8 ± 1.6	0.232
Ca (mg/dl) [8.8–10.4 mg/dl]	9.6 ± 0.1	9.5 ± 0.1	0.851
Serum P (mg/dl) [2.5–4.48 mg/dl]	3.5 ± 0.2	3.4 ± 0.1	0.608
PTH (pg/ml) [10–65 pg/ml]	42.8 ± 9.3	46.8 ± 4.1	0.272
25OH vitamin D (ng/ml) [20–100 ng/ml]	30.2 ± 3.1	27.3 ± 2.7	0.997

Data are shown as mean ± SEM, and P values were calculated by unpaired t-test. Values in squared parenthesis denote normal range.

not feasible due to the loss of cell viability caused by intracellular staining. We found that the level of TGFβ1 mRNA in this Treg-enriched population was higher in the Teriparatide-treated group than in the control group (Fig 1C). *Post hoc* analysis showed that TGFβ1 mRNA levels were higher at 3 months than at baseline in the Teriparatide-treated group. Moreover, at 6 months TGFβ1 mRNA levels were higher in the Teriparatide-treated group than in the control group. Together, these findings demonstrate that Teriparatide treatment expands the number and the activity of circulating human Tregs.

To determine whether Teriparatide targets Tregs directly or indirectly, human peripheral blood CD4⁺CD25⁺ T cells were stimulated *in vitro* with anti-CD3 Ab and IL-2 for 6 days. Vehicle or Teriparatide were added every 2 days for 1 or 24 h. Analysis by flow cytometry revealed that Teriparatide did not increase the relative number of Tregs (CD4⁺CD25⁺Foxp3⁺ cells) in cultures of peripheral blood CD4⁺CD25⁺ T cells (Fig 1D), suggesting that Teriparatide regulates the number of Tregs via indirect mechanisms. We also found that *in vitro* stimulation with Teriparatide does not increase the expression of TGFβ mRNA in sorted peripheral blood CD4⁺CD25⁺ T cells (Fig 1E), confirming that Teriparatide does not directly target Tregs.

iPTH treatment in mice expands the pool of BM Tregs by increasing Treg differentiation

As in human cells, *in vitro* PTH stimulation increases in production of TGFβ1 and IGF-1 by murine osteoblasts [36–38]. However, the effects of iPTH treatment on the production of these factors are largely unknown. To investigate this matter, 6-week-old mice were treated with vehicle or iPTH for 2 weeks. BM was then harvested and cultured for 24 h. ELISAs revealed that iPTH significantly increases the levels of TGFβ1 and IGF-1 in the whole BM culture media (Appendix Fig S1A and B), suggesting that iPTH may regulate Treg differentiation.

To investigate the effect of iPTH treatment on the number of BM Tregs, 6-week-old mice were treated with vehicle or iPTH for 1, 2, or 4 weeks. BM was then harvested and stained for TCRβ, CD4, and Foxp3. iPTH treatment increased the relative and absolute number of BM Tregs (TCRβ⁺CD4⁺Foxp3⁺ cells) during the entire study

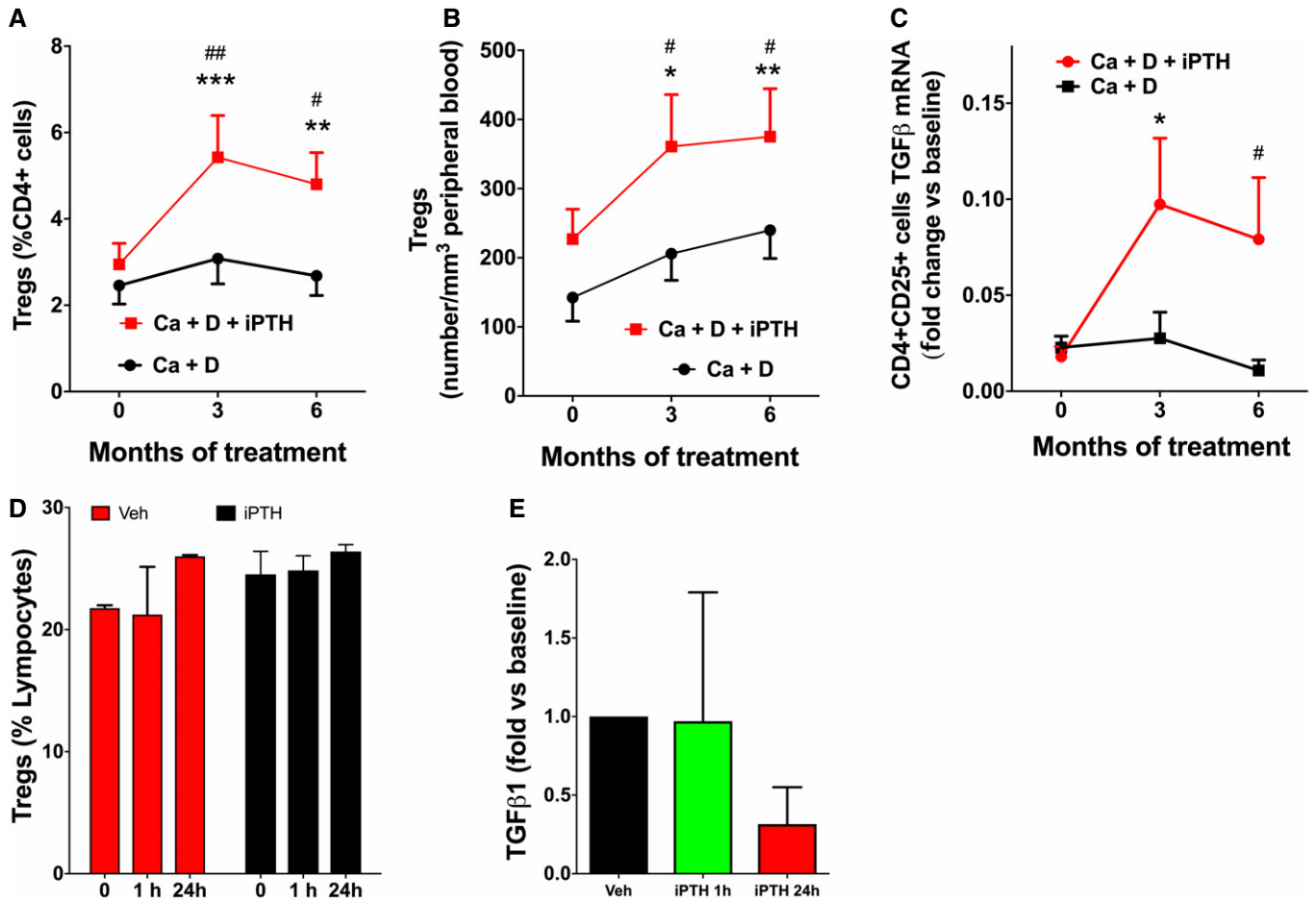


Figure 1. Teriparatide treatment in humans increases the absolute and relative number of Tregs in peripheral blood and TGFβ expression by Tregs.

- A Relative frequency of Tregs in PBMC at 3 and 6 months of treatment. $n = 20$ patients per group.
 B Absolute frequency of Tregs in PBMC at 3 and 6 months of treatment. $n = 20$ patients per group.
 C mRNA levels of TGFβ1 in peripheral blood CD4⁺CD25⁺ T cells at 3 and 6 months of treatment. $n = 9$ patients per group.
 D Relative frequency of Tregs in cultures of peripheral blood CD4⁺CD25⁺ T cells stimulated with vehicle or PTH.
 E mRNA levels of TGFβ1 in peripheral blood CD4⁺CD25⁺ T cells stimulated with vehicle or PTH.

Data information: All data are expressed as mean \pm SEM. All data were normally distributed according to the Shapiro–Wilk normality test and analyzed by two-way ANOVA for repeated measures. $*P < 0.05$, $**P < 0.01$, and $***P < 0.001$ compared to baseline. $^{\#}P < 0.05$ and $^{\#\#}P < 0.01$, compared to Ca + D group.

period (Fig 2A and B). The increase in absolute number of BM Tregs was already significant at 1 week of iPTH treatment, peaked at 2 weeks, and remained significantly increased at 4 weeks of treatment. By contrast, iPTH did not increase the number of splenic, thymic, and intestinal Tregs (Appendix Fig S2A–E).

iPTH could expand the pool of BM Tregs via multiple mechanisms including increasing the differentiation of conventional CD4⁺ T cells into Tregs or the proliferation of Tregs within the BM. To gain mechanistic insights, we determined the effects of iPTH on Treg differentiation, which is defined as the induction of Foxp3 expression in CD4⁺Foxp3⁻ T cells [25]. For this purpose, we made use of B6.Foxp3.eGFP reporter mice, a strain in which eGFP expression is co-expressed with Foxp3 and restricted to CD4⁺ T cells. Conventional CD4⁺ T cells (CD4⁺eGFP⁻) were FACS-sorted from the spleens of B6.Foxp3.eGFP reporter mice and transferred into TCRβ^{-/-} mice, a strain lacking αβ T cells. After 2 weeks, a length of time sufficient for the engraftment and expansion of donor T cells,

recipient mice were treated with vehicle or iPTH for 1–4 weeks. We then determined the number of CD4⁺eGFP⁺ cells in the BM by flow cytometry. Treatment with iPTH increased the relative and the absolute number of CD4⁺eGFP⁺ cell in the BM at 1, 2, and 4 weeks of treatment (Fig 2C and D), demonstrating that iPTH increases the differentiation of BM Tregs. Additional studies that used BrdU incorporation to measure proliferation revealed that iPTH treatment for 1, 2, or 4 weeks does not increase BM Treg proliferation (Appendix Fig S2F). In an additional set of experiments, Tregs (CD4⁺eGFP⁺ cells) were FACS-sorted from the spleens of B6.Foxp3.eGFP reporter mice and transferred into TCRβ^{-/-} mice. Recipient mice were treated with vehicle or iPTH for 2 weeks, starting the day of the Treg transfer. This design was selected to minimize the confounding effect of the partial loss of Foxp3 expression by CD4⁺eGFP⁺ cells, which may occur after Treg transfer into lymphopenic host mice [43]. These studies revealed that iPTH does not affect the relative and the absolute number of CD4⁺eGFP⁺ cells

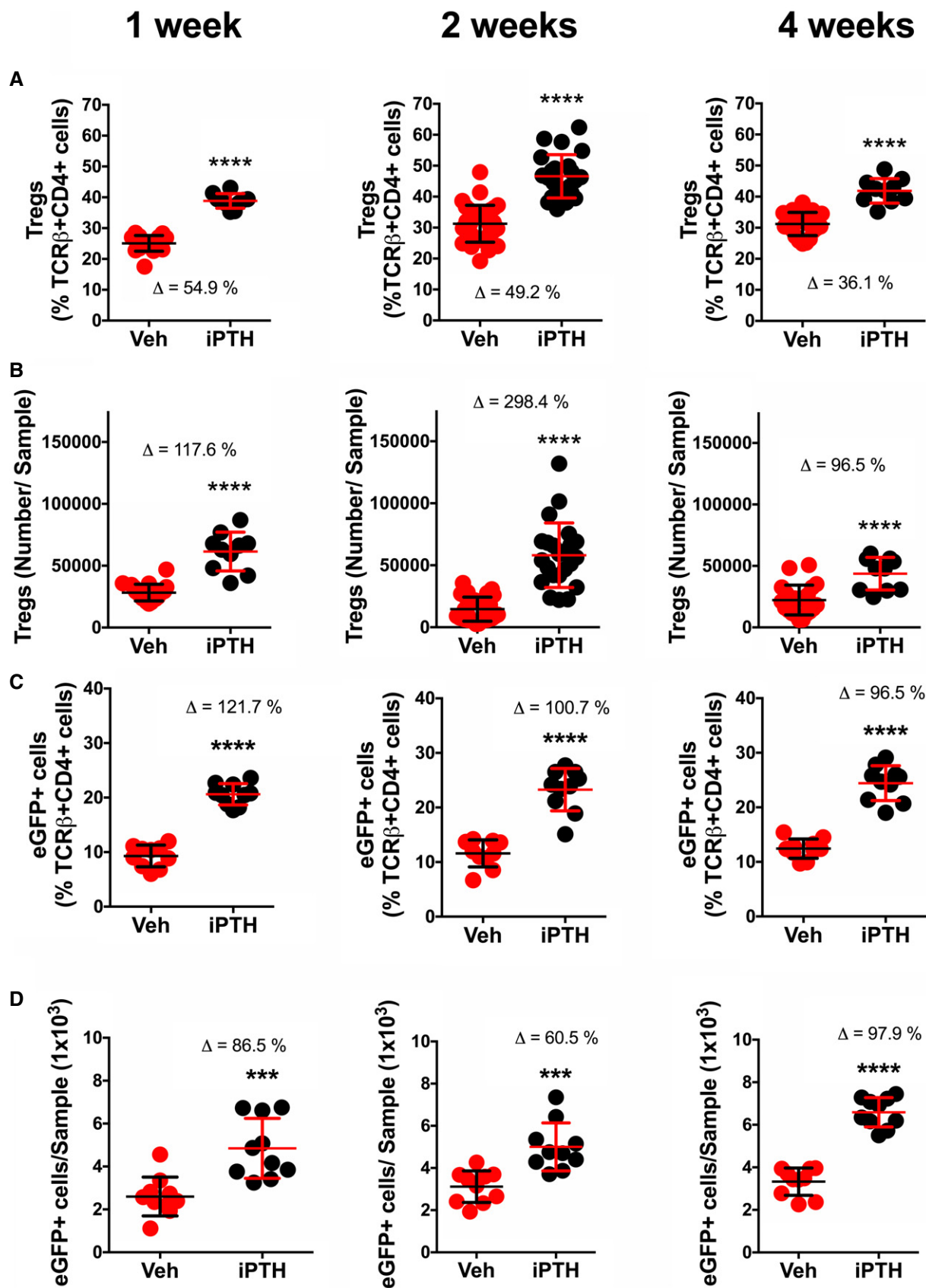


Figure 2.

Figure 2. iPTH treatment increases the number of BM Tregs and Treg differentiation.

To determine the effect of treatment on the number of Tregs, BM $\text{TCR}\beta^+\text{CD4}^+\text{Foxp3}^+$ T cells were counted by flow cytometry following 1, 2, and 4 weeks of treatment with vehicle or iPTH. To assess Treg differentiation, conventional CD4^+ T cells ($\text{TCR}\beta^+\text{CD4}^+\text{eGFP}^-$) from B6.Foxp3.eGFP reporter mice were transferred into $\text{TCR}\beta^{-/-}$ mice. Recipient mice were treated with vehicle or iPTH for 1, 2, or 4 weeks starting 2 weeks after the T-cell transfer. The number of BM $\text{TCR}\beta^+\text{CD4}^+\text{eGFP}^+$ cells was then determined by flow cytometry.

A Relative frequency of BM Tregs at 1, 2, and 4 weeks of treatment. $n = 10$ –32 mice per group.

B Absolute frequency of Tregs at 1, 2, and 4 weeks of treatment. $n = 10$ –32 mice per group.

C Relative frequency of eGFP⁺ Tregs at 1, 2, and 4 weeks of treatment $n = 10$ mice per group.

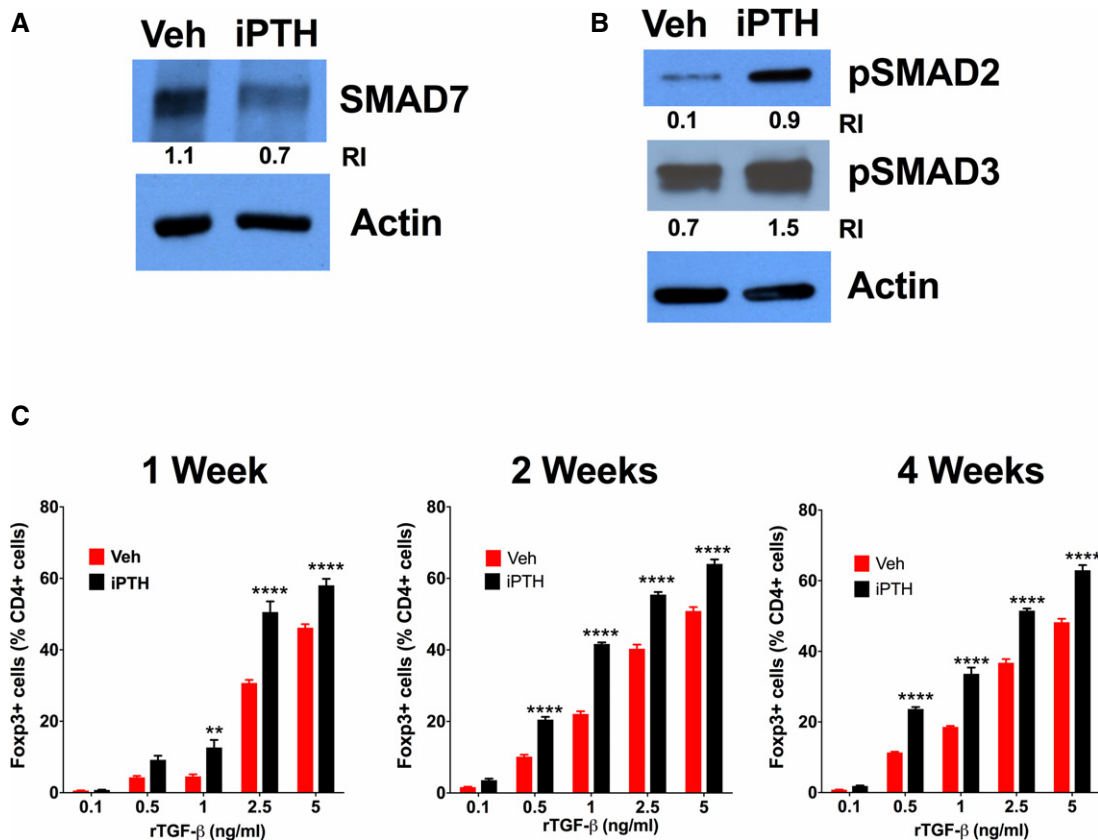
D Absolute frequency of eGFP⁺ Tregs at 1, 2, and 4 weeks of treatment $n = 10$ mice per group.

Data information: Data are expressed as mean \pm SEM. All data were normally distributed according to the Shapiro–Wilk normality test and analyzed by unpaired *t*-tests. *** $P < 0.001$, and **** $P < 0.0001$ compared to the corresponding vehicle.

residing in the BM and the spleen (Appendix Fig S2G–J). These findings, together with a lack of an effect of iPTH on Treg proliferation, indicate that iPTH does not alter the homing of Tregs to the spleen and the BM.

In addition to increasing the BM levels of TGF β and IGF-1 [36–38], iPTH enhances the sensitivity of conventional CD4^+ cells to TGF β . This was disclosed by experiments in which unstimulated splenic $\text{CD4}^+\text{CD25}^-$ cells purified from iPTH-treated mice were

found to express lower levels of the negative regulator of TGF β signaling SMAD7 as compared to $\text{CD4}^+\text{CD25}^-$ cells from vehicle-treated mice (Fig 3A). To ascertain the functional relevance of this finding, splenic $\text{CD4}^+\text{CD25}^-$ cells from vehicle- or iPTH-treated mice were stimulated *in vitro* with CD3/CD28 Ab, IL-2, and TGF β at 2.5 ng/ml for 72 h to induce their differentiation into Tregs [44]. Measurements of phosphorylated SMAD2 and SMAD3 (pSMAD2 and pSMAD3) at the end of the culture period revealed higher

**Figure 3. iPTH treatment increases the sensitivity of conventional CD4^+ T cells to TGF β .**

A Western blotting analysis of SMAD7 levels in unstimulated splenic conventional CD4^+ cells. Data are from 1 representative experiment of a total of four experiments. R.I., relative intensity.

B Western blotting analysis of pSMAD2 and pSMAD3 levels in splenic conventional CD4^+ T cells stimulated with anti-CD3/CD28 Ab, IL-2, and recombinant TGF β 1 (rTGF β 1) at 2.5 ng/ml for 72 h to induce their differentiation into Tregs. Data are from one representative experiment of a total of four experiments. R.I., relative intensity.

C Relative frequency (mean \pm SEM) of Foxp3⁺ Tregs in cultures of conventional CD4^+ T cells stimulated with anti-CD3/CD28 Ab, IL-2, and increasing doses of rTGF β 1. Splenic conventional CD4^+ T cells were obtained after 1, 2, and 4 weeks of treatment with vehicle or iPTH. $n = 10$ mice per group. Data were analyzed by two-way ANOVA and *post hoc* tests applying the Bonferroni correction for multiple comparisons. ** $P < 0.01$ and **** $P < 0.0001$ compared to vehicle.

concentrations of pSMAD2 and pSMAD3 (Fig 3B) in cells from iPTH-treated mice as compared to those from control mice, suggesting that conventional CD4⁺ T cells from iPTH-treated mice have a higher sensitivity to TGFβ. To confirm this hypothesis, splenic CD4⁺CD25⁻ cells were purified from vehicle- or iPTH-treated mice and then cultured *in vitro* for 72 h with anti CD3/CD28 Ab, IL-2, and increasing doses of TGFβ (0.1–5 ng/ml). At each dose of TGFβ, cultures of CD4⁺CD25⁻ T cells from iPTH-treated mice yielded a greater percentage of Foxp3⁺ Tregs than those from vehicle-treated mice (Fig 3C). Together, these findings indicate that CD4⁺ T cells from iPTH-treated mice possess a greater sensitivity to TGFβ, which results in enhanced differentiation of CD4⁺ T cells into Tregs.

An increase in the number of Tregs is required for iPTH to induce bone anabolism in mice

A direct means to investigate the contribution of Tregs to the anabolic activity of iPTH is to assess the effects of iPTH in a model in which the increase in the frequency of Tregs is prevented. The surface marker CD25 is expressed at high levels by most CD4⁺ Foxp3⁺ Tregs [45]. Accordingly, treatment with anti-CD25 Abs capable of deleting CD25^{hi} is used to partially deplete Tregs *in vivo* [46,47]. We thus treated 6-week-old mice with vehicle or iPTH (days 1–28) plus four injections (days -2, 0, 5, and 7) of isotype control Ab or the anti-CD25 Ab PC61 [46,47]. We found CD25^{hi} to be expressed by CD4⁺ T cells and by a negligible fraction of CD8⁺ T cells (Appendix Fig S3A). Anti-CD25 Ab decreased the frequency of CD25^{hi} CD4⁺ T cells but not that of CD25^{lo} CD4⁺ T cells. As previously reported [48], we also found that treatment with anti-CD25 Ab decreased the number of CD25^{hi}Foxp3⁺CD4⁺ T cells, but not the number of CD25^{lo}Foxp3⁻CD4⁺ T cells (Appendix Fig S3B). In addition, treatment with anti-CD25 Ab did not decrease the percentage of BM of conventional CD4⁺ T cells (TCRβ⁺CD4⁺CD25⁺Foxp3⁻ cells) and that of CD8⁺ T cells (TCRβ⁺CD8⁺CD25⁺ cells) (Appendix Fig S3C–F). Together, these findings demonstrate that anti-CD25 Ab specifically depletes Tregs.

At sacrifice control mice treated with anti-CD25 Ab had ~37% fewer Tregs than mice treated with irrelevant (Irr.) Ab (Fig 4A and B). Moreover, treatment with anti-CD25 Ab prevented the increase in BM Tregs induced by iPTH. The partial depletion of Tregs

induced by anti-CD25 Ab did not increase the production of inflammatory and lineage-specific cytokines in the BM. In fact, in both the vehicle- and iPTH-treated groups, BM cells from mice treated with anti-CD25 Ab expressed similar levels of TNF, IL-17A, IL-6, IL-4, and IL-13 mRNAs to those from mice treated with Irr. Ab (Appendix Fig S4). Moreover, iPTH lowered the mRNA levels of IFNγ, in both the Irr. Ab and the anti-CD25 Ab groups but did not affect the other cytokines. Since inflammatory cytokines blunt bone formation [49], these findings indicate treatment with anti-CD25 Ab does not alter the bone anabolic activity of iPTH by inducing inflammation. Analysis by *in vitro* μCT of femurs harvested at sacrifice revealed that iPTH induced a significant increase in trabecular bone volume (BV/TV) in mice treated with Irr. Ab (Fig 4C and D), but not in those treated with anti-CD25 Ab. Trabecular thickness (Tb.Th), trabecular number (Tb.N), and trabecular space (Tb.Sp), which are indices of trabecular structure, were altered by iPTH in mice treated with Irr. Ab, but not in those treated with anti-CD25 Ab (Appendix Fig S5A–C). By contrast, iPTH increases cortical volume (Ct.Vo) (Fig 4C and E) and cortical thickness (Ct.Th) (Appendix Fig S5D) in both groups of mice, confirming that T cells are not implicated in the mechanism by which iPTH increases cortical volume. Together, these findings demonstrate that the anabolic effects of iPTH in trabecular bone are dependent on increased numbers of Tregs.

Analysis of femoral cancellous bone by histomorphometry revealed that iPTH increased the dynamic indices of bone formation mineral apposition rate (MAR) and bone formation rate (BFR/BS) in Treg-replete mice but not in those treated with anti-CD25 Ab (Fig 4F–H). Moreover, iPTH increased two static indices of bone formation, the number of osteoblasts per bone surface (N.Ob/BS) (Fig 4I) and the percentage of surfaces covered by osteoblasts (Ob.S/BS) (Fig 4J) in Treg-replete mice but not in those treated with anti-CD25 Ab. The finding that treatment with anti-CD25 Ab did not decrease bone formation in vehicle-treated mice provides evidence that partial Treg depletion does not cause a nonspecific inhibitory effect of on bone formation. Two indices of bone resorption, the number of OCs per bone surface (N.Oc/BS) and the percentage of surfaces covered by OCs (Oc.S/BS), were not affected by iPTH (Fig 4K–M) in both control and Treg-depleted groups. However, N.Oc/BS was higher in mice treated with iPTH and anti-CD25 Ab, as

Figure 4. Depletion of Tregs by treatment with anti-CD25 Ab prevents the bone anabolic activity of iPTH.

- A, B Relative and absolute frequency of BM Tregs.
- C Images of representative three-dimensional μCT reconstructions of examined femurs from each group.
- D Femoral trabecular bone volume (BV/TV) as measured by μCT scanning.
- E Femoral cortical bone volume (Ct.Vo) by μCT scanning
- F Images are representative sections displaying the calcein double-fluorescence labeling. Original magnification 20×. Scale bar represents 300 μm.
- G Mineral apposition rate (MAR).
- H Bone formation rate per mm bone surface (BFR/BS).
- I The number of osteoblasts per mm bone surface (N.Ob/BS).
- J The percentage of bone surface covered by osteoblasts (Ob.S/BS).
- K The images show tartrate-resistant acid phosphatase (TRAP)-stained sections of the distal femur. Original magnification 40×. Scale bar represents 300 μm.
- L The number of osteoclasts per mm bone surface (N.Oc/BS).
- M The percentage of bone surface covered by osteoclasts (Oc.S/BS).
- N Serum levels of osteocalcin (OCN), a marker of bone formation.
- O Serum levels of type 1 cross-linked C-telopeptide (CTX), a marker of resorption.

Data information: *n* = 10–25 mice per group. Data are expressed as mean ± SEM. All data were normally distributed according to the Shapiro–Wilk normality test and analyzed by two-way ANOVA and *post hoc* tests applying the Bonferroni correction for multiple comparisons. **P* < 0.05, ***P* < 0.01, ****P* < 0.001, and *****P* < 0.0001 compared to the indicated group.

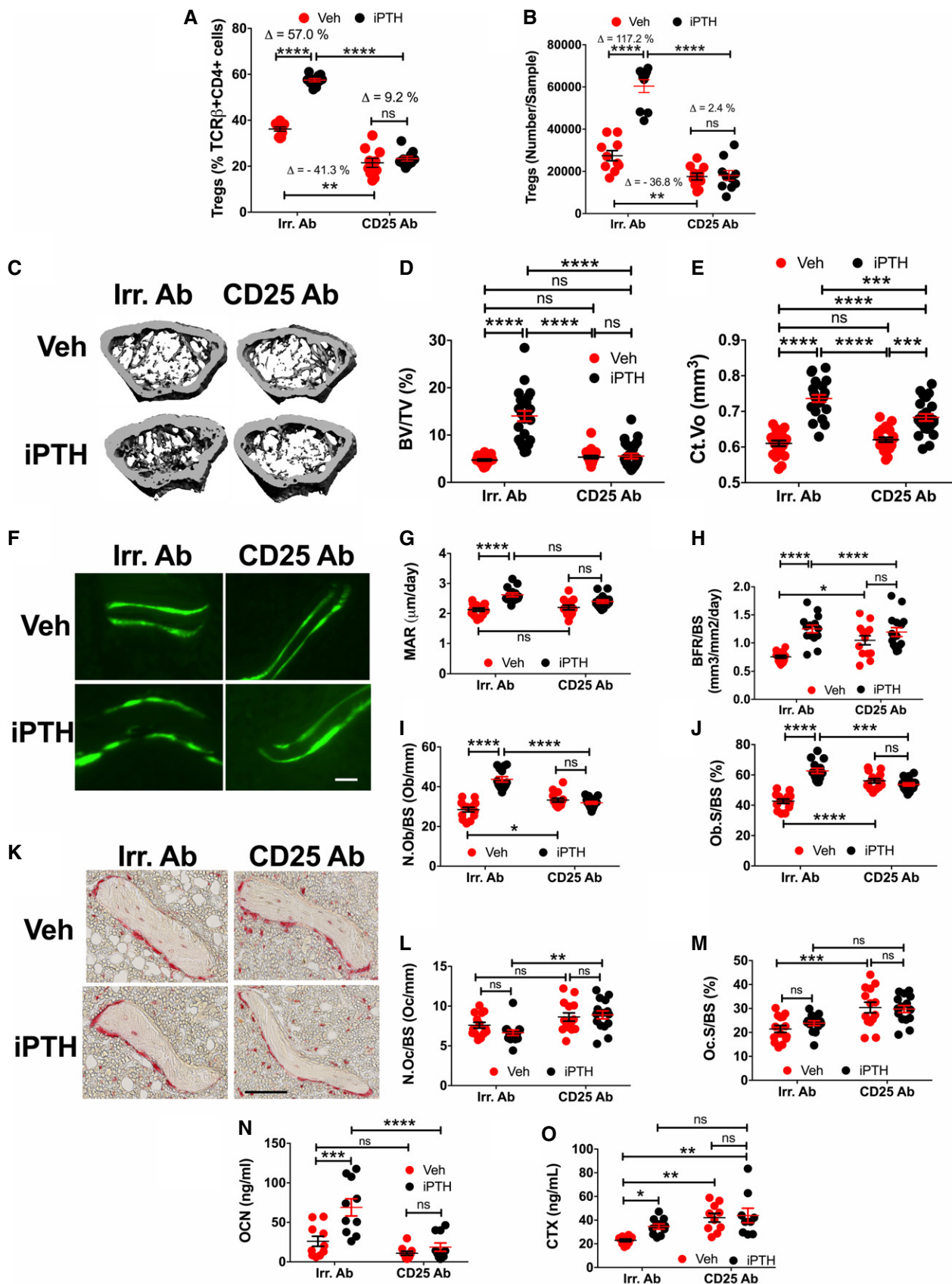


Figure 4.

compared to those treated with iPTH and Irr. Ab, suggesting that Treg depletion may stimulate bone resorption.

Measurements of serum levels of osteocalcin, a marker for bone formation, revealed that iPTH increased bone formation in mice treated with Irr. Ab but not in those treated with anti-CD25 Ab (Fig 4N). Serum CTX, a marker for bone resorption, also increased significantly in response to iPTH in mice treated with Irr. Ab but not in those injected with anti-CD25 Ab (Fig 4O). Moreover, mice treated with anti-CD25 Ab had higher CTX levels than those treated with Irr. Ab, confirming that Treg depletion is associated with an increase in bone resorption. The differences between the CTX data and histomorphometric indices of bone resorption are explained by the fact that CTX reflects cortical and trabecular bone resorption, while the histomorphometric analysis was limited to the trabecular compartment.

To determine the role of Tregs in mediating the effects of iPTH on osteoblastogenesis, BM was harvested at sacrifice and cultured for 1 week to allow SCs to proliferate. SCs were then purified and counted. This analysis revealed that iPTH treatment increases the number of SCs in samples from mice treated with Irr. Ab while it had no effects in those treated with anti-CD25 Ab (Fig 5A). To investigate the mechanism involved, BM was cultured for 1 week, and SCs were purified and used to determine their rate of proliferation and apoptosis. These experiments revealed that iPTH increases significantly the proliferation of SCs from mice treated with Irr. Ab, while it had no effect on the proliferation of SCs from mice treated with anti-CD25 Ab (Fig 5B). iPTH decreased the rate of SC apoptosis in mice treated with Irr. Ab, while it had no effect on SC apoptosis in mice treated with anti-CD25 Ab (Fig 5C). Analysis of the expression levels of osteoblastic genes in SCs revealed that iPTH treatment increased the expression of type 1 collagen (Col1), runt-related transcription factor 2 (Runx2), osterix (Osx), bone sialoprotein (BSP), and osteocalcin (Ocn) mRNAs in SCs from mice treated with Irr. Ab, while it had no effect on SCs from mice treated with anti-CD25 Ab (Fig 5D). These findings demonstrate that iPTH regulates osteoblast proliferation, differentiation, and life span through a Treg-dependent mechanism.

To further investigate the relevance of Tregs for the anabolic activity of iPTH, experiments were conducted utilizing DEREg mice [50], a strain that expresses a fusion protein of the human diphtheria toxin (DT) receptor (hDTR) and eGFP under control of the Foxp3 promoter. Foxp3⁺ Tregs can be selectively depleted upon DT administration to DEREg mice, since WT mice do not express the hDTR receptor and are thus insensitive to DT. DT is known not to cause toxic effects in mice [51]. While Treg ablation in DEREg mice causes scurfy-like symptoms in newborn animals, older mice do not develop autoimmune diseases [50,51] as DT treatment of older DEREg mice causes a partial Treg depletion [52] and the residual Treg population is sufficient to prevent disease in adult mice [52]. We treated 6-week-old mice with DT (1 µg/mouse, i.p. two times per week for 4 weeks), a treatment modality titrated to block the increase in Tregs induced by iPTH. Mice were also treated with vehicle or iPTH for 4 weeks starting after the first two DT injections. Controls included DEREg mice not treated with DT and WT littermate (LM) mice treated with DT. Analysis of BM samples harvested at sacrifice revealed that iPTH had expanded Tregs in control mice but not in DEREg + DT mice (Fig 6A and B). As expected, analysis of vehicle-treated groups showed that DEREg + DT mice had a lower absolute and relative numbers of Tregs as compared to control groups. Analysis by µCT of femurs harvested at sacrifice

revealed that iPTH induced a significant increase in BV/TV in the two control groups but not in DT-treated DEREg mice (Fig 6C and D). Analysis of distal femurs also revealed that Tb.Th, Tb.N, and Tb.Sp were differentially altered by iPTH in Treg-replete and Treg-depleted mice (Appendix Fig S5E–G). By contrast, iPTH increased Ct.Vo (Fig 6C and E) and cortical thickness (Ct.Th) (Appendix Fig S5H) in all groups of mice. Together, these findings confirmed that the anabolic effects of iPTH in trabecular bone are dependent on increased numbers of Tregs.

Analysis of femoral cancellous bone by histomorphometry revealed that iPTH increased the dynamic indices of bone formation MAR and BFR/BS in the two control groups but not in DT-treated DEREg mice (Fig 6F–H). N.Ob/BS and Ob.S/BS, which are static indices of bone formation, were also increased by iPTH in DEREg mice and littermate controls but not in DEREg + DT mice (Fig 6I and J). Two indices of bone resorption, N.Oc/BS and Oc.S/BS, were similar in all groups of mice (Fig 6K–M). Analysis of biochemical markers of bone turnover revealed that iPTH increased serum level of osteocalcin and CTX in control mice but not on Treg-depleted mice (Fig 6N and O), confirming that the increase in the number of BM Treg is required for iPTH to increase bone turnover. In vehicle-treated mice, serum CTX was higher in Treg-depleted mice than in Treg-replete controls, confirming that Treg depletion leads to a stimulation of bone resorption.

Discussion

iPTH treatment is an approved bone anabolic treatment for osteoporosis but its intricate mechanism of action remains largely unknown. We report that *in vivo* iPTH treatment increases the number of BM Tregs in mice. The increase in the BM Treg pool is essential for the bone anabolic activity of iPTH. The increase in the number of Tregs is due to enhanced differentiation of peripherally induced Tregs, a phenomenon driven by the capacity of iPTH to upregulate the levels of TGFβ and IGF-1 in the BM and to increase the sensitivity of naïve CD4⁺ cells to TGFβ.

To translate our findings in humans, we measured the absolute and relative frequency of Tregs in the peripheral blood of osteoporotic women treated with Teriparatide, a form of iPTH treatment. We found that Teriparatide increases the number of Tregs at 3 and 6 months of treatment. Teriparatide also increases TGFβ1 mRNA levels, an indicator of Treg activity. By contrast, we found that *in vitro* treatment of Tregs with PTH does not affect the number of Tregs and TGFβ production, indicating that iPTH regulates human Tregs indirectly.

Tregs are a suppressive population of predominantly CD4⁺ T cells that play a critical role in maintaining immune tolerance and immune homeostasis. Accordingly, defects in Treg numbers and/or activity have been implicated in several chronic inflammatory diseases. Tregs are also known to regulate osteoclast formation [26,29,30], blunt bone resorption [26,27], and prevent ovariectomy-induced bone loss [28]. However, CD4⁺Foxp3⁺ Tregs have not been previously reported to stimulate bone formation, and iPTH treatment was not known to regulate the number of BM Tregs.

Our findings demonstrate that one mechanism by which iPTH expands murine BM Tregs is enhanced differentiation of peripherally induced Tregs. We also found iPTH not to alter Treg

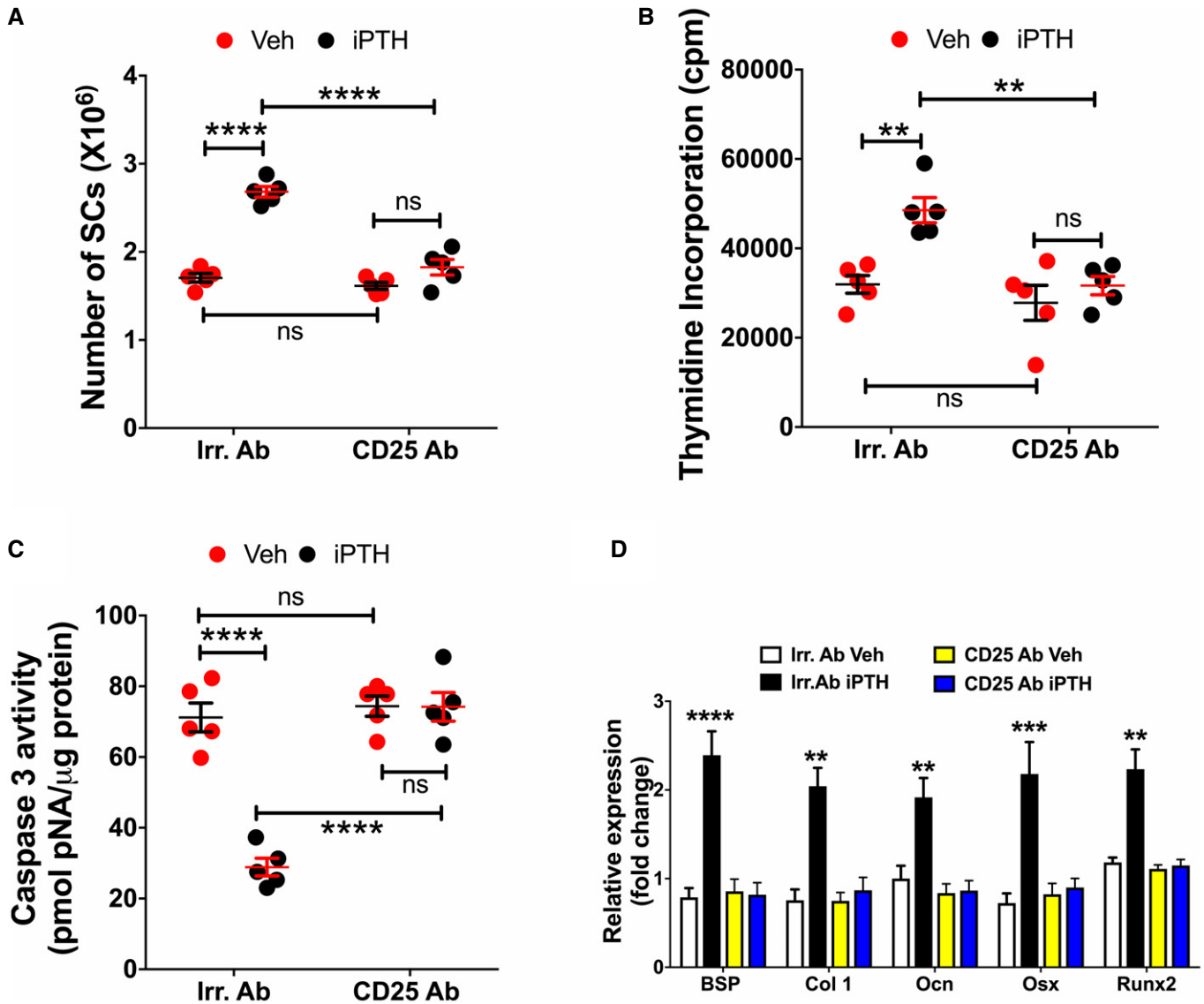


Figure 5. Depletion of Tregs by treatment with anti-CD25 Ab blocks the effects of iPTH on SC number, proliferation, apoptosis, and expression of osteoblast differentiation genes.

A BM harvested at sacrifice was cultured for 1 week and SCs purified and counted.

B SCs were purified from BM cultured for 1 week, seeded in equal number, and pulsed with [3 H]-thymidine for 18 h, to assess their proliferation. Data are expressed in CPM.

C SCs were purified from BM cultured for 1 week and the rate of apoptosis quantified by determinations of caspase-3 activity.

D SCs were purified from BM, cultured for 1 week and the level of OB marker genes, bone sialoprotein (BSP), type I collagen (Col1), osteocalcin (Ocn), osterix (Osx), and runt-related transcription factor 2 (Runx2) analyzed by RT-PCR.

Data information: Data are expressed as mean \pm SEM. $n = 5$ mice per group. All data were analyzed by two-way ANOVA and *post hoc* tests applying the Bonferroni correction for multiple comparisons. ** $P < 0.01$, *** $P < 0.001$, and **** $P < 0.0001$ compared to the indicated group or Irr. Ab vehicle.

proliferation and homing to the BM. Whether additional mechanisms, such as increased life span, contribute to the numeric increase in BM Tregs remains to be determined.

PPR is expressed by conventional CD4⁺ cells and CD8⁺ cells but not by Tregs. On the other hand, iPTH upregulates the BM levels of TGF β and IGF-1, factor capable of inducing Treg differentiation *in vitro* [31–35]. Therefore, iPTH is likely to induce murine Treg differentiation indirectly.

In the mouse, iPTH treatment for 4 weeks did not increase the number of Tregs in the spleen, thymus, and intestinal wall, suggesting that a treatment period longer than 4 weeks might be required for iPTH to expand Tregs in peripheral blood and lymphoid organs, a hypothesis supported by our findings in humans at 3 and 6 months of treatment. It is also likely that the increase in Tregs induced by iPTH occurs first in the BM because of environmental cues. iPTH increases the osteoblastic production of TGF β and the

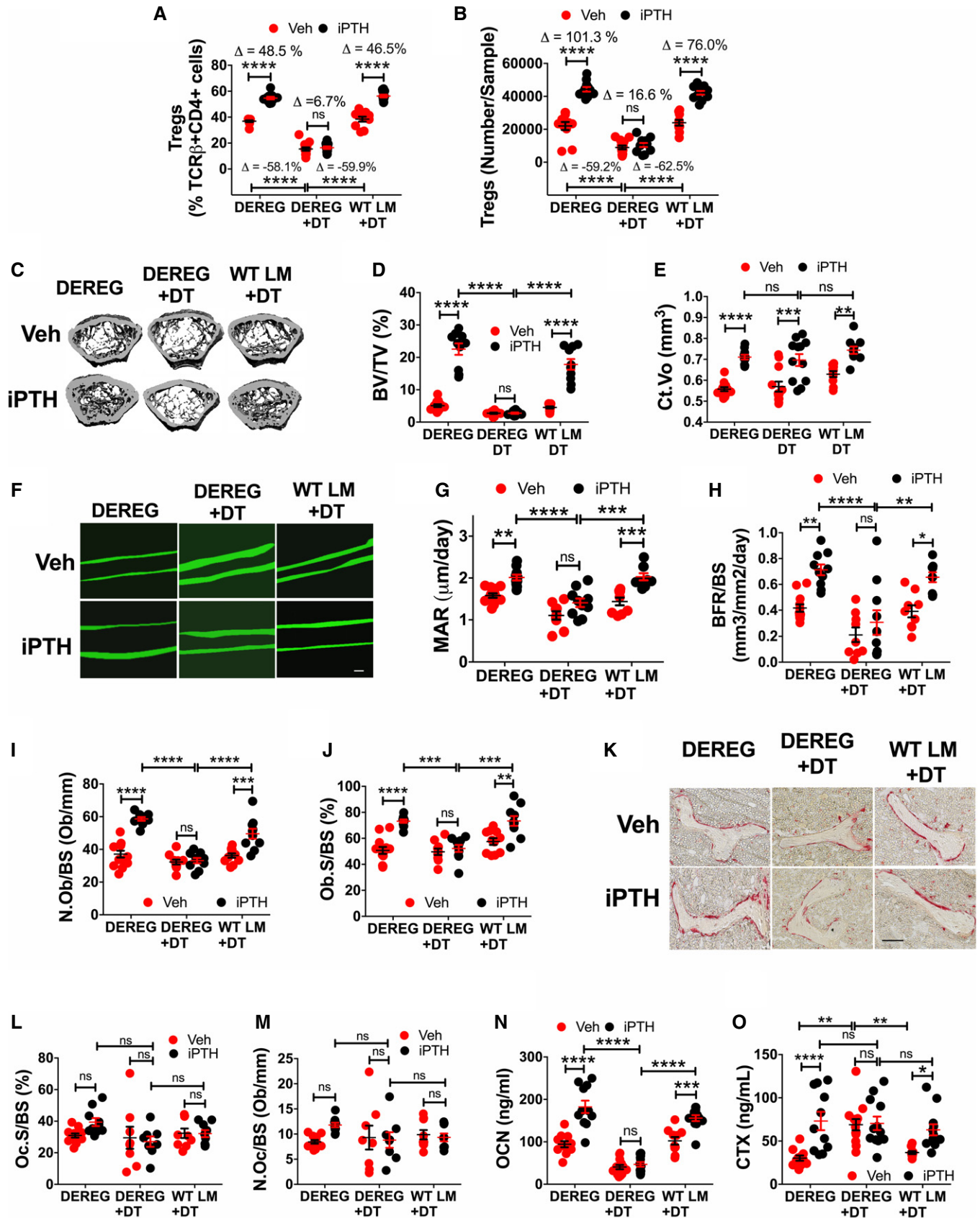


Figure 6.

Figure 6. Depletion of Tregs by treatment of DERE mice with diphtheria toxin (DT) prevents the bone anabolic activity of iPTH.

- A, B Relative and absolute frequency of BM Tregs.
 C Images of representative three-dimensional μ CT reconstructions of examined femurs from each group.
 D Femoral trabecular bone volume (BV/TV) as measured by μ CT scanning.
 E Femoral cortical bone volume (Ct.Vo) by μ CT scanning.
 F Images are representative sections displaying the calcein double-fluorescence labeling. Original magnification 20 \times . Scale bar represents 300 μ m.
 G Mineral apposition rate (MAR).
 H Bone formation rate (BFR).
 I The number of osteoblasts per mm bone surface (N.Ob/BS).
 J The percentage of bone surface covered by osteoblasts (Ob.S/BS).
 K The images show tartrate-resistant acid phosphatase (TRAP)-stained sections of the distal femur. Original magnification 40 \times . Scale bar represents 300 μ m.
 L The number of osteoclasts per mm bone surface (N.Oc/BS).
 M The percentage of bone surface covered by osteoclasts (Oc.S/BS).
 N Serum levels of osteocalcin, a marker of bone formation.
 O Serum levels of type 1 cross-linked C-telopeptide (CTX), a marker of resorption.

Data information: $n = 9$ –13 mice per group. Data are expressed as mean \pm SEM. All data were normally distributed according to the Shapiro–Wilk normality test and analyzed by two-way ANOVA and *post hoc* tests applying the Bonferroni correction for multiple comparisons. * $P < 0.05$, ** $P < 0.01$, *** $P < 0.001$, and **** $P < 0.0001$ compared to the indicated group.

bone matrix is the largest reservoir of TGF β in the body [36,53]. iPTH also increases the osteoblastic production of IGF-1 [36,38]. It is thus likely that in the first 4 weeks of treatment the increase in the number of Tregs induced by iPTH is confined to the BM because of the higher levels of TGF β and IGF-1 present in the BM as compared to the spleen.

We have used two experimental models to assess the relevance of Tregs for the anabolic activity of iPTH in the mouse, depletion of Tregs in WT mice by treatment with anti-CD25 Ab, and depletion of Tregs in DERE mice by treatment with DT. Both strategies prevented the increase in the number of Tregs induced by iPTH. In both cases, blockade of the increase in the number of Tregs prevented the increases in bone formation and trabecular bone volume induced by iPTH, demonstrating that an enlargement of the pool of BM Tregs is required for iPTH to increase trabecular bone mass. By contrast, blockade of Tregs did not blunt the capacity of iPTH to increase cortical bone volume. These findings are in agreement with previous reports from our laboratory demonstrating that T cells do not contribute to iPTH-induced cortical bone anabolism [11,20,22]. We hypothesize that iPTH induces cortical bone anabolism primarily by regulating the osteocytic production of sclerostin.

Recently, there has been an explosion in research investigating the potential to manipulate Tregs for clinical purposes [54–58]. Among these studies are several phase I clinical trials to test whether boosting Treg numbers and/or function is a feasible, safe, and potentially effective way to treat diseases such as graft vs. host disease, type 1 diabetes and to prevent the rejection of transplanted organs [54–58]. Osteoporosis is a common chronic disorder that represents a major source of disability in the elderly. Novel anabolic treatments are needed because the long-term use of current antiresorptive agents is associated with significant adverse events and complications. An increase in the number of Treg is achievable by Treg transfer or treatment with mTOR inhibitors, self-antigens, or cytokines [59], and inhibition of CD28 costimulation (e.g. CTLA-4Ig). Based on our findings, pharmacological Tregs may represent a novel therapeutic modality for osteoporosis or for potentiating the anabolic activity of iPTH. Moreover, the use of iPTH to increase the number of Tregs may find applications in transplant medicine or as a treatment for inflammatory and autoimmune conditions.

Materials and Methods

Human study population

All human studies were approved by the Ethical Committee of the A.O.U. Città della Salute e della Scienza—A.O. Ordine Mauriziano—A.S.L. TO1, Turin, Italy, and informed consent was obtained from all participants. The study population was recruited from the patients of A.O.U. Città della Salute e della Scienza, Turin, Italy. The study population included 40 women affected by PMO. The demographic characteristics of the study population are shown in Table 1. The diagnosis of PMO was established based on WHO criteria [60]: the presence of secondary osteoporosis was ruled out by medical history, physic examination and blood examinations quantifying calcium, phosphorus, 25OH vitamin D, and PTH. Twenty patients were treated with calcium carbonate (1,000 mg/day) and cholecalciferol 800 UI/day (control treatment). The remaining twenty patients were treated with human PTH 1-34 (Teriparatide, Eli Lilly, Indianapolis) 20 μ g/day subcutaneously, calcium carbonate (1,000 mg/day), and cholecalciferol 800 UI/day. Patients in the Teriparatide group had prior fragility fractures, whereas those in the control treatment group had not, according to guide lines for PMO treatment of the Italian Health ministry. Blood samples (40 ml) were collected in EDTA-containing vacuum tubes at baseline and after 3 and 6 months of treatment.

Study design

No randomization procedure was used to assign humans and mice to experimental groups. All murine and human samples were analyzed in blinded fashion. The investigators analyzing the human samples were blind to the identity of the study participant, disease state, treatment status, and all other clinical variables. The investigators analyzing mouse samples were blind to the genotype and treatment group. Congenic WT mice or nontransgenic littermates were used as controls for transgenic mice.

Inclusion and exclusion criteria for the human study population

None of the subjects enrolled were affected by disease states affecting bone health other than PMO. Subjects affected by renal or

hepatic insufficiency or chronic inflammatory conditions such as rheumatoid arthritis, psoriasis, and inflammatory bowel disease were excluded, as these diseases are known to influence bone status. Subjects treated with drugs active on bone turnover such as bisphosphonates, denosumab, teriparatide, hormone replacement therapy, selective estrogen receptor modulator, strontium ranelate, glucocorticoids, androgens, or GnRH agonists for any length of time during the 6 months prior to enrollment were excluded.

Flow cytometric analysis of human samples

Peripheral blood mononuclear cells were purified from 40 ml blood obtained from all patients at each time point using the Ficoll–Paque gradient method, as previously described [61]. The Human Regulatory T-cell Staining Kit (eBioscience Inc., San Diego, CA, USA) was used in accordance with manufacturer's instructions to stain PBMCs for Tregs. Briefly, the following labeled monoclonal antibodies and corresponding isotype controls were used: anti-CD4 (FITC-conjugated), anti-CD25 (APC-conjugated), and anti-Foxp3 (PE-conjugated). After surface staining for CD4 and CD25, cells were washed, fixed, and permeabilized (Fix-Perm Buffer). Cells were then incubated with anti-Foxp3 for intra-nuclear staining. Flow cytometry was performed on an Accuri C6 flow cytometer (BD Biosciences).

Human T-cell immunomagnetic separation

Human CD4⁺CD25⁺ T cells were isolated from whole blood at each time point using The Complete Kit for Human CD4⁺CD25⁺ Regulatory T Cells, which includes RosetteSep CD4⁺ T Cell Enrichment Cocktail and EasySep Human CD25 Positive Selection Kit (STEMCELL Technologies, Auburn, CA, USA) according to the manufacturer's instructions. The purity of CD4⁺CD25⁺ T cells was 93–95% as assessed by flow cytometry.

Real-time RT–PCR and human primers

RT–PCR was used to evaluate the mRNA levels of TGFβ1 in CD4⁺CD25⁺ T cells. RNA was isolated using TRIzol reagent (Ambion, Huntingdon, UK), according to the manufacturer's protocol; 1 μg of RNA was reverse-transcribed to single-stranded cDNA using the High Capacity cDNA Reverse Transcription Kit (Applied-Biosystems). RT–PCR was performed with IQ SYBR Green Supermix (Bio-Rad). The housekeeping control gene was β-actin, and gene expression was quantified using the 2^{-ΔΔC_t} method. The primers used were as follows: 5'-CTCTCCGACCTGCCACAGA-3' (forward) and 3'-TCTCAGTATCCCACGGAAATAACC-5' (reverse) for TGFβ1; 5'-CCTAAAAGCCACCCCACTTCT-3' (forward) and 3'-CACCTCCCCTGTGTGGACTT-5' (reverse) for β-actin.

In vitro PTH treatment of human CD4⁺CD25⁺ T cells

Purified CD4⁺CD25⁺ T cells were cultured for 6 days in RPMI medium containing 10% fetal bovine serum (FBS), 1% penicillin streptomycin (Gibco, Thermo Fisher Scientific, MA, USA), with 500 U/ml rIL-2 (Tebu-bio srl, Milano, Italy) and 2 μg/ml anti-CD3 antibody (Biolegend, San Diego, CA, USA). Human PTH 1-34 (50 ng/ml) or control vehicle was added to the cultures for 1 h or 24 h for three times during the 6-day culture to mimic the anabolic

effects of intermittent PTH 1-34. Cells were then harvested and utilized for flow cytometry and RNA extraction.

Animals

All the animal procedures were approved by the Institutional Animal Care and Use Committee of Emory University. All *in vivo* experiments were carried out in female mice. *In vitro* experiments were conducted using primary cells from female mice or EL4 cells. Female C57BL/6 WT, TCRβ^{-/-}, DEREg, and Foxp3 eGFP knock-in mice were purchased from Jackson Laboratories (Bar Harbor, ME). All mice were maintained under specific pathogen-free conditions and fed sterilized food (5V5R chow) and autoclaved water *ad libitum*.

In vivo iPTH treatment

For the *in vivo* iPTH studies, 80 μg/kg/day of hPTH 1-34 (Bachem California Inc., Torrance, CA, USA) or vehicle was injected daily subcutaneously into female mice for 1–4 weeks starting at the age of 6 weeks, as described [11,20,22,62].

TGFβ1 and IGF-1 ELISA

BM cells from long bones were cultured for 24 h. Supernatants were collected and assayed for TGFβ1 or IGF-1 by ELISA kits (R&D Systems) following the manufacturer's instruction. When checking TGFβ1, the medium without the cells was run as the control of the baseline levels of TGFβ1. To isolate CD4⁺ T cells from BM, BM CD8⁺ T cells were discarded by EasySep Mouse CD8a Positive Selection Kit II (StemCell Technologies). CD4⁺ T cells were then positively isolated using APC-anti-TCRβ antibody and EasySep Mouse APC Positive Selection Kit (StemCell Technologies).

T-cell purification and adoptive transfer

Splenic T cells from 6- to 8-week-old Foxp3 eGFP knock-in mice were enriched by negative selection using EasySep Mouse T Cell Isolation Kit (StemCell Technologies). Next, conventional CD4⁺ T cells (CD4⁺eGFP⁻) were purified from enriched splenic T cells by FACS sorting and transferred into 4-week-old TCRβ^{-/-} recipient mice by IV injection (3 × 10⁶ cells per mouse). Recipient mice were treated with vehicle or iPTH for 1–4 weeks starting 2 weeks after the CD4⁺eGFP⁻ cell transfer. For Treg isolation, CD4⁺eGFP⁺ cells were sorted from enriched splenic T cells of Foxp3 eGFP knock-in mice and injected into 6-week-old TCRβ^{-/-} recipient mice via tail vein (2 × 10⁶ cells per mouse). The purity of CD4⁺eGFP⁺ cells was 99% checked by flow cytometry. Vehicle or iPTH treatment was started the day of the Treg transfer for 2 weeks. At the end of the treatment period, the number of CD4⁺eGFP⁺ cells was determined by flow cytometry in spleen and BM cells.

Small intestine Lamina propria lymphocyte (SILP) isolation

Lamina propria lymphocyte isolation was performed as described [63]. Briefly, the small intestine was removed and flushed of fecal contents, and intestinal segments containing Peyer's patches were excised. The intestine was opened longitudinally and cut into 5-mm pieces. Tissues were transferred into a 50-ml conical tube and

shaken at 250 rpm for 20 min at 37°C in HBSS medium (Life Technologies, Grand Island, NY, USA) supplemented with 5% FBS (Mediatech Inc., Manassas, VA, USA) containing 2 mM EDTA. The tissue suspension was passed through a strainer, and the remaining intestinal tissue was washed and then minced, transferred into a fresh 50-ml conical tube, and shaken for 20 min at 37°C in HBSS + 5% FBS containing type VIII collagenase (Sigma-Aldrich, St. Louis, MO, USA) at 1.5 mg/ml and DNase I at 100 µg/ml (Roche). The tissue suspension was collected, passed through a strainer, and pelleted by centrifugation at 267 g for 5 min. The pellet was suspended in 5 ml HBSS and 5 ml 90% isotonic Percoll, and then transferred into a 15-ml tube and mixed by tilting back and forth. The cell content was layered onto 2 ml of 70% isotonic Percoll. The gradient was centrifuged at 742 g for 20 min. Cells were collected from the interface area. When these cells were used for flow cytometry, the live cells were discriminated by LIVE/DEAD Fixable Yellow Dead Cell Stain Kit (ThermoFisher).

BrdU incorporation studies

Mice were injected IP with 40 mg/kg/day of BrdU solution for 4 days and sacrificed 24 h later. BrdU detection was performed by using the BrdU Flow Kit (BD Biosciences, San Diego, CA) and analyzing cells by flow cytometry. The percentage of BrdU⁺ Treg cells was quantified by gating CD4⁺Foxp3⁺ cells in the TCRβ⁺ cell population.

Anti-CD25 Ab treatment

Six-week-old WT mice were injected daily with vehicle or PTH for 4 weeks (days 1–28). Mice were also injected with anti-CD25 Ab (clone PC61, 500 µg/mouse/injection IP) (BioXCell, West Lebanon, NH, USA) on days –2, 0, 5, and 7 or isotype-matched irrelevant Ab.

DT treatment

DT was purchased from Merck (catalog number 322326), and each lot was tested for toxicity in WT mice and titrated for potency in DERE mice prior to use. DERE and littermate control mice were administered 1 µg DT intraperitoneally on two consecutive days each week for total 4 weeks.

µCT measurements

µCT scanning and analysis of the distal femur were performed as reported previously [20,64,65] using a Scanco µCT-40 scanner (Scanco Medical, Bassersdorf, Switzerland). Femoral trabecular and cortical bone regions were evaluated using isotropic 12-µm voxels. For the femoral trabecular region, we analyzed 140 slices from the 50 slices under the distal growth plate. Femoral cortical bone was assessed using 80 continuous CT slides located at the femoral midshaft. X-ray tube potential was 70 kVp, and integration time was 200 ms.

Quantitative bone histomorphometry

The measurements, terminology, and units used for histomorphometric analysis were those recommended by the Nomenclature

Committee of the American Society of Bone and Mineral Research [66]. Nonconsecutive longitudinal sections of the femur were prepared and analyzed as described previously [65]. Mice were injected subcutaneously with calcein at day 7 and day 2 before sacrifice. Nonconsecutive longitudinal sections (5 µm thick) were cut from methyl methacrylate plastic-embedded blocks along the frontal plane using a Leica RM2155 microtome and were stained with Goldner's trichrome stain for the static measurements. Additional sections were cut at 10 µm and left unstained for dynamic (fluorescent) measurements. Measurements were obtained in an area of cancellous bone that measured ≈ 2.5 mm² and contained only secondary spongiosa, which was located 0.5–2.5 mm proximal to the epiphyseal growth cartilage of the femurs. Measurements of single-labeled and double-labeled fluorescent surfaces and interlabel width were made in the same region of interest using unstained sections. Mineral apposition rate (MAR) and BFR were calculated by the software by applying the interlabel period. Histomorphometry was done using the Bioquant Image Analysis System (R&M Biometrics).

Markers of bone turnover

Serum CTX and osteocalcin were measured by rodent-specific ELISA assays (Immunodiagnostic Systems, Scottsdale, AZ, USA).

Stromal cell purification

BM SCs were purified as previously described [11,20,22]. In brief, BM cells from long bones were cultured for 7 days in α-MEM medium containing 10% FBS, 100 mg/ml of penicillin, and 100 IU/ml of streptomycin, to allow the proliferation of SCs. After removing nonadherent cells, adherent macrophages were eliminated by positive selection using anti-CD11c MACS Microbeads (Miltenyi Biotec, Auburn, CA, USA). The remaining adherent cells were defined as SCs as they express alkaline phosphatase (ALP), type I collagen, and Runx2, and have the capacity to form mineralization nodules when further cultured under mineralizing conditions.

SC thymidine incorporation assay

The proliferation of purified SCs was measured by [³H]-thymidine incorporation assay. SCs were pulsed with [³H]-thymidine (0.5 µCi/10,000 cells) for 18 h and were harvested with a Cell Harvester (Skatron, Inc., Sterling, VA, USA). [³H]-thymidine incorporation was read by a LS 6000 IC Liquid Scintillation Counter (Beckman Coulter, Inc., Fullerton, CA, USA).

SC apoptosis assay

The activity of caspase-3, the critical protease in the induction of apoptosis, was measured in SCs using CaspACE Assay System (Promega Corporation, Madison, WI, USA) according to the manufacturer's protocol.

In vitro Treg differentiation

Assessment of Treg differentiation *in vitro* was carried out as described [67]. Splenic CD4⁺ T cells from WT mice treated with

vehicle or iPTH were purified by negative selection using EasySep Mouse CD4⁺ T Cell Isolation Kit (StemCell Technologies). CD25⁺ cells were then removed using the EasySep Mouse CD25 Regulatory T Cell Positive Isolation Kit (StemCell Technologies). The remaining cells (CD25⁻ enriched CD4⁺ T cells) were cultured in plates coated with anti-CD3 Ab (3 µg/ml) in the presence of anti-CD28 Ab (3 µg/ml), IL-2 (5 ng/ml), and TGFβ1 (0.1–5 ng/ml) for 3 days. Cells were then harvested and analyzed by flow cytometry to enumerate CD4⁺Foxp3⁺ cells.

Western blotting

Resting or cultured conventional CD4⁺ T cells were lysed in lysis buffer (20 mM Tris-HCl, pH 7.5, 150 mM NaCl, 1 mM Na₂EDTA, 1 mM EGTA, 1% Triton X-100, 2.5 mM sodium pyrophosphate, 1 mM β-glycerophosphate, 1 mM Na₃VO₄, and 1 µg/ml leupeptin, Cell Signaling Technology, Danvers, MA, USA). Halt Protease and Phosphatase Inhibitor Cocktail (ThermoFisher Scientific) were added into the reagents before using. Lysates were cleared by centrifugation, and the supernatants were boiled in SDS loading buffer. The same amount of proteins was separated on 10% Mini-PROTEAN TGX Precast Gels (Bio-Rad) and electroblotted to nitrocellulose membrane (ThermoFisher Scientific). Proteins were detected by anti-Smad7 (catalog no. sc-365846, Santa Cruz Biotechnology), anti-phospho-Smad2 (Ser465/467) (catalog no. 3108), or anti-phospho-Smad3 (Ser423/425) (catalog no. 9520) (Cell Signaling Technology, Danvers, MA) antibodies. Anti-beta-actin (catalog no. sc-1616) antibody bought from Santa Cruz Biotechnology was used as the loading control. Western blot analysis was conducted by using Luminata Crescendo Western HRP substrate (EMD Millipore). Band intensities were quantified with Quantity One 1D Analysis Software (Bio-Rad Laboratories) and expressed relative to beta-actin.

Flow cytometry

Flow cytometry was performed on a LSR II system (BD Biosciences, Franklin Lakes, NJ, USA), and data were analyzed using FlowJo software (Tree Star, Inc., Ashland, OR). For intracellular Foxp3 staining, APC-Foxp3 (clone FJK-16s, eBioscience) antibody was added after cell fixation and permeabilization with BD Transcription Factor Buffer Set (BD Biosciences). The following anti-mouse antibodies were used for cell surface staining: purified CD16/32, BV 421-TCRβ (clone H57-597), PerCP/Cy5.5-CD4 (clone RM4-5), PE-CD25 (clone PC61), and BV 711-CD8 (clone 53-6.7) (Biolegend).

Real-time RT-PCR and murine primers

Total RNA was isolated from total BM cells and SCs using TRIzol reagent (ThermoFisher Scientific). cDNA was synthesized with random hexamer primers (Roche) and AMV reverse transcriptase (Roche). mRNA levels of bone sialoprotein (BSP), collagen 1 (Col1), osteocalcin (Ocn), osterix (Osx), and runt-related transcription factor 2 (Runx2) in SCs and that of TNF, IL-6, IFNγ, IL-4, IL-13, and IL-17A in total BM were quantified by real-time PCR. Changes in relative gene expression between vehicle and iPTH groups were calculated using the 2^{-ΔΔC_T} method with normalization to 18S rRNA. The primers used are provided in Appendix Table S1.

Statistical analysis

Human Tregs and human TGFβ1 data were analyzed by ANOVA for repeated measures. Human demographic and clinical data were analyzed by unpaired two-tailed *t*-tests. When murine data were normally distributed according to the Shapiro–Wilk normality test, they were analyzed by unpaired two-tailed *t*-tests, one-way or two-way analysis of variance, as appropriate. This analysis included the main effects for animal strain and treatment plus the statistical interaction between animal strain and treatment. When the statistical interaction between animal strain and treatment group was not statistically significant ($P > 0.05$) nor suggestive of an important interaction ($P > 0.10$), *P*-values for the main effects tests were reported. When the statistical interaction was statistically significant ($P < 0.05$) or suggestive of an important interaction, then *t*-tests were used to compare the differences between the treatment means for each animal strain, applying the Bonferroni correction for multiple comparisons. Data that were not normally distributed (as tested by Shapiro–Wilk normality test) were analyzed by Kruskal–Wallis nonparametric tests.

Expanded View for this article is available online.

Acknowledgements

This study was supported by grants from the National Institutes of Health (RP: DK108842, AR54625, and RR028009; JYL: AR061453; MNW: AG040013, AR068157, and AR070091). MNW was also supported by a grant from the Biomedical Laboratory Research & Development Service of the VA Office of Research and Development (5I01BX000105).

Author contributions

MY, RDP, MNW, and RP designed the animal studies. PDA, FS, and IB designed and performed the human studies and analyzed the human data. MY, CV, AMT, J-YL, EH, and JA performed the research and analyzed the animal data. RP wrote the manuscript.

Conflict of interest

The authors declare that they have no conflict of interest.

References

1. Grey AB, Stapleton JP, Evans MC, Reid IR (1996) Accelerated bone loss in post-menopausal women with mild primary hyperparathyroidism. *Clin Endocrinol (Oxf)* 44: 697–702
2. Potts J (1998) Primary hyperparathyroidism. *Metab Bone Dis* 1: 411–442
3. Uzawa T, Hori M, Ejiri S, Ozawa H (1995) Comparison of the effects of intermittent and continuous administration of human parathyroid hormone (1–34) on rat bone. *Bone* 16: 477–484
4. Jilka RL (2007) Molecular and cellular mechanisms of the anabolic effect of intermittent PTH. *Bone* 40: 1434–1446
5. Zaidi M (2007) Skeletal remodeling in health and disease. *Nat Med* 13: 791–801
6. Calvi LM, Sims NA, Hunzelman JL, Knight MC, Giovannetti A, Saxton JM, Kronenberg HM, Baron R, Schipani E (2001) Activated parathyroid hormone/parathyroid hormone-related protein receptor in osteoblastic cells differentially affects cortical and trabecular bone. *J Clin Invest* 107: 277–286

7. Lanske B, Amling M, Neff L, Guiducci J, Baron R, Kronenberg HM (1999) Ablation of the PTHrP gene or the PTH/PTHrP receptor gene leads to distinct abnormalities in bone development. *J Clin Invest* 104: 399–407
8. Powell WF Jr, Barry KJ, Tulum I, Kobayashi T, Harris SE, Bringhurst FR, Pajevic PD (2011) Targeted ablation of the PTH/PTHrP receptor in osteocytes impairs bone structure and homeostatic calcemic responses. *J Endocrinol* 209: 21–32
9. Rhee Y, Allen MR, Condon K, Lezcano V, Ronda AC, Galli C, Olivos N, Passeri G, O'Brien CA, Bivi N et al (2011) PTH receptor signaling in osteocytes governs periosteal bone formation and intracortical remodeling. *J Bone Miner Res* 26: 1035–1046
10. Saini V, Marengi DA, Barry KJ, Fulzele KS, Heiden E, Liu X, Dedic C, Maeda A, Lotinun S, Baron R et al (2013) Parathyroid hormone (PTH)/PTH-related peptide type 1 receptor (PPR) signaling in osteocytes regulates anabolic and catabolic skeletal responses to PTH. *J Biol Chem* 288: 20122–20134
11. Terauchi M, Li JY, Bedi B, Baek KH, Tawfeek H, Galley S, Gilbert L, Nanes MS, Zayzafoon M, Guldberg R et al (2009) T lymphocytes amplify the anabolic activity of parathyroid hormone through Wnt10b signaling. *Cell Metab* 10: 229–240
12. Cho SW, Soki FN, Koh AJ, Eber MR, Entezami P, Park SI, van Rooijen N, McCauley LK (2014) Osteal macrophages support physiologic skeletal remodeling and anabolic actions of parathyroid hormone in bone. *Proc Natl Acad Sci USA* 111: 1545–1550
13. Qin L, Raggatt LJ, Partridge NC (2004) Parathyroid hormone: a double-edged sword for bone metabolism. *Trends Endocrinol Metab* 15: 60–65
14. Kramer I, Loots GG, Studer A, Keller H, Kneissel M (2010) Parathyroid hormone (PTH)-induced bone gain is blunted in SOST overexpressing and deficient mice. *J Bone Miner Res* 25: 178–189
15. Wan M, Yang C, Li J, Wu X, Yuan H, Ma H, He X, Nie S, Chang C, Cao X (2008) Parathyroid hormone signaling through low-density lipoprotein-related protein 6. *Genes Dev* 22: 2968–2979
16. Keller H, Kneissel M (2005) SOST is a target gene for PTH in bone. *Bone* 37: 148–158
17. Bellido T, Ali AA, Gubrij I, Plotkin LI, Fu Q, O'Brien CA, Manolagas SC, Jilka RL (2005) Chronic elevation of parathyroid hormone in mice reduces expression of sclerostin by osteocytes: a novel mechanism for hormonal control of osteoblastogenesis. *Endocrinology* 146: 4577–4583
18. Silvestrini G, Ballanti P, Leopizzi M, Sebastiani M, Berni S, Di Vito M, Bonucci E (2007) Effects of intermittent parathyroid hormone (PTH) administration on SOST mRNA and protein in rat bone. *J Mol Histol* 38: 261–269
19. Guo J, Liu M, Yang D, Bouxsein ML, Saito H, Galvin RJ, Kuhstoss SA, Thomas CC, Schipani E, Baron R et al (2010) Suppression of Wnt signaling by Dkk1 attenuates PTH-mediated stromal cell response and new bone formation. *Cell Metab* 11: 161–171
20. Li JY, Walker LD, Tyagi AM, Adams J, Weitzmann MN, Pacifici R (2014) The sclerostin-independent bone anabolic activity of intermittent PTH treatment is mediated by T-cell-produced Wnt10b. *J Bone Miner Res* 29: 43–54
21. Pacifici R (2013) Role of T cells in the modulation of PTH action: physiological and clinical significance. *Endocrine* 44: 576–582
22. Bedi B, Li JY, Tawfeek H, Baek KH, Adams J, Vangara SS, Chang MK, Kneissel M, Weitzmann MN, Pacifici R (2012) Silencing of parathyroid hormone (PTH) receptor 1 in T cells blunts the bone anabolic activity of PTH. *Proc Natl Acad Sci USA* 109: E725–E733
23. Bennett CN, Ouyang H, Ma YL, Zeng Q, Gerin I, Sousa KM, Lane TF, Krishnan V, Hankenson KD, MacDougald OA (2007) Wnt10b increases postnatal bone formation by enhancing osteoblast differentiation. *J Bone Miner Res* 22: 1924–1932
24. Abbas AK, Benoist C, Bluestone JA, Campbell DJ, Ghosh S, Hori S, Jiang S, Kuchroo VK, Mathis D, Roncarolo MG et al (2013) Regulatory T cells: recommendations to simplify the nomenclature. *Nat Immunol* 14: 307–308
25. Shevach EM (2009) Mechanisms of Foxp3⁺ T regulatory cell-mediated suppression. *Immunity* 30: 636–645
26. Kim YG, Lee CK, Nah SS, Mun SH, Yoo B, Moon HB (2007) Human CD4⁺CD25⁺ regulatory T cells inhibit the differentiation of osteoclasts from peripheral blood mononuclear cells. *Biochem Biophys Res Commun* 357: 1046–1052
27. Yuan FL, Li X, Lu WG, Xu RS, Zhao YQ, Li CW, Li JP, Chen FH (2010) Regulatory T cells as a potent target for controlling bone loss. *Biochem Biophys Res Commun* 402: 173–176
28. Zaiss MM, Sarter K, Hess A, Engelke K, Bohm C, Nimmerjahn F, Voll R, Schett G, David JP (2010) Increased bone density and resistance to ovariectomy-induced bone loss in FoxP3-transgenic mice based on impaired osteoclast differentiation. *Arthritis Rheum* 62: 2328–2338
29. Zaiss MM, Axmann R, Zwerina J, Polzer K, Guckel E, Skapenko A, Schulze-Koops H, Horwood N, Cope A, Schett G (2007) Treg cells suppress osteoclast formation: a new link between the immune system and bone. *Arthritis Rheum* 56: 4104–4112
30. Kelchtermans H, Geboes L, Mitera T, Huskens D, Leclercq G, Matthys P (2009) Activated CD4⁺CD25⁺ regulatory T cells inhibit osteoclastogenesis and collagen-induced arthritis. *Ann Rheum Dis* 68: 744–750
31. Chen W, Jin W, Hardegen N, Lei KJ, Li L, Marinon N, McGrady G, Wahl SM (2003) Conversion of peripheral CD4⁺CD25[−] naive T cells to CD4⁺CD25⁺ regulatory T cells by TGF-beta induction of transcription factor Foxp3. *J Exp Med* 198: 1875–1886
32. Liu Y, Zhang P, Li J, Kulkarni AB, Perruche S, Chen W (2008) A critical function for TGF-beta signaling in the development of natural CD4⁺CD25⁺Foxp3⁺ regulatory T cells. *Nat Immunol* 9: 632–640
33. Ohkura N, Kitagawa Y, Sakaguchi S (2013) Development and maintenance of regulatory T cells. *Immunity* 38: 414–423
34. Anguela XM, Tafuro S, Roca C, Callejas D, Agudo J, Obach M, Ribera A, Ruzo A, Mann CJ, Casellas A et al (2013) Nonviral-mediated hepatic expression of IGF-I increases Treg levels and suppresses autoimmune diabetes in mice. *Diabetes* 62: 551–560
35. Johannesson B, Sattler S, Semenova E, Pastore S, Kennedy-Lydon TM, Sampson RD, Schneider MD, Rosenthal N, Bilbao D (2014) Insulin-like growth factor-1 induces regulatory T cell-mediated suppression of allergic contact dermatitis in mice. *Dis Model Mech* 7: 977–985
36. Pfeilschifter J, Laukhuf F, Muller-Beckmann B, Blum WF, Pfister T, Ziegler R (1995) Parathyroid hormone increases the concentration of insulin-like growth factor-1 and transforming growth factor beta 1 in rat bone. *J Clin Invest* 96: 767–774
37. Cho SW, Pirih FQ, Koh AJ, Michalski M, Matt E, Ritchie K, Sinder B, Oh S, Al-Dujaili SA, Lee J et al (2013) The soluble interleukin-6 receptor is a mediator of hematopoietic and skeletal actions of parathyroid hormone. *J Biol Chem* 288: 6814–6825
38. McCarthy TL, Centrella M, Canalis E (1989) Parathyroid hormone enhances the transcript and polypeptide levels of insulin-like growth factor I in osteoblast-enriched cultures from fetal rat bone. *Endocrinology* 124: 1247–1253
39. Oursler MJ, Cortese C, Keeting P, Anderson MA, Bonde SK, Riggs BL, Spelsberg TC (1991) Modulation of transforming growth factor-beta

- production in normal human osteoblast-like cells by 17 beta-estradiol and parathyroid hormone. *Endocrinology* 129: 3313–3320
40. Wu Y, Kumar R (2000) Parathyroid hormone regulates transforming growth factor beta1 and beta2 synthesis in osteoblasts via divergent signaling pathways. *J Bone Miner Res* 15: 879–884
 41. Esen E, Lee SY, Wice BM, Long F (2015) PTH promotes bone anabolism by stimulating aerobic glycolysis via IGF signaling. *J Bone Miner Res* 30: 1959–1968
 42. Chaudhry A, Rudensky AY (2013) Control of inflammation by integration of environmental cues by regulatory T cells. *J Clin Invest* 123: 939–944
 43. Duarte JH, Zelenay S, Bergman ML, Martins AC, Demengeot J (2009) Natural Treg cells spontaneously differentiate into pathogenic helper cells in lymphopenic conditions. *Eur J Immunol* 39: 948–955
 44. Karlsson F, Robinson-Jackson SA, Gray L, Zhang S, Grisham MB (2011) *Ex vivo* generation of regulatory T cells: characterization and therapeutic evaluation in a model of chronic colitis. *Methods Mol Biol* 677: 47–61
 45. Roncador G, Brown PJ, Maestre L, Hue S, Martinez-Torrecuadrada JL, Ling KL, Pratap S, Toms C, Fox BC, Cerundolo V et al (2005) Analysis of FOXP3 protein expression in human CD4⁺CD25⁺ regulatory T cells at the single-cell level. *Eur J Immunol* 35: 1681–1691
 46. Tan C, Reddy V, Dannull J, Ding E, Nair SK, Tyler DS, Pruitt SK, Lee WT (2013) Impact of anti-CD25 monoclonal antibody on dendritic cell-tumor fusion vaccine efficacy in a murine melanoma model. *J Transl Med* 11: 148
 47. Setiady YY, Coccia JA, Park PU (2010) *In vivo* depletion of CD4⁺FOXP3⁺ Treg cells by the PC61 anti-CD25 monoclonal antibody is mediated by Fcγ3⁺ phagocytes. *Eur J Immunol* 40: 780–786
 48. Betts RJ, Ho AW, Kemeny DM (2011) Partial depletion of natural CD4(+) CD25(+) regulatory T cells with anti-CD25 antibody does not alter the course of acute influenza A virus infection. *PLoS One* 6: e27849
 49. Bertolini DR, Nedwin GE, Bringman TS, Smith DD, Mundy GR (1986) Stimulation of bone resorption and inhibition of bone formation *in vitro* by human tumor necrosis factor. *Nature* 319: 516–518
 50. Lahl K, Loddenkemper C, Drouin C, Freyer J, Arnason J, Eberl G, Hamann A, Wagner H, Huehn J, Sparwasser T (2007) Selective depletion of Foxp3⁺ regulatory T cells induces a scurfy-like disease. *J Exp Med* 204: 57–63
 51. Klingenberg R, Gerdes N, Badeau RM, Gistera A, Strodtzoff D, Ketelhuth DF, Lundberg AM, Rudling M, Nilsson SK, Olivecrona G et al (2013) Depletion of FOXP3⁺ regulatory T cells promotes hypercholesterolemia and atherosclerosis. *J Clin Invest* 123: 1323–1334
 52. Lahl K, Sparwasser T (2011) *In vivo* depletion of FoxP3⁺ Tregs using the DEREK mouse model. *Methods Mol Biol* 707: 157–172
 53. Koh AJ, Novince CM, Li X, Wang T, Taichman RS, McCauley LK (2011) An irradiation-altered bone marrow microenvironment impacts anabolic actions of PTH. *Endocrinology* 152: 4525–4536
 54. Trzonkowski P, Bieniaszewska M, Juscinska J, Dobyszuk A, Krzystyniak A, Marek N, Mysliwska J, Hellmann A (2009) First-in-man clinical results of the treatment of patients with graft versus host disease with human *ex vivo* expanded CD4⁺CD25⁺CD127⁻ T regulatory cells. *Clin Immunol* 133: 22–26
 55. Brunstein CG, Miller JS, Cao Q, McKenna DH, Hippen KL, Curtsinger J, Defor T, Levine BL, June CH, Rubinstein P et al (2011) Infusion of *ex vivo* expanded T regulatory cells in adults transplanted with umbilical cord blood: safety profile and detection kinetics. *Blood* 117: 1061–1070
 56. Di Ianni M, Falzetti F, Carotti A, Terenzi A, Castellino F, Bonifacio E, Del Papa B, Zei T, Ostini RI, Cecchini D et al (2011) Tregs prevent GVHD and promote immune reconstitution in HLA-haploidentical transplantation. *Blood* 117: 3921–3928
 57. Marek-Trzonkowska N, Mysliwiec M, Dobyszuk A, Grabowska M, Techmanska I, Juscinska J, Wujtewicz MA, Witkowski P, Mlynarski W, Balcerska A et al (2012) Administration of CD4⁺CD25^{high}CD127⁻ regulatory T cells preserves beta-cell function in type 1 diabetes in children. *Diabetes Care* 35: 1817–1820
 58. Feng F, Hu P, Chen L, Tang Q, Lian C, Yao Q, Chen K (2013) Display of human proinsulin on the *Bacillus subtilis* spore surface for oral administration. *Curr Microbiol* 67: 1–8
 59. von Boehmer H, Daniel C (2013) Therapeutic opportunities for manipulating T(Reg) cells in autoimmunity and cancer. *Nat Rev Drug Discov* 12: 51–63
 60. (1984) Osteoporosis. National Institutes of Health Consensus Development Conference Statement. *Natl Inst Health Consens Dev Conf Consens Statement* 5: 6
 61. D'Amelio P, Grimaldi A, Pescarmona GP, Tamone C, Roato I, Isaia G (2005) Spontaneous osteoclast formation from peripheral blood mononuclear cells in postmenopausal osteoporosis. *FASEB J* 19: 410–412
 62. Li JY, Adams J, Calvi LM, Lane TF, DiPaolo R, Weitzmann MN, Pacifici R (2012) PTH expands short-term murine hemopoietic stem cells through T cells. *Blood* 120: 4352–4362
 63. Li JY, Chassaing B, Tyagi AM, Vaccaro C, Luo T, Adams J, Darby TM, Weitzmann MN, Mülle JG, Gewirtz AT et al (2016) Sex steroid deficiency-associated bone loss is microbiota dependent and prevented by probiotics. *J Clin Invest* 126: 2049–2063
 64. Robinson JW, Li JY, Walker LD, Tyagi AM, Reott MA, Yu M, Adams J, Weitzmann MN, Pacifici R (2015) T cell-expressed CD40L potentiates the bone anabolic activity of intermittent PTH treatment. *J Bone Miner Res* 30: 695–705
 65. Li JY, D'Amelio P, Robinson J, Walker LD, Vaccaro C, Luo T, Tyagi AM, Yu M, Reott M, Sassi F et al (2015) IL-17A is increased in humans with primary hyperparathyroidism and mediates PTH-induced bone loss in mice. *Cell Metab* 22: 799–810
 66. Dempster DW, Compston JE, Drezner MK, Glorieux FH, Kanis JA, Malluche H, Meunier PJ, Ott SM, Recker RR, Parfitt AM (2013) Standardized nomenclature, symbols, and units for bone histomorphometry: a 2012 update of the report of the ASBMR Histomorphometry Nomenclature Committee. *J Bone Miner Res* 28: 2–17
 67. Fantini MC, Dominitzki S, Rizzo A, Neurath MF, Becker C (2007) *In vitro* generation of CD4⁺ CD25⁺ regulatory cells from murine naive T cells. *Nat Protoc* 2: 1789–1794